STUDY OF SEEPAGE THROUGH EARTHEN DAM AND FOUNDATION BY NUMERICAL AND CENTRIFUGE MODELING

Thesis submitted by

SMITA TUNG

DOCTOR OF PHILOSOPHY (ENGINEERING)

DEPARTMENT OF CIVIL ENGINEERING
JADAVPUR UNIVERSITY
KOLKATA – 700 032, INDIA

2018

JADAVPUR UNIVERSITY
KOLKATA – 700032, INDIA

INDEX NO.40/14/Engineering

1. Title of the Thesis

STUDY OF SEEPAGE THROUGH EARTHEN DAM AND FOUNDATION BY NUMERICAL AND CENTRIFUGE MODELING

2. Name, Designation and Institution of the Supervisor

Dr. GUPINATH BHANDARI
Associate Professor

(Dr.) SIBAPRIYA MUKHERJEE
Professor

Department of Civil Engineering
Jadavpur University, Kolkata 700032, India

3. List of Publications:

(a) Journal papers (2 published)

(i) International Journal of Geotechnical Engineering, Taylor and Francis Group, Vol. 10, issue 2, pp. 162-173, 2016. "BEHAVIOR OF SHEET PILE AS SEEPAGE CUTOFF BELOW EARTHEN DAM".

(ii) Advanced Engineering Forum, ISSN: 2234- 991X, Trans Tech Publications, Switzerland, Vol. 21, pp 389-396. "STABILITY ANALYSIS OF THE EARTH EMBANKMENTS SUBJECTED TO NATURAL CYCLIC PROCESSES''

(b) Conference papers (3 published)

(i) S.Tung, G. Bhandari, S.P. Mukherjee and K. Deb , (2013) "EFFECT OF SHEET PILE ON SEEPAGE BELOW EARTHEN DAM" , IGC-2013,December, Roorkee.

(ii) S.Tung, G. Bhandari, S.P. Mukherjee, (2015) "EFFECT OF SEEPAGE CUTOFF BELOW EARTHEN DAM UNDER RAPID DRAWSOWN" , IGC-2015, PUNE

(iii) S.Tung, S.P. Mukherjee, G. Bhandari (2016) "EFFECT OF SEEPAGE CUTOFF ON SOME IMPORTANT ASPECTS OF EARTHEN DAM UNDER RISE UP CONDITION BY NUMERICAL MODELLING", GEOTECHNICS FOR INFRASTRUCTURE DEVELOPMENT -2016,KOLKATA.

4. **List of Patents :** NIL

5. List of Presentations in National/International/Conference/workshops:

Presentation in National conferences: 02
Presentation in National conferences: NIL

CERTIFICATE FROM THE SUPERVISORS

This is to certify that the Thesis entitled "STUDY OF SEEPAGE THROUGH EARTHEN DAM AND FOUNDATION BY NUMERICAL AND CENTRIFUGE MODELING " submitted by Smita Tung, Who got his name registered on 29th October, 2014 for the award of Ph.D. (Engineering) degree of Jadavpur University, is absolutely based upon his own work under the joint supervision of Dr. GUPINATH BHANDARI and (Prof) Dr. S.P. MUKHERJEE and that neither his Thesis nor any part of the Thesis has been submitted for any degree / diploma are only other academic award anywhere before.

Dr. GUPINATH BHANDARI
Associate Professor

Dr. SIBAPRIYA MUKHERJEE
Professor

Department of Civil Engineering
Jadavpur University, Kolkata 700032, India

(Signature of Supervisor & date with Official seal)

ACKNOWLEDGEMENT

I wish to express my whole hearted and deep gratitude to Dr. Sibapriya Mukherjee, Professor and Dr. Gupinath Bhandari, Associate Professor of Civil Engineering Department, Jadavpur University, for their valuable guidance, constant support and encouragement throughout my PhD research work without which the thesis could not be completed. This has been a precious opportunity for me not only to gain knowledge and skill but also to learn much more about approaches, attitudes towards work and interpersonal relationship. I am extremely thankful to both the supervisors with their readiness for academic discussions and general help which were of immense value to me.

I am sincerely thankful and indebted to Prof. Dipankar Chakraborty, Head, Civil Engineering Department, Prof. R. B. Sahu, Prof. P. Aitch, Prof. S. K. Biswas and Dr. N. Roy, Faculty members of Soil Mechanics and foundation Engineering Division of Civil Engineering Department, Jadavpur University for their constant encouragement and continuous valuable suggestions throughout my work.

My sincere thanks have been extended to Prof. S. N. Ghosh, Prof. S. Mondal, Prof. A Guha Niyogi, Prof. P. Bhattacharya, Prof. K. Mandal, Prof. S. Roychowdhury, Prof. S. Pal, Prof. S. K. De, Prof. A. Sheuli, Prof. A Dutta, Prof. A. Debsarkar, Prof. S. N. Chakraborty, Prof. S. N. Mukherjee, Prof. T. Hazra.

I sincerely acknowledge with thanks the help rendered by Sharmistha Bhattacharjee, NIELIT, Kolkata Center, Sri. Sabyasachi Mukherjee, Master degree of Civil Engineering, Jadavpur University for helping me a lot throughout my experimental work.

I am also thankful to Soil mechanics Laboratory staff Sri. Robin Pal, Sri. Apurba Banerjee and Sri. Ranjit Kushari and others for their support and cooperation during my experimental work in the laboratory.

Thanks to all other Teachers and Staff members of Civil Engineering Department for extending their kind co-operation towards me during the work.

Finally, but most importantly, my parents, my younger sister and my seniors have always been there for me during the ups and downs, sharing my excitement and frustration. Their love and understanding have allowed me to make this thesis successfully.

DATE: **SMITA TUNG**

PLACE: JADAVPUR

ABSTRACT

A dam is constructed across a river, as a barrier, to impound water in the reservoir to use it for various purposes like irrigation; navigation etc. One of the main problems that affects the design life of an earthen embankment is seepage both steady and transient seepage. The present study consists of experimental and numerical modelling of a model earthen embankment simulating soil conditions of South 24 parganas, West Bengal, India. Both steady and transient cases of seepage have been considered for the study. In case of transient seepage with rise up and drawdown conditions, diurnal tidal head variation has been considered to occur of 3.5 m in 6 hours. It is obvious that seepage through and below an earthen dam plays an important role in determining the stability of a dam. Therefore, the effect of sheet pile as seepage cut off has been studied with variation of the sheet pile length and location under steady state and transient state for both static and seismic conditions. The analysis has been done using FLAC2D version 5.0, SEEP/W version 12.0 after validating the flownet by MATLAB version 14.0, for a dam of top width 1m bottom width 17m and height of 4m with upstream water level of 3.5 m and no downstream head. The study has been done for homogeneous soil medium. It was considered that a soft clayey soil was present down to a depth of 20 m below the dam. The foundation of the dam has also been considered clayey to simulate soil condition of a location at South 24 Parganas in West Bengal, India. Experimental study has been performed by centrifuge modeling to supplement the numerical studies. Considering Scale factor N= 100g, g being acceleration due to gravity, the model has been rotated at a speed of 400 rpm. The circuit of artificial tide control, based on solenoid valve, Arduino, IR sensor has been implemented in the geotechnical centrifugal machine to provide an artificial tide like river in nature. With the help of Raspberry Pi camera module Images have been captured at regular intervals of every few seconds. The images obtained from centrifuge modeling have been thereafter processed through MATLAB- Raspberry Pi interfacing. Particle Image Velocimetry (PIV) processing have been adopted by Fast Fourier Transform (FFT) cross correlation. The PIV results indicate a clear representation of the stream flow and flow vector for variation of sheet pile length and position under steady and transient states. Based on the images obtained from the experiments, streamlines and flow vectors from each experimental model have been compared with numerical results and found to match well for all the cases. Thereafter pore pressures along middle horizontal section of the dam and along different levels of foundation have been obtained from results of numerical and experimental studies. The results indicate that during both steady seepage and transient seepage cases, pore pressure is high on the upstream side of sheet pile and it

suddenly reduces along the sheet pile itself for all sheet pile positions. Sheet pile length had significant effect on pore pressure variation along the sheet pile. The salient observations indicate that, for 5m length to 20m length the decrease of pore pressure is varying from 7.57% to 16.66% for 3*B*/8 position, from downstream end at base, whereas for B/8 position it varies from 18.083% to 28.33% under rise up condition and the same for drawdown condition is varying from 8.48% to 11.71% for 3*B*/8 position; whereas for *B*/8 position it varies from 9.78% to 29.29%. Again in seismic cases under steady state condition as pore water pressure increases the factor of safety is also reduced by 45% to 50% compared to corresponding static cases due to increase of seepage force.

It is observed at the end that in case of the model dam piping failure occurs after subsequent cycles of rise up and drawdown. Pore water pressure during the multiple tidal cycles and this led to serviceability failure, as they encountered cyclic settlement and rebound, resulting in permanent deformation. It has been observed that in case of 120 cycles reduction factor of safety is 8.3%, 26% and 40%, on an average, compared to 80 cycles, 20 cycles and single tidal cycle respectively. The factor of safety against piping has been found to increase with increase of length of sheet pile at fixed location with respect to base width of a dam. When the location of sheet pile of a fixed length was moved towards the downstream side of the dam the factor of safety against piping was found to increase. The overall factor of safety (with consideration of both stability and piping) increased when sheet pile was considered to be placed below a dam compared to the condition when no sheet pile was considered. Under full rise up condition considering 5m of sheet pile at *B*/8 position factor of safety against piping increases up to 37.00% compared to 3*B*/8 position whereas this is approximately 18.75% for 2B/8 position, compared to 3*B*/8 position.

This present research also brings out the effect of tide induced transient seepage on earthen embankments under seismic condition. It has been seen that under seismic condition stability is affected to a large extent, as suggested by reduction of factor of safety. Pore water pressure variation and fluid flow vector in vertical direction was found to be erratic under seismic condition. The effectiveness of sheet pile as seepage cutoff has been found to be very effective for all the cases of steady and transient seepage under seismic and non-seismic conditions.

The outcome of the study is expected to be useful for practical engineers in case of stability analysis of an earthen dam with similar soil condition.

CONTENTS

Chapter 1	INTRODUCTION	Page no.
	1.1 An Overview	1
	1.2 Objective and Scope	2
	1.2.1 Objective	2
	1.2.2 Scope of Work	3
	1.3 The Present Study	4
	1.4 Organization of the Thesis	5
Chapter 2	LITERATURE REVIEW	
	2.1 General	7
	2.2 Steady Seepage	7
	2.3 Unsteady Seepage	9
	2.4 Slope Stability Analysis	18
	2.4.1 Static Condition	18
	2.4.2 Seismic Condition	20
	2.5 Experimental Modeling in Centrifuge of Seepage Analysis	24
	2.6 Summary of Findings From Past Studies	26
	2.7 Research Gap	27
Chapter 3	NUMERICAL MODELING	
	3.1 General	28
	3.2 Parametric study	29
	3.3Modelling by MATLAB	35
	3.3.2 Mathematical background of formulation for PDE analysis in MATLAB	37
	3.4Modelling by FLAC 2D	40
	3.4.1. Detailed analysis in FLAC 2D	40
	3.4.1.1. Generation of mesh and boundary condition	41
	3.4.1.2. Interface element and material properties	41
	3.4.1.3 Effective stress analyses	43
	3.4.1.4Seismic study	43
	3.5. Modeling by GEOSTUDIO	44
	3.5.1 Mathematical formulation	45
	3.5.2 Finite element by GEOSTUDIO	46
	3.5.2.1. Geometry and mesh generation	47
	3.5.2.2 Interface element and boundary condition	47
	3.5.2.3Material properties	48
	3.5.2.4 Deformation based coupled analysis	49
	3.6 Presentation of numerical results	51
	3.6.1 Phreatic surface and flow net in steady state condition (with out cut off)	52
	3.6.1.1. Presentation of result from MATLAB	52

3.6.1.2. Presentation of result from FLAC 2D 52
3.6.1.3. Presentation of result from SEEP/W 53
3.6.2 Phreatic surface and flownet in steady state condition (with cut off) 54
3.6.2.1. Presentation of result from MATLAB 54
3.6.2.2. Presentation of result from FLAC 2D 57
3.6.2.3. Presentation of result from SEEP/W 60
3.6.3 Dynamics of phreatic surface and flow net single tidal cycle: effect of rise-up and draw-down rate (without cut off) 64
3.6.3.1 Presentation of result from MATLAB 64
3.6.3.2 Presentation of result from FLAC 2D 65
3.6.3.3 Presentation of result from SEEP/W 68
3.6.4 Dynamics of phreatic surface and flownet in transient condition: rise up and drawdown (with cut off) 69
3.6.4.1. Presentation of result from MATLAB 69
3.6.4.1.1 Presentation of result for 5 m long sheet pile B/8position from downstream end 70
3.6.4.1.2 Presentation of result for 10 m long sheet pile B/8position from downstream end 71
3.6.4.1.3 Presentation of result for 15 m long sheet pile B/8position from downstream end 73
3.6.4.1.4 Presentation of result for 20 m long sheet pile B/8position from downstream end 74
3.6.4.1.5 Presentation of result for 5 m long sheet pile 2B/8position from downstream end 74
3.6.4.1.6 Presentation of result for 10 m long sheet pile 2B/8position from downstream end 79
3.6.4.1.7 Presentation of result for 15 m long sheet pile 2B/8position from downstream end 81
3.6.4.1.8 Presentation of result for 20 m long sheet pile 2B/8position from downstream end 83
3.6.4.1.9 Presentation of result for 5 m long sheet pile 3B/8position from downstream end 85
3.6.4.1.10 Presentation of result for 10 m long sheet pile 3B/8position from downstream end 86
3.6.4.1.11 Presentation of result for 15 m long sheet pile 3B/8position from downstream end 88
3.6.4.1.12 Presentation of result for 20 m long sheet pile 3B/8position from downstream end 89
3.6.4.2. Presentation of result of FLAC 2D 91
3.6.4.2.1 Presentation of result for 5 m long sheet pile B/8position from downstream end 91
3.6.4.2.2 Presentation of result for 10 m long sheet pile B/8position from downstream end 93

3.6.4.2.3 Presentation of result for 15 m long sheet pile B/8position from downstream end 94
3.6.4.2.4 Presentation of result for 20 m long sheet pile B/8position from downstream end 96
3.6.4.2.5 Presentation of result for 5 m long sheet pile 2B/8position from downstream end 98
3.6.4.2.6 Presentation of result for 10 m long sheet pile 2B/8position from downstream end 99
3.6.4.2.7 Presentation of result for 15 m long sheet pile 2B/8position from downstream end 101
3.6.4.2.8 Presentation of result for 20 m long sheet pile 2B/8position from downstream end 102
3.6.4.2.9 Presentation of result for 5 m long sheet pile 3B/8position from downstream end 104
3.6.4.2.10 Presentation of result for 10 m long sheet pile 3B/8position from downstream end 105
3.6.4.2.11 Presentation of result for 15 m long sheet pile 3B/8position from downstream end 107
3.6.4.2.12 Presentation of result for 20 m long sheet pile 3B/8position from downstream end 108
3.6.4.3. Presentation of result of SEEP/W 109
3.6.4.3.1 Presentation of result for 5 m long sheet pile B/8position from downstream end 110
3.6.4.3.2 Presentation of result for 10m long sheet pile B/8position from downstream end 112
3.6.4.3.3 Presentation of result for 15m long sheet pile B/8position from downstream end 114
3.6.4.3.4 Presentation of result for 20m long sheet pile B/8position from downstream end 115
3.6.4.3.5 Presentation of result for 5m long sheet pile 2B/8position from downstream end 117
3.6.4.3.6 Presentation of result for 10m long sheet pile 2B/8position from downstream end 118
3.6.4.3.7 Presentation of result for 15m long sheet pile 2B/8position from downstream end 119
3.6.4.3.8 Presentation of result for 20m long sheet pile 2B/8position from downstream end 121
3.6.4.3.8 Presentation of result for 20m long sheet pile 2B/8position from downstream end 123
3.6.4.3.10 Presentation of result for 10m long sheet pile 3B/8position from downstream end 125
3.6.4.3.11 Presentation of result for 15m long sheet pile 3B/8position from downstream end 127

3.6.4.3.12 Presentation of result for 20m long sheet pile 3B/8position from downstream end 129
3.6.5 Phreatic surface under Multiple tidal cycle condition 131
3.6.6 Phreatic surface and flownet under seismic condition 132
3.6.6.1 analytical validation 132
3.6.6.2 Presentation of results under steady state (seismic condition) 133
3.6.6.2.1 Presentation of results from FLAC 2D for without sheet pile under steady state (seismic condition) 133
3.6.6.2.2 Presentation of results from SEEP/W for without sheet pile under steady state 133
3.6.6.2.3 Presentation of results from FLAC 2D for with sheet pile under steady state 134
3.6.6.2.4 Presentation of results from SEEP/W without sheet pile under steady state (seismic condition) 146
3.6.6.3 Presentation of results under transient state 139
3.6.6.3.1 Presentation of results from FLAC 2D for without sheet pile under transient state 140
3.6.6.3.2 Presentation of results from FLAC 2D for with sheet pile under transient state 140
3.6.6.3.2.1 Presentation of results for 5m long sheet pile at *B/8*position 141
3.6.6.3.2.2 Presentation of results for 10m long sheet pile at *B/8*position 141
3.6.6.3.2.3 Presentation of results for 15m long sheet pile at *B/8*position 142
3.6.6.3.2.4 Presentation of results for 20m long sheet pile at *B/8*position 143
3.6.6.3.2.5 Presentation of results for 5m long sheet pile at 2*B/8*position 144
3.6.6.3.2.6 Presentation of results for 10 m long sheet pile at 2*B/8*position 145
3.6.6.3.2.7 Presentation of results for 15 m long sheet pile at 2*B/8*position 146
3.6.6.3.2.8 Presentation of results for 20 m long sheet pile at 2*B/8*position 147
3.6.6.3.2.9 Presentation of results for 5 m long sheet pile at 3*B/8*position 148
3.6.6.3.2.10 Presentation of results for 10 m long sheet pile at 3*B/8*position 149
3.6.6.3.2.11 Presentation of results for 15 m long sheet pile at 3*B/8*position 150
3.6.6.3.3.12 Presentation of results for 20 m long sheet pile 151

at 3*B/8*position
3.7 Use of Numerical Results 152
Chapter 4 EXPERIMENTAL INVESTIGATION
4.1 An Overview 153
4.2 Principle of Centrifuge Modelling 154-158
4.2.1 General Principle 154
4.2.2 Mathematical Formulation 155
4.2.3 Centrifugal Modelling for Seepage Analysis 156
4.2.3.1 Determination of actual dimension of the wall and model dam 157
4.2.3.2 Determination of actual *EI* of the wall 157
4.2.3.3 Variation in Gravity field 158
4.3 Test Programme 158-164
4.4 Experimental Set Up 164-169
4.4.1 Details of Centrifuge 164
4.4.2 Fabrication of Seepage Test Box 167
4.4.3 Water Supply Arrangement 168
4.4.3.1Valve control through Arduino 169
4.5 Soil Properties of Model Embankment 170
4.6 Experimental Procedure 171-176
4.6.1 Model Embankment 171
4.6.1.1 Formation of Foundation 171
4.6.1.2 Construction of Embankment 172
4.6.2 Simulation of Seepage for Transient State 174
4.6.3 Instrumentation 174
4.6.3.1 Artificial tidal control circuit 174
4.6.3.2 Digital image capturing through Raspberry Pi camera 176
4.6.4 Acceleration of centrifuge model 176
4.7 Outcome of Experiments 177-179
4.7.1 Digital Image processing 177
4.7.2 Piezometers Readings 179
4.8 Presentation of Experimental Results 179-195
4.8.1 Dynamics of Phreatic Surface 179
4.8.1.1 Dynamics of Phreatic surface under steady state condition 179
4.8.1.2 Dynamics of phreatic surface Single Tidal Cycle: Effect of Rise-Up and Draw-Down 180
4.8.1.3 Dynamics of phreatic surface Single Tidal Cycle: Effect of Rise-Up and Draw-Down rate (B/8 position 5m length) 182
4.8.1.4 Dynamics of phreatic surface Single Tidal Cycle: Effect of Rise-Up and Draw-Down rate (B/8 position 10m length) 183
4.8.1.5 Dynamics of phreatic surface Single Tidal Cycle: Effect of Rise-Up and Draw-Down rate (B/8 position 15m length) 185

4.8.1.6 Dynamics of phreatic surface Single Tidal Cycle: Effect of Rise-Up and Draw-Down rate (B/8 position 20m length) 186
4.8.1.7 Dynamics of phreatic surface Single Tidal Cycle: Effect of Rise-Up and Draw-Down rate (2B/8 position 5m length) 187
4.8.1.8 Dynamics of phreatic surface Single Tidal Cycle: Effect of Rise-Up and Draw-Down rate (2B/8 position 10m length) 188
4.8.1.9 Dynamics of phreatic surface Single Tidal Cycle: Effect of Rise-Up and Draw-Down rate (2B/8 position 15m length) 189
4.8.1.10 Dynamics of phreatic surface Single Tidal Cycle: Effect of Rise-Up and Draw-Down rate (2B/8 position 20m length) 190
4.8.1.11 Dynamics of phreatic surface Single Tidal Cycle: Effect of Rise-Up and Draw-Down rate (3B/8 position 5m length) 191
4.8.1.12 Dynamics of phreatic surface Single Tidal Cycle: Effect of Rise-Up and Draw-Down rate (3B/8 position 10m length) 191
4.8.1.13 Dynamics of phreatic surface Single Tidal Cycle: Effect of Rise-Up and Draw-Down rate (3B/8 position 15m length) 193
4.8.1.14 Dynamics of phreatic surface Single Tidal Cycle: Effect of Rise-Up and Draw-Down rate (3B/8 position 20m length) 194
4.8.2 Presentation of Fluid Flow Vector And Flownet 195
4.8.2.1 Embankment with-out cut off Steady state condition 195
4.8.2.2 Embankment with cut off Steady state condition 196
4.8.2.3 Embankment With-Out Cut Off Transient State Condition 199
4.8.2.4 Embankment With Cut Off Transient State Condition 200
4.8.2.4.1 Flow net and fluid flow vector (B/8 position 5m length) 200
4.8.2.4.2 Flow net and fluid flow vector (B/8 position 10m length) 202
4.8.2.4.3 Flow net and fluid flow vector (B/8 position 15m length) 204
4.8.2.4.4 Flow net and fluid flow vector (B/8 position 20m length) 205
4.8.2.4.5 Flow net and fluid flow vector (2B/8 position 5m length) 207
4.8.2.4.6 Flow net and fluid flow vector (2B/8 position 10m length) 209
4.8.2.4.7 Flow net and fluid flow vector (2B/8 position 15m length) 210
4.8.2.4.8 Flow net and fluid flow vector (2B/8 position 20m length) 212
4.8.2.4.9 Flow net and fluid flow vector (3B/8 position 5m length) 213
4.8.2.4.10 Flow net and fluid flow vector (3B/8 position 10m length) 215

4.8.2.4.11 Flow net and fluid flow vector (3B/8 position 15m length) 216
4.8.2.4.12 Flow net and fluid flow vector (3B/8 position 20m length) 218
4.9 Experimental Observations for fluid flow vector 219
4.10 Use of Experimental Model 224

Chapter 5 **DISCUSSION ON RESULTS**

5.1 General 225
5.2 Flow Net Pattern 225-226
5.2.1. Steady State 225
5.2.2. Transient State 225
5.3 Fluid Flow Vector 226-256
5.3.1 Steady State 227
5.3.1.1 Numerical Observations 227
5.3.1.2 Comparison of Experimental Observations and Numerical Study for Steady State 230
5.3.1.3 Seismic Condition under Steady State 232
5.3.2 Transient State 234-256
5.3.2.1 Numerical Study under Transient State 234
5.3.2.1.1 At 7m from the Top of the Dam 234
5.3.2.1.2 At 12m from the Top of the Dam 244
5.3.2.2 Comparison of Numerical Study and Experimental Observations under Transient State 252
5.3.2.3 Seismic Condition under Transient State 256
5.4 Pore Water Pressure (PWP) Variation 260
5.4.1 PWP variation in foundation 260
5.4.1.1 Steady State 260
5.4.1.1.1 Numerical Observations 261
5.4.1.1.2 Comparison between numerical and experimental results 263
5.4.1.1.3 Observations for Seismic Study 264
5.4.1.2 Transient State 267
5.4.1.2.1 Numerical results 267
5.4.1.2.1.1. Numerical Observations at 7m from the top of the Dam 268
5.4.1.2.1.2. Numerical Observations at 12m from the top of the Dam 274
5.4.1.2.2 Comparison of Pore Water Pressure from Numerical and Experimental Observations 280
5.4.1.2.2.1 Pore Water Pressure Variation at 7m from the top of the Dam 280
5.4.1.2.2.2 Pore Water Pressure Variation at 12m 295

	from the top of the Dam	
	5.4.1.2.3 Observations for Seismic Study	301
	5.4.2 Pore Water Pressure Variation within Dam Body	305
	5.4.2.1 Static Condition	305
	5.4.2.2 Seismic Condition	305
	5.4.2.3. Transient State Condition	306
	5.4.2.3.1 Single tidal cycle under static condition	306
	5.4.2.3.2 Single tidal cycle under seismic condition	309
	5.4.2.3.3 Multiple tidal cycle	310
	5.4.3 Pore Pressure along Base	311
	5.5. Soil Pressure	312
	5.5.1 Steady State	312
	5.5.1.1 Steady State Static Condition	312
	5.5.1.2 Steady State Seismic Condition	314
	5.5.2 Transient Case	315
	5.5.2.1 Transient Static Condition	315
	5.5.2.2 Transient Seismic Condition	317
	5.6 Factor of Safety (FOS)	321
	5.6.1 Overall Factor of Safety	321
	5.6.1.1 Steady State Under Static And Seismic Conditions	321
	5.6.1.2 Transient State (Single Tidal Cycle)	323
	5.6.1.2.1 Effect of rise up and drawdown on Factor of Safety for variation position and length of sheet pile	327
	5.6.1.2.2 Transient State (Multiple Tidal Cycle)	328
	5.6.2 Factor of Safety Against Piping	328
	5.6.2.1 Steady State	329
	5.6.2.2 Transient State	329
	5.7 Statistical Modeling	336-363
	5.7.1 Prediction of factor of safety against piping with fluid flow vector, pore water pressure (Steady State)	336
	5.7.2 Prediction of factor of safety against piping with sheet pile length and position with time (Transient State)	338
	5.7.3 Correlation of overall factor of safety against under static condition between pore water pressure, fluid flow vector, piping with sheet pile length and position with time	339
	5.7.4 Correlation of overall factor of safety against under seismic condition between sheet pile length and position with time	343
	5.7.5 Prediction of Overall Factor of Safety	346-353
Chapter 6	SUMMARY, CONCLUSION AND FURTHER SCOPE	354-360
	6.1 Summary	354-355
	6.2 Conclusions	355-359
	6.3 Future scope of work	360
	REFERENCES	361-368

LIST OF TABLES

Table no.	Name of Tables	Page no.
2.1	Power requirement to generate 20% earthquake at 50Hz of N =100g	20
2.2	Factor of Safety values for static slope stability	23
3.1	Properties of sheet pile material	28
3.2	Nomencleture of parametric model for steady state (under static and seismic condition)	29-30
3.3(a)	Numerical study for transient state with tidal cycle (under seismic and static conditions)	30-34
3.3(b)	Numerical case study for transient state with multiple tidal cycle (under seismic and static conditions)	34
3.4	Peak horizontal acceleration (ms^{-2})	136
4.1	Centrifuge seepage modelling scaling laws	161
4.2	Test programme for steady state (under static condition)	163
4.3(a)	Test programme for transient statewith single tidal cycle (under static conditions	164
4.3(b)	Test programme for (transient state with multiple tidal cycle (under static conditions)	168
4.4	Centrifuge machine details	169
4.5	Soil _Properties_for _Experimental_Model	175
5.1	Factor Of Safety Under Static Condition	342
5.2	Factor Of Safety Under Seismic Condition	343
5.3	Factor Of Safety Against Piping Under Static Condition	351
5.4	Regression Modeling	362
5.5	Generalized Equation	363

LIST OF FIGURES

Fig. no.	Title	Page no.
3.1	Flow chart for numerical analysis	28
3.2(a)	Schematic Diagram of Model Embankment	29
3.2(b)	Flowchart for numerical analysis	30
3.3(a)	Boundary Condition	37
3.3(b)	Formation of Meshing	37
3.4	Triangular mesh with nodal points.	39
3.5(a)	Model dam Geometry with sheet pile	41
3.5(b)	Model dam boundary condition	41
3.6	Time history acceleration data of India (Sikkim)-Nepal-Border	44
3.7(a)	Geometry, boundary condition and generation of mesh(seep/w and sigma/w)	48
3.7(b)	Geometry, boundary condition and generation of mesh(quake/w)	48
3.8	Volumetric Water Content function (as per Modified Kovacs methodology using Grain size distribution) showing plot of Volumetric water content (m^3/m^3) versus Matric Suction (kPa) for clayey Silt (Kovacs method 2003).	49
3.9	Flowchart Defining Methodology followed during seepage analysis	50
3.10	Flowchart Defining Methodology followed during analysis in SIGMA/W	51
3.11	Steady State seepage condition for working head of 3.5 m	52
3.12	Steady State seepage condition for working head of 3.5 m	53
3.13	Steady State seepage condition for working head of 3.5 m	53
3.14(a)	Steady State seepage condition (for 5m long sheet pile *B*/8 position from downstream end) working head of 3.5 m	54
3.14(b)	Steady State seepage condition (for 10m long sheet pile *B*/8 position from downstream end) for working head of 3.5 m	54
3.14(c)	Steady State seepage condition (for 15m long sheet pile *B*/8 position from downstream end) working head of 3.5 m	55
3.14(d)	Steady State seepage condition (for 20m long sheet pile *B*/8 position from downstream end) working head 3.5 m	55
3.14(e)	Steady State seepage condition (for 5m long sheet pile 2*B*/8 position from downstream end) working head of 3.5 m	55
3.14(f)	Steady State seepage condition (for 10m long sheet pile 2*B*/8 position from downstream end) working head of 3.5 m	55
3.14(g)	Steady State seepage condition (for 15m long sheet pile 2*B*/8 position from downstream end) working head of 3.5 m	56

3.14(h)	Steady State seepage condition (for 20m long sheet pile 2*B*/8 position from downstream end) working head of 3.5 m	56
3.14(i)	Steady State seepage condition (for 5m long sheet pile 3*B*/8 position from downstream end) working head of 3.5 m	56
3.14(j)	Steady State seepage condition (for 10m long sheet pile 3*B*/8 position from downstream end) working head of 3.5 m	56
3.14(k)	Steady State seepage condition (for 15m long sheet pile 3*B*/8 position from downstream end) working head of 3.5 m	57
3.14(l)	Steady State seepage condition (for 15m long sheet pile 3*B*/8 position from downstream end) working head of 3.5 m	57
3.15(a)	Steady State seepage condition (for 5m long sheet pile *B*/8 position from downstream end) working head of 3.5 m	58
3.15(b)	Steady State seepage condition (for 10 m long sheet pile *B*/8 position from downstream end) working head of 3.5 m	58
3.15(c)	Steady State seepage condition (for 15 m long sheet pile *B*/8 position from downstream end) working head of 3.5 m	58
3.15(d)	Steady State seepage condition (for 20 m long sheet pile *B*/8 position from downstream end) working head of 3.5 m	58
3.15(e)	Steady State seepage condition (for 5m long sheet pile 2*B*/8 position from downstream end) working head of 3.5 m	59
3.15(f)	Steady State seepage condition (for 10 m long sheet pile 2*B*/8 position from downstream end) working head of 3.5 m	59
3.15(g)	Steady State seepage condition (for 15 m long sheet pile 2*B*/8 position from downstream end) working head of 3.5m	59
3.15(h)	Steady State seepage condition (for 20 m long sheet pile 2*B*/8 position from downstream end) working head of 3.5m	59
3.15(i)	Steady State seepage condition (for 5 m long sheet pile 3*B*/8 position from downstream end) working head of 3.5 m	60
3.15(j)	Steady State seepage condition (for 10 m long sheet pile 3*B*/8 position from downstream end) working head of 3.5m	60
3.15(k)	Steady State seepage condition (for 15 m long sheet pile 3*B*/8 position from downstream end) working head of 3.5m	60
3.15(l)	Steady State seepage condition (for 20 m long sheet pile 3*B*/8 position from downstream end) working head of 3.5m	60
3.16(a)	Steady State seepage condition (for 5 m long sheet pile *B*/8 position from downstream end) working head of 3.5 m	61
3.16(b	Steady State seepage condition (for 10 m long sheet pile *B*/8 position from downstream end) working head of 3.5 m	61
3.16(c)	Steady State seepage condition (for 15 m long sheet pile *B*/8 position from downstream end) working head of 3.5 m	61
3.16(d)	Steady State seepage condition (for 20 m long sheet pile *B*/8 position from downstream end) working head of 3.5 m	61

3.16(e)	Steady State seepage condition (for 5 m long sheet pile 2*B*/8 position from downstream end) working head of 3.5 m	62
3.16(f)	Steady State seepage condition (for 10 m long sheet pile 2*B*/8 position from downstream end) working head of 3.5 m	62
3.16(g)	Steady State seepage condition (for 15 m long sheet pile 2*B*/8 position from downstream end) working head of 3.5 m	62
3.16(h)	Steady State seepage condition (for 20 m long sheet pile 2*B*/8 position from downstream end) working head of 3.5 m	62
3.16(i)	Steady State seepage condition (for 5 m long sheet pile 3*B*/8 position from downstream end) working head of 3.5 m	63
3.16(j)	Steady State seepage condition (for 10 m long sheet pile 3*B*/8 position from downstream end) working head of 3.5 m	63
3.16(k)	Steady State seepage condition (for 15 m long sheet pile 3*B*/8 position from downstream end) working head of 3.5 m	63
3.16(l)	Steady State seepage condition (for 20 m long sheet pile 3*B*/8 position from downstream end) working head of 3.5 m	63
3.17(a)	Development of phreatic surface for 1 Hour	64
3.17(b)	Development of phreatic surface for 5 Hour	65
3.17(c)	Development of phreatic surface for 6 Hour	65
3.17(d)	Development of phreatic surface for 10 Hour	65
3.18(a)	Flow-net under Rise up condition for without sheet pile condition, time = 1.0 hr.	66
3.18(b)	Flow-net under Rise up condition for without sheet pile condition, time = 3.0 hrs.	66
3.18(c)	Flow-net under Rise up condition for without sheet pile condition, time = 5.0 hrs.	66
3.18(d)	Flow-net under Rise up condition for without sheet pile condition, time = 6.0 hrs.	66
3.18(e)	Flow-net under Drawdown condition for without sheet pile condition, time = 8.0 hrs.	67
3.18(f)	Flow-net under Drawdown condition for without sheet pile condition, time = 10.0 hrs.	67
3.18(g)	Flow-net under Drawdown condition for without sheet pile condition, time = 12.0 hrs.	67
3.19(a)	Flow-net under rise up condition for without sheet pile condition, time = 30min.	68
3.19(b)	Flow-net under rise up condition for without sheet pile condition, time = 1hrs.	68
3.19(c)	Flow-net under rise up condition for without sheet pile condition, time = 5hrs.	68
3.19(d)	Flow-net under rise up condition for without sheet pile condition, time = 6hrs.	68

3.19(e)	Flow-net under draw down condition for without sheet pile condition, time = 7 hrs.	69
3.19(f)	Flow-net under draw down condition for without sheet pile condition, time = 10 hrs.	69
3.20(a)	Flow-net under Rise up condition (for 5m long sheet pile at *B*/8 from downstream end, time = 1.0 hr.)	70
3.20(b)	Flow-net under Rise up condition (for 5m long sheet pile at *B*/8 from downstream end, time = 3.0 hrs.)	70
3.20(c)	Flow-net under Rise up condition (for 5m long sheet pile at *B*/8 from downstream end, time = 5.0 hrs.)	70
3.20(d)	: Flow-net under Rise up condition (for 5m long sheet pile at *B*/8 from downstream end, time = 6.0 hrs.)	70
3.20(e)	Flow-net under Rise up condition (for 6m long sheet pile at *B*/8 from downstream end, time = 7.0 hrs.)	71
3.20(f)	Flow-net under Drawdown condition (for 7m long sheet pile at *B*/8 from downstream end, time = 10.0 hrs.)	71
3.20(g)	Flownet under Drawdown condition (for 5m long sheet pile at B/8 from downstream end, time = 11.0 hrs.)	71
3.21(a)	Flow-net under Rise up condition (for 10m long sheet pile at *B*/8 from downstream end, time = 1.0 hr.)	72
3.21(b)	Flow-net under Rise up condition (for 10m long sheet pile at *B*/8 from downstream end, time = 5.0 hrs.)	72
3.21(c)	Flow-net under Rise up condition (for 10m long sheet pile at *B*/8 from downstream end, time = 6.0 hrs.)	72
3.21(d)	Flow-net under Drawdown condition (for 10m long sheet pile at *B*/8 from downstream end, time = 10.0 hrs.)	72
3.21(e)	Flow-net under Drawdown condition (for 10m long sheet pile at *B*/8 from downstream end, time = 11.0 hrs.)	73
3.22(a)	Flow-net under Rise up condition (for 15m long sheet pile at *B*/8 from downstream end, time = 1.0 hr.)	73
3.22(b)	Flow-net under Rise up condition (for 15m long sheet pile at *B*/8 from downstream end, time = 5.0 hrs.)	73
3.22(c)	Flow-net under Rise up condition (for 15m long sheet pile at *B*/8 from downstream end, time = 6.0 hrs.)	74
3.22(d)	Flow-net under Drawdown condition (for 15m long sheet pile at *B*/8 from downstream end, time = 7.0 hrs.)	74
3.22(e)	Flownet under Drawdown condition (for 15m long sheet pile at B/8 from downstream end, time =11.0 hrs.)	74
3.23(a)	Flow-net under Rise up condition (for 20m long sheet pile at *B*/8 from downstream end, time =1.0 hr.)	75
3.23(b)	Flow-net under Rise up condition (for 20m long sheet pile at *B*/8 from downstream end, time =3.0 hrs.)	75

3.23(c)	Flow-net under Rise up condition (for 20m long sheet pile at *B*/8 from downstream end, time =5.0 hrs.)	75
3.23(d)	Flow-net under Rise up condition (for 20m long sheet pile at *B*/8 from downstream end, time =6.0 hrs.)	75
3.23(e)	Flow-net under Drawdown condition (for 20m long sheet pile at *B*/8 from downstream end, time =7.0 hrs.)	76
3.23(f).	Flow-net under Drawdown condition (for 20m long sheet pile at *B*/8 from downstream end, time =10.0 hrs.)	76
3.23(g)	Flownet under Drawdown condition (for 20m long sheet pile at B/8 from downstream end, time =11.0 hrs.)	76
3.24(a)	Flow-net under Rise up condition (for 5m long sheet pile at 2*B*/8 from downstream end, time =1.0 hr.)	77
3.24(b)	Flow-net under Rise up condition (for 5m long sheet pile at 2*B*/8 from downstream end, time =3.0 hrs.)	77
3.24(c)	Flow-net under Rise up condition (for 5m long sheet pile at 2*B*/8 from downstream end, time =5.0 hrs.)	77
3.24(d)	Flow-net under Rise up condition (for 5m long sheet pile at 2*B*/8 from downstream end, time =6.0 hrs.)	77
3.24(e)	Flow-net under Drawdown condition (for 5m long sheet pile at 2*B*/8 from downstream end, time =3.0 hrs.)	78
3.24(f)	Flow-net under Drawdown condition (for 5m long sheet pile at 2*B*/8 from downstream end, time =10.0 hrs.)	78
3.24(g)	Flow-net under Drawdown condition (for 5m long sheet pile at 2*B*/8 from downstream end, time =11.0 hrs.)	78
3.25(a)	Flow-net under Rise up condition (for 10m long sheet pile at 2*B*/8 from downstream end, time =1.0 hr.)	79
3.25(b)	Flow-net under Rise up condition (for 10m long sheet pile at 2*B*/8 from downstream end, time =3.0 hrs.)	79
3.25(c)	Flow-net under Rise up condition (for 10m long sheet pile at 2*B*/8 from downstream end, time =5.0 hrs.)	79
3.25(d)	Flow-net under Rise up condition (for 10m long sheet pile at 2*B*/8 from downstream end, time =6.0 hrs.)	79
3.25(e)	Flow-net under Drawdown condition (for 10m long sheet pile at 2*B*/8 from downstream end, time =7.0 hrs.)	80
3.25(f)	Flow-net under Drawdown condition (for 10m long sheet pile at 2*B*/8 from downstream end, time =7.0 hrs.)	80
3.25(g)	Flow-net under Drawdown condition (for 10m long sheet pile at 2*B*/8 from downstream end, time =11.0 hrs.)	80
3.26(a)	Flow-net under Rise up condition (for 15m long sheet pile at 2*B*/8 from downstream end, time =1.0 hr.)	81
3.26(b)	Flow-net under Rise up condition (for 15m long sheet pile at 2*B*/8 from downstream end, time =3.0 hrs.)	81

3.26(c)	Flow-net under Rise up condition (for 15m long sheet pile at 2*B*/8 from downstream end, time =5.0 hrs.)	81
3.26(d)	Flow-net under Rise up condition (for 15m long sheet pile at 2*B*/8 from downstream end, time =6.0 hrs.)	81
3.26(e)	Flow-net under Drawdown condition (for 15m long sheet pile at 2*B*/8 from downstream end, time =7.0 hrs.)	82
3.26(f)	Flow-net under Drawdown condition (for 15m long sheet pile at 2*B*/8 from downstream end, time =10.0 hrs.)	82
3.26(g)	Flow-net under Drawdown condition (for 15m long sheet pile at 2*B*/8 from downstream end, time =11.0 hrs.)	82
3.27(a)	Flow-net under Rise up condition (for 20m long sheet pile at 2*B*/8 from downstream end, time =1.0 hr.)	83
3.27(b)	Flow-net under Rise up condition (for 20m long sheet pile at 2*B*/8 from downstream end, time =3.0 hrs.)	83
3.27(c)	Flow-net under Rise up condition (for 20m long sheet pile at 2*B*/8 from downstream end, time =5.0 hrs.)	83
3.27(d)	Flow-net under Rise up condition (for 20m long sheet pile at 2*B*/8 from downstream end, time =6.0 hrs.)	83
3.27(e)	Flow-net under Drawdown condition (for 20m long sheet pile at 2*B*/8 from downstream end, time =7.0 hrs.)	84
3.27(f)	Flow-net under Drawdown condition (for 20m long sheet pile at 2*B*/8 from downstream end, time =10.0 hrs.)	84
3.27(g)	Flow-net under Drawdown condition (for 20m long sheet pile at 2*B*/8 from downstream end, time =11.0 hrs.)	84
3.28(a)	Flow-net under Rise up condition (for 5m long sheet pile at 3*B*/8 from downstream end, time =1.0 hr.)	85
3.28(b)	Flow-net under Rise up condition (for 5m long sheet pile at 3*B*/8 from downstream end, time =3.0 hrs.)	85
3.28(c)	Flow-net under Rise up condition (for 5m long sheet pile at 3*B*/8 from downstream end, time =5.0 hrs.)	85
3.28(d)	Flow-net under Rise up condition (for 5m long sheet pile at 3*B*/8 from downstream end, time =6.0 hrs.)	85
3.28(e)	Flow-net under Drawdown condition (for 5m long sheet pile at 3*B*/8 from downstream end, time =11.0 hrs.)	86
3.29(a)	Flow-net under Rise up condition (for 10m long sheet pile at 3*B*/8 from downstream end, time =1.0 hr.)	86
3.29(b)	Flow-net under Rise up condition (for 10m long sheet pile at 3*B*/8 from downstream end, time =3.0 hrs.)	86
3.29(c)	Flow-net under Rise up condition (for 10m long sheet pile at 3*B*/8 from downstream end, time =5.0 hrs.)	87
3.29(d)	Flow-net under Rise up condition (for 10m long sheet pile at 3*B*/8 from downstream end, time =6.0 hrs.)	87

3.29(e)	Flow-net under Drawdown condition (for 10m long sheet pile at 3*B*/8 from downstream end, time =7.0 hrs.)	87
3.29(f)	Flow-net under Drawdown condition (for 10m long sheet pile at 3*B*/8 from downstream end, time =10.0 hrs.)	87
3.30(a)	Flow-net under Rise up condition (for 15m long sheet pile at 3*B*/8 from downstream end, time =1.0 hr.)	88
3.30(b)	Flow-net under Rise up condition (for 15m long sheet pile at 3*B*/8 from downstream end, time =3.0 hrs.)	88
3.30(c)	Flow-net under Rise up condition (for 15m long sheet pile at 3*B*/8 from downstream end, time =5.0 hrs.)	88
3.30(d)	Flow-net under Rise up condition (for 15m long sheet pile at 3*B*/8 from downstream end, time =6.0 hrs.)	88
3.30(e)	Flow-net under Drawdown condition (for 15m long sheet pile at 3*B*/8 from downstream end, time =7.0 hrs.)	89
3.30(f)	Flow-net under Drawdown condition (for 15m long sheet pile at 3*B*/8 from downstream end, time =11.0 hrs.)	89
3.31(a)	Flow-net under Rise up condition (for 20m long sheet pile at 3*B*/8 from downstream end, time =1.0 hr.)	89
3.31(b)	Flow-net under Rise up condition (for 20m long sheet pile at 3*B*/8 from downstream end, time =3.0 hrs.)	89
3.31(c)	Flow-net under Rise up condition (for 20m long sheet pile at 3*B*/8 from downstream end, time =5.0 hrs.)	90
3.31(d)	Flow-net under Rise up condition (for 20m long sheet pile at 3*B*/8 from downstream end, time =6.0 hrs.)	90
3.31(e)	Flow-net under Drawdown condition (for 20m long sheet pile at 3*B*/8 from downstream end, time =7.0 hrs.)	90
3.31(f)	Flow-net under Drawdown condition (for 20m long sheet pile at 3*B*/8 from downstream end, time =11.0 hrs.)	90
3.32(a)	Flow-net under Rise up condition (for 5 m long sheet pile at *B*/8 from downstream end, time = 1.0 hr.)	91
3.32(b)	Flow-net under Rise up condition (for 5 m long sheet pile at *B*/8 from downstream end, time = 5.0 hrs.)	91
3.32(c)	Flow-net under Rise up condition (for 5 m long sheet pile at *B*/8 from downstream end, after 6.0 hrs.)	92
3.32(d)	Flow-net under Drawdown condition (for 5 m long sheet pile at *B*/8 from downstream end, time = 7.0 hrs.)	92
3.32(e)	Flow-net under Drawdown condition (for 5 m long sheet pile at *B*/8 from downstream end, time = 10.0 hrs.)	92
3.32(f)	Flow-net under Drawdown condition (for 5 m long sheet pile at *B*/8 from downstream end, time = 11.0 hrs.)	92
3.33(a)	Flow-net under Rise up condition (for 10 m long sheet pile at *B*/8 from downstream end, time = 1.0 hr.)	93

3.33(b)	Flow-net under Rise up condition (for 10 m long sheet pile at *B*/8 from downstream end, time = 5.0 hrs.	93
3.33(c)	Flow-net under Rise up condition (for 10 m long sheet pile at *B*/8 from downstream end, time = 6 hrs.)	93
3.33(d)	Flow-net under Drawdown condition (for 10 m long sheet pile at *B*/8 from downstream end, time = 7.0 hrs.)	93
3.33(e)	Flow-net under Drawdown condition (for 10 m long sheet pile at *B*/8 from downstream end, time = 10.0 hrs.)	94
3.33(f)	Flow-net under Drawdown condition (for 10 m long sheet pile at *B*/8 from downstream end, time = 11.0 hrs.)	94
3.34(a)	Flow-net under Rise up condition (for 15 m long sheet pile at *B*/8 from downstream end, time = 1.0 hr.)	95
3.34(b)	Flow-net under Rise up condition (for 15 m long sheet pile at *B*/8 from downstream end, time = 5.0 hrs.)	95
3.34(c)	Flow-net under Rise up condition (for 15 m long sheet pile at *B*/8 from downstream end, time = 6.0 hrs.)	95
3.34(d)	Flow-net under Drawdown condition (for 15 m long sheet pile at *B*/8 from downstream end, time = 7.0 hrs.)	95
3.34(e)	Flow-net under Drawdown condition (for 15 m long sheet pile at *B*/8 from downstream end, time = 10.0 hrs.)	96
3.34(f)	Flow-net under Drawdown condition (for 15 m long sheet pile at *B*/8 from downstream end, time = 11.0 hrs.)	96
3.35(a)	Flow-net under Rise up condition (for 20 m long sheet pile at *B*/8 from downstream end, time = 1.0 hr.)	96
3.35(b)	Flow-net under Rise up condition (for 20 m long sheet pile at *B*/8 from downstream end, time = 5.0 hrs.)	96
3.35(c)	Flow-net under Rise up condition (for 20 m long sheet pile at B/8 from downstream end, time = 6.0 hrs.)	97
3.35(d)	Flow-net under Drawdown condition (for 20 m long sheet pile at *B*/8 from downstream end, time = 7.0 hrs.)	97
3.35(e)	Flow-net under Drawdown condition (for 20 m long sheet pile at *B*/8 from downstream end, time = 10.0 hrs.)	97
3.35(f)	Flow-net under Drawdown condition (for 20 m long sheet pile at *B*/8 from downstream end, time = 11.0 hrs.)	97
3.36(a)	Flow-net under Rise up condition (for 5m long sheet pile at 2*B*/8 from downstream end, time = 1.0 hr.)	98
3.36(b)	Flow-net under Rise up condition (for 5m long sheet pile at 2*B*/8 from downstream end, time = 5.0 hrs.)	98
3.36(c)	Flow-net under Rise up condition (for 5m long sheet pile at 2*B*/8 from downstream end, time = 6.0 hrs.)	98
3.36(d)	Flow-net under Drawdown condition (for 5m long sheet pile at 2*B*/8 from downstream end, time = 7.0 hrs.)	98

3.36(e)	Flow-net under Drawdown condition (for 5m long sheet pile at 2*B*/8 from downstream end, time = 10.0 hrs.)	99
3.36(f)	Flow-net under Drawdown condition (for 5m long sheet pile at 2*B*/8 from downstream end, time = 11.0 hrs.)	99
3.37(a)	Flow-net under Rise up condition (for 10m long sheet pile at 2*B*/8 from downstream end, time = 1.0 hr.)	99
3.37(b)	Flow-net under Rise up condition (for 10m long sheet pile at 2*B*/8 from downstream end, time = 5.0 hrs.)	99
3.37(c)	Flow-net under Rise up condition (for 10m long sheet pile at 2*B*/8 from downstream end, time = 6.0 hrs.)	100
3.37(d)	Flow-net under Drawdown condition (for 10m long sheet pile at 2*B*/8 from downstream end, time = 7.0 hrs.)	100
3.37(e)	Flow-net under Drawdown condition (for 10m long sheet pile at 2*B*/8 from downstream end, time = 10.0 hrs.)	100
3.37(f)	Flow-net under Drawdown condition (for 10m long sheet pile at 2*B*/8 from downstream end, time = 11.0 hrs.)	100
3.38(a)	Flow-net under Rise up condition (for 15m long sheet pile at 2*B*/8 from downstream end, time = 1.0 hr.)	101
3.38(b)	Flow-net under Rise up condition (for 15m long sheet pile at 2*B*/8 from downstream end, time = 5.0 hrs.	101
3.38(c)	Flow-net under Rise up condition (for 15m long sheet pile at 2*B*/8 from downstream end, time = 6.0 hrs.)	101
3.38(d)	Flow-net under Drawdown condition (for 15m long sheet pile at 2*B*/8 from downstream end, time = 7.0 hrs.)	101
3.38(e)	Flow-net under Drawdown condition (for 15m long sheet pile at 2*B*/8 from downstream end, time = 10.0 hrs.)	102
3.38(f)	Flow-net under Drawdown condition (for 15m long sheet pile at 2*B*/8 from downstream end, time = 11.0 hrs.)	102
3.39(a)	Flow-net under Rise up condition (for 20m long sheet pile at 2*B*/8 from downstream end, time = 1.0 hr.)	102
3.39(b)	Flow-net under Rise up condition (for 20m long sheet pile at 2*B*/8 from downstream end, time = 5.0 hrs.)	102
3.39(c)	Flow-net under Rise up condition (for 20m long sheet pile at 2*B*/8 from downstream end, time = 6.0 hrs.)	103
3.39(d)	Flow-net under Drawdown condition (for 20m long sheet pile at 2*B*/8 from downstream end, time = 8.0 hrs.)	103
3.39(e)	Flow-net under Drawdown condition (for 20m long sheet pile at 2*B*/8 from downstream end, time = 10.0 hrs.)	103
3.39(f)	Flow-net under Drawdown condition (for 20m long sheet pile at 2*B*/8 from downstream end, time = 11.0 hrs.)	103
3.40(a)	Flow-net under Rise up condition (for 5m long sheet pile at 3*B*/8 from downstream end, time = 1.0 hr.)	104

3.40(b)	Flow-net under Rise up condition (for 5m long sheet pile at 3*B*/8 from downstream end, time = 5.0 hrs.)	104
3.40(c)	Flow-net under Rise up condition (for 5m long sheet pile at 3*B*/8 from downstream end, time = 6.0 hrs.)	104
3.40(d)	Flow-net under Drawdown condition (for 5m long sheet pile at 3*B*/8 from downstream end, time = 7.0 hrs.)	104
3.40(e)	Flow-net under Drawdown condition (for 5m long sheet pile at 3*B*/8 from downstream end, time = 10.0 hrs.)	105
3.40(f)	Flow-net under Drawdown condition (for 5m long sheet pile at 3*B*/8 from downstream end, time = 11.0 hrs.)	105
3.41(a)	Flow-net under Rise up condition (for 10m long sheet pile at 3*B*/8 from downstream end, time = 1.0 hr.)	105
3.41(b)	Flow-net under Rise up condition (for 10m long sheet pile at 3*B*/8 from downstream end, time = 5.0 hrs.)	105
3.41(c)	Flow-net under Rise up condition (for 10m long sheet pile at 3*B*/8 from downstream end, time = 6.0 hrs.)	106
3.41(d)	Flow-net under Drawdown condition (for 10m long sheet pile at 3*B*/8 from downstream end, time = 7.0 hrs.)	106
3.41(e)	Flow-net under Drawdown condition (for 10m long sheet pile at 3*B*/8 from downstream end, time = 10.0 hrs.)	106
3.41(f)	Flow-net under Drawdown condition (for 10m long sheet pile at 3*B*/8 from downstream end, time = 11.0 hrs.)	106
3.42(a)	Flow-net under Rise up condition (for 15 m long sheet pile at 3*B*/8 from downstream end, time = 1.0 hr.)	107
3.42(b)	Flow-net under Rise up condition (for 15 m long sheet pile at 3*B*/8 from downstream end, time = 5.0 hrs.)	107
3.42(c)	Flow-net under Rise up condition (for 15 m long sheet pile at 3*B*/8 from downstream end, time = 6.0 hrs.)	107
3.42(d)	Flow-net under Drawdown condition (for 15 m long sheet pile at 3*B*/8 from downstream end, time = 7.0 hrs.)	107
3.42(e)	Flow-net under Drawdown condition (for 15 m long sheet pile at 3*B*/8 from downstream end, time = 10.0 hrs.)	108
3.42(f)	Flow-net under Drawdown condition (for 15 m long sheet pile at 3*B*/8 from downstream end, time = 11.0 hrs.)	108
3.43(a)	Flow-net under Rise up condition (for 20m long sheet pile at 3*B*/8 from downstream end, time = 1.0 hr.)	108
3.43(b)	Flow-net under Rise up condition (for 20m long sheet pile at 3*B*/8 from downstream end, time = 5.0 hrs.)	108
3.43(c)	Flow-net under Rise up condition (for 20m long sheet pile at 3*B*/8 from downstream end, time = 6.0 hrs.)	109
3.43(d)	Flow-net under Drawdown condition (for 20m long sheet pile at 3*B*/8 from downstream end, time = 7.0 hrs.)	109

3.43(e)	Flow-net under Drawdown condition (for 20m long sheet pile at 3*B*/8 from downstream end, time = 10.0 hrs.)	109
3.43(.f)	Flow-net under Drawdown condition (for 20m long sheet pile at 3*B*/8 from downstream end, time = 11.0 hrs.)	109
3.44(a)	Flownet under rise up condition (for 5m long sheet file at B/8 position from downstream end, time=1 hr.)	110
3.44(b)	Flownet under rise up condition (for 5m long sheet file at B/8 position from downstream end, time=3 hrs.)	110
3.44(c)	Flownet under rise up condition (for 5m long sheet file at B/8 position from downstream end, time=5 hrs.)	110
3.44(d)	Flownet under rise up condition (for 5m long sheet file at B/8 position from downstream end, time=6 hrs.)	110
3.44(e)	Flownet under draw down condition (for 5m long sheet file at B/8 position from downstream end, time=7 hrs.)	111
3.44(f)	Flownet under draw down condition (for 5m long sheet file at B/8 position from downstream end, time=10 hrs.)	111
3.44(g)	Flownet under draw down condition (for 5m long sheet file at B/8 position from downstream end, time=12 hrs.)	111
3.45(a)	Flownet under rise up condition (for 10m long sheet file at B/8 position from downstream end, time=1 hrs.)	112
3.45(b)	Flownet under rise up condition (for 10m long sheet file at B/8 position from downstream end, time=2 hrs.)	112
3.45(c)	Flownet under rise up condition (for 10m long sheet file at B/8 position from downstream end, time=3 hrs.)	112
3.45(d)	Flownet under rise up condition (for 10m long sheet file at B/8 position from downstream end, time=5 hrs.)	112
3.45(e)	Flownet under rise up condition (for 10m long sheet file at B/8 position from downstream end, time=6 hrs.)	113
3.45(f)	Flownet under draw down condition (for 10m long sheet file at B/8 position from downstream end, time=7 hrs.)	113
3.45(g)	Flownet under draw down condition (for 10m long sheet file at B/8 position from downstream end, time=10 hrs.)	113
3.45(h)	Flownet under draw down condition (for 10m long sheet file at B/8 position from downstream end, time=11 hrs.)	113
3.46(a)	Flownet under rise up condition (for 15m long sheet file at B/8 position from downstream end, time=1 hr.)	114
3.46(b)	Flownet under rise up condition (for 15m long sheet file at B/8 position from downstream end, time=2 hrs.)	114
3.46(c)	Flownet under rise up condition (for 15m long sheet file at B/8 position from downstream end, time=6 hrs.)	114
3.46(d)	Flownet under rise up condition (for 15m long sheet file at B/8 position from downstream end, time=5 hrs.)	114

3.46(e)	Flownet under rise up condition (for 15m long sheet file at B/8 position from downstream end, time=3 hrs.)	115
3.46(f)	Flownet under draw down condition (for 15m long sheet file at B/8 position from downstream end, time=11 hrs.)	115
3.47(a)	Flownet under rise up condition (for 20m long sheet file at B/8 position from downstream end, time=3 hrs.)	115
3.47(b)	Flownet under rise up condition (for 20m long sheet file at B/8 position from downstream end, time=5 hrs.)	115
3.47(c)	Flow-net under rise up condition (for 20m long sheet file at B/8 position from downstream end, time=6 hrs.)	116
3.47(d)	Flow-net under rise up condition (for 20m long sheet file at B/8 position from downstream end, time=10 hrs.)	116
3.47(e)	Flow-net under rise up condition (for 20m long sheet file at B/8 position from downstream end, time=11 hrs.)	116
3.48(a)	Flownet under Rise UP condition (for 20m long sheet file at B/8 position from downstream end, time=1 hr.)	117
3.48(b)	Flownet under Rise UP condition (for 20m long sheet file at B/8 position from downstream end, time=5 hrs.)	117
3.48(c)	Flownet under rise up condition (for 5m long sheet file at 2B/8 position from downstream end, time=6 hrs.)	117
3.48(d)	Flownet under draw down condition (for 5m long sheet file at 2B/8 position from downstream end, time=10 hrs.)	117
3.49(a)	Flownet under rise up condition (for 10m long sheet file at 2B/8 position from downstream end, time=1 hr.)	118
3.49(b)	Flownet under rise up condition (for 10m long sheet file at 2B/8 position from downstream end, time=3 hrs.)	118
3.49(c)	Flow-net under rise up condition (for 10m long sheet file at 2B/8 position from downstream end, time=5 hrs.)	118
3.49(d)	Flow-net under draw down condition (for 10 m long sheet file at 2B/8 position from downstream end, time=10 hrs.)	118
3.49(e)	Flow-net under draw down condition (for 10 m long sheet file at 2B/8 position from downstream end, time=12 hrs.)	119
3.50(a)	Flow-net under rise up condition (for 15m long sheet file at 2B/8 position from downstream end, time=1 hr.)	119
3.50(b)	Flow-net under rise up condition (for 15m long sheet file at 2B/8 position from downstream end, time=3 hrs.)	119
3.50(c)	Flow-net under rise up condition (for 15m long sheet file at 2B/8 position from downstream end, time=5 hrs.)	120
3.50(d)	Flow-net under rise up condition (for 15m long sheet file at 2B/8 position from downstream end, time=6 hrs.)	120
3.50(e)	Flow-net under draw down condition (for 10m long sheet file at 2B/8 position from downstream end, time=7 hrs.)	120

3.50(f)	Flow-net under draw down condition (for 10m long sheet file at 2B/8 position from downstream end, time=10 hrs.)	120
3.50(g)	Flow-net under draw down condition (for 10m long sheet file at 2B/8 position from downstream end, time=12 hrs.)	121
3.51(a)	Flow-net under rise up condition (for 15m long sheet file at 2B/8 position from downstream end, time=3 hrs.)	121
3.51(b)	Flow-net under rise up condition (for 15m long sheet file at 2B/8 position from downstream end, time=5 hrs.)	121
3.51(c)	Flow-net under rise up condition (for 15m long sheet file at 2B/8 position from downstream end, time=6 hrs.)	122
3.51(d)	Flow-net under drawn down condition (for 15m long sheet file at 2B/8 position from downstream end, time=7 hrs.)	122
3.51(e)	Flow-net under drawn down condition (for 15m long sheet file at 2B/8 position from downstream end, time=10 hrs.)	122
3.51(f)	Flow-net under drawn down condition (for 15m long sheet file at 2B/8 position from downstream end, time=12 hrs.)	122
3.52(a)	Flow-net under rise up condition (for 20m long sheet file at 2B/8 position from downstream end, time=1 hrs.)	123
3.52(b)	Flow-net under rise up condition (for 20m long sheet file at 2B/8 position from downstream end, time=2 hrs.)	123
3.52(c)	Flow-net under rise up condition (for 20m long sheet file at 2B/8 position from downstream end, time=3 hrs.)	123
3.52(d)	Flow-net under rise up condition (for 20m long sheet file at 2B/8 position from downstream end, time=5 hrs.)	123
3.52(e)	Flow-net under rise up condition (for 20m long sheet file at 2B/8 position from downstream end, time=6 hrs.)	124
3.52(f)	Flow-net under draw down condition (for 20m long sheet file at 2B/8 position from downstream end, time=7 hrs.)	124
3.52(g)	Flow-net under draw down condition (for 20m long sheet file at 2B/8 position from downstream end, time=10 hrs.)	124
3.52(h)	Flow-net under draw down condition (for 20m long sheet file at 2B/8 position from downstream end, time=11 hrs.)	124
3.53(a)	Flow-net under rise up condition (for 5m long sheet file at 3B/8 position from downstream end, time=1 hrs.)	125
3.53(b)	Flow-net under rise up condition (for 5m long sheet file at 3B/8 position from downstream end, time=1 hr.)	125
3.53(c)	Flow-net under rise up condition (for 5m long sheet file at 3B/8 position from downstream end, time=3 hrs.)	125
3.53(d)	Flow-net under rise up condition (for 5m long sheet file at 3B/8 position from downstream end, time=5 hrs.)	125
3.53(e)	Flow-net under rise up condition (for 5m long sheet file at 3B/8 position from downstream end, time=6 hrs.)	126

3.53(f)	Flow-net under draw down condition (for 5m long sheet file at 3B/8 position from downstream end, time=7 hrs.)	126
3.53(g)	Flow-net under draw down condition (for 5m long sheet file at 3B/8 position from downstream end, time=10 hrs.)	126
3.53(h)	Flow-net under draw down condition (for 5m long sheet file at 3B/8 position from downstream end, time=11 hrs.)	126
3.54(a)	Flow-net under rise up condition (for 10m long sheet file at 3B/8 position from downstream end, time=1 hrs.)	127
3.54(b)	Flow-net under rise up condition (for 10m long sheet file at 3B/8 position from downstream end, time=1 hour.)	127
3.54(c)	Flow-net under rise up condition (for 10m long sheet file at 3B/8 position from downstream end, time=3 hrs.)	127
3.54(d)	Flow-net under rise up condition (for 10m long sheet file at 3B/8 position from downstream end, time=5 hrs.)	127
3.54(e)	Flow-net under rise up condition (for 10m long sheet file at 3B/8 position from downstream end, time=6 hrs.)	128
3.54(f)	Flow-net under draw down condition (for 10m long sheet file at 3B/8 position from downstream end, time=7 hrs.)	128
3.54(g)	Flow-net under draw down condition (for 10m long sheet file at 3B/8 position from downstream end, time=10 hrs.)	128
3.55(a)	Flow-net under rise up condition (for 20m long sheet file at 3B/8 position from downstream end, time=1 hrs.)	129
3.55(b)	Flow-net under rise up condition (for 20m long sheet file at 3B/8 position from downstream end, time=2 hrs.)	129
3.55(c)	Flow-net under rise up condition (for 20m long sheet file at 3B/8 position from downstream end, time=3 hrs.)	129
3.55(d)	Flow-net under rise up condition (for 20m long sheet file at 3B/8 position from downstream end, time=5 hrs.)	129
3.55(e)	Flow-net under rise up condition (for 20m long sheet file at 3B/8 position from downstream end, time=6 hrs.)	130
3.55(f)	Flow-net under draw down condition (for 20m long sheet file at 3B/8 position from downstream end, time=7 hrs.)	130
3.55(g)	Flow-net under draw down condition (for 20m long sheet file at 3B/8 position from downstream end, time=10 hrs.)	130
3.55(h)	Flow-net under draw down condition (for 20m long sheet file at 3B/8 position from downstream end, time=11 hrs.)	130
3.56	Isoline for multiple tidal cycle	131
3.57(a)	Flow-net for without sheet pile condition, at steady state condition	133
3.57(b)	Flow-net for without sheet pile condition, at steady state condition	133

3.58(a)	Flownet for 5 m long sheet file at *B*/8 position from downstream end	134
3.58(b)	Flownet for 10 m long sheet file at *B*/8 position from downstream end	134
3.58(c)	Flownet for 15 m long sheet file at *B*/8 position from downstream end	134
3.58(d)	Flownet for 20 m long sheet file at *B*/8 position from downstream end	134
3.58(e)	Flownet for 5 m long sheet file at 2*B*/8 position from downstream end	135
3.58(f)	Flownet for 10 m long sheet file at 2*B*/8 position from downstream end	135
3.58(g)	Flownet for 15 m long sheet file at 2*B*/8 position from downstream end	135
3.58(h)	Flownet for 200 m long sheet file at 2*B*/8 position from downstream end	135
3.58(i)	Flownet for 5 m long sheet file at 3*B*/8 position from downstream end	135
3.58(j)	Flownet for 10 m long sheet file at 3*B*/8 position from downstream end	135
3.58(k)	Flownet for 15 m long sheet file at 3*B*/8 position from downstream end	136
3.58(l)	Flownet for 20 m long sheet file at 3*B*/8 position from downstream end	136
3.59(a)	Flownet for 5 m long sheet file at *B*/8 position from downstream end	137
3.59(b)	Flownet for 10 m long sheet file at *B*/8 position from downstream end	137
3.59(c)	Flownet for 15 m long sheet file at *B*/8 position from downstream end	137
3.59(d)	Flownet for 20 m long sheet file at *B*/8 position from downstream end	137
3.59(e)	Flownet for 5 m long sheet file at 2*B*/8 position from downstream end	138
3.59(f)	Flownet for 10 m long sheet file at 2*B*/8 position from downstream end	138
3.59(g)	Flownet for 15 m long sheet file at 2*B*/8 position from downstream end	138
3.59(h)	Flownet for 20 m long sheet file at 2*B*/8 position from downstream end	138
3.59(i)	Flownet for 5 m long sheet file at 3*B*/8 position from downstream end	139

3.59(j)	Flownet for 10 m long sheet file at 3*B*/8 position from downstream end	139
3.59(k)	Flownet for 20 m long sheet file at 3*B*/8 position from downstream end	139
3.59(l)	Flownet for 20 m long sheet file at 3*B*/8 position from downstream end	139
3.60(a)	Flow-net under Rise up condition for without sheet pile condition, at full rise up condition, t=6.0 hrs.)	140
3.60(b)	Flow-net under Rise up condition for without sheet pile condition, time = 12.0 hr.	140
3.60(c)	Flow-net under Drawdown condition for without sheet pile condition, time = 8.0 hrs.	140
3.61(a)	Flow-net under Rise up condition (for 5 m long sheet pile at *B*/8 from downstream end, time = 1.0 hr.)	141
3.61(b)	Flow-net under Rise up condition (for 5 m long sheet pile at *B*/8 from downstream end, time = 6.0 hrs.)	141
3.61(c)	Flow-net under Rise up condition (for 5 m long sheet pile at *B*/8 from downstream end, time = 8.0 hrs.)	141
3.62(a)	Flow-net under Rise up condition (for 10m long sheet pile at *B*/8 from downstream end, time = 1.0 hr.)	142
3.62(b)	Flow-net under Rise up condition (for 10m long sheet pile at *B*/8 from downstream end, time = 6.0 hrs.)	142
3.62(c)	Flow-net under Drawdown condition (for 10m long sheet pile at *B*/8 from downstream end, time = 8.0 hrs.)	142
3.63(a)	Flow-net under Rise up condition (for 15m long sheet pile at *B*/8 from downstream end, time = 1.0 hr.)	143
3.63(b)	Flow-net under Rise up condition (for 15m long sheet pile at *B*/8 from downstream end, time = 6.0 hrs.)	143
3.63(c)	Flow-net under Drawdown condition (for 15m long sheet pile at *B*/8 from downstream end, time = 8.0 hrs.)	143
3.64(a)	Flow-net under Rise up condition (for 20m long sheet pile at *B*/8 from downstream end, time = 1.0 hr.)	144
3.64(b)	Flow-net under Rise up condition (for 20m long sheet pile at *B*/8 from downstream end, time = 6.0 hrs.)	144
3.64(c)	Flow-net under Drawdown condition (for 20m long sheet pile at *B*/8 from downstream end, time = 8.0 hrs.)	144
3.65(a)	Flow-net under Rise up condition (for 5m long sheet pile at 2*B*/8 from downstream end, time = 1.0 hr.)	145
3.65(b)	Flow-net under Rise up condition (for 5m long sheet pile at 2*B*/8 from downstream end, time = 6.0 hrs.)	145
3.65(c)	Flow-net under Drawdown condition (for 5m long sheet pile at 2*B*/8 from downstream end, time = 10.0 hrs.)	145

3.66(a)	Flow-net under Rise up condition (for 10m long sheet pile at 2*B*/8 from downstream end, time = 1.0 hr.)	146
3.66(b)	Flow-net under Rise up condition (for 10m long sheet pile at 2*B*/8 from downstream end, time = 6.0 hrs.)	146
3.66(c)	Flow-net under Drawdown condition (for 10m long sheet pile at 2*B*/8 from downstream end, time = 10.0 hrs.)	146
3.67(a)	Flow-net under Rise up condition (for 15m long sheet pile at 2*B*/8 from downstream end, time = 1.0 hr.)	147
3.67(b)	Flow-net under Rise up condition (for 15m long sheet pile at 2*B*/8 from downstream end, time = 6.0 hrs.)	147
3.67(c)	Flow-net under Drawdown condition (for 15m long sheet pile at 2*B*/8 from downstream end, time = 10.0 hrs.)	147
3.68(a)	Flow-net under Rise up condition (for 20 m long sheet pile at 2*B*/8 from downstream end, time = 1.0 hrs.)	148
3.68(b)	Flow-net under Rise up condition (for 20 m long sheet pile at 2*B*/8 from downstream end, time = 6.0 hrs.)	148
3.68(c)	Flow-net under Rise up condition (for 20 m long sheet pile at 2*B*/8 from downstream end, time = 10.0 hrs.)	148
3.69(a)	Flow-net under Rise up condition (for 5m long sheet pile at 3*B*/8 from downstream end, time = 1.0 hrs.)	149
3.69(b)	Flow-net under Drawdown condition (for 5m long sheet pile at 3*B*/8 from downstream end, time = 6.0 hrs.)	149
3.69(c)	Flow-net under Drawdown condition (for 5m long sheet pile at 3*B*/8 from downstream end, time = 8.0 hrs.)	149
3.70(a)	Flow-net under Rise up condition (for 10m long sheet pile at 3*B*/8 from downstream end, time = 1.0 hr.)	150
3.70(b)	Flow-net under Rise up condition (for 10m long sheet pile at 3*B*/8 from downstream end, time = 6.0 hr.)	150
3.70(c)	Flow-net under Rise up condition (for 10m long sheet pile at 3*B*/8 from downstream end, time = 8.0 hr.)	150
3.71(a)	Flow-net under Rise up condition (for 15 m long sheet pile at 3*B*/8 from downstream end, time = 1.0 hrs.)	151
3.71(b)	Flow-net under Rise up condition (for 15 m long sheet pile at 3*B*/8 from downstream end, time = 6.0 hrs.)	151
3.71(c)	Flow-net under Rise up condition (for 15 m long sheet pile at 3*B*/8 from downstream end, time = 8.0 hrs.)	151
3.72(a)	Flow-net under Rise up condition (for 20m long sheet pile at 3*B*/8 from downstream end, time = 1.0 hrs.)	152
3.72(b)	Flow-net under Rise up condition (for 20m long sheet pile at 3*B*/8 from downstream end, time = 6.0 hrs.)	152
3.72(c)	Flow-net under Rise up condition (for 20m long sheet pile at 3*B*/8 from downstream end, time = 10.0 hrs.)	152

4.1	Flow Chart for present current experimental and numerical simulation analysis	153
4.2	centrifuge traveling around a circle or circular path	156
4.3	Flowchart for experimental analysis	159
4.3(a)	Top view of Centrifuge with model of dam	165
4.3(b)	Front View of Geotechnical Centrifuge	166
4.3(c)	Top view of Geotechnical Centrifuge	166
4.4	View of the Geotechnical Centrifuge with component details	166
4.5 (a)	Top view of Model Test Box	167
4.5 (b)	Front view of Model Test Box	167
4.6 (a)	Front view of Model Test Box piezometer position	168
4.6 (b)	Top view of Model Test Box piezometer position	168
4.7	Details dimension of the front view of the model box	168
4.8	Arduino Board	169
4.9	Valve control through Arduino	170
4.10	Stage-1, Construction of Bed	172
4.11	Stage-2, installation of sheet pile	172
4.12	Stage-3, Construction of Slope	172
4.13	Top view of Earthen Dam	173
4.14(a)	Front View of Model Embankment	173
4.14(b)	Top view of Model Embankment	173
4.15	Site elevation of Earthen Dam	173
4.16	Solenoid Valve	174
4.17	Artificial tide control circuit	175
4.18(a)	Opening Circuit diagram of Solenoid valve	175
4.18(b)	closing Circuit diagram of Solenoid valve	175
4.19(a)	Digital image capturing Raspberry Pi module	181
4.19(b)	Digital image capturing camera module	176
4.20(a)	Experimental model of Simulation of tidal cycle	177
4.20(b)	Experimental model of Image capturing with camera module	177
4.21(a)	Flow Chart for Image Capturing and Processing	178
4.21(b)	Output image of embankment model of Image Capturing and Processing	178
4.22(a)	Front View Model Test Box piezometer position during test	179
4.22(b)	Top view Model Test Box piezometer position during test	179
4.23	Steady State seepage condition for working head of 3.5 m	180
4.24(a)	Development of phreatic surface for 2 hrs.	181
4.24(b)	Development of phreatic surface for 3 hrs.	181
4.24(c)	Development of phreatic surface for 4 hrs.	181
4.24(d)	Development of phreatic surface for 5 hrs.	181
4.24(e)	Development of phreatic surface for 6 hrs.	181
4.25(a)	Development of phreatic surface for 1 hour	182

4.25(b)	Development of phreatic surface for 2 hrs	182
4.25(c)	Development of phreatic surface for 3 hrs.	182
4.25(d)	Development of phreatic surface for 4 hrs.	182
4.25(e)	Development of phreatic surface for 5 hrs.	183
4.25(f)	Development of phreatic surface for 6 hrs.	183
4.25(g)	Development of phreatic surface for 10 hrs.	183
4.26(a)	Development of phreatic surface for 1 hour	184
4.26(b)	Development of phreatic surface for 3 hour	184
4.26(c)	Development of phreatic surface for 5 hrs.	184
4.26(d)	Development of phreatic surface for 6 hrs.	184
4.27(a)	Development of phreatic surface for 1 hour	185
4.27(b)	Development of phreatic surface for 2 hrs.	185
4.27(c)	Development of phreatic surface for 4 hrs.	185
4.27(d)	Development of phreatic surface for 7 hrs.	185
4.28(a)	Development of phreatic surface for 2 hrs.	186
4.28(b)	Development of phreatic surface for 5 hrs.	186
4.28(c)	Development of phreatic surface for 7 hrs.	186
4.29(a)	Development of phreatic surface for 1 hour	187
4.29(b)	Development of phreatic surface for 3 hrs.	187
4.29(c)	Development of phreatic surface for 5 hrs.	187
4.29(d)	Development of phreatic surface for 6 hrs.	187
4.30(a)	Development of phreatic surface for 1 hour	188
4.30(b)	Development of phreatic surface for 3 hrs.	188
4.30(c)	Development of phreatic surface for 4 hrs.	188
4.30(d)	Development of phreatic surface for 6 hrs.	188
4.31(a)	Development of phreatic surface for 1 hour	189
4.31(b)	Development of phreatic surface for 3 hrs.	189
4.31(c)	Development of phreatic surface for 6 hrs.	189
4.32(a)	Development of phreatic surface for 1 hour	190
4.32(b)	Development of phreatic surface for 3 hrs.	190
4.32(c)	Development of phreatic surface for 5 hrs.	190
4.32(d)	Development of phreatic surface for 6 hrs.	190
4.33(a)	Development of phreatic surface for 3 hrs.	191
4.33(b)	Development of phreatic surface for 6 hrs.	191
4.34(a)	Development of phreatic surface for 1 hour	192
4.34(b)	Development of phreatic surface for 3 hrs.	192
4.34(c)	Development of phreatic surface for 4 hrs.	192
4.34(d)	Development of phreatic surface for 5 hrs.	192
4.34(e)	Development of phreatic surface for 7 hrs.	193
4.35(a)	Development of phreatic surface for 1 hour	193
4.35(b)	Development of phreatic surface for 3 hrs.	193
4.35(c)	Development of phreatic surface for 5 hrs.	194

4.35(d)	Development of phreatic surface for 6 hrs.	194
4.36(a)	Development of phreatic surface for 1 hour	194
4.36(b)	Development of phreatic surface for 3 hrs.	194
4.36(c)	Development of phreatic surface for 6 hrs.	195
4.37(a)	Phreatic Surface Development for steady state condition	196
4.38(a)	Flownet for *B*/8 position 5m long sheet pile	196
4.38(b)	Flownet for *B*/8 position 10m long sheet pile	196
4.38(c)	Flownet for *B*/8 position 15m long sheet pile	197
4.38(d)	Flownet for *B*/8 position 20m long sheet pile	197
4.38(e)	Flownet for*2B*/8 position 5m long sheet pile	197
4.38(f)	Flownet for*2B*/8 position 10m long sheet pile	197
4.38(g)	Flownet for*2B*/8 position 15m long sheet pile	198
4.38(h)	Flownet for*2B*/8 position 20m long sheet pile	198
4.38(i)	Flownet for*3B*/8 position 5m long sheet pile	198
4.38(j)	Flownet for*3B*/8 position 10m long sheet pile	198
4.38(k)	Flownet for*3B*/8 position 15m long sheet pile	199
4.38(l)	Flownet for*3B*/8 position 20m long sheet pile	199
4.39(a)	Phreatic Surface Development for tidal cycle 2 hrs.	199
4.39(b)	Phreatic Surface Development for tidal cycle 4 hrs.	200
4.39(c)	Phreatic Surface Development for tidal cycle 6 hrs.	200
4.40(a)	Flownet under rise up condition (for 5 m long sheet file at *B*/8 from downstream end, time=1 hour.)	201
4.40(b)	Flownet under rise up condition (for 5 m long sheet file at *B*/8 from downstream end, time=3 hrs.)	201
4.40(c)	Flownet under rise up condition (for 5 m long sheet file at *B*/8 from downstream end, time=5 hrs.)	201
4.40(d)	Flownet under rise up condition (for 5 m long sheet file at *B*/8 from downstream end, time=7 hrs.)	201
4.41(a)	Flownet under rise up condition (for 10 m long sheet file at *B*/8 from downstream end, time=1 hour.)	202
4.41(b)	Flownet under rise up condition (for 10 m long sheet file at *B*/8 from downstream end, time=2 hrs.)	202
4.41(c)	Flownet under rise up condition (for 10 m long sheet file at *B*/8 from downstream end, time=3 hrs.)	203
4.41(d)	Flownet under rise up condition (for 10 m long sheet file at *B*/8 from downstream end, time=4 hrs.)	203
4.41(e)	Flownet under rise up condition (for 10 m long sheet file at *B*/8 from downstream end, time=6 hrs.)	203
4.41(f)	Flownet under rise up condition (for 10 m long sheet file at *B*/8 from downstream end, time=8 hour)	203
4.42(a)	Flownet under rise up condition (for 15 m long sheet file at *B*/8 from downstream end, time=1 hour)	204

4.42(b)	Flownet under rise up condition (for 15 m long sheet file at *B*/8 from downstream end, time=3 hrs.)	204
4.42(c)	Flownet under rise up condition (for 15 m long sheet file at *B*/8 from downstream end, time=4 hrs.)	205
4.42(d)	Flownet under rise up condition (for 15 m long sheet file at *B*/8 from downstream end, time=6 hrs.)	205
4.43(a)	Flownet under rise up condition (for 20 m long sheet file at *B*/8 from downstream end, time=1 hour)	206
4.43(b)	Flownet under rise up condition (for 20 m long sheet file at *B*/8 from downstream end, time=2 hrs.)	206
4.43(c)	Flownet under rise up condition (for 20 m long sheet file at *B*/8 from downstream end, time=3 hrs.)	206
4.43(d)	Flownet under rise up condition (for 20 m long sheet file at *B*/8 from downstream end, time=5 hrs.)	206
4.43(e)	Flownet under rise up condition (for 20 m long sheet file at *B*/8 from downstream end, time=7 hrs.)	207
4.44(a)	Flownet under rise up condition (for 5 m long sheet file at 2*B*/8 from downstream end, time=1 hour)	208
4.44(b)	Flownet under rise up condition (for 5 m long sheet file at 2*B*/8 from downstream end, time=2 hrs.)	208
4.44(c)	Flownet under rise up condition (for 5 m long sheet file at 2*B*/8 from downstream end, time=3 hrs.)	208
4.44(d)	Flownet under rise up condition (for 5 m long sheet file at 2*B*/8 from downstream end, time=5 hrs.)	208
4.44(e)	Flownet under rise up condition (for 5 m long sheet file at 2*B*/8 from downstream end, time=7 hrs.)	209
4.45(a)	Flownet under rise up condition (for 10 m long sheet file at 2*B*/8 from downstream end, time=1 hour)	210
4.45(b)	Flownet under rise up condition (for 10 m long sheet file at 2*B*/8 from downstream end, time=3 hrs.)	210
4.45(c)	Flownet under rise up condition (for 10 m long sheet file at 2*B*/8 from downstream end, time=6 hrs.)	210
4.46(a)	Flownet under rise up condition (for 15 m long sheet file at 2*B*/8 from downstream end, time=1 hour)	211
4.46(b)	Flownet under rise up condition (for 15 m long sheet file at 2*B*/8 from downstream end, time=2 hrs.)	211
4.46(c)	Flownet under rise up condition (for 15 m long sheet file at 2*B*/8 from downstream end, time=5 hrs.)	211
4.46(d)	Flownet under rise up condition (for 15 m long sheet file at 2*B*/8 from downstream end, time=7 hrs.)	211
4.47(a)	Flownet under rise up condition (for 20 m long sheet file at 2*B*/8 from downstream end, time=1 hour)	212

4.47(b)	Flownet under rise up condition (for 20 m long sheet file at 2*B*/8 from downstream end, time=2 hrs.)	212
4.47(c)	Flownet under rise up condition (for 20 m long sheet file at 2*B*/8 from downstream end, time=4 hrs.)	213
4.47(d)	Flownet under rise up condition (for 20 m long sheet file at 2*B*/8 from downstream end, time=6 hrs.)	213
4.48(a)	Flownet under rise up condition (for 5 m long sheet file at 3*B*/8 from downstream end, time=1 hour)	214
4.48(b)	Flownet under rise up condition (for 5 m long sheet file at 3*B*/8 from downstream end, time=3 hrs.)	214
4.48(c)	Flownet under rise up condition (for 5 m long sheet file at 3*B*/8 from downstream end, time=5 hrs.)	214
4.48(d)	Flownet under rise up condition (for 5 m long sheet file at 3*B*/8 from downstream end, time=7 hrs.)	214
4.49(a)	Flownet under rise up condition (for 10 m long sheet file at 3*B*/8 from downstream end, time=1 hour)	215
4.49(b)	Flownet under rise up condition (for 10 m long sheet file at 3*B*/8 from downstream end, time=2 hrs.)	215
4.49(c)	Flownet under rise up condition (for 10 m long sheet file at 3*B*/8 from downstream end, time=3 hrs.)	216
4.49(d)	Flownet under rise up condition (for 10 m long sheet file at 3*B*/8 from downstream end, time=5 hrs.)	216
4.49(e)	Flownet under rise up condition (for 10 m long sheet file at 3*B*/8 from downstream end, time=6 hrs.)	216
4.49(f)	Flownet under rise up condition (for 10 m long sheet file at 3*B*/8 from downstream end, time=8 hrs.)	216
4.50(a)	Flownet under rise up condition (for 15 m long sheet file at 3*B*/8 from downstream end, time=1 hour)	217
4.50(b)	Flownet under rise up condition (for 15 m long sheet file at 3*B*/8 from downstream end, time=3 hrs.)	217
4.50(c)	Flownet under rise up condition (for 15 m long sheet file at 3*B*/8 from downstream end, time=5 hrs.)	217
4.50(d)	Flownet under rise up condition (for 15 m long sheet file at 3*B*/8 from downstream end, time=7 hrs.)	217
4.51(a)	Flownet under rise up condition (for 20 m long sheet file at 3*B*/8 from downstream end, time=1 hour)	218
4.51(b)	Flownet under rise up condition (for 20 m long sheet file at 3*B*/8 from downstream end, time=3 hrs.)	218
4.51(c)	Flownet under rise up condition (for 20 m long sheet file at 3*B*/8 from downstream end, time=5 hrs.)	219
4.51(d)	Flownet under rise up condition (for 20 m long sheet file at 3*B*/8 from downstream end, time=7 hrs.)	219

4.52	Results from experimental investigation *B/*8 position 5m length (a) 5m from the top of dam (b) 10 m from the top of dam	220
4.53	Results from experimental investigation *B/*8 position 10m length at 5m from the top of dam	220
4.54	Result from experimental investigation *B/*8 position 15m length (a) 5m from the top of dam (b) 15 m from the top of dam	221
4.55	Result from experimental investigation 20m long sheet pile for *B/*8 position (a) 5m from the top of dam (b) 10 m from the top of dam	221
4.56	Result from experimental investigation 2*B/*8 position 5m length (a) 5m from the top of dam (b) 10 m from the top of dam	221
4.57	Result from experimental investigation 2*B/*8 position 10m length (a) 5m from the top of dam (b) 10 m from the top of dam	222
4.58	Result from experimental investigation 2*B/*8 position 15m length (a) 5m from the top of dam (b) 10 m from the top of dam (c)15 m from the top of dam	222
4.59	Result from experimental investigation 2*B/*8 POSITION 20m length (a) 5m from the top of dam (b) 15 m from the top of dam	223
4.60	Result from experimental investigation 3*B/*8 position 5m length (a) 5m from the top of dam (b) 10 m from the top of dam	223
4.61	Result from experimental investigation 3*B/*8 position 10m length (a) 5m from the top of dam (b) 15 m from the top of dam	223
4.62	Result from experimental investigation 3*B/*8 position 15m length (a) 10m from the top of dam (b) 15 m from the top of dam	224
4.63	Result from experimental investigation 3*B/*8 position 20m length (a) 5m from the top of dam (b) 10 m from the top of dam	224
5.1(a)	Fluid flow vector of embankment with-out sheet pile (OBTAINED FROM FLAC2D)	228
5.1(b)	Fluid flow vector of embankment with sheet pile condition (OBTAINED FROM FLAC2D)	228
5.2(a)	Typical graph showing fluid flow vector in vertical direction for different sheet pile position (5m from the top)	228

5.2(b)	Fluid flow vector in vertical direction for different sheet pile length at fixed position of 3*B*/8 (5m from the top)..	229
5.2(c)	Typical graph showing fluid flow vector in vertical direction for different sheet pile position (12m from the top)	229
5.2(d)	Fluid flow vector in vertical direction for different sheet pile length at fixed position of 3*B*/8 (12 m from the top).	230
5.3 (a)	Result From experimental investigation and numerical analysis for *B*/8 position at 7 m from the top of dam	231
5.3 (b)	Result From experimental investigation and numerical analysis for *5m* length of sheet pile at 7m from the top of dam	232
5.4 (a)	Fluid flow vector in vertical direction of 15 m length for *B*/8 position from the downstream end for acceleration time= 37.25 sec, 69.25 sec, 169.25 sec. (at 7m from the top)	232
5.4 (b)	Fluid flow vector in vertical direction of 15 m length for 3*B*/8 position from the downstream end for acceleration time= 37.25 sec, 69.25 sec, 169.25 sec. (at 7 m from the top)	233
5.4 (c):	Fluid flow vector in vertical direction of 15 m length for 3*B*/8 position from the downstream end for acceleration time= 37.25 sec, 69.25 sec, 169.25 sec. (at 12 m from the top)	233
5.5 (a)	Fluid flow vector in vertical direction for 10 m long sheet pile with position at 3*B*/8 from the downstream end	234
5.5 (b)	Fluid flow vector in vertical direction for 15 m long sheet pile with position at 3*B*/8 from the downstream end	235
5.5(c)	Fluid flow vector in vertical direction for 10 m long sheet pile with position at 2*B*/8 from the downstream end	235
5.5(d)	Fluid flow vector in vertical direction for 15 m long sheet pile with position at 2*B*/8 from the downstream end	235
5.5(e)	Fluid flow vector in vertical direction for 10 m long sheet pile with position at *B*/8 from the downstream end	236
5.5(f)	Fluid flow vector in vertical direction for 15 m long sheet pile with position at *B*/8 from the downstream end	236
5.6 (a)	Fluid flow vector in vertical direction for 5m long sheet pile at 7m from the top under full drawdown condition	237
5.6 (b)	Fluid flow vector in vertical direction for 5m long sheet pile at 7m from the top under full rise up condition	237
5.6(c)	Fluid flow vector in vertical direction for 10m long sheet pile at 7m from the top under full drawdown condition	238
5.6(d)	Fluid flow vector in vertical direction for 10m long sheet pile at 7m from the top under full rise up condition	238
5.6(e)	Fluid flow vector in vertical direction for 15m long sheet pile at 7m from the top under drawdown condition	239
5.6(f)	Fluid flow vector in vertical direction for 15m long sheet pile at 7m from the top under rise up condition	239
5.6(g)	Fluid flow vector in vertical direction for 20m long sheet pile at 7m from the top under drawdown condition	240

5.6(h):	Fluid flow vector in vertical direction for 20m long sheet pile at 7m from the top under rise up condition	241
5.6(i)	Fluid flow vector in vertical direction at 3*B*/8 position for different sheet pile length at 7m from the top under drawdown condition	241
5.6(j)	Fluid flow vector in vertical direction at 3*B*/8 position for different sheet pile length at 7m from the top under rise up condition	241
5.6(k)	Fluid flow vector in vertical direction at 3*B*/8 position for different sheet pile length at 7m from the top under full rise up condition	242
5.6(l)	Fluid flow vector in vertical direction at 2*B*/8 position for different sheet pile length at 7m from the top under full drawdown condition	242
5.6(m)	Fluid flow vector in vertical direction at 2*B*/8 position for different sheet pile length at 7m from the top under rise up condition	242
5.6(n)	Fluid flow vector in vertical direction at 2*B*/8 position for different sheet pile length at 7m from the top under full rise up condition	243
5.6(o)	Fluid flow vector in vertical direction at *B*/8 position for different sheet pile length at 7m from the top under full drawdown condition	243
5.6(p)	Fluid flow vector in vertical direction at *B*/8 position for different sheet pile length at 7m from the top under rise up condition	244
5.6(q)	Fluid flow vector in vertical direction at *B*/8 position for different sheet pile length at 7m from the top under full rise up condition	244
5.7 (a)	Fluid flow vector in vertical direction of 5 m length for 3*B*/8 position from the downstream end	245
5.7 (b)	Fluid flow vector in vertical direction of 10 m length for 3*B*/8 position from the downstream end	245
5.7(c)	Fluid flow vector in vertical direction of 15 m length for 3*B*/8 position from the downstream end	246
5.7(d)	Fluid flow vector in vertical direction of 20 m length for 3*B*/8 position from the downstream end	246
5.7(e)	Fluid flow vector in vertical direction of 5 m length for 2*B*/8 position from the downstream end	247
5.7(f)	Fluid flow vector in vertical direction of 10 m length for 2*B*/8 position from the downstream end	247
5.7(g)	Fluid flow vector in vertical direction of 15 m length for 2*B*/8 position from the downstream end	248
5.7(h)	Fluid flow vector in vertical direction of 20 m length for 2*B*/8 position from the downstream end	248
5.7(i)	Fluid flow vector in vertical direction of 5 m length for *B*/8 position from the downstream end	249
5.7(j)	Fluid flow vector in vertical direction of 10 m length for *B*/8 position from the downstream end	249

5.7(k)	Fluid flow vector in vertical direction of 10 m length for *B*/8 position from the downstream end	250
5.7(l)	Fluid flow vector in vertical direction of 20 m length for *B*/8 position from the downstream end	250
5.7(m)	Fluid flow vector in vertical direction at 2*B*/8 position for different sheet pile length at 12m from the top under full drawdown condition	251
5.7(n)	Fluid flow vector in vertical direction at 2*B*/8 position for different sheet pile length at 12m from the top under rise up condition	251
5.7(o)	Fluid flow vector in vertical direction at 2*B*/8 position for different sheet pile length at 12m from the top under full rise up condition	252
5.8 (a)	Fluid flow vector in vertical direction for *B*/8 position from the downstream end at 7m from the top (Numerical and experimental investigation)	253
5.8 (b)	Fluid flow vector in vertical direction for 2*B*/8 position from the downstream end at 7m from the top (Numerical and experimental investigation)	253
5.8(c)	Fluid flow vector in vertical direction for 3*B*/8 position from the downstream end at 7m from the top (Numerical and experimental investigation)	254
5.8(d)	Fluid flow vector in vertical direction for 5m length at different position from the downstream end at 7m from the top (Numerical and experimental investigation)	254
5.8(e)	Fluid flow vector in vertical direction for 15m length at different position from the downstream end at 10m from the top (Numerical and experimental investigation)	255
5.8(f)	Fluid flow vector in vertical direction for 15m length at different position from the downstream end at 7m from the top (Numerical and experimental investigation)	255
5.8(g)	Fluid flow vector in vertical direction for 20m length at different position from the downstream end at 7m from the top (Numerical and experimental investigation)	256
5.9(a)	Fluid flow vector in vertical direction for 3*B*/8 position from the downstream end for different sheet pile length at 7m from the top	257
5.9 (b)	Fluid flow vector in vertical direction for 2*B*/8 position from the downstream end for different sheet pile length at 7m from the top	257
5.9 (c)	Fluid flow vector in vertical direction for *B*/8 position from the downstream end for different sheet pile length at 7m from the top	258

5.9(d)	Fluid flow vector in vertical direction for *15 m* long sheet pile from the at different position from downstream end at 7m from the top	258
5.9(e)	Fluid flow vector in vertical direction for 3*B*/8 position from the downstream end for different sheet pile length at 12m from the top	259
5.9(f)	Fluid flow vector in vertical direction for 2*B*/8 position from the downstream end for different sheet pile length at 12m from the top	259
5.9(g)	Fluid flow vector in vertical direction for *B*/8 position from the downstream end for different sheet pile length at 12m from the top	260
5.10(a)	Pore pressure variation for 20m length sheet pile for different sheet pile positions 2m below the base of earthen dam at 7m from the top of dam	261
5.10(b)	Pore pressure variation (along the sheet pile) for 20m long sheet pile for different sheet pile positions	262
5.10(c)	Pore pressure variation (along the sheet pile) for different sheet pile lengths for a *B*/8 sheet pile position.	262
5.11(a)	Pore pressure variation (along the sheet pile) for different sheet pile positions for a 5m length sheet pile (at 7m from the top of the dam)	263
5.11(b)	Pore pressure variation for different sheet pile length for 3*B*/8 position (at 7m from the top of the dam)	263
5.11(c)	Pore pressure variation at for different sheet pile length at 3*B*/8 position sheet pile (at 12m from the top of the dam)	264
5.11(d)	Pore pressure variation for different sheet pile positions for a 10m length sheet pile (at 12m from the top of the dam)	264
5.12(a)	Pore pressure variation for different sheet pile positions for a 5m length sheet pile position at 7m from the top of the dam.	265
5.12(b)	Pore pressure variation for different sheet pile positions for a 10m length sheet pile position at 7m from the top of the dam.	265
5.12(c)	Pore pressure variation for 2B/8 position from downstream end for different length of sheet pile at 7m from the top of the dam	266
5.12(d)	Pore pressure variation for different sheet pile positions for a 10m length sheet pile position at 12m from the top of the dam.	266
5.12(e)	Pore pressure variation for different sheet pile positions for a 15m length sheet pile position at 12m from the top of the dam.	267
5.13(a)	Pore water pressure variation of 5 m length for 3*B*/8 position from the downstream end	268

5.13(b)	Pore water pressure variation of 10 m length for 3*B*/8 position from the downstream end	268
5.13(c)	Pore water pressure variation of 15 m length for 3*B*/8 position from the downstream end	269
5.13(d)	Pore water pressure variation of 20 m length for 3*B*/8 position from the downstream end	269
5.13(e)	Pore water pressure variation of 5 m length for 2*B*/8 position from the downstream end	270
5.13(f)	Pore water pressure variation of 10 m length for 2*B*/8 position from the downstream end	270
5.13(g)	Pore water pressure variation of 15 m length for 2*B*/8 position from the downstream end	271
5.13(h)	Pore water pressure variation of 20 m length for 2*B*/8 position from the downstream end	271
5.13(i)	Pore water pressure variation of 5m length for *B*/8 position from the downstream end	272
5.13(j)	Pore water pressure variation of 10m length for *B*/8 position from the downstream end	272
5.13(k)	Pore water pressure variation of 15m length for *B*/8 position from the downstream end	273
5.13(l)	Pore water pressure variation of 20m length for *B*/8 position from the downstream end	273
5.14(a)	Pore water pressure variation of 5m length for 3*B*/8 position from the downstream end (at 12m from the top of dam)	274
5.14(b)	Pore water pressure variation of 10m length for 3*B*/8 position from the downstream end (at 12m from the top of dam)	274
5.14(c)	Pore water pressure variation of 15m length for 3*B*/8 position from the downstream end (at 12m from the top of dam)	275
5.14(d)	Pore water pressure variation of 20m length for 3*B*/8 position from the downstream end (at 12m from the top of dam)	275
5.14(e)	Pore water pressure variation of 5m length for 2*B*/8 position from the downstream end (at 12m from the top of dam)	276
5.14(f)	Pore water pressure variation of 10m length for 2*B*/8 position from the downstream end (at 12m from the top of dam)	276
5.14(g)	Pore water pressure variation of 15m length for 2*B*/8 position from the downstream end (at 12m from the top of dam)	277
5.14(h)	Pore water pressure variation of 20m length for 2*B*/8 position from the downstream end (at 12m from the top of dam)	277
5.14(i)	Pore water pressure variation of 5m length for *B*/8 position from the downstream end (at 12m from the top of dam)	278
5.14(j)	Pore water pressure variation of 10m length for *B*/8 position from the downstream end (at 12m from the top of dam)	278
5.14(k)	Pore water pressure variation of 15m length for *B*/8 position from the downstream end (at 12m from the top of dam)	279
5.14(l)	Pore water pressure variation of 20m length for *B*/8 position from the downstream end (at 12m from the top of dam)	279

5.15(a)	Pore water pressure variation of 5m long sheet pile at 3*B*/8 position under full rise up and drawdown condition at 7m position (Experimental and numerical investigation)	281
5.15(b)	Pore water pressure variation of 10m long sheet pile at 3*B*/8 position under full rise up and drawdown condition at 7m position (Experimental and numerical investigation)	281
5.15(c)	Pore water pressure variation of 3*B*/8 position under full rise up and drawdown condition at 7m position (Experimental and numerical investigation)	282
5.15(d)	Pore water pressure variation of 3*B*/8 position under full rise up and drawdown condition at 7m position (Experimental and numerical investigation)	282
5.15(e)	Pore water pressure variation of 2*B*/8 position under full rise up and drawdown condition at 7m position (Experimental and numerical investigation)	283
5.15(f)	Pore water pressure variation of 2*B*/8 position under full rise up and drawdown condition at 7m position (Experimental and numerical investigation)	283
5.15(g)	Pore water pressure variation of 2*B*/8 position under full rise up and drawdown condition at 7m position (Experimental and numerical investigation)	284
5.15(h)	Pore water pressure variation of 2*B*/8 position under full rise up and drawdown condition at 7m position (Experimental and numerical investigation)	284
5.15(i)	Pore water pressure variation of *B*/8 position under full rise up and drawdown condition at 7m position (Experimental and numerical investigation)	285
5.15(j)	Pore water pressure variation of *B*/8 position under full rise up and drawdown condition at 7m position (Experimental and numerical investigation)	285
5.15(k)	Pore water pressure variation of *B*/8 position under full rise up and drawdown condition at 7m position (Experimental and numerical investigation)	286
5.15(l)	Pore water pressure variation of *B*/8 position under full rise up and drawdown condition at 7m position (Experimental and numerical investigation)	286
5.16(a)	Pore water pressure variation of 5m long sheet pile under full drawdown condition at 7m position (Experimental and numerical investigation)	287
5.16(b)	Pore water pressure variation of 5m long sheet pile under full drawdown condition at 7m position (Experimental and numerical investigation)	287
5.16(c)	Pore water pressure variation of 10m long sheet pile under full drawdown condition at 7m position (Experimental and numerical investigation)	288
5.16(d)	Pore water pressure variation of 10m long sheet pile under full rise up condition at 7m position (Experimental and numerical investigation)	288

5.16(e)	Pore water pressure variation of 15m long sheet pile under full drawdown condition at 7m position (Experimental and numerical investigation)	289
5.16(f)	Pore water pressure variation of 15m long sheet pile under full rise up condition at 7m position (Experimental and numerical investigation)	289
5.16(g)	Pore water pressure variation of 20m long sheet pile under full drawdown condition at 7m position (Experimental and numerical investigation)	290
5.16(h)	Pore water pressure variation of 20m long sheet pile under full rise up condition at 7m position (Experimental and numerical investigation)	290
5.16(i)	Pore water pressure variation of different length of sheet pile at 3*B*/8 position under full drawdown condition at 7m position (Experimental and numerical investigation)	291
5.16(j)	Pore water pressure variation of different length of sheet pile at 3*B*/8 position under full rise up condition at 7m position (Experimental and numerical investigation)	291
5.16(k)	Pore water pressure variation of different length of sheet pile at 2*B*/8 position under full rise up condition at 7m position (Experimental and numerical investigation)	292
5.16(l)	Pore water pressure variation of different length of sheet pile at 2*B*/8 position under full drawdown condition at 7m position (Experimental and numerical investigation)	292
5.16(m)	Pore water pressure variation of different length of sheet pile at *B*/8 position under full rise up condition at 7m position (Experimental and numerical investigation)	293
5.16(n)	Pore water pressure variation of different length of sheet pile at *B*/8 position under full drawdown condition at 7m position (Experimental and numerical investigation)	293
5.17(a)	Pore water pressure variation of 3*B*/8 position under full rise up and drawdown condition at 12m position (Experimental and numerical investigation)	295
5.17(b)	Pore water pressure variation of 3*B*/8 position under full rise up and drawdown condition at 12m position (Experimental and numerical investigation)	296
5.17(c)	Pore water pressure variation of 3*B*/8 position under full rise up and drawdown condition at 12m position (Experimental and numerical investigation)	296
5.17(d)	Pore water pressure variation of 3*B*/8 position under full rise up and drawdown condition at 12m position (Experimental and numerical investigation)	297
5.17(e)	Pore water pressure variation of 2B/8 position under full rise up and drawdown condition at 12m position (Experimental and numerical investigation)	297
5.17(f)	Pore water pressure variation of 5m long sheet pile under full drawdown condition at 12m position (Experimental and numerical investigation)	298

5.17(g)	Pore water pressure variation of 5m long sheet pile under full rise up condition at 12m position (Experimental and numerical investigation)	298
5.17(h)	Pore water pressure variation of 10m long sheet pile under full rise up condition at 12m position (Experimental and numerical investigation)	299
5.17(i)	Pore water pressure variation of B/8 position sheet pile under full rise up condition at 12m position (Experimental and numerical investigation)	299
5.17(j)	Pore water pressure variation of 5m long sheet pile under full rise up condition at 12m position (Experimental and numerical investigation)	300
5.17(k)	Pore water pressure variation of 5m long sheet pile under full rise up condition	300
5.18(a)	Pore water pressure variation of 5m long sheet pile under full drawdown condition (at 7m position from top)	302
5.18(b)	Pore water pressure variation of 5m long sheet pile under full rise up condition (at 12m position from top)	302
5.18(c)	Pore water pressure variation of 5m long sheet pile under rise up condition (at 12m position from top)	303
5.18(d)	Pore water pressure variation of 10m long sheet pile under full drawdown condition (at 7m position from top)	303
5.18(e)	Pore water pressure variation of 10m long sheet pile under rise up condition (at 7m position from top)	304
5.18(f)	Pore water pressure variation of 10m long sheet pile under rise up condition (at 12m position from top)	304
5.19(a)	Pore water pressure variation in steady state condition for *B*/8 position 5m length at 2m from the top.	305
5.19(b)	Pore water pressure variation in steady state condition	306
5.20 (a)	Pore water pressure variation in rise up condition (Numerical)	307
5.20 (b)	Pore water pressure variation in drawdown condition (Numerical)	307
5.20 (c)	Pore water pressure variation in rise up and drawdown condition (Numerical)	308
5.20 (d)	Pore water pressure variation (Experimental and numerical investigation)	308
5.20(e)	Pore water pressure variation with respect to time (For different location	309
5.20(f)	Pore water pressure variation with respect to time (For different location	310
5.21(a)	variation of pore water pressure for 3*B*/8 position 5 m length	310
5.21(b)	Variation of pore water pressure at the dam body	311
5.22 (a)	Pore water pressure variation at the foundation level in drawdown condition	311
5.22 (b)	Pore water pressure variation at the foundation level in drawdown condition (Numerical)	312
5.23(a)	Soil pressure diagram for different sheet pile length at 2*B*/8 position	313

5.23(b)	Soil pressure diagram for different sheet pile position for 20m long sheet pile	313
5.23(c)	Soil pressure diagram for different sheet pile length under seismic condition	314
5.23(d):	Soil pressure diagram for different sheet pile position of 20 m length under seismic condition	314
5.24(a):	Soil pressure diagram for different sheet pile position of 15 m length under rise up condition	315
5.24(b):	Soil pressure diagram for different sheet pile position of 15 m length under drawdown condition	316
5.24(c):	Soil pressure diagram for different sheet pile position of 20 m length under rise up condition	316
5.24(d):	Soil pressure diagram for different sheet pile position of 20 m length under drawdown condition	317
5.24(e):	Soil pressure diagram for *B*/8 position under drawdown condition	317
5.24(f):	Soil pressure diagram for 5m long sheet pile under rise up condition (seismic)	318
5.24(g):	Soil pressure diagram for 10m long sheet pile under rise up condition (seismic condition)	318
5.24(h):	Soil pressure diagram for 15m long sheet pile under rise up condition (seismic condition)	319
5.24(i):	Soil pressure diagram for 20m long sheet pile under rise up condition (seismic condition)	319
5.24(j):	Soil pressure diagram for 3*B*/8 position under rise up condition (seismic condition)	320
5.24(k):	Soil pressure diagram for 2*B*/8 position under rise up condition (seismic condition)	320
5.25(a):	Variation of Overall Factor of safety with different sheet pile positions under static condition	322
5.25(b):	Variation of Overall Factor of safety with different sheet pile positions under seismic condition	322
5.25 (c)	Factor of safety against time for different sheet pile condition	325
5.25 (d)	Factor of safety against time at different position for 15m long sheet pile under static condition	325
5.25 (e)	Factor of safety against time at different position for 15m long sheet pile under seismic condition	326
5.25 (f)	Factor of safety against time at *B*/8 position for different sheet pile length under static condition	326
5.25 (g)	Factor of safety against time at *B*/8 position for different sheet pile length under seismic condition	327
5.25 (h)	Factor of safety against time at *B*/8 position for different sheet pile length under multiple tidal cycle	328

5.26(a)	Variation of factor of safety against piping with sheet pile length	329
5.26(a)	Factor of safety against piping for different sheet pile condition	330
5.26(b)	Factor of safety against piping for *B*/8position sheet pile position	331
5.26(c)	Factor of safety against piping for 2*B*/8position sheet pile position	331
5.26(d)	Factor of safety against piping for 3*B*/8position sheet pile position	332
5.26(e)	Factor of safety against piping for 5m long sheet pile	332
5.26(f)	Factor of safety against piping for 10m long sheet pile	333
5.26(g)	Factor of safety against piping for 15m long sheet pile	333
5.26(h)	Factor of safety against piping for 20m long sheet pile	334
5.27 (a) & (b)	Crack developed under effect of tidal cycle a) in the centrifuge model b)Real time crack developed in embankment at Sundar ban site. (Reference: www.google.co.in/search sundarban crack developed)	335
5.27 (c)	Crack developed under effect of tidal cycle in MATLAB Software at *B*/8 position 10m long sheet pile (Theoretical)	335
5.27 (d)	Crack developed under effect of tidal cycle in MATLAB Software at 2*B*/8 position 10m long sheet pile (Theoretical)	336
5.28	Statistical modeling corelating dependent and independent variable (a) contour (b)coordinate(c) 3D surface	337
5.29	Statistical modeling corelating dependent and independent variable (a) contour (b) 3D surface	338
5.30(a)	Sheet pile position Residual Plot	339
5.30(b)	Sheet pile position Line Fit Plot	339
5.30(c)	Sheet pile length Residual Plot	340
5.30(d)	Sheet pile length Line Fit Plot	340
5.30(e)	Fluid flow vector Residual Plot	340
5.30(f)	Fluid flow vector Line Fit Plot	341
5.30(g)	Pore Water Pressure Residual Plot	341
5.30(h)	Pore Water Pressure Line Fit Plot	341
5.30(i)	Time Residual Plot	342
5.30(j)	Time Line Fit Plot	342
5.30(k)	Normal Probability Plot	342
5.31(a)	Sheet pile position Residual Plot	344
5.31(b)	Sheet pile position Line fit Plot	344
5.31(c)	Sheet pile Length Residual Plot	344
5.31(d)	Sheet pile Length line fit Plot	345
5.31(e)	Time residual Plot	345
5.31(f)	Time Line fit Plot	345

5.31(g)	Normal probability Plot	346
5.32 (a)	Scatter plot for prediction model for B/H ratio and factor of safety (FOS) as predictors using PCA	347
5.32 (b)	Scatter plot for prediction model using slope and factor of safety (FOS) s predictors using PCA	347
5.33(a)	True response and predicted response using PCA in predictor model for static condition	348
5.33(b)	Residuals vs. True response using PCA in predictor model for static condition	349
5.33(c)	Residuals vs. Record number using PCA in predictor model for static condition	349
5.33(d)	True response and predicted response using PCA in predictor model for seismic condition	350
5.33(e)	Residuals vs. True response using PCA in predictor model for seismic condition	351
5.33(f)	Residuals vs. Record number using PCA in predictor model for seismic condition	351
5.33(g)	Optimization of factor of safety with respect to sheet pile position and sheet pile length under static condition	352
5.33(h)	Optimization of factor of safety with respect to sheet pile position and sheet pile length under seismic condition	353
5.33(i)	Optimization of factor of safety with respect to sheet pile position and sheet pile length under both static and seismic condition	353

Symbols and Notations

A	-Cross-sectional area for the sheet pile wall per m
A_Δ	-The area of the triangle
$\bar{a}$	-centrifugal acceleration
B	-Base width of dam
C	-A 2-by-2 matrix function on Ω
C_1	-A constant and given by $7600(D_r)^{-2.5}$
C_2	-A constant given by $0.4/C_1$
c, a, f	-complex functions defined on Ω
D_r	-The relative density
D_r	-Relative density maintained at 65%
D1 to D6	-Time in drawdown after 6 hours to 12 hours respectively
E_{steel}	-The Young's modulus for the sheet pile wall
E'	-Stiffness of the soil under effective stress conditions
EI	-stiffness of sheet pile
EMB	-Nomenclature of embankment without sheet pile
$\Delta\varepsilon^p$	-The change in volumetric strain
ε_{vd}	-The change in the volumetric strain.
€	-Strains in the scaled model
F_x & F_y	-Body forces
G	-Shear modulus of elasticity
γ_s	-The shear strain in the soil
h	-Unit matrix
Δh	-Difference in head between Upstream and downstream
h'	-Section depth

$\Delta h/N_d$	-Head drop between two successive equipotential lines
i_e	-Exit gradient
i_c / i_e	-Factor of safety against piping
I	-Moment of inertia for the sheet pile wall
i, j, and k	-Unit vectors
k	-Permeability of soil
K	-Bulk modulus
K_b	-Bulk modulus of elasticity
K_s	-Shear stiffness of the interface
K_n	-Normal stiffness of the interface
L5	- 5m length of Sheet pile
L10	- 10m length of Sheet pile
L15	-15m length of Sheet pile
L20	- 20m length of Sheet pile
L_{max}	-The maximum edge-length of the triangle
M	-block structure of mass
l'	-Length of mass structure
b'	-width of mass structure
h'	-height of mass structure
M_s	-The constrained modulus of the soil
ΣMsf	-Total multiplier
N	-Scaling factor
N_d	-Number of head drops per flow channel
p	-The fluid pressure
P	-The mass density
$\bar{u}, \bar{v}$	-velocities in the x and y directions

u	-A solution of the differential equation
Δu	-The change in the pore water pressure
μ	-The molecular viscosity
U	-Unknown solution complex functions defined on Ω
υ′	-Poisson ratio under effective stress conditions
R1 to R6	-Time in rise up after 1 to 6 hours respectively
r	-Radius of circular path
ρ	-Density of water
T	-The out-of-plane dimension
T2.1	-Sheet pile position at B/8 position from downstream end
T4.2	-Sheet pile position at 2B/8 position from downstream end
T6.3	-Sheet pile position at 3B/8 position from downstream end
θ	-Angular velocity
θ_k	-Angular velocity of the sphere
σ_x, σ_y, τ_{xy}	-Stress components
σ_{vm}	-vertical stress
Ω	-A bounded domain in the plane
$\boldsymbol{X}_m$	-Model parameter
$\boldsymbol{X}_p$	-Prototype parameter
Δz_{min}	-Minimum width of the neighboring zone

CHAPTER ONE

INTRODUCTION

1.1 AN OVERVIEW:

Geotechnical engineers face problems while designing dams in respect of hydraulic failure and instability of slope. These two aspects therefore play major role in dam design. Further failure due to stability of slope causes complete collapse of the dam. Thus, hydraulic failure as well as failure of slope particularly on downstream side becomes the main factors affecting overall stability of the dam. Fogg and Senger (1985) observed that accurate construction of flow nets could be very difficult in heterogeneous, anisotropic media or in regional cross sections. Desai (1983) analyzed earthen dam for seepage and slope stability and found that factor of safety was affected for both the cases of steady seepage and transient flow. Due to the gravitational effect of the Sun and Moon on the rotating Earth, water-bodies face a gravitational pull resulting in periodic rise and fall of water surface levels, called 'tides'. The condition in which there is a rise in water level is called flow tide, whereas the falling tide is termed as ebb tide. These tides have predominant effects in case of shallow depth of water bodies with constrained landmasses. The embankment may experience two types of seepage conditions: steady seepage and unsteady seepage, depending on the upstream and downstream hydrodynamic conditions. Hydraulic failure in earthen dam is influenced by the pore pressure, flow distribution and their variations with time. This may further affect the stability of the dam. David et al (2010) and Hansen et al (2012) investigated the effect of water dynamics on earth dam based in transient simulation seepage condition using two-dimensional numerical model. Rakhshandehroo et al (2013) analyzed transient pore water pressure fluctuations of dam using 3-D finite element model. It was found that dynamics of water on upstream side affected saturated zone within the dam and also thereby affected factor of safety against slope stability. For the survival of the dam, factor of safety of downstream slope has been considered an important factor as cyclic loading produced by fluctuations in the level of pool causes strain softening and a critical loss.

In case of hydraulic failure seepage must be reduced by providing cut off as seepage barrier. The downstream sheet pile is usually used to decrease the exit gradient at the downstream side of the structure in order to reduce the risk of soil piping in this side. Even though the existence of this sheet pile reduces the exit gradient, the risk of piping is still significant,

hence an usual practice is to adopt a certain protection at the downstream side of the structure. The length of protection required is usually decided upon the desired factor of safety against piping. Duncan (2008) described the mechanism of sheet pile wall as flood protection and erosion criteria and also investigated the failure mechanism of embankment using sheet pile wall. H. Al-Suhaili (1990) found an analytical solution using the Shwarz-Christoffel transformation for exit gradient variation on downstream side of inclined sheet pile. It had been estimated that the exit gradient was decreased as the angle was increased. The results indicated low variation of this protection length with the angle of inclination. Lee and Benson (2000) evaluated the effectiveness of seepage barriers.

Further seismic activity is associated with complex oscillating patterns of accelerations and ground motions, which generate transient dynamic loads due to the inertia of the dam and the retained body of water. The seismic action plays an important role in determining the acceptability of the performance of the earthen dam.

The embankments in South 24 Parganas, which are constructed using locally available soil are facing severe problem of erosion at the downstream end. The present study has been formulated, to measure the effectiveness of sheet pile as seepage barrier to reduce the possibility of toe failure in case of tidal variation, considering the Rise up and Draw down conditions. During flood season water disappears within a relatively short period of time thus creating a rapid draw-down scenario on the embankment. In such scenarios, the heightened pore-water pressures present in the embankment during the flooding have been studied which may be triggering slope failures. Furthermore, in this study, considering the real situation in the field where water level on the upstream face can rise and fall, unsteady flow through an earthen dam has been analyzed including the seepage surface on the upstream side. The objective and scope of the present study have been outlined as follows on the basis of detailed literature review presented in Chapter 2.

1.2 OBJECTIVE AND SCOPE:

The objective and scope of the present work have been outlined as follows:

1.2.1 OBJECTIVE:

Based on the detailed literature review presented in chapter two the objectives of the study have been presented as follows:

i) To obtain top flow line of a model dam with different working heads under steady seepage, rise up and drawdown conditions by geotechnical centrifuge modeling.

ii) To obtain flow-nets under steady seepage, rise up and drawdown conditions by MATLAB software after validation of top flow lines in both the cases.

iii) To study the dynamics of the phreatic surface of an earthen embankment during transient stages under rise up and drawdown conditions of a single tidal cycle and multiple cycles.

iv) To estimate the pore water pressure distribution within the embankment during transient stages under rise up and drawdown conditions for a single tidal cycle and multiple cycles.

v) To conduct the slope stability analysis during steady and transient states under rise up and drawdown conditions for model embankment in single and multiple tidal cycles.

1.2.2 SCOPE OF WORK:

The scope of the present work is depicted as follows:

1) To obtain top flow lines for different cases under steady seepage and rise up-drawdown conditions by geotechnical centrifuge.
2) To validate the flow lines obtained by experimental output with that of finite element analysis (using MATLAB and SEEP/W) along with finite difference analysis (using FLAC 2D) under the experimental conditions.
3) To conduct the slope stability analysis during steady and transient states (rise up and drawdown conditions) for model embankment in cases of single and multiple tidal cycles.

4) To study the following flow and stress parameters under steady and transient states for both static and seismic conditions in case of a model dam with and without sheet pile :

A. Flow parameters:

a) Fluid flow vector

b) Factor of safety against piping failure

B. Stress parameters:

a) Pore water pressure

b) Soil pressure on sheet pile

c) Factor of safety against failure of slope

5) Development of statistical model for prediction of Factor of safety against piping, Overall Factor of safety, Pore water pressure with the variable input parameters of embankment.

1.3 THE PRESENT STUDY:

In the present study an attempt has been made to investigate the seepage behavior of a model earthen dam with and without sheet pile of varying length and position from the downstream end. For this purpose an experimental study has been carried out by modeling with geotechnical centrifuge for both steady and transient states of seepage. The top flow line and other flow lines have been obtained by particle image velocimetry (PIV) analysis performed on the images obtained from the outputs of centrifuge testing. The flow lines obtained from centrifuge modeling for both steady and transient conditions have been validated through MATLAB software (version 2014a), FLAC 2D (version 5.0) and SEEP/W (version 12.0). Finite element and finite difference methods have been adopted for both steady and transient states to obtain flow nets for different cases. In the present investigation, parametric studies have been carried out to observe variation of pore water pressure, fluid flow vector, soil pressure on sheet pile, factor of safety against piping (F_p) and overall factor of safety (F_s). It has been observed during steady state that flow vector reduces with increase of sheet pile

length. At the downstream end pore pressure becomes of similar order irrespective of sheet pile location. In case of rise up and drawdown conditions, the factor of safety changes from 15% to 35%, on an average, under both rise up and drawdown conditions for any position of sheet pile.

Overall factor of safety increases by maximum 16% to 17% for both static and seismic conditions with sheet pile, compared to factor of safety without sheet pile condition. Under full rise up condition considering 5m long sheet pile at *B*/8 position from downstream end of base, factor of safety against piping increases up to 37.00% compared to minimum value at 3*B*/8 position; whereas this is approximately 18.75% for 2B/8 position, compared to 3*B*/8 position. In seismic cases under steady state condition as pore water pressure increases the factor of safety is also reduced by 45% to 50% compared to corresponding static cases due to increase of seepage force. After Statistical Analysis, it has been found that most advantageous location and length of sheet pile become *B/7* from downstream end and 0.88 times the bottom width of the dam respectively under both static and seismic condition for both steady and transient seepage.

1.4 ORGANISATION OF THE THESIS:

The thesis has been primarily divided into the following eight chapters along with an **ABSTRACT** of the entire thesis presented at the beginning.

- **CHAPTER 1 - INTRODUCTION:** This chapter highlights the overview of the present study, research objectives and scope of work along with organization of the thesis.
- **CHAPTER 2 - LITERATURE REVIEW:** This chapter contains the reviews of past studies pertinent to the present research work.
- **CHAPTER 3 - NUMERICAL MODELING:** This chapter deals with numerical analysis adopted for the present study highlighting salient aspects of finite element and finite difference methods including principles of different softwares used for the present study - MATLAB (version 2014 a), FLAC 2D (version 5.0) and GEOSTUDIO (version 12.0).

- **CHAPTER 4 - EXPERIMENTAL INVESTIGATION:** This chapter deals with the test program for centrifuge model, materials and equipment used, experimental set up, test procedures, PIV analysis and presentation of experimental results.
- **CHAPTER 5 –DISCUSSION ON RESULTS:** This chapter presents a detailed discussion on experimental and numerical results obtained from the present study.
- **CHAPTER 6 - SUMMARY, CONCLUSION AND FURTHER SCOPE:** This chapter summarizes the current research and presents the major conclusions of this study and also it further recommends the direction of future research work which may be carried out in the relevant field.
- **REFERENCES:** The references, cited in the thesis, have been furnished at the end.

CHAPTER TWO

LITERATURE REVIEW

2.1 GENERAL

In this chapter an attempt has been made to present relevant past works. It has been found that there are several works in the fields of steady seepage, unsteady seepage and slope stability analysis. The works under each of these fields have been presented in separate sections in chronological order as follows. At the end of the chapter an attempt has also been made to bring out the research gap to supplement the objective and scope of the present work.

2.2 STEADY SEEPAGE

A number of theoretical and numerical studies have been done by different researchers and these are presented as follows:

The differential equation governing two-dimensional steady seepage flows through a porous medium has been derived by Laplace (1880) as:

$$k_x \frac{\partial^2 h}{\partial x^2} + k_y \frac{\partial^2 h}{\partial y^2} = 0 \qquad (2.1)$$

Where h = total available head under which steady seepage occurs; x, y = two mutually perpendicular direction *i.e.* horizontal and vertical direction respectively; k_x, k_y = permeability in horizontal and vertical direction respectively. If the medium is isotropic and homogeneous, then $k_x = k_y = k$ (say) and the Eq. 2.1 is reduced to

$$k\left(\frac{\partial^2 h}{\partial x^2} + \frac{\partial^2 h}{\partial y^2}\right) = 0 \qquad (2.2)$$

Forchheimer (1880) demonstrated that the distribution of water pressure and velocity within a seepage medium was governed by the Laplace differential equation. **Richardson (1990)** had been obtained an approximate solution of the Laplace's equation. This method was not widely used for earth dams. Exit gradient from flow net had been investigated by Casagrande (1937. **Bligh (1910)** and **Lane (1935)** developed empirical methods and **Khosla et al (1954)** developed a method based on independent variable for finding exit gradient on downstream side of an earthen dam.

After that the solution of the Laplace equation by the graphical procedure or with electric models had been adopted as standard procedure for seepage analysis (Sherard et al., 1963).

Fogg and Senger (1985) developed accurate construction of flow nets by automatically generating streamlines using conventional ground – water flow modeling algorithms in heterogeneous, anisotropic media or in regional cross sections where vertical exaggeration of scale was great. Possible boundary conditions included prescribed stream function (Dirichlet type) and prescribed stream function gradient (Neumann type). The method was generally not appropriate when sources or sinks occur inside the flow region, and it will not handle transient conditions. **Fenton and Griffiths (1996)** conducted monte Carlo simulation to predict seepage flow through randomly heterogeneous earth dams with various geometries and the amount of drawdown of the free surface on the downstream face of the dam. **Fenton and Griffiths (1997)** computed the location of free surface using boundary elements method with large aspect ratios as the free surface drops towards the base of the mesh. **Boufadel et al. (1999)** studied the effect of capillary flow on steady seepage in trenches and dams. A model was developed and compared with formulation to see the effects of unsaturated zone on seepage face heights and outflows from hypothetical anisotropic rectangular domains. It was seen that seepage occurred in unconfined groundwater flows as well. Nomo graphs were developed for rectangular domains and trapezoidal dams.

Boufadel et al. (1999) carried out seepage analysis of a model dam under anisotropic condition**.** The work addressed issues related to scaling of physical systems and by investigating steady seepage in an anisotropic trapezoidal domain simulating a dam. It was suggested that the requirement of proper scaling down from anisotropic to isotropic was essential, as pointed out in this study; else error in the estimation of seepage was almost 60 percent. A comprehensive discussion on the mechanisms of piping and internal erosion in dams was presented by **McCook (2004). Fell and Wan (2005)** presented methods for estimating the probability of failure of embankment dams by internal erosion, piping within the foundation, and piping from the embankment to the foundation. The determination of phreatic line for a steady state two-dimensional unconfined flow through a homogeneous levee with a horizontal toe drain resting on an impervious base was studied by **Mishra et al. (2005).** At first to determine the phreatic line, they used the method of fragments. Unlike in Kozeny's method, the hydraulic resistance of the soil in a levee bounded by an equipotential parabolic surface and the straight upstream sloping face has been considered in the computation of the seepage and location of the phreatic line. They derived equation of

equipotential lines and streamlines, and also for seepage quantities through the levee. These equations were extended to analyze seepage characteristics through a zoned levee having an upstream rock-fill part and a downstream clayey part. The location of the filter that was provided to safeguard against capillary rise for greater stability of downstream side of levee was also derived. The results of the analysis were compared with those obtained from Kozeney's solution and Numerov's solution.

Richard et al. (2005) determined stability of an embankment dam of 408.4 m long 13.7 m high located in the United States under extreme flooding conditions. The embankment configured with 2H:1V downstream slope and a flatter upstream slope with a 15.2 m wide crest. The dam is underlain by an alluvium soil foundation of depth 24m. Mohr Coulomb model adopted for analyzing this steady state condition with uncoupled flow assigning head water and tail pore pressure at the far edges of model. They evaluated the factor of safety with variation of friction angle value in FLAC 2D software. But they did not include the study of pore pressure variation within and below the embankment.

Hasani et al. (2013) proposed a procedure using the changes in pore pressures calculated by finite-element seepage analyses to estimate changes in buoyancy and seepage forces that occurred as a result of seepage barrier construction.

2.3 UNSTEADY SEEPAGE:

A number of theoretical, numerical and experimental studies have been done by different researchers and these are presented as follows:

During a transient process if the total stresses remain constant, the differential equation governing three-dimensional transient case through a porous medium when the controlling parameters change with respect to has been can be written as,

$$\frac{\partial}{\partial x}\left(k_x\frac{\partial h}{\partial x}\right)+\frac{\partial}{\partial y}\left(k_x\frac{\partial h}{\partial y}\right)+\frac{\partial}{\partial z}\left(k_x\frac{\partial h}{\partial z}\right)=m_\gamma\frac{\partial h}{\partial t} \qquad (2.3)$$

where h = total available head under which unsteady seepage occurs; x, y= two mutually perpendicular directions *i.e.* horizontal and vertical direction respectively; k_x, k_y= permeability in horizontal and vertical directions respectively; m_γ=storage co-efficient.

Turnbull and Mansur (1961) also explained the importance of underground storage on under-seepage and excess hydrostatic pressure during relatively low high waters and high waters of short duration. They noted that during a high water, if the ground water table is low, drainage into subsurface storage landward of the levee reduces hydrostatic pressures and seepage rising to the surface. However, if the ground water table is high or the flood is of long duration, this factor has little effect on substratum hydrostatic pressures. In general, piezometric data obtained during the 1950 high water indicated that ground water storage landward of the levees was filled by the time a high flood stage developed. Approximate theoretical critical gradients for silty sands and silts is approximately 0.85 and for silty clay and clay is 0.80 (Turnbull and Mansur, 1961).

Dvinhoff and Harr (1971) had presented an alternate direction implicit procedure (ADEP) to solve the partial Differential equation governing two-dimensional unsteady-seepage flow for locating the phreatic surface of the earth embankment due to instantaneous or rapid drawdown of reservoir level. The exit point was determined by equating the quantity of water that had flowed over the surface of seepage in time t to the volume of water that had been lost from space bounded by the initial and final positions of the surface. After locating the phreatic line independently, the governing differential equation for two-dimensional seepage flow was solved using ADEP technique locating the phreatic surface as a function of time. The solution was extended to the case of instantaneous drawdown for partial pool also. A parabolic equation defining the geometry of the phreatic surface was obtained from the tests conducted with 'hele-shaw' viscous flow models and the agreement found to be satisfactory.

Marsal and Resendiz (1971) discussed short-term and long-term mechanisms that may be in effect in dams with seepage barriers and discuss design considerations for seepage barriers in dams. **Ahmed-Zeki et al. (2000)** presented an assessment of the long-term performance of a Seepage barrier. An assessment of the effectiveness of the seepage barrier observed in Maintaining sufficiently low uplift pressures beneath the dam to maintain sliding and overturning stability.

Li et al. (1983) developed a model using finite element method for stress, seepage and stability analysis of dams and earth banks. The seepage analysis was based on a residual flow scheme involving saturated and unsaturated zones in which the original mesh remains invariant during transient flow and interactions. Factor of safety had been incorporated against stability of embankment with time during rise or drawdown in reservoir level. The

procedure had been found to provide satisfactory correlation with analytical solutions and field observations for a number of problems. It could be useful and appropriate for a nonlinear stress, seepage and stability analysis of dams and earth banks.

Cargill and Ko (1983) performed centrifugal tests on embankment to simulate the transient flow phenomena. Four types of soil which were reconstituted mixture of sand and silt, namely as original, coarse removed, same $D_{10,}$ same $C_{u.}$ The centrifuge test was carried out at 1.36m centrifuge 50g, 37.5g and 25g acceleration respectively.

A transient analysis for seepage involving unsaturated – saturated criteria in FEM model, was carried out for the western dyke of Wallace dam (Lake Oconee, Georgia, USA) by Aral and Maslia (1983). The water level fluctuation was about 0.46 m. The effect of presence of chimney drain, 1.8 m wide, on this zoned dam was also studied. The unsteady state was governed by a partial differential equation, which was numerically solved by Galerkin formulation. It was observed that, flow vector to the chimney drain showed that it was very effective in reducing seepage pressures.

Davies and Parry (1985) conducted centrifuge test to check the performance of low embankment founded on soft clay soil during and after the construction. The foundation was constructed with Spes-white kaolin clay material and the embankment was of sand material. The test was carried out at 100g acceleration. A cake of kaolin clay of width 0.675m, 0.18m high and 0.2m deep was consolidated from slurry. Embankment was constructed by pouring sand from specially arranged hopper during centrifuge test. 11 numbers of miniature piezo-electric pore pressure transducers were embedded into the embankment at the middle depth of 90mm. They monitored displacement and pore pressure variation to observe the progressive failure. They carried out total and effective stress analyses of the embankment stability. From total stress analyses they estimate factor of safety to be 1.04 and from effective stress analysis it was 0.90. Pore pressure was increased as much as 18% after the end of the construction.

Yang H. Huang (1986) estimated the position of phreatic surface in earthen dams due to unsteady flow, as a function of time. This procedure followed the methodology of **Cedergren (1977),** where the phreatic surface in impervious horizontal base earthen dams using transient flow-nets was developed and compared with a viscous fluid model. With time, while the upper end of the phreatic surface remained still at entry point water level, the same moved

horizontally along the impervious base towards the downstream end. The same was assumed to be a straight line to be on the conservative side.

Chang (1987) adopted Boundary Element method (BEM**)** had been presented for seepage analysis of earthen dams involving drawdown of the water level in the reservoir. The boundary element method was adopted for solving the seepage problem involving free surface, because the boundary element method requires discretization only on the boundary rather than over the whole region, as required in FEM. This paper reported an evaluation of the applicability of the boundary element method to the seepage analysis of earth dams due to drawdown of the water level in reservoir. Dam heights used in this evaluation range from 15 inches to 100 feet. The evaluation was based on comparisons between calculated response and measured results from laboratory model test and field observations, for types of soil ranging from coarse sand to clayey sand. They concluded that Boundary Element Method yielded more appropriate results compared to FEM.

Desai (1988) discussed the various merits and de-merits of seepage analysis in uncoupled mode. In coupled analysis, both displacement and pore water pressures were assumed to be the unknown parameters in FEM. In uncoupled analysis, the residual flow procedure (i.e. same mesh was used for stress and seepage) was coupled with a non-linear finite element with elasto-plastic models for soils. Case studies discussed included- (i) Transient Seepage Analysis of River Mississippi (ii) Time dependant head fluctuation analysis of Sherman Dam (iii) Consolidation and Seepage in deformable soils using Biot's Coupled Approach and Uncoupled approach by Residual flow procedure.

Meyer (1994) studied the dam is stable against piping but potentially locally unstable against heaving. They studied that Factor of Safety against heave and piping reduced because hydraulic gradients in the blockage increased as water levels rise.

During flood season water disappears within a relatively short period of time thus creating a rapid draw-down scenario on the embankment. In such scenarios, the heightened pore-water pressures present in the embankment during the flooding have been studied which may be triggering slope failures.

Lee and Benson (2000) conducted experimental study to evaluate the effectiveness of seepage barriers. The study included intact barriers and barriers with defects and investigated the effects of keying them into an aquitard. But none of them reported any study regarding

seepage barrier (sheet pile etc.) for unconfined seepage flow (to and below earthen dam) and no study regarding the position and length of sheet pile are not observed in the study.

Thieu et al. (2001) studied 2D Steady state conditions, transient conditions and 3D steady state conditions. The role of permeability and water storage with variations in suction pressure was studied experimentally and compared with available literature. In solving for the flow-nets during both steady and transient conditions, the boundary conditions were used as Partial Differential Equation for seepage. Solutions indicated that the phreatic line positions were very sensitive to the transient state seepage. Predictions at early times and in the long run they were found to lie significantly close to that of the steady state.

Das (2005) studied the identification of probable causes of failure of existing earthen embankment around Sundarban. The shear strength value of the subsoil and embankment of the study area was low. The failure of the embankments in the Sundarban deltaic system had different causes but it was found that their slopes were stable, except few cases especially when reservoir was full. But the factor of safety was found unsafe in the base shear (upstream and downstream) in most of the cases.

Wenjun Dong and Schwanz (2005) This paper presents the results of Finite Element Soil-Pile-Interaction Analysis of Floodwall in Soft Clay. Soil parameters were very important in finite element modeling of soil structure/sheet pile interactions. By using appropriate soil parameters, interaction effects had been modeled in the finite element model. Soil-pile interaction was evaluated using a set of p-y curves in the discrete model based on the conventional approach of a 1D beam on an elastic foundation. The proposed procedure for soil-pile interaction in a plane strain model was mainly based on the calibration with a lateral pile load test and parametric study using the Matlock p-y curve, based procedure. More efforts will be needed for the investigation of the theoretical mechanism behind these numerical observations, possibly using the recently developed soil strain wedge concept.

Schmertmann (2006) observed that permeability and shear strength of each soil varies with the degree of saturation. Thus, saturated and nearly saturated conditions may cause reduction of stability of slopes, dam and earth dikes. He investigated that significant reductions in slope stability occurred as a result of mounding in transient seepage analysis. He estimated that mounding reduces the stability of an earth dam slope as much as 50%.

Robert et al. (2008) in transient seepage analyses they evaluated possible uplift pressures of Rueter-Hess Dam of 61-meter, high zoned embankment. During the transient seepage analyses, developed unsaturated hydraulic conductivity functions and non-linear transient boundary conditions, and investigated the model sensitivity.

Alsenousi and Hasan G. Mohamed (2008) presented the solution of the governing equations of groundwater seepage under hydraulic structures on the basis of finite element approximations, a two-dimensional numerical model. The goal was to study the effect of inclined cutoffs, permeability ratio, and foundation soil depth on exit gradient, uplift pressure and flow rate. The model calculated the piezometric head at all nodal points in the problem solution domain for steady and unsteady flow conditions. Using these head values, the exit gradient, uplift pressure and flow rate were determined. The model results indicated that the finite element technique gave comparable values for similar cases solved with other solution methods and offer a more general approach that permits the usage of the desired permeability, foundation soil depth, and flow type.

Huang et al. (2009) investigated the influence of transient seepage on stability of dam under rapid drawdown condition. It was evaluated using finite element method that lowest factor of safety induced on the upstream side of dam immediately after drawdown and the factor of safety of upstream slope increases rapidly with time.

David et al. (2010) investigated the effect of water dynamics on earth dam based in transient simulation seepage condition using two-dimensional numerical model based on Richards' equation for water flow in porous medium.

Freduland (2011) analyzed the effects of the pore water pressures and the stability of the earth dam under rapid drawdown condition focusing on the changing of pore-water pressures in the levee in an uncoupled fashion. It was found that in an earth dam the impact of rapid draw-down can vary significantly based on the hydraulic conductivity of the individual layers.

Hansen et al. (2012) studied a numerical parametric study of flow through rock fill dam using a finite-difference scheme that directly incorporated the exponent of a power law that replaced Darcy's law. Convergence, use of specialty nodes, nodal density, and boundary condition effects were quantitatively investigated. The flow-field angle of the toe was found

to be a useful starting point in studying the potential for unraveling failure. It was investigated that the Factors of safety tends to drop below unity under the seepage face primarily because of the strength of the exit gradient near the toe of the structure and secondarily because of the overflow velocity.

Perri et al (2012) analyzed the influence of the pore water pressures in the calculated factor of safety of an embankment with and without cut off wall in steady state condition of full flooding stage using finite element method. Mohr- Coulomb model was adopted for the study to show the seepage mitigation on slope stability. They observed that using cut off wall there was significant decrease of seepage gradient and thereby increase of Factor of Safety. They also observed that increase of cohesion value in the characterization of the materials increases factor of safety. But they did not carry out deformation analysis and variation of pore pressure of embankment.

Moayed et al. (2012) deals with the effectiveness of different types of drainage filters used in toe of earthen embankment dams. A model was developed in finite element software Abaqus (Simulia) and drawdown was simulated by transient loading in 15 steps (each representing 1m daily drawdown), in addition to static loading. The mesh was made of 1473 6-noded iso-parametric Quad-Triangular elements. The phreatic line, for different cases of filter was plotted. The conclusion was that chimney drain is most effective, in dissipation of pore pressures.

Khassaf et (2013) studied finite element used to determine the factor of safety of Mandali dam under rapid drawdown with seismic load (0.07g) effect for one and two direction. They found that the factor of safety of upstream decrease when rapid drawdown condition and seismic load effect and the upstream slope is still stable during rapid drawdown.

A 3-D finite element model of the Doroodzan Dam on Kor River (Iran) was developed and analyzed for steady and transient conditions **by Rakhshandehroo and Pourtouiserkani (2013).** Transient pore water pressure fluctuations were predicted at different piezometer locations for a 21-day rapid drawdown of 23.9m. It was found that seepage through the dam was not sensitive to hydraulic conductivity of downstream dam body, apparently due to the effective hydraulic behavior of the chimney drainage there. Under rapid drown down conditions, a maximum of 11.8m excess pore water pressure on upstream part of the dam was observed (compared to the steady state conditions) while no significant excess pressure was

seen at the downstream part of the dam. Dynamics of the phreatic line location during the 21-day rapid drawdown was monitored in four 5.25-day time steps. Phreatic line at the upstream face of the dam closely followed the reservoir level rapid drawdown. However, phreatic line at the interior sections of the dam did not drop as fast. As a result, a gradient towards upstream face of the dam was developed after 10 days which might jeopardize slope stability there. In general, rapid drawdown was cautiously analyzed in dams, especially those with short emptying times, as it may reverse the seepage direction, endanger the slope stability, and not allow excess pore water pressure to dissipate. A 4-year period (1999 to 2002) field data was used for calibrating the model and the results were verified. It was observed that unsaturated zone has a considerable effect on slope stability, safety factor, and deformation of dams, however, it did not change overall flow conditions and hydraulic behavior of the dam considerably.

Lopez et al. (2013) the stability of an earthen embankment during drawdown (viz. Fully Slow drawdown, fully rapid drawdown, transient drawdown) was analyzed using commercially available FEM software's PLAXIS 2D and PLAXFLOW. In modeling of fully slow drawdown, uncoupled drained analysis was made, for fully rapid drawdown, uncoupled undrained analysis and for transient drawdown, undrained analysis coupled with deformation was made. The influence of soil permeability, drawdown -rate and drawdown ratio on the stability of embankment was also studied, for the three modes mentioned above. Moreover, the selection of type of model, i.e. Mohr-Coulomb, Hardening Soil Model, on the stability analysis has also been discussed.

Le et al. (2013) focused on study on the stability and deformation of sheet pile wall constructed along with riverside areas in the Mekong river delta. Factor of safety analyzed based of design depth of sheet pile using Limit equilibrium method. It had been observed that predicted maximum lateral movement of the wall matched well with field measurements.

Khalilzad et al. (2014) focused on the effect of various parameters (geometry of the embankment and hydraulic loading in terms of intensity, duration, and cycles of loading and unloading as a result of the rise and fall of the water level in the reservoir) on the deformation response of embankment dams and the corresponding performance limit states. The analysis of a model embankment dam was conducted using the finite-element approach (15 nodded triangular plane strain using PLAXIS 2D software) and the results were incorporated into simplified deformation-based probabilistic analyses. The effect of the change in geometry on

shear strains and horizontal deformations and the corresponding probabilities of exceeding three predefined limit states were presented. The constitutive model of the analysis domain had been defined by the hardening soil (HS) model in comparison with the Mohr-Coulomb model.

Vandenberge et al. (2015) investigated external water level variations, such as rapid drawdown or flood loading, change the internal pore pressures in an embankment as a result of changes in the boundary conditions. Three different effects resulting were : (1) changes in water pressure on the slope change the seepage boundary conditions, (2) changes in the total stress applied by the weight of the water on the slope change the confining pressure on the soil, and (3) changes in the stabilizing load from the reservoir cause changes in shear stress. . In principle, the stability of a slope can be evaluated using either total stress (undrained) or effective stress (drained) strength parameters. Effective stress analyses use drained strengths, which are often easier to measure and tend to be less dependent on the direction of loading or loading stress path. For these reasons, effective stress analyses are attractive for embankments experiencing changing water levels, such as RDD or flood loading. Uncoupled transient seepage analyses, which consider only the change of water pressure on slope, are increasingly being advocated as an appropriate means to calculate pore pressures for effective stress stability analyses following water level changes. This paper discusses the limitations of uncoupled transient seepage analyses for calculating pore pressures during drawdown, explains the requirements for more appropriate analyses, and gives examples that show the errors incumbent on the use of uncoupled analyses Examples are provided that illustrate the shortcomings of using uncoupled transient seepage for stability analyses

Athania et al. (2015) presented the results of seepage and stability analyses of the considered earth dam using finite element method. The seepage analysis had been divided into two categories viz. Steady state and Transient analyses. Based on the parametric sensitivity analysis, both the seepage and stability studies have brought out the importance of considering the coupled effects on the overall stability of the earth dam. The results of finite element modelling of the stability and seepage analyses of the earth dam used PLAXIS 3D software. The two main parameters which were varied in the study to identify the changes in the stability of the earth dam are the Young's modulus (E) and angle of internal friction (φ). The stability of the dam had been checked for the following conditions (1) Full (High) reservoir level of the dam (2) Rapid drawdown (RDD 1 and RDD2) in 5 and 10-days' duration (3) Slow drawdown in 50 days duration and (4) Low water level of the dam. The

study showed that increase in the Young's modulus of core and shell resulted in the decrease of the maximum crest displacement and the variation in angle of internal friction plays a vital role in the fulfillment of the overall stability criteria. The factor of safety (FoS) was greater than 1.6 for both the full (high) reservoir condition and low reservoir condition whereas, the FoS values were found to be less than the stipulated values for the other stability considerations.

For each test the size of models was same. Four miniature semiconductor pressure transducers were used to measure the pore pressure. In centrifuge two sets of test-transient and steady state flow test for each soil were carried out. In transient water flow condition, the equipotential were increased with the rise up of head water for original soil. They observed that relative changes in consistency due to change in permeability due to migration of fine particles and change in saturation.

2.4 SLOPE STABILITY ANALYSIS

2.4.1 Static Condition

Lane and Griffith (2000) analyzed factor of safety of a homogenous earthen dam in different stages of drawdown condition using finite element method. They developed generation of charts, based on FEM, for slope stability analysis on complex geometries and conditions (submergence & drawdown). The finite-element program was for 2D, plane strain, slope stability analysis by finite elements using eight-node quadrilateral elements of elastic-visco-plastic soil with a Mohr-Coulomb failure criterion and a non-associated flow rule. In partial submergence / Slow Drawdown (Drained condition), neglecting seepage conditions, FOS of slope in drawdown condition had been computed for various Depth of Drawdown with respect to Embankment top to Height of Embankment. In the initial stages of partial submergence slow drawdown ($L/H < 0.7$), the increased weight of the slope had a proportionately greater destabilizing effect than the increased frictional strength and the FOS falls. At higher drawdown levels ($L/H > 0.7$), however, the increased frictional strength starts to have a greater influence than the increased weight and the FOS rises. In the finite-element program rapid drawdown was modeled when the piezometric surface is specified as per the original water level, but the face loads were based on the drawdown reservoir level, which in this case is below that of the piezometric values. In totality, FOS charts were developed for

Slow as well as Rapid drawdown, for different drawdown ratios (L/H) in order to get the minimum FOS to be used in design.

The key problem lies in determination of the position of phreatic surface in transient simulations, when water table level dramatically changes during extreme floods (**Chen, Zhang, 2006**). During the design of the slope stability in the Three Gorges Reservoir Zone, the methods adopted for determining the ground water table and hydrodynamic forces during reservoir drawdown were mostly empirical.

To improve the methods, a simplified formula of the phreatic-line in landslide mass was proposed by **Zheng et al. (2005)** during reservoir drawdown, based on the Boussinesq's differential equation of unsteady-seepage, and deduced by Laplace's transform. In the end, the amended formula was proved by a large-scale model test. The test shows that the value obtained is much close to that by the amended formula, with the error within 5%.

Das and Viswanadham (2010) performed centrifuge modelling to simulate the seepage induced slope failure. They conducted the tests with and without the use of discrete and randomly distributed geo-fibers to check the deformation and stability behaviour of 2V:1H slope. They used soil of 80% sand size particles, 10% silt size particles and 10% clay size particles; and an average size of particles was d_{50}=0.25mm. They classified the soil as SM soil as per USCS classification. Polyester fibers of specific gravity 1.33, tensile strength 600MPa and tri-angular cross section were used as geo- fibers in the test. They performed the test on 4.5m radius and 250g ton capacity centrifuge. The slope model was prepared within a metal strong box of internal dimension760mmx200mmx410mm with one side made up of a thick acrylic sheet to observe the slope model during the centrifuge test. The slope model was prepared considering half portion of an embankment of height 7.2m height and 7.5m crest width of prototype and scale factor of 30.A water-tank of dimensions 80 mm x 360 mm x200 mm and made up of a 10 mm thick acrylic sheet, was kept inside the strong box to simulate the water seepage from side of the slope. Three Linearly variable differential transformers (LVDT) were used at the top of the slope and five miniature pore-pressure transducers (PPT) were used at the toe level to monitor the deformation and pore-pressure changes. The test was performed at 30g acceleration. Water seepage was allowed by switching on a solenoid valve connected with surge tank and seepage simulator. Two sets of model tests were carried for unreinforced and reinforced soils. They observed that the slope settlement of unreinforced model was about 32% of the height of 7.2m. For reinforced model it was about 0.7% of the

slope height. They concluded from centrifuge tests that the slope settlement reduction and stability enhancement could be done by use of geo-fiber reinforcement.

Rice (2010) described the mechanism of sheet pile wall as flood protection and erosion criteria and also investigated the failure mechanism of embankment using sheet pile wall. They studied that seepage barriers drastically increase hydraulic gradients around the boundaries of the barrier. **Stark et al. (2017)** investigated seepage analysis of San Luis Dam on upstream slide to evaluate the pore-water pressures at failure and progression of the phreatic surface through the fine-grained core for drawdown stability analyses. It was studied that, van Genuchten parameter significantly influences unsaturated soil response during drawdown. For the survival of the dam, factor of safety of downstream slope has been considered an important factor as cyclic loading produced by fluctuations in the level of pool causes strain softening and a critical loss.

2.4.2 Seismic Condition

The dynamic programming method can be combined with a finite element stress analysis to provide a more complete solution for the analysis of slope stability because the technique overcomes the primarily difficulties associated with limit equilibrium methods.

Zou et al. (1995) proposed an improved dynamic programming technique that used essentially the same method as that introduced by Yamagami and Ueta (1988). The modification made by Zou et al. was that the critical slip surface might contain a segment connecting two state points located in the same stage. The stability of a trial dam in Nong Ngu Hao, Bangkok, Thailand, was analyzed as part of the study of the proposed procedure.

Pham and Freduland (2003) computed critical surface using a finite element stress analysis. Results obtained when using analytical programmed DYNPROG were compared with those obtained when using several well-known limit equilibrium methods. The comparisons demonstrate that the dynamic programming method provides a superior solution when compared with conventional limit equilibrium methods. Analyses conducted also show that factors of safety computed when using the dynamic programming method are generally slightly lower than those computed using conventional limit equilibrium methods of slices. For Poisson's ratio approaches 0.5, the computed factors of safety from the dynamic programming method and the limit equilibrium method appear to become similar.

A number of works have been done on experimental models. **Schofield et al (1988)** discussed about the seismic behaviour of soil model placed over shaking table mounted on geotechnical centrifuge. They had discussed that shaking mass could be reduced if the model rest on the sliding plate within a container. The power required to generate a 20% earthquake at 50Hz in a 100g centrifugal model flight were shown in Table 2.1.

Table 2.1: Power requirement to generate 20% earthquake at 50Hz of *N=100g*

Shaken mass(kg)	50	300	1000
Force(kN)	10	60	200
Power(kW)	3	19	63

They had discussed different types of soil models that were tested in different conditions.

In the 12inch stacked ring apparatus fine sand was filled in saturated condition and placed on geotechnical centrifuge. The pore-pressure at different heights was measured. It was observed that the pore –pressure was increased at the top pore-pressure transducer. After 3 to 4 cycles an upward hydraulic gradient was observed which leads to liquefaction of the soil. In the centrifuge model test on a single pile soil system it was concluded that the for granular soil system the distribution of shear modulus with depth was proportional to root of the effective confining pressure and void ratio.

Chakraborty and Chaudhury (2009) analyzed the failing of tailing earthen dams due to earthquake by various software. They performed static and seismic analysis. They considered a tailing dam of prototype dimensions-44 m height and 4m core and 1:2.5 upstream and downstream slopes. They modelled the dam using core and performed the seepage analysis at FLAC 3D software. They verified the phreatic surface obtained from FLAC 3D software with the SEEP/W software inputting the same properties. They performed static and seismic analysis. They used Mohr-Coulomb plasticity model for analysis in FLAC 3D software. From the FLAC 3D analysis, they obtained displacement, acceleration, time-history, stresses, strains at various locations of the dam due to critical load combination. They took horizontal and vertical seismic coefficient as 0.15 and 0.075. They had done static analysis by FLAC 3D, TALREN4 and SLOPE/W software. They evaluated the factor of safety that had been listed in Table 2.2.

Table 2.2: Factor of Safety values for static slope stability

FLAC 3D	TALREN4	SLOPE/W
1.22	1.34	1.386

In static analysis maximum displacement was 3.5 cm and that of seismic analysis it was 66.7cm. Hence, they concluded that at seismic loading the displacement was 19 times that of static condition. From displacement data they concluded that the acceleration was amplified from base to crest of the dam. From static analysis they concluded that for safety obtained at FLAC 3D was maximum value of 1.22. But from TALREN4 analysis they obtained the seismic factor of safety was 0.89. From this analysis they concluded that the slope of tailing earthen dam was not safe under seismic loading condition.

Hata et al. (2011) had evaluated the size of earthquake induced slope failure based on maximum slip surface**.** They had discussed the slope failure with reference of two case histories-a) 2001 Geiyo earthquake (Mj6.7) and b) 2009 Suruga Bay Earthquake (Mj6.5). They had discussed that the actual slip surface, maximum slip surface and the critical slip surface could not be calculated by considering the homogeneous soil strength condition. They had approached a probabilistic method by the Monte Carlo simulation to calculate the propagation of the critical, maximum and actual slip surface with the soil heterogeneity condition. They had concluded that the calculated slip surface in homogeneous embankment model in the conventional method was less that the observed slip surface. The slip surface calculated by Monte Carlo method was more realistic considering the heterogeneity of soil strength.

Chatterjee et al.(2012) had analyzed the seismic behavior of soil slope by analytical and numerical approaches. They model had three regions-foundation, embankment, canal-bunds. The slope of embankment and bunds were 2(H):1(V) and the foundation width, depth of embankment and bunds were 10m,6m, 6.5m respectively.

They performed the dynamic analysis by calculating the vibration period T=0.33 from Bathurst and Hatami equation.

From the analyses it had been concluded that FOS was maximum at embankment stage of construction and decreased in canal full of water stage. The displacement at the top of the slope was maximum and decreased towards toe. The displacement was minimum at stiff clay and maximum at loose sand. There was negligible displacement at the bottom of the slope. With the increase in cohesive property the displacement was decreased, hence the stability could be achieved with the increment of cohesive property. The displacement of slope along the face was influenced by acceleration and stage of construction hence it was affecting the stability of the slope. In Pseudo-Static analysis with the increase in k_h value Factor of safety decreased with change in construction stages from embankment to canal bunds full of water stages.

Higo et al. (2013) conducted centrifuge test on unsaturated road embankment with and without seepage flow through the soil model to study the stability against earthquake.

They used Yodogawa-levee sand of embankment of Yodo river near Kansai area. The embankment was constructed in eight layers (three layers of base ground and five layers of embankment) and a supply tank was attached to model for water supply. Seepage through three slits at the side wall at an interval of 1.5m. The laser displacement sensors were placed to quantify the displacement between before and after test by the Particle tracking Velocimetry (PTV) technique. Pore Pressure. Transducers and accelerometers were also used to determine pore pressure and acceleration. The centrifuge was rotated at 50g acceleration. Two sets of test were carried out without and with seepage of water through the soil. From the tests they observed without seepage the soil was remained unsaturated and with seepage condition the pore pressure increased.

They analyzed the data with multi-phase coupled liquefaction analyses method. They concluded from the centrifuge test and numerical analyses that the infiltration of water into the unsaturated embankment had induced the large deformation in the seepage area due to the generation of pore water pressure in the embankment.

2.5 EXPERIMENTAL MODELING OF SEEPAGE ANALYSIS IN CENTRIFUGE

The basic principle is that 1/*N* scale model of a prototype in the enhanced gravity field of a geotechnical centrifuge. The gravity is increased by the same geometric factor *N* relative to the normal earth's gravity field. In case of using same soil in the centrifuge model and the prototype, it should be expected the same hydraulic conductivity k for the soil in both. The hydraulic gradient, however, is defined as the change in pressure head over a given distance, and this is different in the model and the prototype

$$i_{model}/i_{prototype}=[dp/ds]_{model}/[dp/ds]_{prototype} \qquad (2.4)$$

However, the pressure head in the centrifuge model and prototype will be the same, although they occur over much smaller distance in the centrifuge model. This distances scale by a factor N as seen in the following equation

$$i_{model}/i_{prototype}=[ds]_{model}/[ds]_{prototype}=N \qquad (2.5)$$

In this section an attempt has been made to present the summary of past works done on seepage analysis in chronological order as follows:

He discussed about the modeling of base motion with the basic criteria of prototype and model particle velocity at homologous points would be same. He also discussed that the time scaling between diffusion and inertial phenomena could be increased with the increase of fluid viscosity. The use of silicone oil, glycerol mixed with water and cellulose based water mixtures instead of water could increase the viscosity. He stated that the use of non-reflecting barriers near the end plates could help to avoid stress waves reflection. Dux seal, silicone rubber, urethane foam were materials which could be used for this purpose.

He concluded that to validate mitigation measures, validate numerical modeling and study the efficacy of new geotechnical structural systems this study can help.

Xu et al. (2005) investigated experimentally factor of safety against stability in soft ground in Huai-He rivers levee. Based on centrifuge (Cap. 400 g ton) experiments on soft ground made from the remolded clay cakes from in-situ soft ground of Huai-He River's levee of a flood channel to Huang sea, in China. The test section with lowest Factor of Safety against stability

was taken for the Centrifuge Test. The behavior of the levee at end of construction & sudden drawdown was simulated & analyzed in two separate centrifuge tests. The experiment was conducted in plane strain condition with dimensions 1.1 m by 0.4 m wide by 0.55 m height. It was found that concerning the instability behavior of levee on soft foundation at the end of construction, the sliding surface is a deep seated one, which passes through the soft ground. investigated experimentally factor of safety against stability in soft ground in Huai-He rivers levee. It was found that mechanism of instability during sudden drawdown of floodwater, preceded with a local failure of slope instability in embankment slope, whose slip surface passes through the toe of slope. Rapid rise of water also causes wetting of unsaturated region in the structure result in slope failures.

Thusyanthan et al. (2003) analysed the scaling law of seepage velocity with the help of Darcy's law and Kozney-Carmen's equations to clarify whether the scaling is of Darcy's permeability or of hydraulic gradient. They had used energy gradient as a driving force on the pore fluid. They pointed out from Darcy's law that the rate of fluid flow through a porous medium is proportional to the potential energy gradient within that fluid. The Darcy's equation of flow velocity is given by Equation. 2.6 , as follows:

$$v=ki \qquad (2.6)$$

Here k is the Darcy's permeability and i is the hydraulic conductivity. From this equation it was concluded that Darcy's permeability was scaled.

From Muskat's equation $k= (K\gamma)/\mu= (K\rho g)/\mu$ *(2.7)*

and from Kozney-Carmen's equation $(d_m^2/180)x(n^3/(1-n)^2)$ *(2.8)*

They concluded intrinsic permeability was independent of gravity. They analyzed if the potential gradient in the Darcy's law was replaced by total energy gradient then the hydraulic gradient was scaled.

Manzari (1996) analyzed the catastrophic failure of dam due to earthquake with the centrifuge modelling technique. He prepared the model with sand as core and silt as outer surface. Pore pressure transducer, accelerometer, linearly variable differential transducer was used in centrifuge tests.

From the transducers they found that shear stress ratio was varied between 0.54 to 0.74 at the middle most portion pore pressure was more than the top and bottom. High initial shear stress ratios were generated at the interface of the core of sandy soil and silty layer. He explained that it may be due to dilative behavior. He analyzed that at the top transducer E the pore pressure increment was high after a few second due to base liquefaction. The interface pore pressure readings were negative due to dilative action and high shear stress ratio. A quasi-static analysis was conducted with effective stress approach on geotechnical centrifuge model and coupled stress-flow formulation was used to represent stress-strain behavior of soil. From the test it was seen that the sand core remained stable after shaking than the silt layer which was flowed off towards the toes of the embankment. He concluded that the effective stress approach would be useful to predict seismic stability of saturated soil embankment.

2.6 SUMMARY OF FINDINGS FROM PAST STUDIES

A summary of past studies relevant to this research has been presented below

- Several researchers have worked elaborately on steady state seepage conditions.
- Transient stage analyses have been performed by several researchers. A lot of literature, both numerical and experimental was found for transient stage induced by draw-down conditions. Although several publications have brought out numerical analysis for both cohesive and cohesionless type of soils, yet experimentation models based on cohesive soils only a few.
- Full scale model centrifuge tests are also been done by some researchers. However, some literature is available which deals with numerical or experimental analysis of transient seepage conditions induced by continuous rise-up and draw-down conditions with multiple cycles, as in case of embankments exposed to diurnal tidal cycles.

2.7 RESEARCH GAP

Research gap as understood from the literature review presented in this chapter has been indicated below:

- Transient stage analysis has been performed by several researchers. A lot of literature presenting both numerical and experimental works was found for transient stage induced by draw-down conditions. Seepage under drawdown condition has been studied only, whereas, rise up condition has not been addressed properly.
- Effect of sheet pile as fluid barrier is not well addressed.
- The effects of tidal cycle under static and seismic conditions have not been properly addressed.
- Determination of flow-net by experimental modeling has not been well addressed by earlier researchers.

On this basis the objective and scope of the present study has been framed as presented in Chapter 1.

Based on the detailed literature review and the research gap as mentioned above the objectives and scope of the present research work have been outlined, as presented in Chapter 1.

CHAPTER THREE

NUMERICAL MODELING

3.1 General

Study of seepage requires flownet with particulars to steady and unsteady conditions under static and seismic cases. In order to, draw flownet it is essential to locate top flow line, which is upper boundary of the flownet. It is a free water surface and is also referred to as the phreatic line or top flow line. The top flow line may therefore be defined as the line above which there is no excess pore water pressure. To locate the top line of seepage, as well as to draw flownet the following software's, have been used in the present study,

1. MATLAB
2. FLAC 2D
3. SEEP/W

In MATLAB flownet has been drawn by solving Laplace's partial differential equation and top flow line, flownet and exit gradient have been compared with the results of analyses using FLAC 2D and SEEP/W softwares. The parametric variation has been analyzed with the help of FLAC 2D and SEEP/W. Slope stability analysis has been studied using SLOPE/W. In seismic condition stability analysis has been done by QUAKE/W software. The flowchart of the numerical analysis has been presented in Figure 3.1.

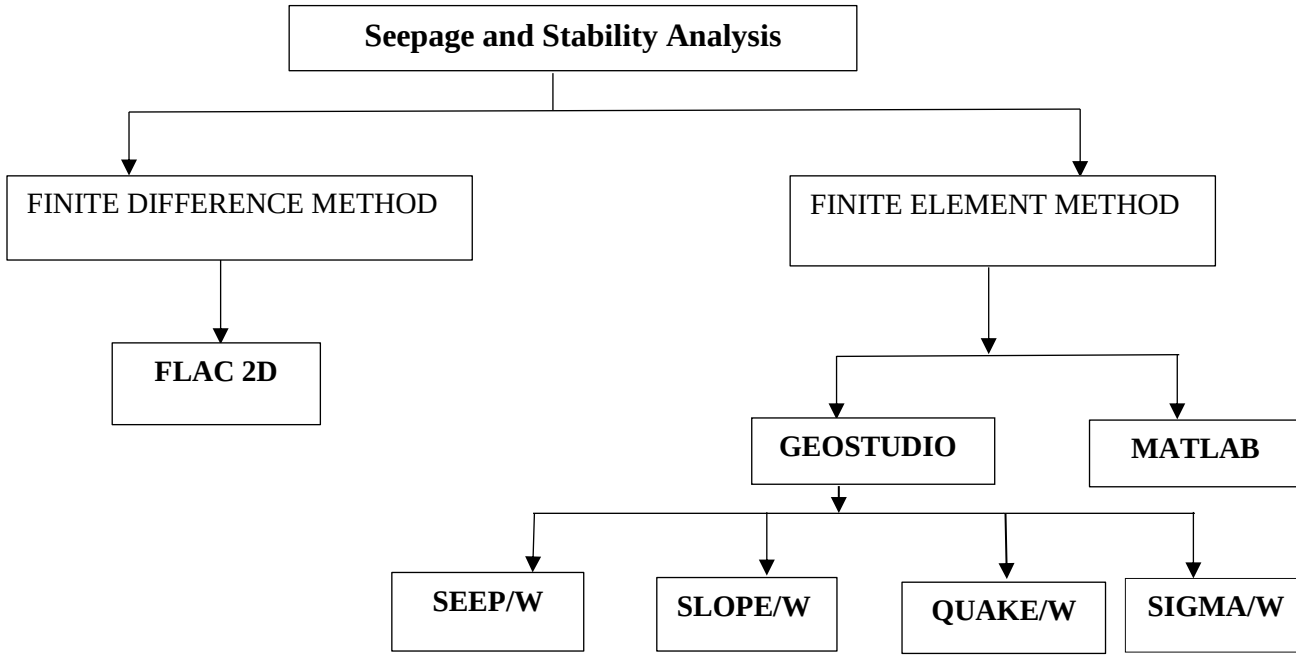

Fig. 3.1: Flow chart for numerical analysis

Bore log of South 24 parganas has been provided by S GHOSH & ASSOCIATES PVT. LTD. The stratification of subsoil of the selected area of South 24 parganas, West Bengal have been obtained from the bore log data sheets of different locations. An average value has been considered for

analysis in the present study and has been presented in Figure. 3.2(a). The cross-sectional details of existing embankment of typical model dam studied by numerical analysis has been presented in Figure. 3.2(a). The study has been done for working head of 3.5m in steady state and transient state of single tidal cycle and also for multiple tidal cycle. Time history acceleration data of India (Sikkim)-Nepal-Border of Lat. of 27.6 N Long. of 88.2 E recorded of origin Time of 18/9/2011 at about 12:40:47 has been adopted for the present study (Reference: http://www.pesmos.in/). The model has been studied considering peak acceleration = (-) 0.156 m/s^2 for a duration of 169.845 sec. Figure 3.2(b) presents flowchart of the numerical study showing different parametric variation.

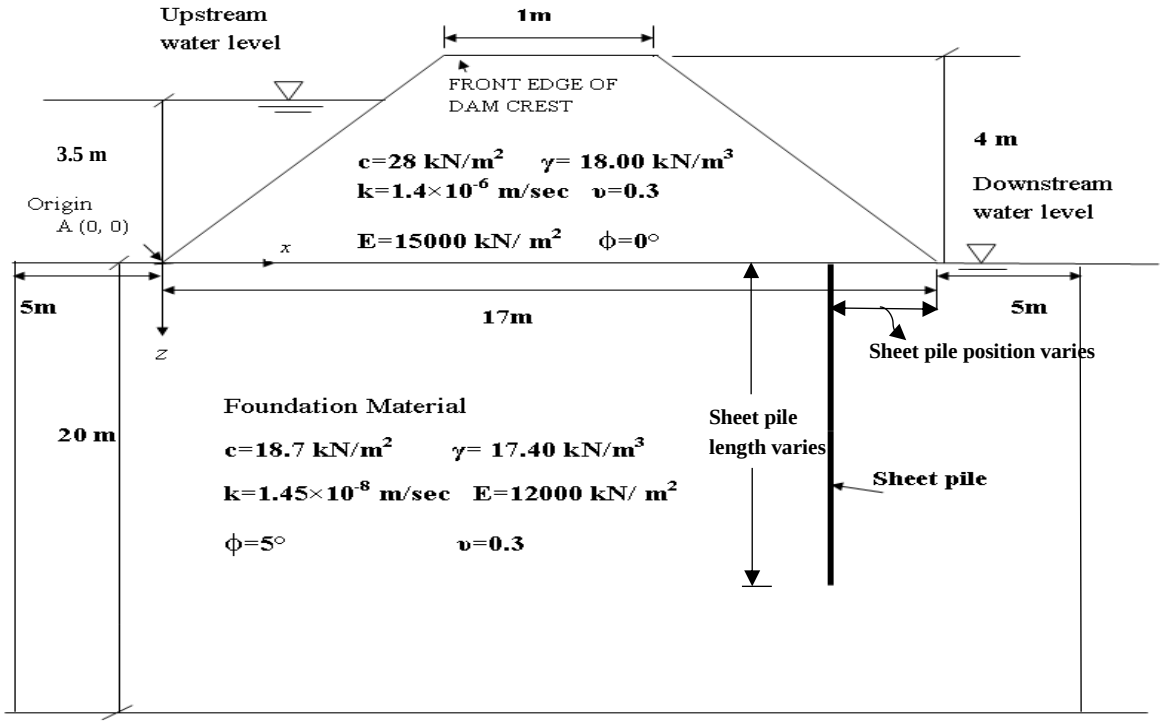

Figure 3.2(a) – Schematic Diagram of Model Embankment

Table 3.1 presents sheet pile properties used in present study for steady seepage and transient condition.

Table 3.1: Properties of sheet pile material

Area of cross section per meter	**0.03**
Moment of Inertia per meter	0.00225
E_{steel} (N/m^2)	2×10^{11}

3.2 PARAMETRIC STUDY

Figure 3.2 b represents the flow chart of numerical analysis for current study considering variation of parameter of sheet pile length and sheet pile position considering steady state and transient state of time variation of 1hr., 2hrs., 3hrs.,4 hrs.,5hrs.,6hrs.,7hrs.,8hrs.,9hrs.,10hrs.,11hrs.,12hrs. respectively. Table 3.2 presents numerical cases for steady seepage conditions for both static and seismic conditions. Table 3.3(a) presents numerical cases for transient state for single tidal cycle considering both static and seismic conditions. Table 3.3(b) presents numerical cases for transient state for multiple tidal cycle considering both static and seismic conditions.

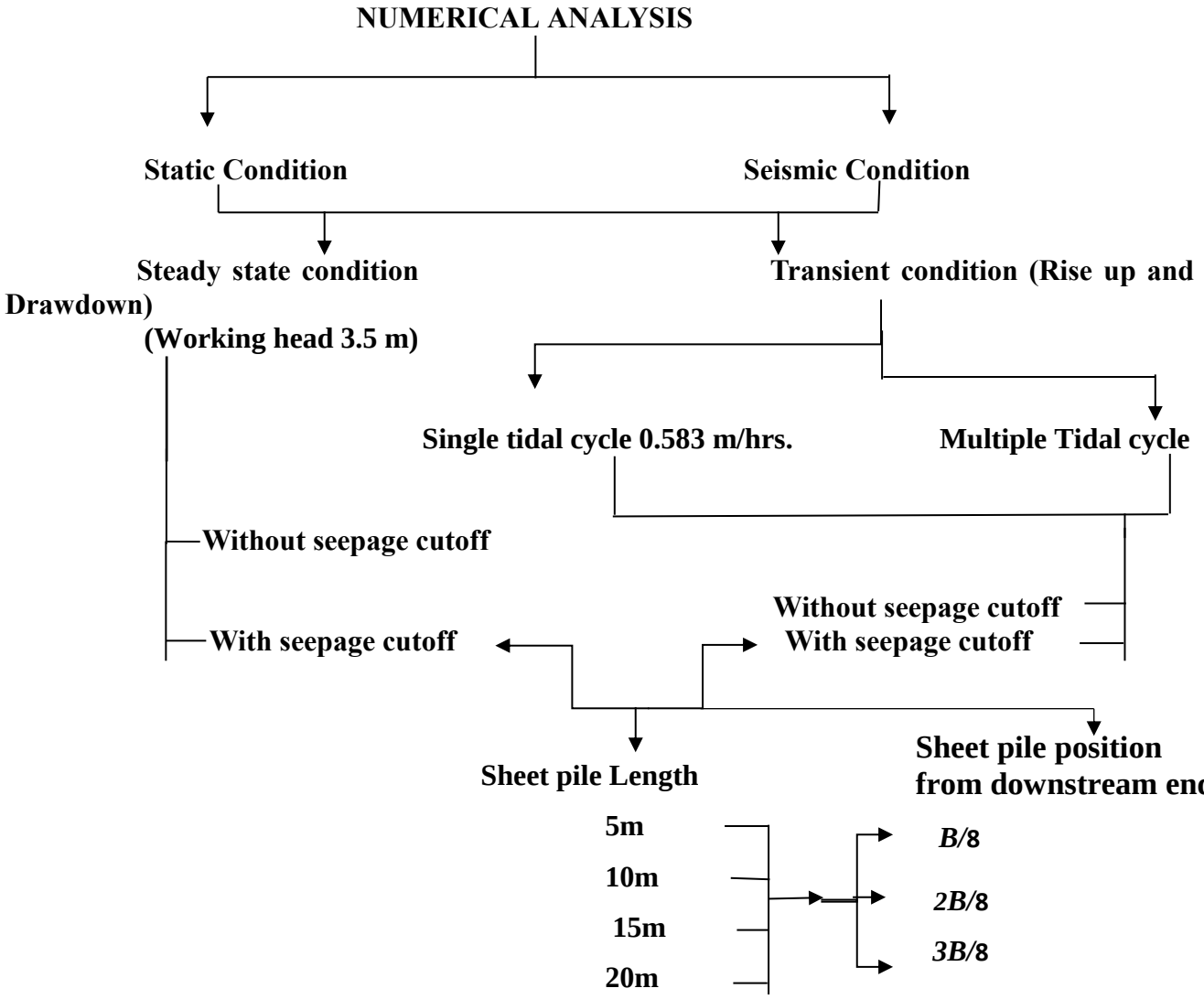

Fig. 3.2b Flowchart for numerical analysis

TABLE 3.2: LIST OF NUMERICAL CASES FOR STEADY STATE (UNDER STATIC AND SEISMIC CONDITION)

Sl. no.	Nomenclature	Sheet pile length in meter	Sheet pile position from Downstream end
1	EMB	N.A	N.A
2	T2.1L5	5	B/8
3	T2.1L10	10	
4.	T2.1L15	15	
5	T2.1L20	20	
6	T4.2L5	5	2B/8
7	T4.2L10	10	
8	T4.2L15	15	
9	T4.2L20	20	
10	T6.3L5	5	3B/8
11	T6.3L10	10	
12	T6.3L15	15	
13	T6.3L20	20	

TABLE 3.3(a): LIST OF NUMERICAL CASES FOR TRANSIENT STATE WITH SINGLE TIDAL CYCLE (UNDER SEISMICAND STATIC CONDITIONS)

Serial No.	Model Nomenclature	Rate of rise and fall (m/hour)	Half Cycle Time(hour)		Number of Cycles	Remarks
			Rise up	Drawdown		
1	EMBR1	0.583 m/hour 0.583 m/hour	1	-	0.5	Single Tidal cycle
2	EMBR2		2		0.5	
3	EMBR3		3		0.5	
4	EMBR4		4		0.5	
5	EMBR5		5		0.5	
6	EMBR6		6		0.5	
7	EMBD1			7	0.5	
8	EMBD2			8	0.5	
9	EMBD3			9	0.5	
10	EMBD4			10	0.5	
11	EMBD5			11	0.5	
12	EMBD6			12	0.5	
13	T2.1L5R1		1	-	0.5	Single Tidal cycle
14	T2.1L5R2		2		0.5	
15	T2.1L5R3		3		0.5	
16	T2.1L5R4		4		0.5	
17	T2.1L5R5		5		0.5	
18	T2.1L5R6		6		0.5	

19	T2.1L5D1			7	0.5	
20	T2.1L5D2			8	0.5	
21	T2.1L5D3			9	0.5	
22	T2.1L5D4			10	0.5	
23	T2.1L5D5			11	0.5	
24	T2.1L5D6			12	0.5	
25	T2.1L10R1		1	-	0.5	
26	T2.1L10R2		2		0.5	
27	T2.1L10R3		3		0.5	
28	T2.1L10R4		4		0.5	
29	T2.1L10R5		5		0.5	
30	T2.1L10R6		6		0.5	
31	T2.1L10D1			7	0.5	
32	T2.1L10D2			8	0.5	
33	T2.1L10D3			9	0.5	
34	T2.1L10D4			10	0.5	
35	T2.1L10D5			11	0.5	
36	T2.1L10D6			12	0.5	
37	T2.1L15R1		1	-	0.5	
38	T2.1L15R2		2		0.5	
39	T2.1L15R3		3		0.5	
40	T2.1L15R4		4		0.5	
41	T2.1L15R5		5		0.5	
42	T2.1L15R6		6		0.5	
43	T2.1L15D1			7	0.5	
44	T2.1L15D2			8	0.5	
45	T2.1L15D3			9	0.5	
46	T2.1L15D4			10	0.5	
47	T2.1L15D5			11	0.5	
48	T2.1L15D6			12	0.5	
49	T2.1L20R1		1	-	0.5	
50	T2.1L20R2		2		0.5	
51	T2.1L20R3		3		0.5	
52	T2.1L20R4		4		0.5	
53	T2.1L20R5		5		0.5	
54	T2.1L20R6		6		0.5	
55	T2.1L20D1			7	0.5	
56	T2.1L20D2			8	0.5	
57	T2.1L20D3			9	0.5	
58	T2.1L20D4			10	0.5	
59	T2.1L20D5			11	0.5	Single Tidal cycle
60	T2.1L20D6			12	0.5	
61	T4.2L5R1		1	-	0.5	
62	T4.2L5R2		2		0.5	
63	T4.2L5R3		3		0.5	
64	T4.2L5R4		4		0.5	

65	T4.2L5R5		5		0.5	
66	T4.2L5R6		6		0.5	
67	T4.2L5D1			7	0.5	
68	T4.2L5D2			8	0.5	
69	T4.2L5D3			9	0.5	
70	T4.2L5D4			10	0.5	
71	T4.2L5D5			11	0.5	
72	T4.2L5D6			12	0.5	
73	T4.2L10R1		1	-	0.5	
74	T4.2L10R2		2		0.5	
75	T4.2L10R3		3		0.5	
76	T4.2L10R4		4		0.5	
77	T4.2L10R5		5		0.5	
78	T4.2L10R6		6		0.5	
79	T4.2L10D1			7	0.5	
80	T4.2L10D2			8	0.5	
81	T4.2L10D3			9	0.5	
82	T4.2L10D4			10	0.5	
83	T4.2L10D5			11	0.5	
84	T4.2L10D6			12	0.5	
85	T4.2L15R1		1	-	0.5	
86	T4.2L15R2		2		0.5	
87	T4.2L15R3		3		0.5	
88	T4.2L15R4		4		0.5	
89	T4.2L15R5		5		0.5	
90	T4.2L15R6		6		0.5	
91	T4.2L15D1			7	0.5	
92	T4.2L15D2			8	0.5	
93	T4.2L15D3			9	0.5	
94	T4.2L15D4			10	0.5	
95	T4.2L15D5			11	0.5	
96	T4.2L15D6			12	0.5	
97	T4.2L20R1		1	-	0.5	
98	T4.2L20R2		2		0.5	
99	T4.2L20R3		3		0.5	
100	T4.2L20R4		4		0.5	
101	T4.2L20R5		5		0.5	
102	T4.2L20R6		6		0.5	
103	T4.2L20D1			7	0.5	
104	T4.2L20D2			8	0.5	
105	T4.2L20D3			9	0.5	
106	T4.2L20D4			10	0.5	
107	T4.2L20D5			11	0.5	
108	T4.2L20D6			12	0.5	
109	T6.3L5R1		1	-	0.5	
110	T6.3L5R2		2		0.5	

111	T6.3L5R3		3		0.5	
112	T6.3L5R4		4		0.5	
113	T6.3L5R5		5		0.5	
114	T6.3L5R6		6		0.5	
115	T6.3L5D1			7	0.5	
116	T6.3L5D2			8	0.5	
117	T6.3L5D3			9	0.5	
118	T6.3L5D4			10	0.5	
119	T6.3L5D5			11	0.5	
120	T6.3L5D6			12	0.5	
121	T6.3L10R1		1	-	0.5	
122	T6.3L10R2		2		0.5	
123	T6.3L10R3		3		0.5	
124	T6.3L10R4		4		0.5	
125	T6.3L10R5		5		0.5	
126	T6.3L10R6		6		0.5	
127	T6.3L10D1			7	0.5	
128	T6.3L10D2			8	0.5	
129	T6.3L10D3			9	0.5	
130	T6.3L10D4			10	0.5	
131	T6.3L10D5			11	0.5	
132	T6.3L10D6			12	0.5	
133	T6.3L15R1		1	-	0.5	
134	T6.3L15R2		2		0.5	
135	T6.3L15R3		3		0.5	
136	T6.3L15R4		4		0.5	
137	T6.3L15R5		5		0.5	
138	T6.3L15R6		6		0.5	
139	T6.3L15D1			7	0.5	
140	T6.3L15D2			8	0.5	
141	T6.3L15D3			9	0.5	
142	T6.3L15D4			10	0.5	
143	T6.3L15D5			11	0.5	
144	T6.3L15D6			12	0.5	
145	T6.3L20R1		1	-	0.5	
146	T6.3L20R2		2		0.5	
147	T6.3L20R3		3		0.5	
148	T6.3L20R4		4		0.5	
149	T6.3L20R5		5		0.5	
150	T6.3L20R6		6		0.5	
151	T6.3L20D1			7	0.5	
152	T6.3L20D2			8	0.5	
153	T6.3L20D3			9	0.5	
154	T6.3L20D4			10	0.5	
155	T6.3L20D5			11	0.5	
156	T6.3L20D6			12	0.5	

TABLE 3.3(b): LIST OF NUMERICAL CASES (TRANSIENT STATE WITH MULTIPLE TIDAL CYCLE (UNDER STATIC CONDITION)

Serial No.	Model Nomenclature	Rate of rise and fall	No of cycle	REMARK
1	E	0.583 m/hour	120 (considering 60 days duration)	Multiple tidal cycle
2	T2.1L5			
3	T2.1L10			
4	T2.1L15			
5	T2.1L20			
6	T4.2L5			
7	T4.2L10			
8	T4.2L15			
9	T4.2L20			
10	T6.3L5			
11	T6.3L10			
12	T6.3L15			
13	T6.3L20			

**** Sheet pile position from toe of the embankment has been denoted by T. T2.1 represents sheet pile is at *B*/8 position from the downstream end. T4.2 represents sheet pile is at 2*B*/8 position from the downstream end. T6.3 represents sheet pile is at 3*B*/8 position from the downstream end.**

****Sheet pile length has been denoted by L. L5 represents sheet pile of 5m length. L10represents sheet pile of 10m length. L15 represents sheet pile of 15m length. L20 represents sheet pile of 20m length.**

**** Rise up time have been denoted by R. R1, R2, R3, R4, R5, R6 represents time in hour for a half cycle for 1hour interval i.e. 1 hr.,2hrs.,3hrs.,4hrs.,5hrs.,6hrs. respectively.**

***Drawdown time have been denoted by D. D1, D2, D3, D4, D5, D6 represents time in hour for a half cycle for 1hour interval i.e. 7 hrs.,8hrs.,9hrs.,10hrs.,11hrs.,12hrs. respectively.**

3.3 MODELLING BY MATLAB:

Numerical analyses have been done to study the effects of sheet pile location and length on different seepage parameters such as fluid flow vector, pore water pressure variation, exit gradient as well as soil pressure on sheet pile. The details of the parametric study are mentioned in Figure 3.2(b). To establish the reliability of the study, flownet has been also drawn by solving partial differential equation (Eq. 3.1) with the help of partial differential equation (PDE) solver in MATLAB. The PDE solver uses the finite element method for solving steady state seepage analysis defined on

bounded domain in the plane. The PDE Solver assembles a PDE problem by using finite element formulation. The basic Elliptic Equation used in PDE Solver is

$$-\nabla.(c\nabla u) + au = f \text{ in } \Omega \qquad (3.1)$$

where Ω is a bounded domain in the plane. c, a, f, and the unknown solution u are complex functions defined on Ω. c can also be a 2-by-2 matrix function on Ω. The boundary conditions specify a combination of u and its normal derivative on the boundary. The unknown vector u contains the values of the approximate solution at the mesh points. (Reference: MATLAB manual 20014a)

The steps for constructing flownet have been adopted as follows:

1. **Drawing of Geometry:** The geometry has been defined in terms of Cartesian co-ordinate system.
2. **Boundary conditions:** Boundary conditions are defined in MATLAB in the form of Neumann and Dirichlet condition in PDE Solver. Where a Neumann condition usually refers to the case q = 0. Dirichlet boundary condition applies in this study at the position of upstream and downstream head has been shown in Figure.3.3(a).
3. **Initializing Mesh:** triangular mesh has been considered on the domain Ω. The toolbox has mesh generating and mesh refining facilities. A mesh is described by three matrices of fixed format that contain information about the mesh points, the boundary segments, and the triangles. Triangular mesh elements have been shown in Figure 3.3(b)
4. **Refining Mesh:** Mesh has been refined for accurate adjustment of result. Foundation materials were modeled using high order triangular elements with a finer mesh in the soil wedges adjacent to vertical sheet piles.
5. **Solving through PDE tool bar:** The approximate solution to the elliptic PDE is found by steps: The geometry of the domain Ω defining the boundary conditions has been described interactively using PDE tool. A triangular mesh has been then generated on the bounded domain Ω in the plane, described by three matrices containing information about mesh points, boundary segment and triangle. PDE with discretized boundary conditions along with the generated mesh finally helps to obtain a linear system.

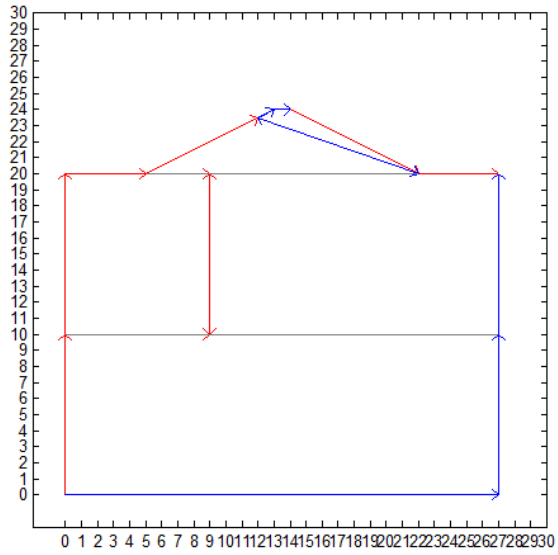

Figure. 3.3(a): Boundary Condition

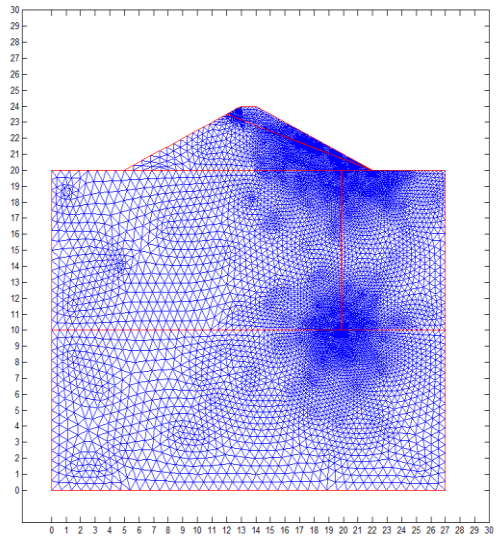

Figure. 3.3(b): Formation of Meshing

3.3.2 MATHEMATICAL BACKGROUND OF FORMULATION FOR PDE ANALYSIS IN MATLAB:

In MAT LAB version 2014 a PDE Solver tool bar, flownet of earthen dam with or without sheet pile has been drawn by using Eq. 3.1. In the current study a combination of Dirichlet and Generalized Neumann boundary *i.e.* mixed boundary condition have been applied where,

- Dirichlet: $hu - r$ on the boundary $\partial\Omega$.
- Generalized Neumann: $\vec{n}.(c\nabla u) + qu = g$ on $\partial\Omega$. *(3.2)*

Generalized Neumann conditions have been assumed on the whole boundary, since Dirichlet conditions can be approximated by generalized Neumann conditions. In the simple case of a unit matrix h, Dirichlet condition yields because division with a very large q cancels the normal derivative terms. The mixed boundary condition of the system case requires a more complicated treatment, described in the elliptic system. Assuming that u is a solution of the differential equation, the equation has been multiplied with an arbitrary test function *v* and integrate on Ω as follows:

$$\int_{\Omega} -\big(\nabla.(c\nabla_u)\big)v + auvdx) = \int_{\Omega} fvdx \qquad (3.3)$$

Integrating using Green's formula) the following expression have been obtained,

$$\int_{\Omega} (\mathrm{c}\nabla\mathrm{u}).\nabla v + auv\,dx - \int_{\partial\Omega} \vec{n}.(\mathrm{c}\nabla\mathrm{u})v\,ds = \int_{\Omega} fv\,dx \qquad (3.4)$$

The boundary integral can be replaced by the boundary condition:

$$\int_{\Omega} (\mathrm{c}\nabla \mathrm{u}).\nabla v + auv\, dx - \int_{\partial\Omega}(-\mathrm{qu} + \mathrm{g})v\, ds = \int_{\Omega} fv\, dx \qquad (3.5)$$

Replacing the original problem to find *u* such have been depicted in the following expression,

$$\left(\int_{\Omega} (\mathrm{c}\nabla \mathrm{u}).\nabla v + auv - fv\, dx - \int_{\partial\Omega}(-\mathrm{qu} + \mathrm{g})v\, ds\right) = 0 \qquad (3.6)$$

This Eq.3.6 is called the variational form of the differential equation. The solution *u* and the test functions *v* belong to some function subspace. By choosing an Np-dimensional subspace the differential equation has been projected onto a finite-dimensional function space *i.e.* to lie in *u* and *v* rather than V.

The solution of the finite dimensional problem turns out to be the element of that lies closest to the weak solution when measured in the energy norm. Due to linearity of differential operator, the variational equation is satisfied for *Np* test-functions $\emptyset_i$ that form a basis, i.e.,

$$\int_{\Omega} (\mathrm{c}\nabla \mathrm{u}).\nabla \phi_i + au\phi_{\mathrm{i}} - f\phi_{\mathrm{i}}\, dx - \int_{\partial\Omega}(-\mathrm{qu} + \mathrm{g})\phi_{\mathrm{i}}\, ds = 0, \qquad \mathrm{i} = 1,2,\ldots,N_{\mathrm{p}} \qquad (3.7)$$

Where, $i = 1,2,\ldots,N_p$

Expanding *u* in the same basis of V_{N_p}

$$u(x) = \sum_{j=1}^{N_r} U_j \phi_j(x) \qquad (3.8)$$

and the following system of equations has been obtained:

$$\sum_{j=1}^{N_r}\left(\int_{\Omega}\left(c\nabla\phi_j\right).\nabla\phi_i + \alpha\phi_i\phi_j dx + \int_{\partial\Omega} q\phi_i\phi_j\, ds\right)U_j = \int_{\Omega} f\phi_i dx + \int_{\partial\Omega} g\phi_i\, ds \qquad (3.9)$$

Where,

$$K_{i,j} = \int_{\Omega}(c\nabla\phi_j).\nabla\phi_i dx \quad \text{(Stiffness matrix)} \qquad (3.10)$$

$$M_{i,j} = \int \alpha\phi_i\phi_j dx \quad \text{(Mass matrix)} \qquad (3.11)$$

$$Q_{i,j} = \int_{\partial\Omega} q\phi_i\phi_j\, ds \qquad (3.12)$$

$$F_i = \int_{\Omega} f\phi_i dx \qquad (3.13)$$

$$G_i = \int_{\partial\Omega} g\phi_i\, ds. \qquad (3.14)$$

The system has been rewriten in the form $(K + M + Q)U = F + G) \geq 0$ and $q(x) \geq 0'$ on some part of $\partial\Omega$, then, if $U \neq 0$.

If c(x)= d > 0, a(x) ≥0 and q(x)>0 on some part of $\partial\Omega, then, if\ (U \neq 0)$.

$$U^T(K + M + Q)U = \int_\Omega c|\nabla u|^2 + \alpha u^2 dx + \int_{\partial\Omega} qu^2 ds > 0, \text{ if } U \neq 0 \qquad (3.15)$$

$$u(x_i)=\sum_{j=0}^{N_P} U_j \emptyset_j(x_i)=U_i \qquad (3.16)$$

A triangle has been considered with the nodes P1, P2, and P3 as shown in the following Figure. 3.4

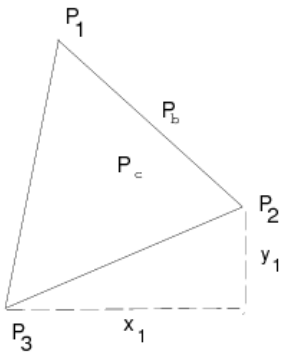

Figure 3.4: Triangular mesh with nodal points.

The simplest computations, for the local mass matrix m has been given as

$$m_{i,j} = \int_{\nabla P_1P_2P_3} a(P_c)\phi_i(x)\phi_j(x)\ dx = a(P_c)\frac{\text{area }(\nabla P_1P_2P_3)}{12}\left(1 + \delta_{i,j}\right) \qquad (3.17)$$

Where P_c is the center of mass of $\Delta P_1P_2P_3$, i.e.,

$$P_c = \frac{\nabla P_1P_2P_3}{3} \qquad (3.18)$$

The contribution to the right side *f* is just

$$f_i = f(P_c)\frac{\text{area }(\nabla P_1P_2P_3)}{3} \qquad (3.19)$$

If functions $\emptyset_1, \emptyset_2$ and $\emptyset_3$ such that $\emptyset(P_i) = 1$. If $P_2 - P_3 = [x_1, y_1]^T$ then

$$\nabla\phi_1 = \frac{1}{2\ \text{area}(\Delta P_1P_2P_3)}\begin{bmatrix} y_1 \\ -x_1 \end{bmatrix} \qquad (3.20)$$

and after integration (taking c as a constant matrix on the triangle

$$k_{i,j} = \frac{1}{4\ \text{area}(\Delta P_1 P_2 P_3)} \left[y_j - x_j\right] c(P_c) \begin{bmatrix} y_1 \\ -x_1 \end{bmatrix} \quad (3.21)$$

$$Q_{i,j} = q(P_b) \frac{|P_1 - P_2|}{6} \left(1 + \delta_{i,j}\right), \quad i,j = 1,2 \quad (3.22)$$

and

$$G_{i,j} = g(P_b) \frac{|P_1 - P_2|}{6}, \quad i = 1,2 \quad (3.23)$$

Where P_b is the midpoint of P_1P_2.

3.4 MODELLING BY FLAC 2D:

FLAC 2D was originally developed for mining and geotechnical engineers (Coetzee *et al.*, 1998) by Itasca Consultants in 1994. Following the guidelines set out by USACE (1989), a finite difference formulation FLAC (FAST LAGRANGIAN ANALYSIS OF CONTINUA) (Itasca, 2005) was selected to model present study. Numerical modeling has been developed for the model earthen dam with and without Sheet pile of varying position and length in FLAC 2D version 5.0. The basic calculation scheme of FLAC is based on the explicit method, where the variables are at discrete points in space and the shape function is undefined. The working methodology is based on the following steps,

Step 1: The velocities and displacements have been calculated from stresses and forces using equations of motion for equilibrium conditions;

Step 2: stresses have been determined using constitutive laws;

Step 3: The boundary conditions and newly determined stresses have been used to determine the nodal forces;

Step 4: Equilibrium conditions have been used to calculate new velocities at the grid points; The basic concept of this FLAC explicit method is to keep the calculation speed ahead of the physical speed using relatively small-time steps in comparison to the implicit method.

3.4.1. DETAILED ANALYSIS IN FLAC 2D

The model dam studied is presented with its dimension and the relevant soil parameters have been indicated in Figure. 3.2(a). The origin shown in figure 3.2(a) is the end point of the embankment on upstream side at the base that is, point A (0, 0) shown in the figure. Two-dimensional numerical analyses have been carried out with the help of FLAC-2D.

3.4.1.1. Generation of mesh and Boundary condition

The standard boundary conditions have been used in the numerical model, *i.e.* fixed in horizontal direction on the vertical boundaries of the domain and fixed along both *x* and *y* directions along the bottom of the model. Boundary condition and Geometry of the present study has been shown in Fig. 3.5(a) and Fig. 3.5(b) for embankment with sheet pile fixed at top and free at bottom. A minimum element size of 0.5m × 0.5m, with gradually increasing element size outside the cofferdam area was used. The ratio for increasing the element size outside the uniform mesh size was 1.05. Ground water flow configuration was used to model the effective stress condition with pore water pressures defined in all mesh zones. FLAC function automatically adjusts total stresses due to any change in pore pressure imposed externally (e.g. due to dewatering or lowering water level manually).

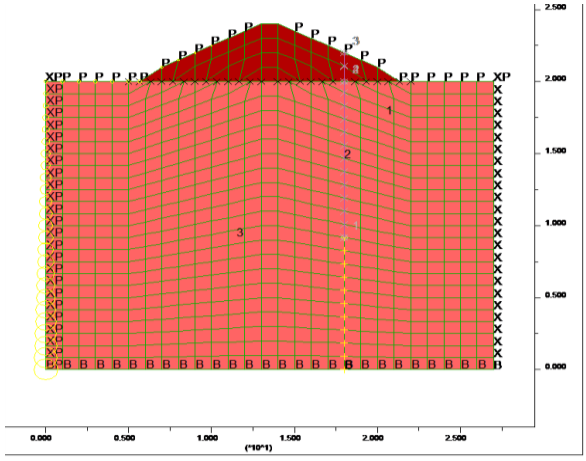

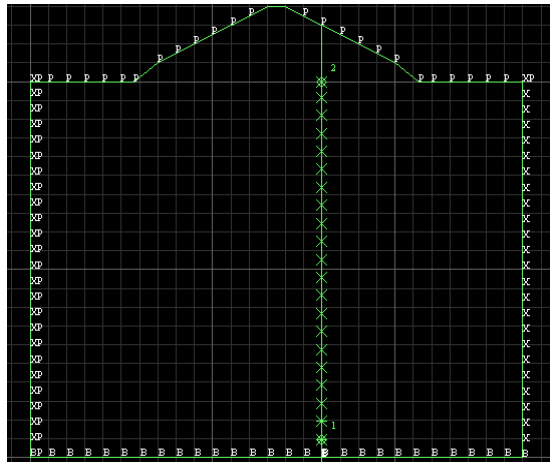

Fig. 3.5(a): Model dam Geometry with sheet pile **Fig. 3.5(b): Model dam boundary condition**

3.4.1.2. Interface element and material properties

Beam element has been adopted to model the sheet pile. Interface elements have been considered between the soil and sheet pile elements. The interfaces have been considered on both sides of the sheet pile so that no relative slip occurs. The interface properties include normal stiffness (K_n), shear stiffness (K_s) and shear strength parameters of the interface. The normal and shear stiffness has been selected such that the stiffness become approximately 10 times the equivalent stiffness of the stiffest neighboring zone as suggested by the FLAC manual (Itasca 2005).

The interface stiffness has been calculated as follows:

$$K_n = K_s = 10.\ max\left[\frac{(K+\frac{4G}{3})}{\Delta Z_{\min}}\right] \qquad (3.24)$$

Where K_n = normal stiffness of the interface; K_s = shear stiffness of the interface and Δz_{min}= minimum width of the neighboring zone. Table 1 presents the properties of interface elements in terms of interface friction angle, normal and shear stiffness, adhesion. The interface friction angle has been set as two-thirds of the maximum soil friction angle. (Reference: Itasca 2005)

The Young's modulus (E_{steel}), cross-sectional area (A), and moment of inertia (I) were specified for the sheet pile wall. Considering unit length along the length of the wall, cross sectional area (A) has been calculated. Mohr-Coulomb model, considering elastic- perfectly plastic soil behavior has been adapted for foundation and embankment soils. (Ref: Pham et al (2013) used Mohr Columb model in their Study of Stability of Slope and Seepage Analysis in Earth Dam obtained realistic result. The strength parameters of soil used in their study indicating Mohr Columb model and the present study is similar to, that used in analysis. That's why Mohr Columb model has been used in our present study).

As FLAC uses bulk modulus (K) and shear modulus (G) elasticity as stiffness parameters, drained bulk and shear modulus for the various soil layers have been calculated using the following relationships:

Bulk modulus of elasticity K_b,

$$K_b = \frac{E'}{3\,(1-2\upsilon')} \qquad (3.25)$$

Shear modulus of elasticity G,

$$G = \frac{E'}{2\,(1+2\upsilon')} \qquad (3.26)$$

where,

υ' = Poisson ratio under effective stress conditions

E' = Stiffness of the soil under effective stress conditions

FLAC requires that the coefficient of pore pressure term in Darcy's equation (known as mobility coefficient) is defined as ratio of intrinsic permeability to the fluid dynamic viscosity as given by the following equation. (3.27)

$$K_{\text{FLAC}} = \frac{K}{\rho \cdot g} \qquad (3.27)$$

Where;

k = Permeability of soil

ρ = Density of water

The sheet piles have been considered to be impermeable. Steel Sheet pile have been considered used in vertical direction in the cross sectional of embankment. The pile stiffness has been calculated from the yield strength.

3.4.1.3 Effective stress analyses

Various load cases have been analyzed independently to assess the stability of an earth-dam at each key load stage and after construction for global stability checks. A multi-stage analysis was undertaken to capture the stability due to the changes to the pore water pressure variation.

To assess the overall failure mode of the structure, soil-fill and interface strength have been gradually reduced for each set of analyses to check the stability under each reduced strength based on strength reduction technique. Calculation of a factor of safety has been executed by reducing the strength parameters of the soil (Phi-c reduction). In the Phi-c reduction approach the strength parameters tanØ and c of the soil are successively reduced until failure of the structure occurs. The total multiplier ΣMsf is used to define the value of the soil strength parameters at a given stage in the analysis as given by equation. (3.28)

$$\sum Msf = \frac{\tan \phi_{input}}{\tan \phi_{reduced}} = \frac{c_{input}}{c_{reduced}} \qquad (3.28)$$

3.4.1.4 STUDY OF SEISMIC EFFECT

In order to carry out study of seepage under seismic condition as given by equation. (3.29), the following stiffness contribution (in units of force/distance) has been made from each of the three grid points of the sub-zone for, each triangular sub-zone:

$$K = (K + \frac{4\,G}{3})\,[\frac{(Lmax)\text{^}2}{6\mathrm{A}\,\Delta}]T \qquad (3.29)$$

where L_{max} is the maximum edge-length of the triangle, A_{Δ} is the area of the triangle and T is the out-of-plane dimension, equal to 1.0 for a plane-strain analysis. Thus, for the full quadrilateral zone, the total contribution to each of the four grid-points is the summation of those for the three triangles meeting at the grid point. Numerical analysis for the seismic response of modeling of earthen dams requires the discretization of a region of the material adjacent to the foundation. The seismic input has been normally represented by plane waves propagating upward through the underlying material.

The boundary conditions at the sides of the model must account for the free-field motion which would exist in the absence of the structure. These boundaries have been placed at sufficient distances to minimize wave reflections and achieve free-field conditions. For soils with high material damping, this condition can be obtained with a relatively small distance (Seed et al., 1975). In the numerical analyses, the pore water pressures within the saturated zone have been estimated using 'Finn model'. Martin et al. (1975) have proposed 'Finn model' and later this model is modified by Byrne et al. (1991). In the 'Finn model', the change in the pore water pressure is given by:

$$\Delta u = M_s \Delta \varepsilon^p \qquad (3.30)$$

where Δu is the change in the pore water pressure, M_s is the constrained modulus of the soil. $\Delta \varepsilon^p$ is the change in volumetric strain and is given by $\gamma_s C_1 \exp(-C_2\, \varepsilon_{vd}/\gamma_s)$, where, ε_{vd} is the change in the volumetric strain. C_1 is a constant and given by $7600(D_r)^{-2.5}$. C_2 is another constant and given by $0.4/C_1$. D_r is the relative density and γ_s is the shear strain in the soil. As mentioned earlier, the relative density (D_r) is maintained at 65% in the model tests. Time history acceleration data of India(Sikkim)-Nepal-Border has been adopted for the present study as shown in Figure. 3.6.

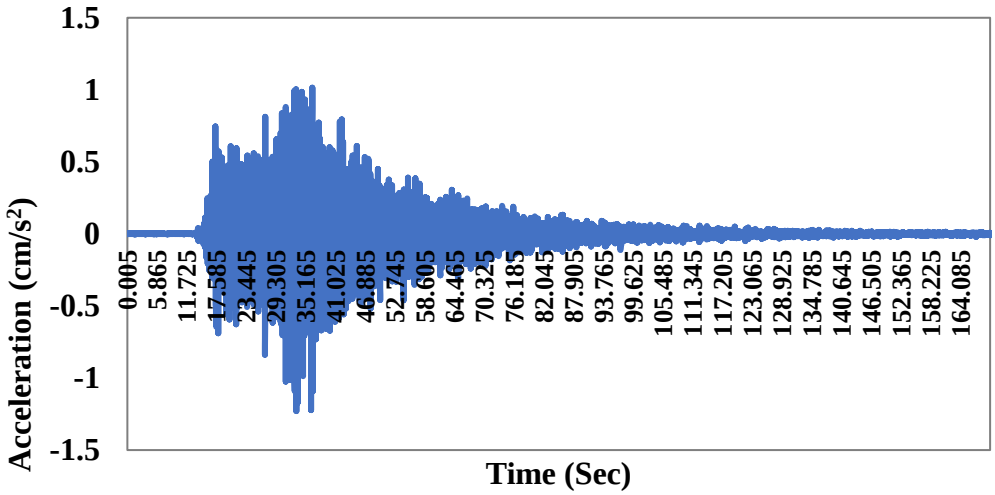

Figure. 3.6.: Time history acceleration data of India (Sikkim)-Nepal-Border (Reference: http://www.pesmos.in/)

Numerical modeling has been studied in the analysis after baseline correction.

3.5. MODELING BY GEOSTUDIO

Seepage and Slope stability analyses have been carried out using Geo-Studio (GEO-SLOPE International 2012) software packages considering both steady and transient seepage. The latest

version of the U.S. Bureau of Reclamation (USBR) recommends the use of the effective stress approach to analyze stability with pore pressures in transient seepage analyses. (Reference: USSD, February 2007).

3.5.1 MATHEMATICAL FORMULATION

From the principle of mass conservation,

$$\frac{\partial \rho}{\partial t} + \frac{\partial}{\partial x}(\rho \bar{u}) + \frac{\partial}{\partial y}(\rho \bar{v}) = 0 \qquad (3.31)$$

Where, ρ = mass density, u, υ = velocities in the x and y directions respectively. Also, F_x and F_y are body forces in the appropriate directions. Conservation of mass leads to:

$$\frac{\partial \rho}{\partial t} + \frac{\partial}{\partial x}(\rho \bar{u}) + \bar{u}\frac{\partial}{\partial y}(\rho \bar{v}) = 0 \qquad (3.32)$$

Where (σ_x, σ_y, τ_{xy}) are stress components as defined for solids.

μ = the molecular viscosity,
λ= -2/3μ and p=the fluid pressure the following form of the stress equations is reached:

Further "Navier-stokes" equation can be written a

$$\frac{\partial \bar{u}}{\partial t} + \bar{u}\frac{\partial \bar{u}}{\partial x} + v\frac{\partial \bar{u}}{\partial y} = \frac{1}{\rho}F_x - \frac{1}{\rho}\frac{\partial p}{\partial x} + \frac{1}{3}\frac{\mu}{\rho}\frac{\partial}{\partial x}\left(\frac{\partial \bar{u}}{\partial x} + \frac{\partial v}{\partial y}\right) + \frac{\mu}{\rho}\left(\frac{\partial^2 \bar{u}}{\partial x^2} + \frac{\partial^2 \bar{u}}{\partial y^2}\right) \qquad (3.33)$$

$$\frac{\partial \bar{v}}{\partial t} + u\frac{\partial \bar{v}}{\partial x} + \bar{v}\frac{\partial \bar{v}}{\partial y} = \frac{1}{\rho}F_y - \frac{1}{\rho}\frac{\partial p}{\partial y} + \frac{1}{3}\frac{\mu}{\rho}\frac{\partial}{\partial y}\left(\frac{\partial \bar{u}}{\partial x} + \frac{\partial \bar{v}}{\partial y}\right) + \frac{\mu}{\rho}\left(\frac{\partial^2 \bar{v}}{\partial x^2} + \frac{\partial^2 \bar{u}}{\partial y^2}\right) \qquad (3.34)$$

For incompressibility condition,

$$\frac{\partial \bar{u}}{\partial t} + \bar{u}\frac{\partial \bar{u}}{\partial x} + \bar{v}\frac{\partial \bar{u}}{\partial y} = \frac{1}{\rho}F_x - \frac{1}{\rho}\frac{\partial p}{\partial x} + \frac{\mu}{\rho}\left(\frac{\partial^2 \bar{u}}{\partial x^2} + \frac{\partial^2 \bar{u}}{\partial y^2}\right) \qquad (3.35)$$

$$\frac{\partial \bar{v}}{\partial t} + \bar{u}\frac{\partial \bar{v}}{\partial x} + \bar{v}\frac{\partial \bar{v}}{\partial y} = \frac{1}{\rho}F_y - \frac{1}{\rho}\frac{\partial p}{\partial y} + \frac{\mu}{\rho}\left(\frac{\partial^2 \bar{v}}{\partial x^2} + \frac{\partial^2 \bar{v}}{\partial y^2}\right) \qquad (3.36)$$

For steady state conditions, the terms ($\partial\bar{u}/\partial t$) and ($\partial\bar{v}/\partial t$) have been dropped. the steady state equations have been presented are,

$$\bar{u}\frac{\partial v}{\partial x} + \bar{v}\frac{\partial \bar{u}}{\partial y} + \frac{1}{\rho}\frac{\partial p}{\partial y} - \frac{\mu}{\rho}\left(\frac{\partial^2 \bar{u}}{\partial x^2} + \frac{\partial^2 \bar{u}}{\partial y^2}\right) = 0 \qquad (3.37)$$

$$\bar{u}\frac{\partial v}{\partial x} + \bar{v}\frac{\partial \bar{u}}{\partial y} + \frac{1}{\rho}\frac{\partial p}{\partial y} - \frac{\mu}{\rho}\left(\frac{\partial^2 \bar{v}}{\partial x^2} + \frac{\partial^2 \bar{v}}{\partial y^2}\right) = 0 \qquad (3.38)$$

The shape functions applied to all variables are given with the help of these shape function equation. (3.37) and equation. (3.38) have been modified as:

$$\bar{u} = N\bar{u}, \qquad \bar{v} = N\bar{v}, \qquad p = Np$$

$$\bar{u}\frac{\partial N}{\partial x}u + \bar{v}\frac{\partial N}{\partial y}\bar{u} + \frac{1}{\rho}\frac{\partial N}{\partial x}p - \frac{\mu}{\rho}\frac{\partial^2 N}{\partial x^2}\bar{u} + \frac{\mu}{\rho}\frac{\partial^2 N}{\partial y^2}\,\bar{u} = 0 \qquad (3.39)$$

$$\bar{u}\frac{\partial N}{\partial x}\bar{v} + \bar{v}\frac{\partial N}{\partial y}\bar{v} + \frac{1}{\rho}\frac{\partial N}{\partial x}p - \frac{\mu}{\rho}\frac{\partial^2 N}{\partial x^2}\bar{v} + \frac{\mu}{\rho}\frac{\partial^2 N}{\partial y^2}\,\bar{v} = 0 \qquad (3.40)$$

Integrating after multiplying by the weighting functions,

$$\iint N\bar{u}\frac{\partial N}{\partial x}\bar{u}\,dx\,dy + \iint N\bar{v}\frac{\partial N}{\partial y}\bar{u}\,dx\,dy + \frac{1}{\rho}\iint N\frac{\partial N}{\partial x}p\,dx\,dy - -\frac{\mu}{\rho}\iint N\frac{\partial^2 N}{\partial x^2}\bar{u}\,dx\,dy - \frac{\mu}{\rho}\iint N\frac{\partial^2 N}{\partial y^2}\bar{u}\,dx\,dy = 0 \quad (3.41)$$

$$\iint N\bar{u}\frac{\partial N}{\partial x}\bar{v}\,dx\,dy + \iint N\bar{v}\frac{\partial N}{\partial y}\bar{v}\,dx\,dy + \frac{1}{\rho}\iint N\frac{\partial N}{\partial y}p\,dx\,dy - \frac{\mu}{\rho}\iint N\frac{\partial^2 N}{\partial x^2}\bar{v}\,dx\,dy - \frac{\mu}{\rho}\iint N\frac{\partial^2 N}{\partial y^2}\bar{v}\,dx\,dy = 0 \quad (3.42)$$

The set of equations of the continuity condition

$$\iint N\left(\frac{\partial N}{\partial x}\,\bar{u} + \frac{\partial N}{\partial y}\bar{v}\right)dx\,dy = 0$$

The equilibrium equation in the terms of ($\bar{u}, \bar{v}$, p) are as belows,

$$\begin{bmatrix} C_{11} & C_{12} & C_{13} \\ C_{21} & C_{22} & C_{23} \\ C_{31} & C_{32} & C_{33} \end{bmatrix}\begin{Bmatrix} \bar{u} \\ p \\ \bar{v} \end{Bmatrix} = \begin{Bmatrix} 0 \\ 0 \\ 0 \end{Bmatrix} \quad (3.43)$$

Where:

$$C_{11} = \iint \left(N\bar{u}\frac{\partial N}{\partial x} + N\bar{v}\frac{\partial N}{\partial x} + \frac{\mu}{\rho}\frac{\partial N}{\partial x}\frac{\partial N}{\partial x} + \frac{\mu}{\rho}\frac{\partial N}{\partial y}\frac{\partial N}{\partial y}\right)dx\,dy$$

$$C_{12} = \iint \frac{1}{\rho}N\frac{\partial N}{\partial x}\,dx\,dy$$

$$C_{13} = 0$$

$$C_{21} = \iint N\frac{\partial N}{\partial x}\,dx\,dy$$

$$C_{22} = 0$$

$$C_{23} = \iint N\frac{\partial N}{\partial y}\,dx\,dy$$

$$C_{31} = 0$$

$$C_{32} = \iint \frac{1}{\rho}N\frac{\partial N}{\partial y}\,dx\,dy$$

$$C_{31} = C_{11}$$

3.5.2 FINITE ELEMENT ANALYSIS BY GEOSTUDIO

The finite element method involved central requirement that the field quantities (e.g., stress and displacement) vary throughout each element in a prescribed fashion, using specific functions controlled by parameters to minimize error terms or energy terms. In numerical model finite element method internal flow in porous media, interstitial pore pressure, gradient, seepage, saturated and unsaturated flow has been taken in the account. A finite-element program developed by Griffiths (1996) and has been extended Lane and Griffiths (1997) to include any combination of submergence and drawdown conditions and to allow for the automatic generation of pore-water pressures. The

program utilizes the finite-element method to account for potentially complex geometries and material properties, but was used to develop a chart based approach for the operation of dams to minimize the risk of slope failure under drawdown conditions. In this research, seepage analysis in earth dam using cut off has been done by SEEP/W software in order to evaluate flownet, determine the phreatic surface through the cross-section of the dam. SLOPE/W software has been used under different conditions to evaluate slope stability of the dam.

3.5.2.1. GEOMETRY AND MESH GENARATION:

In finite element analysis, the model has been discretized into 611 numbers of quadratic elements with 653 nodes. For the accuracy of the numerical result medium coarseness has been adopted in mesh generation technique. Mesh refining has been done after an optimization to lower mesh size. The finite element mesh used in this analysis is as shown in Figure.3.7(a) and Figure 3.7(b) containing 3 nodded triangular elements to describe the domains in SEEP/W analysis and QUAKE/W analysis. SIGMA/W software has been used for coupled analysis and QUAKE/W software has been used in the present study to analyze for seismic condition. The method of analyses used is the limit equilibrium method (LEM) according to Morgenstern-price. Foundation materials have been modeled using high order triangular elements with a finer mesh in the soil wedges adjacent to vertical sheet piles.

3.5.2.2 INTERFACE ELEMENT AND BOUNDARY CONDITION

Interface elements have been introduced between the soil and sheet pile elements and a strength reduction factor have been applied for soil-sheet pile interface. The standard fixity boundary conditions were used in the finite element model, i.e. fixed in horizontal direction on the vertical boundaries and fixed in both x and y directions on the bottom of the model. A close boundary condition was also set on the bottom boundary of the model during the groundwater seepage calculations. The Rise up and Drawdown conditions have been defined as hydraulic head which is a linear function of tidal cycle time. In this particular analysis, the number of cycles has been taken over two months, i.e. 60 days with 120 cycles.

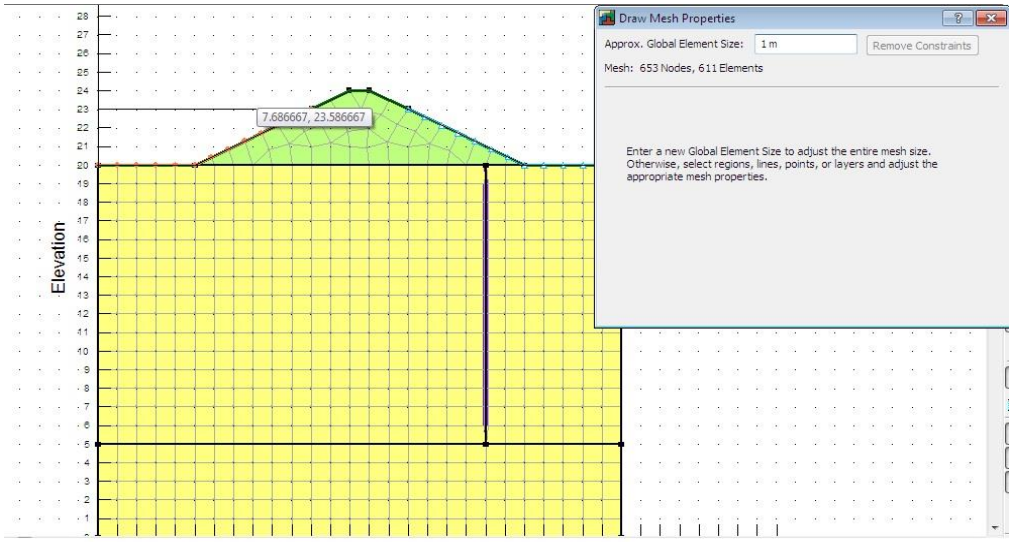

Figure.3.7(a): GEOMETRY, BOUNDARY CONDITION AND GENARATION OF MESH (SEEP/W AND SIGMA/W)

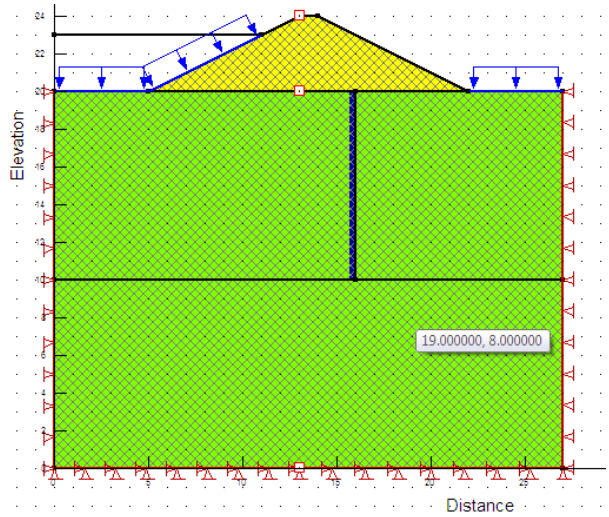

Figure. 3.7(b): GEOMETRY, BOUNDARY CONDITION AND GENARATION OF MESH (QUAKE/W)

3.5.2.3 Material Properties

Material nonlinearity has been considered for the soil using Mohr –Coulomb failure theory and elastic-perfectly plastic behavior of soil. In transient analysis the volumetric water content function and the hydraulic conductivity function play important role (Minasay, 2004). As it has been recorded from site data, that the embankments have been constructed with the locally available top soil layer the volumetric water content function has been developed on the basis of, Modified Kovacs method (2003) using Grain Size distribution, Liquid limit, Porosity, Co-efficient of volume compressibility. The Hydraulic conductivity function has been estimated from the Volumetric water content function

as a data point function using the Van Genuchten methodology (1980), with saturated permeability and residual water content has been shown in Figure. 3.8.

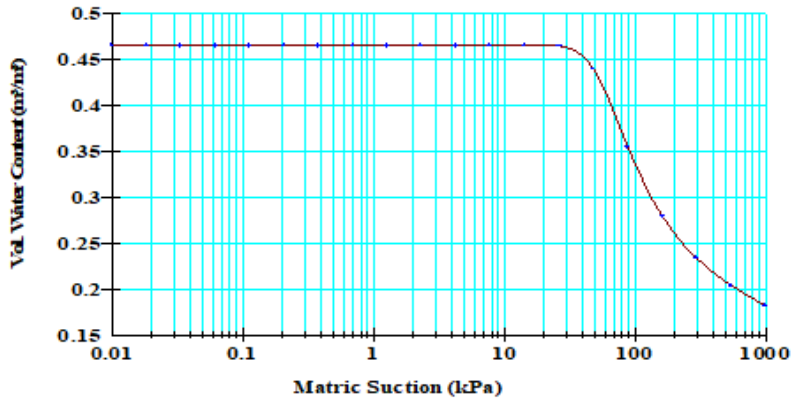

Figure-3.8: Volumetric Water Content function (as per Modified Kovacs methodology using Grain size distribution) showing plot of Volumetric water content (m^3/m^3) versus Matric Suction (kPa) for clayey Silt (Kovacs method ,2003).

3.5.2.4 Deformation based Analysis

A stress – strain type in-situ stage has been developed as the base for the analysis in SIGMA/W. The Low Tide Level (LTL) has been selected as initial stress conditions. A deformation boundary condition with the bottom as fixed and the vertical sides as roller supported has been provided. The material type was selected as Effective parameters with Pore water pressure change. A Stress / PWP mode of analysis have been done for the tidal cycle stage.

Figure. 3.9 and Figure.3.10 represents Flowchart Defining Methodology followed during analysis accordingly. The influence of transient flow to the earthen dam by investigating failure mechanism have been done by using finite element analysis.

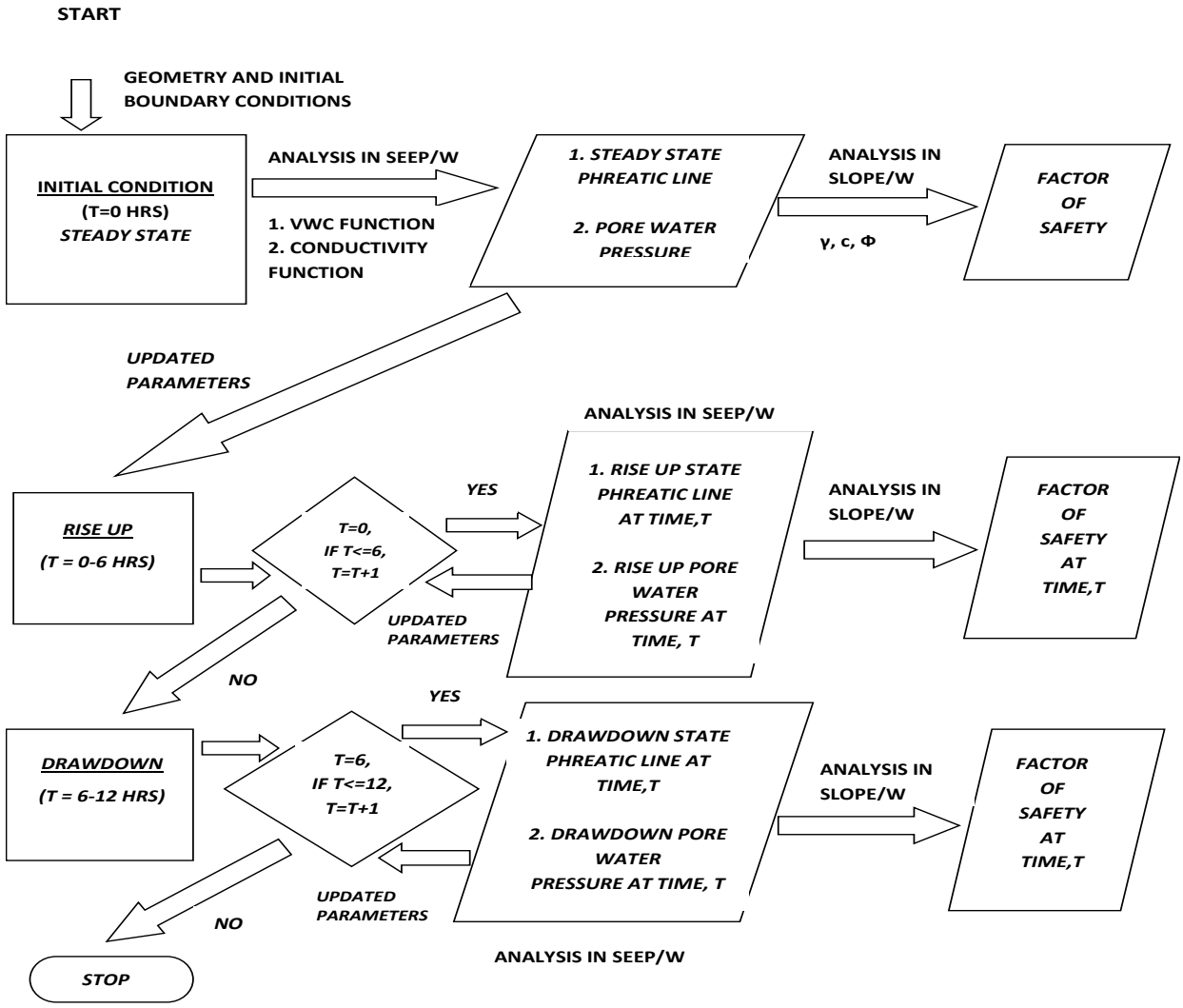

Figure. 3.9: Flowchart Defining Methodology followed during seepage analysis

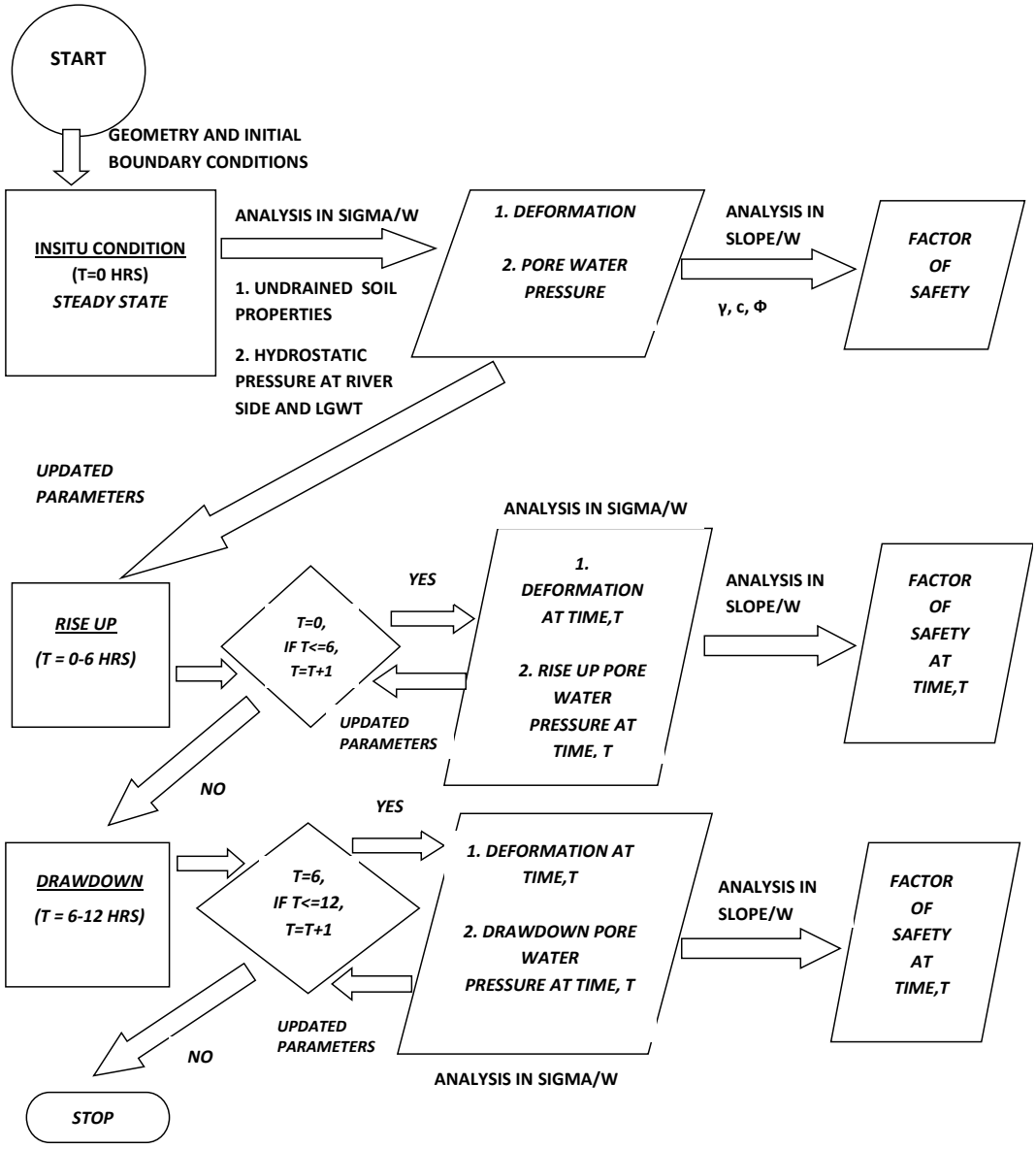

Figure. 3.10: Flowchart Defining Methodology followed during analysis in SIGMA/W

3.6 PRESENTATION OF NUMERICAL RESULTS:

The seepage analysis in the present study has been carried out considering different cases; for both steady and transient seepage condition using the MATLAB version 2014a, FLAC 2D version 5.0, SEEP/W version 12.0. The results of numerical analyses have been furnished below.

3.6.1 PHREATIC SURFACE AND FLOWNET IN STEADY STATE CONDITION (WITH OUT CUT OFF)

3.6.1.1. PRESENTATION OF RESULTS FROM MATLAB

The flownet obtained by MATLAB software under steady state condition with working head of 3.5 m have been presented in Figure 3.11 for the earthen dam without sheet pile condition. The variation of the flownet in upstream side with respect to working head condition has also been shown in the respective figures.

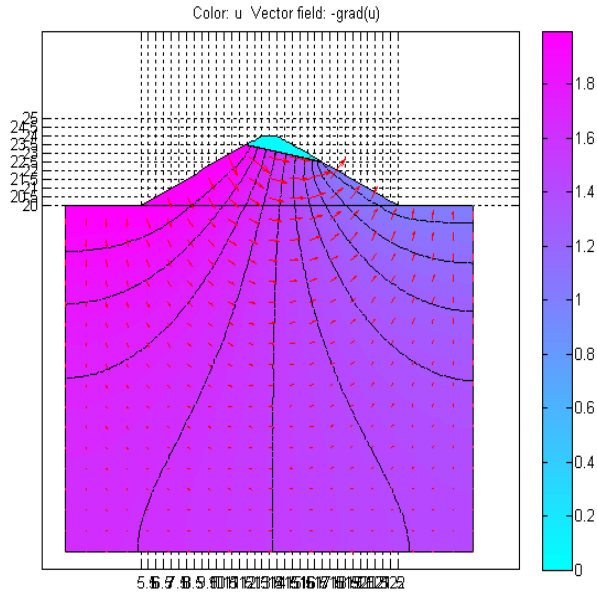

Figure. 3.11: Steady State seepage condition for working head of 3.5 m

3.6.1.2. PRESENTATION OF RESULTS FROM FLAC 2D

The flownet under similar condition without sheet pile condition under steady state condition has been presented in Figure 3.12 using FLAC 2D respectively. It appears from the figures that the corresponding flownets for without sheet pile condition obtained from FLAC 2D match with MATLAB and SEEP/W results each other.

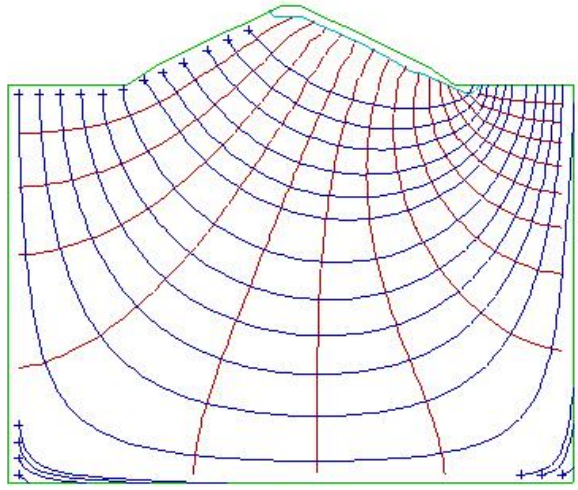

Figure. 3.12: Steady State seepage condition for working head of 3.5 m

3.6.1.3. PRESENTATION OF RESULTS FROM SEEP/W

The flownet without sheet pile condition under steady state condition has been presented in Figure 3.13 using SEEP/W respectively. The patterns of the flownets are similar as obtained from FLAC 2D, SEEP/W and MATLAB. Hence it may be inferred that the boundary conditions are properly modeled.

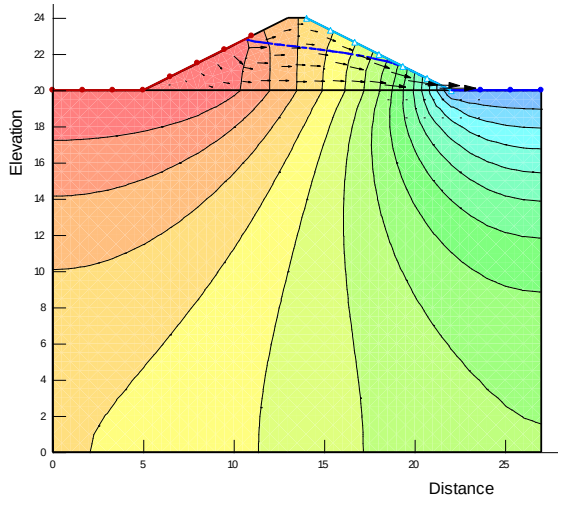

Figure. 3.13: Steady State seepage condition for working head of 3.5 m

3.6.2PHREATIC SURFACE AND FLOWNET IN STEADY STATE CONDITION (WITH CUT OFF)

3.6.2.1. PRESENTATION OF RESULTS FROM MATLAB

Figure 3.14(a) to 3.14(d) presents flownet for the model embankment with sheet pile of length 5m, 10m, 15m and 20m respectively for position of sheet pile at *B*/8 from the downstream end of the dam. Figure 3.14(e) to 3.14(h) presents flownet for the model embankment with sheet pile of length 5m, 10m, 15m and 20m respectively for position of sheet pile at 2*B*/8 from the downstream end of the dam. Figure 3.14(i) to 3.14(l) presents flownet for the model embankment with sheet pile of length 5m, 10m, 15m and 20m respectively for position of sheet pile at 3*B*/8 from the downstream end of the dam. Where *B* represents bottom width of the dam. The variation of the flownet in upstream side with respect to working head condition has also been shown in the respective figures.

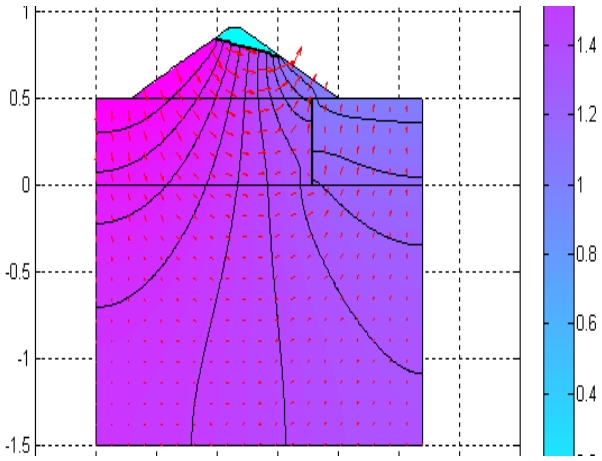

Figure. 3.14(a): Steady State seepage condition (for 5m long sheet pile *B*/8 position from downstream end) working head of 3.5 m

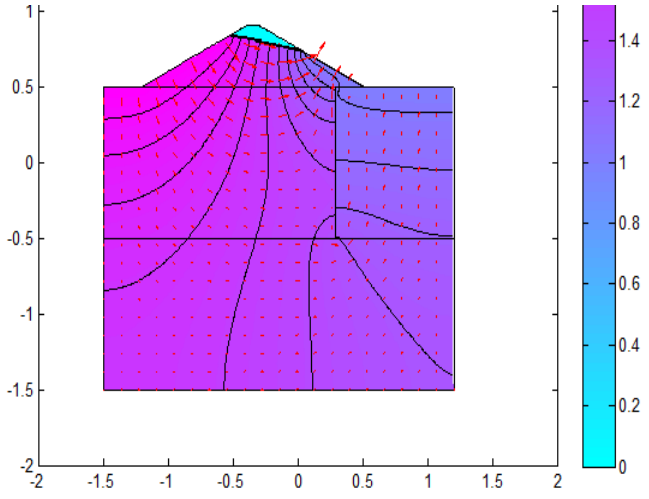

Figure. 3.14(b): Steady State seepage condition (for 10m long sheet pile *B*/8 position from downstream end) for working head of 3.5 m

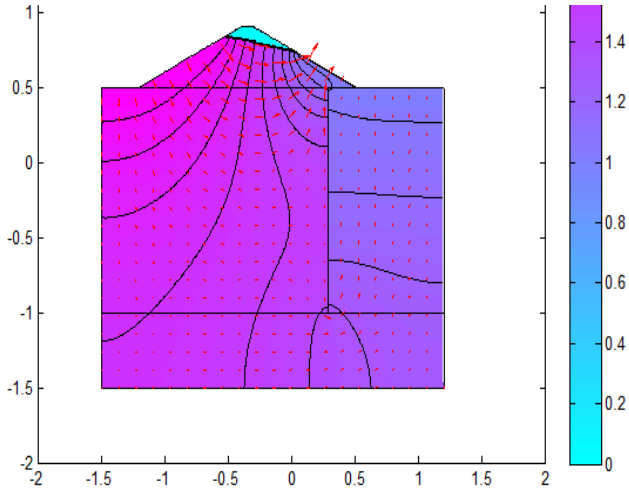

Figure. 3.14(c): Steady State seepage condition (for 15m long sheet pile *B*/8 position from downstream end) working

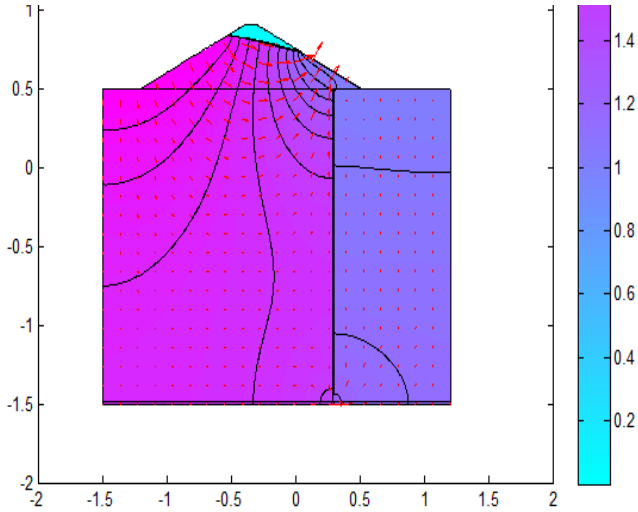

Figure. 3.14(d): Steady State seepage condition (for 20m long sheet pile *B*/8 position from downstream end) working

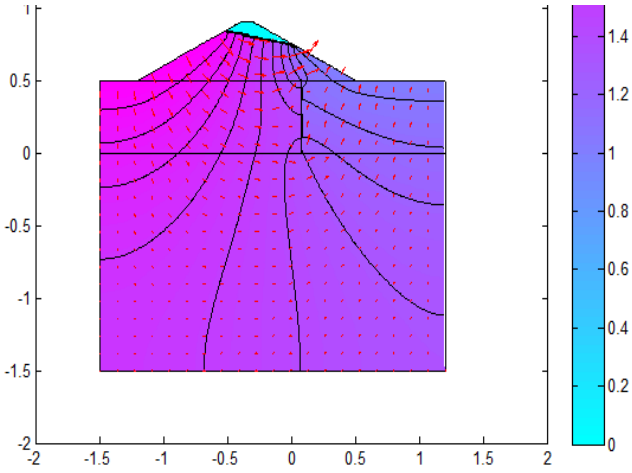

Figure.3.14(e): Steady State seepage condition (for 5m long sheet pile 2*B*/8 position from downstream end) working head of 3.5 m

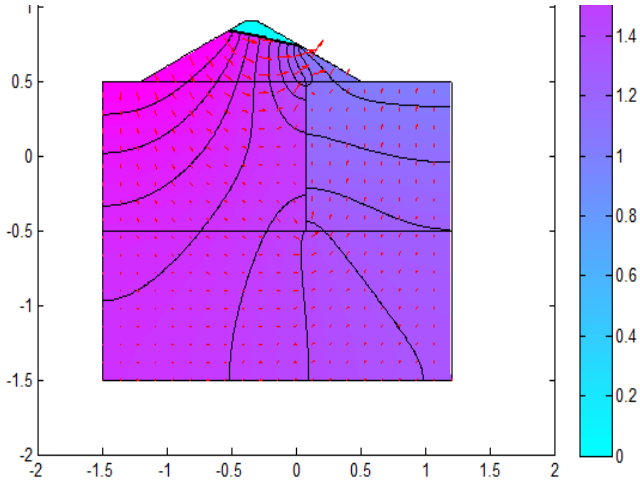

Figure.3.14(f): Steady State seepage condition (for 10m long sheet pile 2*B*/8 position from downstream end) working head of 3.5 m

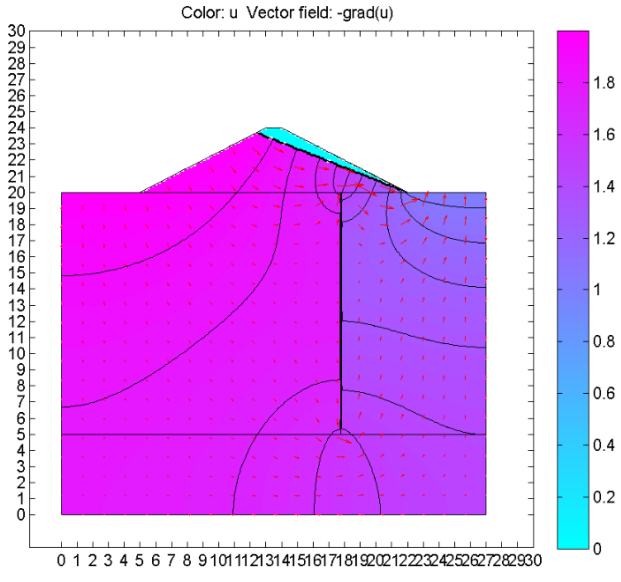

Figure.3.14(g): Steady State seepage condition (for 15m long sheet pile 2*B*/8 position from downstream end) working head of 3.5 m

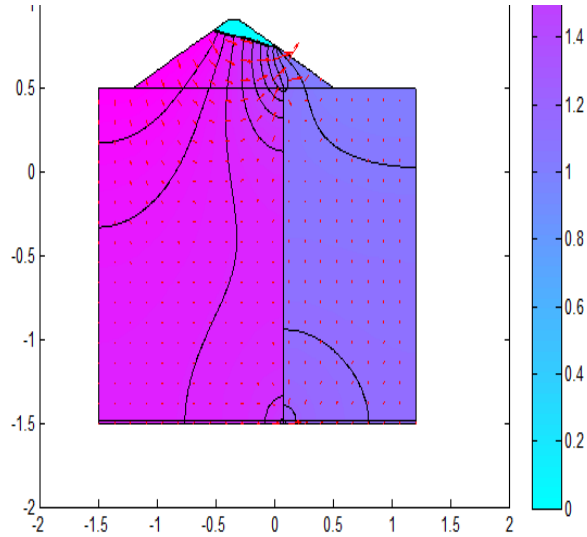

Figure.3.14(h): Steady State seepage condition (for 20m long sheet pile 2*B*/8 position from downstream end) working head of 3.5 m

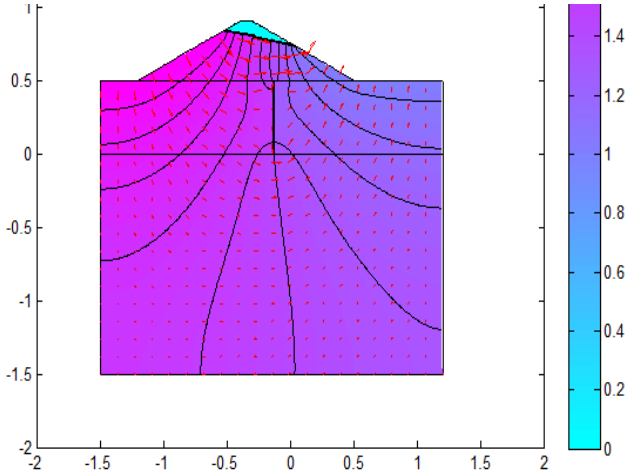

Figure.3.14(i): Steady State seepage condition (for 5m long sheet pile 3*B*/8 position from downstream end) working head of 3.5 m

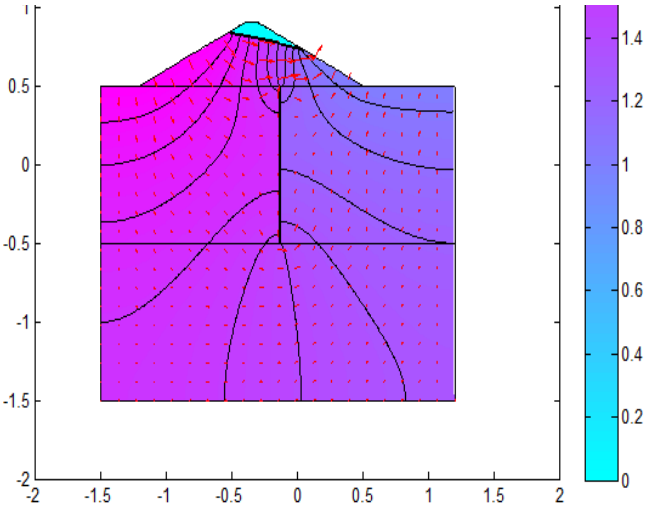

Figure.3.14(j): Steady State seepage condition (for 10m long sheet pile 3*B*/8 position from downstream end) working head of 3.5 m

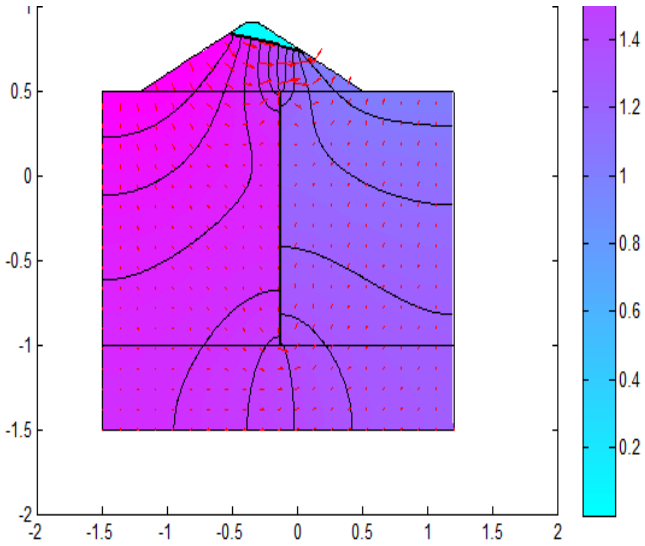

Figure.3.14(k): Steady State seepage condition (for 15m long sheet pile 3*B*/8 position from downstream end) working head of 3.5 m

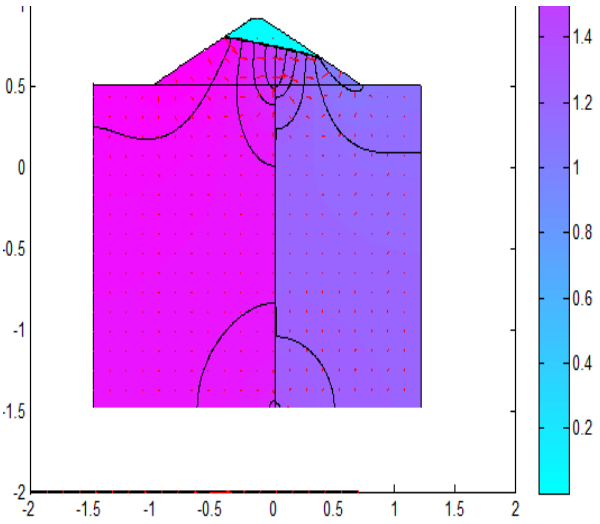

Figure.3.14(l): Steady State seepage condition (for 15m long sheet pile 3*B*/8 position from downstream end) working head of 3.5 m

3.6.2.2. PRESENTATION OF RESULTS FROM FLAC 2D

The flownet without sheet pile condition under steady state for working head of 3.5 m has been presented in this section using FLAC 2D in this section. Figure 3.15(a), Figure 3.15(b), 3.15(c) and 3.15(d) represent the flownet for earthen dam with sheet pile condition for *B*/8 position 5m, 10m, 15 m length, 20 m length respectively. Figure 3.15(e), Figure 3.15(f), 3.15(g) and 3.15(h) represent the earthen dam with sheet pile condition for 2*B*/8 position 5m, 10m, 15 m length, 20 m length respectively. Figure 3.14(i), Figure 3.14(j), 3.15(k) and 3.15(l) represent the earthen dam with sheet pile condition for 3*B*/8 position 5m, 10m, 15 m length, 20 m length respectively.

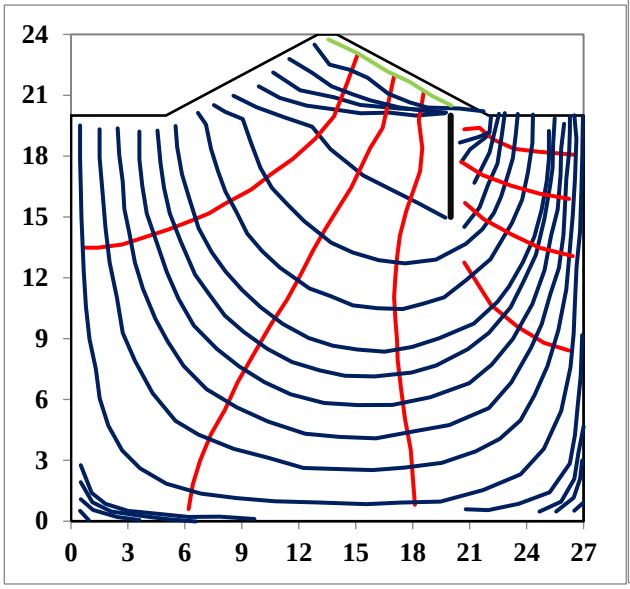

Figure 3.15(a): Steady State seepage condition (for 5m long sheet pile *B*/8 position from downstream end) working head of 3.5 m

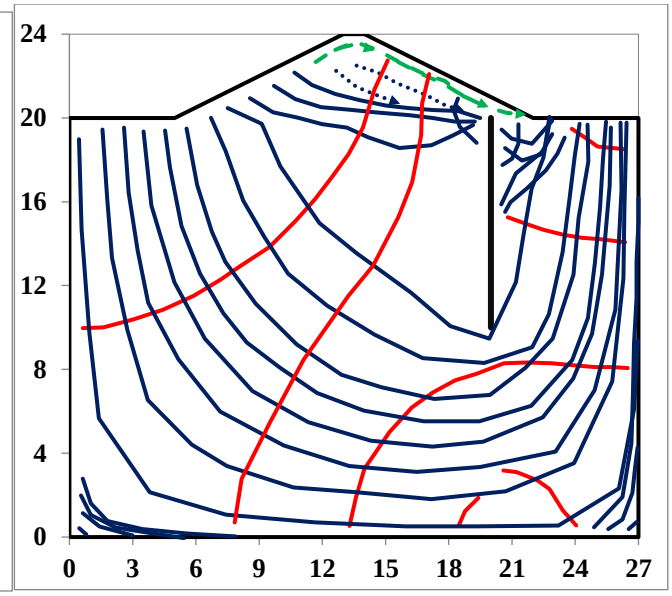

Figure 3.15(b): Steady State seepage condition (for 10 m long sheet pile *B*/8 position from downstream end) working head of 3.5 m

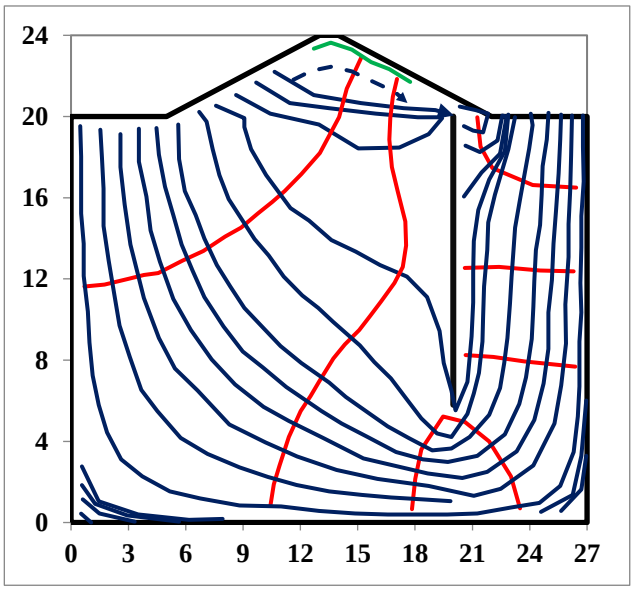

Figure 3.15(c): Steady State seepage condition (for 15 m long sheet pile *B*/8 position from downstream end) working head of 3.5 m

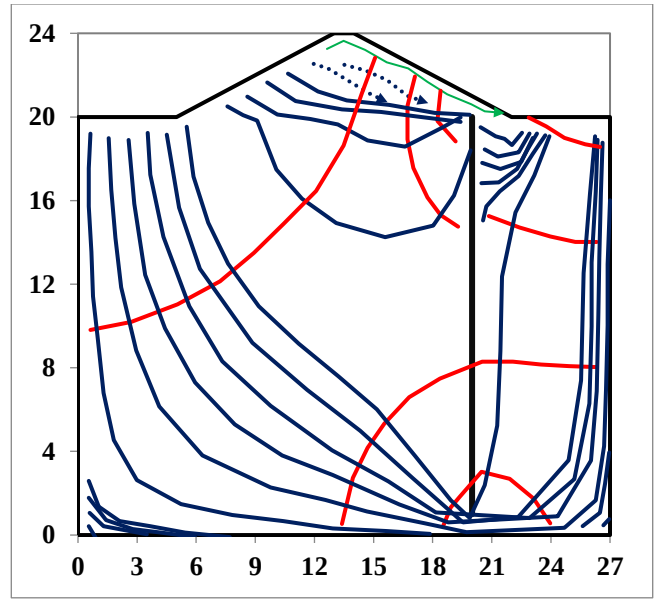

Figure 3.15(d): Steady State seepage condition (for 20 m long sheet pile *B*/8 position from downstream end) working

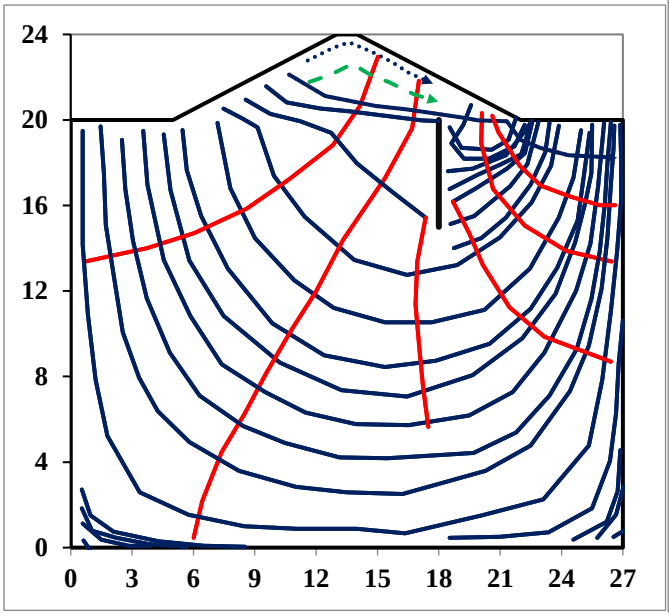

Figure 3.15(e): Steady State seepage condition (for 5m long sheet pile 2*B*/8 position from downstream end) working head of 3.5 m

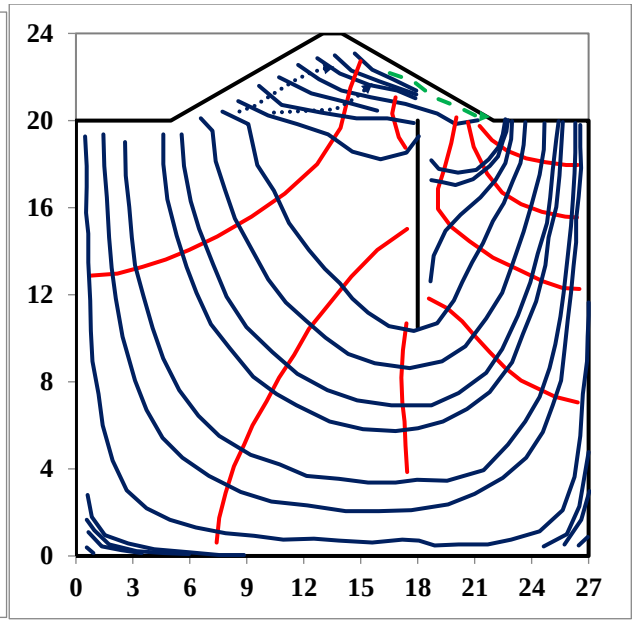

Figure 3.15(f): Steady State seepage condition (for 10 m long sheet pile 2*B*/8 position from downstream end) working head of 3.5 m

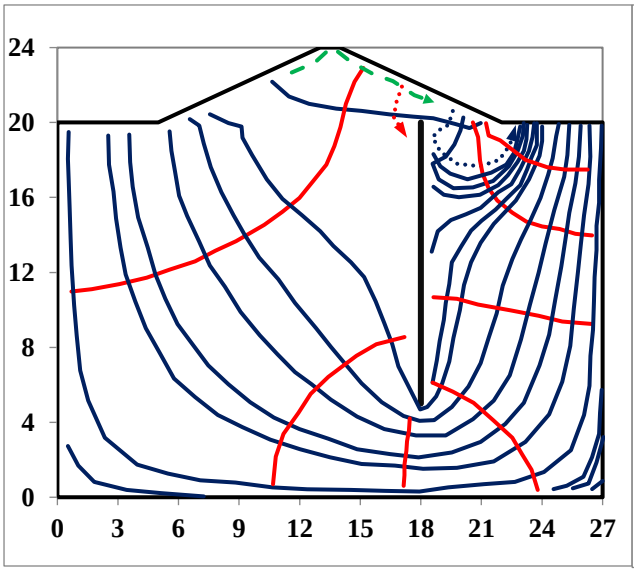

Figure 3.15(g): Steady State seepage condition (for 15 m long sheet pile 2*B*/8 position from downstream end) working head of 3.5 m

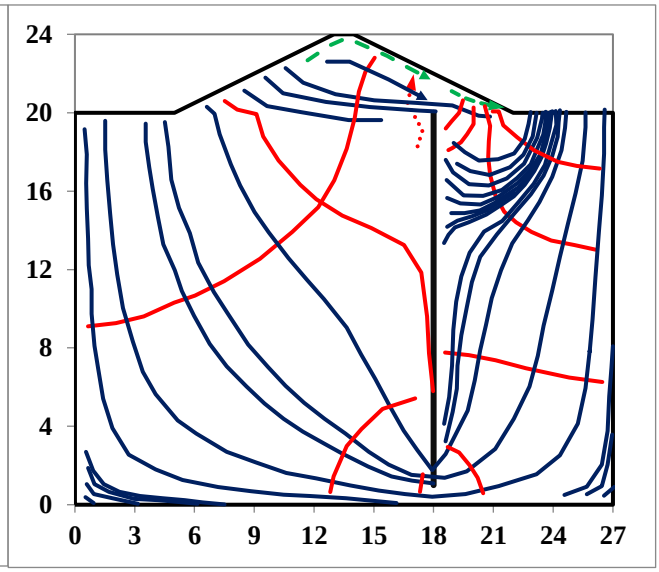

Figure 3.15(h): Steady State seepage condition (for 20 m long sheet pile 2*B*/8 position from downstream end) working head

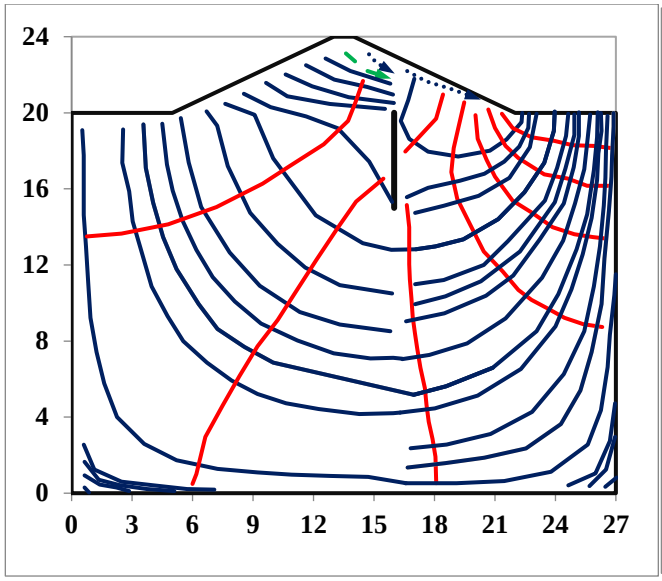

Figure 3.15(i): Steady State seepage condition (for 5 m long sheet pile 3*B*/8 position from downstream end) working head of 3.5 m

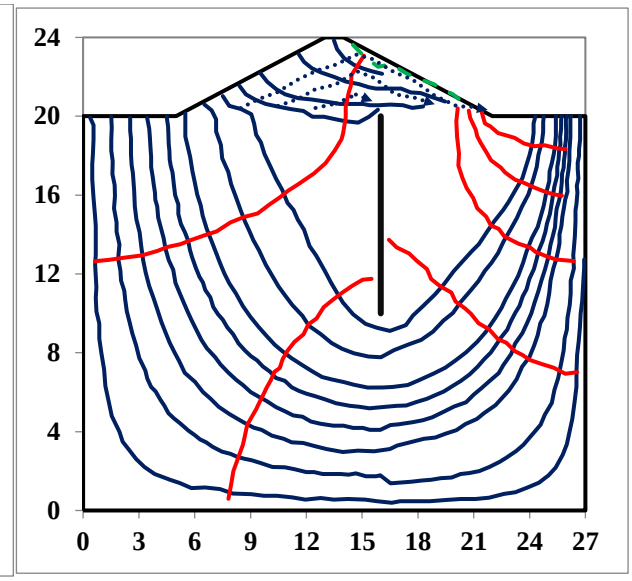

Figure 3.15(j): Steady State seepage condition (for 10 m long sheet pile 3*B*/8 position from downstream end) working head of 3.5 m

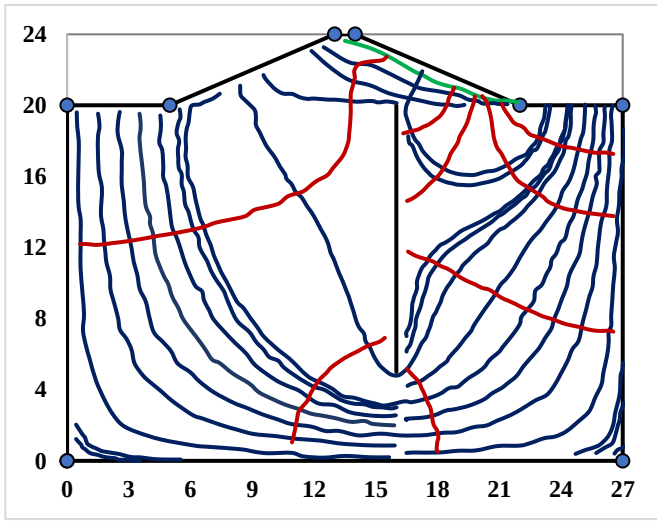

Figure 3.15(k): Steady State seepage condition (for 15 m long sheet pile 3*B*/8 position from downstream end) working head of 3.5 m

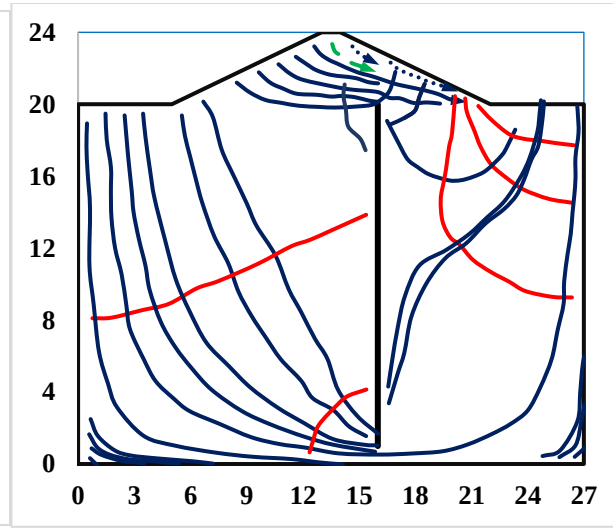

Figure 3.15(l): Steady State seepage condition (for 20 m long sheet pile 3*B*/8 position from downstream end) working head of 3.5 m

3.6.2.3. PRESENTATION OF RESULTS FROM SEEP/W

The steady state analysis in each case has been considered without respect to time and the distribution of total head are shown in the following figures. Figure 3.16(a), Figure 3.16(b), 3.16(c), 3.16(d) represents the flownet for the earthen dam with sheet pile condition for *B*/8 position 5m,

10m, 15 m length, 20 m length respectively. Figure 3.16(e), Figure 3.16(f), 3.16(g), 3.16(h) represents the flownet for earthen dam with sheet pile condition for 2*B*/8 position 5m, 10m, 15 m length, 20 m length respectively. Figure 3.16(i), Figure 3.16(j), 3.16(k), 3.16(l) represents the flownet for earthen dam with sheet pile condition for 3*B*/8 position 5m, 10m, 15 m length, 20 m length respectively. The phreatic surface has been painted as a thick blue line, which smoothly across the dam. The vertical lines are the total head isolines begin at from downstream to upstream. The stream line has been obtained in case of steady seepage analysis with cut off as a barrier. It has been shown that above the phreatic surface there are isolines at negative values, which is because of the suction considered in the software by default.

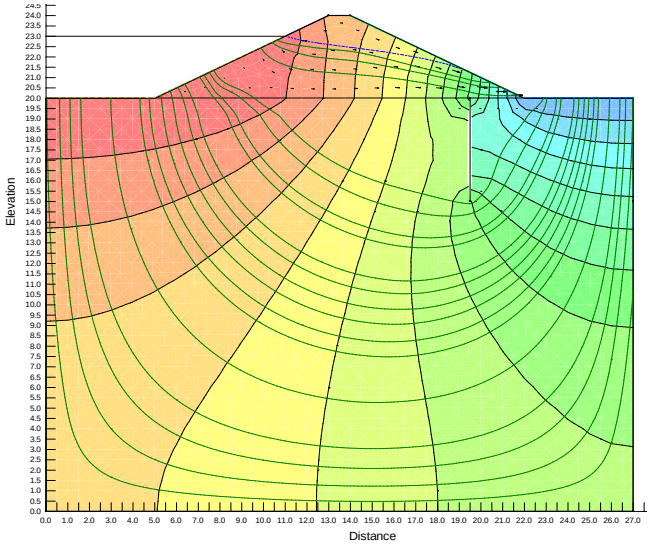

Figure 3.16(a): Steady State seepage condition (for 5 m long sheet pile *B*/8 position from downstream end) working head of 3.5

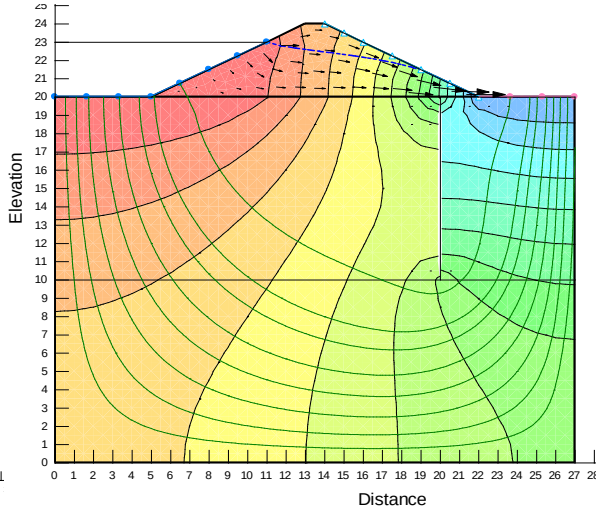

Figure 3.16(b): Steady State seepage condition (for 10 m long sheet pile *B*/8 position from downstream end) working head of 3.5 m

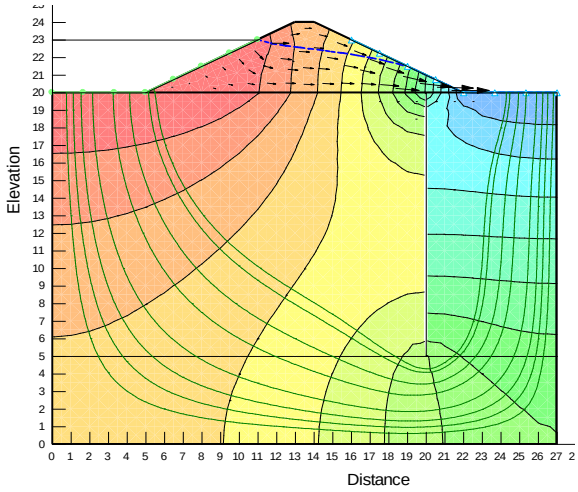

Figure 3.16(c): Steady State seepage condition (for 15 m long sheet pile *B*/8 position from downstream end) working head of 3.5 m

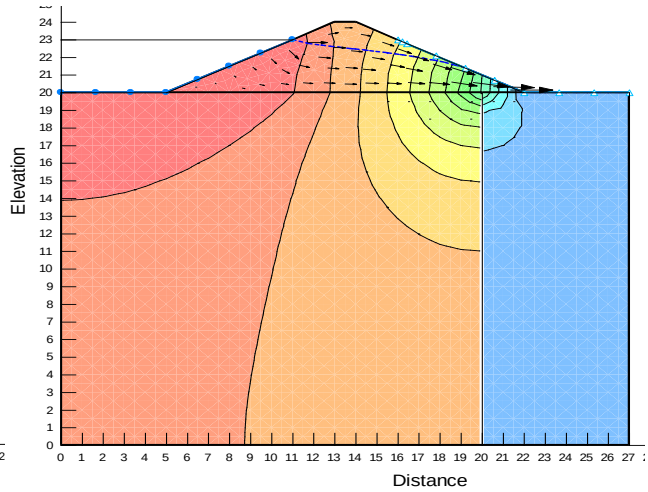

Figure 3.16(d): Steady State seepage condition (for 20 m long sheet pile *B*/8 position from downstream end) working head of 3.5 m

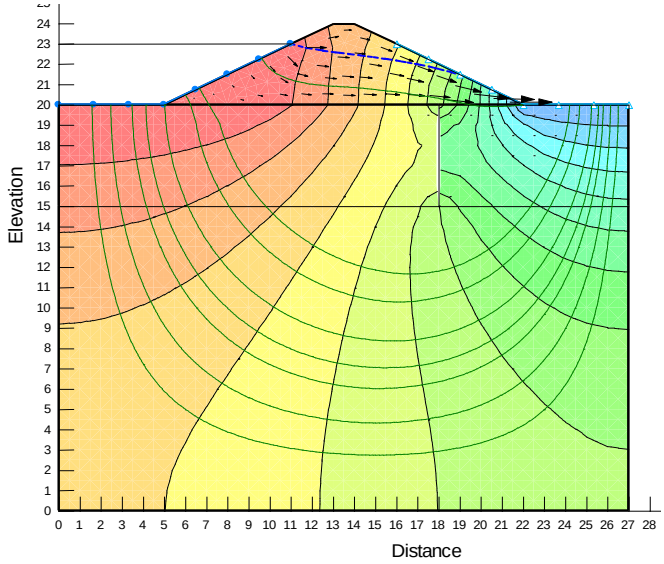

Figure 3.16(e): Steady State seepage condition (for 5 m long sheet pile 2*B*/8 position from downstream end) working head of 3.5 m

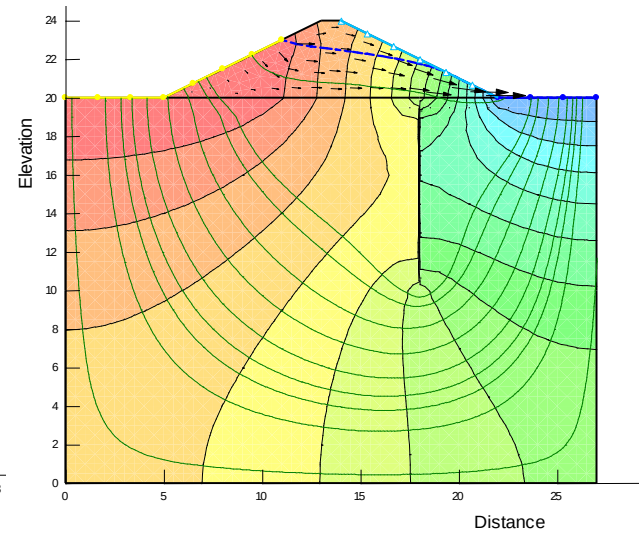

Figure 3.16(f): Steady State seepage condition (for 10 m long sheet pile 2*B*/8 position from downstream end) working

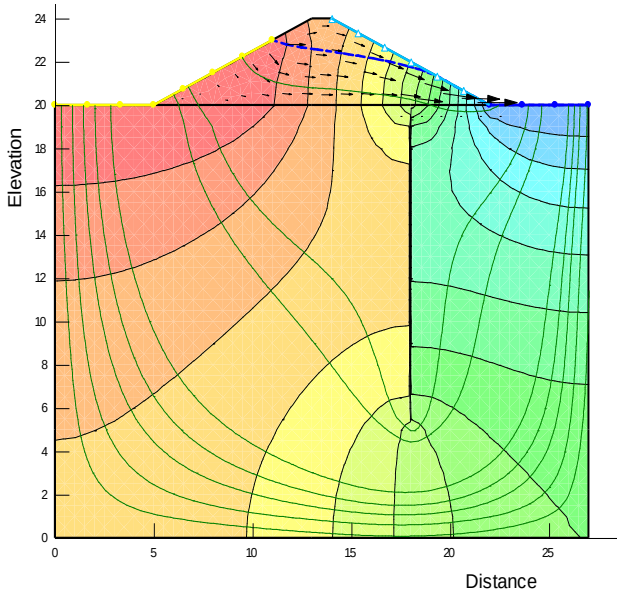

Figure 3.16(g): Steady State seepage condition (for 15 m long sheet pile 2*B*/8 position from downstream end) working head of 3.5 m

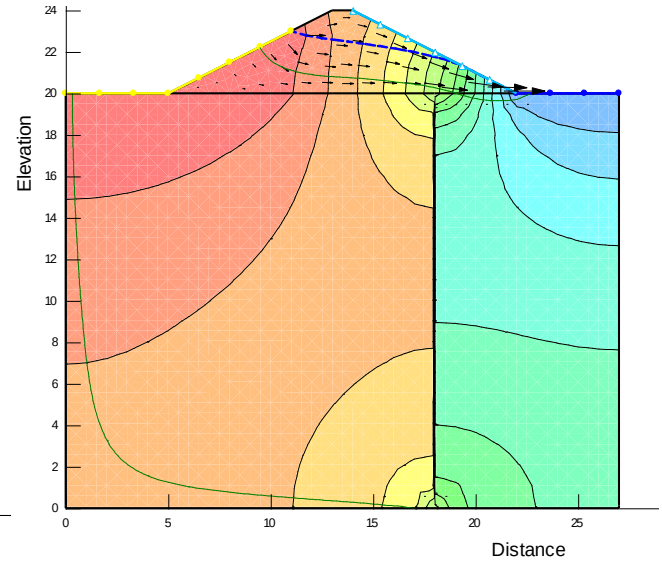

Figure 3.16(h): Steady State seepage condition (for 20 m long sheet pile 2*B*/8 position from downstream end) working head of 3.5 m

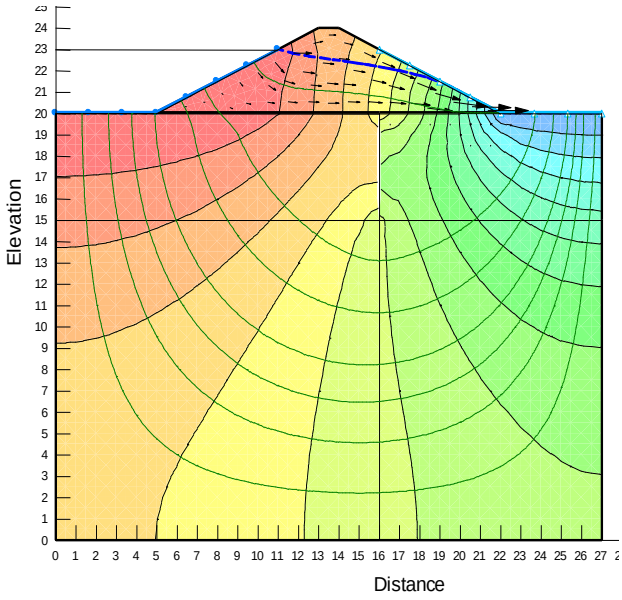

Figure 3.16(i): Steady State seepage condition (for 5 m long sheet pile 3*B*/8 position from downstream end) working head of 3.5 m

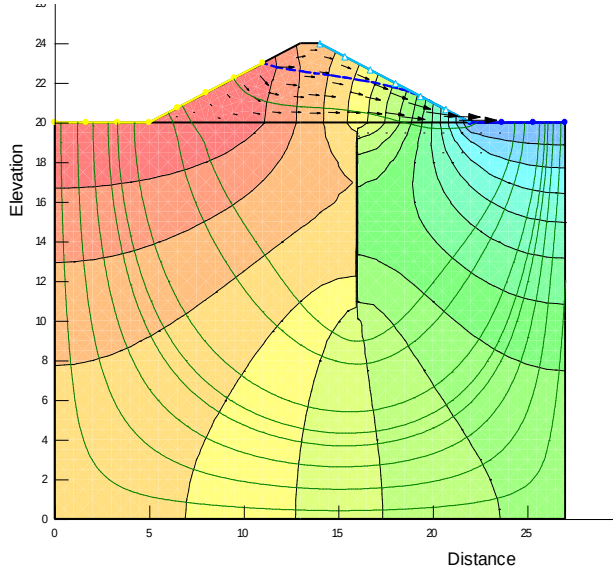

Figure 3.16(j): Steady State seepage condition (for 10 m long sheet pile 3*B*/8 position from downstream end) working head of 3.5 m

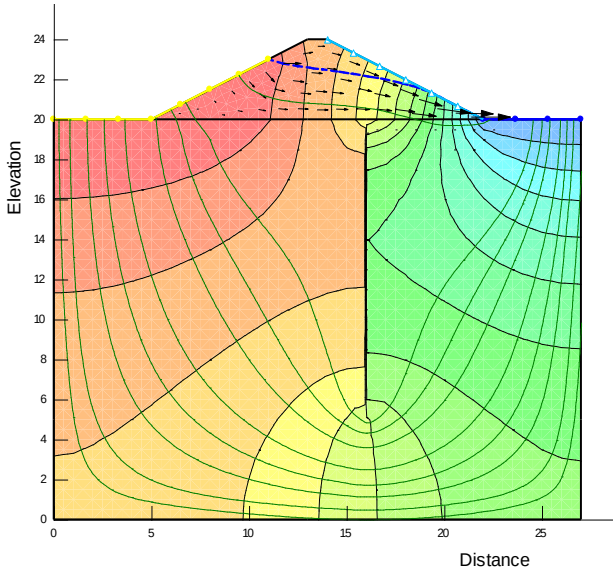

Figure 3.16(k): Steady State seepage condition (for 15 m long sheet pile 3*B*/8 position from downstream end) working head of 3.5 m

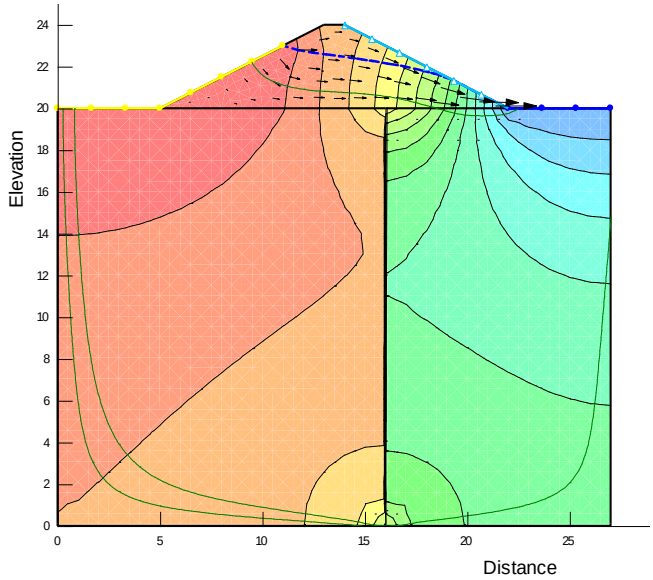

Figure 3.16(l): Steady State seepage condition (for 20 m long sheet pile 3*B*/8 position from downstream end) working head of 3.5 m

3.6.3 DYNAMICS OF PHREATIC SURFACE AND FLOWNET SINGLE TIDAL CYCLE: EFFECT OF RISE UP AND DRAWDOWN RATE (WITH OUT CUT OFF)

The analysis for transient cases is actually an unsteady analysis taking steady-state as the initial condition. In this present study, the water level fluctuates to 4 meters in 6 hours in upstream side of earthen embankment to EGL. In the modeling of Rise up condition final stage of Drawdown condition has been taken as initial condition. In drawdown condition unstable seepage have been developed due to the changes of pore-water pressures at different points. The unsaturated region continuously reflected that the location of phreatic line intermittently dropped and has a tendency to be stable with the elapse of the time.

3.6.3.1 PRESENTATION OF RESULTS FROM MATLAB

During single cycle tests with different rates of Rise Up / Drawdown the variation in dynamics in flownet has been shown in **Figures –3.17(a),3.17(b),3.17(c),3.17(d)** for different time interval under rise up and drawdown conditions. The variation of the flownet in upstream side with respect to cycle time has also been shown in the respective figures obtained from MATLAB. The LTL has been kept at zero position and HTL has been kept as 3.5 m from the base. The increase and decrease in water level from LTL to HTL and HTL to LTL respectively have been considered in the present analyses.

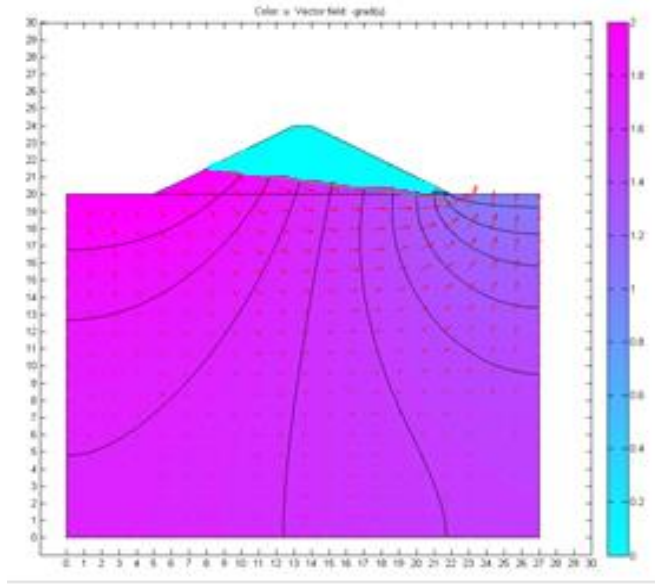

Figures – 3.17(a): Development of phreatic surface for 1 Hour

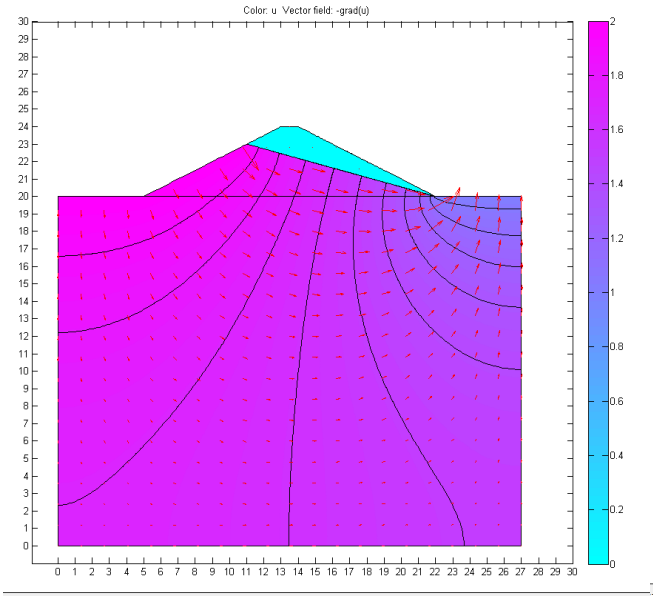

Figures – 3.17(b): Development of phreatic surface for 5 Hour

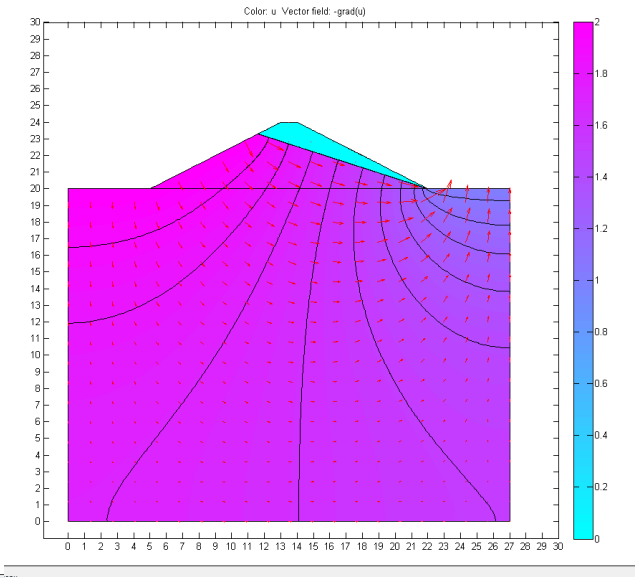

Figures – 3.17(c): Development of phreatic surface for 6 Hour

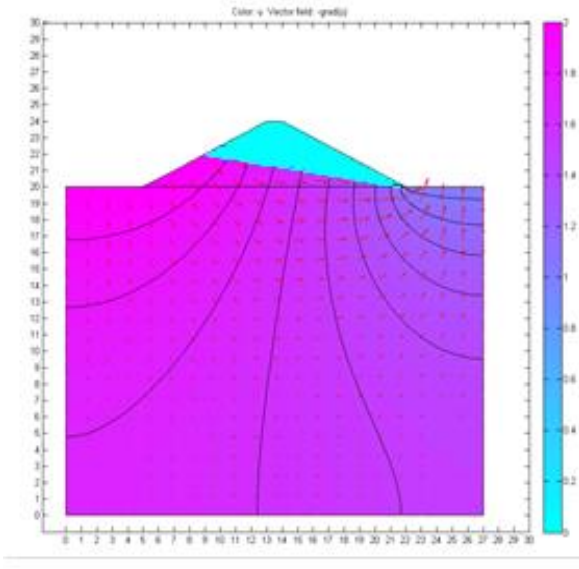

Figure 3.17(d): Development of phreatic surface for 10 Hours

3.6.3.2 PRESENTATION OF RESULTS FROM FLAC 2D

During single cycle tests with different rates of Rise up / Drawdown, the variation in dynamics in flownet has been shown in **Figures –3.18(a),3.18(b),3.18(c),3.18(d),3.18(e),3.18(f),3.18(g)** for different time intervals. The variation of the flownet in upstream side with respect to cycle time has also been shown in the respective figures obtained from FLAC 2D.

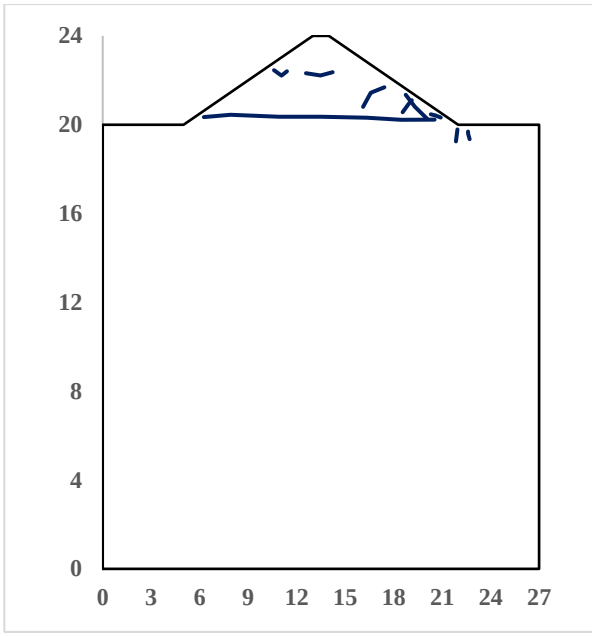

Figure 3.18(a): (Flownet under Rise up condition for without sheet pile condition, time = 1.0 hr.)

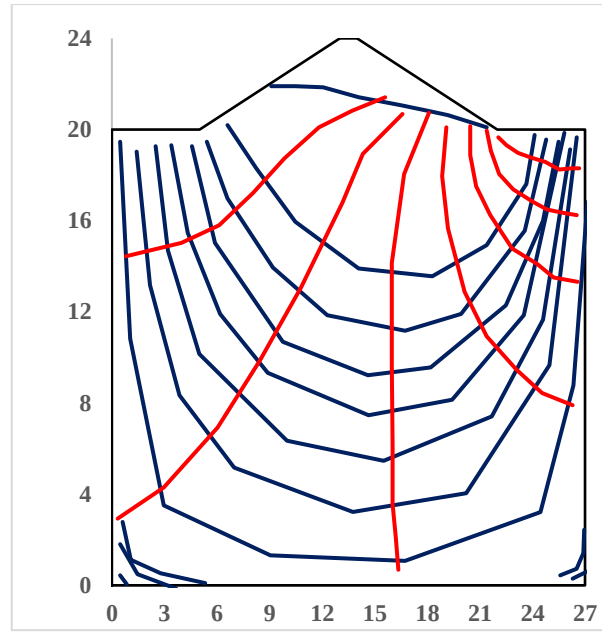

Figure 3.18(b): (Flownet under Rise up condition for without sheet pile condition, time = 3.0 hrs.)

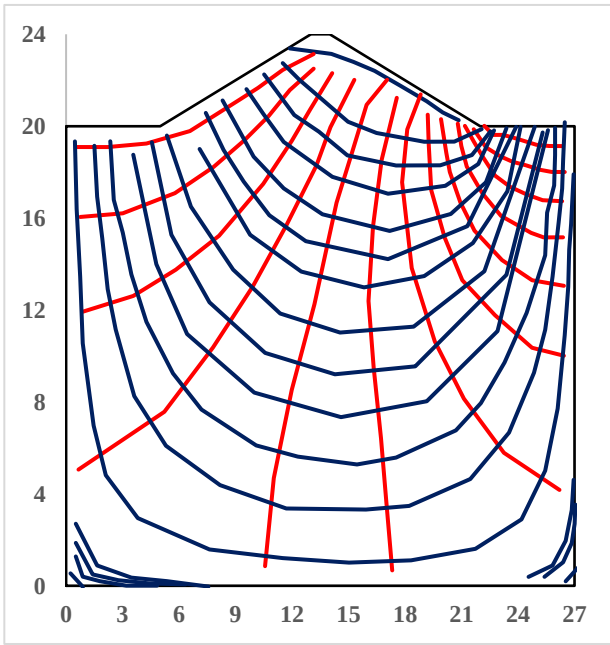

Figure 3.18(c): (Flownet under Rise up condition for without sheet pile condition, time = 5.0 hrs.)

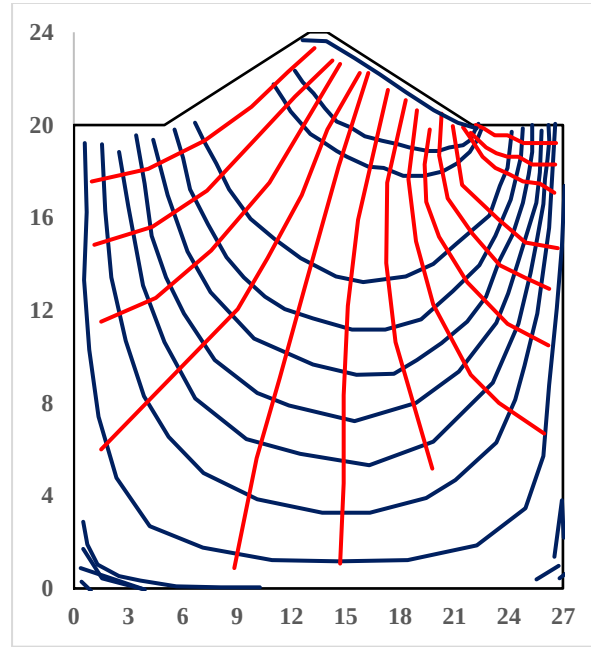

Figure 3.18(d): (Flownet under Rise up condition for without sheet pile condition, time = 6.0 hrs.)

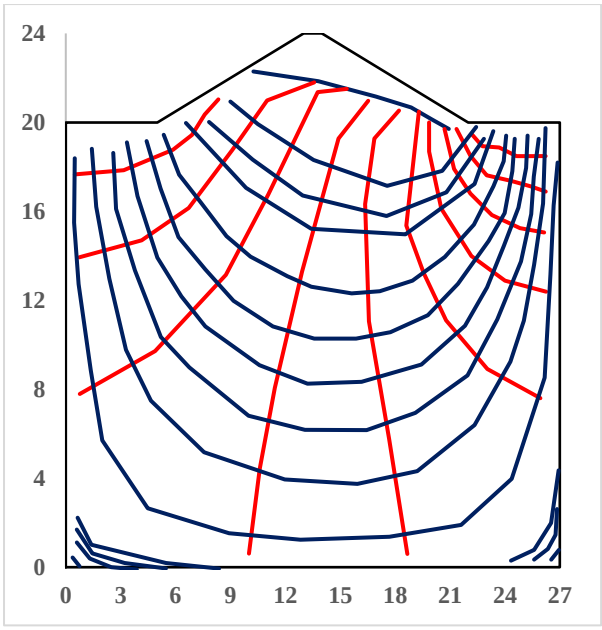

Figure 3.1(e): (Flownet under Drawdown condition for without sheet pile condition, time = 8.0 hrs.)

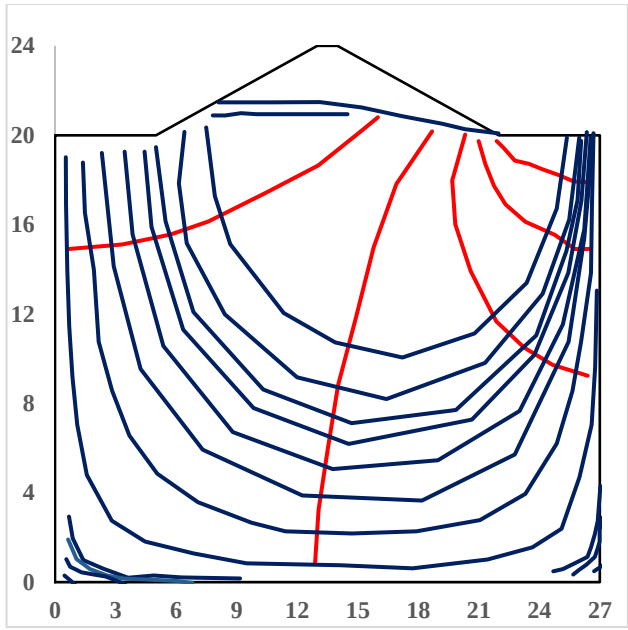

Figure 3.18(f): (Flownet under Drawdown condition for without sheet pile condition, time = 10.0 hrs.)

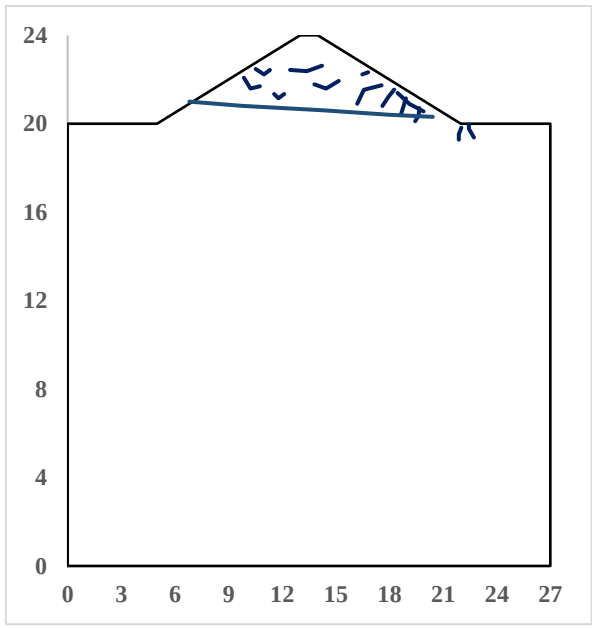

Figure 3.18(g): (Flownet under Drawdown condition for without sheet pile condition, time = 12.0 hrs.)

3.6.3.3 PRESENTATION OF RESULTS FROM SEEP/W

During single cycle tests with different rates of Rise up / Drawdown the variation in dynamics in flownet has been shown in **Figures –3.19(a),3.19(b),3.19(c),3.1(d),3.19(e),3.19(f)** for different time intervals. The variation of the flownet in upstream side with respect to cycle time has also been shown in the respective figures obtained from SEEP/W.

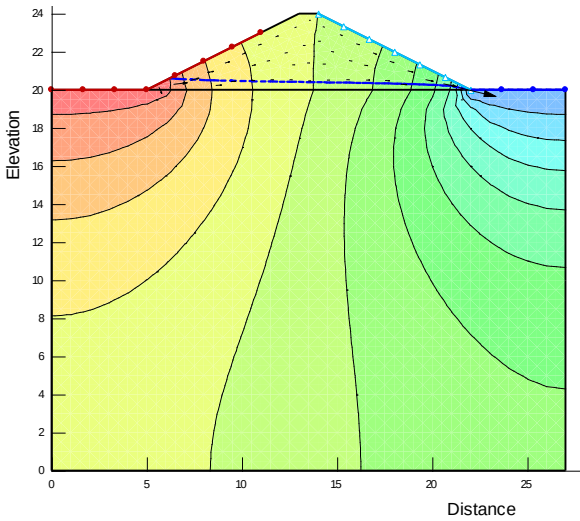

Figure 3.19(a): (Flownet under rise up condition for without sheet pile condition, time = 1 hr.)

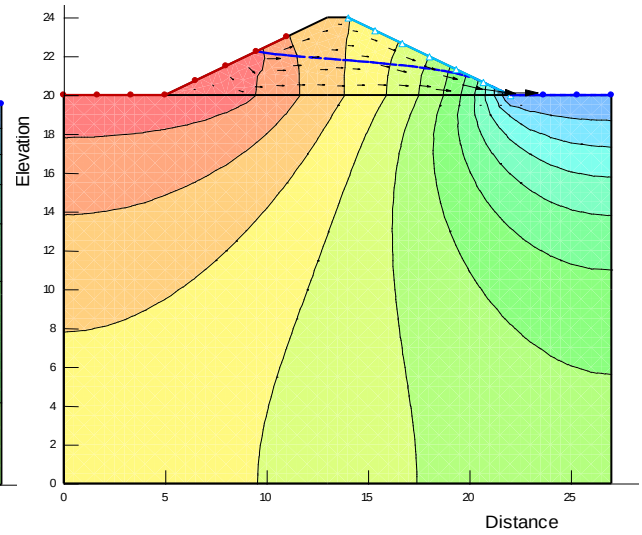

Figure 3.19(b): (Flownet under rise up condition for without sheet pile condition, time = 5 hrs.)

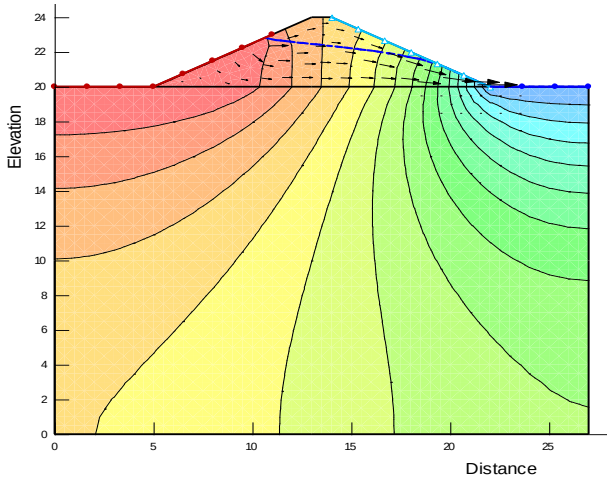

Figure 3.19(c): (Flownet under rise up condition for without sheet pile condition, time = 6 hrs.)

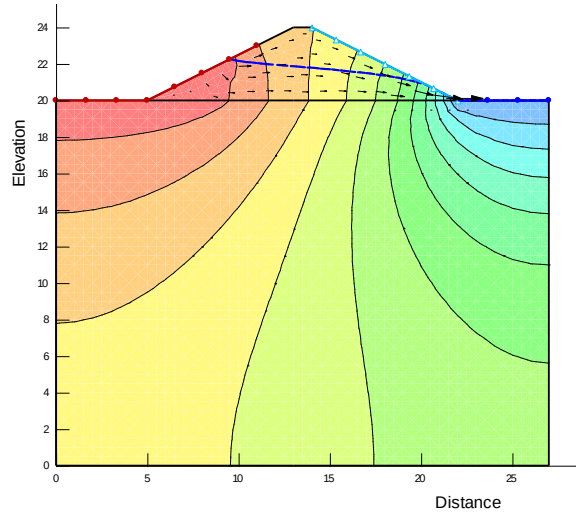

Figure 3.19(d): (Flownet under rise up condition for without sheet pile condition, time = 7 hrs.)

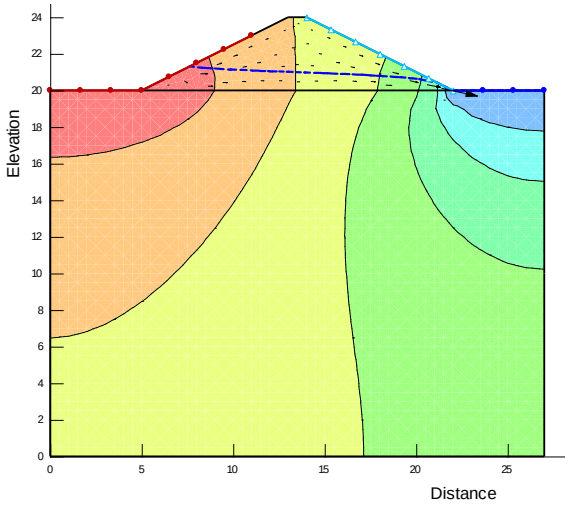

Figure 3.19(e): (Flownet under draw down condition for without sheet pile condition, time = 10 hrs.)

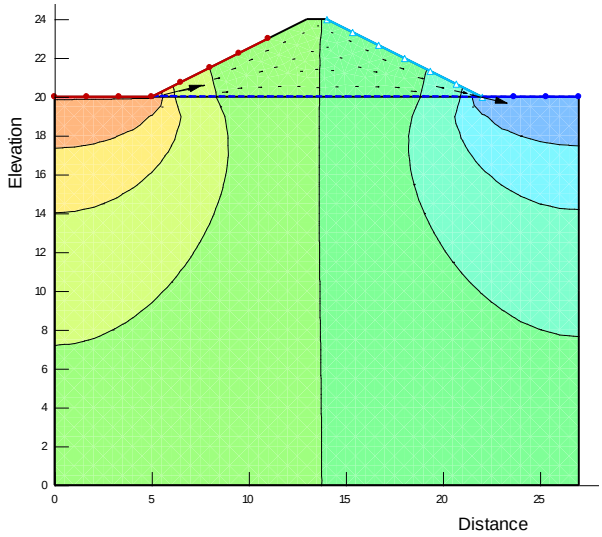

Figure 3.19(f): (Flownet under draw down condition for without sheet pile condition, time = 12 hrs.)

3.6.4 DYNAMICS OF PHREATIC SURFACE AND FLOWNET IN TRANSIENT CONDITION: RISE UP AND DRAWDOWN (WITH CUT OFF)

The transient analysis is actually an unsteady analysis taking steady-state as the initial condition. In this present study, the water level fluctuates to 3.5 meters in 6 hours in upstream side of earthen embankment to EGL. In drawdown condition unstable seepage has been developed due to the changes of pore-water pressures at different points. The unsaturated region continuously reflected that the location of phreatic line intermittently dropped and has a tendency to be stable with the lapse of the time. In the modeling of rise up, final stage of drawdown has been taken as initial head.

3.6.4.1. PRESENTATION OF RESULTS FROM MATLAB

During single cycle tests with different rates of rise up / drawdown the variation in dynamics in flownet has been discussed in this section under rise up and drawdown condition. The variation of the flownet in upstream side with respect to cycle time has also been shown in the respective figures obtained from MATLAB.

3.6.4.1.1 Presentation of results for 5 m long sheet pile at *B*/8 position from downstream end

The variation of the flownet in upstream side with respect to cycle time has also been shown in the respective **Figures –3.20(a),3.20(b),3.20(c),3.20(d),3.20(e),3.20(f),3.20(g)** obtained from MATLAB.

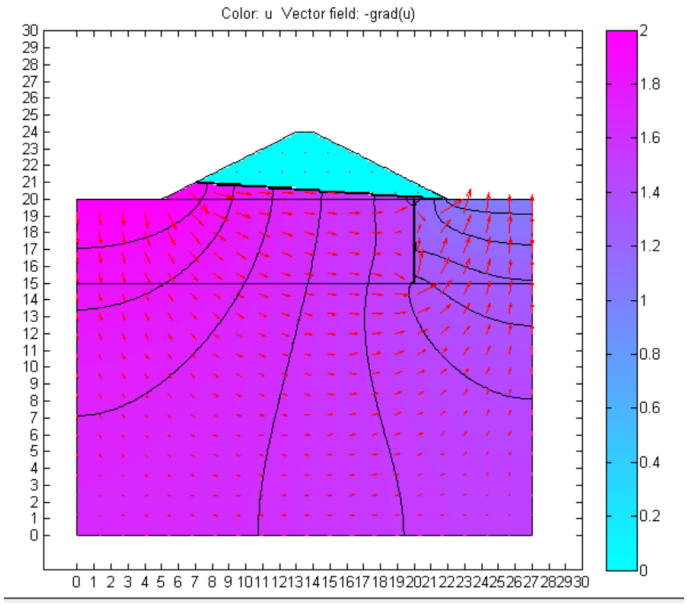

Figure 3.20(a): Flownet under Rise up condition (for 5m long sheet pile at *B*/8 from downstream end, time = 1.0 hr.)

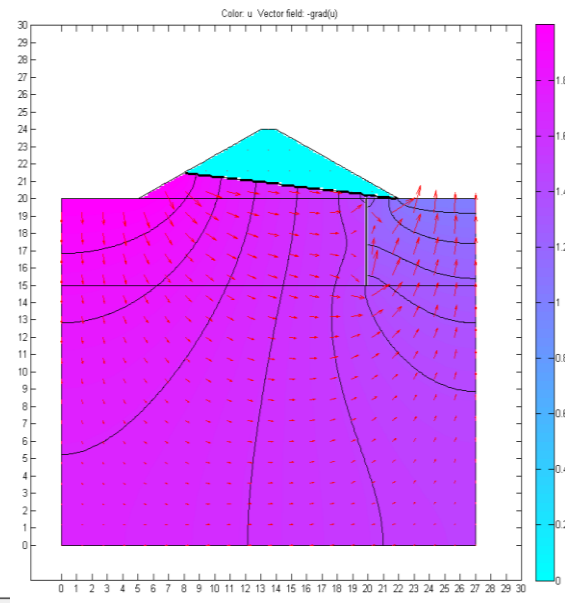

Figure 3.20(b): Flownet under Rise up condition (for 5m long sheet pile at *B*/8 from downstream end, time = 3.0 hrs.)

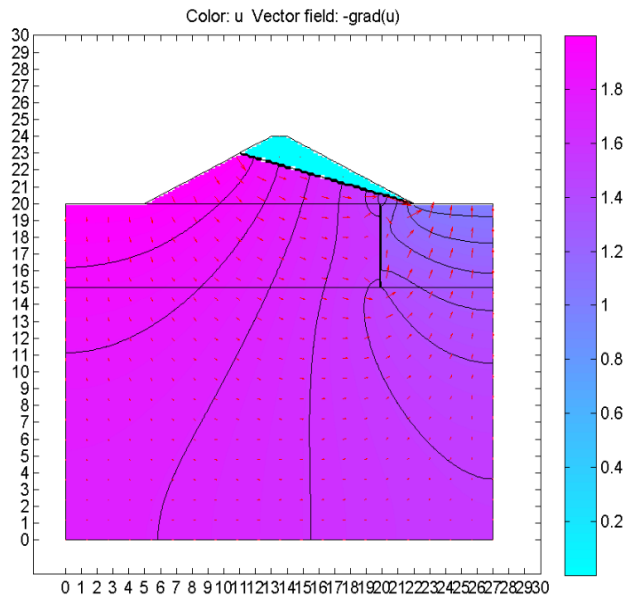

Figure 3.20(c): Flownet under Rise up condition (for 5m long sheet pile at *B*/8 from downstream end, time = 5.0 hrs.)

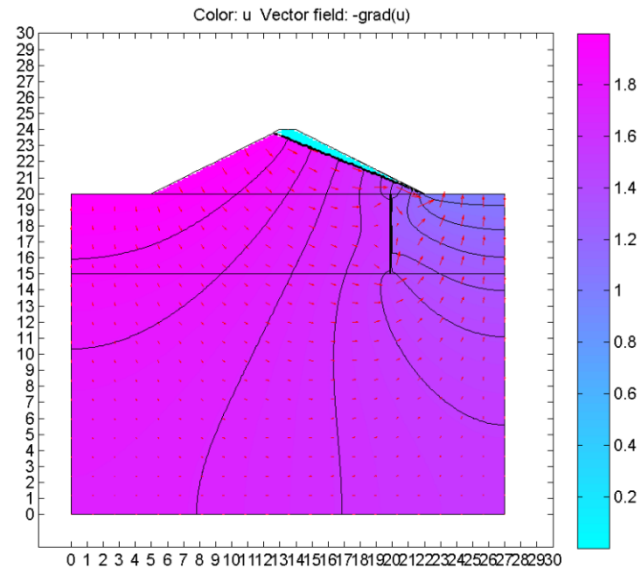

Figure 3.20(d): Flownet under Rise up condition (for 5m long sheet pile at *B*/8 from downstream end, time = 6.0 hrs.)

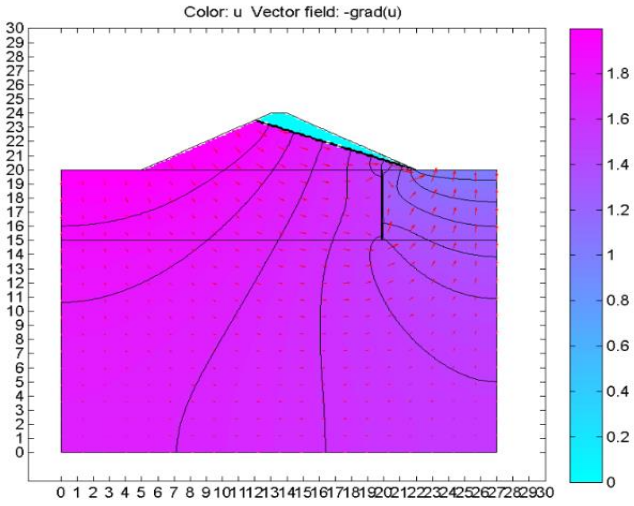

Figure 3.20(e): Flownet under Rise up condition (for 6m long sheet pile at *B*/8 from downstream end, time = 7.0 hrs.)

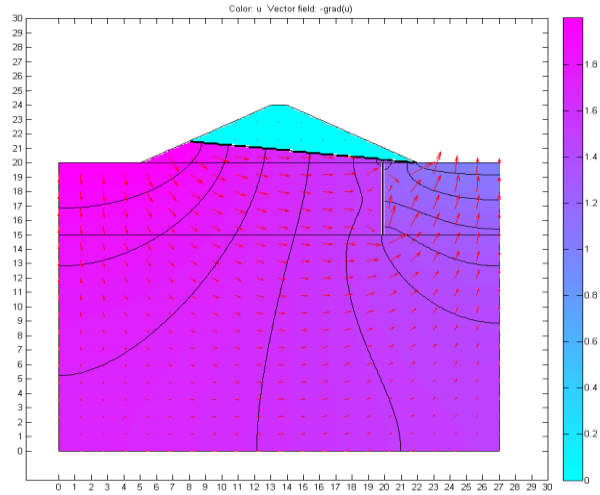

Figure 3.20(f): Flownet under Drawdown condition (for 7m long sheet pile at *B*/8 from downstream end, time = 10.0 hrs.)

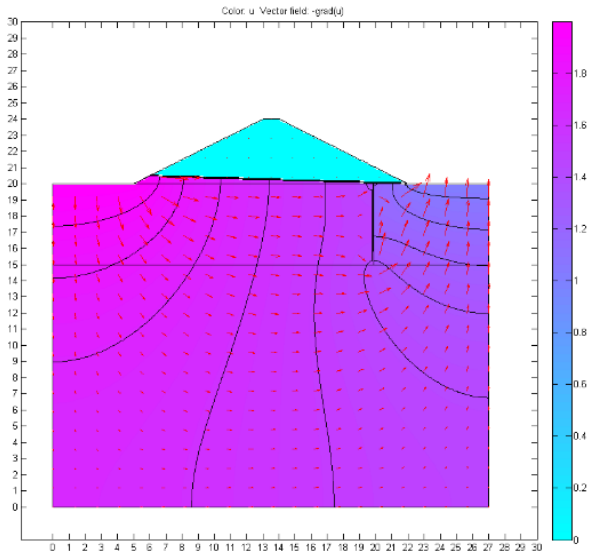

Figure 3.20(g): Flownet under Drawdown condition (for 5m long sheet pile at *B*/8 from downstream end, time = 11.0 hrs.)

3.6.4.1.2 Presentation of results for 10 m long sheet pile at *B*/8 position from downstream end

The variation of the flownet in upstream side with respect to cycle time has also been shown in the respective **Figures –3.21(a),3.21(b),3.21(c),3.21(d),3.21(e)** obtained from MATLAB.

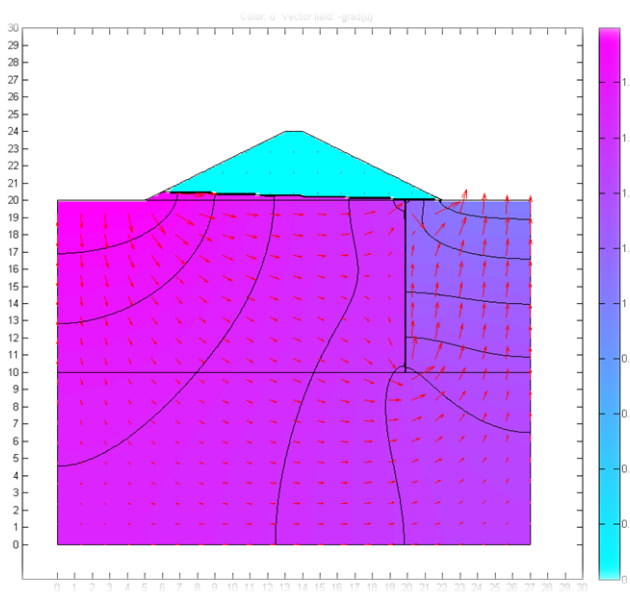

Figure 3.21(a): Flownet under Rise up condition (for 10m long sheet pile at *B*/8 from downstream end, time = 1.0 hr.)

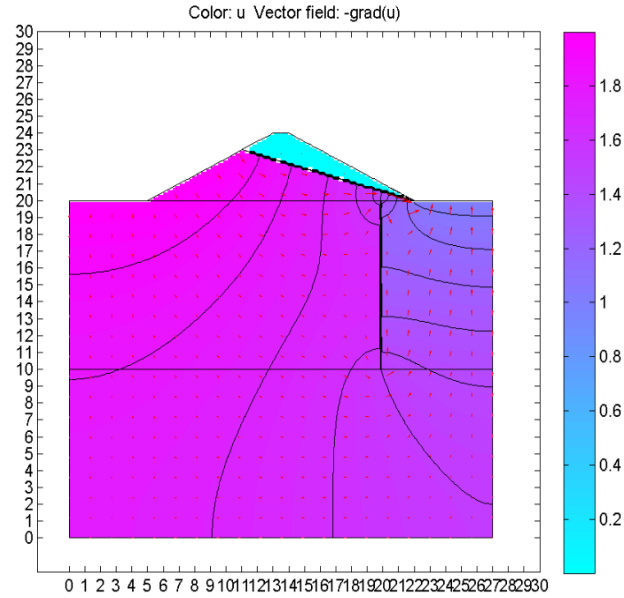

Figure 3.21(b): Flownet under Rise up condition (for 10m long sheet pile at *B*/8 from downstream end, time = 5.0 hrs.)

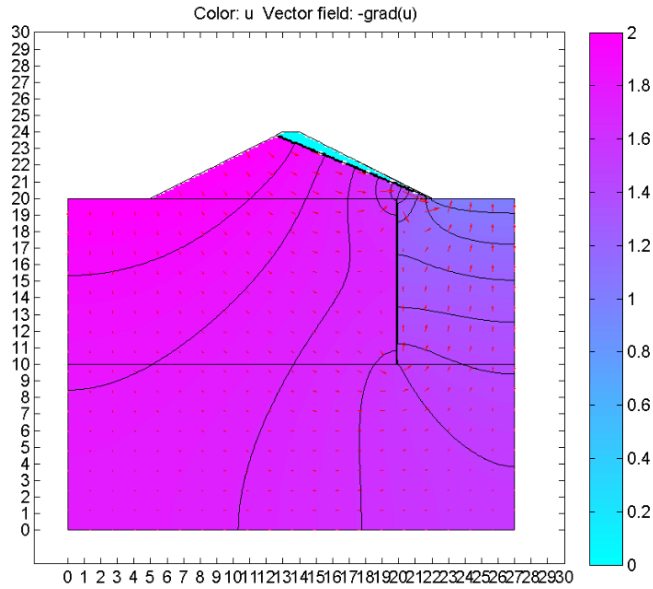

Figure 3.21(c): Flownet under Rise up condition (for 10m long sheet pile at *B*/8 from downstream end, time = 6.0 hrs.)

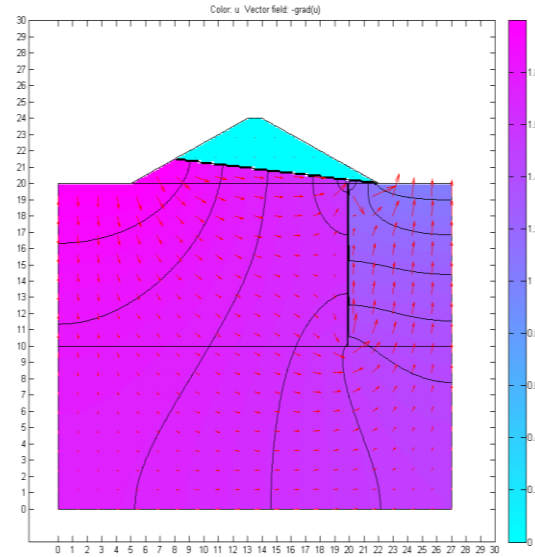

Figure 3.21(d): Flownet under Drawdown condition (for 10m long sheet pile at *B*/8 from downstream end, time = 10.0 hrs.)

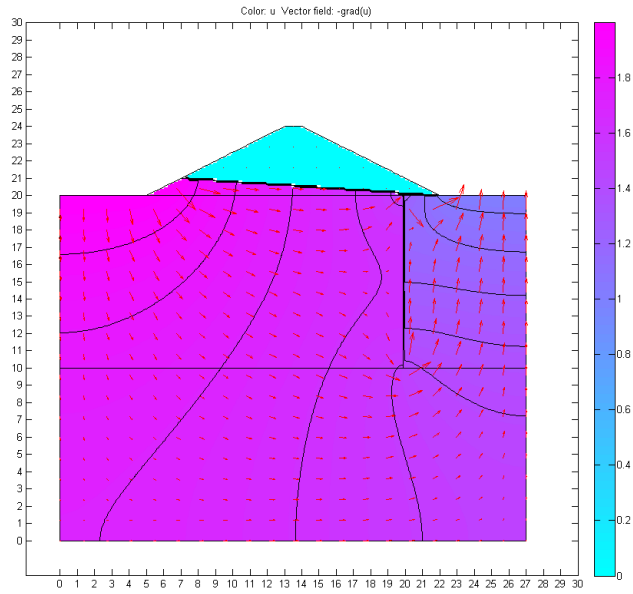

Figure 3.21(e): Flownet under Drawdown condition (for 10m long sheet pile at *B*/8 from downstream end, time = 11.0 hrs.)

3.6.4.1.3 Presentation of results for 15 m long sheet pile at *B*/8 position from downstream end

The variation of the flownet in upstream side with respect to cycle time has also been shown in the respective **Figures –3.22(a),3.22(b),3.22(c),3.22(d),3.22(e)** obtained from MATLAB.

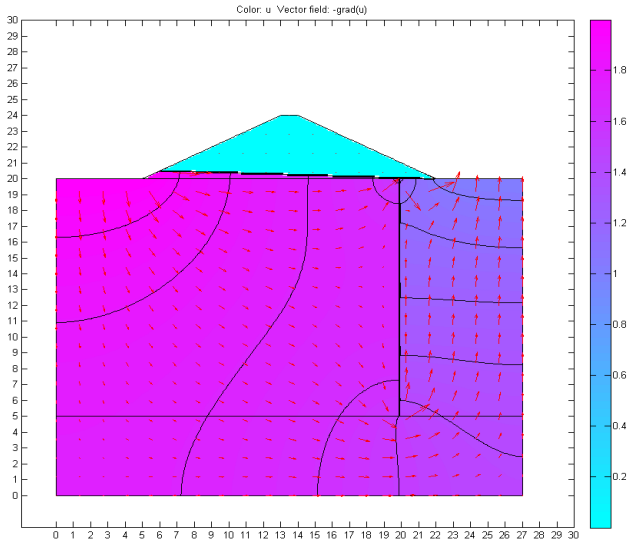

Figure 3.22(a): Flownet under Rise up condition (for 15m long sheet pile at *B*/8 from downstream end, time = 1.0 hr.)

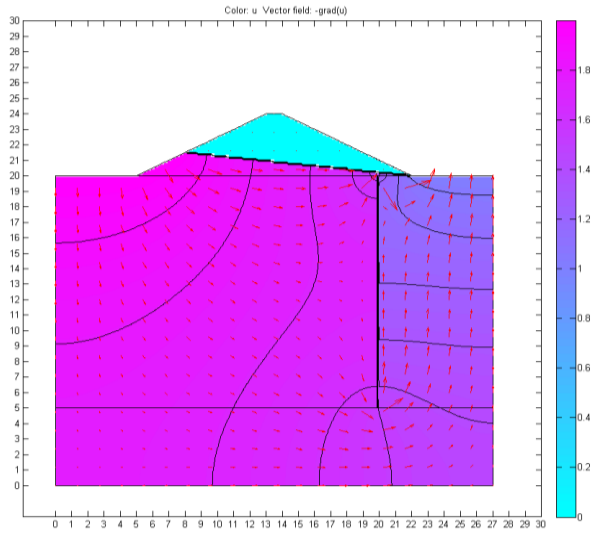

Figure 3.22(b): Flownet under Rise up condition (for 15m long sheet pile at *B*/8 from downstream end, time = 5.0 hrs.)

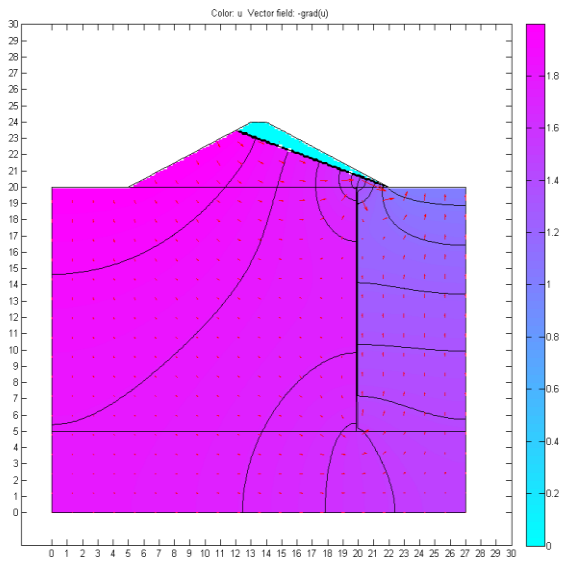

Figure 3.22(c): Flownet under Rise up condition (for 15m long sheet pile at *B*/8 from downstream end, time = 6.0 hrs.)

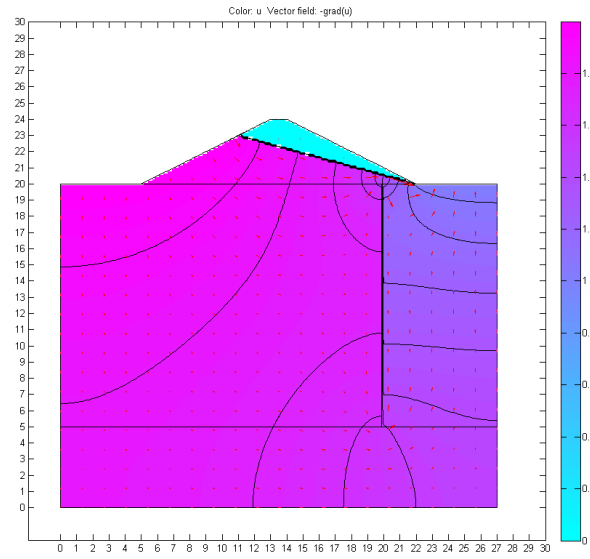

Figure 3.22(d): Flownet under Drawdown condition (for 15m long sheet pile at *B*/8 from downstream end, time = 7.0 hrs.)

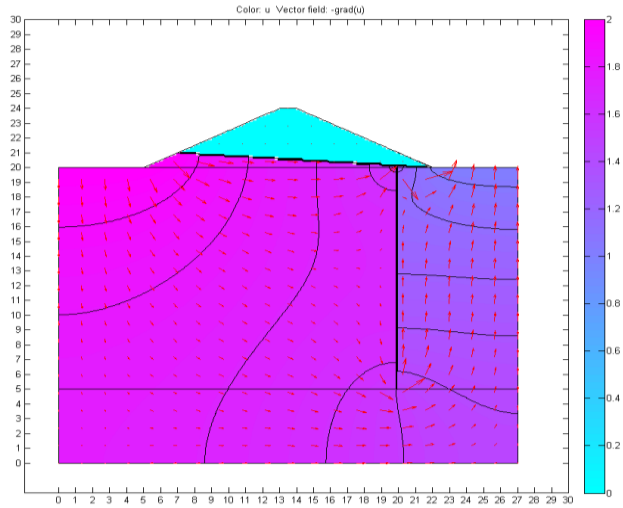

Figure 3.22(e): Flownet under Drawdown condition (for 15m long sheet pile at *B*/8 from downstream end, time =11.0 hrs.)

3.6.4.1.4 Presentation of results for 20 m long sheet pile at *B*/8 position from downstream end

The variation of the flownet due to the variation of upstream side with respect to cycle time has also been shown in the respective **Figures –3.23(a),3.23(b),3.23(c),3.23(d),3.23(e),3.23(f),3.23(g)** obtained from MATLAB.

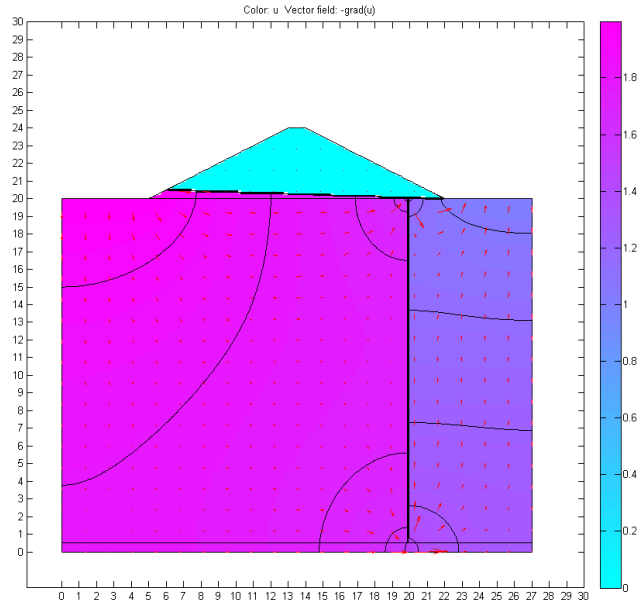

Figure 3.23(a): Flownet under Rise up condition (for 20m long sheet pile at *B*/8 from downstream end, time =1.0 hr.)

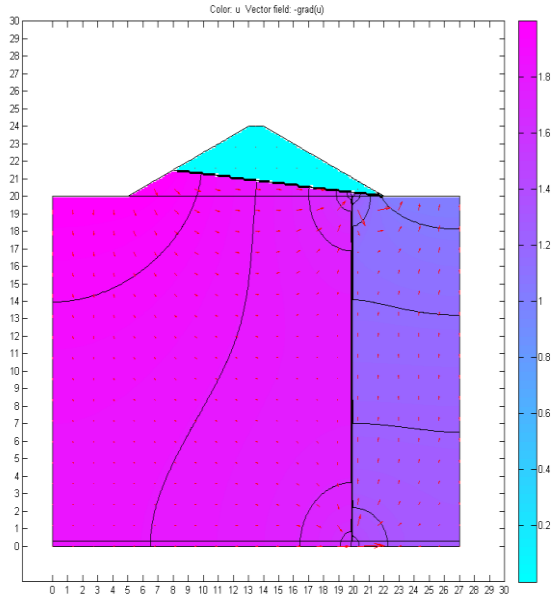

Figure 3.23(b): Flownet under Rise up condition (for 20m long sheet pile at *B*/8 from downstream end, time =3.0 hrs.)

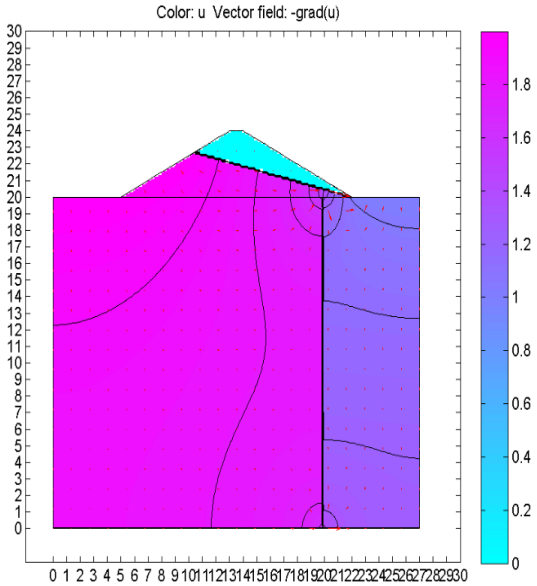

Figure 3.23(c): Flownet under Rise up condition (for 20m long sheet pile at *B*/8 from downstream end, time =5.0 hrs.)

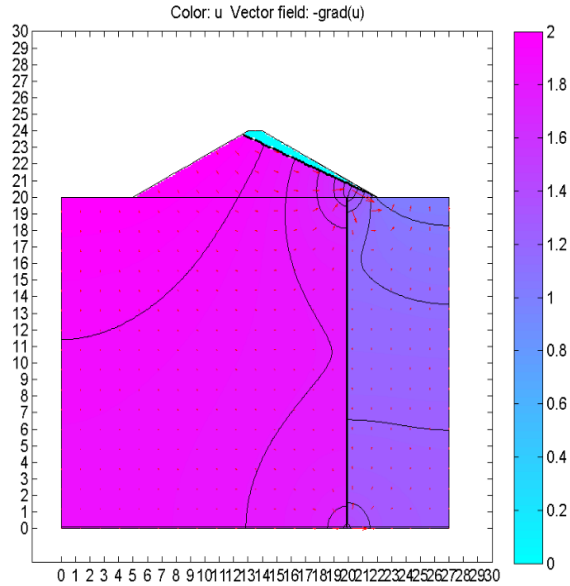

Figure 3.23(d): Flownet under Rise up condition (for 20m long sheet pile at *B*/8 from downstream end, time =6.0 hrs.)

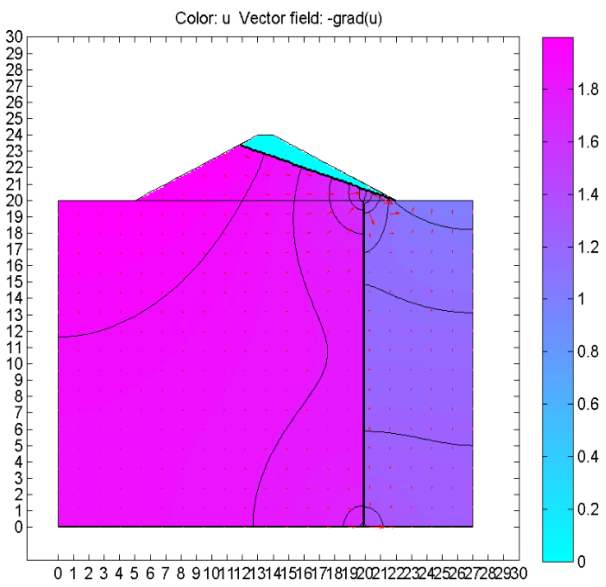

Figure 3.23(e): Flownet under Drawdown condition (for 20m long sheet pile at *B*/8 from downstream end, time =7.0 hrs.)

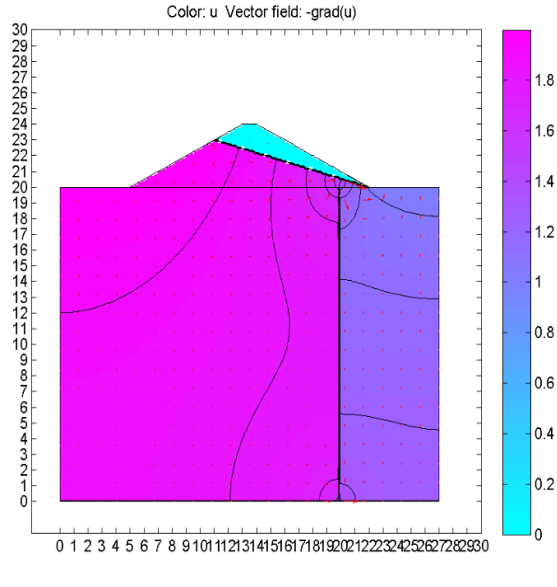

Figure 3.23(f): Flownet under Drawdown condition (for 20m long sheet pile at *B*/8 from downstream end, time =10.0 hrs.)

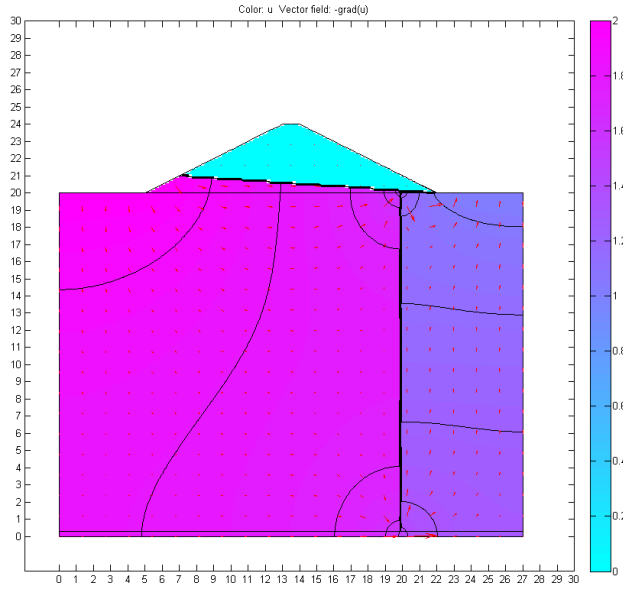

Figure 3.23(g): Flownet under Drawdown condition (for 20m long sheet pile at *B*/8 from downstream end, time =11.0 hrs.)

3.6.4.1.5 Presentation of results for 5 m long sheet pile at 2*B*/8 position from downstream end

The variation of the flownet due to the variation of upstream side with respect to cycle time has also been shown in the respective **Figures –3.24(a),3.24(b),3.24(c),3.24(d),3.24(e),3.24(f),3.24(g)** obtained from MATLAB.

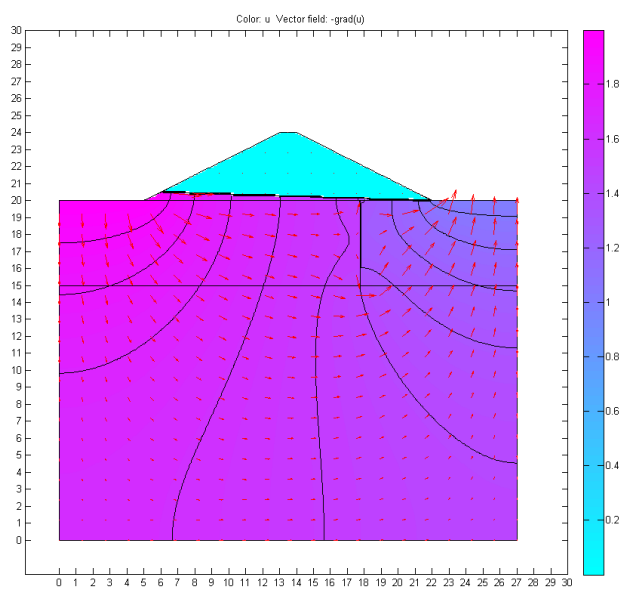

Figure 3.24(a): Flownet under Rise up condition (for 5m long sheet pile at 2*B*/8 from downstream end, time =1.0 hr.)

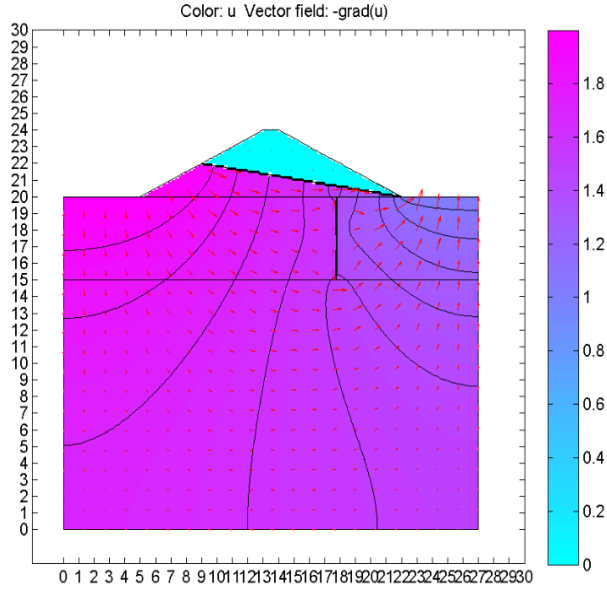

Figure 3.24(b): Flownet under Rise up condition (for 5m long sheet pile at 2*B*/8 from downstream end, time =3.0 hrs.)

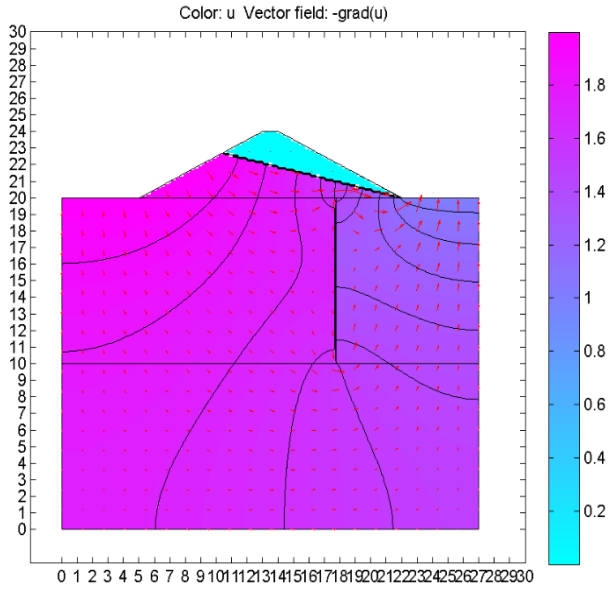

Figure 3.24(c): Flownet under Rise up condition (for 5m long sheet pile at 2*B*/8 from downstream end, time =5.0 hrs.)

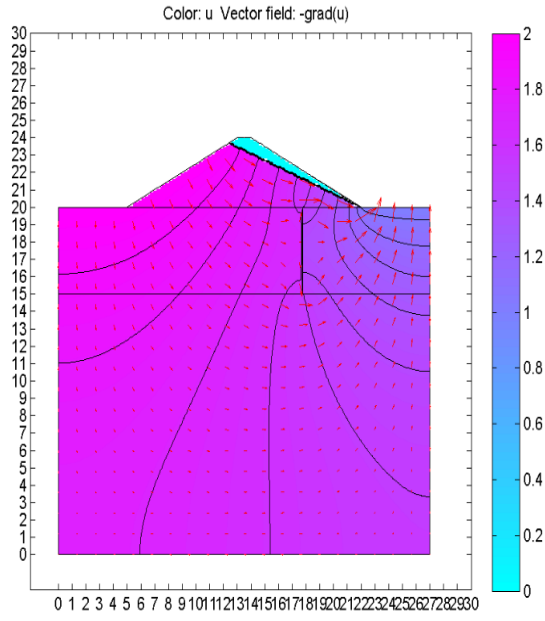

Figure 3.24(d): Flownet under Rise up condition (for 5m long sheet pile at 2*B*/8 from downstream end, time =6.0 hrs.)

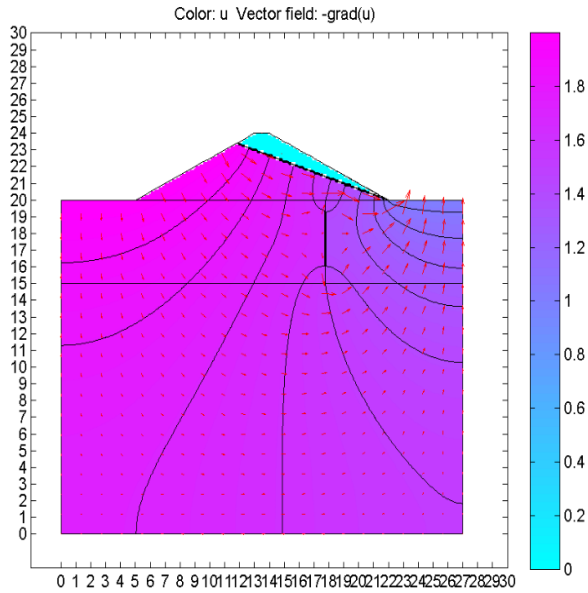

Figure 3.24(e): Flownet under Drawdown condition (for 5m long sheet pile at 2*B*/8 from downstream end, time =3.0 hrs.)

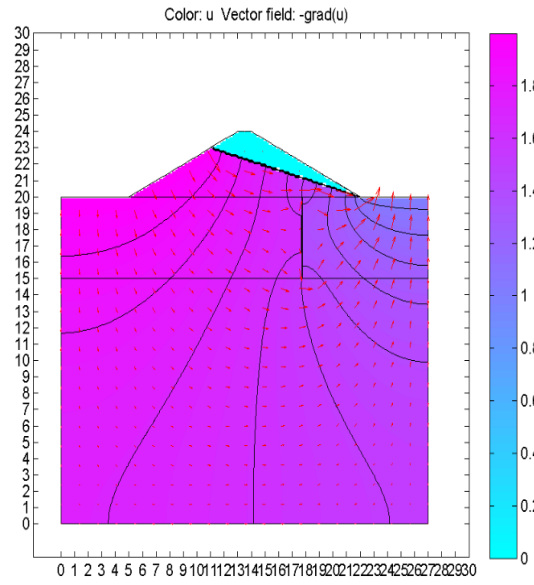

Figure 3.24(f): Flownet under Drawdown condition (for 5m long sheet pile at 2*B*/8 from downstream end, time =10.0 hrs.)

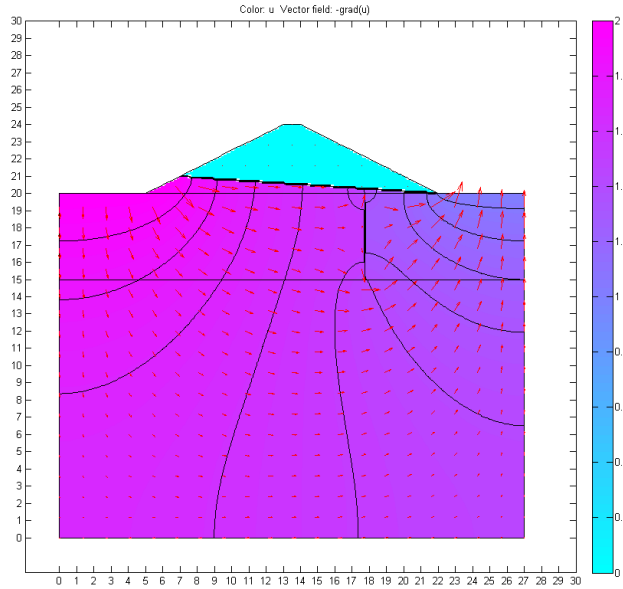

Figure 3.24(g): Flownet under Drawdown condition (for 5m long sheet pile at 2*B*/8 from downstream end, time =11.0 hrs.)

3.6.4.1.6 Presentation of results for 10 m long sheet pile at 2*B*/8 position from downstream end

The variation of the flownet due to the variation of upstream side with respect to cycle time has also been shown in the respective **Figures –3.25(a),3.25(b),3.25(c),3.25(d),3.25(e),3.25(f),3.25(g)** obtained from MATLAB.

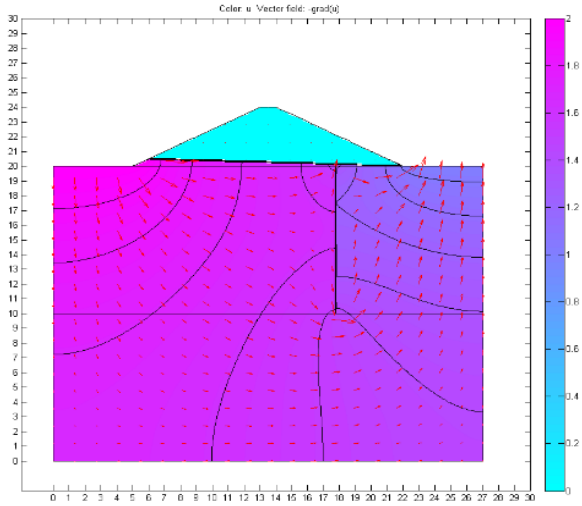

Figure 3.25(a): Flownet under Rise up condition (for 10m long sheet pile at 2*B*/8 from downstream end, time =1.0 hr.)

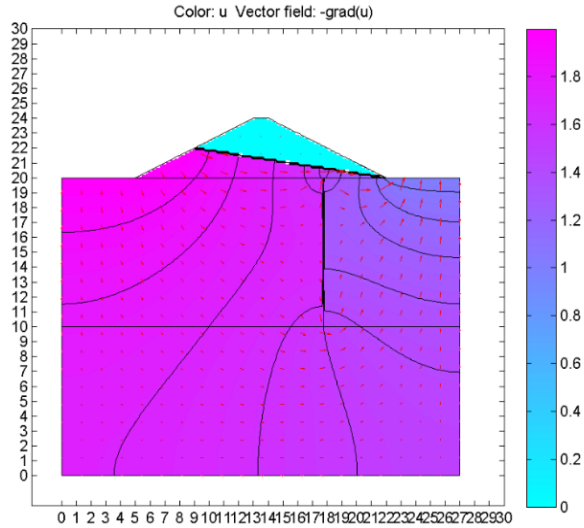

Figure 3.25(b): Flownet under Rise up condition (for 10m long sheet pile at 2*B*/8 from downstream end, time =3.0 hrs.)

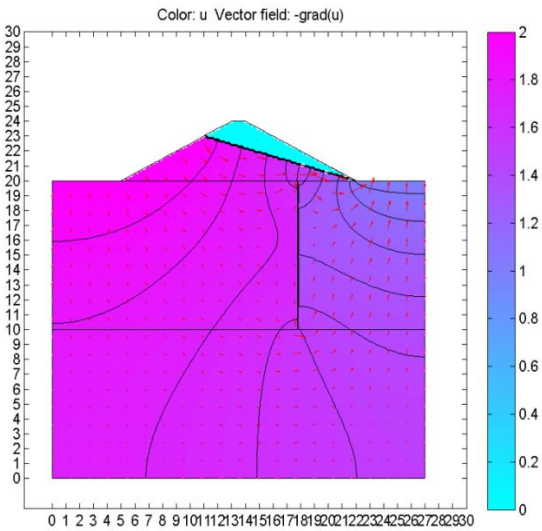

Figure 3.25(c): Flownet under Rise up condition (for 10m long sheet pile at 2*B*/8 from downstream end, time =5.0 hrs.)

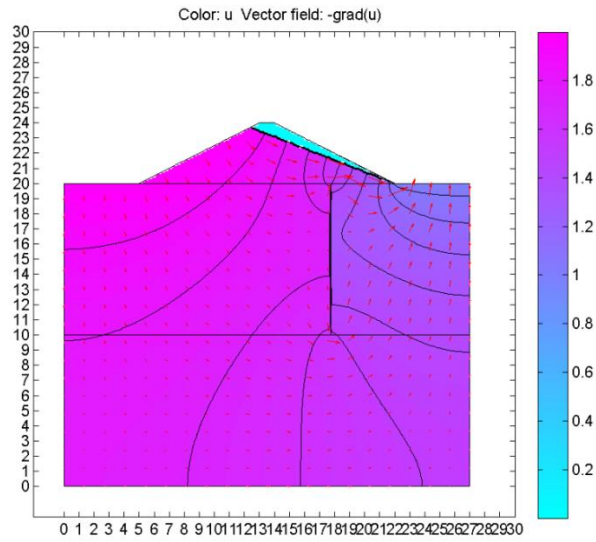

Figure 3.25(d): Flownet under Rise up condition (for 10m long sheet pile at 2*B*/8 from downstream end, time =6.0 hrs.)

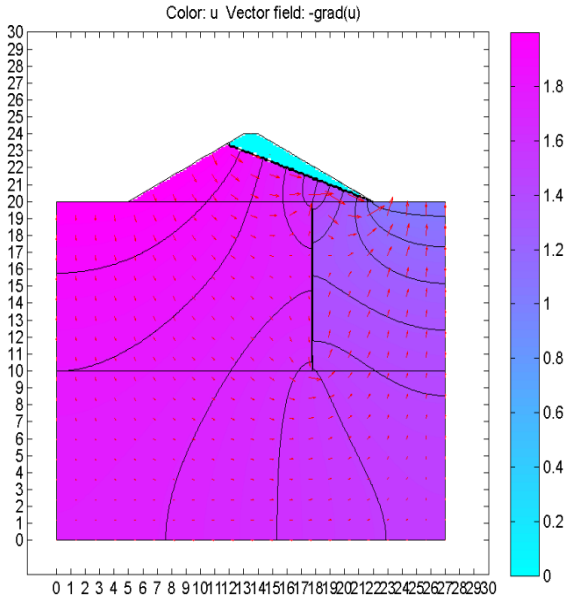

Figure 3.25(e): Flownet under Drawdown condition (for 10m long sheet pile at 2*B*/8 from downstream end, time =7.0 hrs.)

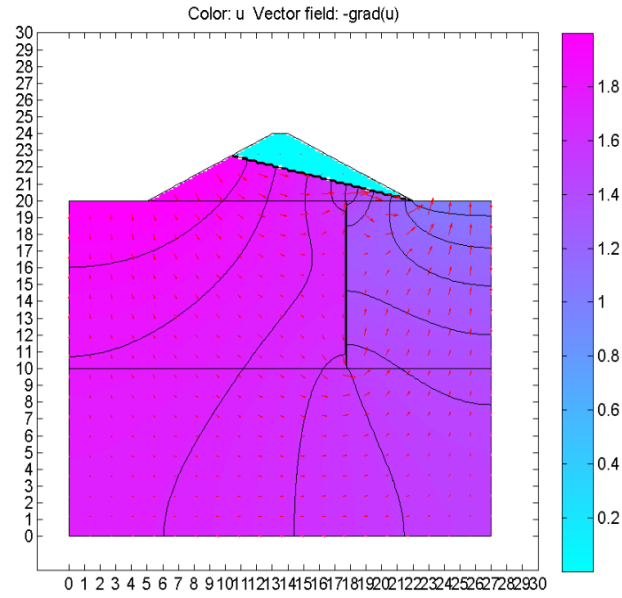

Figure 3.25(f): Flownet under Drawdown condition (for 10m long sheet pile at 2*B*/8 from downstream end, time =10.0 hrs.)

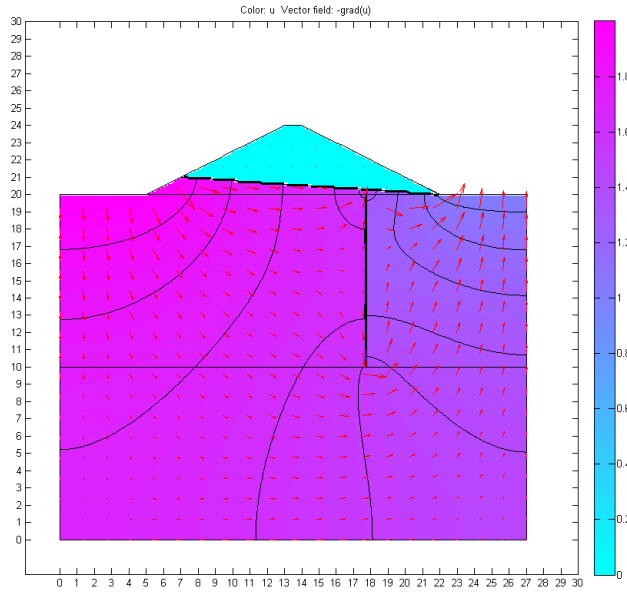

Figure 3.25(g): Flownet under Drawdown condition (for 10m long sheet pile at 2*B*/8 from downstream end, time =11.0 hrs.)

3.6.4.1.7 Presentation of results for 15 m long sheet pile at 2*B*/8 position from downstream end

The variation of the flownet due to the variation of upstream side with respect to cycle time has also been shown in the respective **Figures –3.26(a),3.26(b),3.26(c),3.26(d),3.26(e),3.26(f),3.26(g)** obtained from MATLAB.

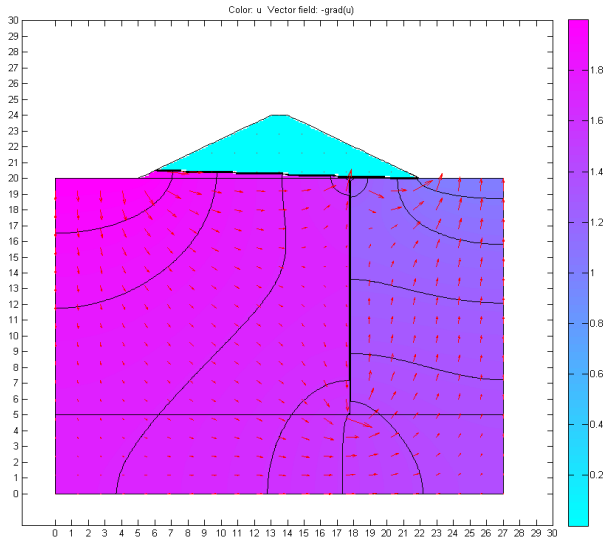

Figure 3.26(a): Flownet under Rise up condition (for 15m long sheet pile at 2*B*/8 from downstream end, time =1.0 hr.)

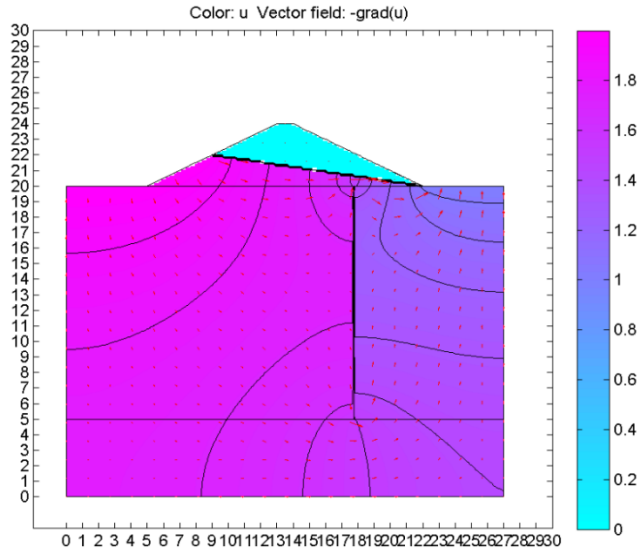

Figure 3.26(b): Flownet under Rise up condition (for 15m long sheet pile at 2*B*/8 from downstream end, time =3.0 hrs.)

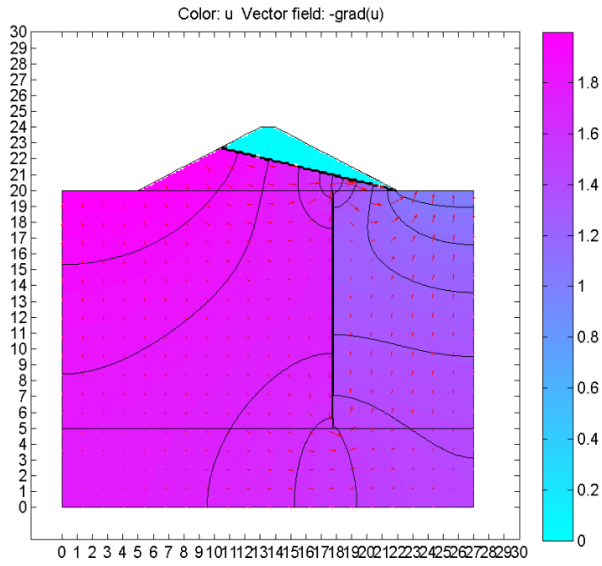

Figure 3.26(c): Flownet under Rise up condition (for 15m long sheet pile at 2*B*/8 from downstream end, time =5.0 hrs.)

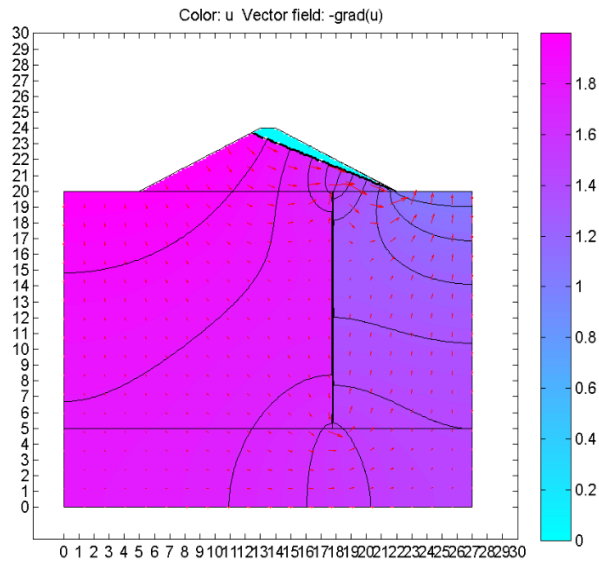

Figure 3.26(d): Flownet under Rise up condition (for 15m long sheet pile at 2*B*/8 from downstream end, time =6.0 hrs.)

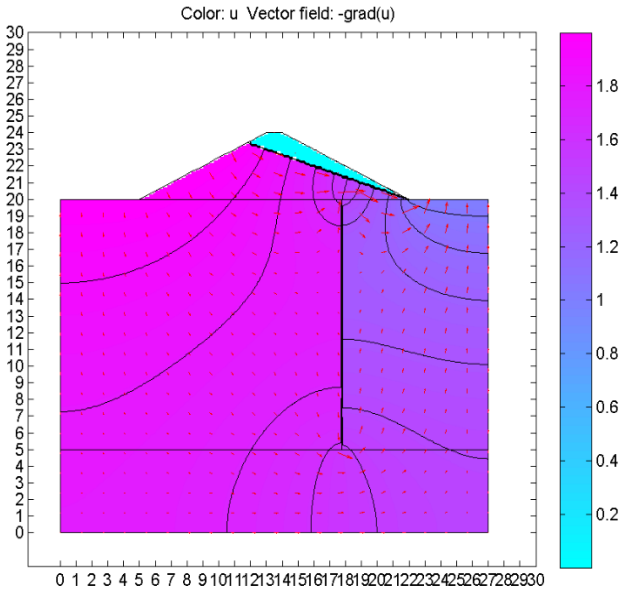

Figure 3.26(e): Flownet under Drawdown condition (for 15m long sheet pile at 2*B*/8 from downstream end, time =7.0 hrs.)

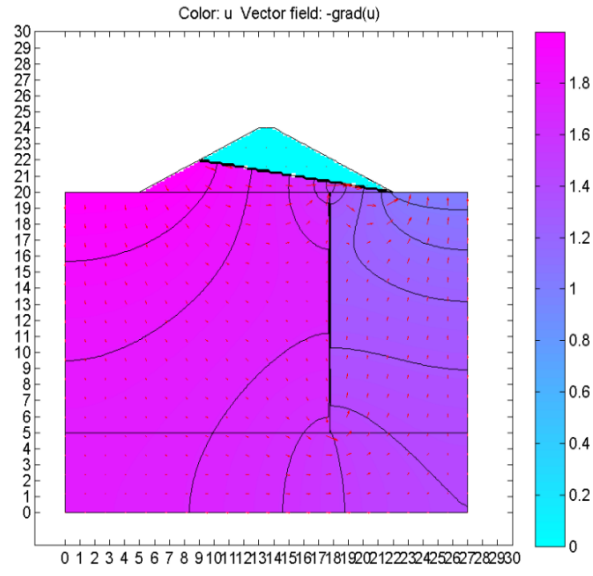

Figure 3.26(f): Flownet under Drawdown condition (for 15m long sheet pile at 2*B*/8 from downstream end, time =10.0 hrs.)

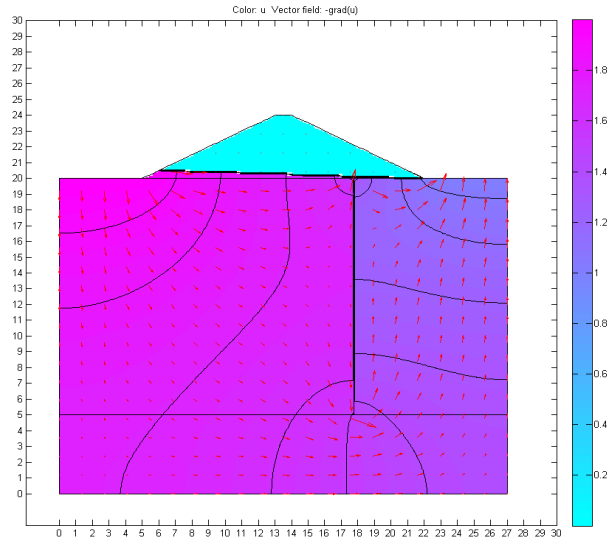

Figure 3.26(g): Flownet under Drawdown condition (for 15m long sheet pile at 2*B*/8 from downstream end, time =11.0 hrs.)

3.6.4.1.8 Presentation of results for 20 m long sheet pile at 2*B*/8 position from downstream end

The variation of the flownet due to the variation of upstream side with respect to cycle time has also been shown in the respective **Figures –3.27(a),3.27(b),3.27(c),3.27(d),3.27(e),3.27(f),3.27(g)** obtained from MATLAB.

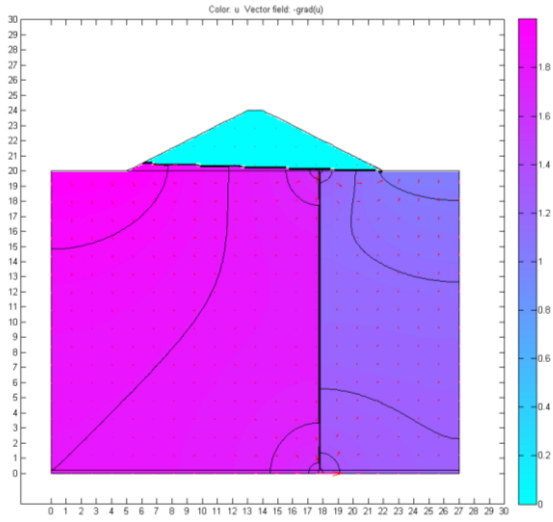

Figure 3.27(a): Flownet under Rise up condition (for 20m long sheet pile at 2*B*/8 from downstream end, time =1.0 hr.)

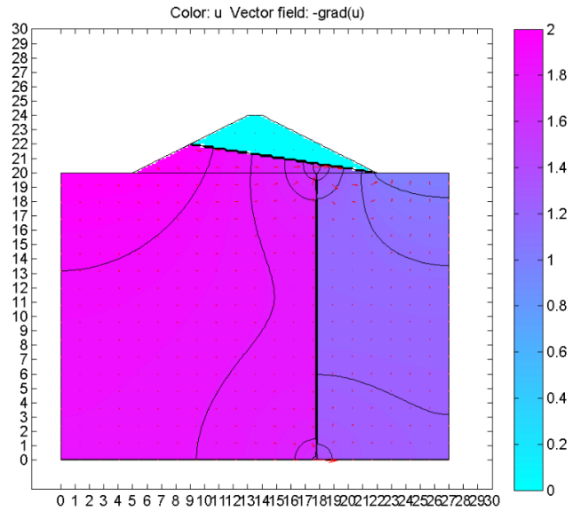

Figure 3.27(b): Flownet under Rise up condition (for 20m long sheet pile at 2*B*/8 from downstream end, time =3.0 hrs.)

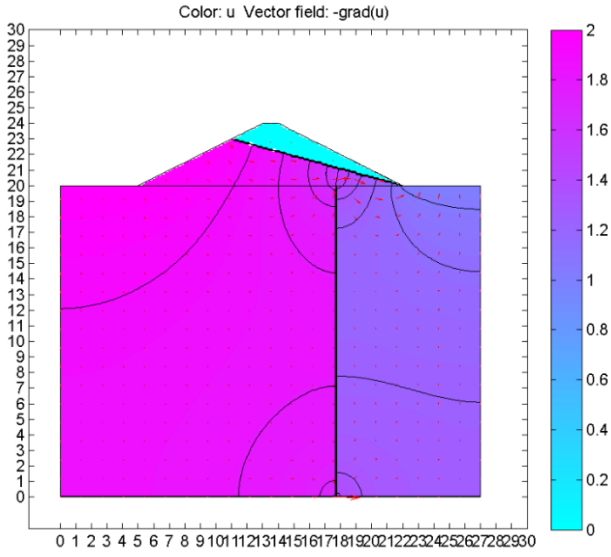

Figure 3.27(c): Flownet under Rise up condition (for 20m long sheet pile at 2*B*/8 from downstream end, time =5.0 hrs.)

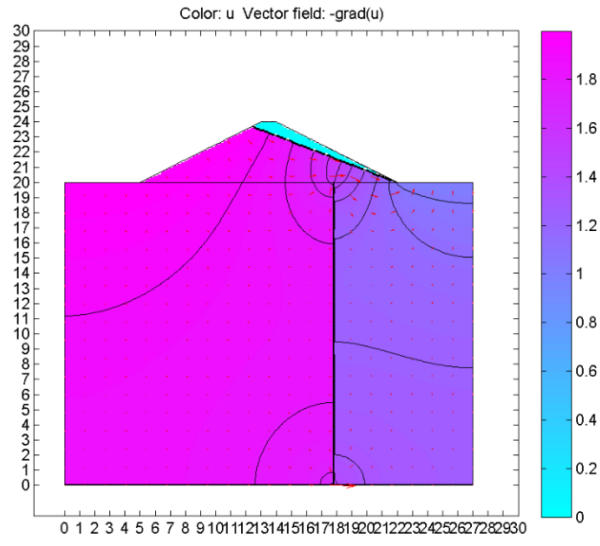

Figure 3.27(d): Flownet under Rise up condition (for 20m long sheet pile at 2*B*/8 from downstream end, time =6.0 hrs.)

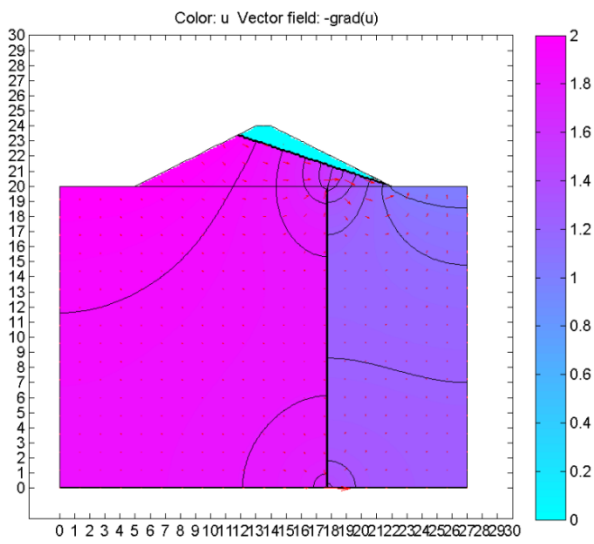

Figure 3.27(e): Flownet under Drawdown condition (for 20m long sheet pile at 2*B*/8 from downstream end, time =7.0 hrs.)

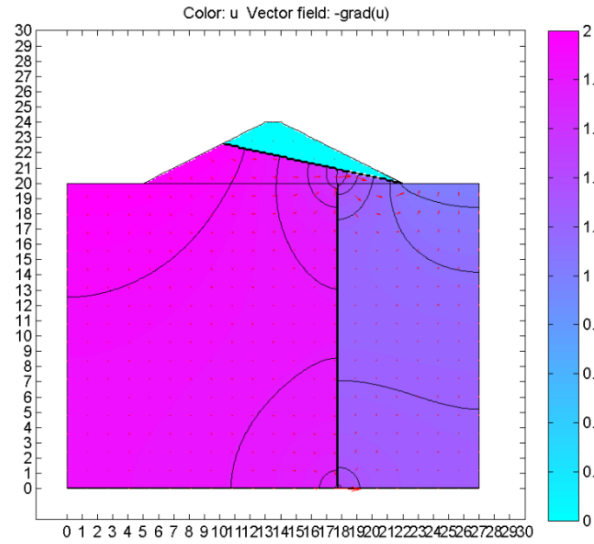

Figure 3.27(f): Flownet under Drawdown condition (for 20m long sheet pile at 2*B*/8 from downstream end, time =10.0 hrs.)

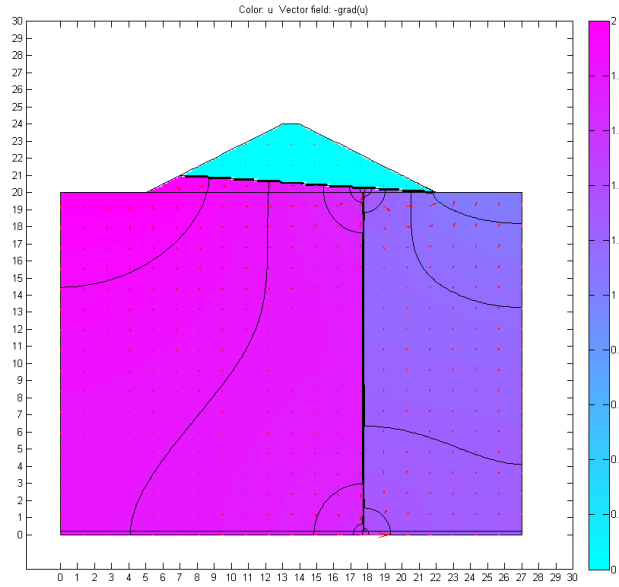

Figure 3.27(g): Flownet under Drawdown condition (for 20m long sheet pile at 2*B*/8 from downstream end, time =11.0 hrs.)

3.6.4.1.9 Presentation of results for 5 m long sheet pile at 3*B*/8 position from downstream end

The variation of the flownet due to the variation of upstream side with respect to cycle time has also been shown in the respective **Figures –3.28(a),3.28(b),3.28(c),3.28(d),3.28(e)** obtained from MATLAB.

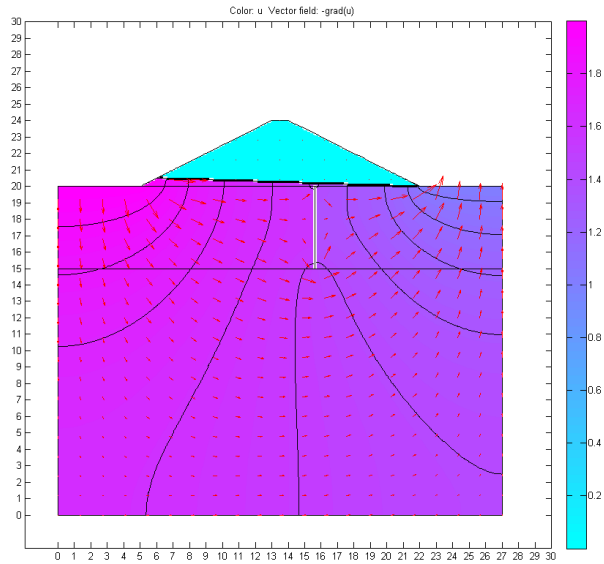

Figure 3.28(a): Flownet under Rise up condition (for 5m long sheet pile at 3*B*/8 from downstream end, time =1.0 hr.)

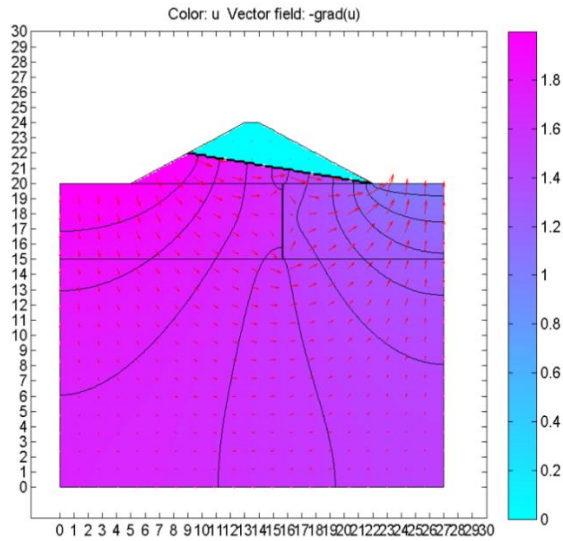

Figure 3.28(b): Flownet under Rise up condition (for 5m long sheet pile at 3*B*/8 from downstream end, time =3.0 hrs.)

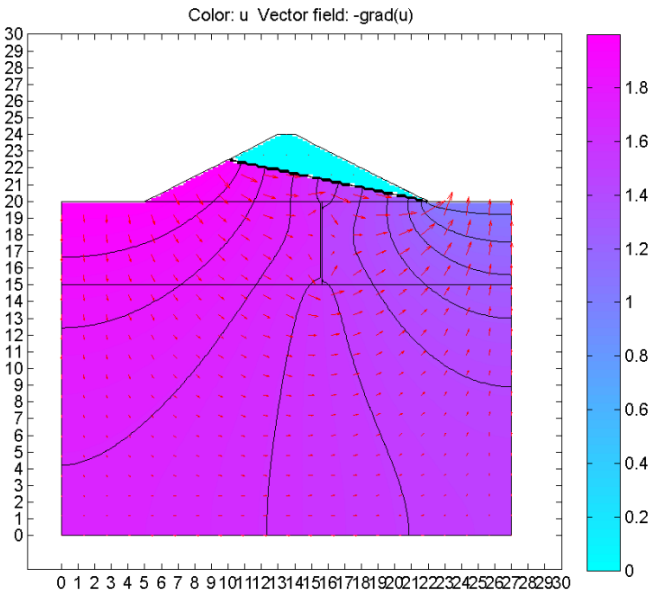

Figure 3.28(c): Flownet under Rise up condition (for 5m long sheet pile at 3*B*/8 from downstream end, time =5.0 hrs.)

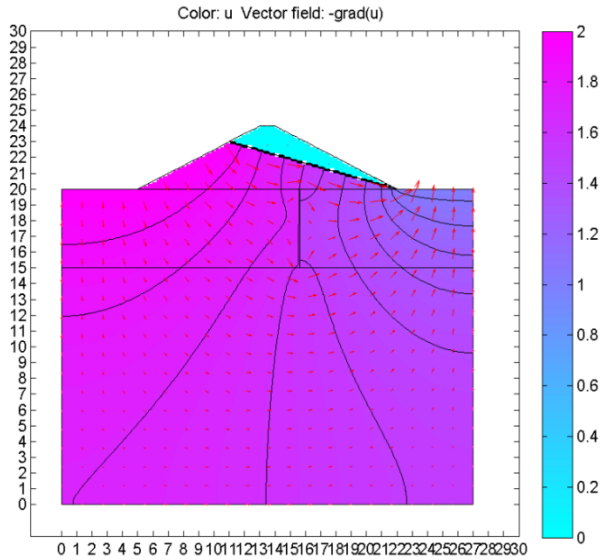

Figure 3.28(d): Flownet under Rise up condition (for 5m long sheet pile at 3*B*/8 from downstream end, time =6.0 hrs.)

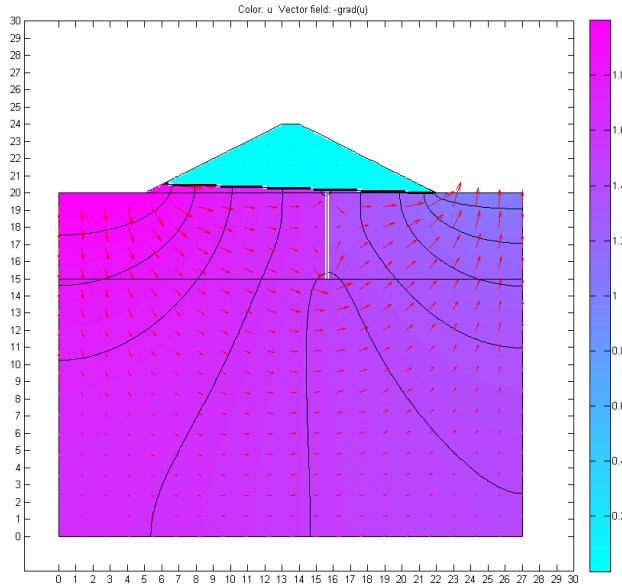

Figure 3.28(e): Flownet under Drawdown condition (for 5m long sheet pile at 3*B*/8 from downstream end, time =11.0 hrs.)

3.6.4.1.10 Presentation of results for 10 m long sheet pile at 3*B*/8 position from downstream end

The variation of the flownet due to the variation of upstream side with respect to cycle time has also been shown in the respective **Figures –3.29(a),3.29(b),3.29(c),2.29(d),3.29(e),3.29(f)** obtained from MATLAB.

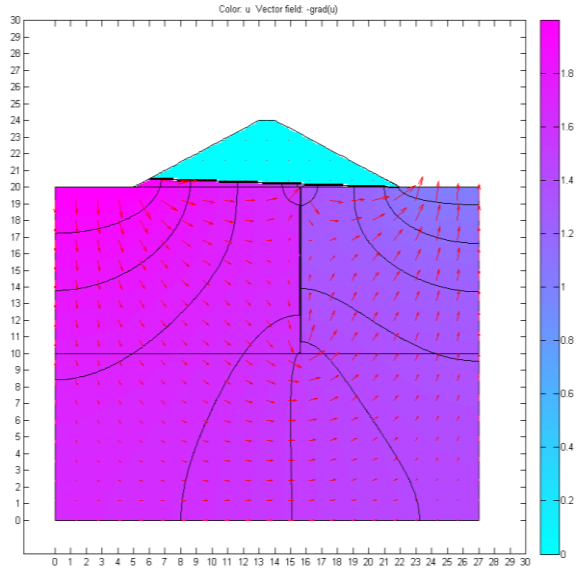

Figure 3.29(a): Flownet under Rise up condition (for 10m long sheet pile at 3*B*/8 from downstream end, time =1.0 hr.)

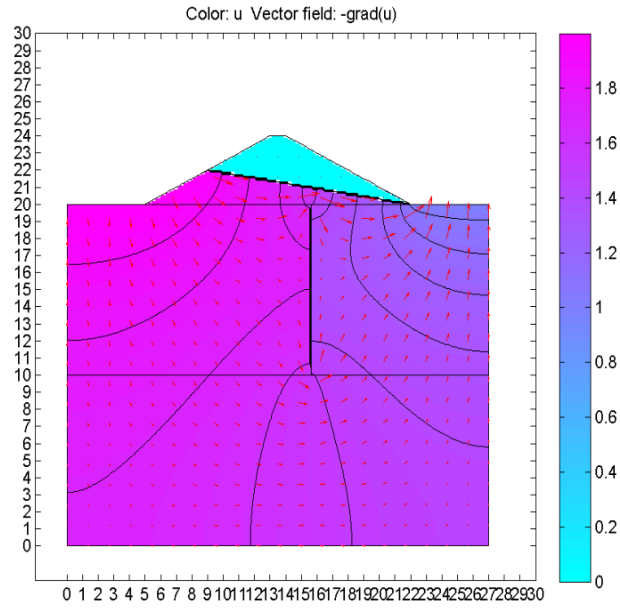

Figure 3.29(b): Flownet under Rise up condition (for 10m long sheet pile at 3*B*/8 from downstream end, time =3.0 hrs.)

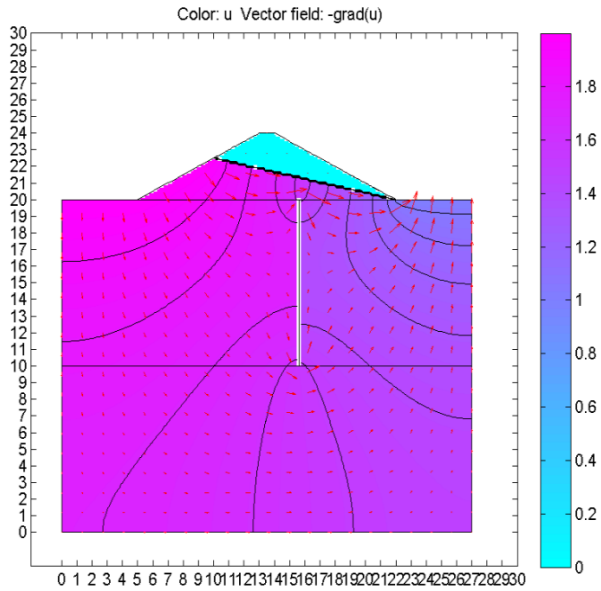

Figure 3.29(c): Flownet under Rise up condition (for 10m long sheet pile at 3*B*/8 from downstream end, time =5.0 hrs.)

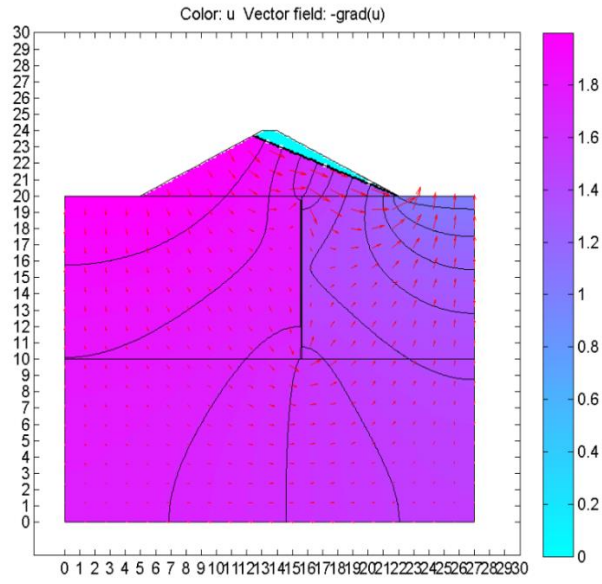

Figure 3.29(d): Flownet under Rise up condition (for 10m long sheet pile at 3*B*/8 from downstream end, time =6.0 hrs.)

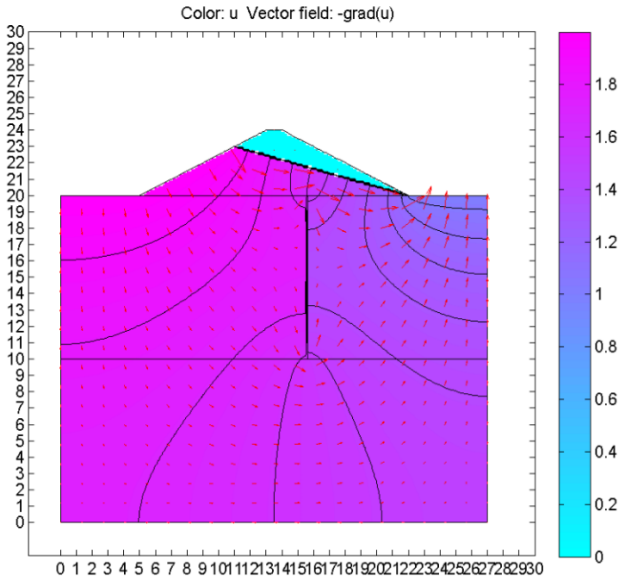

Figure 3.29(e): Flownet under Drawdown condition (for 10m long sheet pile at 3*B*/8 from downstream end, time =7.0 hrs.)

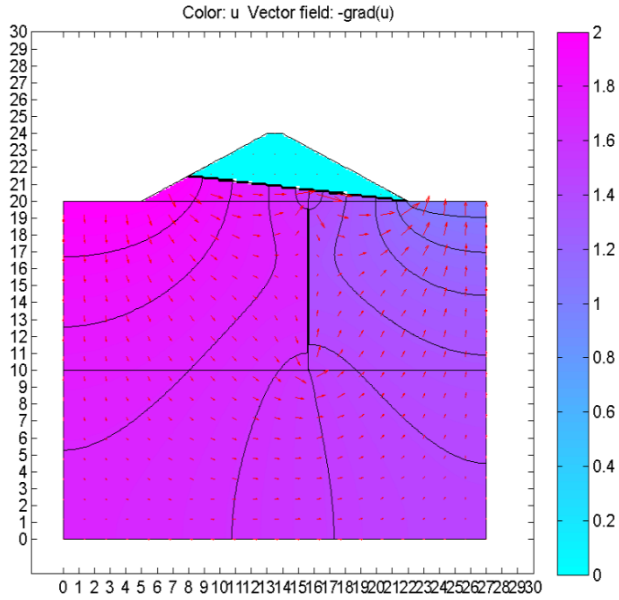

Figure 3.29(f): Flownet under Drawdown condition (for 10m long sheet pile at 3*B*/8 from downstream end, time =10.0 hrs.)

3.6.4.1.11 Presentation of results for 15 m long sheet pile at 3*B*/8 position from downstream end

The variation of the flownet due to the variation of upstream side with respect to cycle time has also been shown in the respective **Figures –3.30(a),3.30(b),3.30(c),3.30(d),3.30(e),3.30(f)** obtained from MATLAB.

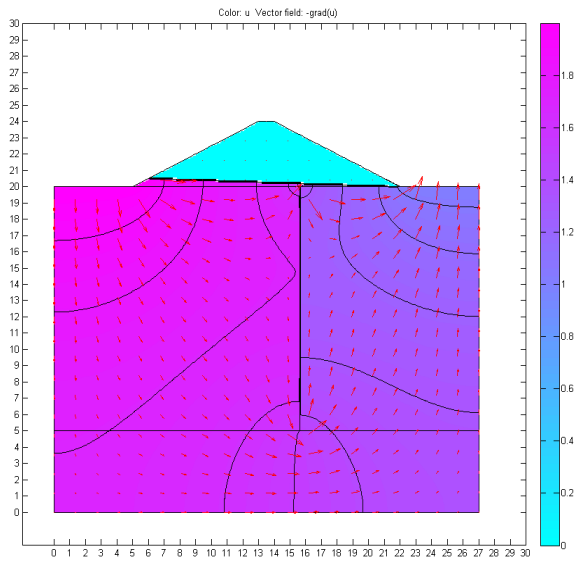

Figure 3.30(a): Flownet under Rise up condition (for 15m long sheet pile at 3*B*/8 from downstream end, time =1.0 hr.)

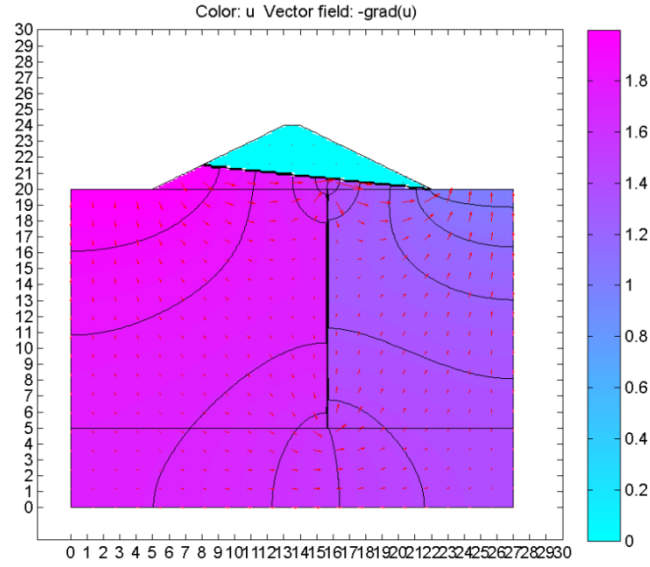

Figure 3.30(b): Flownet under Rise up condition (for 15m long sheet pile at 3*B*/8 from downstream end, time =3.0 hrs.)

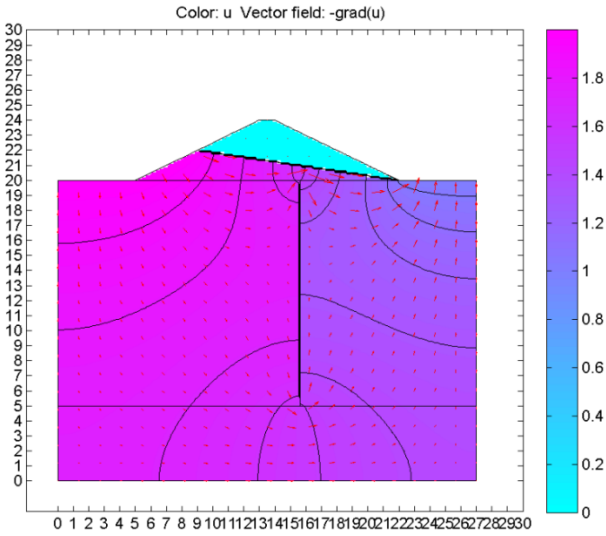

Figure 3.30(c): Flownet under Rise up condition (for 15m long sheet pile at 3*B*/8 from downstream end, time =5.0 hrs.)

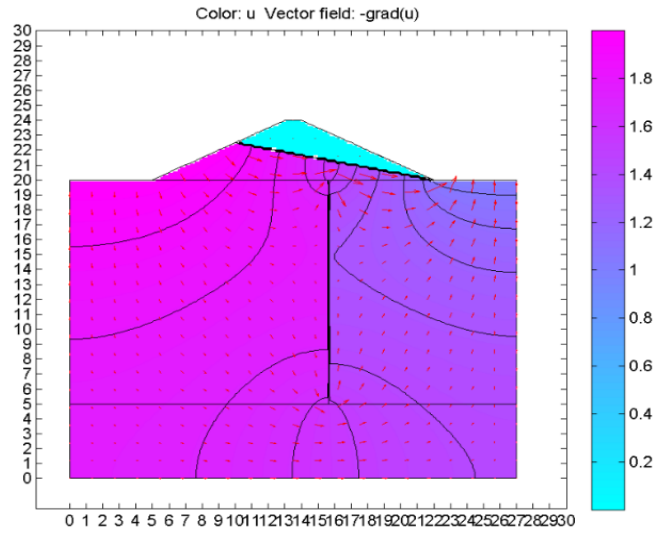

Figure 3.30(c): Flownet under Rise up condition (for 15m long sheet pile at 3*B*/8 from downstream end, time =6.0 hrs.)

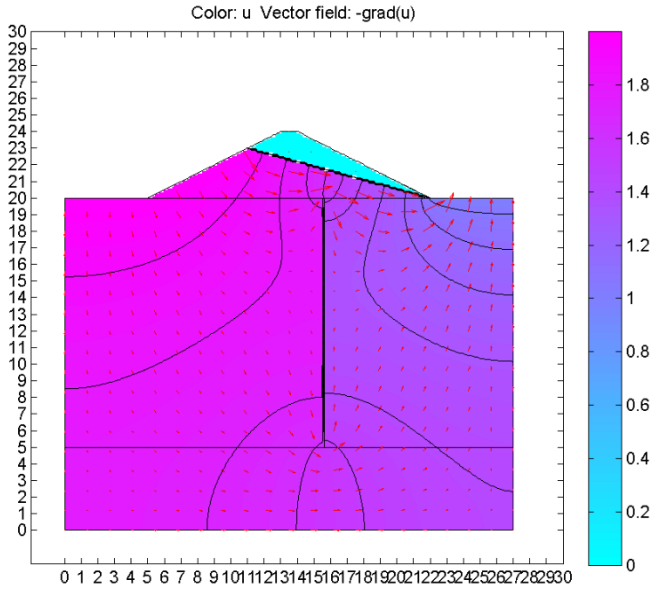

Figure 3.30(e): Flownet under Drawdown condition (for 15m long sheet pile at 3*B*/8 from downstream end, time =7.0 hrs.)

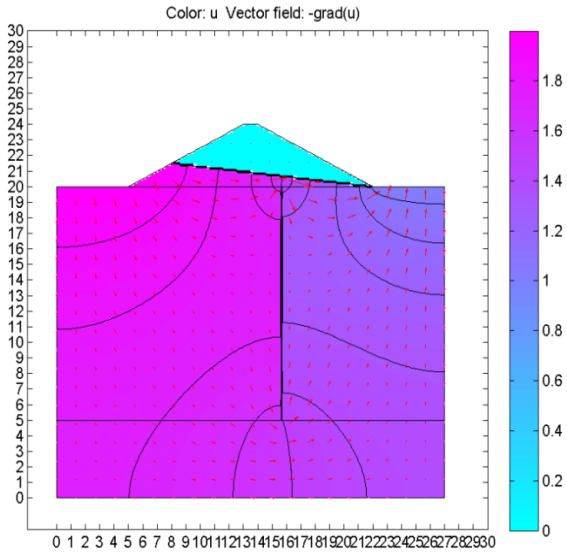

Figure 3.30(f): Flownet under Drawdown condition (for 15m long sheet pile at 3*B*/8 from downstream end, time =11.0 hrs.)

3.6.4.1.12 Presentation of results for 20 m long sheet pile at 3*B*/8 position from downstream end

The variation of the flownet due to the variation of upstream side with respect to cycle time has also been shown in the respective **Figures –3.31(a),3.31(b),3.31(c),3.31(d),3.31(e),3.31(f)** obtained from MATLAB.

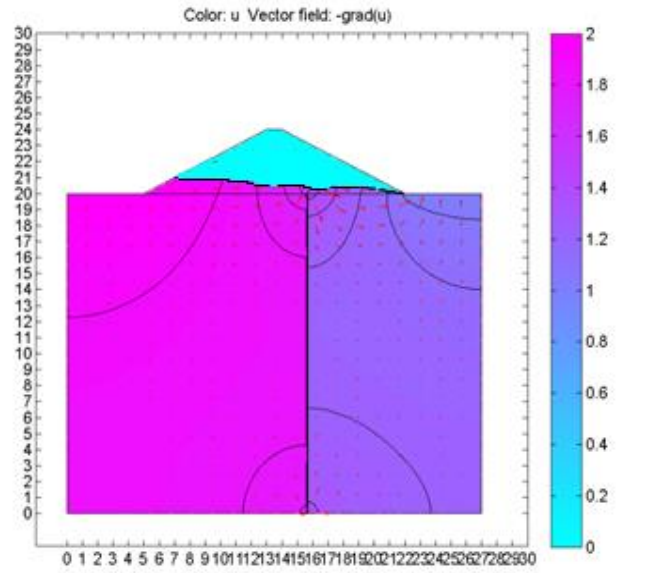

Figure 3.31(a): Flownet under Rise up condition (for 20m long sheet pile at 3*B*/8 from downstream end, time =1.0 hr.)

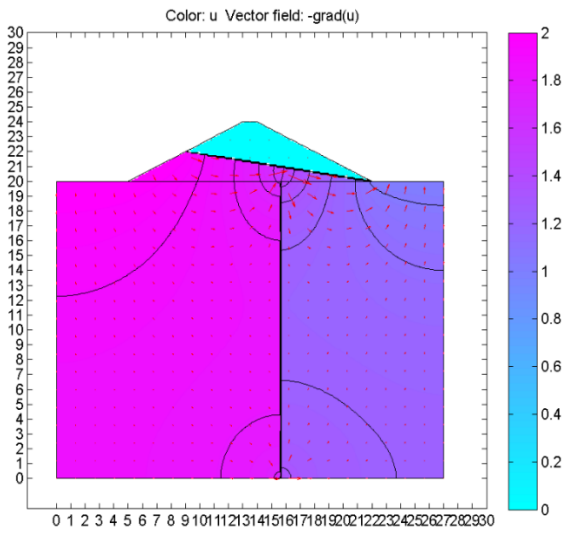

Figure 3.31(b): Flownet under Rise up condition (for 20m long sheet pile at 3*B*/8 from downstream end, time =3.0 hrs.)

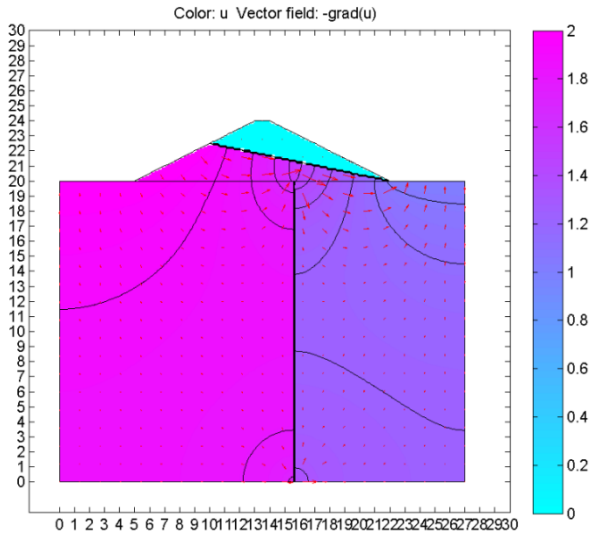

Figure 3.31(c): Flownet under Rise up condition (for 20m long sheet pile at 3*B*/8 from downstream end, time =5.0 hrs.)

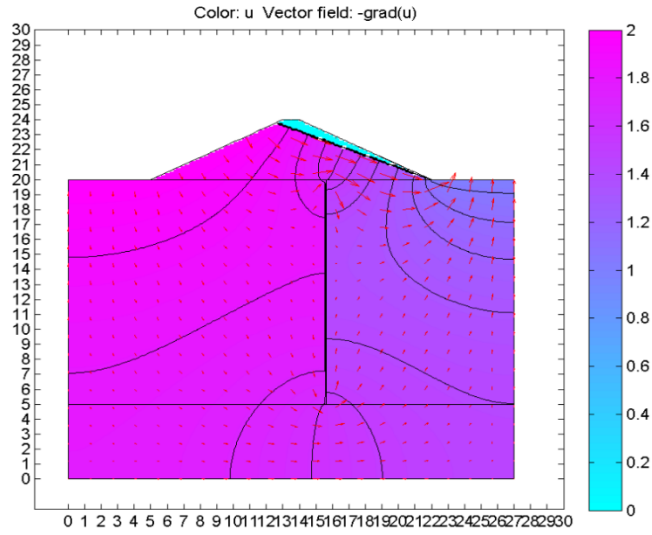

Figure 3.31(d): Flownet under Rise up condition (for 20m long sheet pile at 3*B*/8 from downstream end, time =6.0 hrs.)

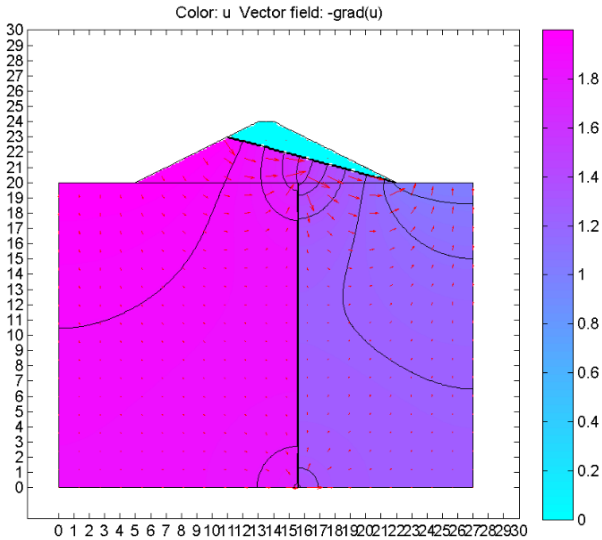

Figure 3.31(e): Flownet under Drawdown condition (for 20m long sheet pile at 3*B*/8 from downstream end, time =7.0 hrs.)

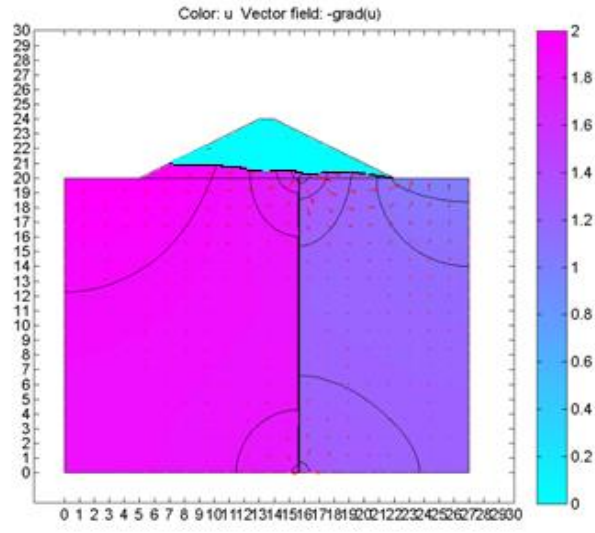

Figure 3.31(f): Flownet under Drawdown condition (for 20m long sheet pile at 3*B*/8 from downstream end, time =11.0 hrs.)

3.6.4.2. PRESENTATION OF RESULTS OF FLAC 2D

During single cycle tests with different rates of Rise up / Drawdown the variation in dynamics in flownet has been shown in in **this section** for different time interval of rise up and drawdown conditions. The variation of the flownet in upstream side with respect to cycle time has also been shown in the respective figures obtained from FLAC 2D.

3.6.4.2.1 Presentation of results for 5 m long sheet pile at *B*/8 position from downstream end

The variation of the flownet due to the variation of upstream side with respect to cycle time has also been shown in the respective **Figures –3.32(a),3.32(b),3.32(c),3.32(d),3.32(e),3.32(f)** obtained from FLAC 2D.

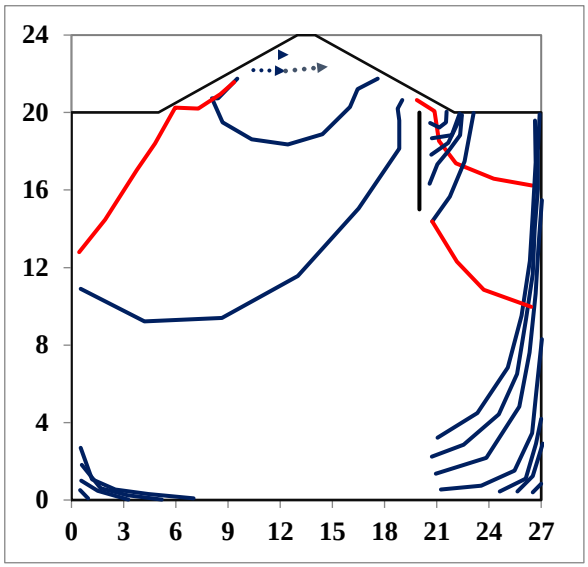

Figure 3.32(a): Flownet under Rise up condition (for 5 m long sheet pile at *B*/8 from downstream end, time = 1.0

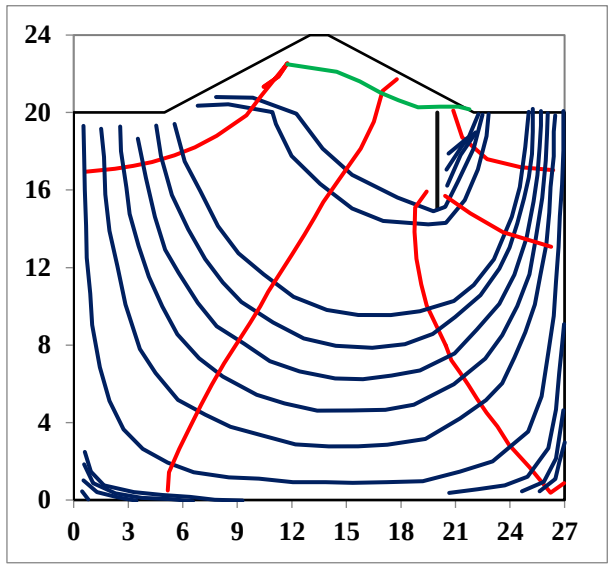

Figure 3.32(b): Flownet under Rise up condition (for 5 m long sheet pile at *B*/8 from downstream end, time = 5.0 hrs.)

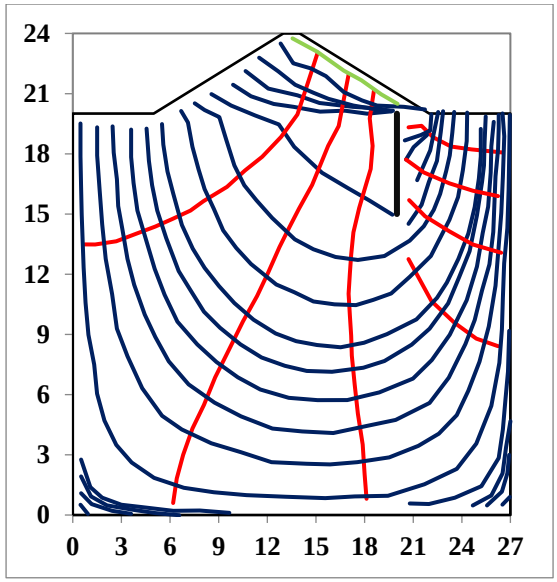

Figure 3.32(c): Flownet under Rise up condition (for 5 m long sheet pile at *B*/8 from downstream end, after 6.0 hrs.)

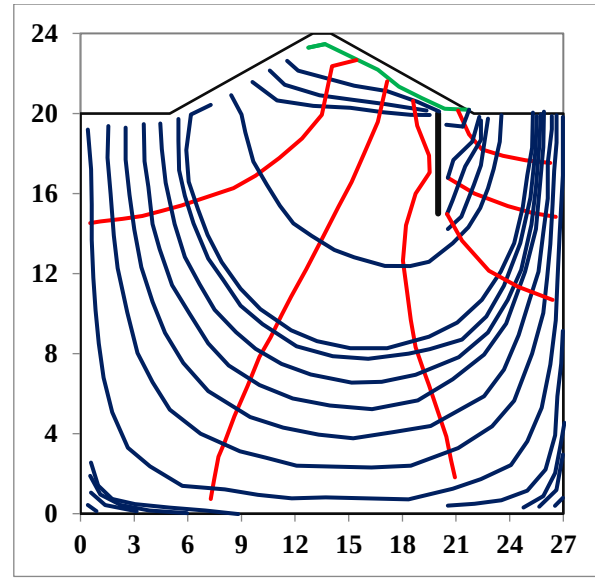

Figure 3.32(d): Flownet under Drawdown condition (for 5 m long sheet pile at *B*/8 from downstream end, time = 7.0 hrs.)

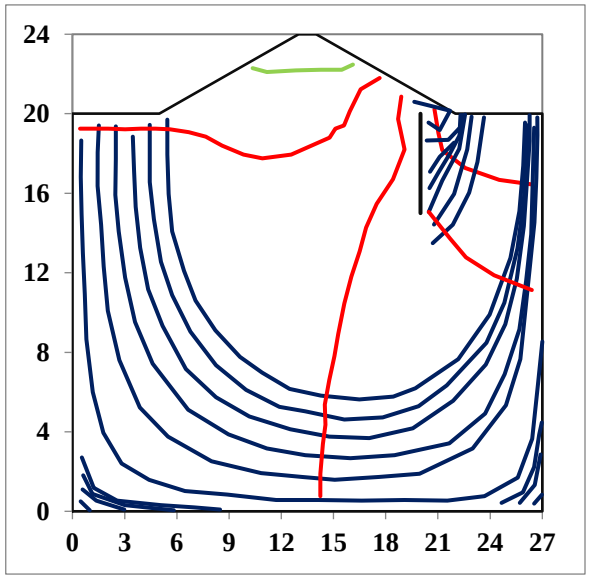

Figure 3.32(e): Flownet under Drawdown condition (for 5 m long sheet pile at *B*/8 from downstream end, time = 10.0 hrs.)

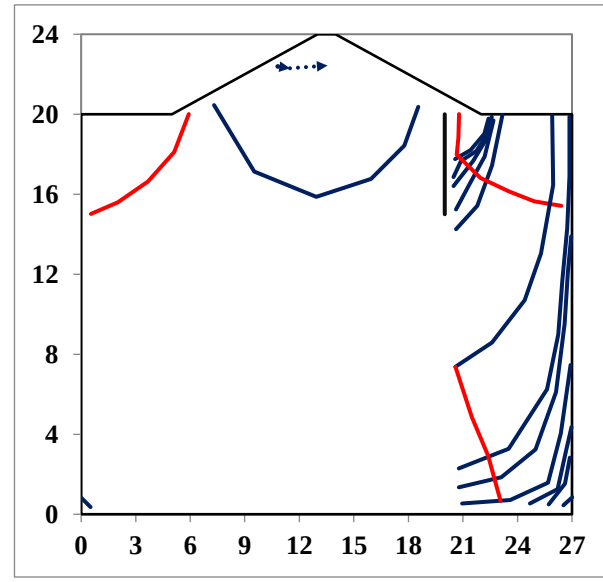

Figure 3.32(f): Flownet under Drawdown condition (for 5 m long sheet pile at *B*/8 from downstream end, time = 11.0 hrs.)

3.6.4.2.2 Presentation of results for 10 m long sheet pile at *B*/8 position from downstream end

The variation of the flownet due to the variation of upstream side with respect to cycle time has also been shown in the respective **Figures –3.33(a),3.33(b),3.33(c),3.33(d),3.3(e),3.33(f)** obtained from FLAC 2D.

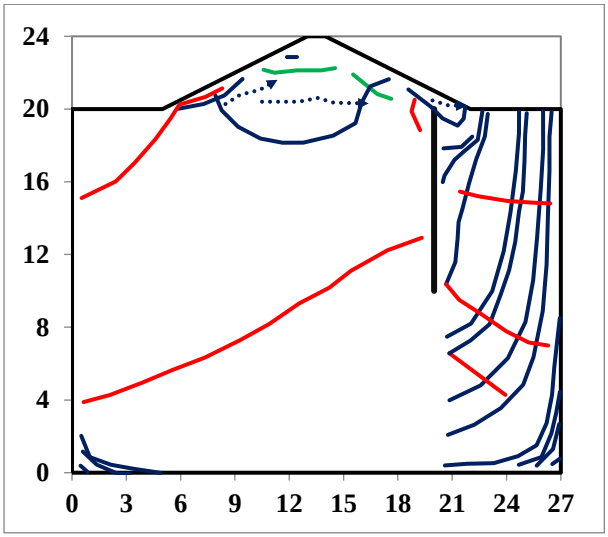

Figure 3.33(a): Flownet under Rise up condition (for 10 m long sheet pile at *B*/8 from downstream end, time = 1.0 hr.)

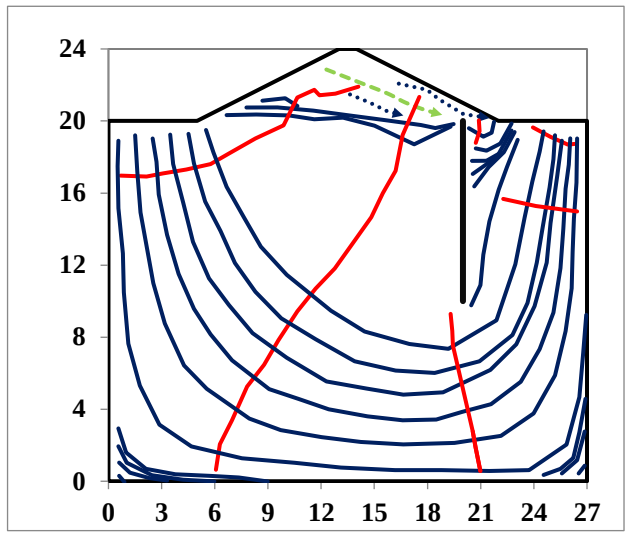

Figure 3.33(b): Flownet under Rise up condition (for 10 m long sheet pile at *B*/8 from downstream end, time = 5.0 hrs.

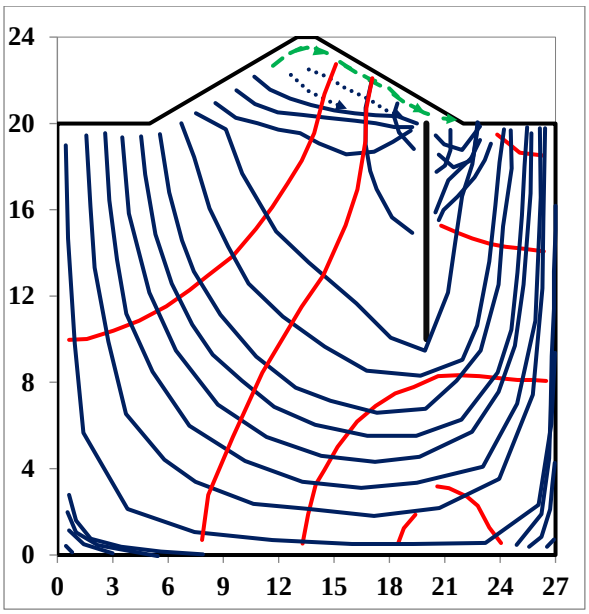

Figure 3.33(c): Flownet under Rise up condition (for 10 m long sheet pile at *B*/8 from downstream end, time = 6 hrs.)

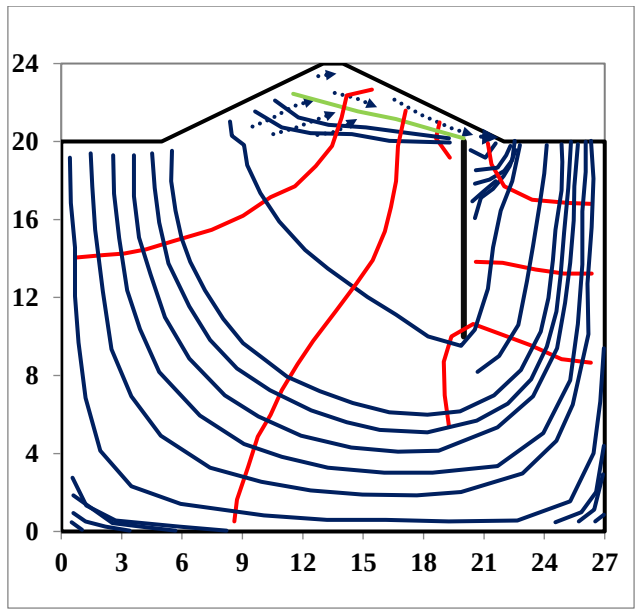

Figure 3.33(d): Flownet under Drawdown condition (for 10 m long sheet pile at *B*/8 from downstream end, time = 7.0 hrs.)

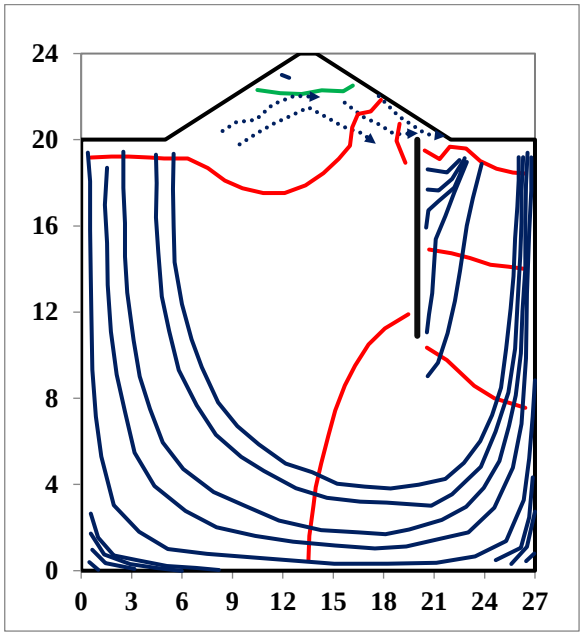

Figure 3.33(e): Flownet under Drawdown condition (for 10 m long sheet pile at *B*/8 from downstream end, time = 10.0 hrs.)

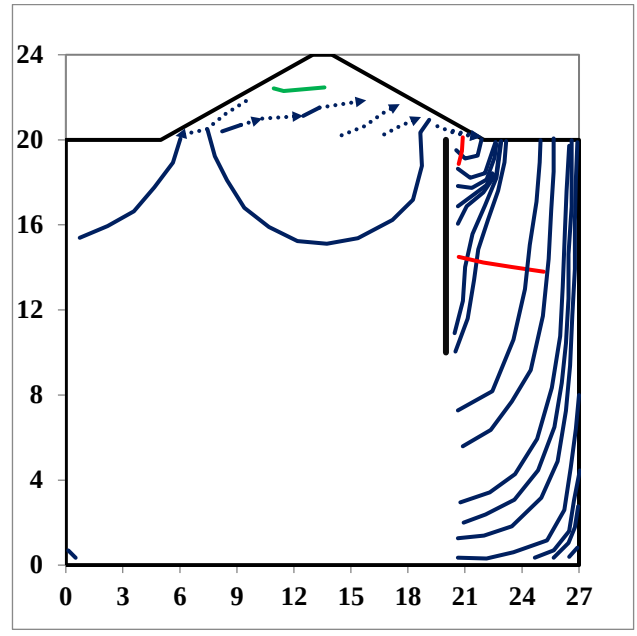

Figure 3.33(f): Flownet under Drawdown condition (for 10 m long sheet pile at *B*/8 from downstream end, time = 11.0 hrs.)

3.6.4.2.3 Presentation of results for 15 m long sheet pile at *B*/8 position from downstream end

The variation of the flownet due to the variation of upstream side with respect to cycle time has also been shown in the respective **Figure-3.34(a),3.34(b),3.34(c),3.34(d),3.34(e),3.34(d)** obtained from FLAC 2D.

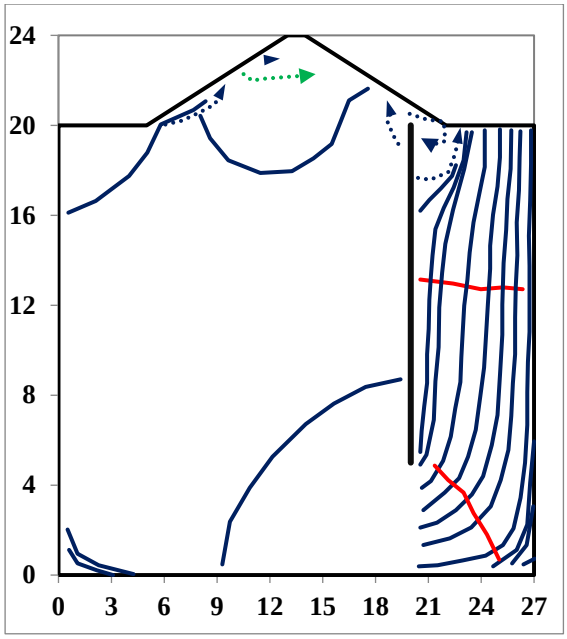

Figure 3.34(a): Flownet under Rise up condition (for 15 m long sheet pile at *B*/8 from downstream end, time = 1.0 hr.)

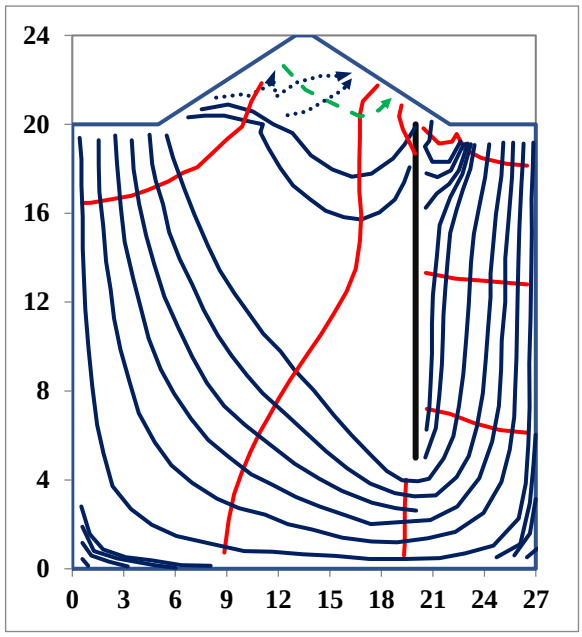

Figure 3.34(b): Flownet under Rise up condition (for 15 m long sheet pile at *B*/8 from downstream end, time = 5.0 hrs.)

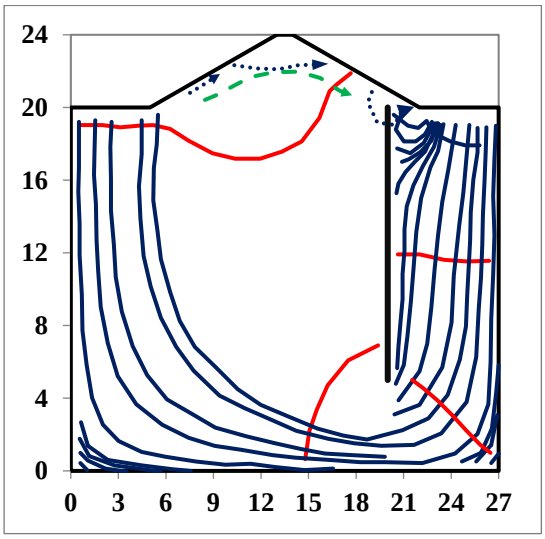

Figure 3.34(c): Flownet under Rise up condition (for 15 m long sheet pile at *B*/8 from downstream end, time = 6.0 hrs.)

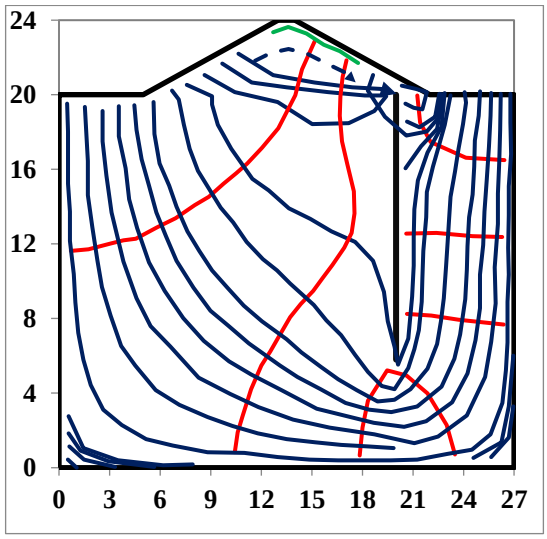

Figure 3.34(d): Flownet under Drawdown condition (for 15 m long sheet pile at *B*/8 from downstream end, time = 7.0 hrs.)

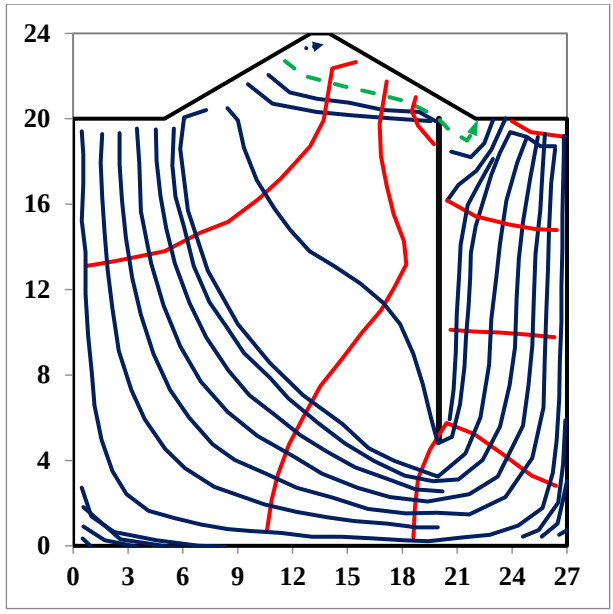

Figure 3.34(e): Flownet under Drawdown condition (for 15 m long sheet pile at *B*/8 from downstream end, time = 10.0 hrs.)

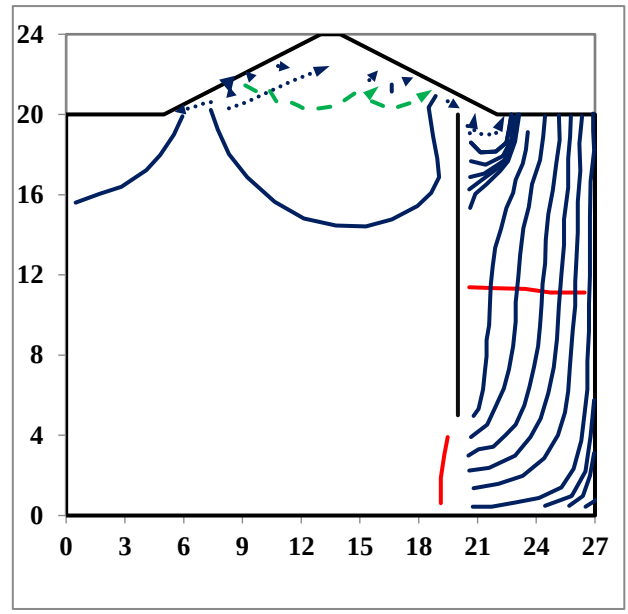

Figure 3.34(f): Flownet under Drawdown condition (for 15 m long sheet pile at *B*/8 from downstream end, time = 11.0 hrs.)

3.6.4.2.4 Presentation of results for 20 m long sheet pile at *B*/8 position from downstream end

The variation of the flownet due to the variation of upstream side with respect to cycle time has also been shown in the respective **Figures –3.35(a),3.35(b),3.35(c),3.35(d),3.35(e),3.35(f)** obtained from FLAC 2D.

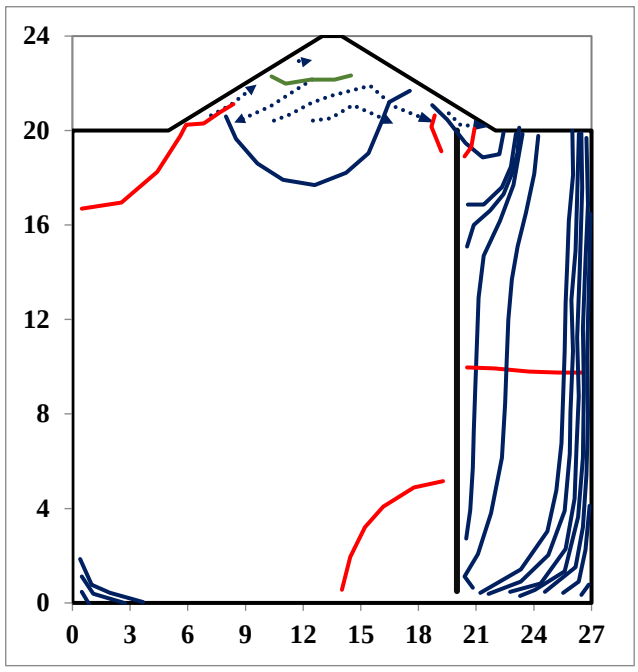

Figure 3.35(a): Flownet under Rise up condition (for 20 m long sheet pile at *B*/8 from downstream end, time = 1.0 hr.)

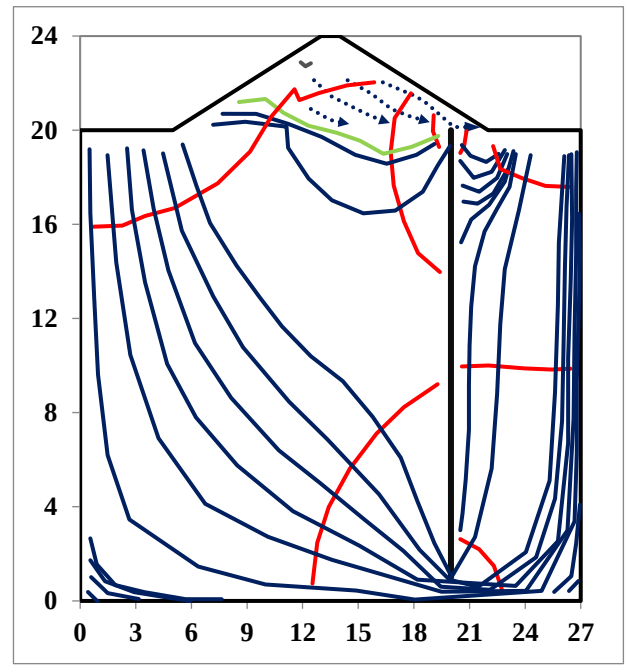

Figure 3.35(b): Flownet under Rise up condition (for 20 m long sheet pile at *B*/8 from downstream end, time = 5.0 hrs.)

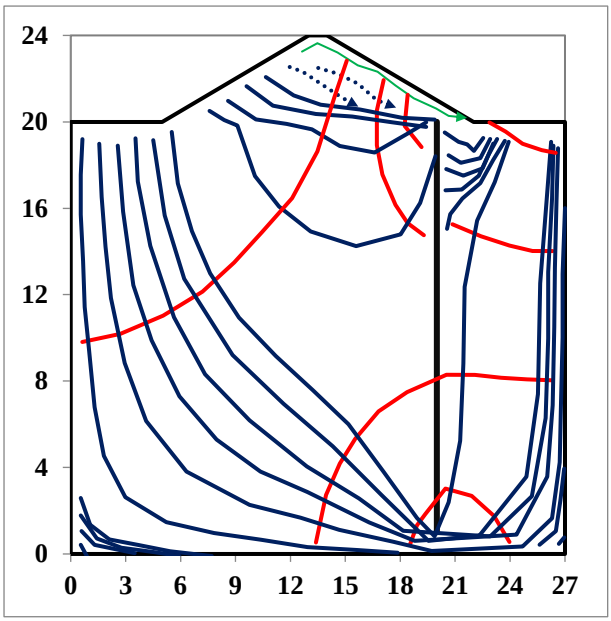

Figure 3.3.5(c): Flownet under Rise up condition (for 20 m long sheet pile at B/8 from downstream end, time = 6.0 hrs.)

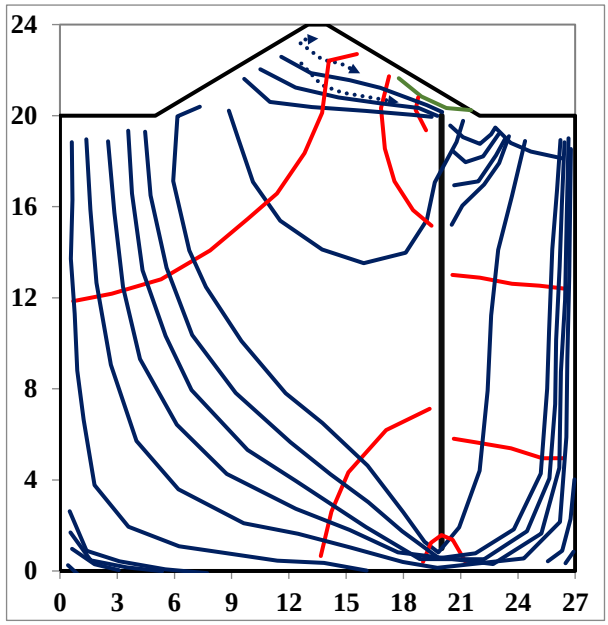

Figure 3.35(d): Flownet under Drawdown condition (for 20 m long sheet pile at *B*/8 from downstream end, time = 7.0 hrs.)

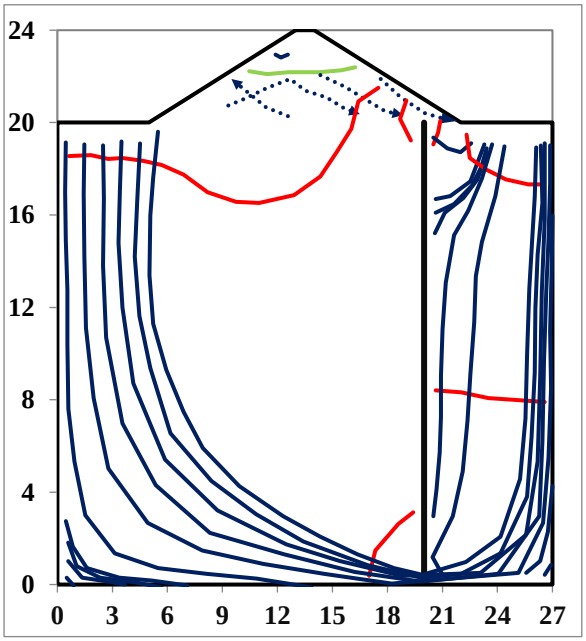

Figure 3.35(e): Flownet under Drawdown condition (for 20 m long sheet pile at *B*/8 from downstream end, time = 10.0 hrs.)

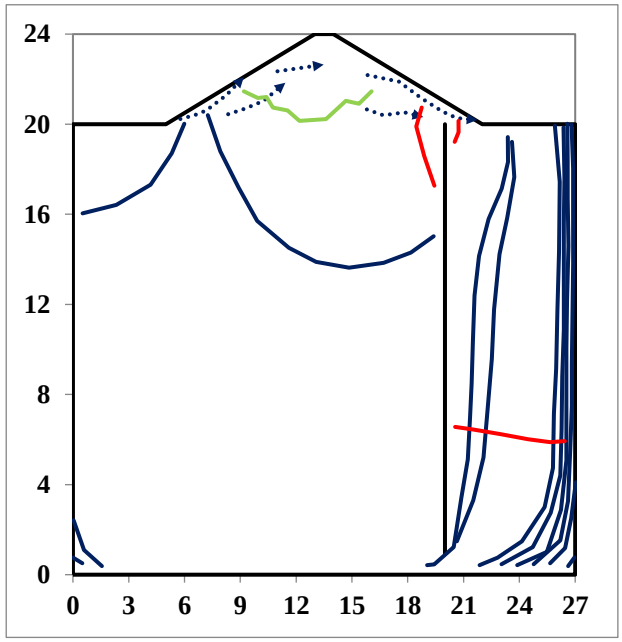

Figure 3.35(f): Flownet under Drawdown condition (for 20 m long sheet pile at *B*/8 from downstream end, time = 11.0 hrs.)

3.6.4.2.5 Presentation of results for 5 m long sheet pile at 2*B*/8 position from downstream end

The variation of the flownet due to the variation of upstream side with respect to cycle time has also been shown in the respective **Figures –3.36(a),3.36(b),3.36(c),3.36(d),3.36(e),3.36(f)** obtained from FLAC 2D.

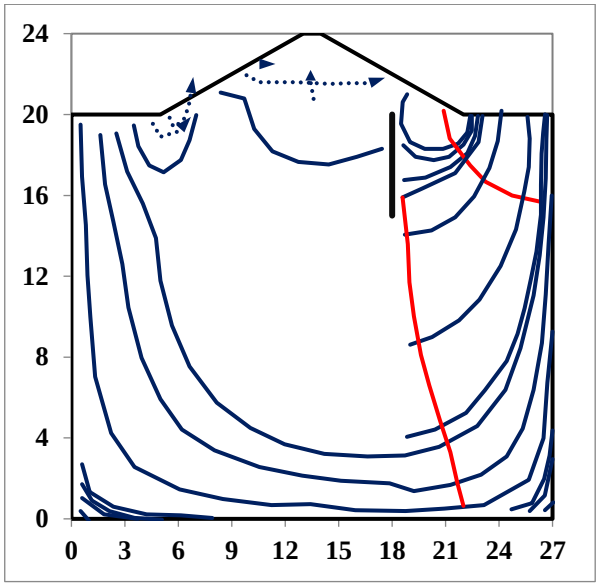

Figure 3.36(a): Flownet under Rise up condition (for 5m long sheet pile at 2*B*/8 from downstream end, time = 1.0 hr.)

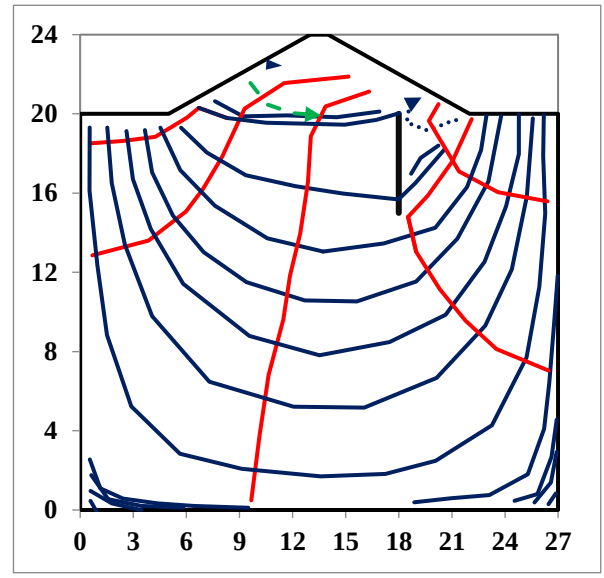

Figure 3.36(b): Flownet under Rise up condition (for 5m long sheet pile at 2*B*/8 from downstream end, time = 5.0 hrs.)

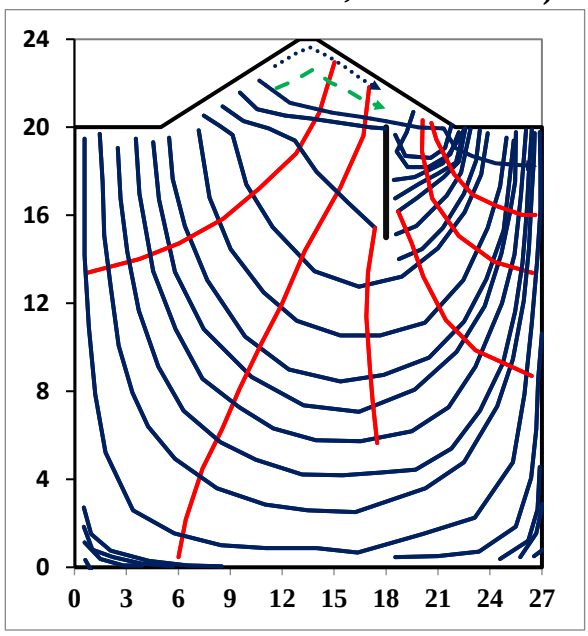

Figure 3.36(c): Flownet under Rise up condition (for 5m long sheet pile at 2*B*/8 from downstream end, time = 6.0 hrs.)

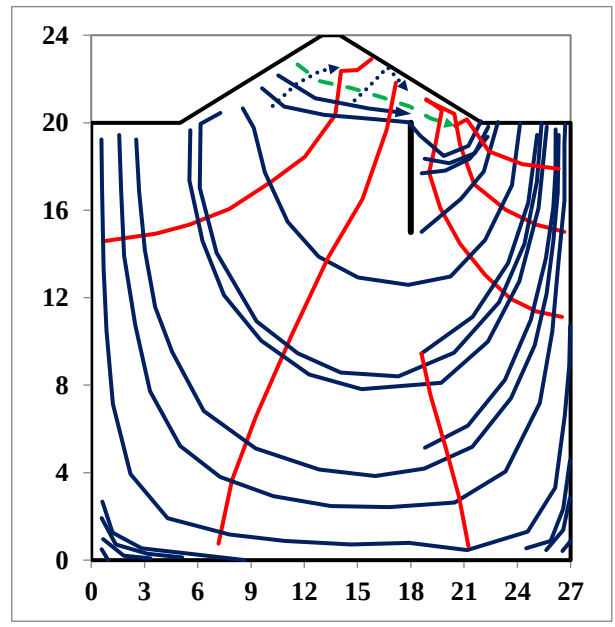

Figure 3.36(d): Flownet under Drawdown condition (for 5m long sheet pile at 2*B*/8 from downstream end, time = 7.0 hrs.)

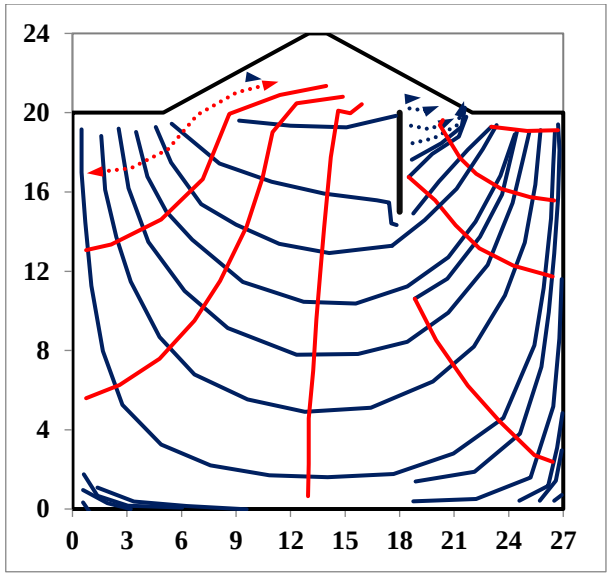

Figure 3.35(e): Flownet under Drawdown condition (for 5m long sheet pile at 2*B*/8 from downstream end, time = 10.0 hrs.)

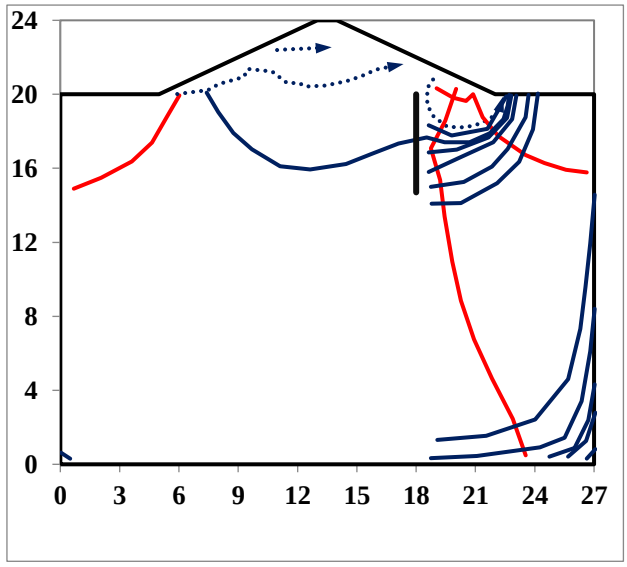

Figure 3.36(f): Flownet under Drawdown condition (for 5m long sheet pile at 2*B*/8 from downstream end, time = 11.0 hrs.)

3.6.4.2.6 Presentation of results for 10 m long sheet pile at 2*B*/8 position from downstream end

The variation of the flownet due to the variation of upstream side with respect to cycle time has also been shown in the respective **Figures –3.37(a),3.37(b),3.37(c),3.37(d),3.37(e),3.37(f)** obtained from FLAC 2D.

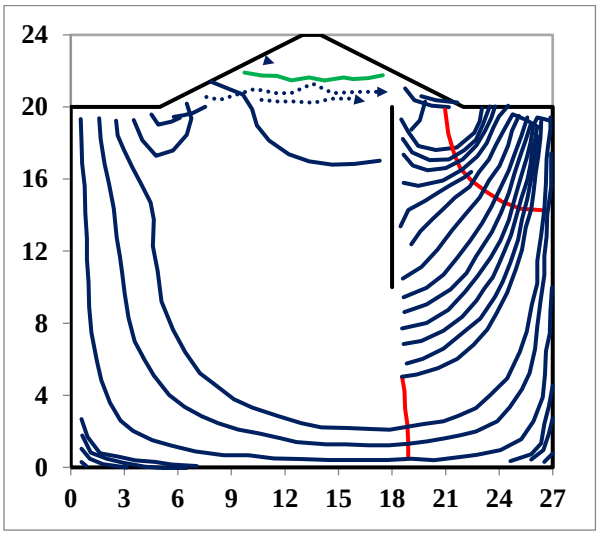

Figure 3.37(a): Flownet under Rise up condition (for 10m long sheet pile at 2*B*/8 from downstream end, time = 1.0 hr.)

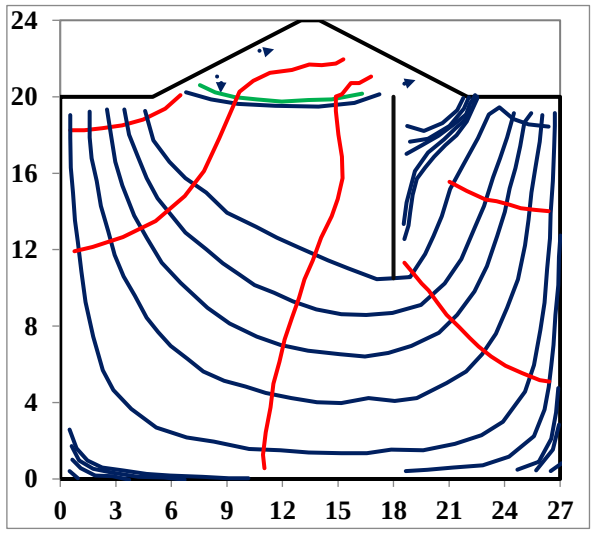

Figure 3.37(b): Flownet under Rise up condition (for 10m long sheet pile at 2*B*/8 from downstream end, time = 5.0 hrs.)

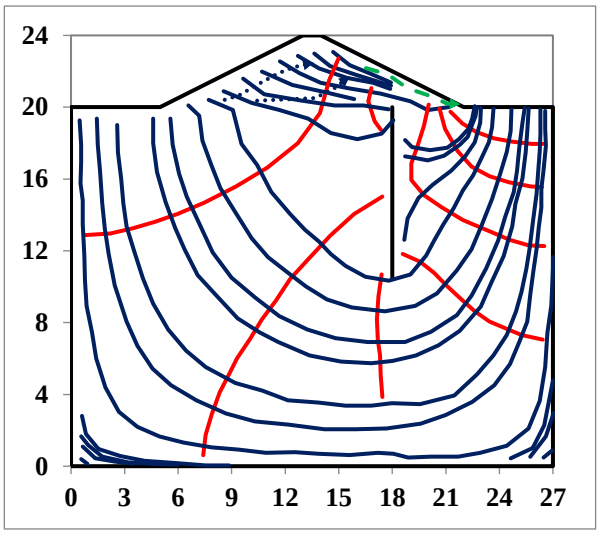

Figure 3.37(c): Flownet under Rise up condition (for 10m long sheet pile at 2*B*/8 from downstream end, time = 6.0 hrs.)

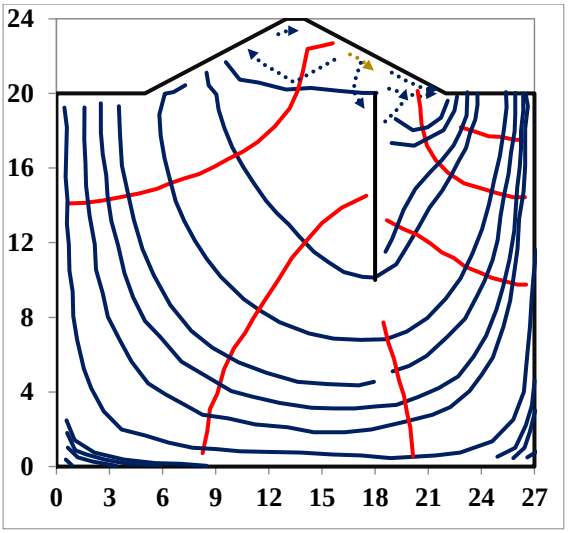

Figure 3.37(d): Flownet under Drawdown condition (for 10m long sheet pile at 2*B*/8 from downstream end, time = 7.0 hrs.)

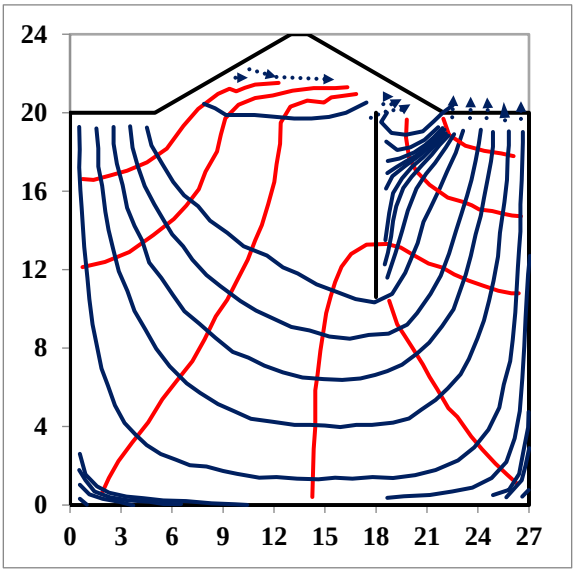

Figure 3.37(e): Flownet under Drawdown condition (for 10m long sheet pile at 2*B*/8 from downstream end, time = 10.0 hrs.)

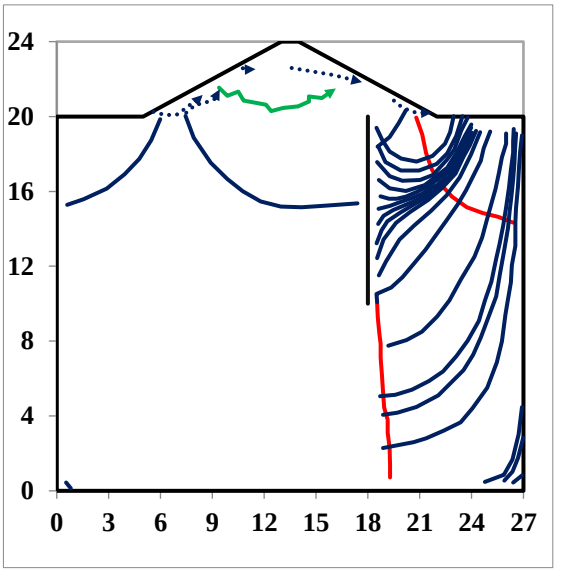

Figure 3.37(f): Flownet under Drawdown condition (for 10m long sheet pile at 2*B*/8 from downstream end, time = 11.0 hrs.)

3.6.4.2.7 Presentation of results for 15 m long sheet pile at 2*B*/8 position from downstream end

The variation of the flownet due to the variation of upstream side with respect to cycle time has also been shown in the respective **Figures –3.38(a),3.38(b),3.38(c),3.38(d),3.38(e),3.38(f)** obtained from FLAC 2D.

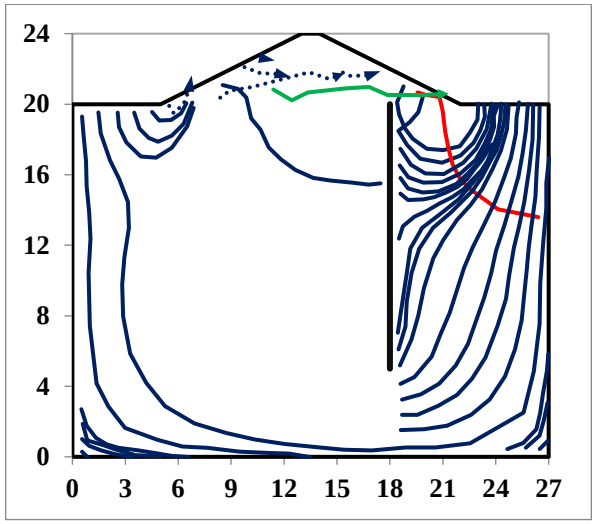

Figure 3.38(a): Flownet under Rise up condition (for 15m long sheet pile at 2*B*/8 from downstream end, time = 1.0 hr.)

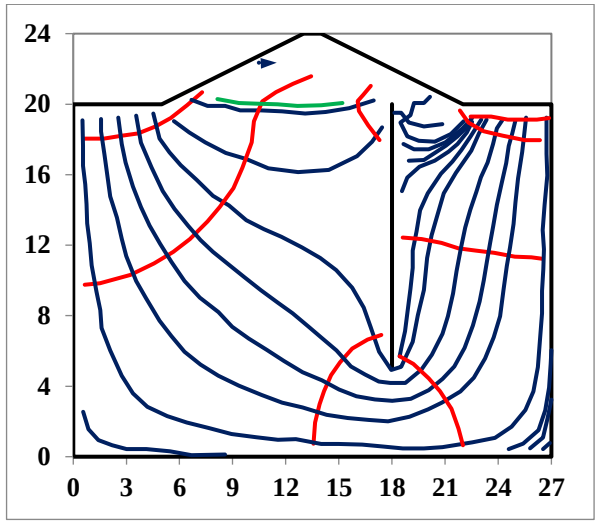

Figure 3.38(b): Flownet under Rise up condition (for 15m long sheet pile at 2*B*/8 from downstream end, time = 5.0 hrs.)

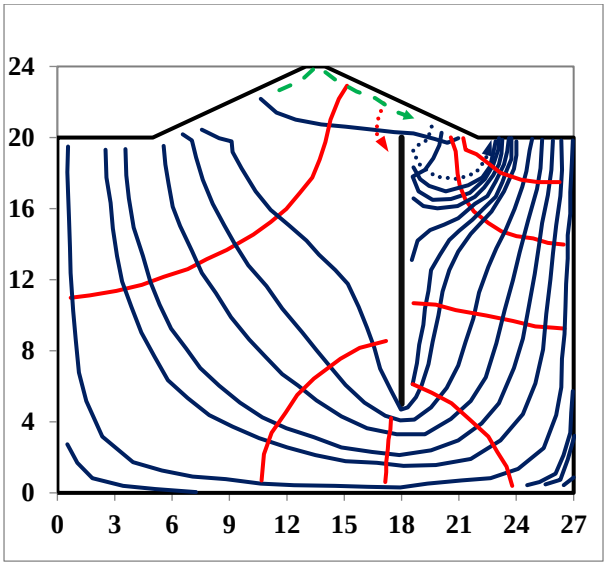

Figure 3.38(c): Flownet under Rise up condition (for 15m long sheet pile at 2*B*/8 from downstream end, time = 6.0 hrs.)

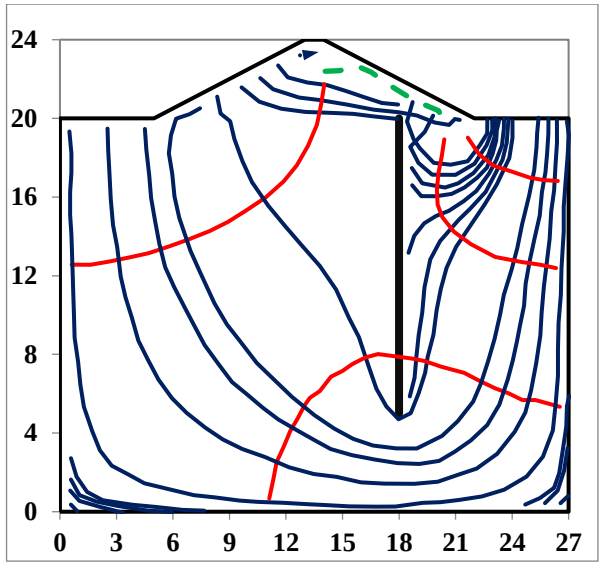

Figure 3.38(d): Flownet under Drawdown condition (for 15m long sheet pile at 2*B*/8 from downstream end, time = 7.0 hrs.)

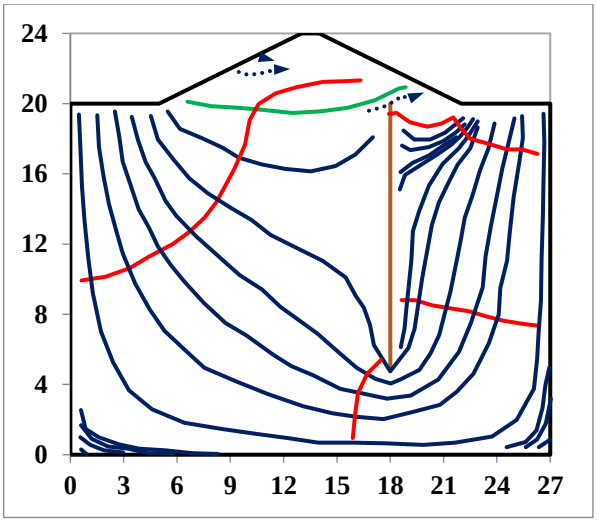

Figure 3.38(e): Flownet under Drawdown condition (for 15m long sheet pile at 2*B*/8 from downstream end, time = 10.0 hrs.)

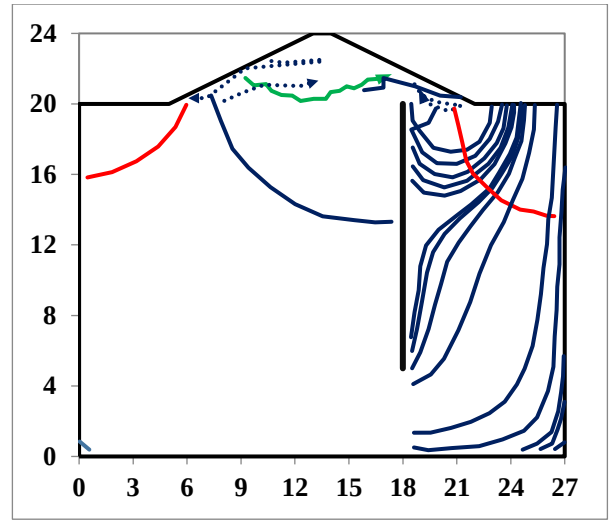

Figure 3.38(f): Flownet under Drawdown condition (for 15m long sheet pile at 2*B*/8 from downstream end, time = 11.0 hrs.)

3.6.4.2.8 Presentation of results for 20 m long sheet pile at 2*B*/8 position from downstream end

The variation of the flownet due to the variation of upstream side with respect to cycle time has also been shown in the respective **Figures –3.39(a),3.39(b),3.39(c),3.39(d),3.39(e),3.39(f)**obtained from FLAC 2D.

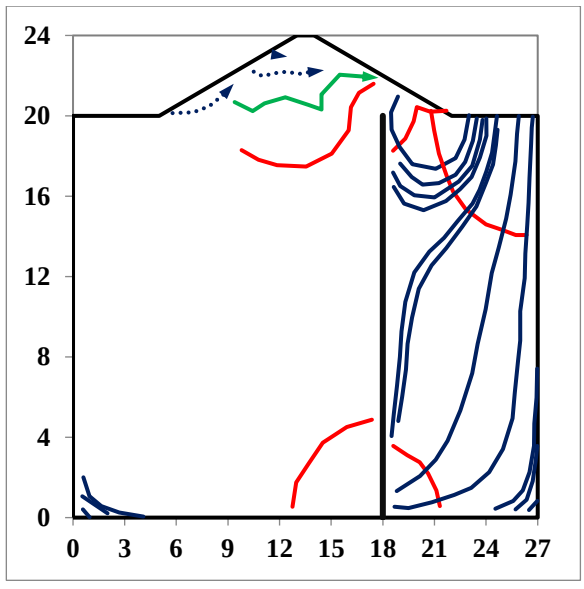

Figure 3.39(a): Flownet under Rise up condition (for 20m long sheet pile at 2*B*/8 from downstream end, time = 1.0 hr.)

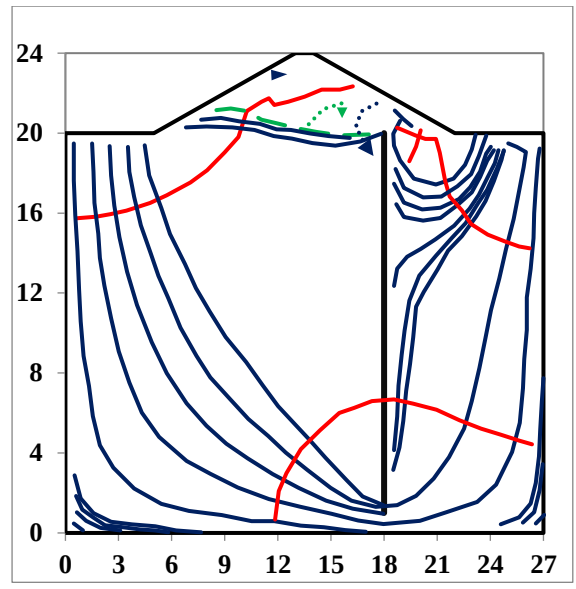

Figure 3.39(b): Flownet under Rise up condition (for 20m long sheet pile at 2*B*/8 from downstream end, time = 5.0 hrs.)

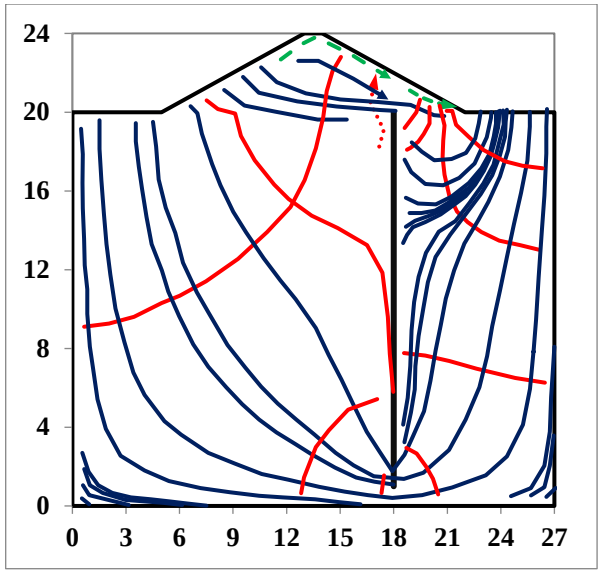

Figure 3.39(c): Flownet under Rise up condition (for 20m long sheet pile at 2*B*/8 from downstream end, time = 6.0 hrs.)

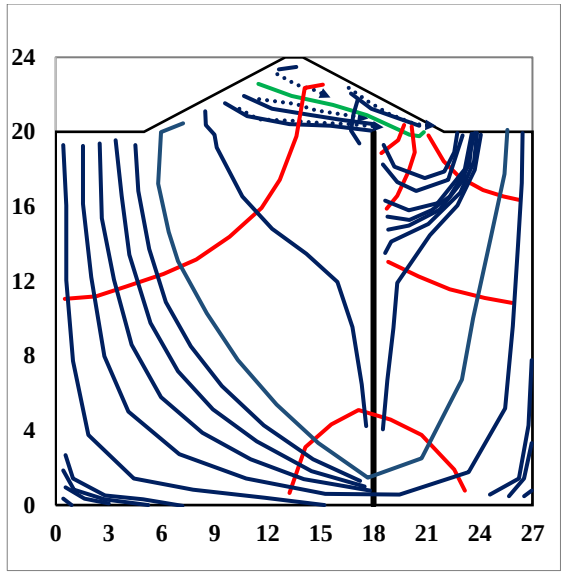

Figure 3.39(d): Flownet under Drawdown condition (for 20m long sheet pile at 2*B*/8 from downstream end, time = 8.0 hrs.)

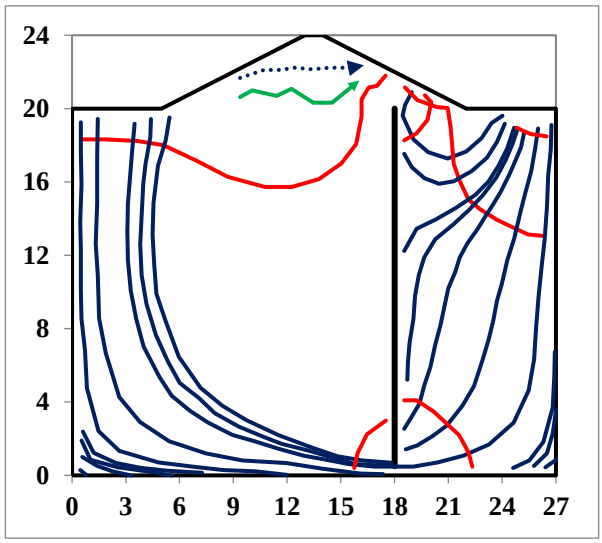

Figure 3.39(e): Flownet under Drawdown condition (for 20m long sheet pile at 2*B*/8 from downstream end, time = 10.0 hrs.)

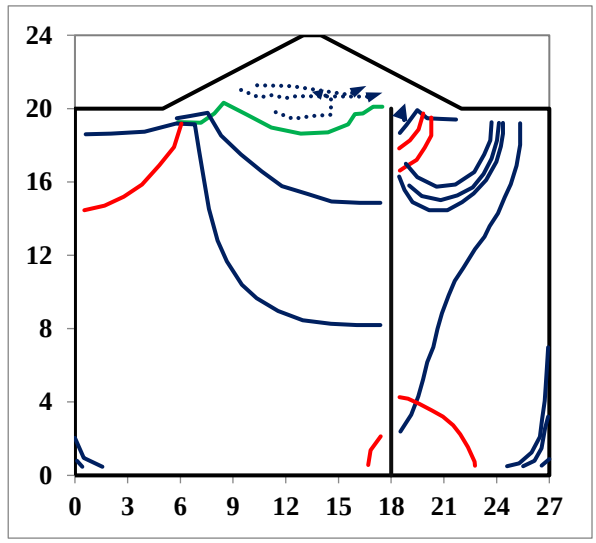

Figure 3.39(f): Flownet under Drawdown condition (for 20m long sheet pile at 2*B*/8 from downstream end, time = 11.0 hrs.)

3.6.4.2.9 Presentation of results for 5 m long sheet pile AT 3*B*/8 position from downstream end

The variation of the flownet due to the variation of upstream side with respect to cycle time has also been shown in the respective **Figures –3.40(a),3.40(b),3.40(c),3.40(d),3.40(e),3.40(f)** obtained from FLAC 2D.

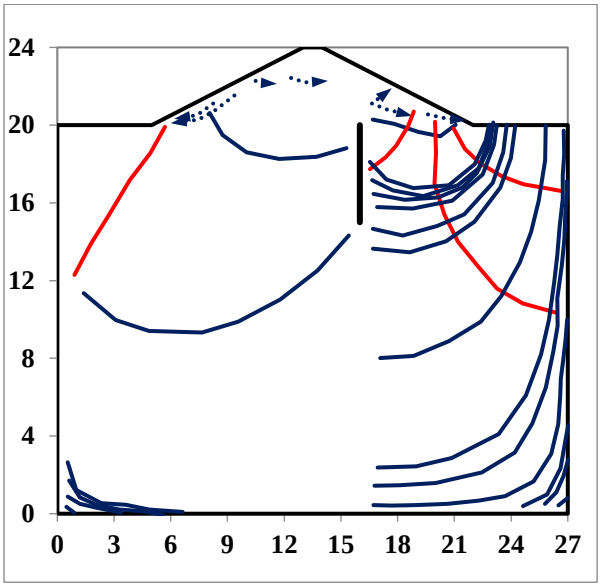

Figure 3.40(a): Flownet under Rise up condition (for 5m long sheet pile at 3*B*/8 from downstream end, time = 1.0 hr.)

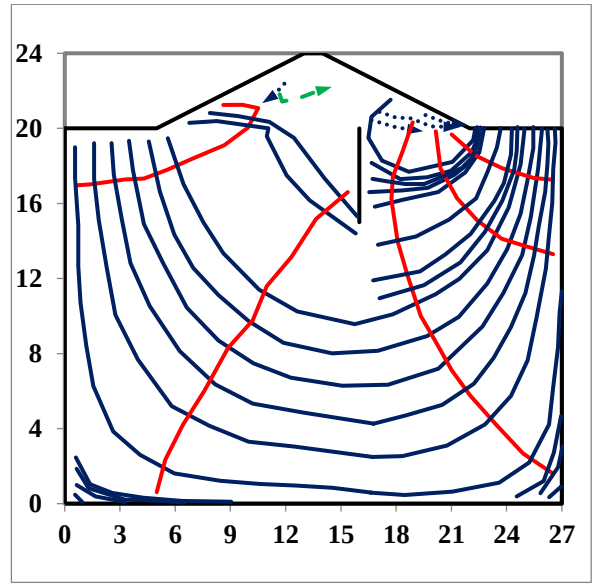

Figure 3.40(b): Flownet under Rise up condition (for 5m long sheet pile at 3*B*/8 from downstream end, time = 5.0 hrs.)

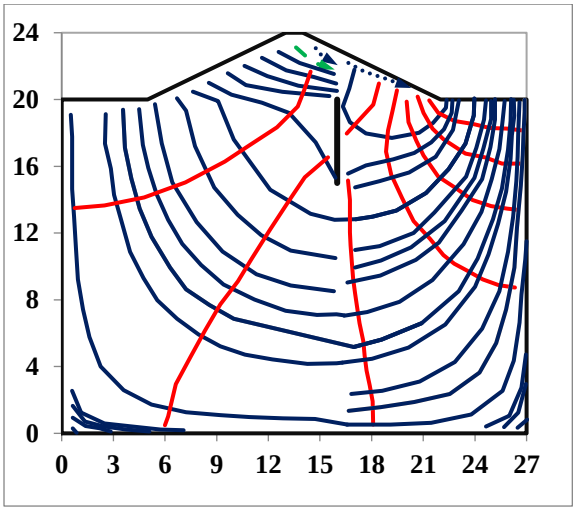

Figure 3.40(c): Flownet under Rise up condition (for 5m long sheet pile at 3*B*/8 from downstream end, time = 6.0 hrs.)

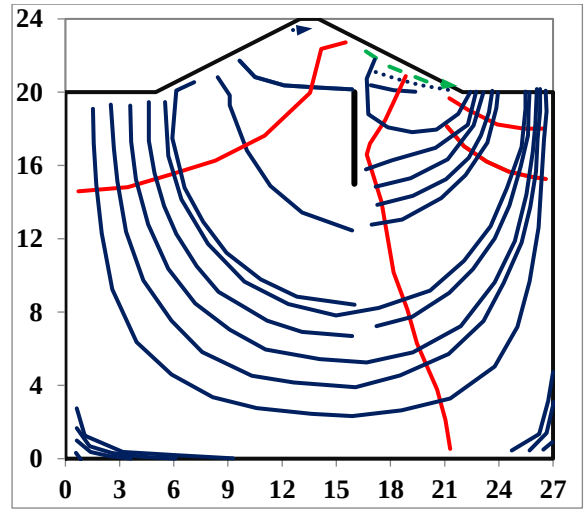

Figure 3.40(d): Flownet under Drawdown condition (for 5m long sheet pile at 3*B*/8 from downstream end, time = 7.0 hrs.)

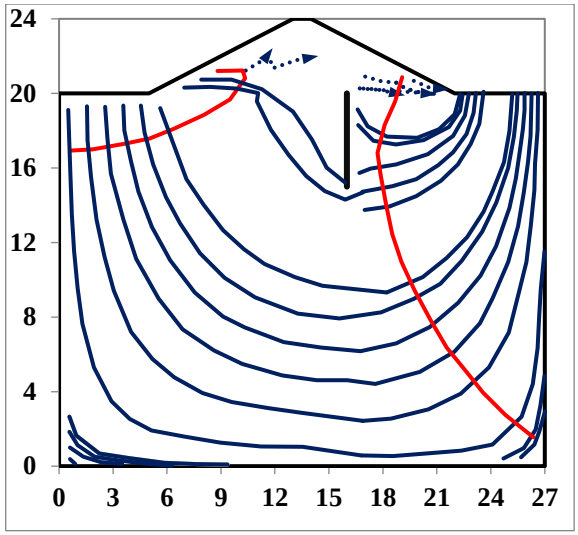

Figure 3.40(e): Flownet under Drawdown condition (for 5m long sheet pile at 3*B*/8 from downstream end, time = 10.0 hrs.)

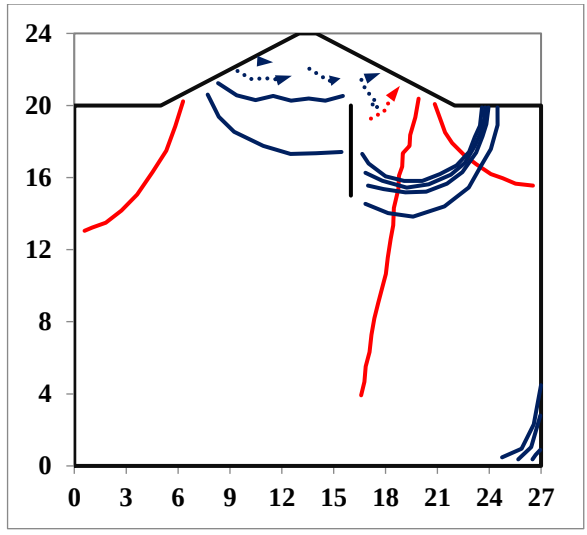

Figure 3.40(f): Flownet under Drawdown condition (for 5m long sheet pile at 3*B*/8 from downstream end, time = 11.0 hrs.)

3.6.4.2.10 Presentation of results for 10 m long sheet pile at 3*B*/8 position from downstream end

The variation of the flownet due to the variation of upstream side with respect to cycle time has also been shown in the respective **Figures –3.41(a),3.41(b),3.41(c),3.41(d),3.41(e),3.41(f)**obtained from FLAC 2D.

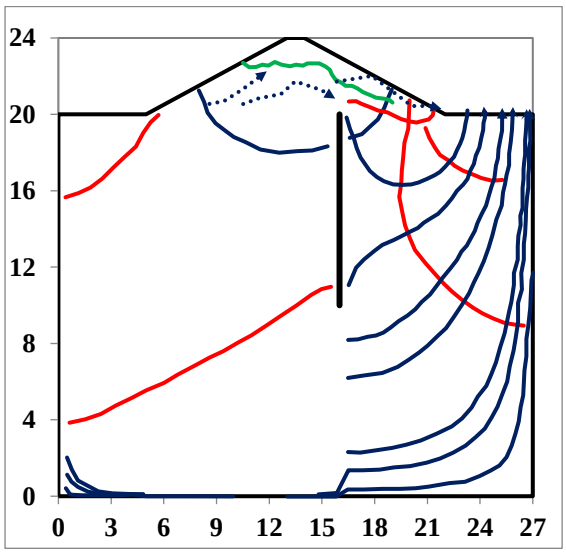

Figure 3.41(a): Flownet under Rise up condition (for 10m long sheet pile at 3*B*/8 from downstream end, time = 1.0 hr.)

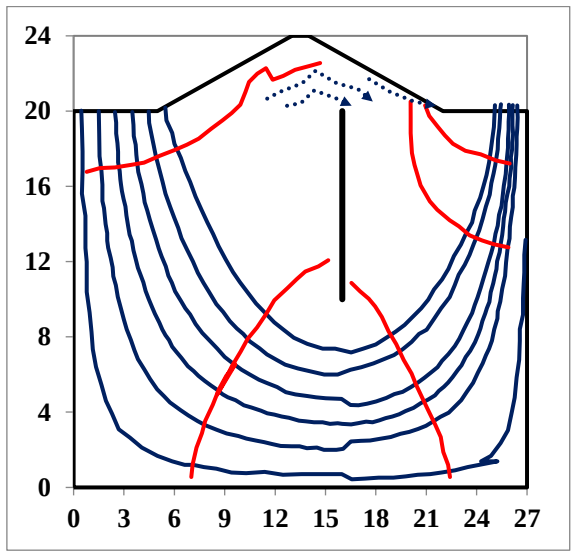

Figure 3.41(b): Flownet under Rise up condition (for 10m long sheet pile at 3*B*/8 from downstream end, time = 5.0 hrs.)

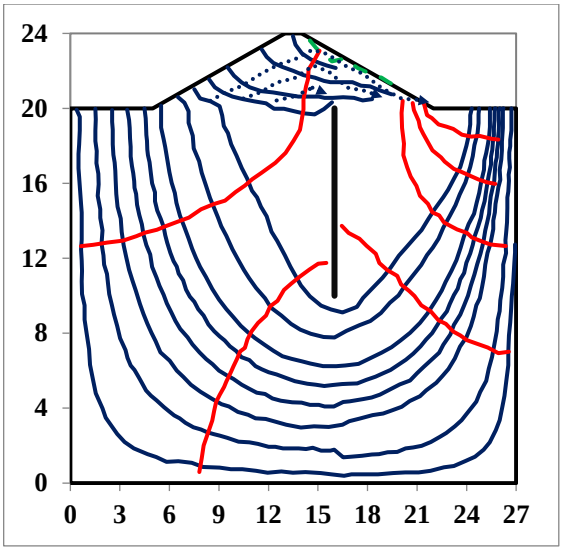

Figure 3.41(c): Flownet under Rise up condition (for 10m long sheet pile at 3*B*/8 from downstream end, time = 6.0 hrs.)

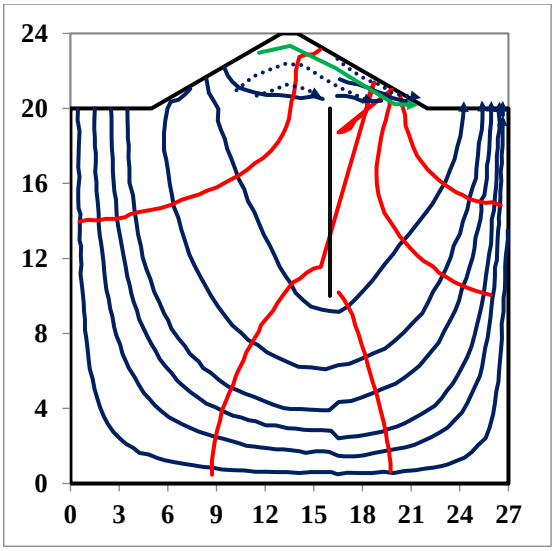

Figure 3.41(d): Flownet under Drawdown condition (for 10m long sheet pile at 3*B*/8 from downstream end, time = 7.0 hrs.)

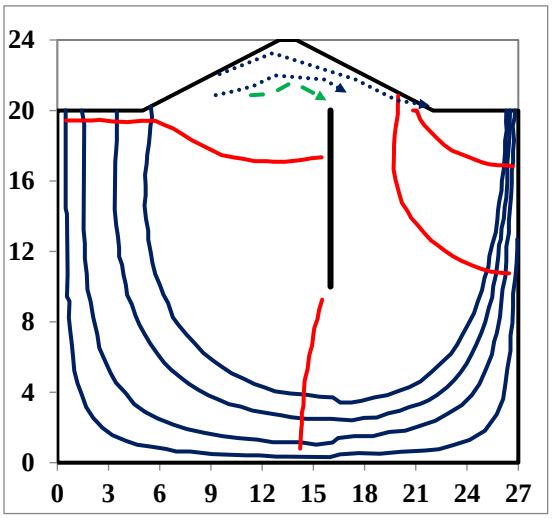

Figure 3.41(e): Flownet under Drawdown condition (for 10m long sheet pile at 3*B*/8 from downstream end, time = 10.0 hrs.)

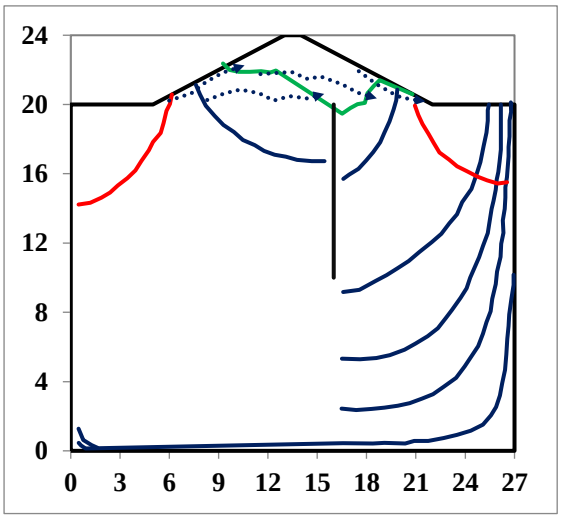

Figure 3.41(f): Flownet under Drawdown condition (for 10m long sheet pile at 3*B*/8 from downstream end, time = 11.0 hrs.)

3.6.4.2.11 Presentation of results for 15 m long sheet pile at 3*B*/8 position from downstream end

The variation of the flownet due to the variation of upstream side with respect to cycle time has also been shown in the respective **Figures –3.42(a),3.42(b),3.42(c),3.42(d),3.42(e),3.42(f)** obtained from FLAC 2D.

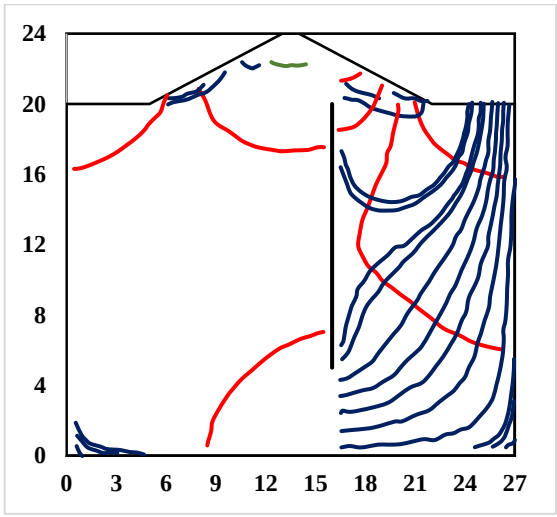

Figure 3.42(a): Flownet under Rise up condition (for 15 m long sheet pile at 3*B*/8 from downstream end, time = 1.0 hr.)

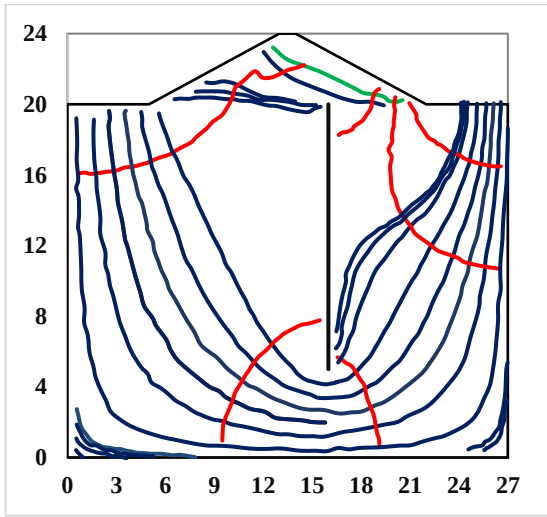

Figure 3.42(b): Flownet under Rise up condition (for 15 m long sheet pile at 3*B*/8 from downstream end, time = 5.0 hrs.)

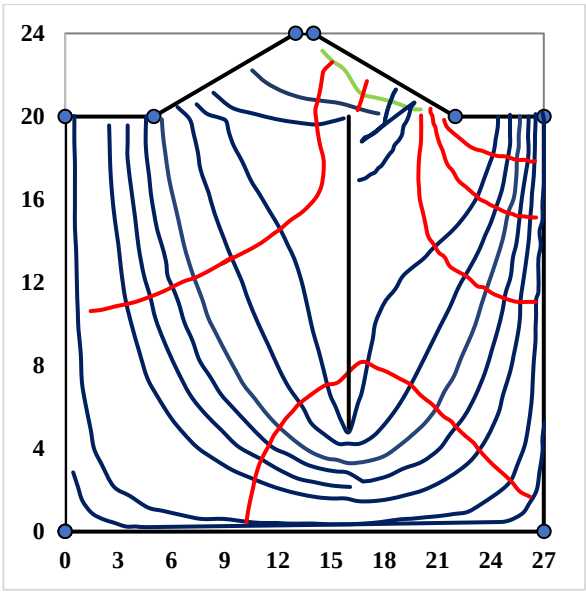

Figure 3.42(c): Flownet under Rise up condition (for 15 m long sheet pile at 3*B*/8 from downstream end, time = 6.0 hrs.)

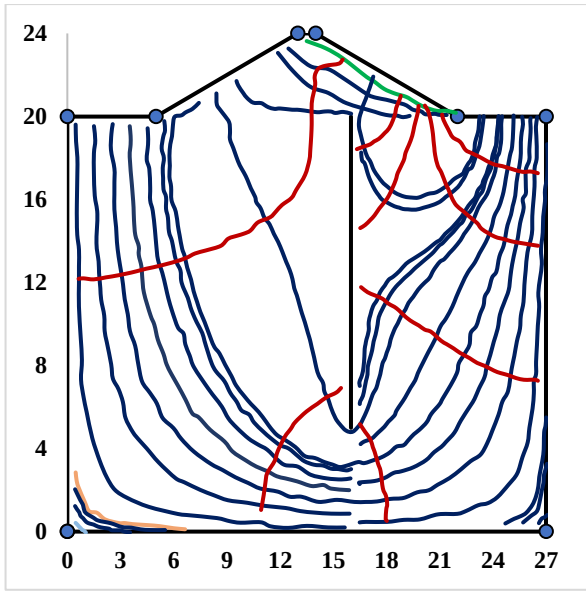

Figure 3.42(d): Flownet under Drawdown condition (for 15 m long sheet pile at 3*B*/8 from downstream end, time = 7.0 hrs.)

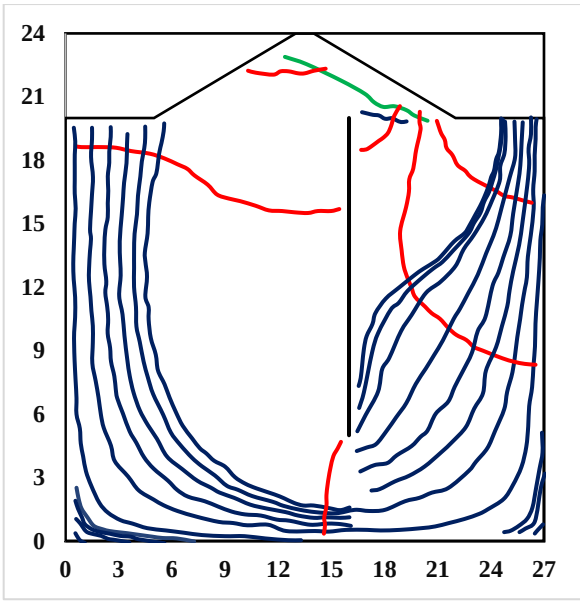

Figure 3.42(e): Flownet under Drawdown condition (for 15 m long sheet pile at 3*B*/8 from downstream end, time = 10.0 hrs.)

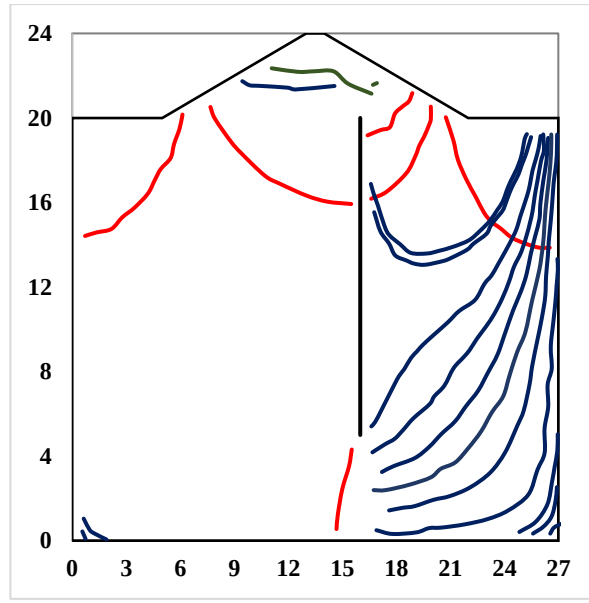

Figure 3.42(f): Flownet under Drawdown condition (for 15 m long sheet pile at 3*B*/8 from downstream end, time = 11.0 hrs.)

3.6.4.2.12 Presentation of results for 20 m long sheet pile at 3*B*/8 position from downstream end

The variation of the flownet in upstream side with respect to cycle time has also been shown in the respective **Figures –3.43(a),3.43(b),3.43(c),3.43(d),3.43(e),3.43(f)** obtained from FLAC 2D.

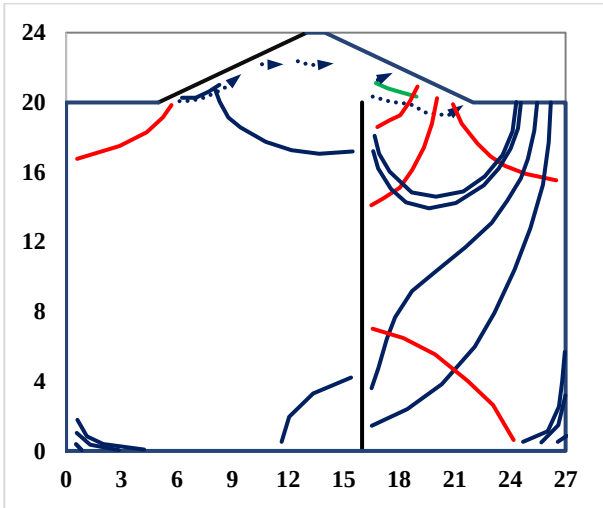

Figure 3.43(a): Flownet under Rise up condition (for 20m long sheet pile at 3*B*/8 from downstream end, time = 1.0 hr.)

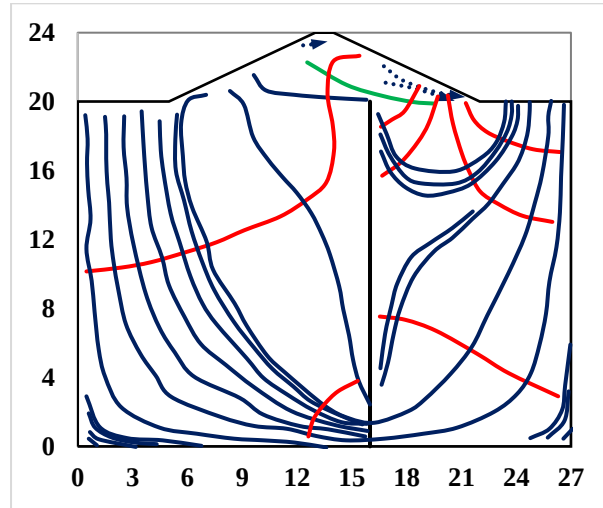

Figure 3.43(b): Flownet under Rise up condition (for 20m long sheet pile at 3*B*/8 from downstream end, time = 5.0 hrs.)

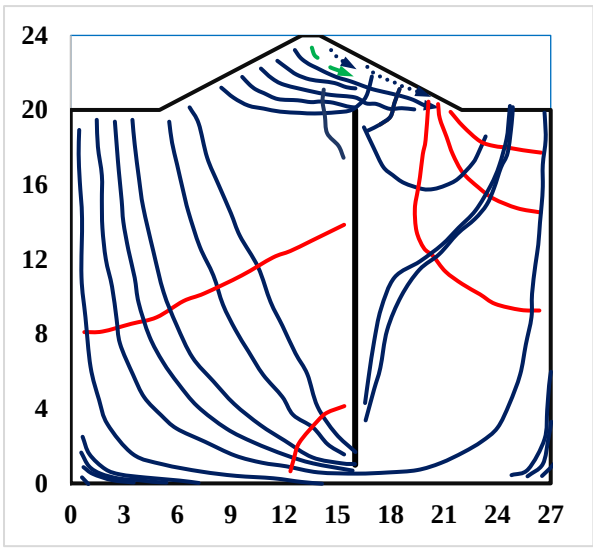

Figure 3.43(c): Flownet under Rise up condition (for 20m long sheet pile at 3*B*/8 from downstream end, time = 6.0 hrs.)

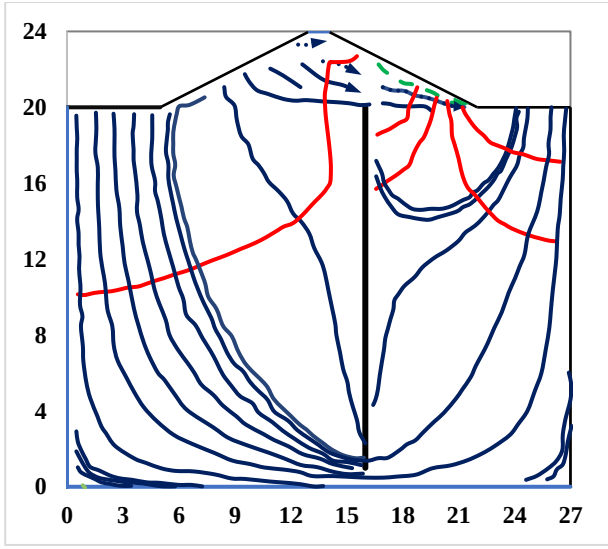

Figure 3.43(d): Flownet under Drawdown condition (for 20m long sheet pile at 3*B*/8 from downstream end, time = 7.0 hrs.)

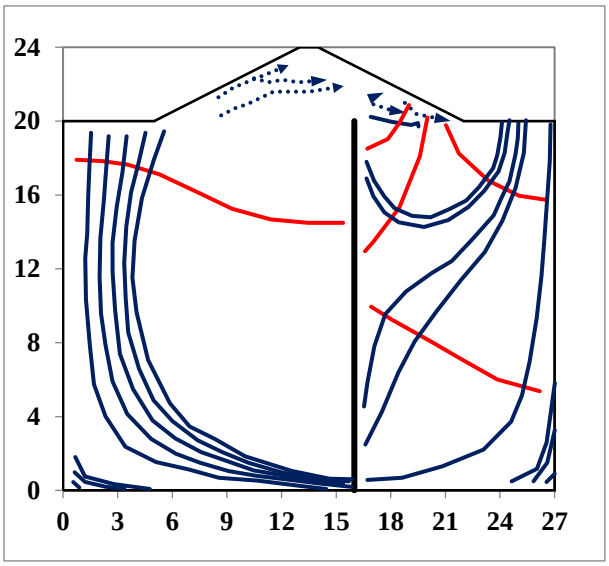

Figure 3.43(e): Flownet under Drawdown condition (for 20m long sheet pile at 3*B*/8 from downstream end, time = 10.0 hrs.)

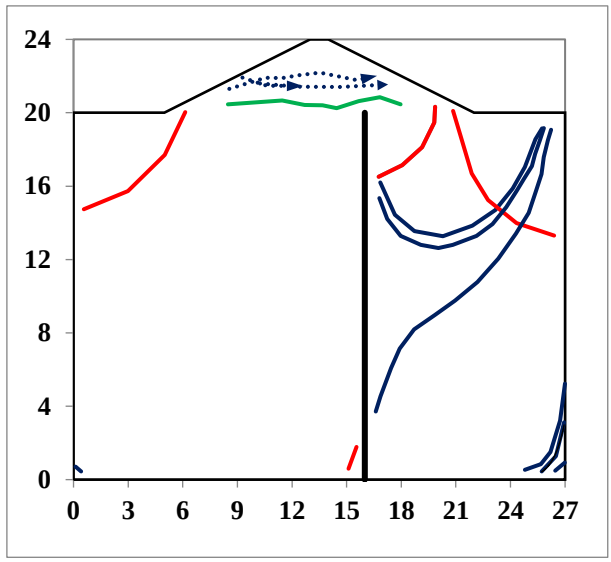

Figure 3.43(f): Flownet under Drawdown condition (for 20m long sheet pile at 3*B*/8 from downstream end, time = 11.0 hrs.)

3.6.4.3. PRESENTATION OF RESULTS OF SEEP/W

During single cycle tests with different rates of Rise up / Drawdown the variation in dynamics in flownet has been shown in **this section** for different time interval of rise up and drawdown condition. The variation of the flownet in upstream side with respect to cycle time has also been shown in the respective figures obtained from SEEP/W.

3.6.4.3.1 Presentation of results for 5 m long sheet pile at *B*/8 position from downstream end

The variation of the flownet in upstream side with respect to cycle time has also been shown in the respective **Figures –3.44(a),3.44(b),3.44(c),3.44(d),3.44(e),3.44(f),3.44(g)** obtained from SEEP/W.

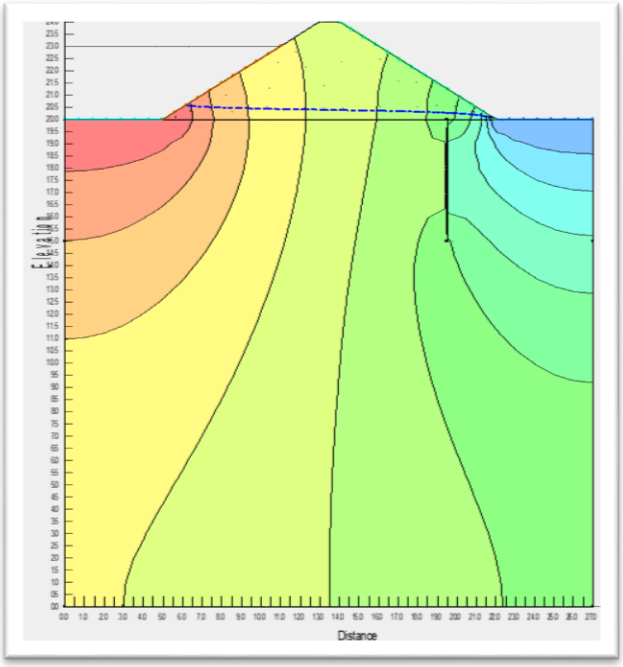

Figure 3.44(a): Flownet under rise up condition (for 5m long sheet file at *B*/8 position from downstream end, time=1 hr.)

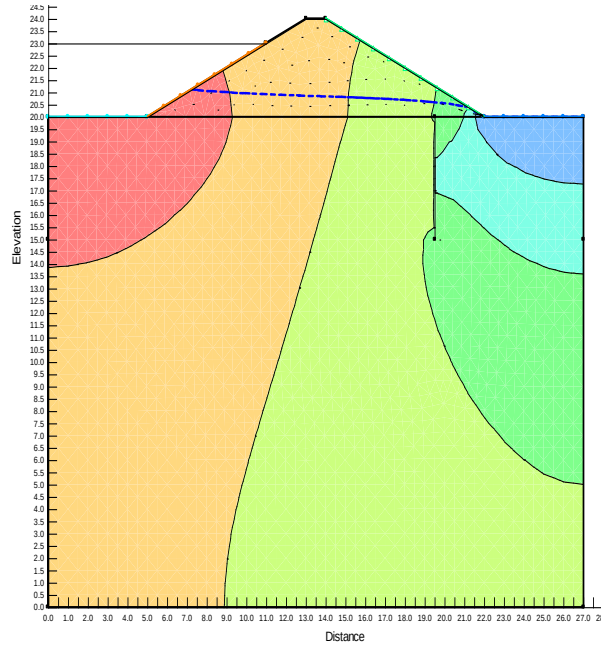

Figure 3.44(b): Flownet under rise up condition (for 5m long sheet file at *B*/8 position from downstream end, time=3 hrs.)

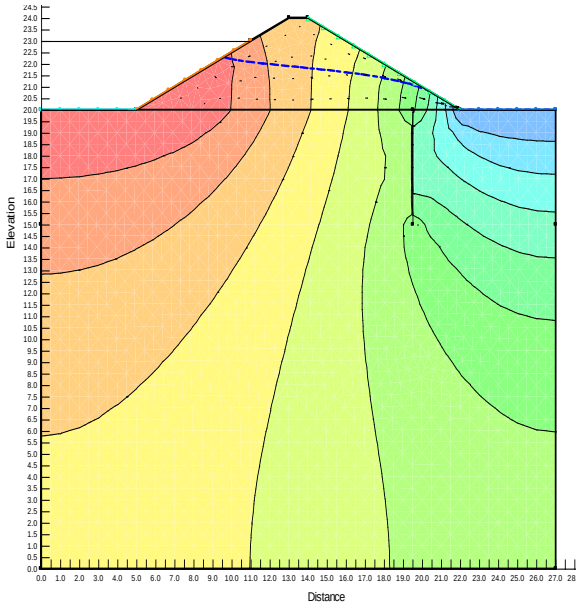

Figure 3.44(c): Flownet under rise up condition (for 5m long sheet file at *B*/8 position from downstream end, time=5 hrs.)

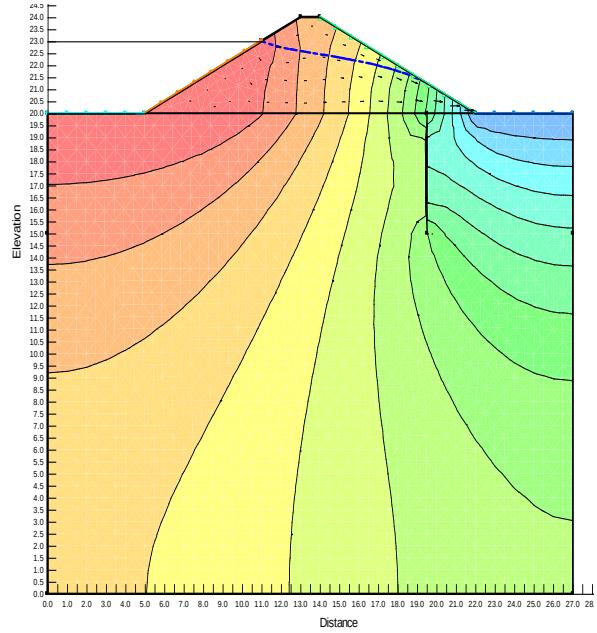

Figure 3.44(d): Flownet under rise up condition (for 5m long sheet file at *B*/8 position from downstream end, time=6 hrs.)

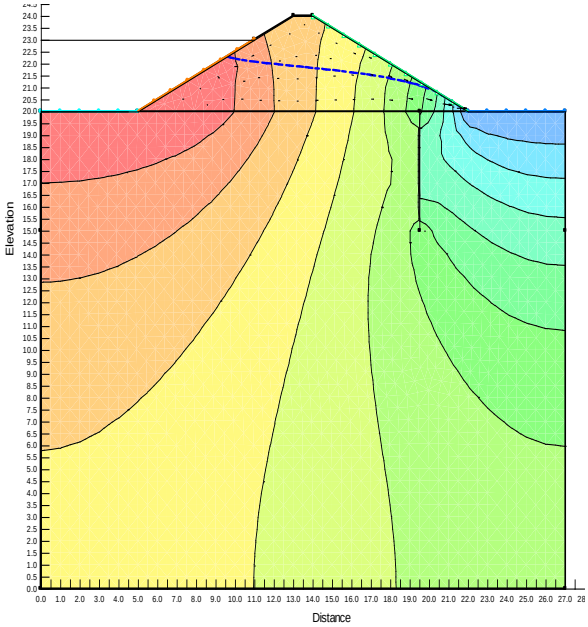

Figure 3.44(e): Flownet under draw down condition (for 5m long sheet file at *B*/8 position from downstream end, time=7 hrs.)

Figure 3.44(f): Flownet under draw down condition (for 5m long sheet file at *B*/8 position from downstream end, time=10 hrs.)

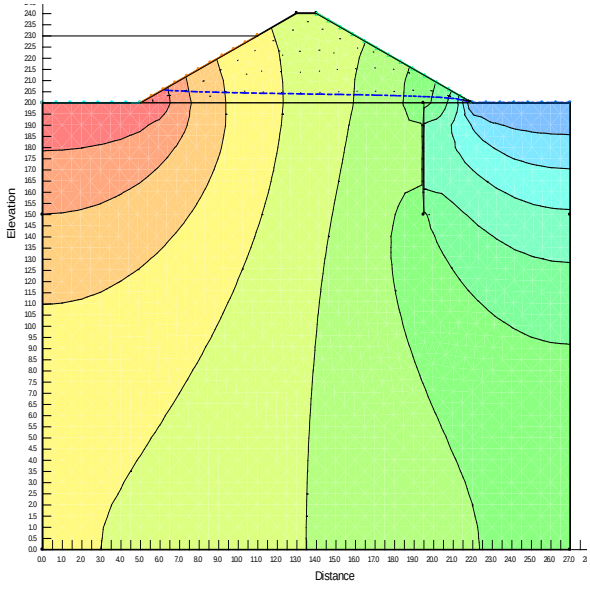

Figure 3.44(g): Flownet under draw down condition (for 5m long sheet file at *B*/8 position from downstream end, time=12hrs.)

3.6.4.3.2 Presentation of results for 10m long sheet pile at *B*/8 position from downstream end

The variation of the flownet in upstream side with respect to cycle time has also been shown in the respective **Figures –3.45(a),3.45(b),3.45(c),3.45(d),3.45(e),3.45(f),3.45(g),3.45(h)** obtained from SEEP/W.

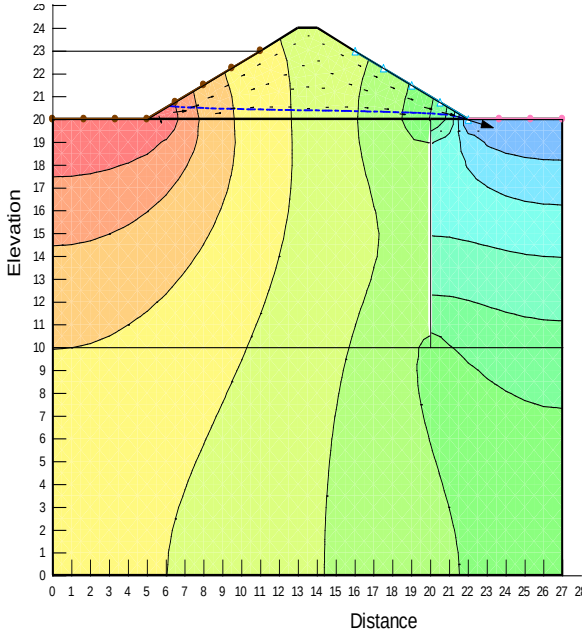

Figure 3.45(a): Flownet under rise up condition (for 10m long sheet file at *B*/8 position from downstream end, time=1 hr.)

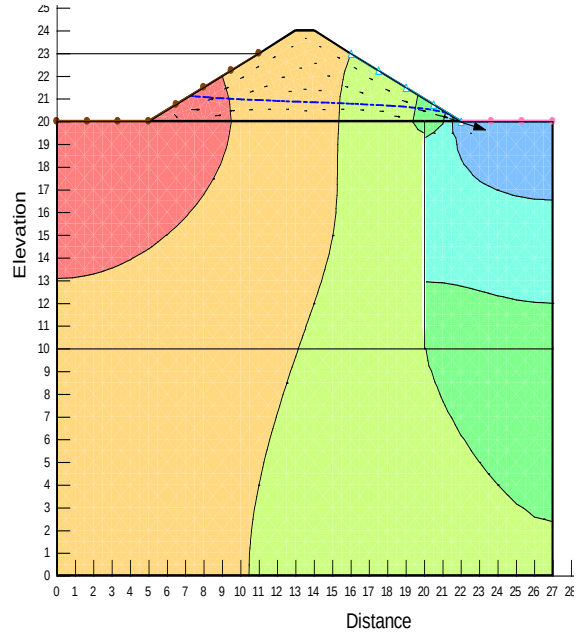

Figure 3.45(b): Flownet under rise up condition (for 10m long sheet file at *B*/8 position from downstream end, time=2 hrs.)

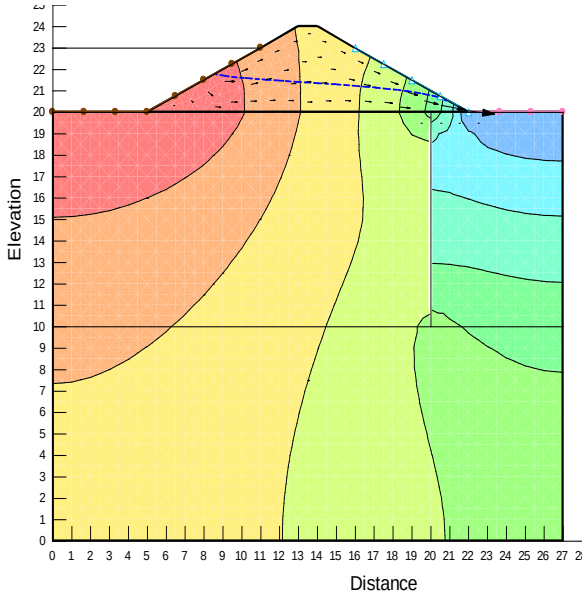

Figure 3.45(c): Flownet under rise up condition (for 10m long sheet file at *B*/8 position from downstream end, time=3 hrs.)

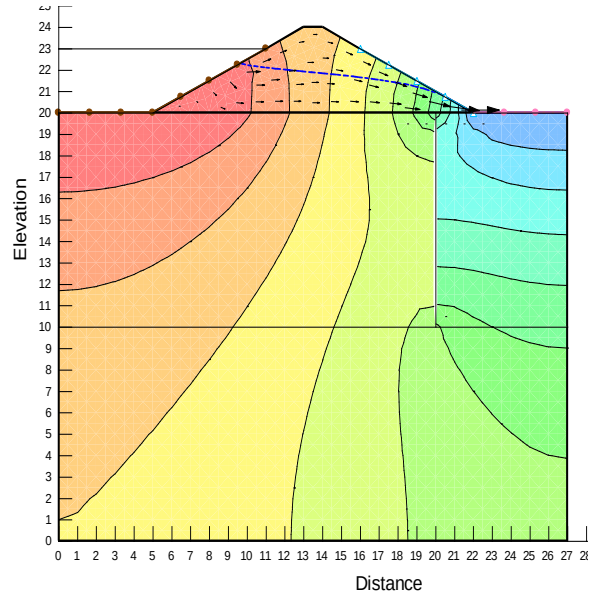

Figure 3.45(d): Flownet under rise up condition (for 10m long sheet file at *B*/8 position from downstream end, time=5 hrs.)

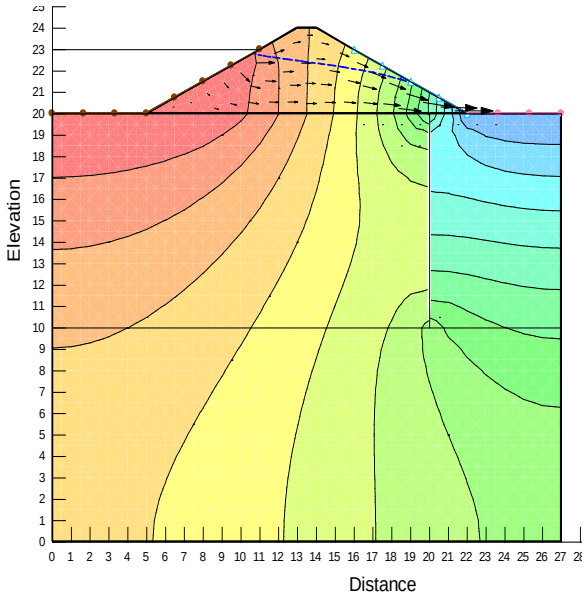

Figure 3.45(e): Flownet under rise up condition (for 10m long sheet file at *B*/8 position from downstream end, time=6 hrs.)

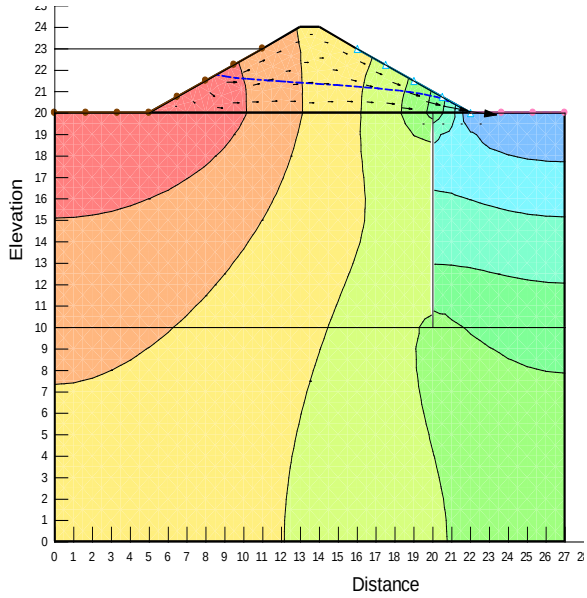

Figure 3.45(f): Flownet under draw down condition (for 10m long sheet file at *B*/8 position from downstream end, time=7 hrs.)

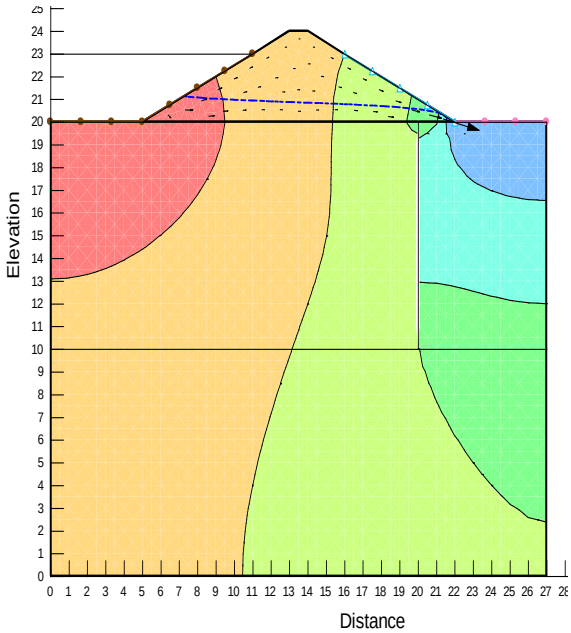

Figure 3.45(g): Flownet under draw down condition (for 10m long sheet file at *B*/8 position from downstream end, time=10 hrs.)

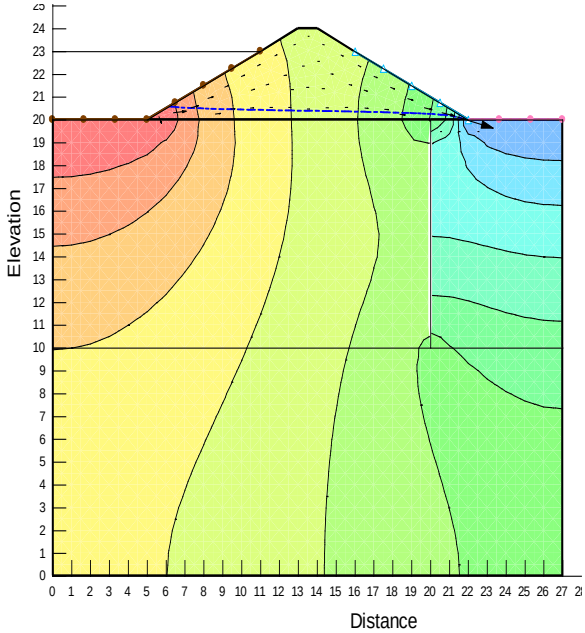

Figure 3.45(h): Flownet under draw down condition (for 10m long sheet file at *B*/8 position from downstream end, time=11 hrs.)

3.6.4.3.3 Presentation of results for 15m long sheet pile at *B*/8 position from downstream end

The variation of the flownet in upstream side with respect to cycle time has also been shown in the respective **Figures –3.46(a),3.46(b),3.46(c),3.46(d),3.46(e),3.46(f),3.46(g),3.46(h),3.46(i)** obtained from SEEP/W.

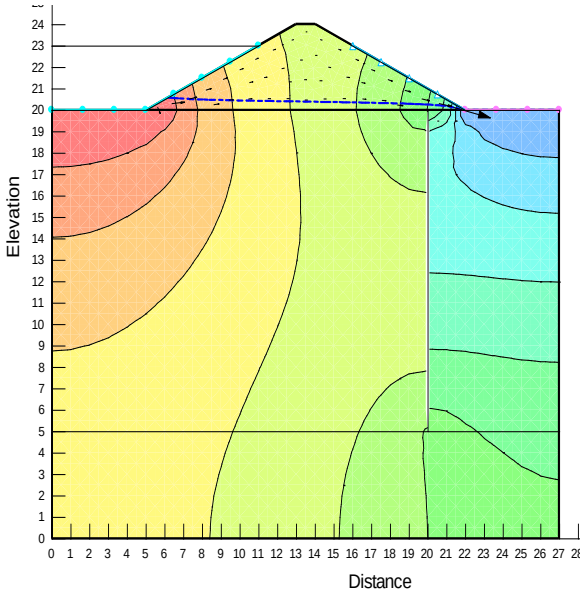

Figure 3.46(a): Flownet under rise up condition (for 15m long sheet file at *B*/8 position from downstream end, time=1 hr.)

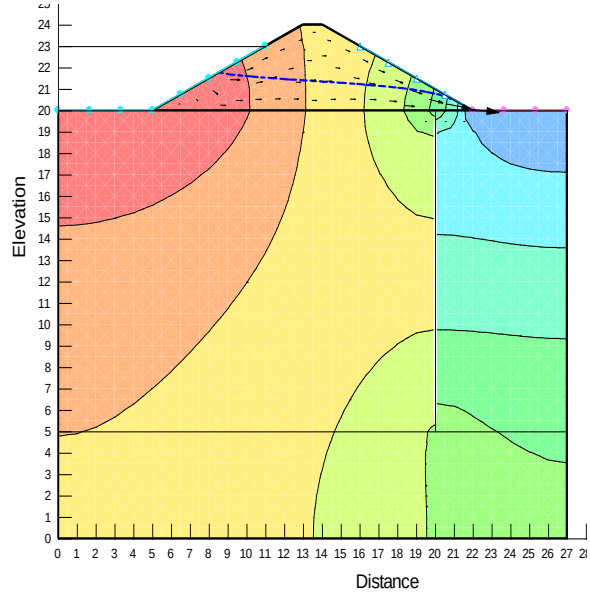

Figure 3.46(b): Flownet under rise up condition (for 15m long sheet file at *B*/8 position from downstream end, time=2 hrs.)

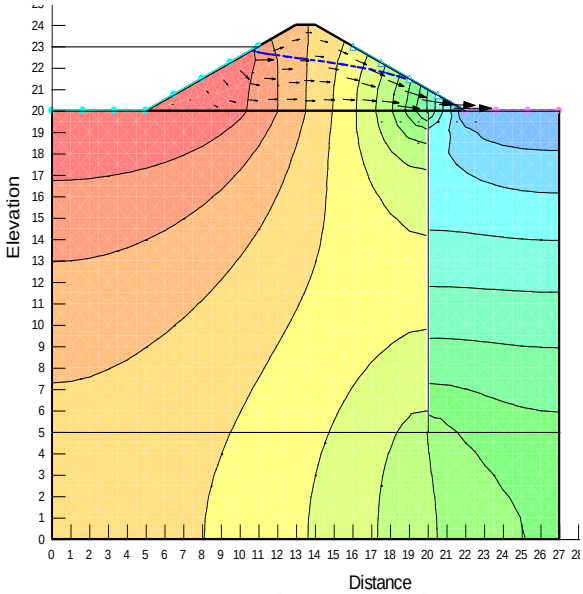

Figure 3.46(c): Flownet under rise up condition (for 15m long sheet file at *B*/8 position from downstream end, time=6 hrs.)

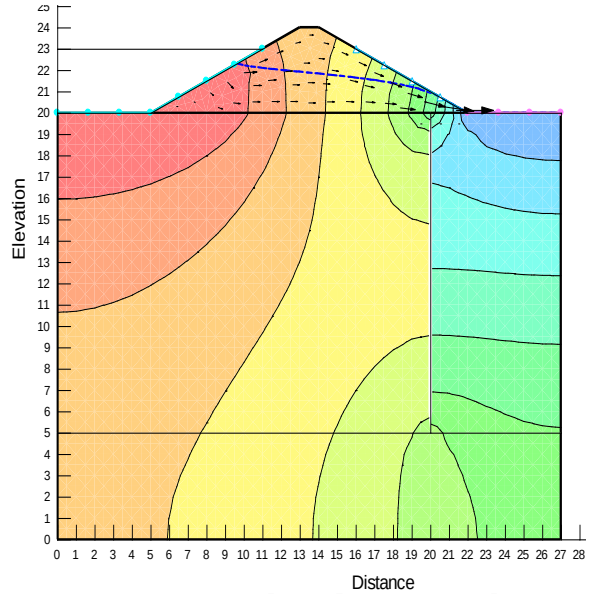

Figure 3.46(d): Flownet under rise up condition (for 15m long sheet file at *B*/8 position from downstream end, time=5 hrs.)

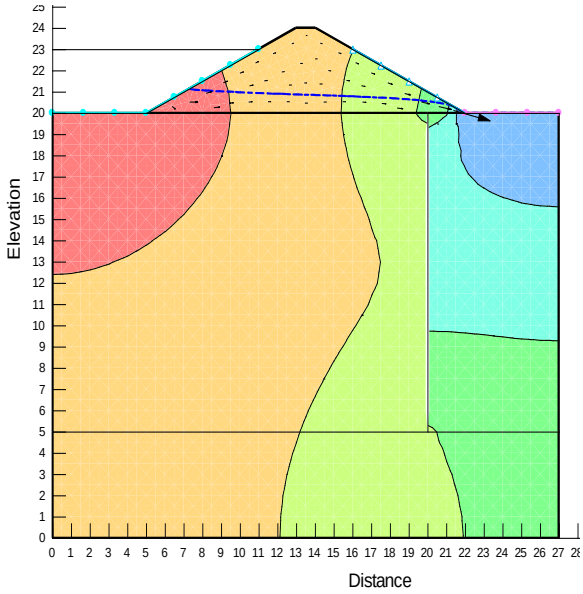

Figure 3.46(e): Flownet under rise up condition (for 15m long sheet file at *B*/8 position from downstream end, time=9 hrs.)

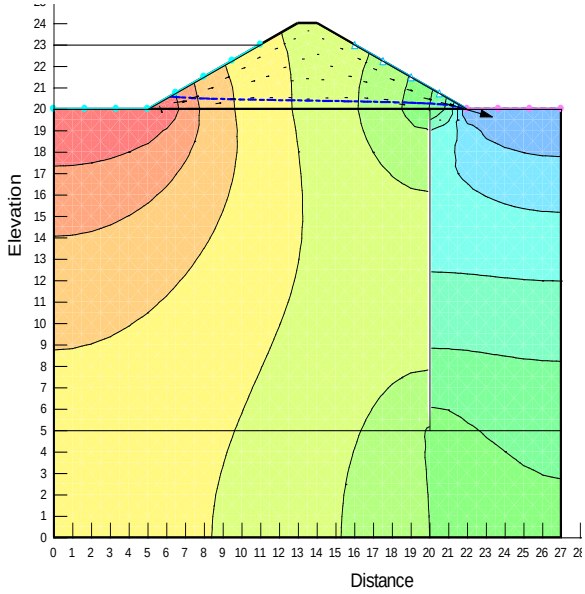

Figure 3.46(f): Flownet under draw down condition (for 15m long sheet file at *B*/8 position from downstream end, time=11 hrs.)

3.6.4.3.4 Presentation of results for 20m long sheet pile at *B*/8 position from downstream end

The variation of the flownet in upstream side with respect to cycle time has also been shown in the respective **Figures –3.47(a),3.47(b),3.47(c)** obtained from SEEP/W.

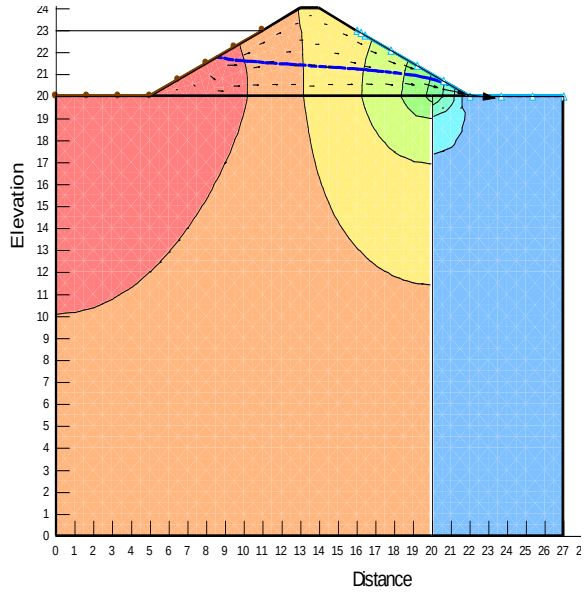

Figure 3.47(a): Flownet under rise up condition (for 20m long sheet file at *B*/8 position from downstream end, time=3 hrs.)

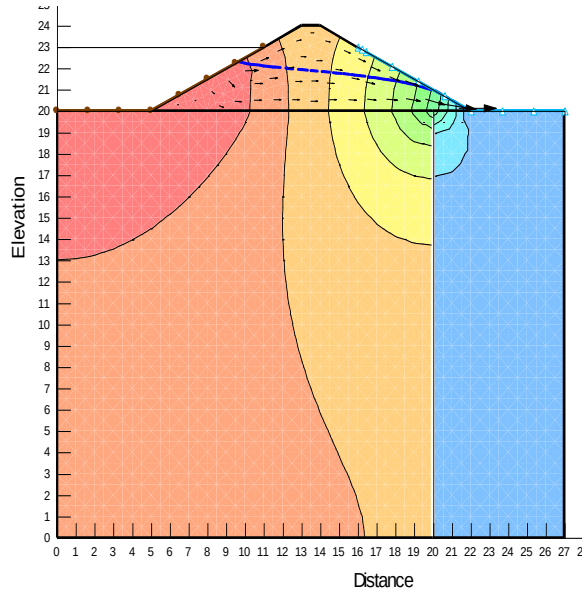

Figure 3.47(b): Flownet under rise up condition (for 20m long sheet file at *B*/8 position from downstream end, time=5 hrs.)

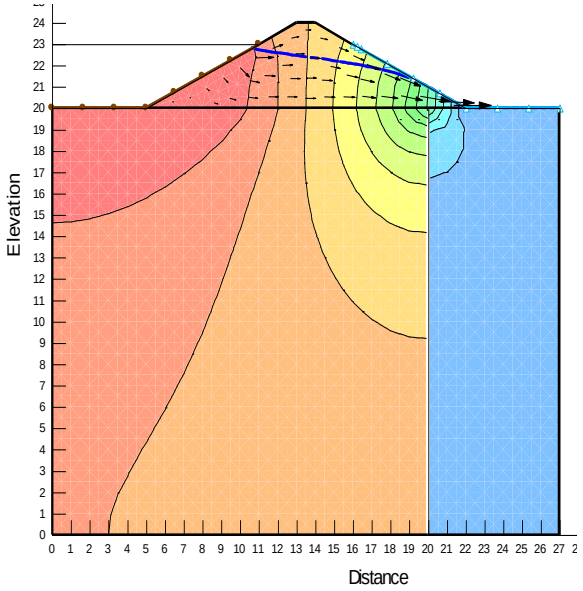

Figure 3.47(c): Flownet under rise up condition (for 20m long sheet file at *B*/8 position from downstream end, time=6 hrs.)

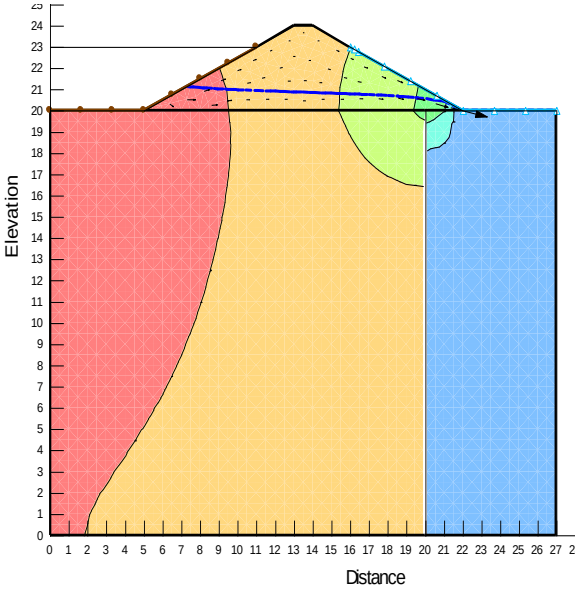

Figure 3.47(d): Flownet under rise up condition (for 20m long sheet file at *B*/8 position from downstream end, time=10 hrs.)

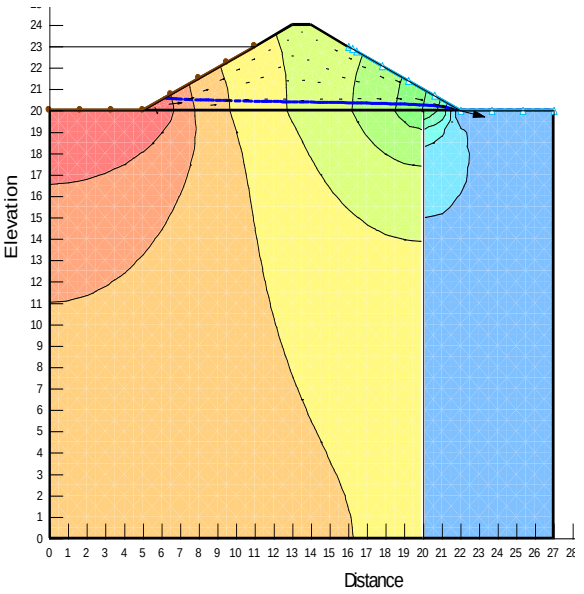

Figure 3.47(e): Flownet under rise up condition (for 20m long sheet file at *B*/8 position from downstream end, time=11 hrs.)

3.6.4.3.5 Presentation of results for 5m long sheet pile at 2*B*/8 position from downstream end

The variation of the flownet in upstream side with respect to cycle time has also been shown in the respective **Figures –3.48(a),3.48(b,)3.48(c),3.48(d)** obtained from SEEP/W.

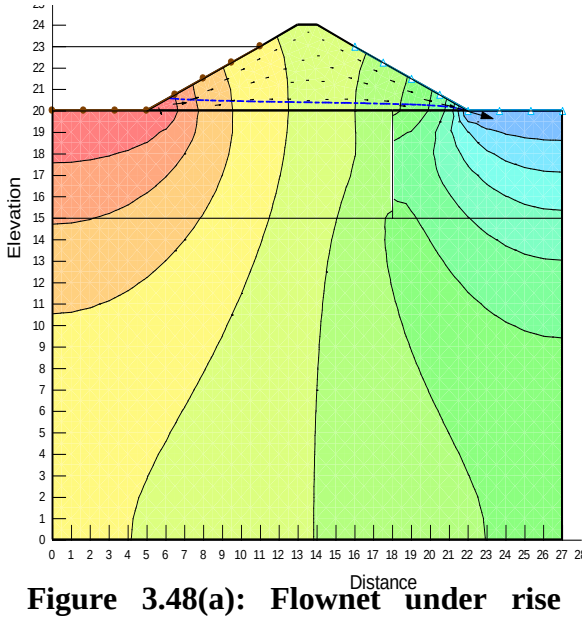

Figure 3.48(a): Flownet under rise up condition (for 20m long sheet file at 2B/8 position from downstream end, time=1 hr.)

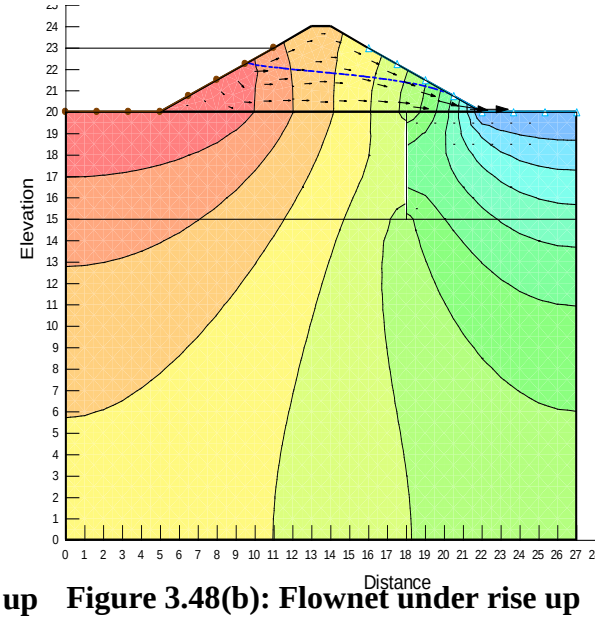

Figure 3.48(b): Flownet under rise up condition (for 20m long sheet file at 2*B*/8 position from downstream end, time=5 hrs.)

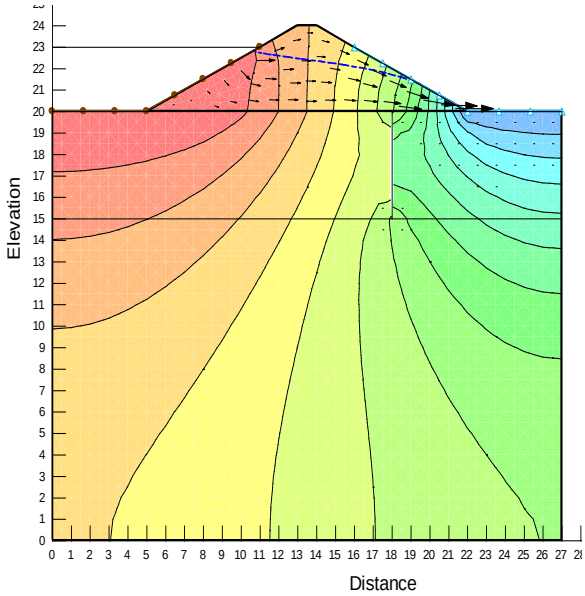

Figure 3.48(c): Flownet under rise up condition (for 5m long sheet file at 2*B*/8 position from downstream end, time=6 hrs.)

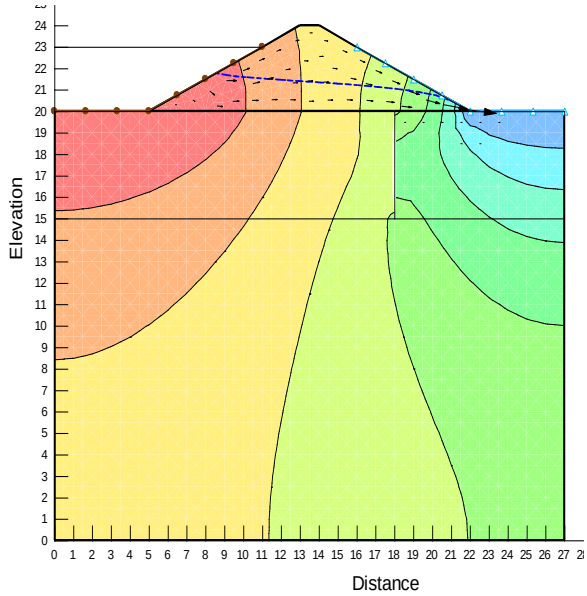

Figure 3.48(d): Flownet under draw down condition (for 5m long sheet file at 2B/8 position from downstream end, time=10 hrs.)

3.6.4.3.6 Presentation of results for 10m long sheet pile at 2*B*/8 position from downstream end

The variation of the flownet in upstream side with respect to cycle time has also been shown in the respective **Figures –3.49(a),3.49(b),3.49(c),3.49(d),3.49(e)** obtained from SEEP/W.

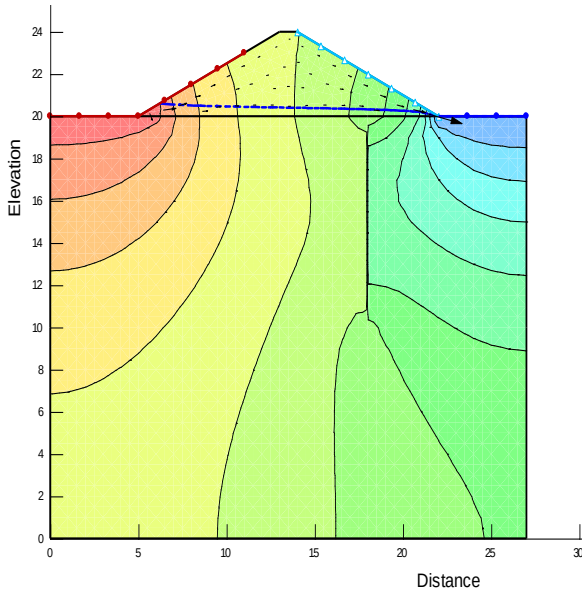

Figure 3.49(a): Flownet under rise up condition (for 10m long sheet file at 2*B*/8 position from downstream end, time=1 hr.)

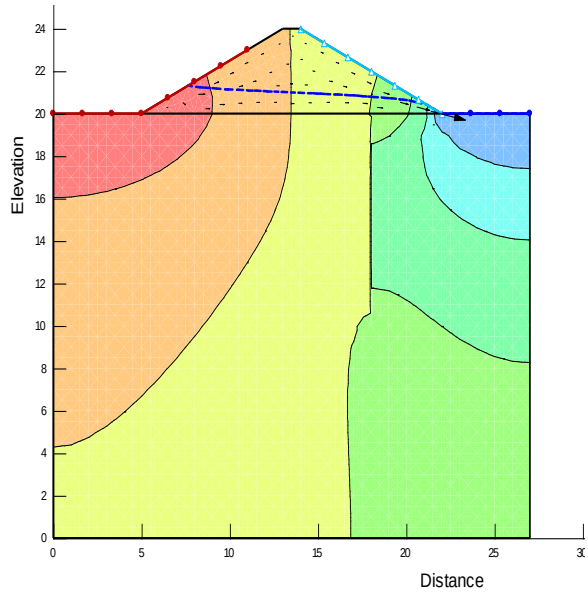

Figure 3.48(b): Flownet under rise up condition (for 10m long sheet file at 2*B*/8 position from downstream end, time=3 hrs.)

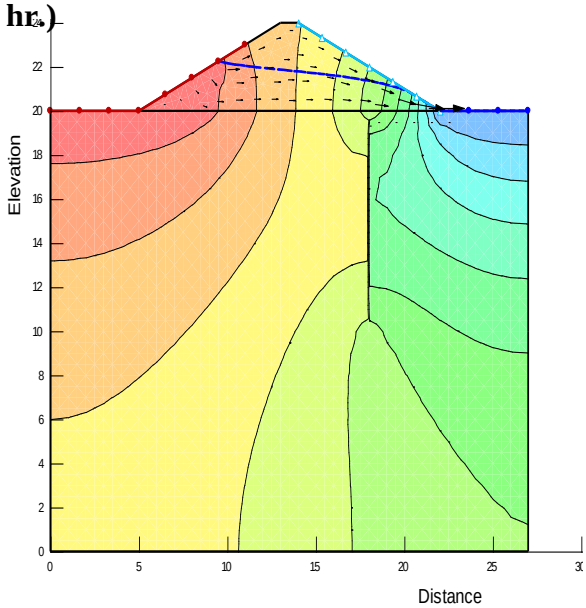

Figure 3.49(c): Flownet under rise up condition (for 10m long sheet file at 2*B*/8 position from downstream end, time=5 hrs.)

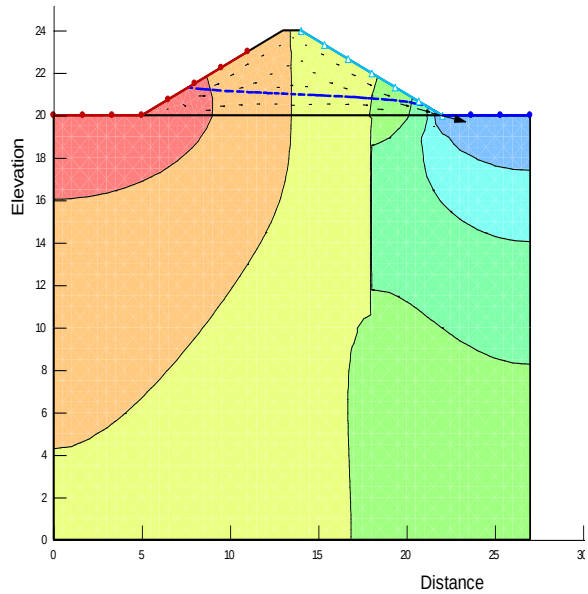

Figure 3.49(d): Flownet under draw down condition (for 10 m long sheet file at 2*B*/8 position from downstream end, time=10 hrs.)

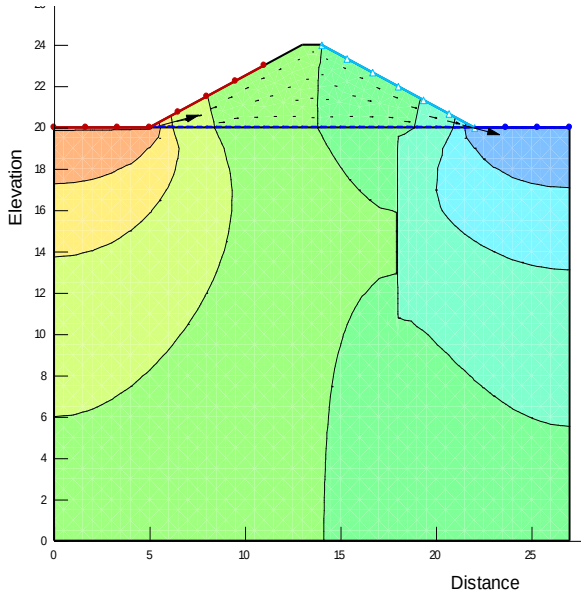

Figure 3.49(e): Flownet under draw down condition (for 10 m long sheet file at 2*B*/8 position from downstream end, time=12 hrs.)

3.6.4.3.7 presentation of results for 15m long sheet pile at 2*B*/8 position from downstream end

The variation of the flownet in upstream side with respect to cycle time has also been shown in the respective **Figures –3.50(a),3.50(b),3.50(c),3.50(d),3.50(e),3.50(f),3.50(g),3.50(h)** obtained from SEEP/W.

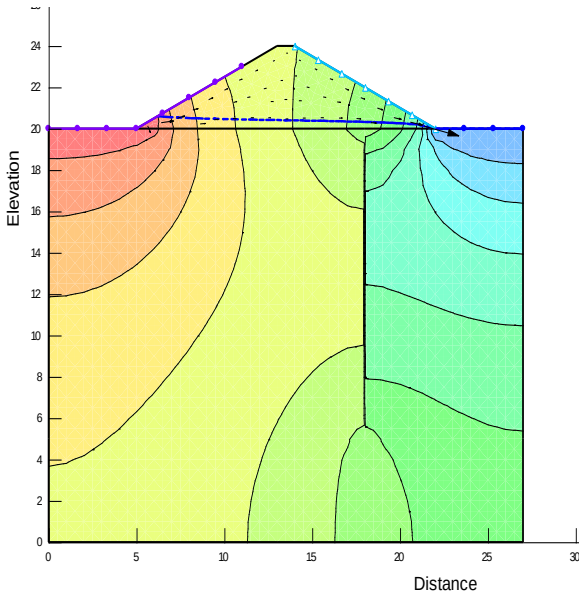

Figure 3.50(a): Flownet under rise up condition (for 15m long sheet file at 2*B*/8 position from downstream end, time=1 hr.)

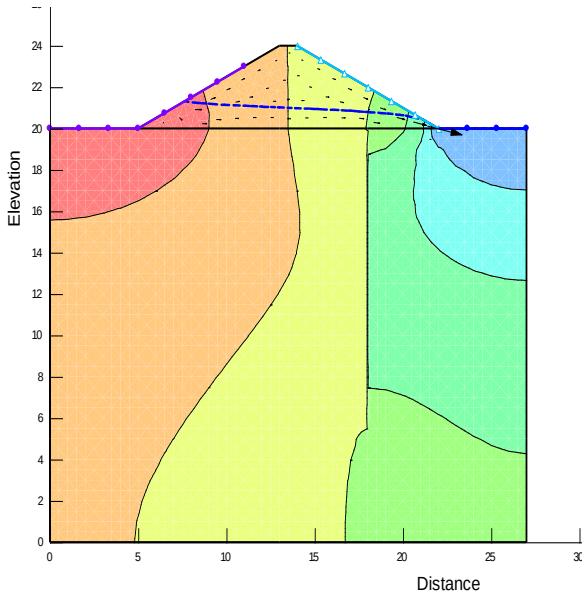

Figure 3.50(b): Flownet under rise up condition (for 15m long sheet file at 2*B*/8 position from downstream end, time=3 hrs.)

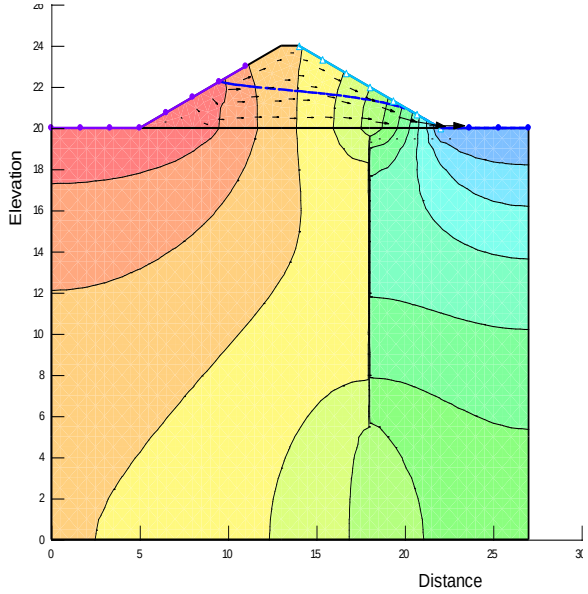

Figure 3.50(c): Flownet under rise up condition (for 15m long sheet file at 2*B*/8 position from downstream end, time=5 hrs.)

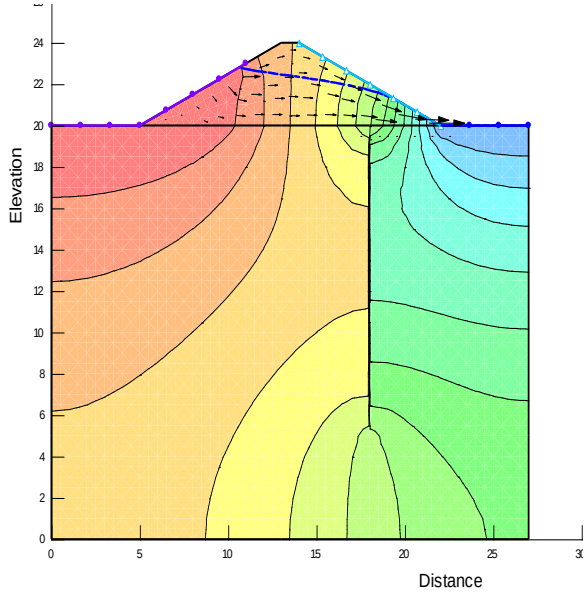

Figure 3.50(d): Flownet under rise up condition (for 15m long sheet file at 2*B*/8 position from downstream end, time=6 hrs.)

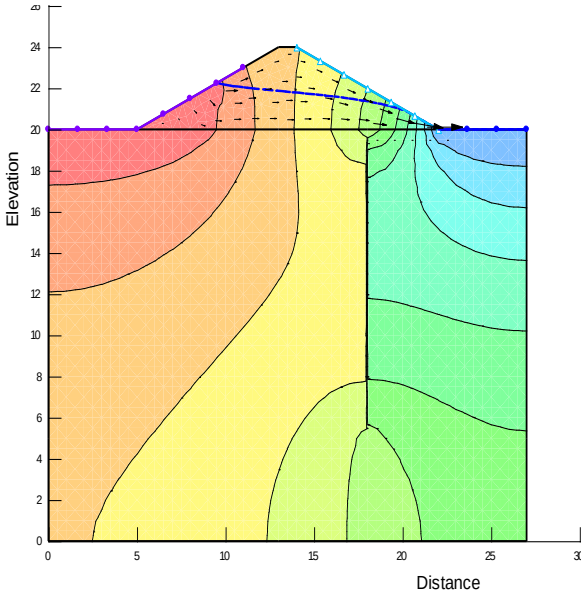

Figure 3.50(e): Flownet under draw down condition (for 15m long sheet file at 2*B*/8 position from downstream end, time=7 hrs.)

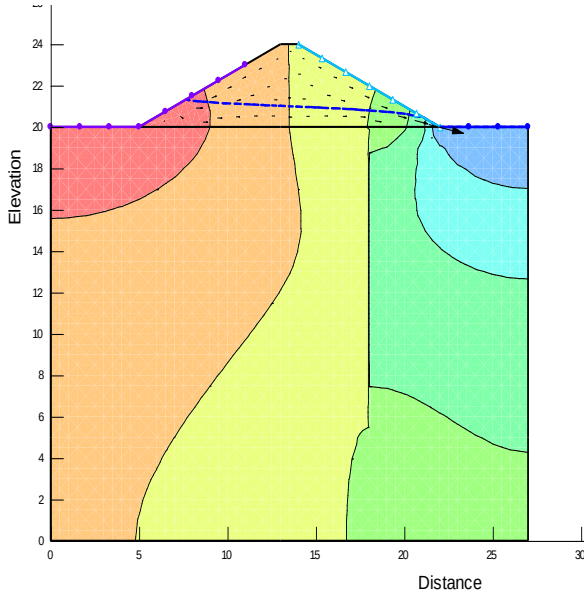

Figure 3.50(f): Flownet under draw down condition (for 15m long sheet file at 2*B*/8 position from downstream end, time=10 hrs.)

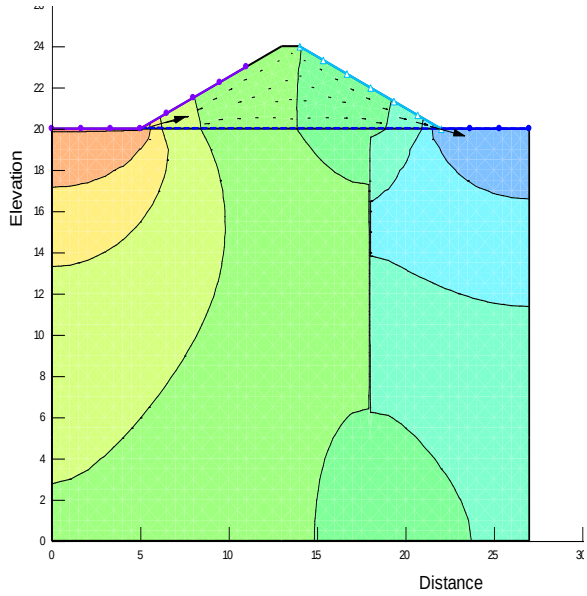

Figure 3.50(g): Flownet under draw down condition (for 15m long sheet file at 2*B*/8 position from downstream end, time=12 hrs.)

3.6.4.3.8 presentation of results for 20m long sheet pile at 2*B*/8 position from downstream end

The variation of the flownet in upstream side with respect to cycle time has also been shown in the respective **Figures –3.51(a),3.51(b),3.51(c),3.51(d),3.51(e),3.51(f)** obtained from SEEP/W.

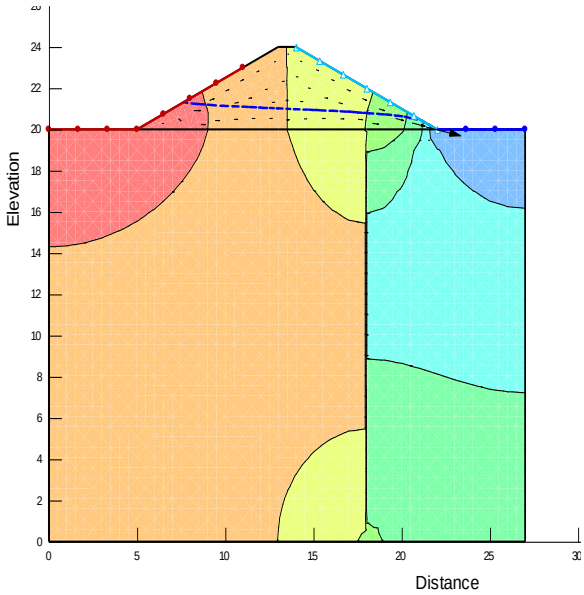

Figure 3.51(a): Flownet under rise up condition (for 20m long sheet file at 2*B*/8 position from downstream end, time=3 hrs.)

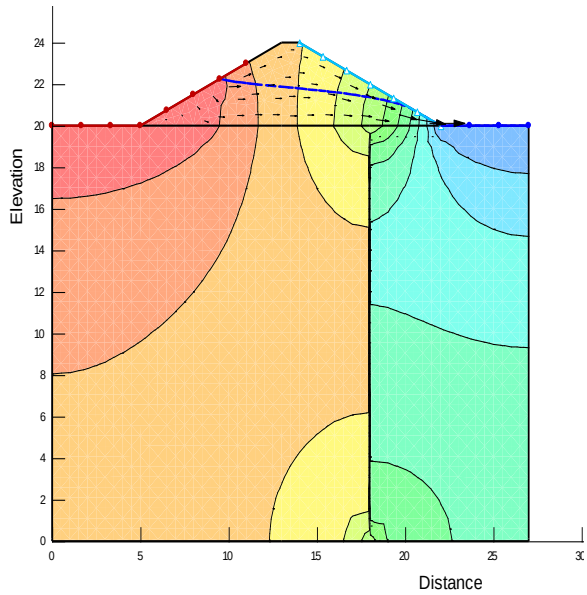

Figure 3.51(b): Flownet under rise up condition (for 20m long sheet file at 2*B*/8 position from downstream end, time=5 hrs.)

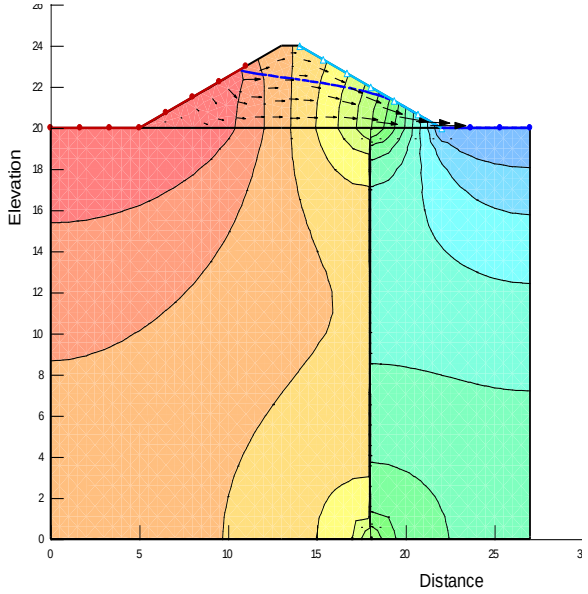

Figure 3.51(c): Flownet under rise up condition (for 20m long sheet file at 2*B*/8 position from downstream end, time=6 hrs.)

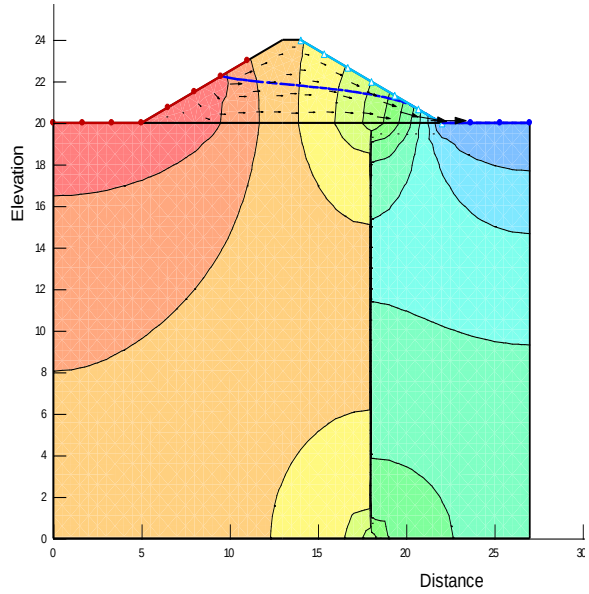

Figure 3.51(d): Flownet under drawn down condition (for 20m long sheet file at 2*B*/8 position from downstream end, time=7 hrs.)

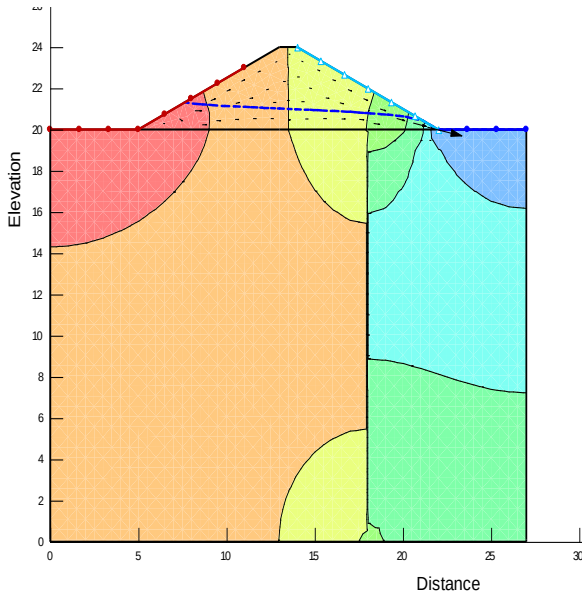

Figure 3.51(e): Flownet under drawn down condition (for 20m long sheet file at 2*B*/8 position from downstream end, time=10 hrs.)

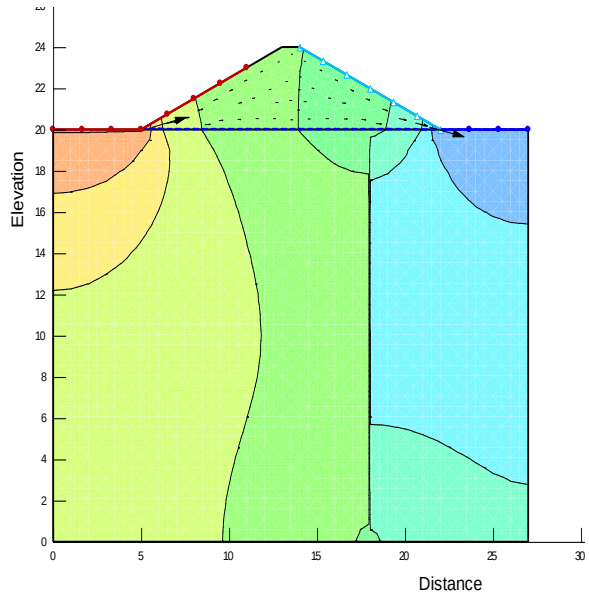

Figure 3.51(f): Flownet under drawn down condition (for 20m long sheet file at 2*B*/8 position from downstream end, time=12 hrs.)

3.6.4.3.9 Presentation of results for 5m long sheet pile at 3*B*/8 position from downstream end

The variation of the flownet in upstream side with respect to cycle time has also been shown in the respective **Figures –3.52(a),3.52(b),3.52(c),3.52(d),3.52(e),3.52(f),3.52(g),3.52(h)** obtained from SEEP/W.

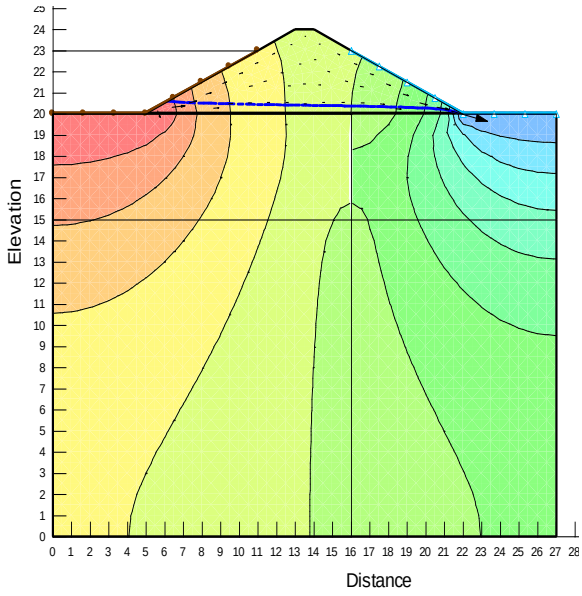

Figure 3.52(a): Flownet under rise up condition (for 5m long sheet file at 3*B*/8 position from downstream end, time=1 hr.)

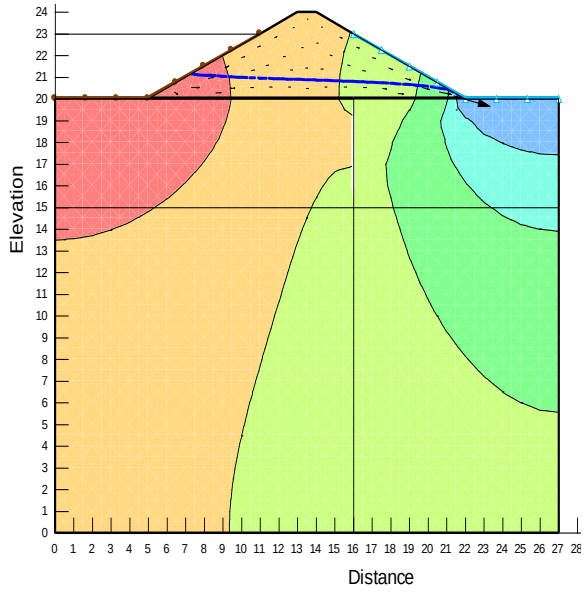

Figure 3.52(b): Flownet under rise up condition (for 5m long sheet file at 3*B*/8 position from downstream end, time=2 hrs.)

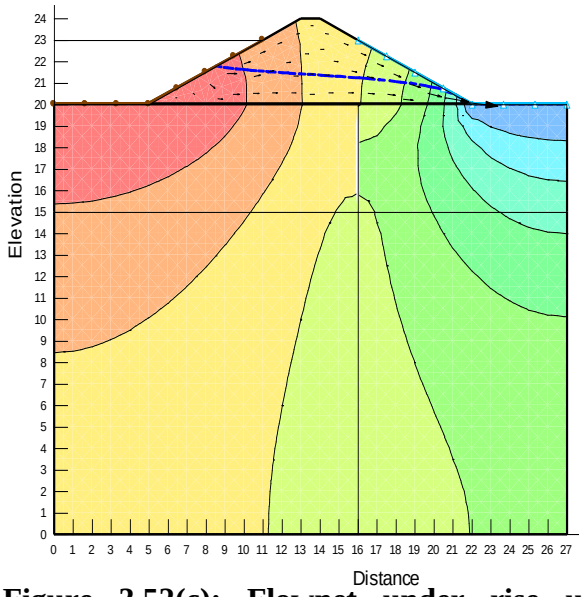

Figure 3.52(c): Flownet under rise up condition (for 5m long sheet file at 3*B*/8 position from downstream end, time=3 hrs.)

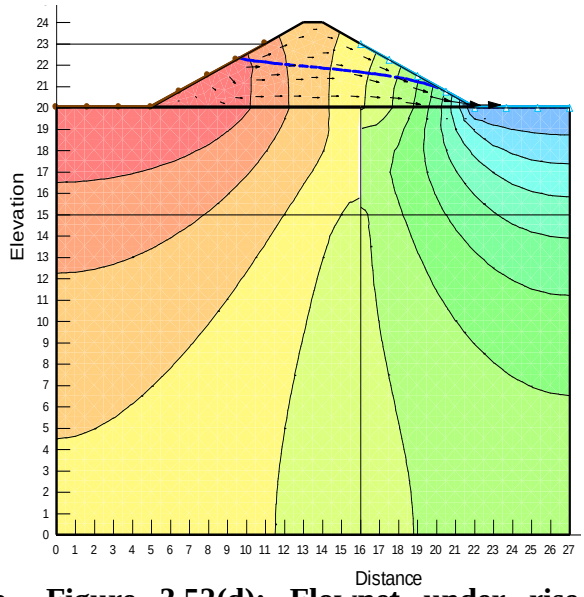

Figure 3.52(d): Flownet under rise up condition (for 5m long sheet file at 3*B*/8 position from downstream end, time=5

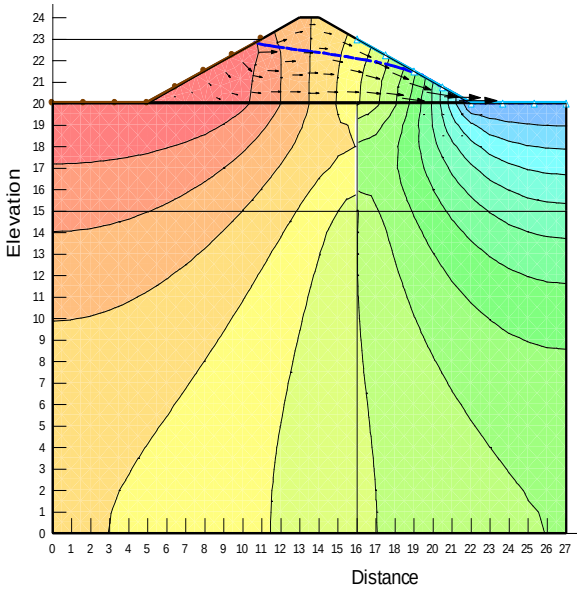

Figure 3.52(e): Flownet under rise up condition (for 5m long sheet file at 3*B*/8 position from downstream end, time=6 hrs.)

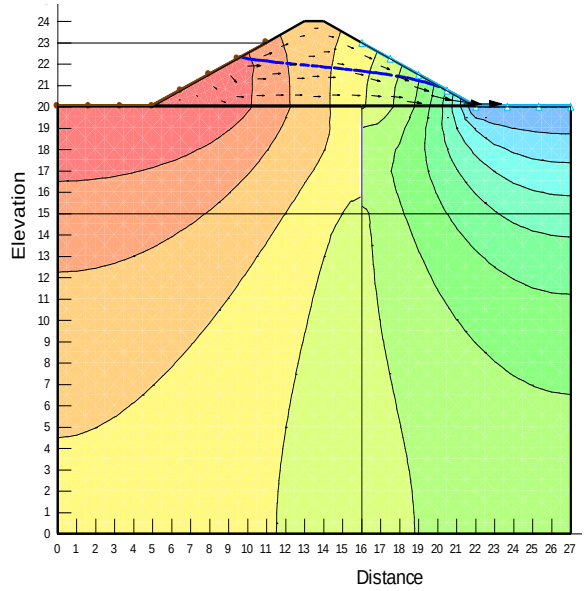

Figure 3.52(f): Flownet under draw down condition (for 5m long sheet file at 3*B*/8 position from downstream end, time=7 hrs.)

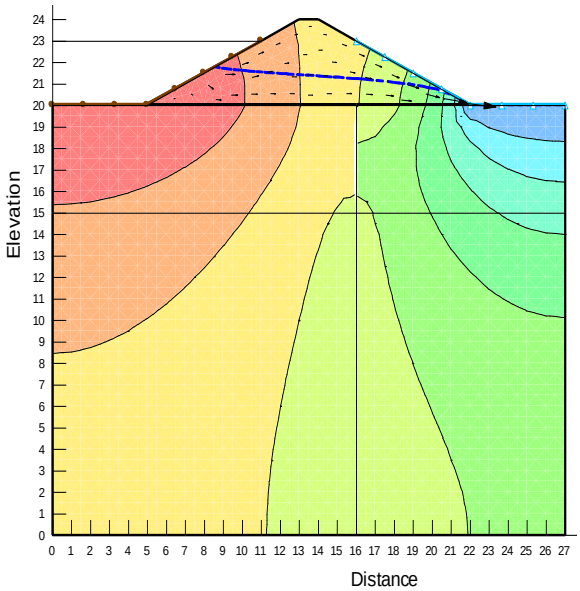

Figure 3.52(g): Flownet under draw down condition (for 5m long sheet file at 3*B*/8 position from downstream end, time=10 hrs.)

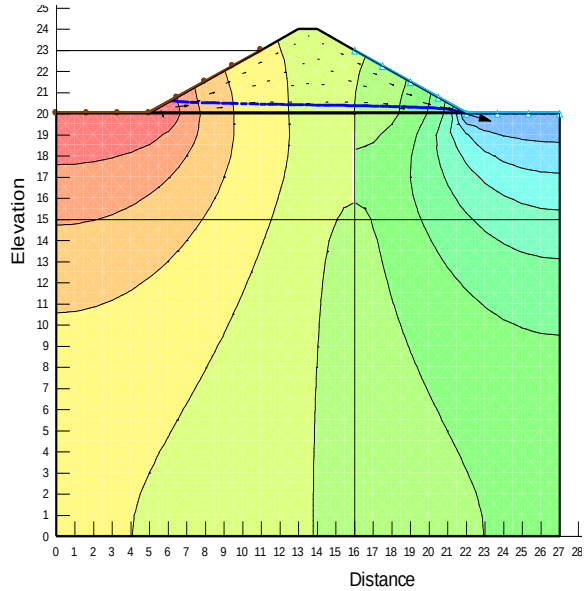

Figure 3.52(h): Flownet under draw down condition (for 5m long sheet file at 3*B*/8 position from downstream end, time=11 hrs.)

3.6.4.3.10 Presentation of results for 10m long sheet pile at 3*B*/8 position from downstream end

The variation of the flownet in upstream side with respect to cycle time has also been shown in the respective **Figures –3.53(a),3.53(b),3.53(c),3.53(d),3.53(e),3.53(f),3.53(g),3.53(h)** obtained from SEEP/W.

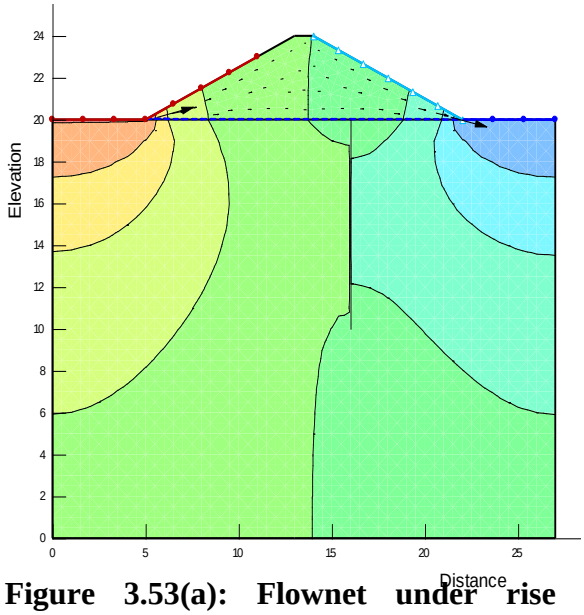

Figure 3.53(a): Flownet under rise up condition (for 10m long sheet file at 3*B*/8 position from downstream end, time=1 hr.)

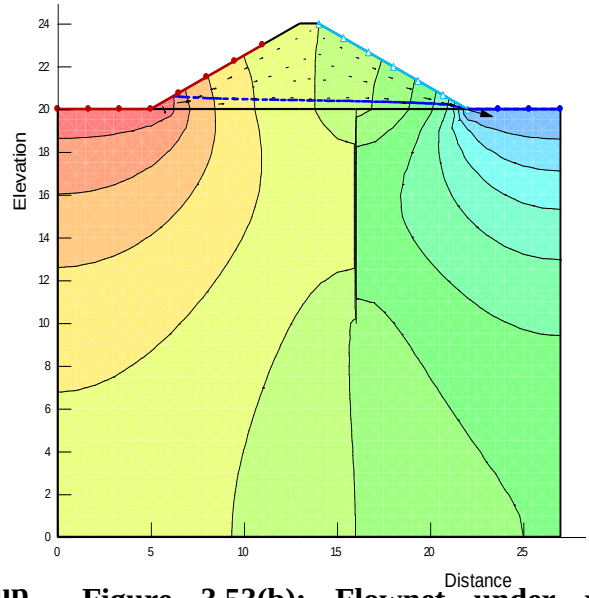

Figure 3.53(b): Flownet under rise up condition (for 10m long sheet file at 3*B*/8 position from downstream end, time=2 hrs.)

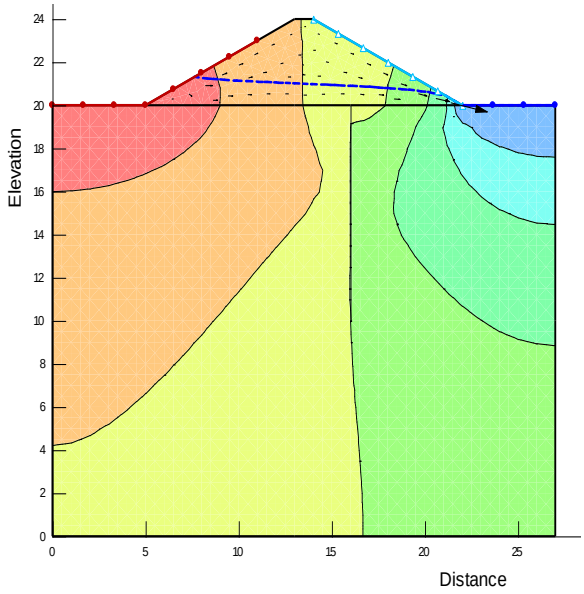

Figure 3.53(c): Flownet under rise up condition (for 10m long sheet file at 3*B*/8 position from downstream end, time=3 hrs.)

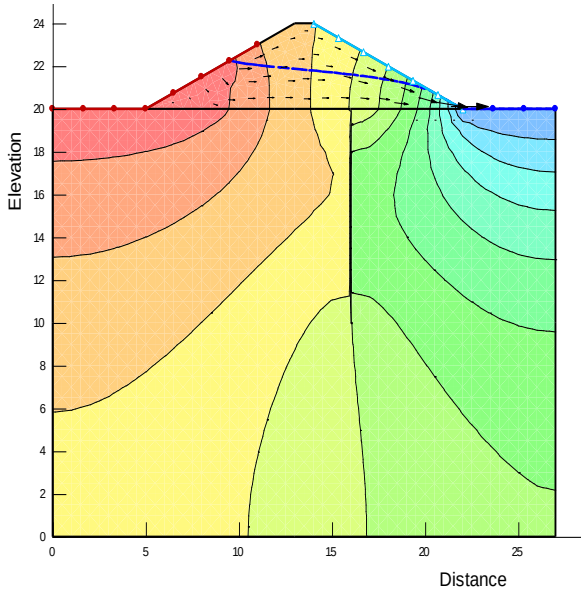

Figure 3.53(d): Flownet under rise up condition (for 10m long sheet file at 3*B*/8 position from downstream end, time=5 hrs.)

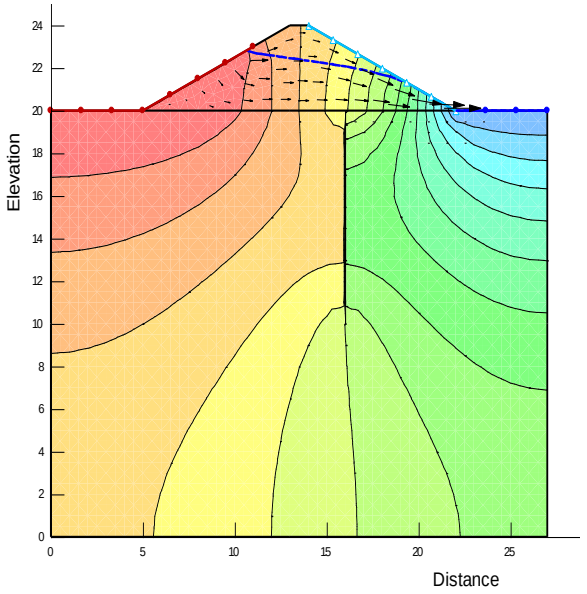

Figure 3.53(e): Flownet under rise up condition (for 10m long sheet file at 3*B*/8 position from downstream end, time=6 hrs.)

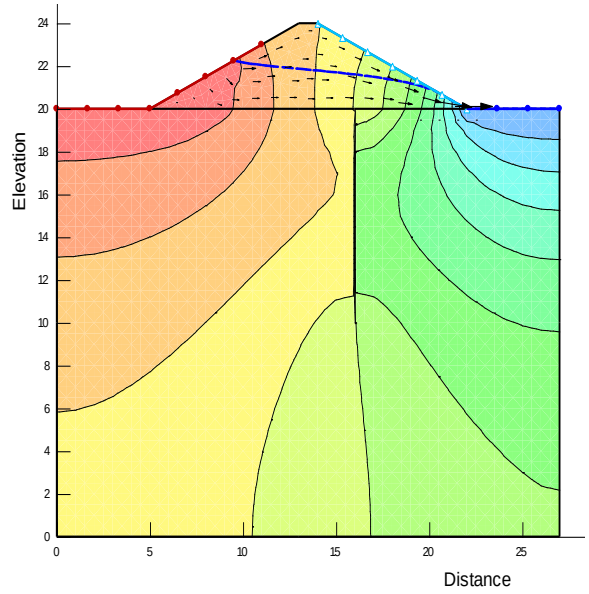

Figure 3.53(f): Flownet under draw down condition (for 10m long sheet file at 3*B*/8 position from downstream end, time=7 hrs.)

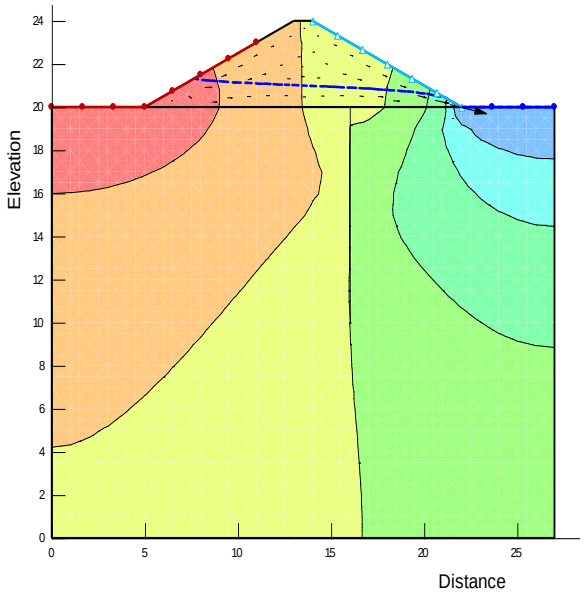

Figure 3.53(g): Flownet under draw down condition (for 10m long sheet file at 3*B*/8 position from downstream end, time=10 hrs.)

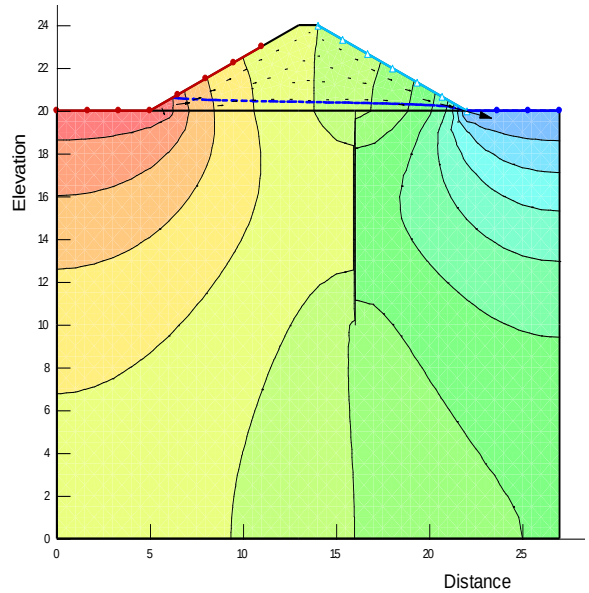

Figure 3.53(h): Flownet under draw down condition (for 10m long sheet file at 3*B*/8 position from downstream end, time=12 hrs.)

3.6.4.3.11 Presentation of results for 15m long sheet pile at 3*B*/8 position from downstream end

The variation of the flownet in upstream side with respect to cycle time has also been shown in the respective **Figures –3.54(a),3.54(b),3.54(c),3.54(d),3.54(e),3.54(f),3.54(g),3.54(h)** obtained from SEEP/W.

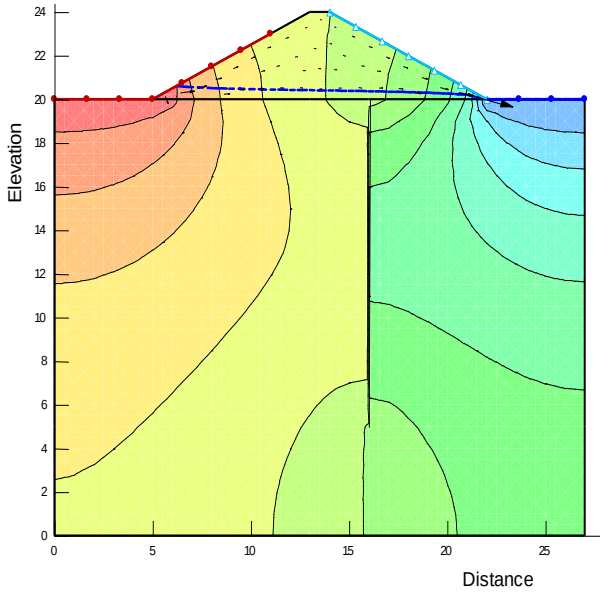

Figure 3.54(a): Flownet under rise up condition (for 15m long sheet file at 3*B*/8 position from downstream end, time=1 hr.)

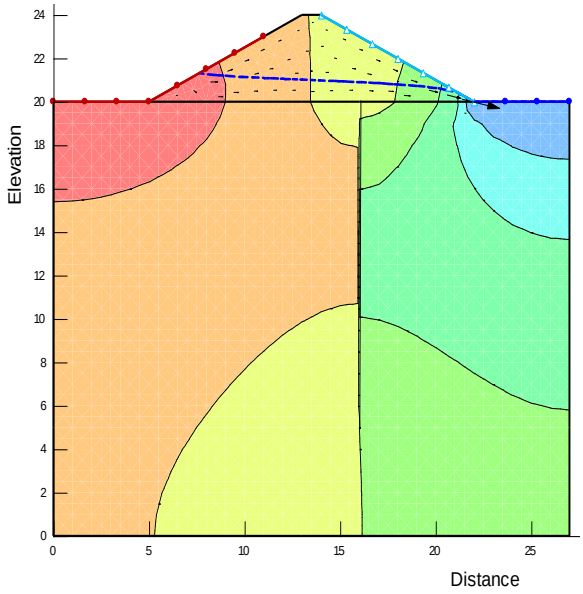

Figure 3.54(b): Flownet under rise up condition (for 15m long sheet file at 3*B*/8 position from downstream end, time=3hrs.)

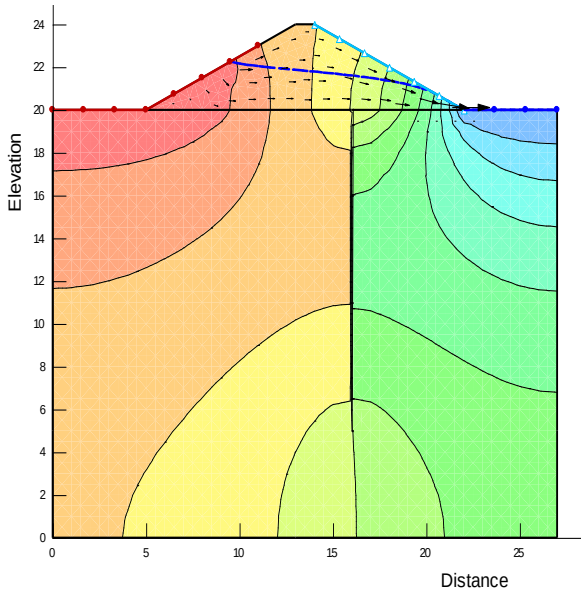

Figure 3.54(c): Flownet under rise up condition (for 15m long sheet file at 3*B*/8 position from downstream end, time=5 hrs.)

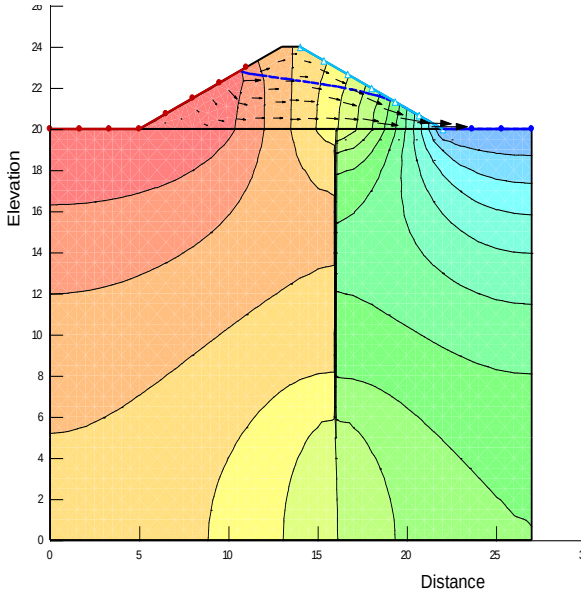

Figure 3.54(d): Flownet under rise up condition (for 15m long sheet file at 3*B*/8 position from downstream end, time=6 hrs.)

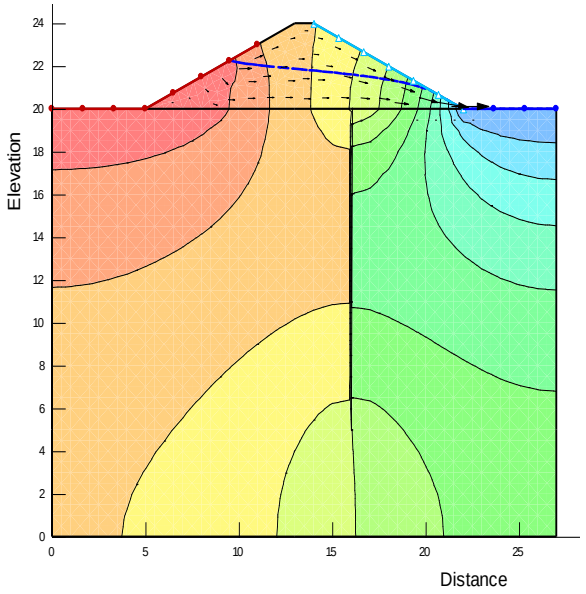

Figure 3.54 (e) : Flownet under rise up condition (for 15m long sheet file at 3*B*/8 position from downstream end, time=7 hrs.)

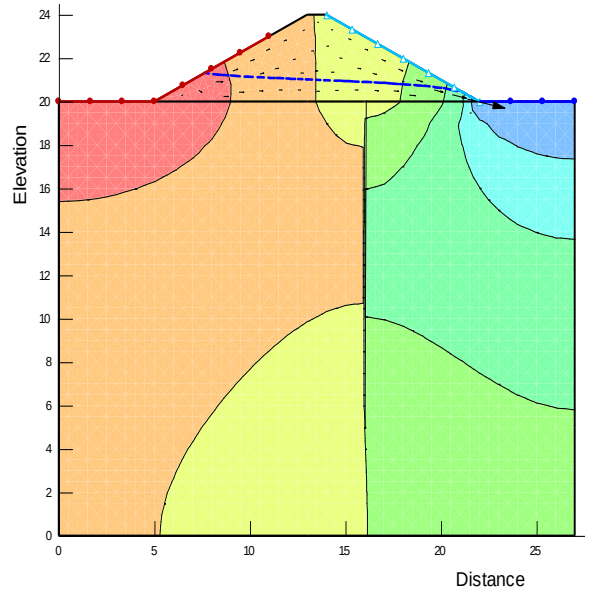

Figure 3.54(f): Flownet under draw down condition (for 15m long sheet file at 3*B*/8 position from downstream end, time=10 hrs.)

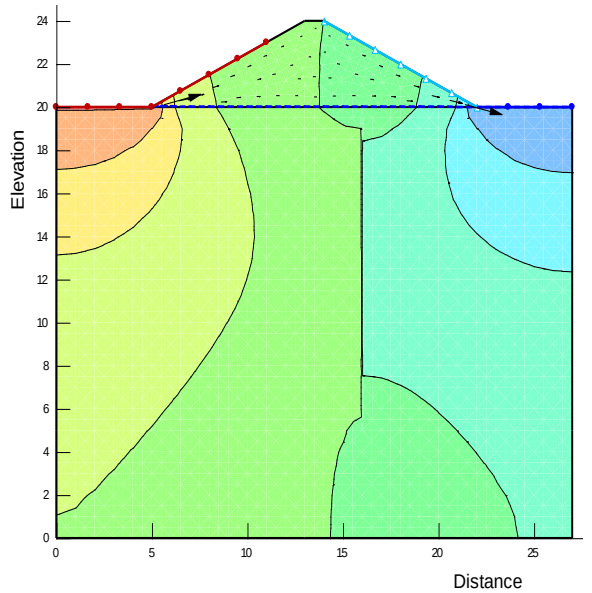

Figure 3.54(g): Flownet under draw down condition (for 15m long sheet file at 3*B*/8 position from downstream end, time=12 hrs.)

3.6.4.3.12 Presentation of results for 20m long sheet pile at 3*B*/8 position from downstream end

The variation of the flownet in upstream side with respect to cycle time has also been shown in the respective **Figures –3.55(a),3.55(b),3.55(c),3.55(d),3.55(d),3.55(f),3.55(g),3.55(h)** obtained from SEEP/W.

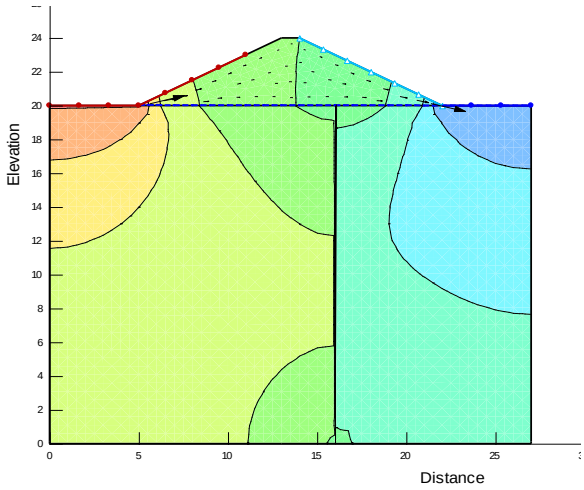

Figure 3.55(a): Flownet under rise up condition (for 20m long sheet file at 3*B*/8 position from downstream end, time=1 hr.)

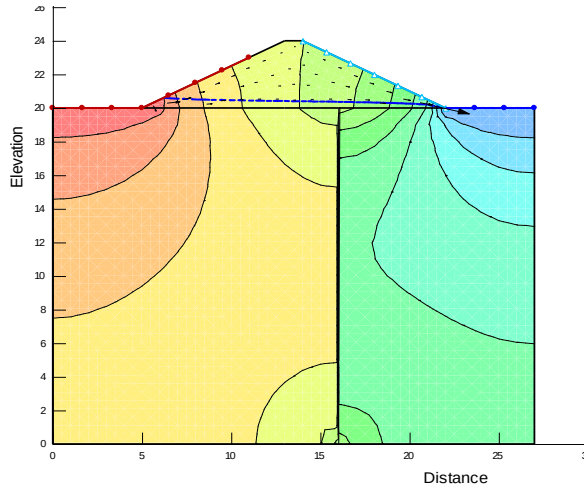

Figure 3.55(b): Flownet under rise up condition (for 20m long sheet file at 3*B*/8 position from downstream end, time=2hrs.)

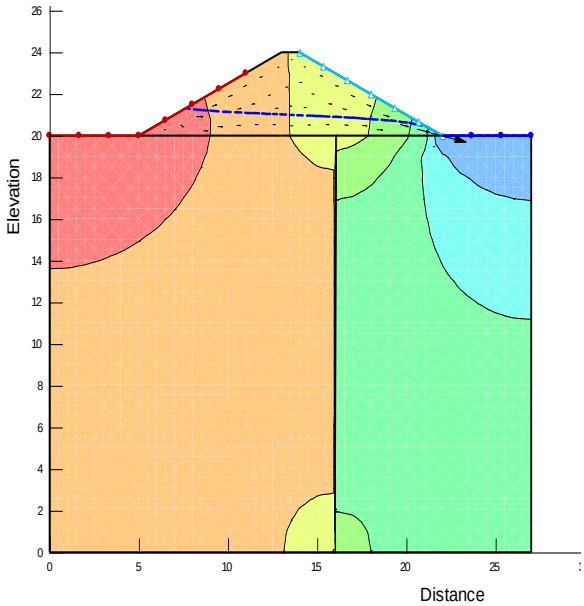

Figure 3.55(c): Flow-net under rise up condition (for 20m long sheet file at 3*B*/8 position from downstream end, time=3 hrs.)

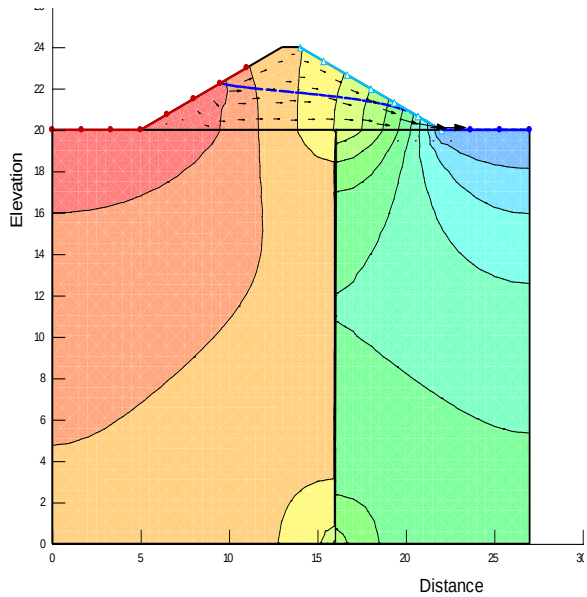

Figure 3.55(d): Flow-net under rise up condition (for 20m long sheet file at 3*B*/8 position from downstream end, time=5 hrs.)

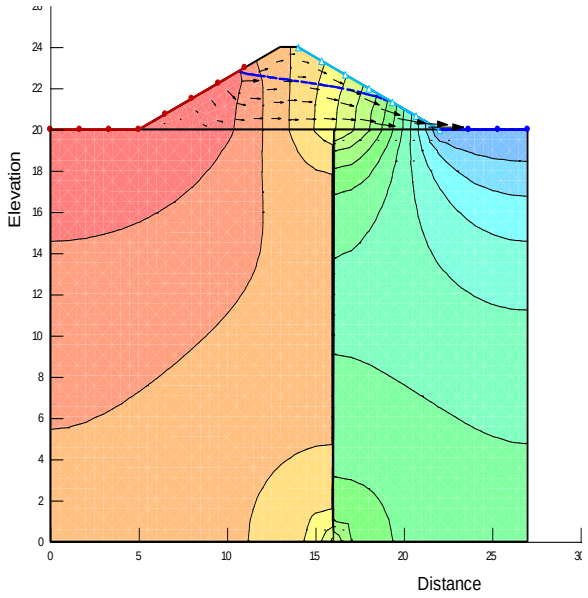

Figure 3.55(e): Flow-net under rise up condition (for 20m long sheet file at 3B/8 position from downstream end, time=6 hrs.)

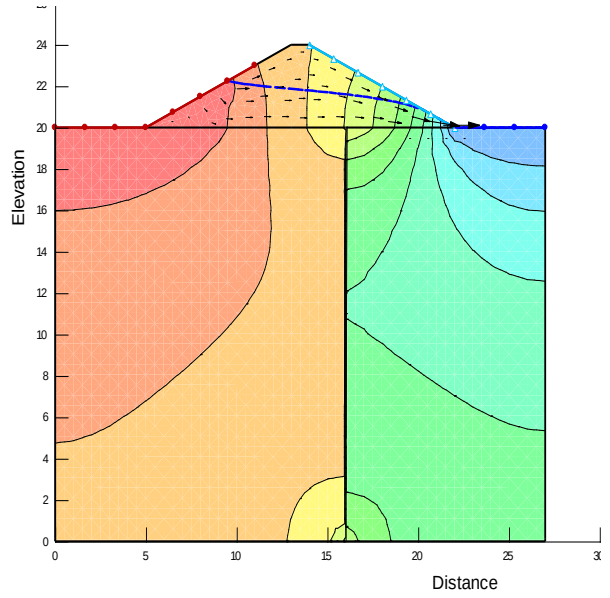

Figure 3.55(f): Flow-net under draw down condition (for 20m long sheet file at 3B/8 position from downstream end, time=7 hrs.)

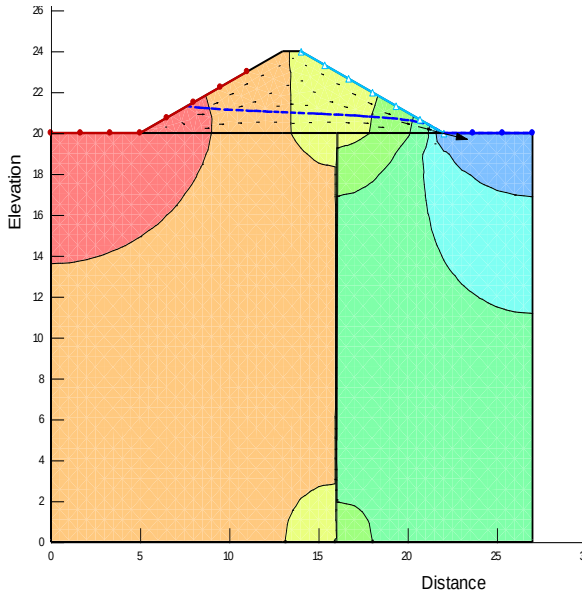

Figure 3.55(g): Flow-net under draw down condition (for 20m long sheet file at 3*B*/8 position from downstream end, time=10 hrs.)

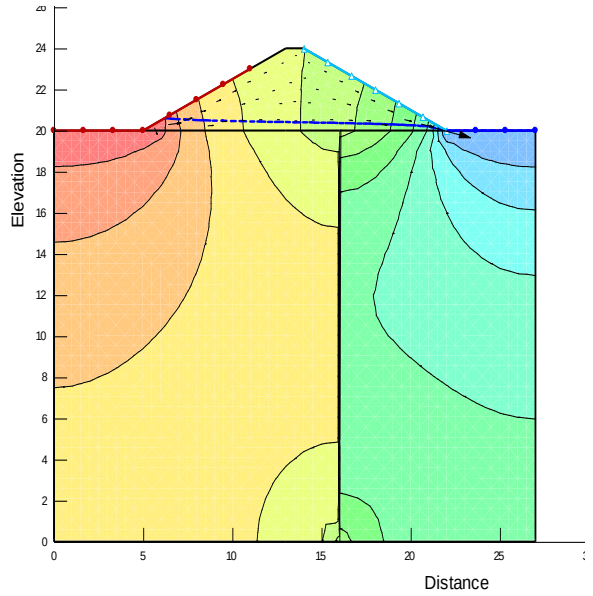

Figure 3.55(h): Flow-net under draw down condition (for 20m long sheet file at 3*B*/8 position from downstream end, time=11 hrs.)

3.6.5 PHREATIC SURFACE UNDER MULTIPLE TIDAL CYCLE CONDITION

All other boundary conditions remain same as per single cycle. In this particular analysis, the number of cycles was taken over two months, i.e. 60 days with 120 cycles. An attempt has been made to study the impact of multiple tidal cycles on the dynamics of the phreatic surface of the current study. The number of tidal cycles selected is based over 60 days' time i.e for 120 cycles. The results have been illustrated in Figure-3.56 after satisfying all numerical cases for multiple tidal cycle. The upper dotted line indicates the phreatic surface position after running of 120 cycles. It has been observed from figure 3.56 that the location of the phreatic surface shifts to a slightly higher elevation within a particular zone after each corresponding cycle. The variation is observed up to a certain distance from the River-Embankment interface, beyond which no variation in phreatic line is observed. At the end of 120 cycles, this zone has been measured as 0.25m approximately from the upper slope for this particular study. However, the elevational shift in phreatic surface is marginal. This phenomenon is similar for all numerical studies of varying sheet pile position and length in an embankment.

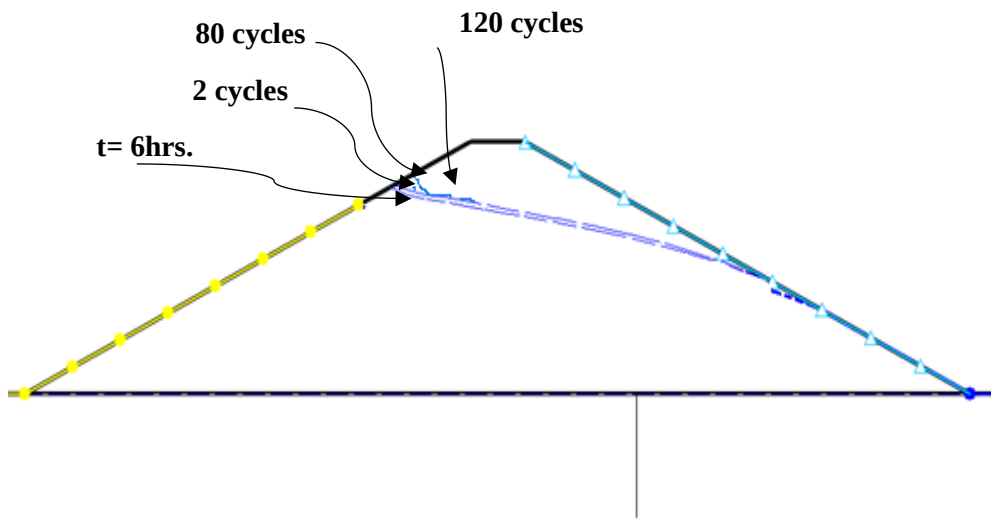

Figure 3.56: Isoline for multiple tidal cycle

3.6.6 PHREATIC SURFACE AND FLOWNET UNDER SEISMIC CONDITION

Phreatic surface and flownet under seismic condition have been discussed in this section. After study of all numerical cases for all transient flow under seismic condition. The phreatic surface appears to be erratic.

3.6.6.1 Analytical Validation

Chakraborty and Chaudhury (2009) analyzed the failing of tailing earthen dams due to earthquake by various software. They performed static and seismic analysis. They considered a tailing dam of prototype dimensions-44 m height and 4m core and 1:2.5 upstream and downstream slopes. They modelled the dam using core and performed the seepage analysis at FLAC 3D software. They verified the phreatic surface obtained from FLAC 3D software with the SEEP/W software inputting the same properties. They performed static and seismic analysis. They evaluated the factor of safety for static and seismic cases. The analysis for the same geometry has been done by using same methodology of the present research with FLAC 2D and SLOPEP/W software. It has been found that there is a good agreement of numerical result with the results of Chakraborty and Chaudhury (2009) obtained as may be observed in Table 3.4. Hence FLAC 2D and SEEP/W has been taken as the tool for the present analysis. From this analysis they concluded that the slope of tailing earthen dam was not safe under seismic loading condition.

Table 3.4: Peak horizontal acceleration (ms^{-2})

Study	+11 m above existing ground level	+22 m above existing ground level	+33 m above existing ground level	Crest level
Chakraborty and Chaudhury (2009) FLAC 3D	1.793	2.27	3.656	4.765
Present method FLAC 2D	2.4	3.8	5.67	7.565

The variation of result may be due to the use of two dimensional and three-dimensional version of FLAC software. Therefore, the FLAC 2D software has been adopted for our further part of the study of embankment with or without sheet pile. The results have further been obtained with the help of QUAKE/W software for seismic cases.

3.6.6.2 PRESENTATION OF RESULTS UNDER STEADY STATE (SEISMIC CONDITION)

Considering seismic effect, the result of phreatic surface and flownet has been observed from FLAC 2D and QUAKE/W analysis

3.6.6.2.1 Presentation of results from FLAC 2D for without sheet pile under steady state (seismic condition)

The result from FLAC 2D has been plotted in Figure. 3.57(a) using FLAC 2D software. In this study the pattern of stream line has not been observed.

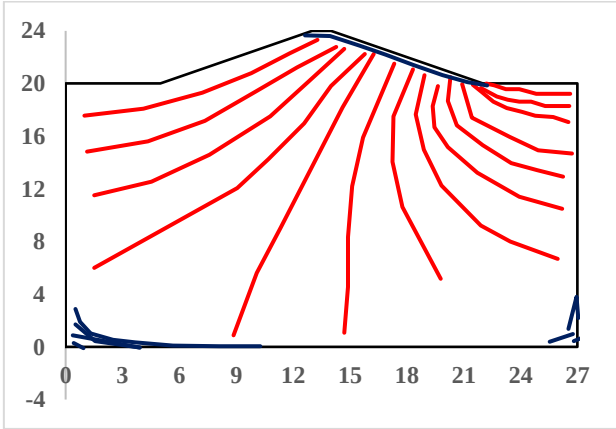

Figure 3.57(a): Flownet for without sheet pile condition, at steady state condition

3.6.6.2.2 Presentation of results from SEEP/W for without sheet pile under steady state

The result from SEEP/W has been plotted in Figure. 3.57(b) using SEEP/W software. In this study the pattern of stream line has not been observed.

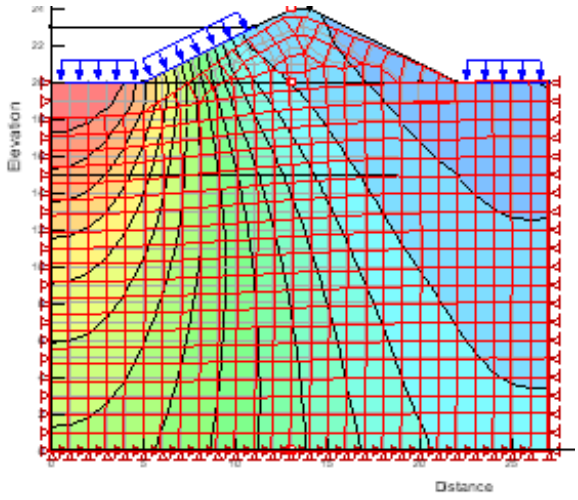

Figure 3.57(b): Flownet for without sheet pile condition, at steady state condition

3.6.6.2.3 Presentation of results from FLAC 2D for with sheet pile under steady state

The variation of the flownet in upstream side has been from plotted in Figure. 3.58(a) to 3.58(l) using FLAC 2D software. Figure 3.58(a) to 3.58(d) presents flownet for the model embankment with sheet pile of length 5m, 10m, 15m and 20m respectively for position of sheet pile at *B*/8 from the downstream end of the dam. Figure 3.58(e) to 3.58(h) presents flownet for the model embankment with sheet pile of length 5m, 10m, 15m and 20m respectively for position of sheet pile at 2*B*/8 from the downstream end of the dam. Figure 3.58(i) to 3.58(l) presents flownet for the model embankment with sheet pile of length 5m, 10m, 15m and 20m respectively for position of sheet pile at 3*B*/8 from the downstream end of the dam. Where *B* represents bottom width of the dam. The variation of the flownet in upstream side with respect to working head condition has also been shown in the respective figures.

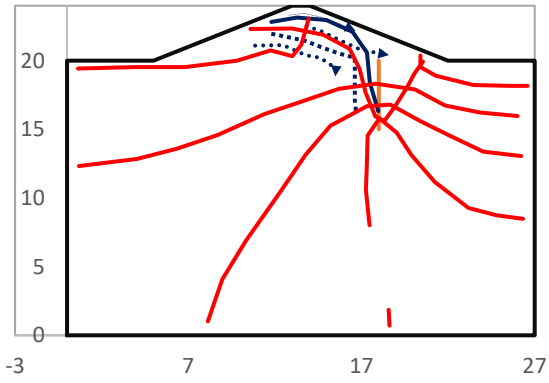

Figure 3.58(a): Flownet for 5 m long sheet file at *B*/8 position from downstream end

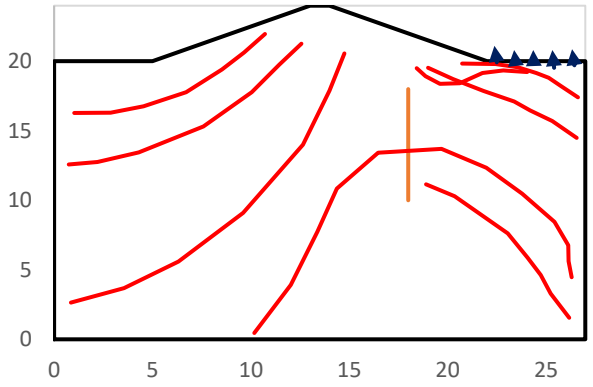

Figure 3.58(b): Flownet for 10 m long sheet file at *B*/8 position from downstream end

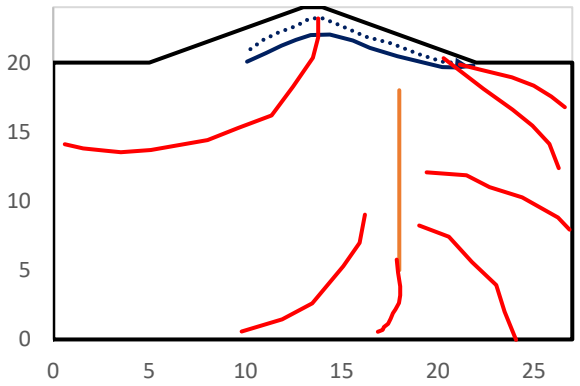

Figure 3.58(c): Flownet for 15 m long sheet file at *B*/8 position from downstream end

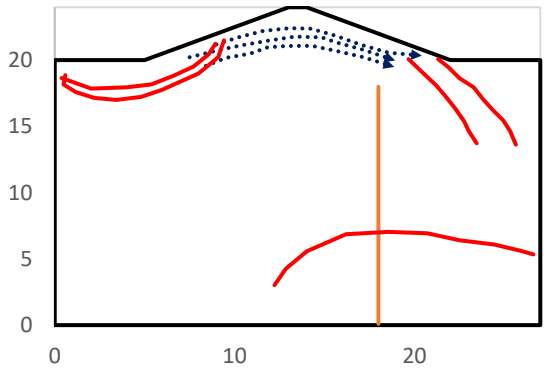

Figure 3.58(d): Flownet for 20 m long sheet file at *B*/8 position from downstream end

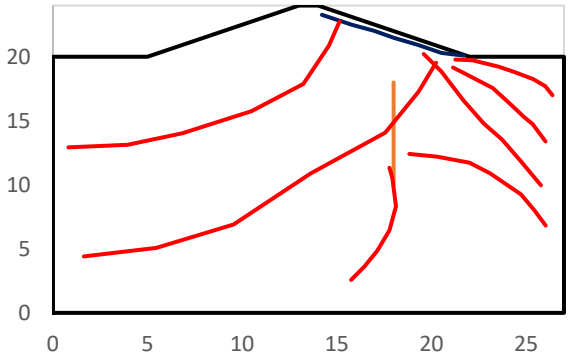

Figure 3.58(e): Flownet for 5 m long sheet file at 2*B*/8 position from downstream end

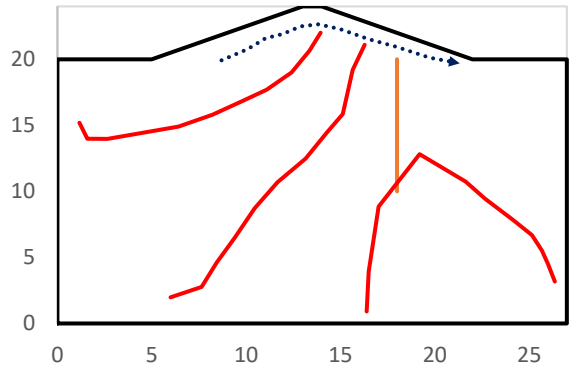

Figure 3.58(f): Flownet for 10 m long sheet file at 2*B*/8 position from downstream end

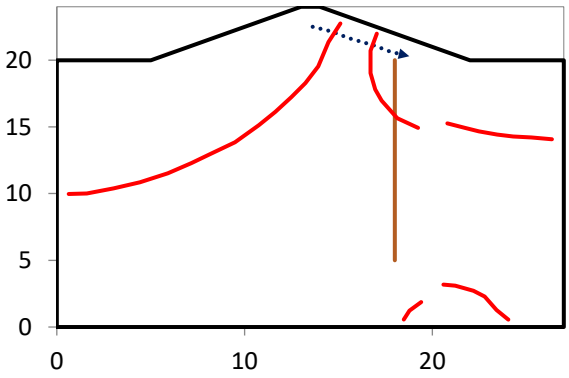

Figure 3.58(g): Flownet for 15 m long sheet file at 2*B*/8 position from downstream end

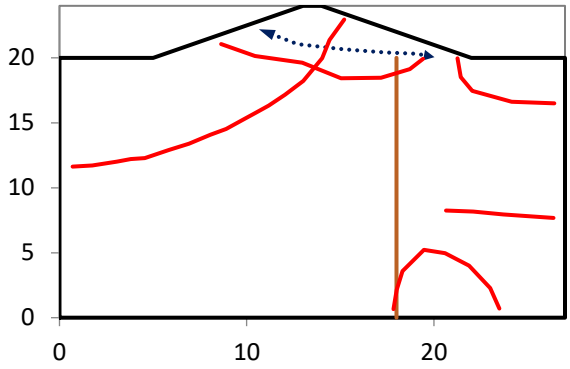

Figure 3.58(h): Flownet for 20 m long sheet file at 2*B*/8 position from downstream end

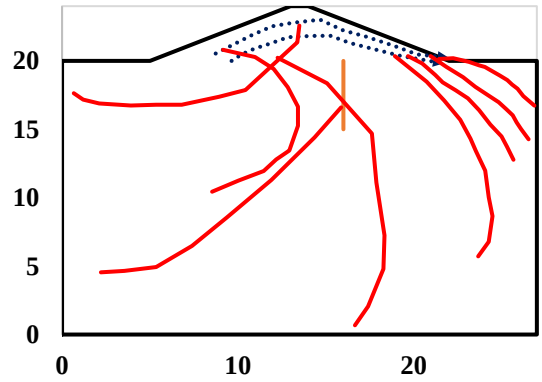

Figure 3.58(i): Flownet for 5 m long sheet file at 3*B*/8 position from downstream end

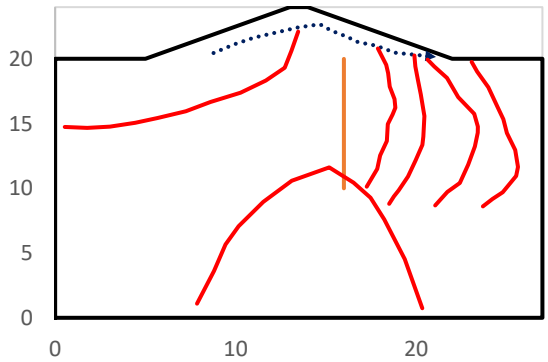

Figure 3.58(j): Flownet for 10 m long sheet file at 3*B*/8 position from downstream end

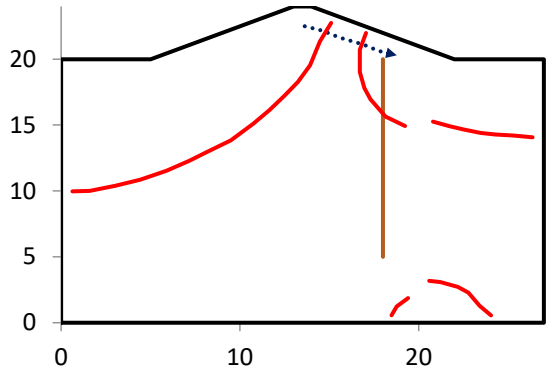

Figure 3.58(k): Flownet for 15 m long sheet file at 3*B*/8 position from downstream end

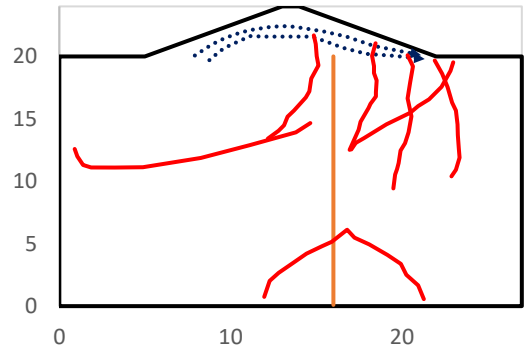

Figure 3.58(l): Flownet for 20 m long sheet file at 3*B*/8 position from downstream end

3.6.6.2.4 Presentation of results from SEEP/W without sheet pile under steady state (seismic condition)

In the study under seismic condition three cases; full rise up, full drawdown condition and intermediate conditions have been modelled. The variation of the flownet in upstream side has been from plotted in Figure. 3.58(a) to 3.58(l) using FLAC 2D software. Figure 3.59(a) to 3.59 (d) presents flownet for the model embankment with sheet pile of length 5m, 10m, 15m and 20m respectively for position of sheet pile at *B*/8 from the downstream end of the dam. Figure 3.59 (e) to 3.59 (h) presents flownet for the model embankment with sheet pile of length 5m, 10m, 15m and 20m respectively for position of sheet pile at 2*B*/8 from the downstream end of the dam. Figure 3.59 (i) to 3.59 (l) presents flownet for the model embankment with sheet pile of length 5m, 10m, 15m and 20m respectively for position of sheet pile at 3*B*/8 from the downstream end of the dam. Where *B* represents bottom width of the dam. The variation of the flownet in upstream side with respect to working head condition has also been shown in the respective figures. The variation of the flownet in upstream side with respect to working head condition has also been shown in the respective figures.

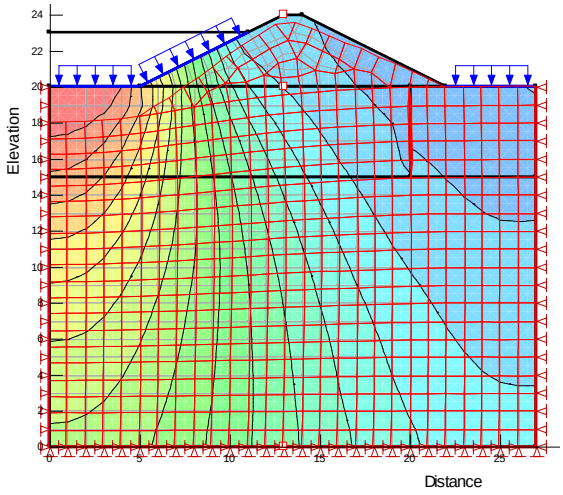

Figure 3.59(a): Flownet for 5 m long sheet file at *B*/8 position from downstream end

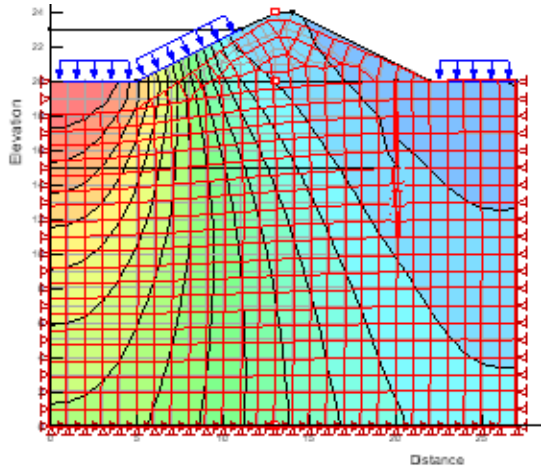

Figure 3.59(b): Flownet for 10 m long sheet file at *B*/8 position from downstream end

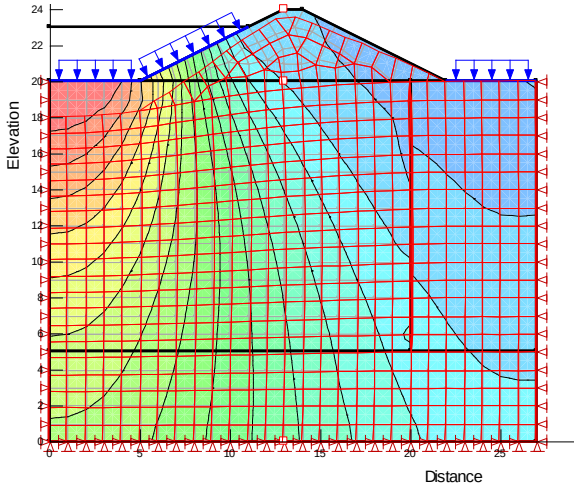

Figure 3.59(c): Flownet for 15 m long sheet file at *B*/8 position from downstream end

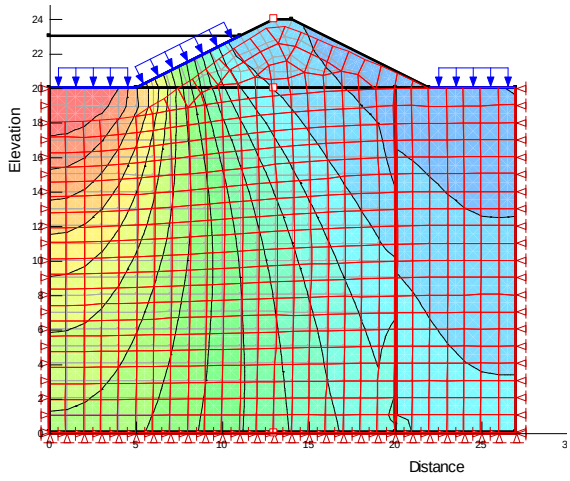

Figure 3.59(d): Flownet for 20 m long sheet file at *B*/8 position from downstream end

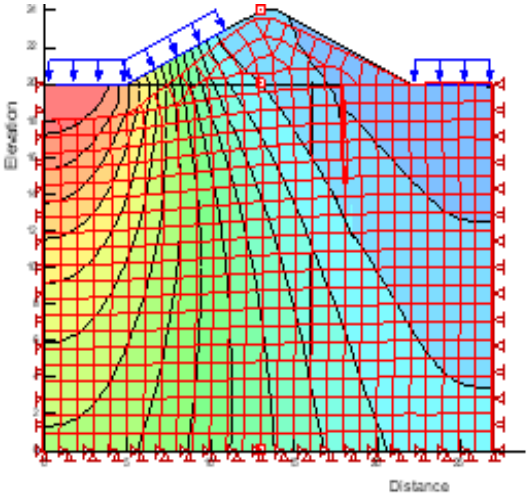

Figure 3.59(e): Flownet for 5 m long sheet file at 2*B*/8 position from downstream end

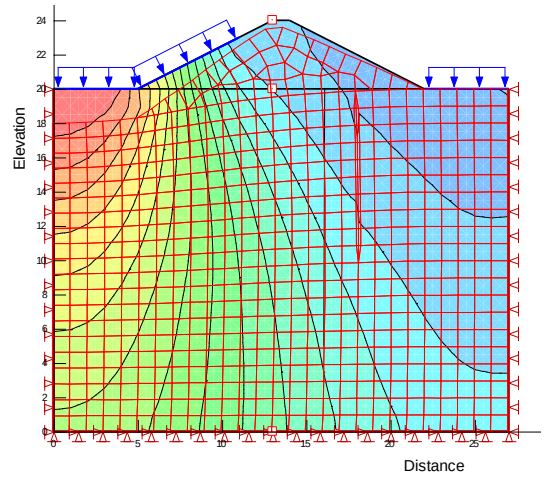

Figure 3.58(f): Flownet for 10 m long sheet file at 2*B*/8 position from downstream end

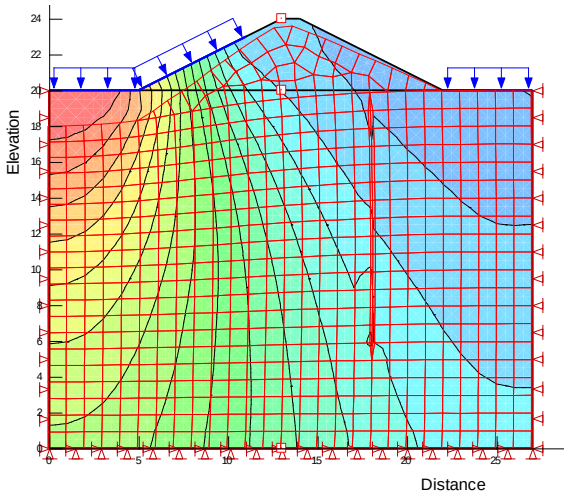

Figure 3.59(g): Flownet for 15 m long sheet file at 2*B*/8 position from downstream end

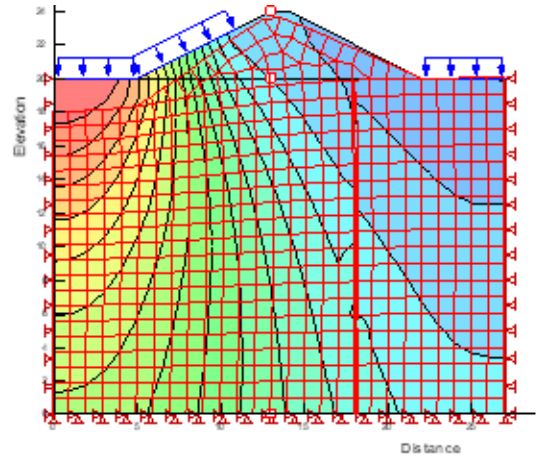

Figure 3.59(h): Flownet for 20 m long sheet file at 2*B*/8 position from downstream end

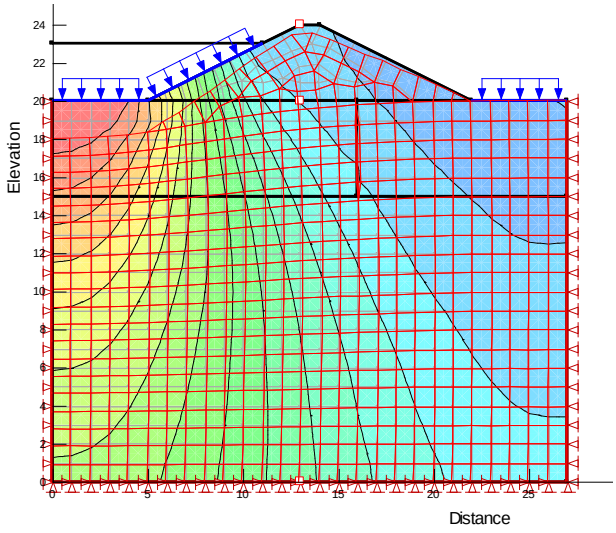

Figure 3.59(i): Flownet for 5 m long sheet file at 3*B*/8 position from downstream end

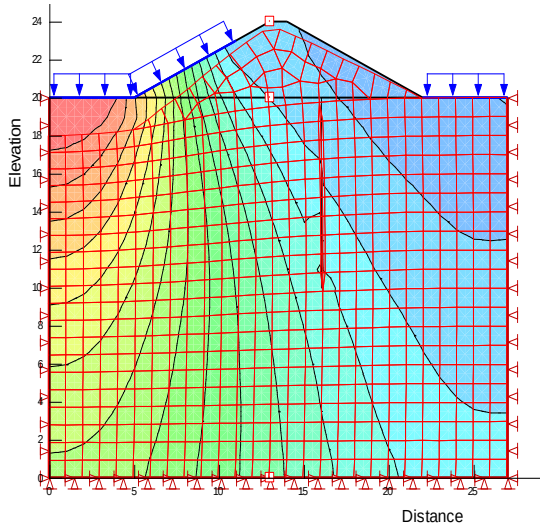

Figure 3.58(j): Flownet for 10 m long sheet file at 3*B*/8 position from downstream end

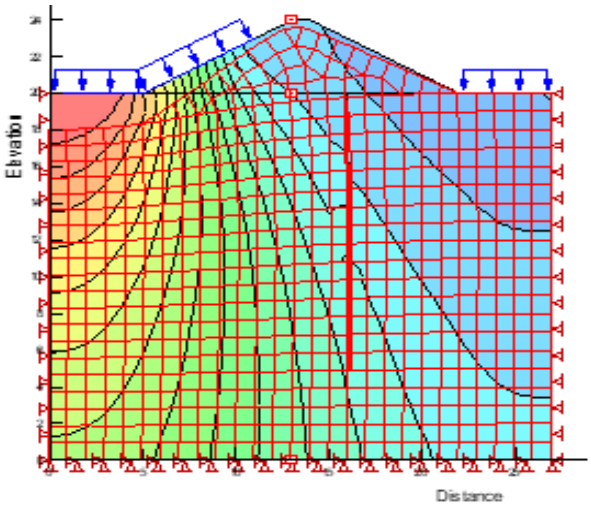

Figure 3.59(k): Flownet for 20 m long sheet file at 3*B*/8 position from downstream end

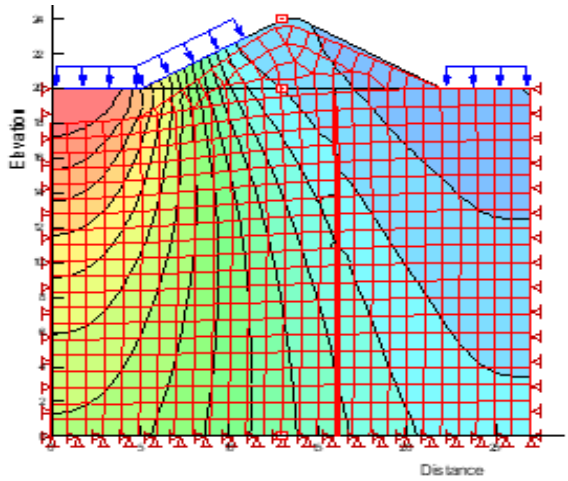

Figure 3.59(l): Flownet for 20 m long sheet file at 3*B*/8 position from downstream end

3.6.6.3 PRESENTATION OF RESULTS UNDER TRANSIENT STATE

In the modeling of seismic effect under transient condition each stage has been taken as steady state.

In this study the pattern of stream line has not been observed.

3.6.6.3.1 PRESENTATION OF RESULTS FROM FLAC 2D FOR WITH OUT SHEET PILE UNDER TRANSIENT STATE

The variation of the flownet in upstream side with respect to cycle time has been represented from Figure. 3.60(a) to 3.60(c) using FLAC 2D software. In this study the pattern of stream line has not been observed.

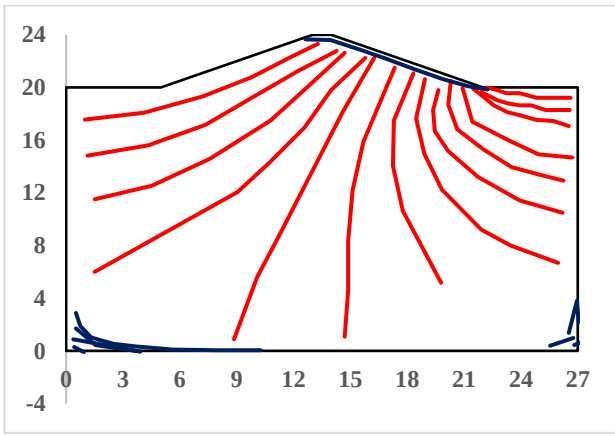

Figure 3.60(a): Flownet under Rise up condition for without sheet pile condition, at full rise up condition, t=6.0 hrs.)

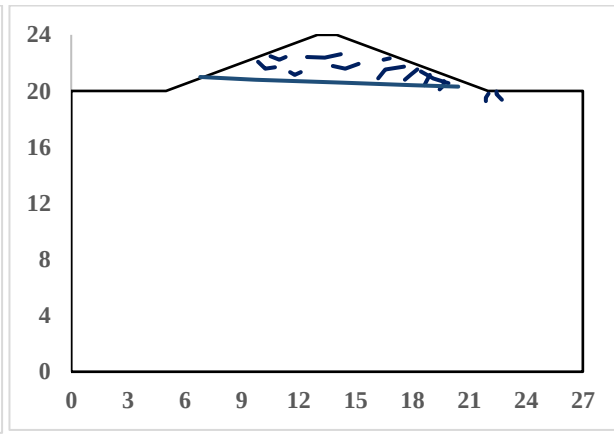

Figure 3.60(b): Flownet under Rise up condition for without sheet pile condition, time = 12.0 hrs.

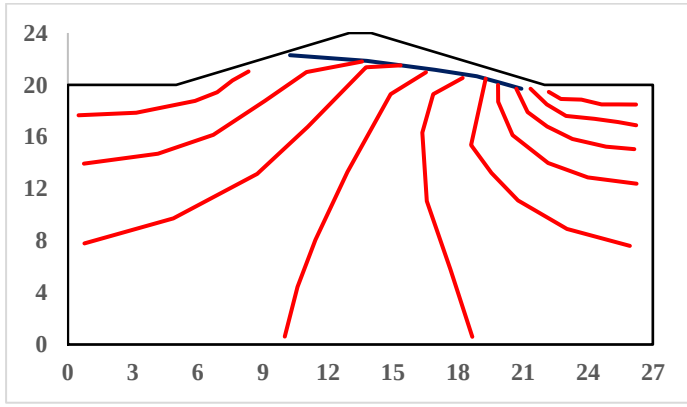

Figure 3.60(c): Flownet under Drawdown condition for without sheet pile condition, time = 8.0 hrs.

3.6.6.3.2 PRESENTATION OF RESULTS FROM FLAC 2D FOR WITH SHEET PILE UNDER TRANSIENT STATE BY FLAC 2D

The variation of the flownet in upstream side with respect to cycle time from FLAC 2D has been plotted and represented from Figure. 3.61(a) to 3.72(c).

3.6.6.3.2.1 Presentation of results for 5m long sheet pile at *B*/8 position

Flownet have been plotted from Figure 3.61(a) to 3.61(c) for the earthen dam with sheet pile condition for *B*/8 position 5m length for full drawdown condition (1 hr.) , full rise up condition (6 hrs.) and for 8.0 hrs.

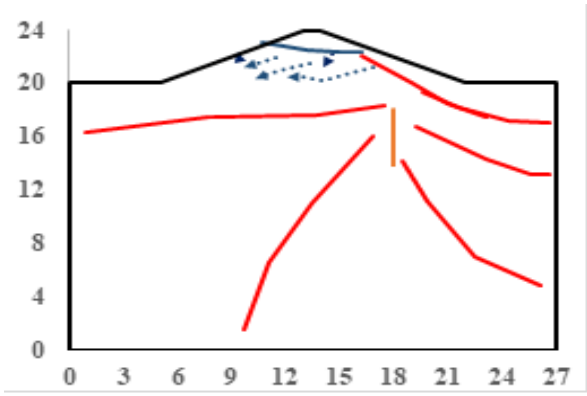

Figure 3.61(a): Flownet under Rise up condition (for 5 m long sheet pile at *B*/8 from downstream end, time = 1.0 hr.)

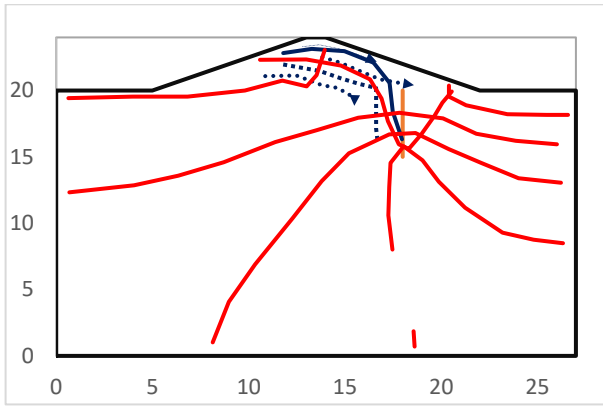

Figure 3.61(b): Flownet under Rise up condition (for 5 m long sheet pile at *B*/8 from downstream end, time = 6.0 hrs.)

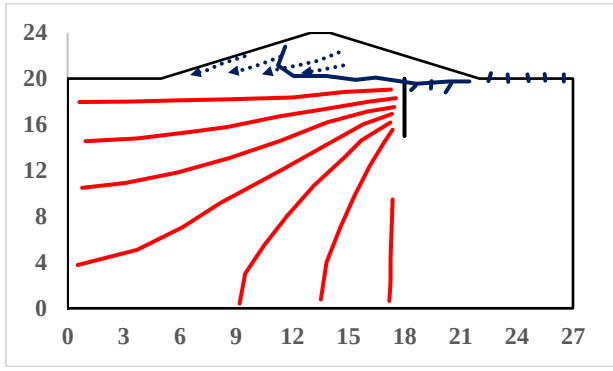

Figure 3.61(c): Flownet under Rise up condition (for 5 m long sheet pile at *B*/8 from downstream end, time = 8.0 hrs.)

3.6.6.3.2.2 Presentation of results for 10m long sheet pile at *B*/8 position

Flownet have been plotted from Figure 3.62(a) to 3.62(c) for the earthen dam with sheet pile condition for *B*/8 position 10m length for full drawdown condition (1 hr.) , full rise up condition (6 hrs.) and for 8.0 hrs.

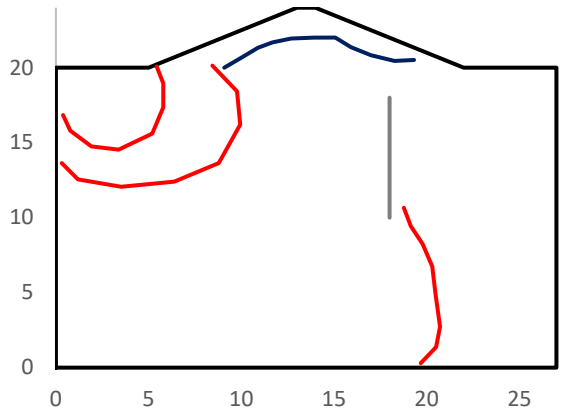

Figure 3.62(a): Flownet under Rise up condition (for 10 m long sheet pile at *B*/8 from downstream end, time = 1.0 hr.)

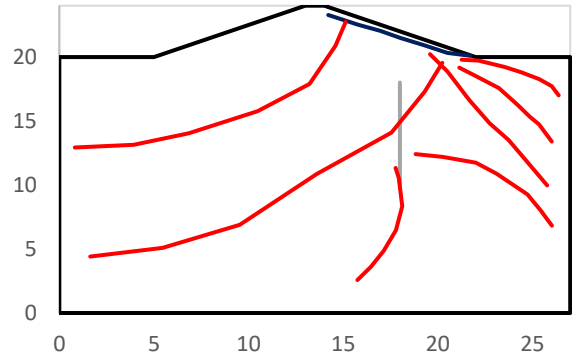

Figure 3.62(b): Flownet under Rise up condition (for 10 m long sheet pile at *B*/8 from downstream end, time = 6.0 hrs.)

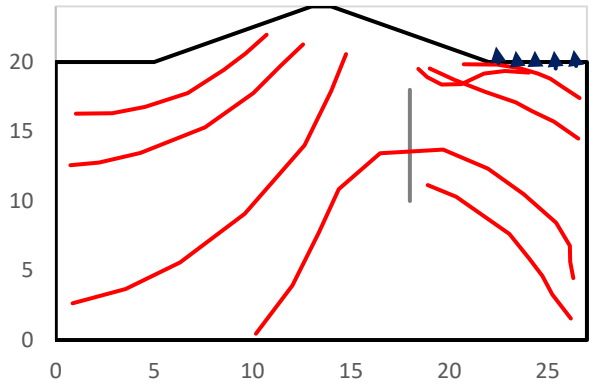

Figure 3.62(c): Flownet under Rise up condition (for 10 m long sheet pile at *B*/8 from downstream end, time = 8.0 hrs.)

3.6.6.3.2.3 Presentation of results for 15m long sheet pile at *B*/8 position

Flownet have been plotted from Figure 3.63(a) to 3.63(c) for the earthen dam with sheet pile condition for *B*/8 position 15m length for full drawdown condition (1 hr.) , full rise up condition (6 hrs.) and for 8.0 hrs.

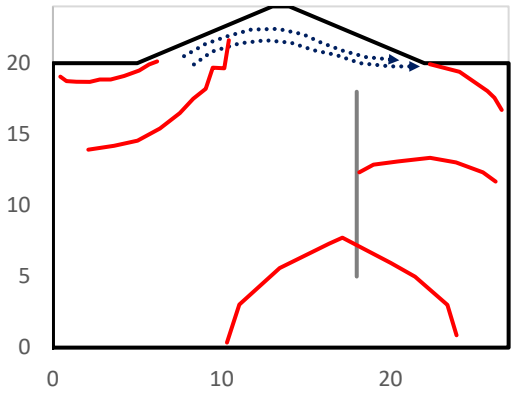

Figure 3.63(a): Flownet under Rise up condition (for 15 m long sheet pile at *B*/8 from downstream end, time = 1.0 hr.)

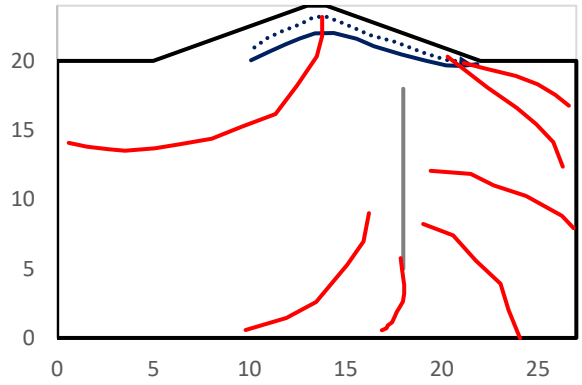

Figure 3.63(b): Flownet under Rise up condition (for 15 m long sheet pile at *B*/8 from downstream end, time = 6.0 hrs.)

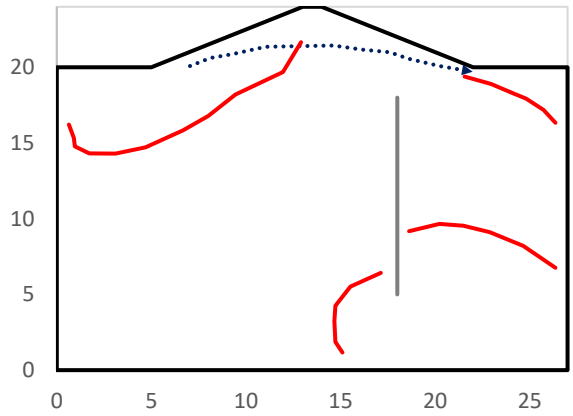

Figure 3.63(c): Flownet under Rise up condition (for 15 m long sheet pile at *B*/8 from downstream end, time = 8.0 hrs.)

3.6.6.3.2.4 Presentation of results for 20m long sheet pile at *B*/8 position

Flownet have been plotted from Figure 3.64(a) to 3.64(c) for the earthen dam with sheet pile condition for *B*/8 position 20m length for full drawdown condition (1 hr.) , full rise up condition (6 hrs.) and for 8.0 hrs.

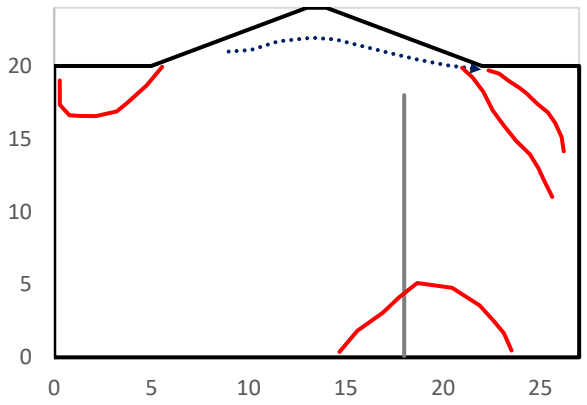

Figure 3.64(a): Flownet under Rise up condition (for 20 m long sheet pile at *B*/8 from downstream end, time = 1.0 hr.)

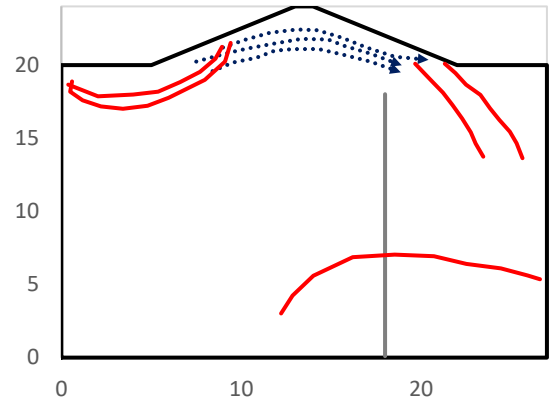

Figure 3.64(b): Flownet under Rise up condition (for 20 m long sheet pile at *B*/8 from downstream end, time = 6.0 hrs.)

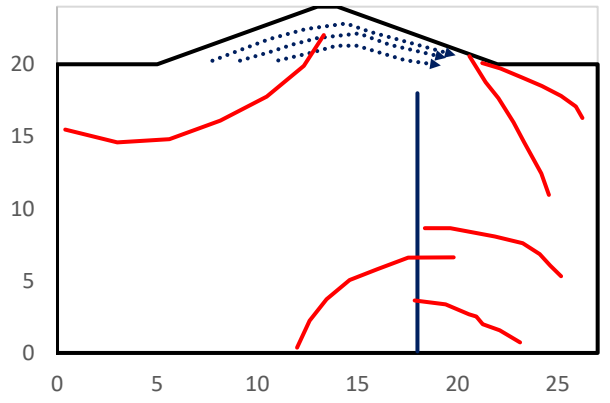

Figure 3.64 (c): Flownet under Rise up condition (for 20 m long sheet pile at *B*/8 from downstream end, time = 8.0 hrs.)

3.6.6.3.2.5 Presentation of results for 5m long sheet pile at 2*B*/8 position

Flownet have been plotted from Figure 3.65(a) to 3.65(c) for the earthen dam with sheet pile condition for 2*B*/8 position 5m length for full drawdown condition (1 hr.), full rise up condition (6 hrs.) and for 8.0 hrs.

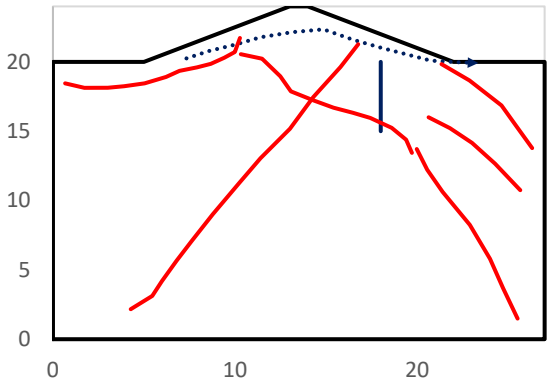

Figure 3.65(a): Flownet under Rise up condition (for 5m long sheet pile at 2*B*/8 from downstream end, time = 1.0 hr.)

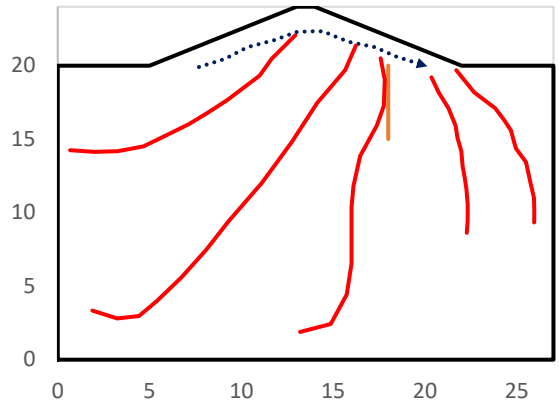

Figure 3.65(b): Flownet under Rise up condition (for 5m long sheet pile at 2*B*/8 from downstream end, time = 6.0 hrs.)

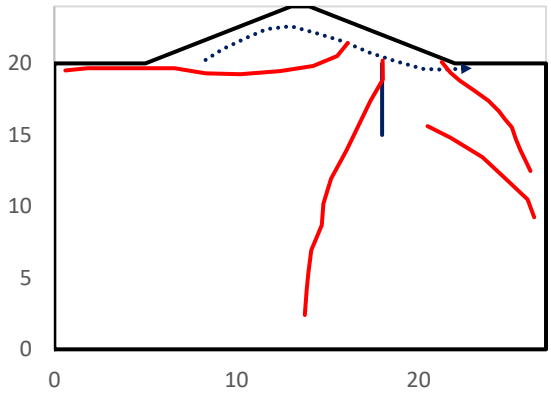

Figure 3.65(c): Flownet under Drawdown condition (for 5m long sheet pile at 2*B*/8 from downstream end, time = 8.0 hrs.)

3.6.6.3.2.6 Presentation of results for 10 m long sheet pile at 2*B*/8 position

Flownet have been plotted from Figure 3.66(a) to 3.66(c) for the earthen dam with sheet pile condition for 2*B*/8 position 10m length for full drawdown condition (1 hr.) , full rise up condition (6 hrs.) and for 8.0 hrs.

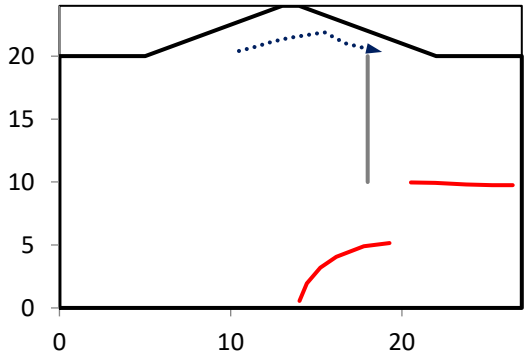

Figure 3.66(a): Flownet under Rise up condition (for 10m long sheet pile at 2*B*/8 from downstream end, time = 1.0 hr.)

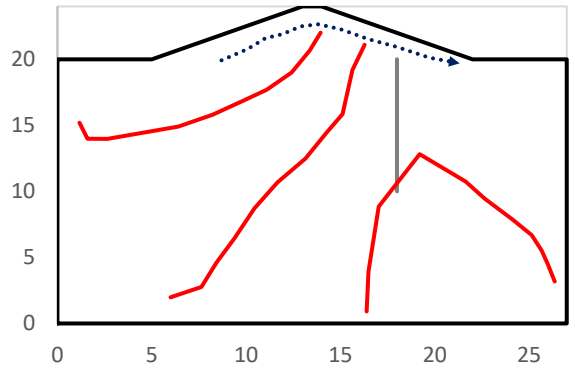

Figure 3.66(b): Flownet under Rise up condition (for 10m long sheet pile at 2*B*/8 from downstream end, time = 6.0 hrs.)

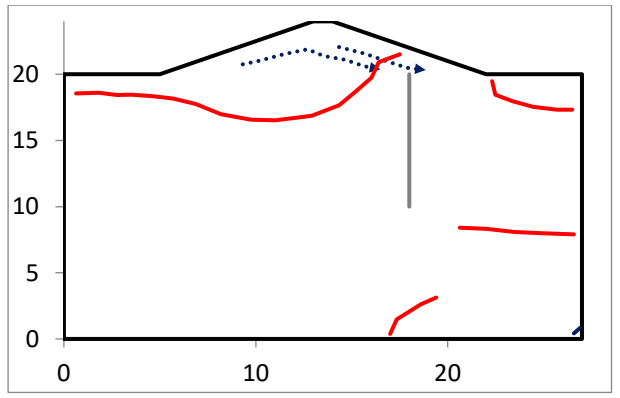

Figure 3.66(e): Flownet under Drawdown condition (for 10m long sheet pile at 2*B*/8 from downstream end, time = 8.0 hrs.)

3.6.6.3.2.7 Presentation of results for 15 m long sheet pile at 2*B*/8 position

Flownet have been plotted from Figure 3.67(a) to 3.67(c) for the earthen dam with sheet pile condition for 2*B*/8 position 10m length for full drawdown condition (1 hr.) , full rise up condition (6 hrs.) and for 10.0 hrs.

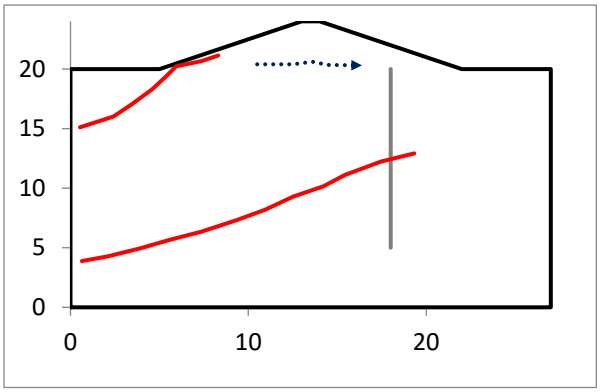

Figure 3.67(a): Flownet under Rise up condition (for 15m long sheet pile at 2*B*/8 from downstream end, time = 1.0 hr.)

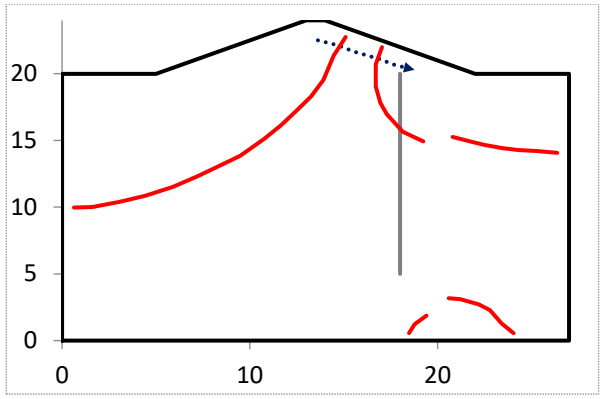

Figure 3.64(b): Flownet under Rise up condition (for 15m long sheet pile at 2*B*/8 from downstream end, time = 6.0 hrs.)

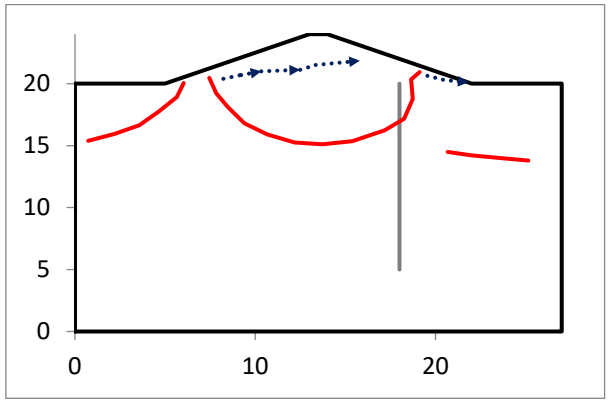

Figure 3.67(c): Flow-net under Drawdown condition (for 15m long sheet pile at 2*B*/8 from downstream end, time = 10.0 hrs.)

3.6.6.3.2.8 Presentation of results for 20 m long sheet pile at 2*B*/8 position

Flownet have been plotted from Figure 3.68(a) to 3.68(c) for the earthen dam with sheet pile condition for 2*B*/8 position 20m length for full drawdown condition (1 hr.) , full rise up condition (6 hrs.) and for 10.0 hrs.

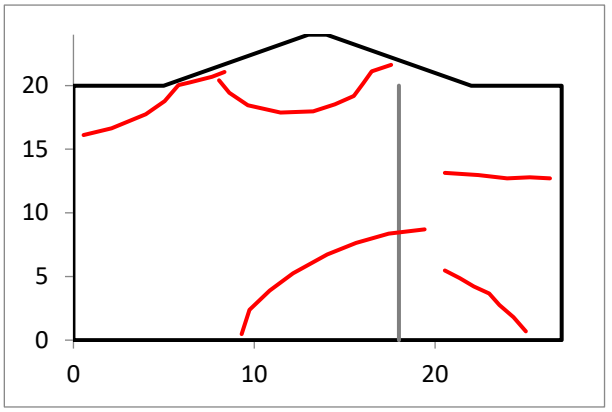

Figure 3.68(a): Flownet under Rise up condition (for 20m long sheet pile at 2*B*/8 from downstream end, time = 1.0 hr.)

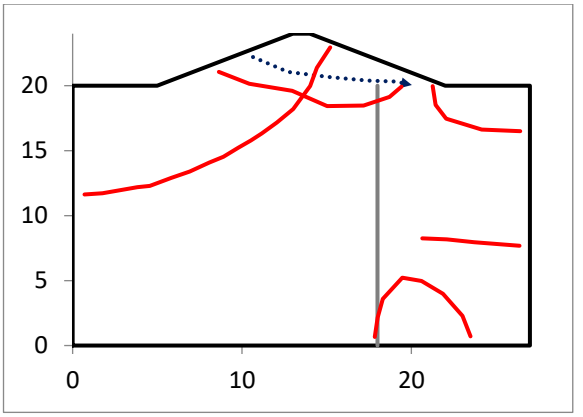

Figure 3.68(b): Flownet under Rise up condition (for 20m long sheet pile at 2*B*/8 from downstream end, time = 6.0 hrs.)

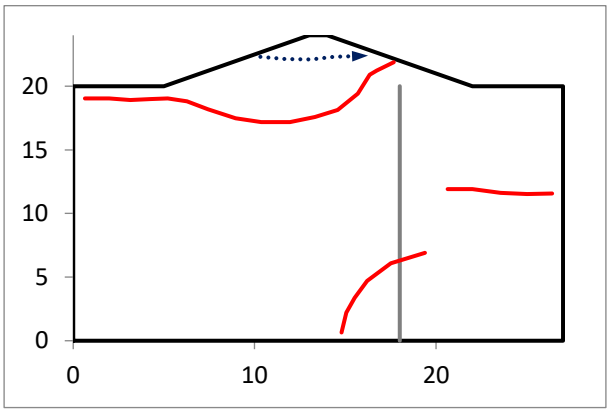

Figure 3.68(c): Flownet under Drawdown condition (for 20m long sheet pile at 2*B*/8 from downstream end, time = 10.0 hrs.)

3.6.6.3.2.9 Presentation of results for 5 m long sheet pile at 3*B*/8 position

Flownet have been plotted from Figure 3.69(a) to 3.69(c) for the earthen dam with sheet pile condition for 3*B*/8 position 5m length for full drawdown condition (1 hr.) , full rise up condition (6 hrs.) and for 8.0 hrs.

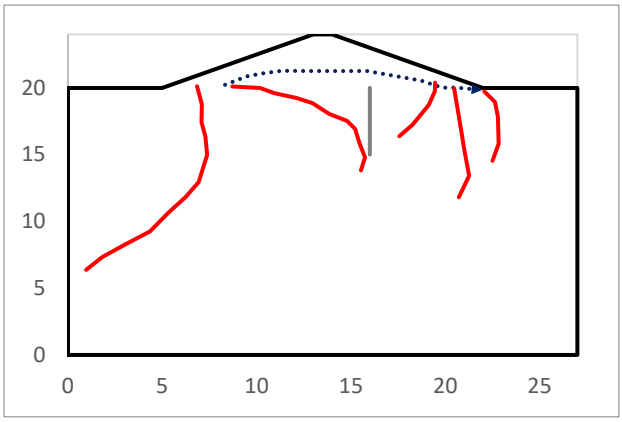

Figure 3.69(a): Flownet under Rise up condition (for 5m long sheet pile at 3*B*/8 from downstream end, time = 1.0 hr.)

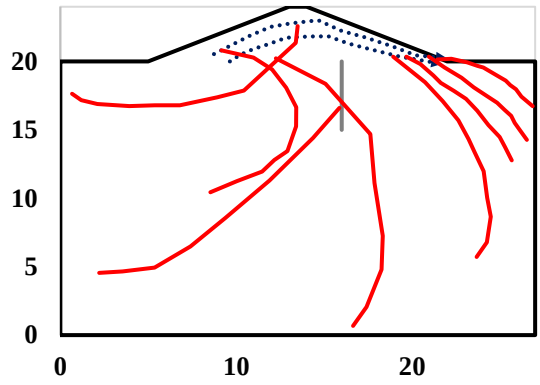

Figure 3.69(b): Flownet under Rise up condition (for 5m long sheet pile at 3*B*/8 from downstream end, time = 6.0 hrs.)

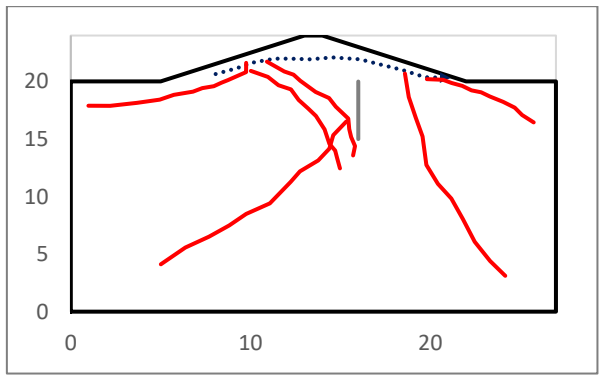

Figure 3.69(c): Flownet under Drawdown condition (for 5m long sheet pile at 3*B*/8 from downstream end, time = 8.0 hrs.)

3.6.6.3.2.10 Presentation of results for 10 m long sheet pile at 3*B*/8 position

Flownet have been plotted from Figure 3.70(a) to 3.70(c) for the earthen dam with sheet pile condition for 3*B*/8 position 10 m length for full drawdown condition (1 hr.) , full rise up condition (6 hrs.) and for 8.0 hrs.

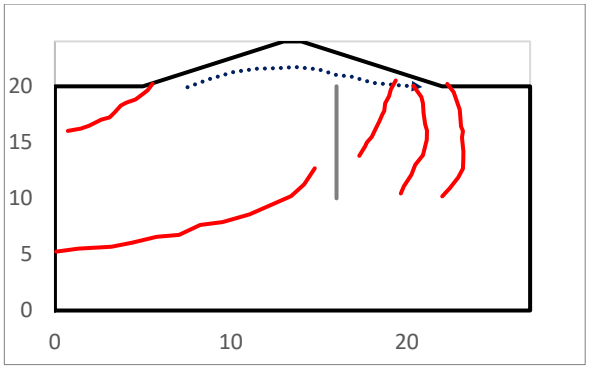

Figure 3.70(a): Flownet under Rise up condition (for 10m long sheet pile at 3*B*/8 from downstream end, time = 1.0 hr.)

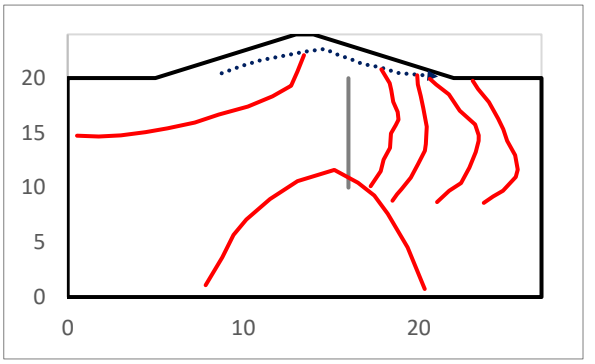

Figure 3.70(b): Flownet under Rise up condition (for 10m long sheet pile at 3*B*/8 from downstream end, time = 6.0 hrs.)

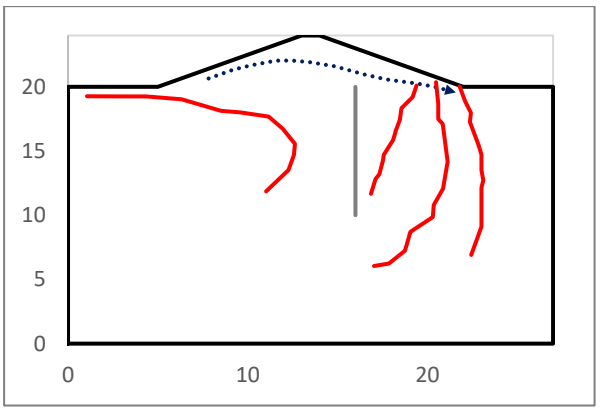

Figure 3.70(c): Flownet under Drawdown condition (for 10m long sheet pile at 3*B*/8 from downstream end, time = 8.0 hrs.)

3.6.6.3.2.11 Presentation of results for 15 m long sheet pile at 3*B*/8 position

Flownet have been plotted from Figure 3.71(a) to 3.71(c) for the earthen dam with sheet pile condition for 3*B*/8 position 10 m length for full drawdown condition (1 hr.) , full rise up condition (6 hrs.) and for 8.0 hrs.

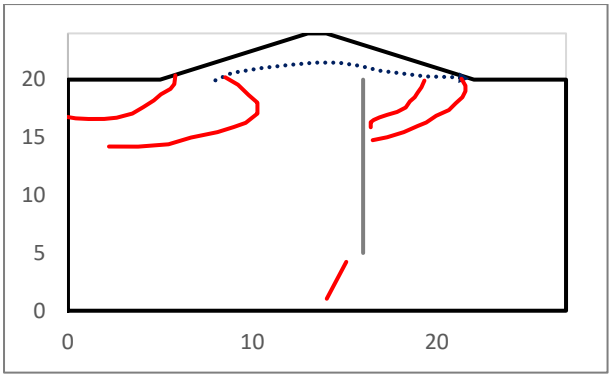

Figure 3.71(a): Flownet under Rise up condition (for 15 m long sheet pile at 3*B*/8 from downstream end, time = 1.0 hr.)

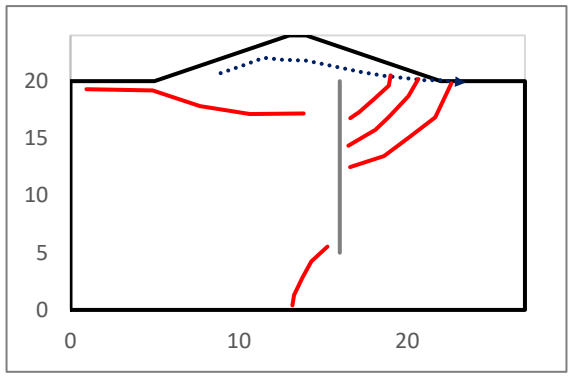

Figure 3.71(b): Flownet under Rise up condition (for 15 m long sheet pile at 3*B*/8 from downstream end, time = 6.0 hrs.)

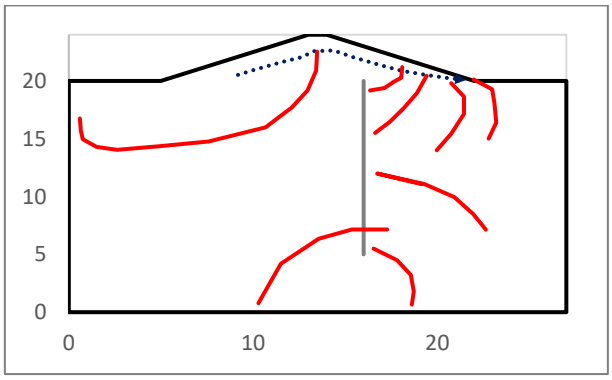

Figure 3.71(c): Flownet under Rise up condition (for 15 m long sheet pile at 3*B*/8 from downstream end, time = 8.0 hrs.)

3.6.6.3.3.12 Presentation of results for 20 m long sheet pile at 3*B*/8 position

Flownet have been plotted from Figure 3.72(a) to 3.72(c) for the earthen dam with sheet pile condition for 3*B*/8 position 10 m length for full drawdown condition (1 hr.) , full rise up condition (6 hrs.) and for 10.0 hrs.

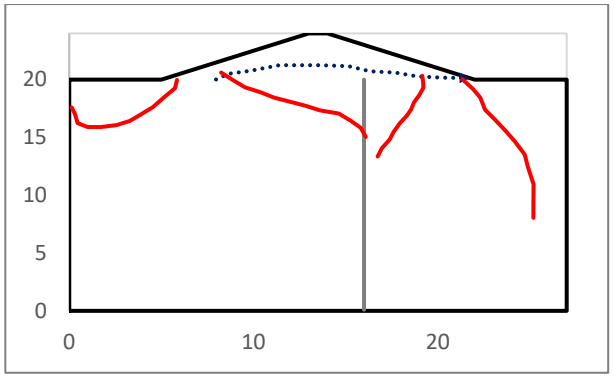

Figure 3.72(a): Flownet under Rise up condition (for 20m long sheet pile at 3*B*/8 from downstream end, time = 1.0 hr.)

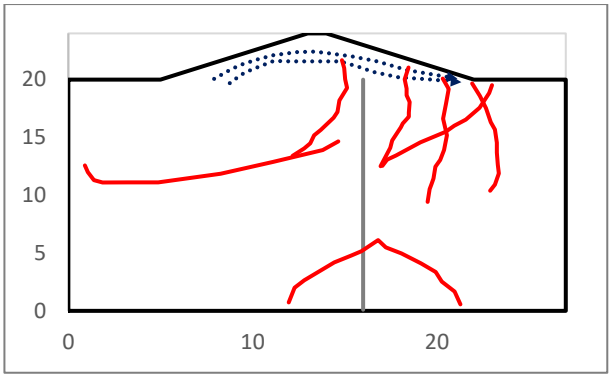

Figure 3.72(b): Flownet under Drawdown condition (for 20m long sheet pile at 3*B*/8 from downstream end, time = 6.0 hrs.)

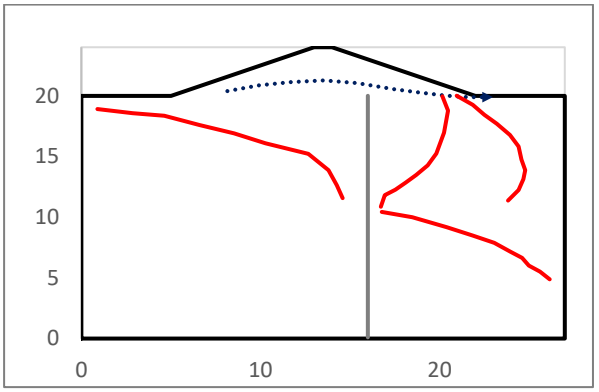

Figure 3.72(c): Flownet under Drawdown condition (for 20m long sheet pile at 3*B*/8 from downstream end, time = 10.0 hrs.)

3.7 USE OF NUMERICAL RESULTS

The numerical results presented in this chapter for different software for different cases of steady and transient seepage, each under static and seismic conditions. The findings of the results are summarized and discussed and they have been compared with experimental results in chapter five.

EXPERIMENTAL INVESTIGATION

4.1 AN OVERVIEW:

An experimental investigation has been undertaken using geotechnical centrifuge to study the effect of steady seepage as well as tide induced transient seepage on earthen embankments. A set-up to study the same was developed in the Geotechnical Engineering Laboratory, Civil Engineering Department, Jadavpur University, Kolkata. The details of the set-up have been given in the upcoming sub-sections of this chapter. The model selected for study is the typical embankment as considered for numerical analysis in the present chapter. The centrifuge technique combines the advantages of modelling a prototype system in an appropriate small-scale test. In recent years, centrifuge has become a more accepted and useful modeling tool in geotechnical problems. In this present research centrifuge has been used to study the flow path using sheet pile as a barrier in the downstream side of an earthen dam and to evaluate the effectiveness of the sheet pile by predicting its stability against piping and failure of slope as well. In order to, do this a properly scaled model has been designed. A series of tests have been performed to study the flow path and fluid flow vector, pore water pressure variation in the seepage analysis of the model earthen dam. It has been possible in centrifuge modeling to generate the real stress field but at the same time with the advantage of faster seepage flow. Figure 4.1 represents the flow chart of current experimental and numerical simulation.

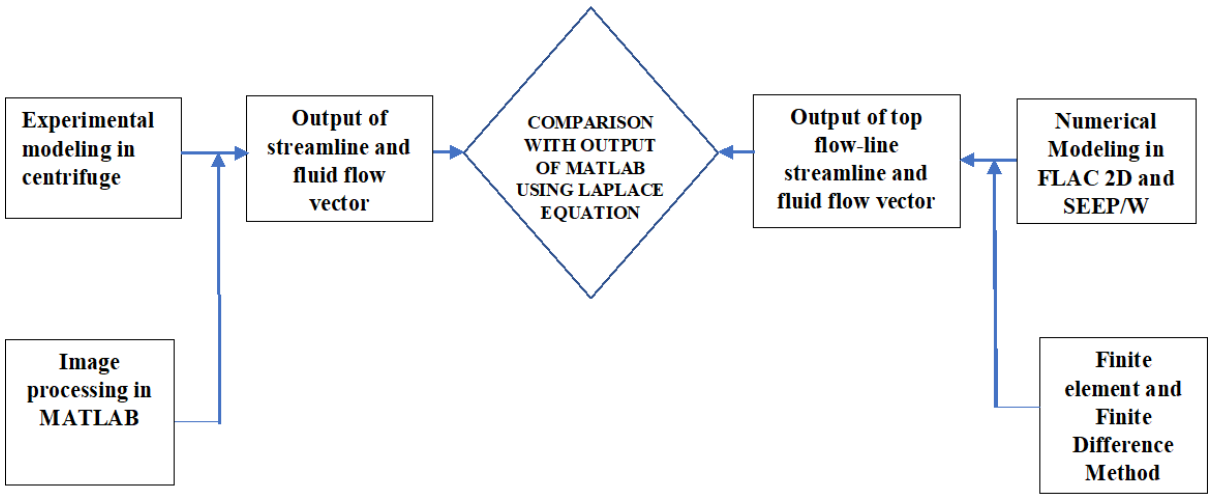

Figure 4.1: Flow Chart for present current experimental and numerical simulation analysis

4.2 PRINCIPLE OF CENTRIFUGE MODELLING

Centrifuge modelling is a technique which involves physical modelling of geotechnical structures which are subjected to gravity forces. The main strength of centrifuge modelling is to capture the correct failure mechanism in the boundary value problems. Through centrifuge modelling it has been possible to analyze complex studies by constructing small-scale physical models and testing them in an enhanced gravity field of a geotechnical centrifuge.

In case of testing of centrifuge modeling, true plain strain models or fully three-dimensional models can be developed as required. In centrifuge modelling a rotating soil body mounted on a geotechnical centrifuge to represent a scale model of a given prototype we are trying to model. The diameter of the centrifuge of 0.55m. The turner beam carries scaled model at one end and a counter weight at the other, each mounted on a swing platform. As the centrifuge starts to spin about the central vertical axis, the swing platforms rotate about a pivot until they become horizontal.

4.2.1 GENERAL PRINCIPLE

The basic principle is that a $\frac{1}{N}$ ($\frac{1}{N}$ =$\boldsymbol{X}$ = $\boldsymbol{X}_m$ / $\boldsymbol{X}_p$, where $\boldsymbol{X}_m$and $\boldsymbol{X}_p$are parameter values in the model and prototype respectively) scale model have been tested of a prototype in the enhanced gravity field of a geotechnical centrifuge. The gravity is increased by the same geometric factor *N* relative to the normal earth's gravity field.

Considering a block structure of mass M and with dimensions *l' ×b'× h'* sited at a horizontal soil bed, the average vertical stress exerted by this block on the soil can be calculated as

$$\sigma_v = \frac{Mg}{L \text{ X } B} \tag{4.1}$$

And, Vertical strain induced for a characteristic length (α) as $\epsilon = \frac{\delta\alpha}{\alpha}$ (4.2)

Where, δα= change in characteristic length

Considering, a scale model in which the dimensions are scaled down by a factor *N*, as all the dimensions are scaled sown the mass of the block will be M/N^3. When scale model is placed in the increased gravity field of N x earth's gravity. vertical stress of scaled model (σ_{vm})

$$\sigma_{vm} = \frac{\left(\frac{M}{N^3}\right) \text{x } (Ng)}{\left(\frac{L}{N}\right) \text{x } \left(\frac{B}{N}\right)} = \frac{Mg}{LX\ B} \tag{4.3}$$

Thus, the vertical stress below this scale model of the block is the same as that below the larger block obtained in equation.4.3. Strains in the scaled model is given by equation 4.4

$$€=\frac{(\frac{\delta\alpha}{N})}{(\frac{\alpha}{N})}=\frac{\delta\alpha}{\alpha} \quad (4.4)$$

Increased gravity acting on scaled model by placing it in a geotechnical centrifuge. When the centrifuge rotating with an angular velocity of θ, the centrifugal acceleration at any radius r is given by $\bar{a}=r\,\theta^2$ (4.5)

$$Ng=r\,\theta^2 \quad (4.6)$$

Where, θ= angular velocity with which centrifuge rotate.

The centrifugal acceleration changes with the radial distance from the axis of rotation of the centrifuge as indicated in equation.4.6.

4.2.2 MATHEMATICAL FORMULATION

Mathematical formulation of the centrifuge modelling considering the uniform circular motion traveling around a circle or circular path at a constant speed has been discussed in this section. Considering a solid sphere travelling around in a circular path of radius *r*. The sphere is travelling at a uniform speed of *v* has been shown in Figure 4.2. However, its velocity $\bar{v}$ is constantly changing as the sphere changes its direction of travel as it goes around the circular path. In uniform circular motion the acceleration of the particle occurs because of change in direction of the velocity although the magnitude of velocity (speed) remains constant.

The sphere is rotating about the center of the circle with an angular speed $\dot{\theta}$. Let a set of unit vectors *i, j* and *k* as defined as shown in figure.4.2. The angular velocity of the sphere is θ_k. It must be noted that in Cartesian system of coordinates, the unit vectors i, j, and *k* are always fixed in direction, so their time derivatives are zero.

The position vector of the sphere at a given instant shown in figure can be written as

$\bar{r} = r\cos\theta_i + r\sin\theta_j$---------- (4.6)

we can obtain the velocity of the sphere by differentiating the position vector in equation

$\bar{v}=(d\bar{r}/dt)= r(-\sin\theta)\,\theta_i + r(\cos\theta)\theta_j$----- ------ (4.7)

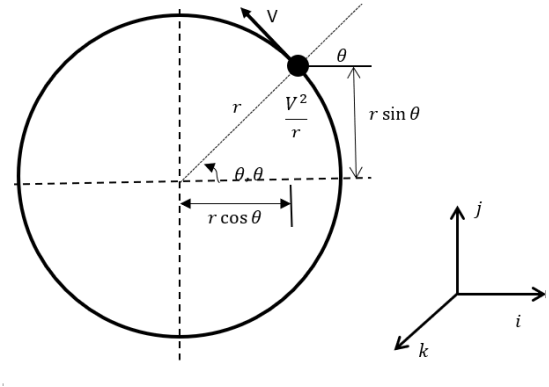

Figure 4.2. centrifuge traveling around a circle or circular path

In order to get the acceleration of the sphere, we can differentiate the velocity vector $\bar{v}$.

$\bar{a}=(d\bar{v}/dt)=-v(cos\theta)\theta_i + v(-sin\theta)\dot{\theta_j}$---------- (4.8)

substituting for the angular speed ϴ̇ from equation into equation (4.9), can write:

$\bar{a}=-(v^2/r)(cos\theta)i -(v^2/r)(sin\theta)j=(-(v^2/r))(cos\theta_i+sin\theta_j)$---------- (4.9)

the magnitude of this acceleration is therefore (v^2/r) and the minus sign indicates that it acts toward the center of the circular path. This acceleration is termed as centripetal acceleration to the model container. The direction of the centripetal acceleration is always towards the central vertical axis of the centrifuge about which it rotates.

4.2.3 CENTRIFUGAL MODELLING FOR SEEPAGE ANALYSIS

Scaling laws are relationships that relate the behavior of the centrifuge model and prototype, these are required to relate the observed behavior of the scale model in the centrifuge experiment to the behavior of a prototype. This is to be assumed that the prototype and the field structure are closely related, and all the essential features of the field structure are present in the prototype. For geometric and stress similitude, model dimensions are N times smaller than the equivalent prototype, where N is the acceleration scale factor (i.e. for testing at 100 times Earth's gravity, N =100 and the model is 100 times smaller than at full scale). The 'prototype' is a theoretical replica or simplification of the full-scale structure, designed to capture the pertinent phenomena. Other experimental parameters affected by accelerating the model above Earth's gravity are shown in Table 4.1.

Table 4.1 Centrifuge seepage modelling scaling laws.

Sr. No.	Parameters	Scale Factors
1	**Acceleration , g**	***N***
2	**Length , l**	***1/N***
3	**Angle of friction , φ**	**1**
4	**Apparent cohesion , c**	**1**
5	**Soil density , ρ**	**1**
6	**Effective stress , σ'**	**1**
7	**Hydraulic Conductivity , k**	***1***
8	**Hydraulic gradient , i**	***N***
9	**Pore pressure , u**	***1***
10	**Seepage velocity , v**	***N***
11	**Flow rate , Q**	***1/N***
12	**Time(kinematic),t**	***$1/N^2$***

A centrifuge machine provide model gravity as desired by applying linear scale factor. The ratio of the acceleration in the model earthen dam and prototype is inversely proportional to the ratio of their linear dimensions. The ratio of linear prototype dimension to the centrifuge model when *N*, then the ratio of area is N^2 and volume N^3. It has been indicated from the scaling relation that the forces in the prototype is N^2 times and moments N^3 of the corresponding model. Deformation in the prototype is *N* times larger than in the model, but strains (deformation per unit length) are the same. The pressure of the same material for both prototype and model are same. In the experiment it was necessary to design model wall to a similar stiffness of prototype per unit width (*EI*). The ratio of stiffness of prototype is N^3 times of that of the model. In the present study *N* has been adopted as 100. The model was 1/100 of the prototype linear dimension, and the model acceleration was 100 times of normal terrestrial gravity.

4.2.3.1Determination of actual dimension of the wall and model dam:

In order to determine the dimension of the modeled sheet pile wall and earthen dam, $EI_{model}=EI_{prototype}/N$

4.2.3.2 Determination of actual *EI* of the wall:

In order to determine the true stiffness *(EI*) of the modeled sheet pile wall, $EI_{model}=EI_{prototype}/N^3$

Steel sheet pile has been considered as protype structure. Modulus of Elasticity of Steel Sheet pile ($E_{prototype}$) = 2×10^{11} N/m^2. Moment of Inertia per meter of steel sheet pile ($I_{prototype}$)=0.00225 m^3. In the present seepage study Perspex sheet has been used as modeled sheet pile. Modulus of Elasticity (E_{model}) of the Perspex= 2.0×10^9 Pa. Moment of Inertia per unit width (I) of a rectangular cross section is $\frac{(h')^3}{12}$, where h is the section depth. In the present experimental study 20 cm length of Perspex when modeled as sheet pile, Moment of Inertia per unit width (I_{model}) = 2.49×10^{-7} m^3/m.

$EI_{model}=2.0\times10^9\times2.49\times10^{-7}$= 498 N-m/m.

4.2.3.3 Variation in Gravity field:

However, in a centrifuge small-scale models are tested in a gravity field, which is linear function of the distance from the center of rotation. Thus, the gravity field varies linearly with radius from the center of rotation and as a square of the angular velocity ϴ of the centrifuge.

4.3 TEST PROGRAMME:

In order to illustrate the test program a flow chart has been presented in Figure 4.3 and the test programme for the steady state and transient state cases have been presented in Table 4.2, Table 4.3(a) and Table 4.3(b) respectively. In case of transient state rise up and drawdown have been considered by varying the rise up half cycle time (t_{RU}) and drawdown Half Cycle time (t_{DD}) for respective tests. A uniform rate of 0.583 m/hour has been maintained for rise up and drawdown for each test.

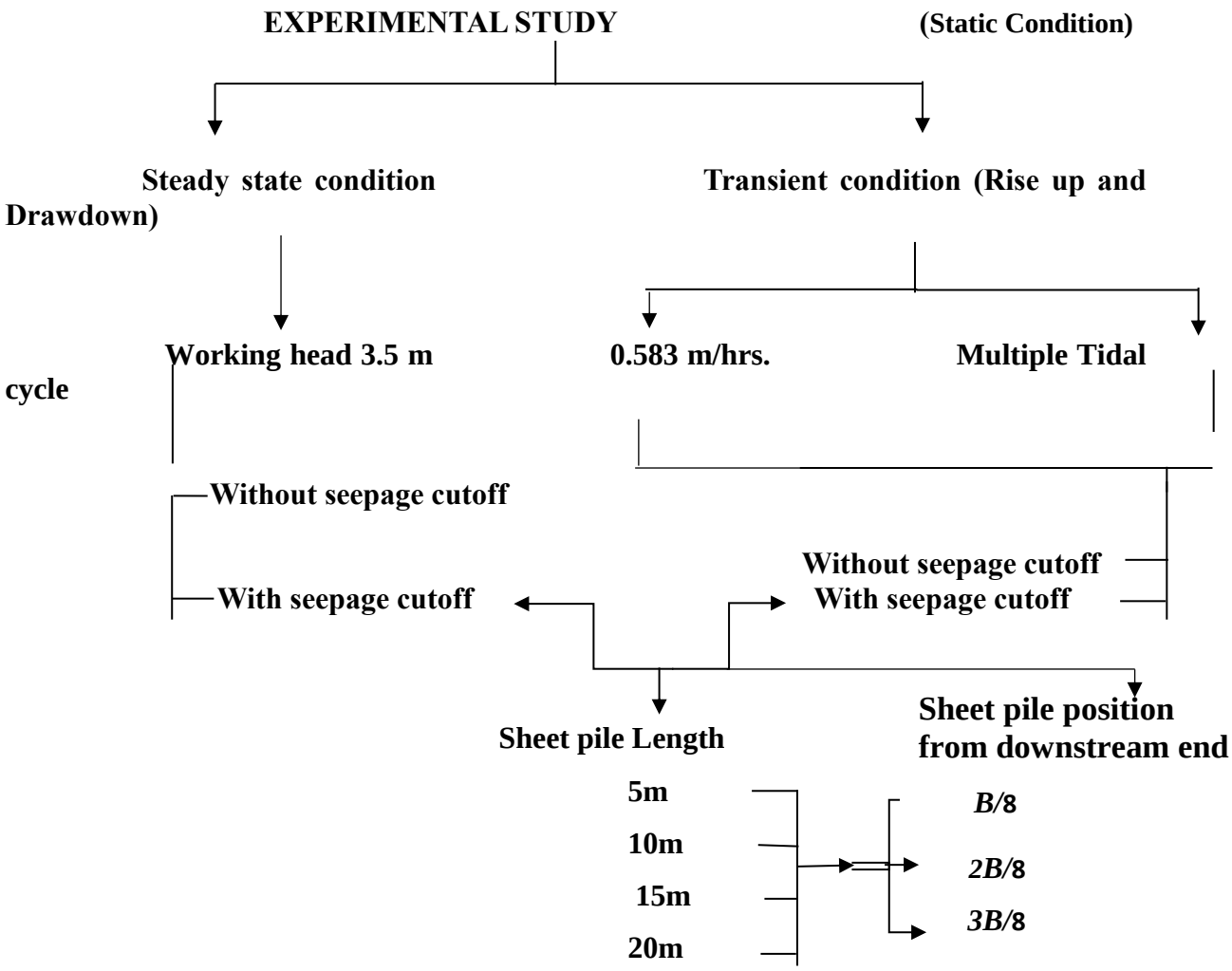

Fig. 4.3 Flowchart for experimental analysis

TABLE 4.2: TEST PROGRAMME FOR STEADY STATE (UNDER STATIC CONDITION)

Sl. no.	Nomenclature	Sheet pile length in meter	Sheet pile position from Downstream end
1	EMB	N.A	N.A
2	T2.1L5	5	B/8
3	T2.1L10	10	
4.	T2.1L15	15	
5	T2.1L20	20	
6	T4.2L5	5	2B/8
7	T4.2L10	10	
8	T4.2L15	15	
9	T4.2L20	20	
10	T6.3L5	5	3B/8
11	T6.3L10	10	
12	T6.3L15	15	
13	T6.3L20	20	

TABLE 4.3(a): TEST PROGRAMME FOR TRANSIENT STATE WITH SINGLE TIDAL CYCLE (UNDER STATIC CONDITIONS)

Serial No.	Model Nomenclature	Rate of rise and fall (m/hour)	Half Cycle Time(hour)		Number of Cycles	Remarks
			Rise up	Drawdown		
1	ER1	0.583 m/hour	1	-	0.5	Single Tidal cycle
2	ER2		2		0.5	
3	ER3		3		0.5	
4	ER4		4		0.5	
5	ER5		5		0.5	
6	ER6		6		0.5	
7	ED1			7	0.5	
8	ED2			8	0.5	
9	ED3			9	0.5	
10	ED4			10	0.5	
11	ED5			11	0.5	
12	ED6			12	0.5	
13	T2.1L5R1	0.583 m/hour	1	-	0.5	Single Tidal cycle
14	T2.1L5R2		2		0.5	
15	T2.1L5R3		3		0.5	
16	T2.1L5R4		4		0.5	
17	T2.1L5R5		5		0.5	
18	T2.1L5R6		6		0.5	
19	T2.1L5D1			7	0.5	
20	T2.1L5D2			8	0.5	
21	T2.1L5D3			9	0.5	
22	T2.1L5D4			10	0.5	
23	T2.1L5D5			11	0.5	
24	T2.1L5D6			12	0.5	
25	T2.1L10R1		1	-	0.5	
26	T2.1L10R2		2		0.5	
27	T2.1L10R3		3		0.5	
28	T2.1L10R4		4		0.5	
29	T2.1L10R5		5		0.5	
30	T2.1L10R6		6		0.5	
31	T2.1L10D1			7	0.5	
32	T2.1L10D2			8	0.5	
33	T2.1L10D3			9	0.5	

34	T2.1L10D4			10	0.5	
35	T2.1L10D5			11	0.5	
36	T2.1L10D6			12	0.5	
37	T2.1L15R1		1	-	0.5	
38	T2.1L15R2		2		0.5	
39	T2.1L15R3		3		0.5	
40	T2.1L15R4		4		0.5	
41	T2.1L15R5		5		0.5	
42	T2.1L15R6		6		0.5	
43	T2.1L15D1			7	0.5	
44	T2.1L15D2			8	0.5	
45	T2.1L15D3			9	0.5	
46	T2.1L15D4			10	0.5	
47	T2.1L15D5			11	0.5	
48	T2.1L15D6			12	0.5	
49	T2.1L20R1		1	-	0.5	
50	T2.1L20R2		2		0.5	
51	T2.1L20R3		3		0.5	
52	T2.1L20R4		4		0.5	
53	T2.1L20R5		5		0.5	
54	T2.1L20R6		6		0.5	
55	T2.1L20D1			7	0.5	
56	T2.1L20D2			8	0.5	
57	T2.1L20D3			9	0.5	
58	T2.1L20D4			10	0.5	
59	T2.1L20D5			11	0.5	Single Tidal cycle
60	T2.1L20D6			12	0.5	
61	T4.2L5R1		1	-	0.5	
62	T4.2L5R2		2		0.5	
63	T4.2L5R3		3		0.5	
64	T4.2L5R4		4		0.5	
65	T4.2L5R5		5		0.5	
66	T4.2L5R6		6		0.5	
67	T4.2L5D1			7	0.5	
68	T4.2L5D2			8	0.5	
69	T4.2L5D3			9	0.5	
70	T4.2L5D4			10	0.5	
71	T4.2L5D5			11	0.5	
72	T4.2L5D6			12	0.5	
73	T4.2L10R1		1	-	0.5	
74	T4.2L10R2		2		0.5	
75	T4.2L10R3		3		0.5	
76	T4.2L10R4		4		0.5	

77	T4.2L10R5		5		0.5	
78	T4.2L10R6		6		0.5	
79	T4.2L10D1			7	0.5	
80	T4.2L10D2			8	0.5	
81	T4.2L10D3			9	0.5	
82	T4.2L10D4			10	0.5	
83	T4.2L10D5			11	0.5	
84	T4.2L10D6			12	0.5	
85	T4.2L15R1		1	-	0.5	
86	T4.2L15R2		2		0.5	
87	T4.2L15R3		3		0.5	
88	T4.2L15R4		4		0.5	
89	T4.2L15R5		5		0.5	
90	T4.2L15R6		6		0.5	
91	T4.2L15D1			7	0.5	
92	T4.2L15D2			8	0.5	
93	T4.2L15D3			9	0.5	
94	T4.2L15D4			10	0.5	
95	T4.2L15D5			11	0.5	
96	T4.2L15D6			12	0.5	
97	T4.2L20R1		1	-	0.5	
98	T4.2L20R2		2		0.5	
99	T4.2L20R3		3		0.5	
100	T4.2L20R4		4		0.5	
101	T4.2L20R5		5		0.5	
102	T4.2L20R6		6		0.5	Single Tidal cycle
103	T4.2L20D1			7	0.5	
104	T4.2L20D2			8	0.5	
105	T4.2L20D3			9	0.5	
106	T4.2L20D4			10	0.5	
107	T4.2L20D5			11	0.5	
108	T4.2L20D6			12	0.5	
109	T6.3L5R1		1	-	0.5	
110	T6.3L5R2		2		0.5	
111	T6.3L5R3		3		0.5	
112	T6.3L5R4		4		0.5	
113	T6.3L5R5		5		0.5	
114	T6.3L5R6		6		0.5	
115	T6.3L5D1			7	0.5	
116	T6.3L5D2			8	0.5	
117	T6.3L5D3			9	0.5	
118	T6.3L5D4			10	0.5	
119	T6.3L5D5			11	0.5	

120	T6.3L5D6			12	0.5	
121	T6.3L10R1		1	-	0.5	
122	T6.3L10R2		2		0.5	
123	T6.3L10R3		3		0.5	
124	T6.3L10R4		4		0.5	
125	T6.3L10R5		5		0.5	
126	T6.3L10R6		6		0.5	
127	T6.3L10D1			7	0.5	
128	T6.3L10D2			8	0.5	
129	T6.3L10D3			9	0.5	
130	T6.3L10D4			10	0.5	
131	T6.3L10D5			11	0.5	
132	T6.3L10D6			12	0.5	
133	T6.3L15R1		1	-	0.5	
134	T6.3L15R2		2		0.5	
135	T6.3L15R3		3		0.5	
136	T6.3L15R4		4		0.5	
137	T6.3L15R5		5		0.5	
138	T6.3L15R6		6		0.5	
139	T6.3L15D1			7	0.5	
140	T6.3L15D2			8	0.5	
141	T6.3L15D3			9	0.5	
142	T6.3L15D4			10	0.5	
143	T6.3L15D5			11	0.5	
144	T6.3L15D6			12	0.5	
145	T6.3L20R1		1	-	0.5	
146	T6.3L20R2		2		0.5	
147	T6.3L20R3		3		0.5	
148	T6.3L20R4		4		0.5	
149	T6.3L20R5		5		0.5	
150	T6.3L20R6		6		0.5	
151	T6.3L20D1			7	0.5	
152	T6.3L20D2			8	0.5	
153	T6.3L20D3			9	0.5	
154	T6.3L20D4			10	0.5	
155	T6.3L20D5			11	0.5	
156	T6.3L20D6			12	0.5	

TABLE 4.3(b) TEST PROGRAMME FOR (TRANSIENT STATE WITH MULTIPLE TIDAL CYCLE (UNDER STATIC CONDITIONS)

Serial No.	Model Nomenclature	Rate of rise and fall	No of cycle	REMARK
1	E	0.583 m/hour	120 (Considering 60 days duration)	Multiple tidal cycle
2	T2.1L5			
3	T2.1L10			
4	T2.1L15			
5	T2.1L20			
6	T4.2L5			
7	T4.2L10			
8	T4.2L15			
9	T4.2L20			
10	T6.3L5			
11	T6.3L10			
12	T6.3L15			
13	T6.3L20			

4.4 EXPERIMENTAL SET UP:

The current study has been done considering *N*=100g in centrifuge experimental modeling.

The main objective of the experimental study in centrifuge was to investigate the effects of dynamics of phreatic surface, flownet, fluid flow vector, pore water pressure with variation of sheet pile position and length.

4.4.1 DETAILS OF CENTRIFUGE

This geotechnical centrifuge at the Geotechnical Engineering Laboratory, Civil Engineering Department, Jadavpur University is made by ELTEK ^{R} is a 4 pole 500 Hz induction motor with 3 phase system and of 1.5m radius with maximum payload capacity 8.5 tons at 400g. In centrifuge modelling a rotating soil body mounted on a geotechnical centrifuge to represent a scale model of a given prototype which is to be modelled are trying to model. The diameter of the centrifuge is 0.55m. The turner beam carries scaled model at one end and a counter weight at the other, each mounted on a swing platform. As the centrifuge starts to spin about the central vertical axis, the swing platforms rotate about a pivot until they become horizontal. Table 4.4 presents the centrifuge machine details including those of the basket used in the current study. Figure 4.3(a) and Figure 4.3(b) represent geotechnical centrifuge

top view with details. Figure 4.4 presents top view of the Geotechnical Centrifuge with component details.

Table 4.4 Centrifuge Machine Details

Manufacturer – ELTEK
Diameter from the axis of rotation to basket base : 1.1 m
Maximum rpm- 700
Acceleration range at 1.5m radius : 10g to 200g
Payload at 100g : 2125 Kg
Soil model size : 26.4cm×26.4cm× 29.0cm×
Bucket base dimension(clear) : 32cm× 32cm
Run up time : 1.40 minutes to reach 100g

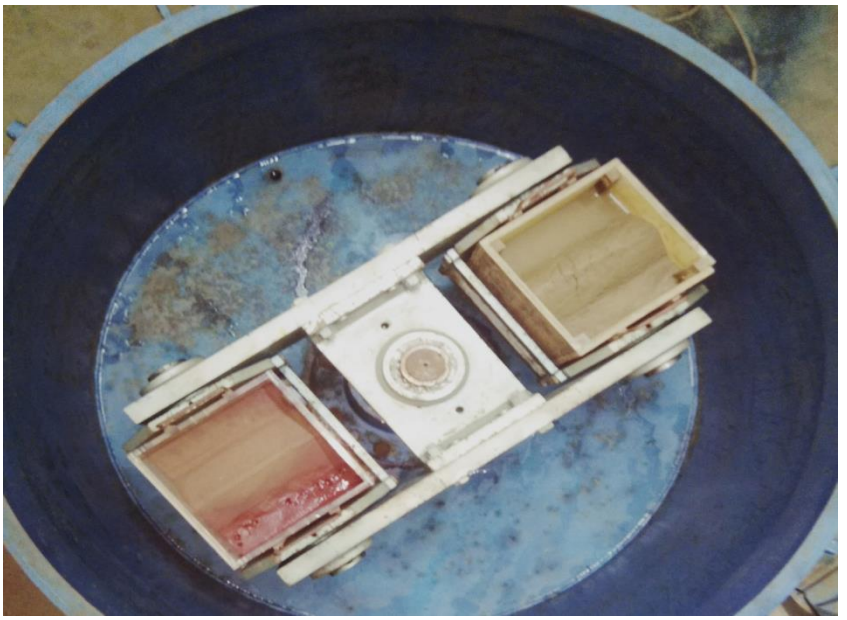

Figure 4.3(a): Top view of Centrifuge with model of dam

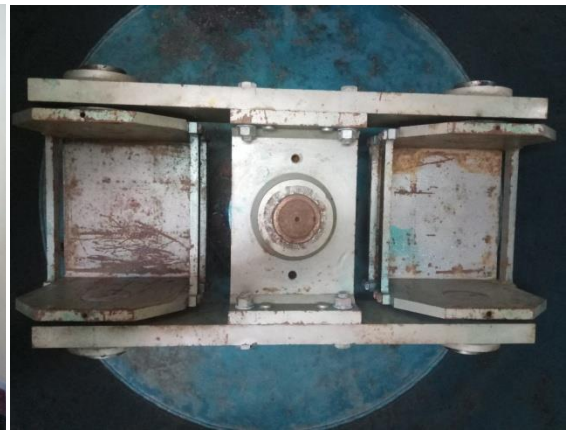

Fig 4.3(b) **Fig 4.3(c)**

Fig 4.3 Geotechnical Centrifuge (a) Top View with model (b) Front View (c) Top view

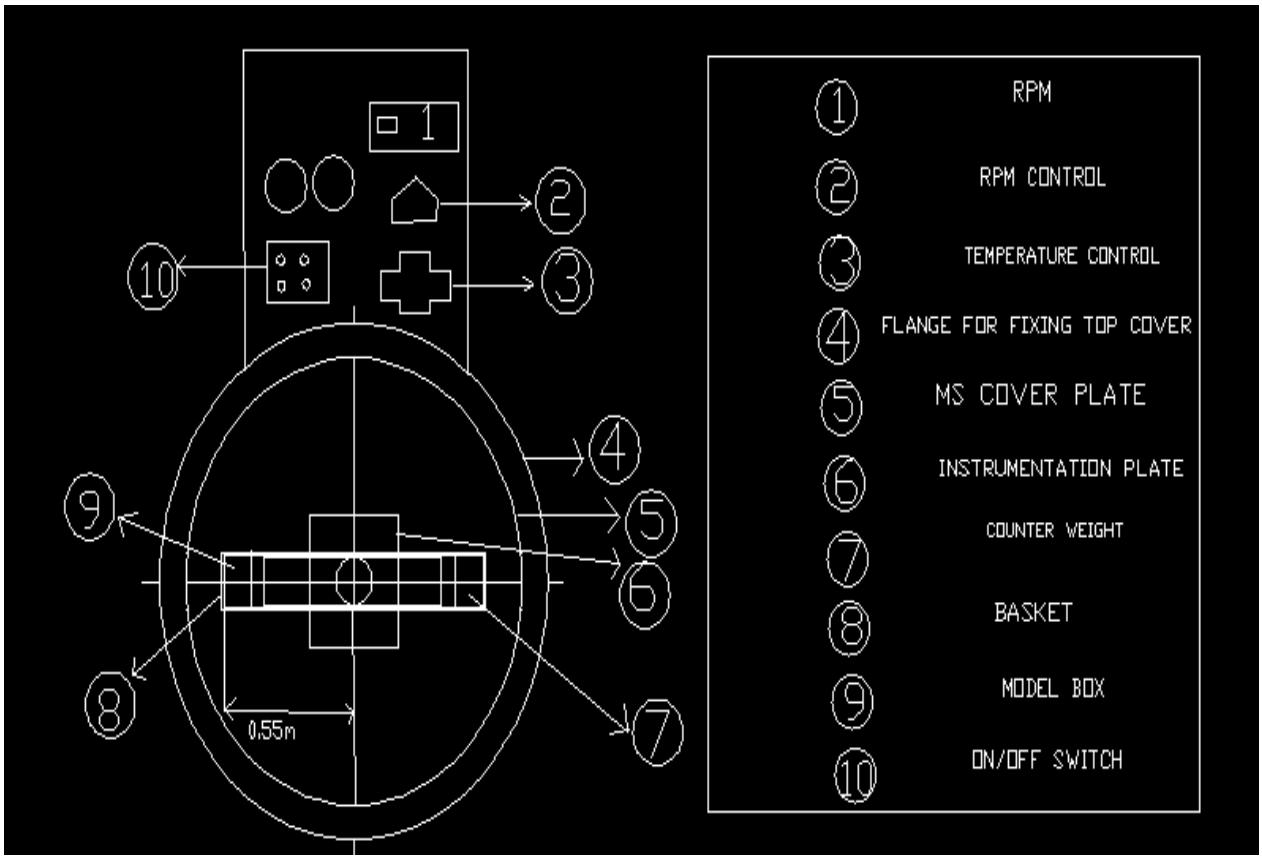

Figure-4.4:Top view of the Geotechnical Centrifuge with component details

In the geotechnical centrifuge considering 100g the calculated rpm calculation has been described as below,

N=100, g=9.81cm/s^2 , r=0.55m

$\omega^2 R = ng$ (4.10)

400 rpm =$\frac{400\times2\pi}{60}$ = 41.67 radian/sec

n= 100, radius(R) = 1.1/2 = 0.55 m

ω = $\sqrt{\frac{100\times9.81}{0.55}}$ = 42.23 rad/s=404rpm

4.4.2 FABRICATION OF SEEPAGE TEST BOX

The scaled model and the counter weight have been mounted at two ends of a swing platform. A seepage tank has been used to simulate three dimensional conditions was fabricated accordingly. A square tank has been fabricated with steel frame, supporting 10 mm thick transparent perspex sheet on all sides. Perspex sheet is transparent and strong enough to bear the loads that may come during testing in centrifuge. The fabric is cubical in shape of external dimensions 290 mm (internal sides 270mm) having top face open and fixed in thin mild steel ribs, and handles in order to support and handle it. The dimensions of the tank are 26.7cm (Length) by 26.7cm (Width) by 26.7cm (Height). The tank has been made waterproof by M-Seal and further lay by GP-Silicone both on the interior and exterior faces. The front and top views of the model test box have been shown in Figure 4.5 (a) and Figure 4.5 (b) respectively. The piezometer positions in model test box has been shown in figure 4.6 (a) and Figure 4.6 (b). The test box contains a circular hole of 30mm diameter on one face, who acts as drainage for downstream side. This whole assembly of the test box is fit according to its space in centrifuge. Figure 4.7 represents the detailed dimension of test box.

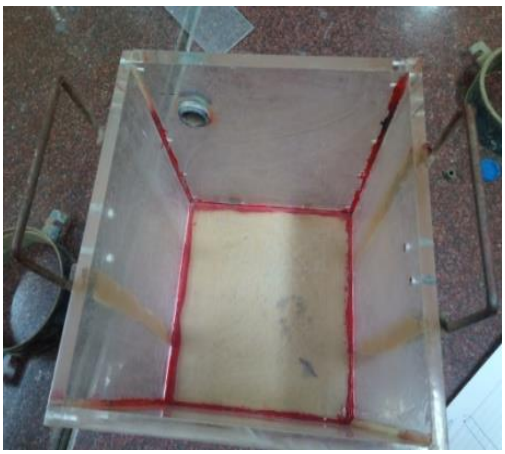

Fig 4.5 (a)

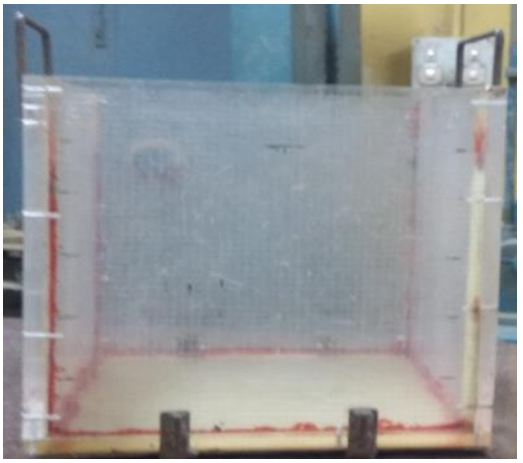

Fig 4.5 (b)

Fig 4.5 Model Test Box (a) Top View (b) Front view

Fig 4.6 (a)

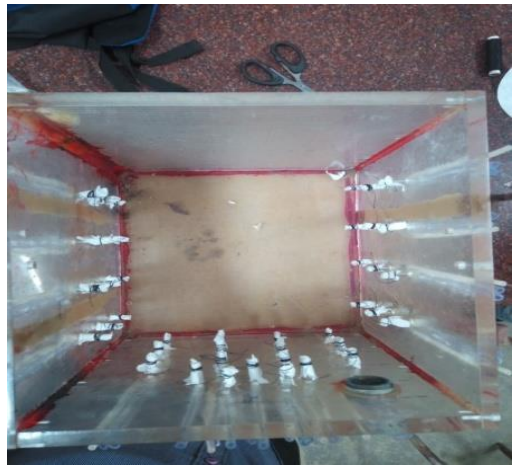

Fig 4.6 (b)

Fig 4.6 Model Test Box piezometer position (a) Front View (b) Top view

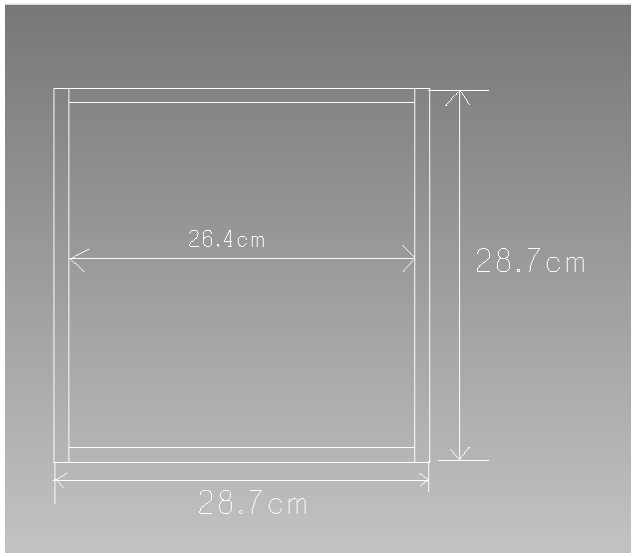

Figure-4.7: Details dimension of the front view of the model box

4.4.3 WATER SUPPLY ARRANGEMENT

The water supply to the tank has been made from a reservoir of maximum capacity of 1.5litres. The reservoir has been placed above the top of tank and flow from reservoir to tank was by virtue of centrifugal acceleration. A total of two valves – one water inlet valve at upstream side of tank and one drainage valves at the upstream side and one at the downstream side of tank respectively were attached to regulate flow to and from the tank.

4.4.3.1 Valve control through Arduino

In this study Arduino ATMEGA 2560 board has been used to control inlet and outlet valve shown in Figure 5.12. This Arduino board is based on the ATmega2560 (datasheet). It has 54 digital input/output pins including 14 PWM outputs pins, 16 analog input pins, 4 UARTs (hardware serial ports), a 16MHz crystal oscillator, an USB connection, a power jack, an ICSP header, and a reset button. Using USB cable and power have been supplied through adapteror battery. 220 Volt DC valve connected through Arduino ATMEGA 2560 to simulated transient seepage condition are shown in Figure 4.8.

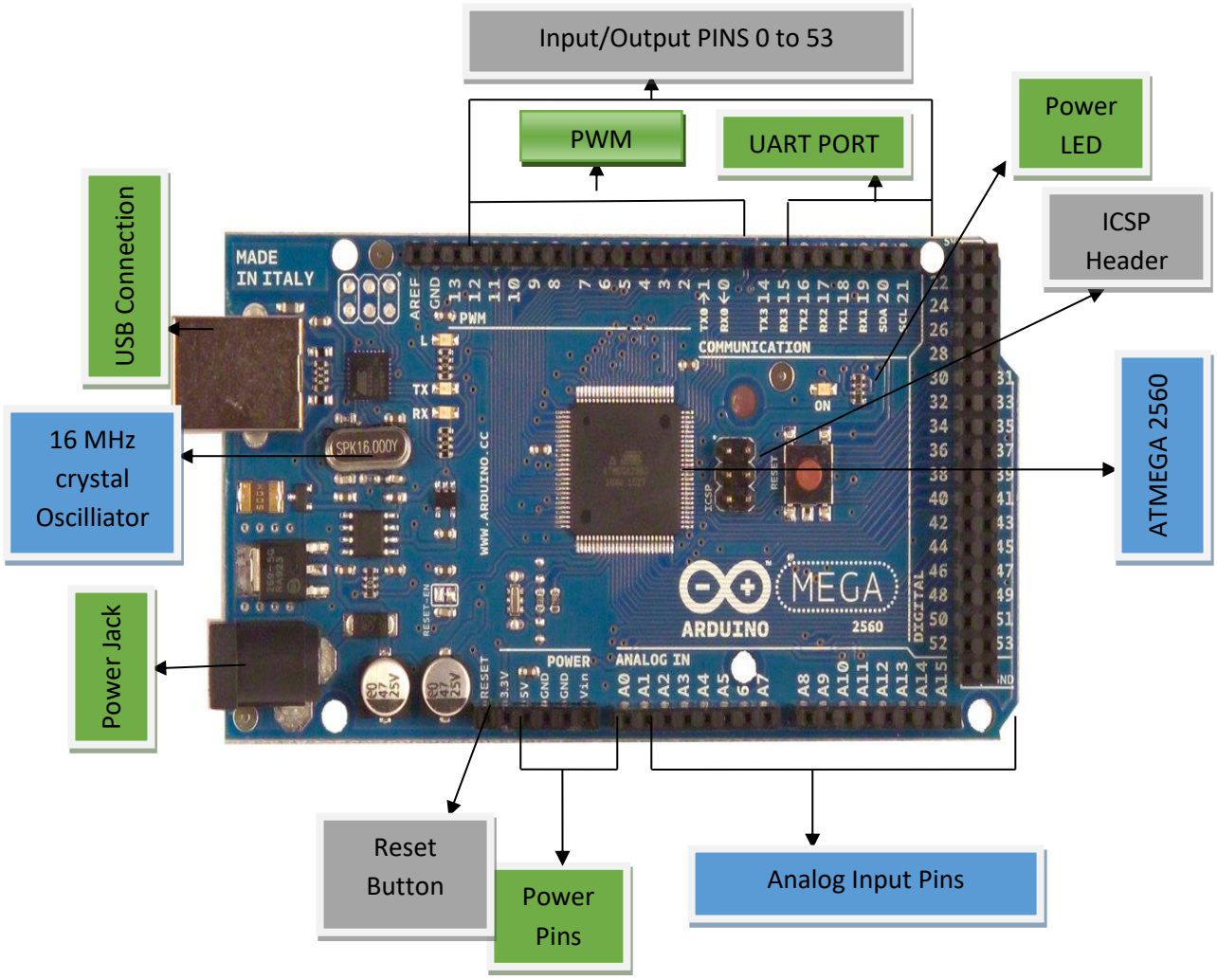

Fig. 4.8 Arduino Board

An artificial tide control circuit to provide an interface to complete the experimental work. A **solenoid valve** is an electromechanically operated valve. This circuit of about artificial tide control, based on Arduino, Infra-Red sensor (IR Sensor) and it has been implemented in the

geotechnical centrifugal machine to provide artificial tide as occur in use of a river in nature. The circuit has been processed by providing internal energy source. this circuit is controllable and have been controlled by infrared remote from a certain distance.

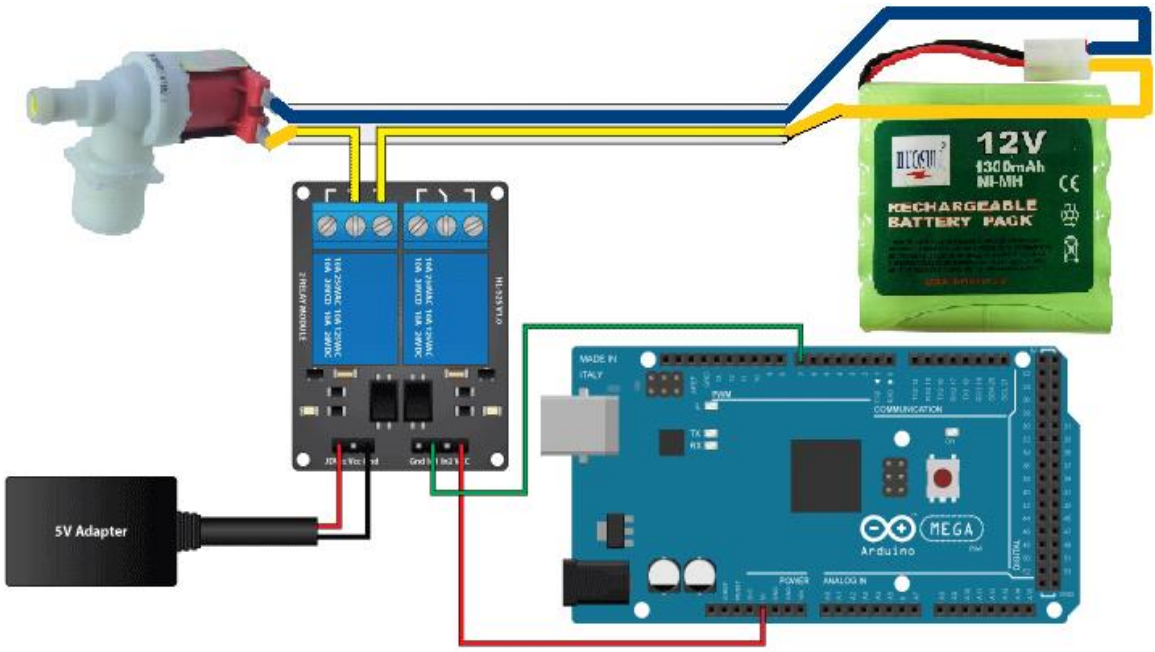

Fig. 4.9 Valve control through Arduino

4.5 SOIL PROPERTIES OF MODEL EMBANKMENT

Disturbed soil sample has been obtained from south 24 parganas embankment site, of the Irrigation and Waterways Department, Government of West-Bengal. This soil has been utilized for construction of the embankment and preliminary testing for soil properties.

The properties obtained by conducting routine tests with this soil are furnished in **Table-4.5**

TABLE-4.5: Soil Properties for Experimental Model

Property tested	Value for test results
Physical Description	Greyish Silty Clay / Clayey Silt
Liquid Limit (%)	40.7
Plastic Limit (%)	23.1
Percentage of Sand (%)	12
Percentage of Silt (%)	64
Percentage of Clay (%)	24
Maximum Dry Density (kN/m^3)	17.0
Optimum Moisture Content (%)	17
Saturated Hydraulic Conductivity (m/sec)	1.450×10^{-8}
Cohesion, C (kN/m^2) at OMC	25
Angle of Internal Friction, Φ (degree) at OMC	5

4.6 EXPERIMENTAL PROCEDURE

4.6.1 MODEL EMBANKMENT

The embankment model was formed as a typical earthen Embankment with desired dimensions and properties and a centrifuge scale of *N*= 100.

4.6.1.1 Formation of Foundation Bed

A 20 cm thick bed was constructed in five layers. Initially, the soil sample was oven dried. Then the lumps were pulverized and particles with 100 percent passing 4.75 mm sieve were taken. Water was added as per optimum moisture content. Hand mixing was done in small quantities not more than 4 kg of dry soil sample. Compaction was achieved by blows from a Standard Proctor Hammer of 4.5 kg falling over a height of 300 mm. The number of blows was adjusted as per density requirement. The targeted density was 95 percent of Standard Proctor density.

4.6.1.2 Construction of Embankment

The main embankment was constructed at level to the desired level of 17 cm from tank base. The side slopes were kept at 2(H):1(V). Sheet piles were used as a cutoff in the experimental model in centrifuge. The methods of compaction and consolidation were utilized as discussed above. The main embankment was made from the foundation level to the desired level of 24 cm from tank base. The side slopes was kept at 2(H) : 1(V). Different stages during formation of the embankment and the completed embankment have been shown in **Figures 4.10, 4.10, 4.11, 4.13 and 4.14** sequentially**.** Figure 4.15 presents site elevation of earthen model dam.

Fig. 4.10 Stage-1, Construction of Bed

Fig.4.11 Stage-2, installation of sheet pile

Fig. 4.12 Stage-3, Construction of Slope

Fig. 4.13 Top view of Earthen Dam

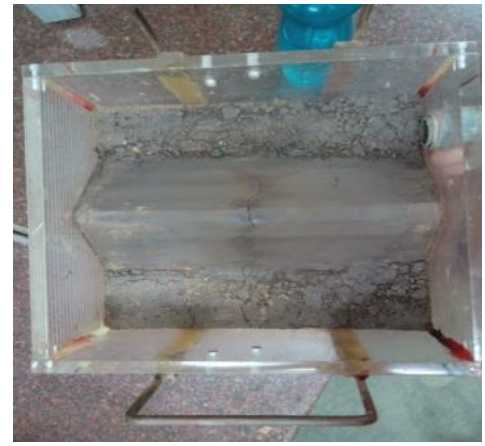

Fig 4.14 (a) **Fig 4.14 (b)**

Fig 4.14 Model Embankment (a) Front View (b) Top view

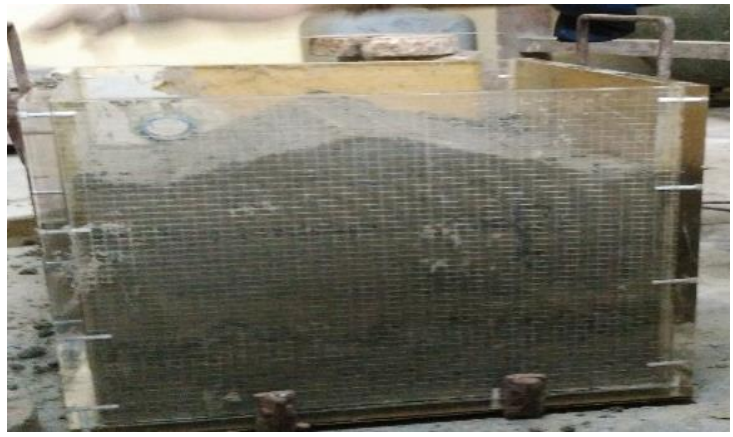

Fig. 4.15 Site elevation of Earthen Dam

4.6.2 SIMULATION OF SEEPAGE FOR TRANSIENT STATE

A steady state has been established between top (EL + 24.0 cm) and the low tide level (EL + 20.0 cm). The tidal effect was simulated on the basis of hydrostatic head which varied with cycle time. The tidal cycle consisting of Rise up and Drawdown half cycles were generated by raising and falling the water level from the Low Tide Level (LTL) (EL + 20.0 cm) to the High Tide Level (HTL) (EL + 24.0 cm) and back to the Low Tide Level(EL + 20.0 cm), respectively. This was done with the help of inlet and drainage valves. The time duration of Rise up and Drawdown half cycle was varied with subsequent tests. The tidal head was maintained on a linear pattern. Rise up Half Cycle time (t_{RU}) is defined as the time duration to complete each Rise up half cycle, i.e. time taken by the riverside water to rise from LTL to HTL. Drawdown Half Cycle time (t_{DD}) has been defined as the time duration to complete each Drawdown half cycle, i.e. time taken by the riverside water to fall from HTL to LTL. The Full cycle time (t_F) is the summation of the Rise up and Drawdown half cycle time. Methylene blue Dye and Red Dye was used during the later stage tests to obtain the flow lines and the Zone of Influence of Rise up.

4.6.3 INSTRUMENTATION

The instrumentation of tidal control and digital image capturing have been illustrated in this section.

4.6.3.1 Artificial tidal control circuit

A **solenoid valve** is an electromechanically operated valve have been shown in Figure.4.16. An artificial tide control circuit to provide an interface to complete the experimental work has been shown in Figure 4.17.

Figure. 4.16 Solenoid Valve

The main component of the circuit is Arduino which helps to receive acknowledgement signal using an IR sensor connected with the pin no 2. Arduino receives signal through pin 2 and then the signal in terms of Hex code decode in the Arduino and as per the signal the output pin have been sent data to the relay. key of IR remote generates Infrared signal in terms of hex code then this Hex code has been received by Arduino board through the port via PIN 2. Then the Arduino board decode the hex code and generates output signal in digital code. The digital code has been converted in to analog signal to activate the Relay. Relay when gets energized by Arduino acknowledge signal which helps to start the solenoid valve, then solenoid valve allows the water to flow.

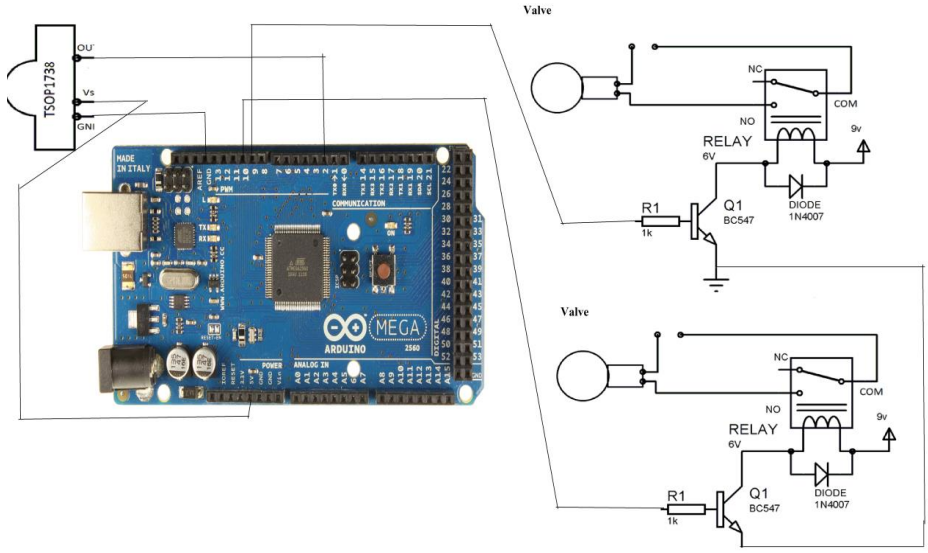

Figure 4.17 Artificial tide control circuit

There solenoid valve, which has been operated by relay by pressing the on/off button to remote the Arduino receive signal shown in Figure.4.18(a) and Figure 4.18(b). Water has been started to flow by generating new signal to activate relay and after a certain period the first valve has been closed and after generation of next signal second valve has been opened to help to operate next cycle of the Tide.

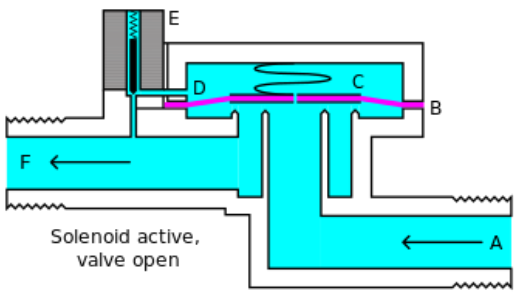

Figure. 4.18 (a)

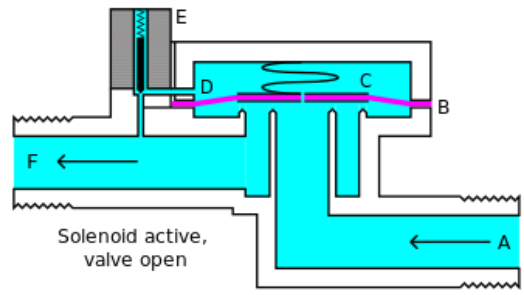

Figure. 4.18(b)

Figure 4.18: Circuit diagram of Solenoid valve (a) opening (b) closing

4.6.3.2 Digital image capturing through Raspberry Pi camera

With the help of digital cameras, it has been possible to capture the digital image of the centrifuge model by mounting camera on the model and viewing the cross-section through transparent side. To fulfill the objective Raspberry pi 3B model has been used with a preinstalled Wi-Fi hardware module shown in Figure.4.19(a). A remote SSH client PuTTY has been used to access raspberry pi command prompt to establish the wireless connection. After logging in to Raspberry Pi using PuTTY "sudo raspi-config" has been used for auto configuration.

The camera has been connected to the BCM2835/BCM2836 processor on the Raspberry Pi microcontroller via the CSI bus, a higher bandwidth link which carries pixel data from the camera back to the processor. The camera has been shown in figure 4.19(b). It supports 2592 x 1944-pixel static images, and also supports 1080p30, 720p60 and 640x480p60/90 video. The Camera Serial interface (CSI) interface has been capable of carrying extremely high rates pixel data. The camera supports the latest version of Raspbian, Raspberry Pi' operating system. Cameras store images at regular intervals onto a memory chip at the real time at the time of centrifuge test.

Figure. 4.19(a)

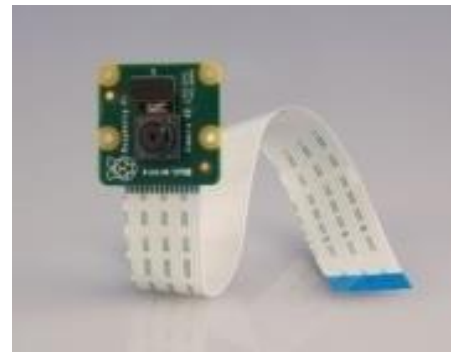

Figure. 4.19(b)

Figure 4.19: Digital image capturing (a) Raspberry Pi module (b) camera module

4.6.4 Acceleration of centrifuge model

The experimental set up of valve control to simulate tidal cycle and image capturing has been shown in Figure. 4.20(a) and 4.20(b). Considering Scale factor *N*= 100g the model has been accelerated at 400 rpm. The *N*g gravity field in the centrifuge varies linearly with the depth of the smaller centrifuge, requiring gravity field of *N*g at a particular depth within the model. The increase in g-acceleration to *N*g 's causes an increase in the soil unit weight by *N* and thereby an increase in pressure. Images have been captured at regular intervals up to one

image of every few seconds. Lighting on the centrifuge packages has improved with the use of LED lights. Polarizing plates have been used to remove unwanted reflections from the Perspex sides of the centrifuge models appearing in the digital images.

Figure. 4.20(a)

Figure. 4.20(b)

Figure 4.20: Experimental model (a) Simulation of tidal cycle (b) Image capturing with camera module

4.7 OUTCOME OF EXPERIMENTS

Based on the images obtained from the experiments and pore pressures obtained from piezometer readings streamlines, flow vectors and pore pressures have been obtained from each experimental model and these have been illustrated in the following sections.

4.7.1 Digital Image processing

The results of the test have been obtained by processing the captured image through MATLAB programming PIV. High-resolution images that can be obtained from centrifuge model test has been processed to give the displacement vectors, fluid flow vector by Particle Image velocimetry (PIV) technique. Digital image can be viewed as a two-dimensional matrix of brightness at different pixel locations. The two-dimensional matrix of brightness is obtained in the image space. The main idea of the velocimetry analysis relies on comparing successive images from a centrifuge test. Each image is divided into a set number of patches. The movement of each patch between the images is tracked. This is done by comparing the intensity of two images by calculating a cross-correlation function in the PIV analysis. The movement of each patch from image 1 to image 2 captured within two consecutive seconds have been obtained. Comparing these two images the flow vector has been finally obtained. The flow chart for image capturing and image processing has been shown in Figure 4.21(a).

Figure. 4.21(b) presents the result of output image of embankment model of Image Capturing and Processing.

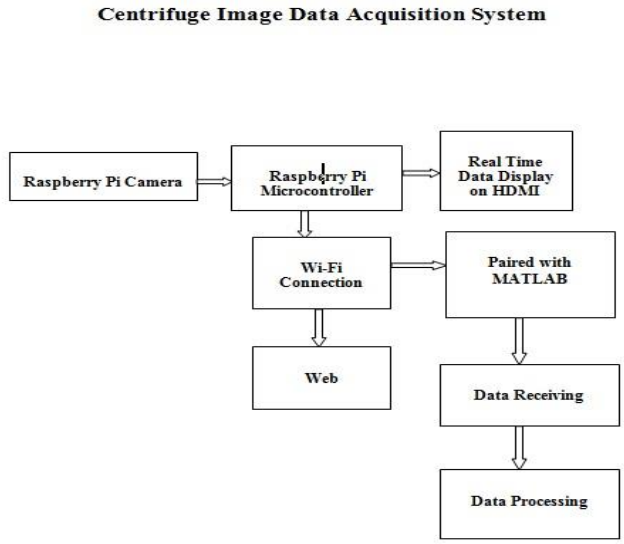

Fig. 4.21(a): Flow Chart for Image Capturing and Processing

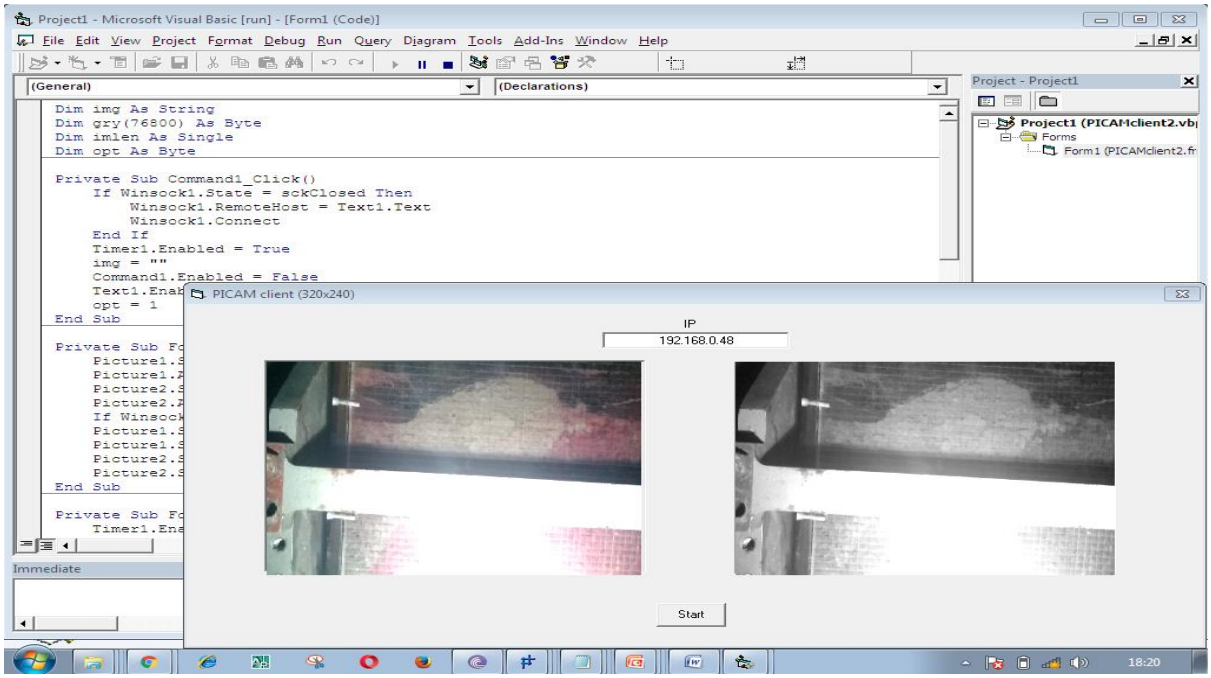

Fig. 4.21(b): Output image of embankment model of Image Capturing and Processing.

Particle Image Velocimetry (PIV) is a non-intrusive velocity field mapping technique that makes use of captured optical images to produce instantaneous vector measurement. The PIV is the statistical evaluation of PIV images in order to determine the streamline. Before the digitalization of this flow tracking technique, flows were interrogated manually. Interrogations were performed on images with relatively sparse seeding which allowed the

tracking of individual particles. Furthermore, PIV allows for the visualization of magnitudes and gives values the x-y components of velocity for the flow different points, at different times in matrix form.

4.7.2 PIEZOMETERS READINGS

Pore pressures have been obtained at different locations in case of each model from piezometers readings. These have helped to study the variation of pore pressure in the body of the dam and foundation along different horizontal planes. A cross section of the earthen dam indicating the locations of all the piezometers has been illustrated in the following Figure 4.22(a) and Figure.4.22(b).

Fig 4.22(a)

Fig 4.22(b)

Fig 4.22 Model Test Box piezometer position during test (a) Front View (b) Top view

4.8 PRESENTATION OF EXPERIMENTAL RESULTS

The digital image of the centrifuge model interfacing through Raspberry Pi camera module has been presented in this section as output images for different time intervals. From this output images the phreatic surface of the earthen dam and movement of the seepage flow for different time intervals have been clearly investigated.

4.8.1 DYNAMICS OF PHREATIC SURFACE

4.8.1.1 Dynamics of Phreatic surface under steady state condition

During steady state tests with working head of 3.5 m the flownet pattern has been shown in **Figures – 4.23.** The variation of the flownet in upstream side with respect to working head

condition has also been shown in the respective figures. Points A, B, C, D, E has been marked with progress of time to illustrate the propagation of flow.

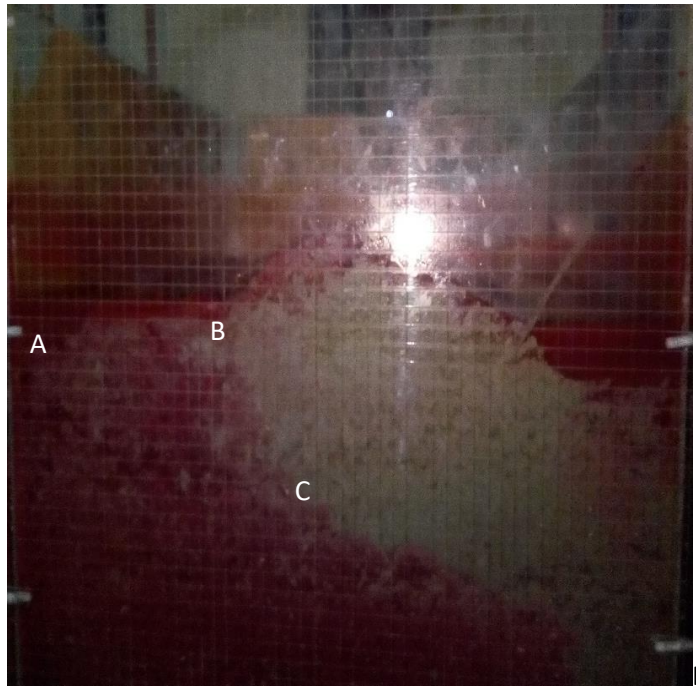

Figures – 4.23: Steady State seepage condition for working head of 3.5 m

4.8.1.2 Dynamics of phreatic surface Single Tidal Cycle: Effect of Rise up and Drawdown

During single cycle tests with a rate of rise up / drawdown, the variation in dynamics in phreatic surface has been shown in **Figures –4.24(a), 4.24(b), 4.24(c), 4.24(d),4.24(e)**. The variation of the phreatic surface in upstream side with respect to time=1hr., 3hrs.,4hrs.,5hrs.,6hrs. respectively has also been shown in the respective figures. The LTL has been kept at zero position and only the increase and decrease in water level from LTL to HTL and HTL to LTL has been made. Points A, B, C, D, E has been marked with progress of time to illustrate the propagation of flow.

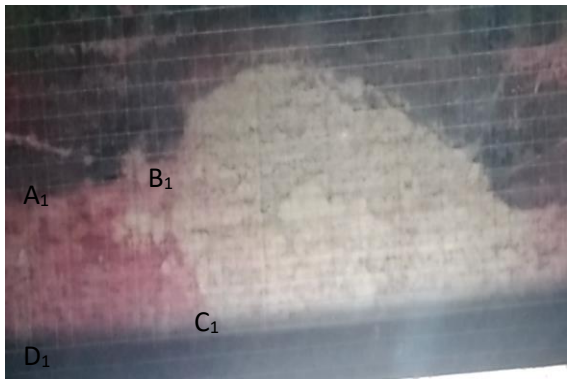

Fig 4.24(a): Development of phreatic surface for 2 hrs.

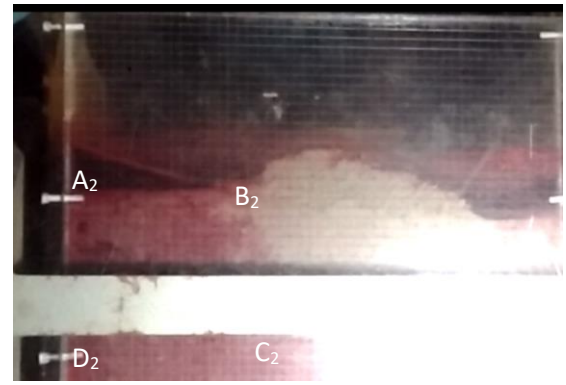

Fig 4.24(b): Development of phreatic surface for 3 hrs.

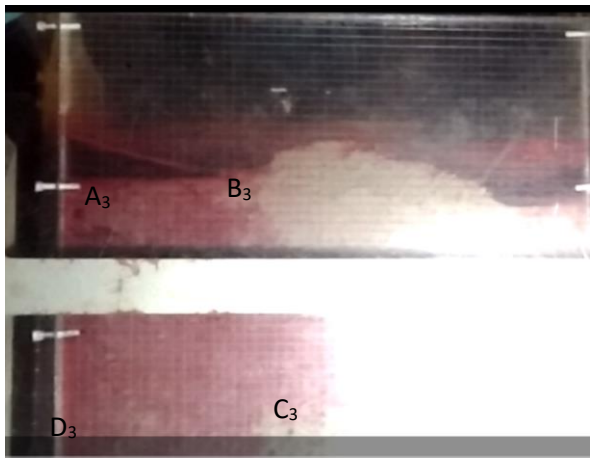

Fig 4.24(c): Development of phreatic surface for 4 hrs.

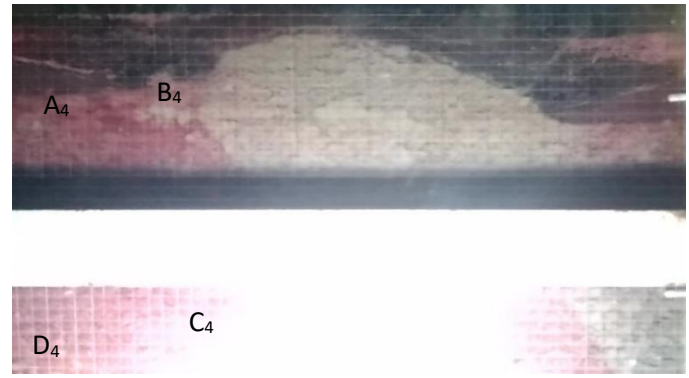

Fig 4.24(d): Development of phreatic surface for 5 hrs.

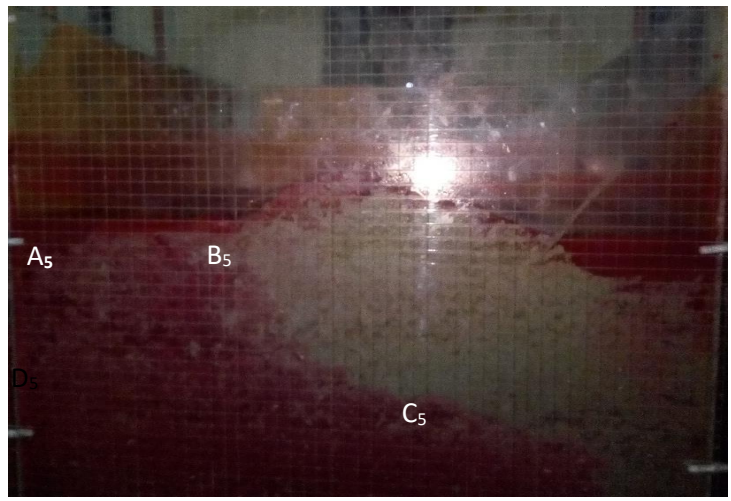

Figure 4.24(e): Development of phreatic surface for 6 hrs.

4.8.1.3 Dynamics of phreatic surface Single Tidal Cycle: Effect of Rise up and Drawdown rate (*B*/8 position 5m length)

During single cycle tests with a rate of rise up / drawdown, the variation in dynamics in phreatic surface has been shown in **Figures –4.25(a), 4.25(b), 4.25(c), 4.25(d), 4.25(e), 4.25(f), 4.25(g)**. The variation of the phreatic surface in upstream side with respect to time=1hr., 2hrs., 3hrs., 4hrs., 5hrs., 6hrs. and 10hrs. respectively has also been shown in the respective figures. The LTL has been kept at zero position and only the increase and decrease in water level from LTL to HTL and HTL to LTL has been made. Points A, B, C, D, E has been marked with progress of time to illustrate the propagation of flow.

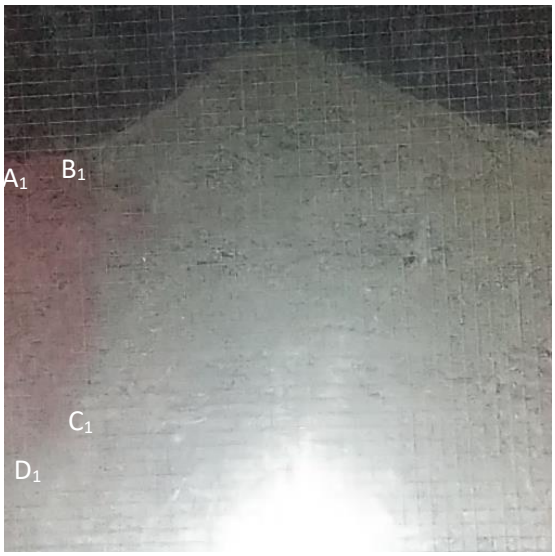

Fig 4.25(a): Development of phreatic surface for 1 hour

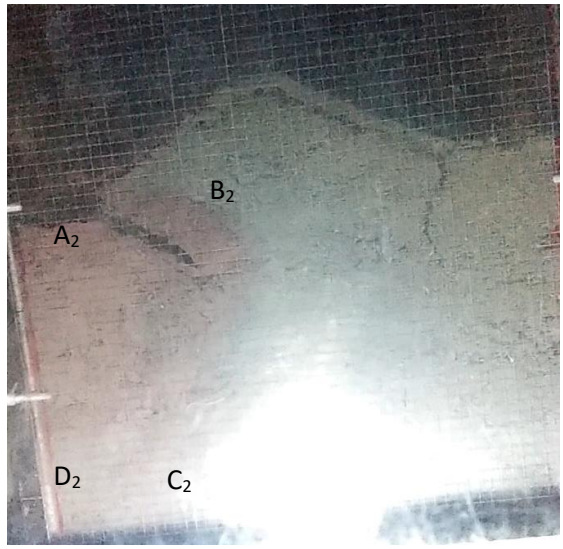

Fig 4.25(b): Development of phreatic surface for 2 hrs.

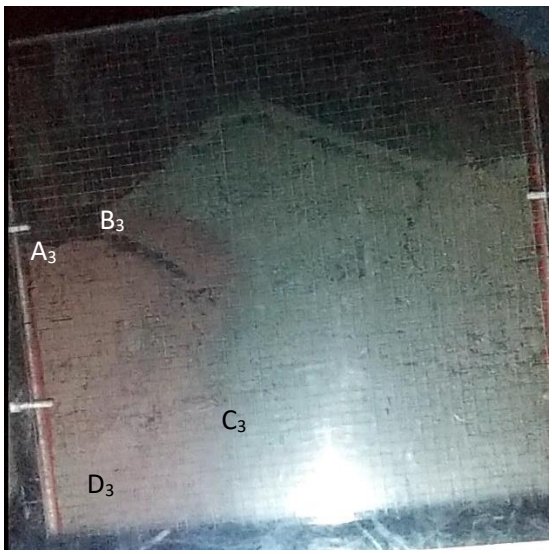

Fig 4.25(c): Development of phreatic surface for 3 hrs.

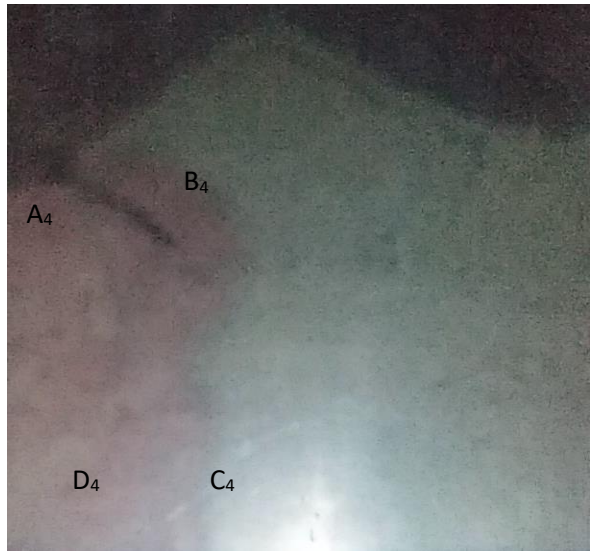

Fig 4.25(d): Development of phreatic surface for 4 hrs.

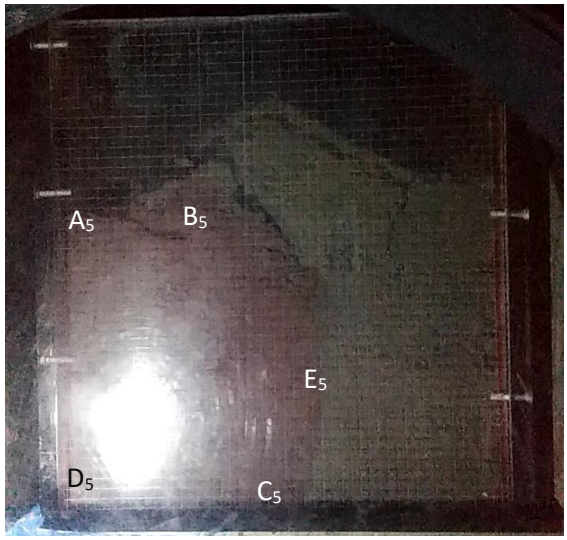

Fig 4.25(e): Development of phreatic surface for 5 hrs.

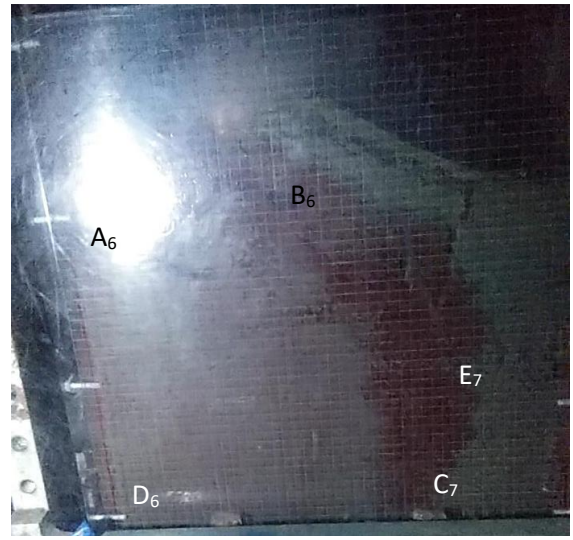

Fig 4.25(f): Development of phreatic surface for 6 hrs.

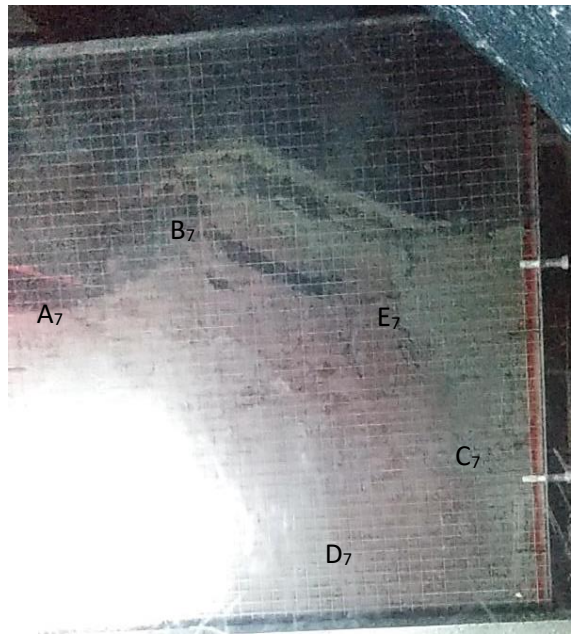

Figure 4.25(g): Development of phreatic surface for 10 hrs.

4.8.1.3 Dynamics of phreatic surface Single Tidal Cycle: Effect of Rise up and Drawdown rate (*B*/8 position 10m length)

During single cycle tests with a rate of rise up / drawdown, the variation in dynamics in phreatic surface has been shown in **Figures –4.26(a),4.26(b),4.26(c),4.26(d)**. The variation of the phreatic surface in upstream side with respect to time=1hr., 3hrs., 5hrs.,6hrs. and 7hrs.

respectively has also been shown in the respective figures. The LTL has been kept at zero position and only the increase and decrease in water level from LTL to HTL and HTL to LTL has been made. Points A, B, C, D, E has been marked with progress of time to illustrate the propagation of flow.

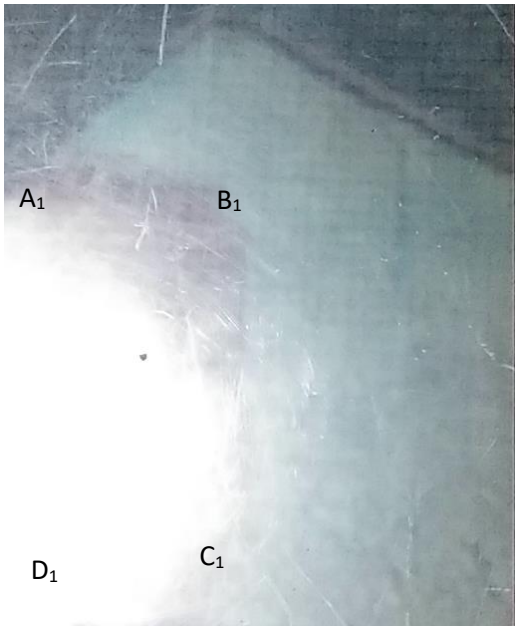

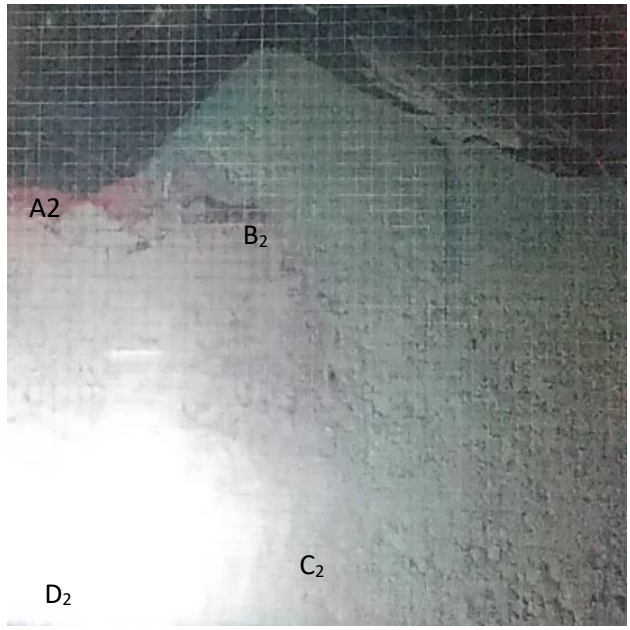

Fig 4.26(a): Development of phreatic surfac

Fig 4.26(b): Development of phreatic surface for 3 hour for 1 hour

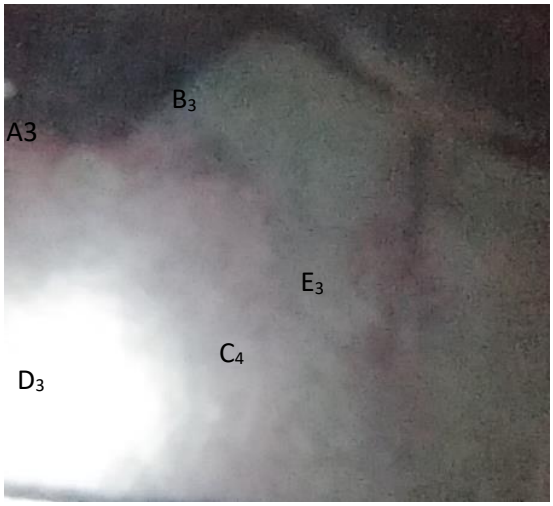

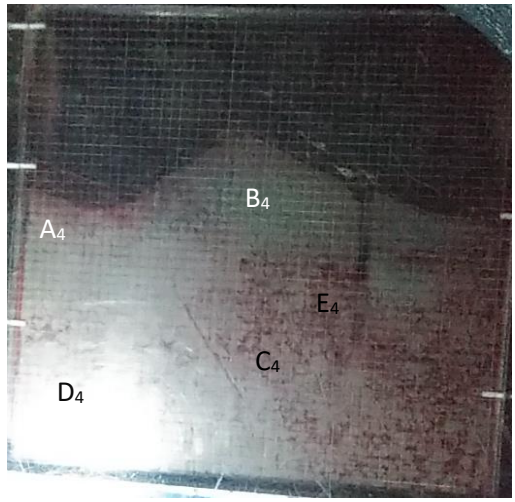

Fig 4.26(c): Development of phreatic surface for 5 hrs.

Fig 4.26(d): Development of phreatic surface for 6 hrs.

4.8.1.4 Dynamics of phreatic surface Single Tidal Cycle: Effect of Rise up and Drawdown rate (*B*/8 position 15m length)

During single cycle tests with a rate of rise up / drawdown, the variation in dynamics in phreatic surface has been shown in **Figures –4.27(a),4.27(b),4.27(c),4.27(d)**. The variation of the phreatic surface in upstream side with respect to time=1hr.,2hrs., 4hrs. and 7hrs. respectively has also been shown in the respective figures. The LTL has been kept at zero position and only the increase and decrease in water level from LTL to HTL and HTL to LTL has been made. Points A, B, C, D, E has been marked with progress of time to illustrate the propagation of flow.

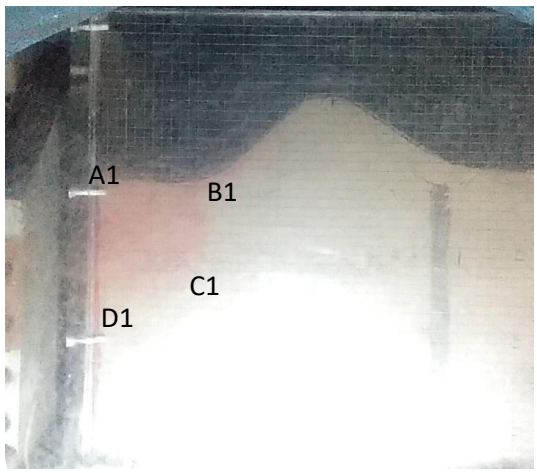

Fig 4.27(a): Development of phreatic surface for 1 hour

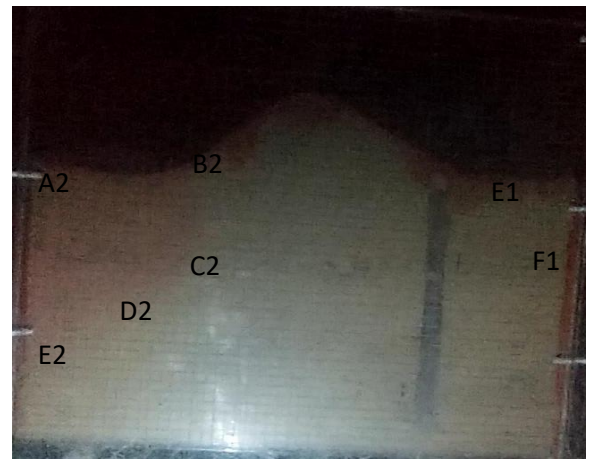

Fig 4.27(b): Development of phreatic surface for 2 hrs.

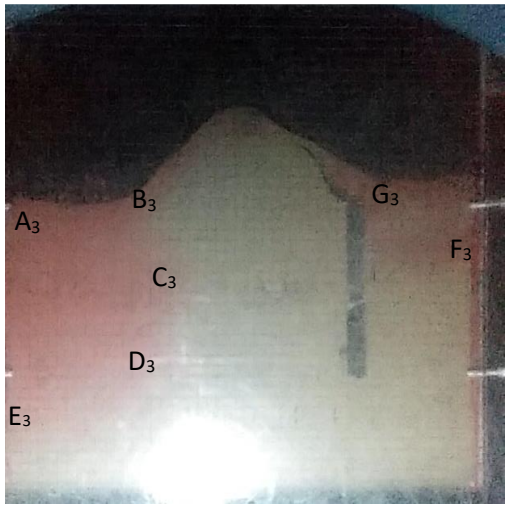

Fig 4.27(c): Development of phreatic surface for 4 hrs.

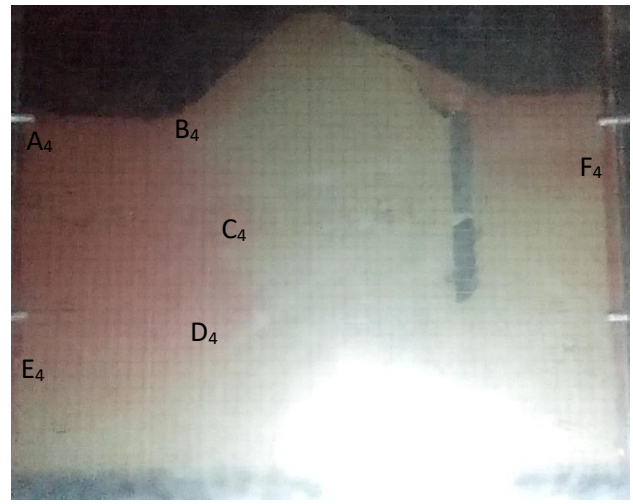

Fig 4.27(d): Development of phreatic surface for 7 hrs.

4.8.1.5 Dynamics of phreatic surface Single Tidal Cycle: Effect of Rise up and Drawdown rate (*B*/8 position 20m length)

During single cycle tests with a rate of rise up / drawdown, the variation in dynamics in phreatic surface has been shown in **Figures –4.28(a),4.28(b),4.28(c)**. The variation of the phreatic surface in upstream side with respect to time=2hrs., 5hrs. and 7hrs. respectively has also been shown in the respective figures. The LTL has been kept at zero position and only the increase and decrease in water level from LTL to HTL and HTL to LTL has been made. Points A, B, C, D, E has been marked with progress of time to illustrate the propagation of flow.

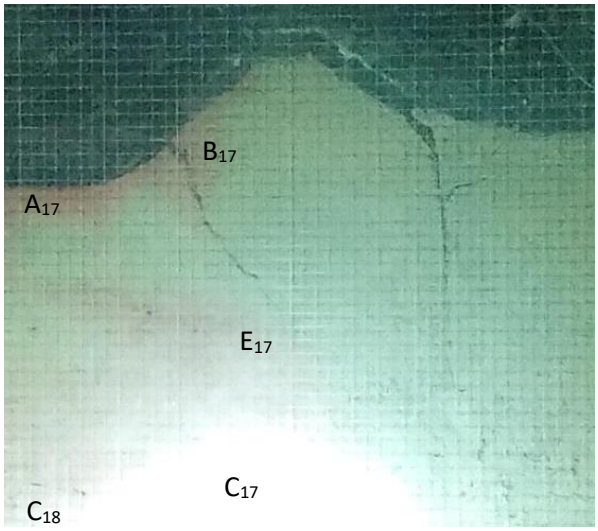

Fig 4.28(a): Development of phreatic surface for 2 hrs.

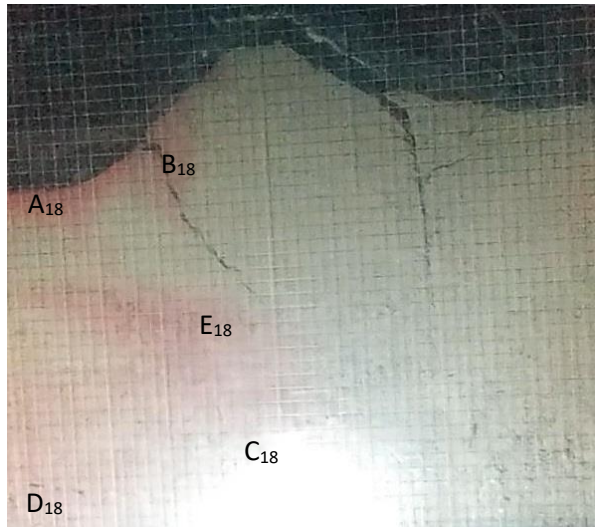

Fig 4.28(b): Development of phreatic surface for 5 hrs.

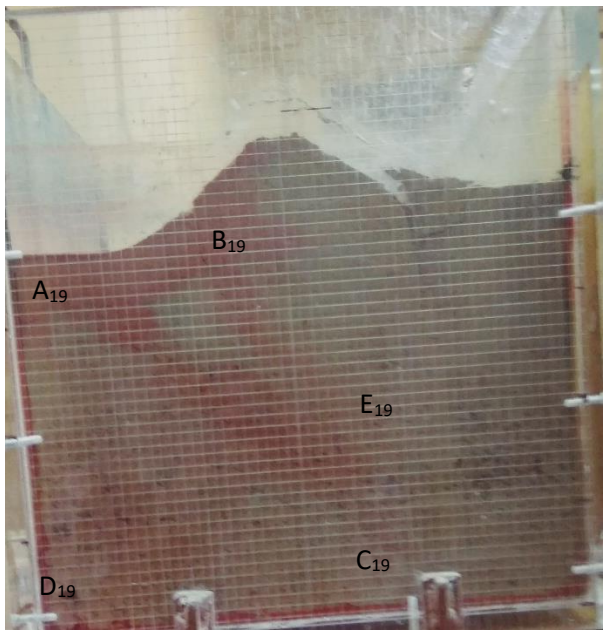

Fig 4.28(c): Development of phreatic surface for 7 hrs.

4.8.1.6 Dynamics of phreatic surface Single Tidal Cycle: Effect of Rise up and Drawdown rate (2*B*/8 position 5m length)

During single cycle tests with a rate of rise up / drawdown, the variation in dynamics in phreatic surface has been shown in **Figures –4.29(a),4.29(b),4.29(c),4.29(d)**. The variation of the phreatic surface in upstream side with respect to time=1hr., 3hrs., 5hrs. and 6hrs. respectively has also been shown in the respective figures. The LTL has been kept at zero position and only the increase and decrease in water level from LTL to HTL and HTL to LTL has been made. Points A, B, C, D, E has been marked with progress of time to illustrate the propagation of flow.

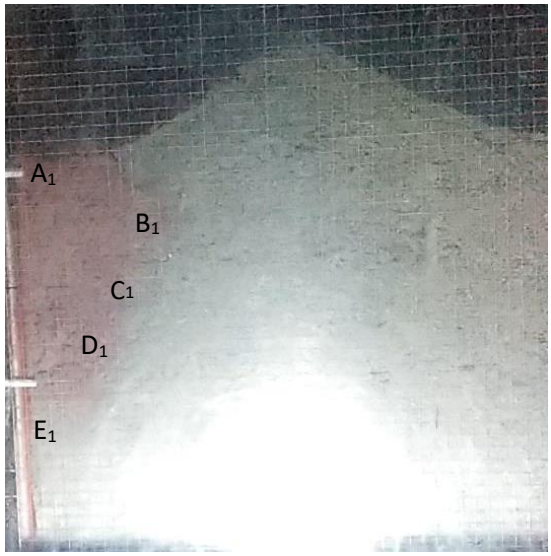

Fig: 4.29(a): Development of phreatic surface for 1 hour

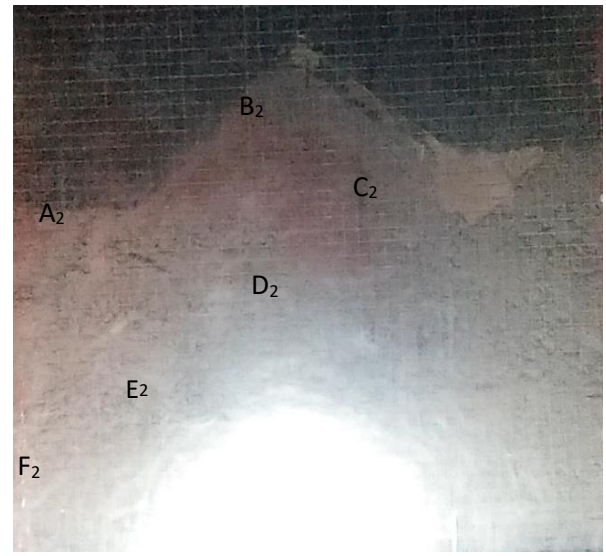

Fig 4.29(b): Development of phreatic surface for 3 hrs.

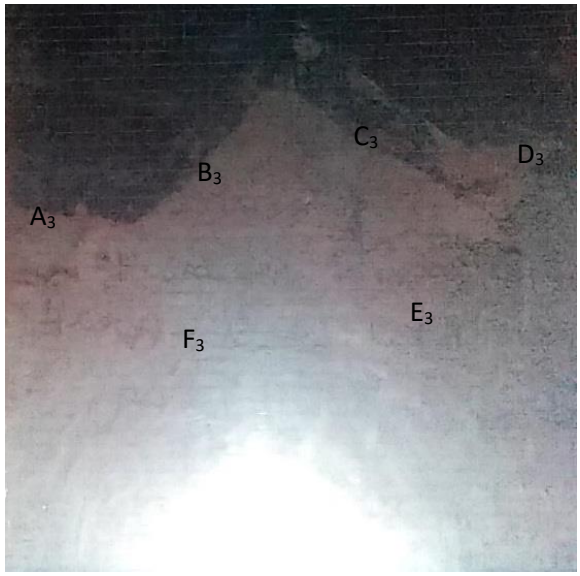

Fig 4.29(c): Development of phreatic surface for 5 hrs.

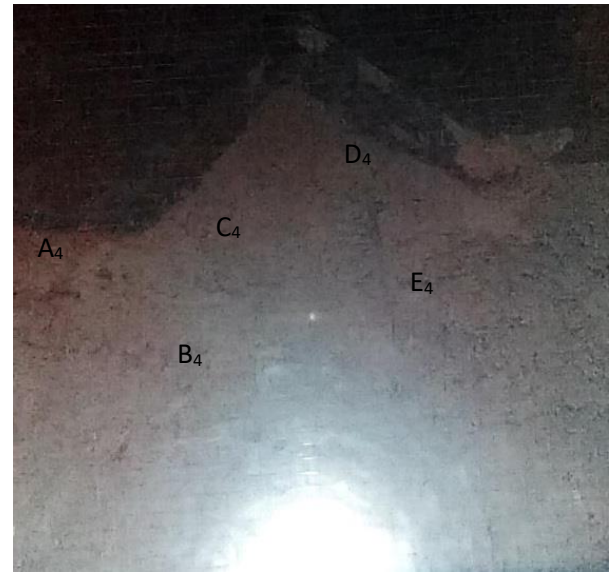

Fig 4.29(d): Development of phreatic surface for 6 hrs.

4.8.1.7 Dynamics of phreatic surface Single Tidal Cycle: Effect of Rise up and Drawdown rate (2*B*/8 position 10m length)

During single cycle tests with a rate of rise up / drawdown, the variation in dynamics in phreatic surface has been shown in **Figures –4.30(a),4.30(b),4.30(c),4.30(d)**. The variation of the phreatic surface in upstream side with respect to time=1hr., 3hrs., 4hrs.and 6hrs. respectively has also been shown in the respective figures. The LTL has been kept at zero position and only the increase and decrease in water level from LTL to HTL and HTL to LTL has been made. Points A, B, C, D, E has been marked with progress of time to illustrate the propagation of flow.

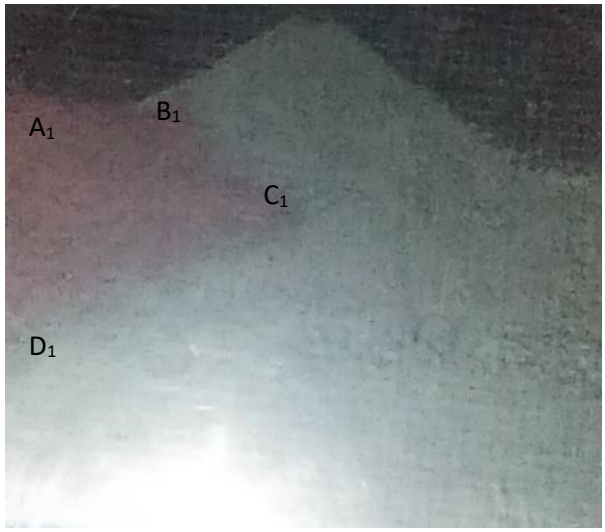

Fig 4.30(a): Development of phreatic surface for 1 hr.

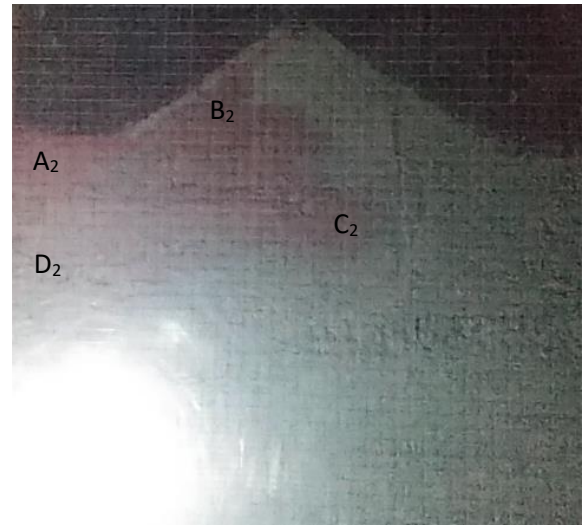

Fig 4.30(b): Development of phreatic surface for 3 hrs.

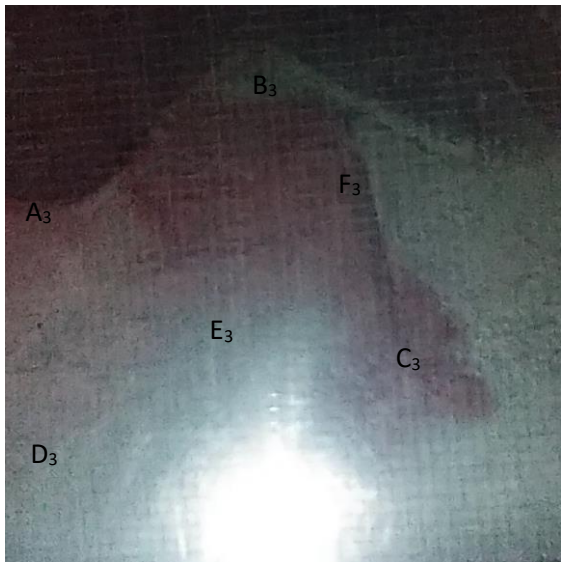

Fig 4.30(c): development of phreatic surface for 4 hrs.

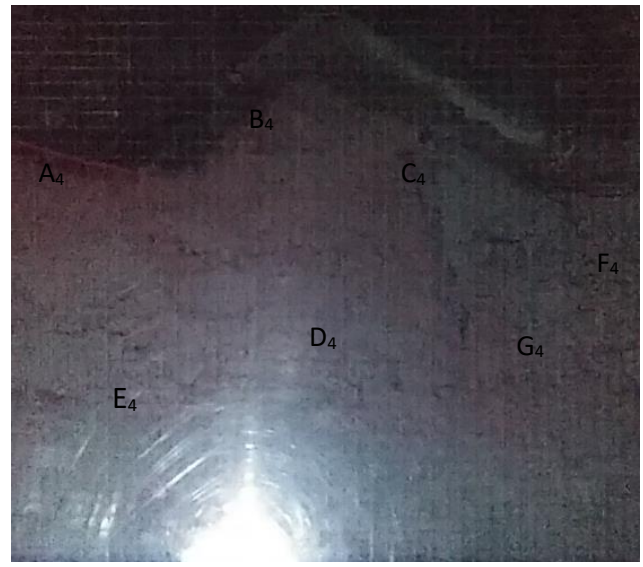

Fig 4.30(d): Development of phreatic surface for 6 hrs.

4.8.1.8 Dynamics of phreatic surface Single Tidal Cycle: Effect of Rise up and Drawdown rate (2*B*/8 position 15m length)

During single cycle tests with a rate of rise up / drawdown, the variation in dynamics in phreatic surface has been shown in **Figures –4.31(a),4.31(b),4.31(c)**. The variation of the phreatic surface in upstream side with respect to time=1hr., 3hrs. and 6hrs. respectively has also been shown in the respective figures. The LTL has been kept at zero position and only the increase and decrease in water level from LTL to HTL and HTL to LTL has been made. Points A, B, C, D, E has been marked with progress of time to illustrate the propagation of flow.

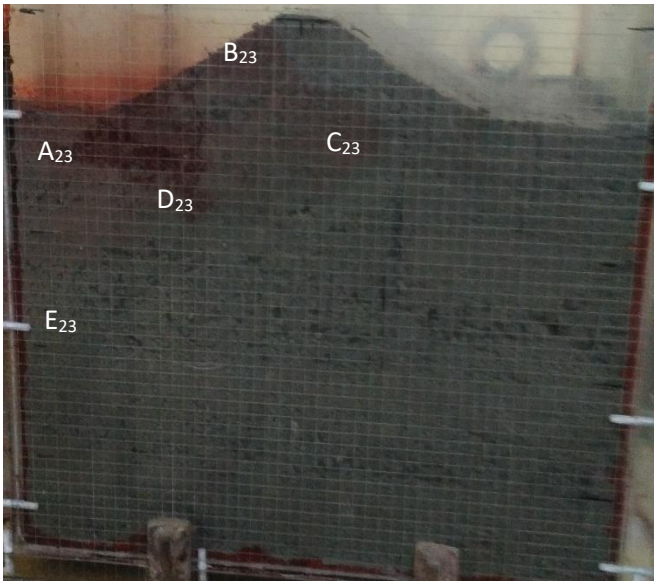

Fig 4.31(a): Development of phreatic surface for 1 hour

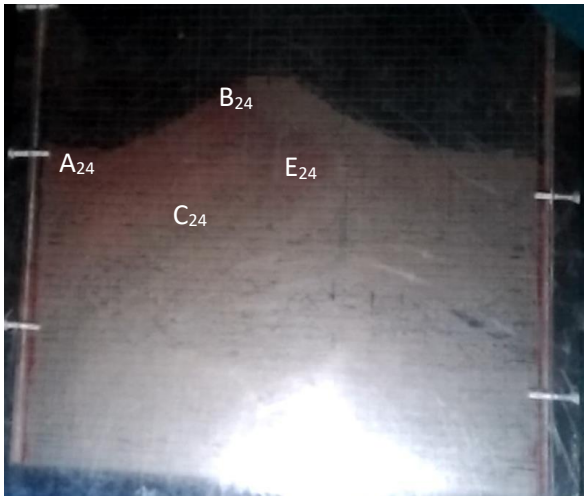

Fig 4.31(b): Development of phreatic surface for 3 hrs.

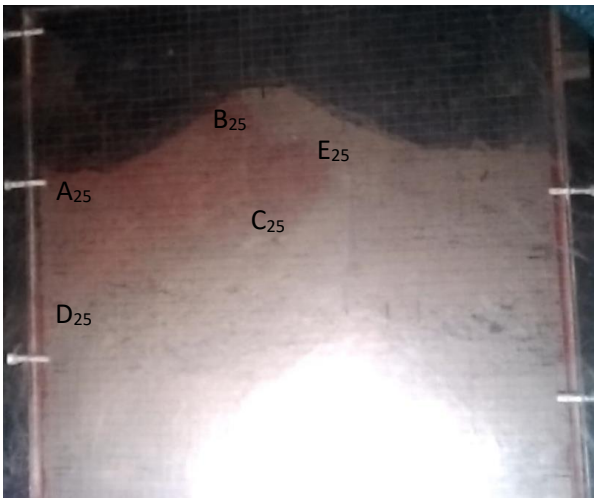

Fig 4.31(c): Development of phreatic surface for 6 hrs.

4.8.1.9 Dynamics of phreatic surface Single Tidal Cycle: Effect of Rise up and Drawdown rate (2*B*/8 position 20m length)

During single cycle tests with a rate of rise up / drawdown, the variation in dynamics in phreatic surface has been shown in **Figures –4.32(a),4.32(b),4.32(c),4.32(d)**. The variation of the phreatic surface in upstream side with respect to time=1hr., 3hrs.,5hrs. and 6hrs. respectively has also been shown in the respective figures. The LTL has been kept at zero position and only the increase and decrease in water level from LTL to HTL and HTL to LTL has been made. Points A, B, C, D, E has been marked with progress of time to illustrate the propagation of flow.

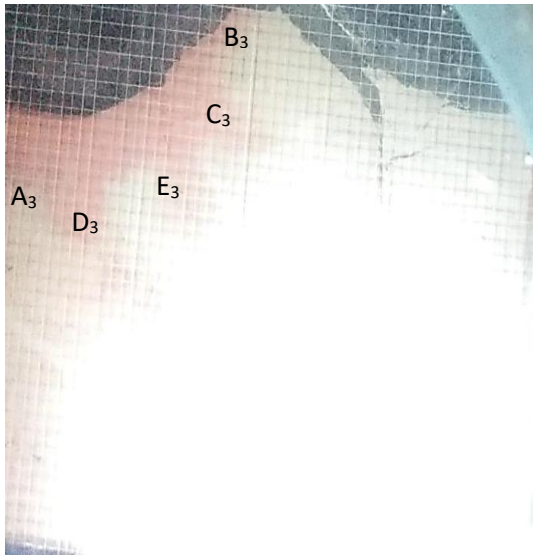

.

Fig 4.32(a): Development of phreatic surface for 1 hour

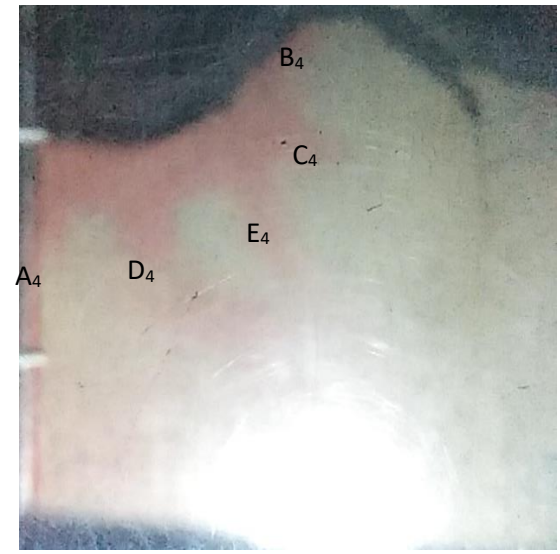

Fig 4.32(b): Development of phreatic surface for 3 hrs.

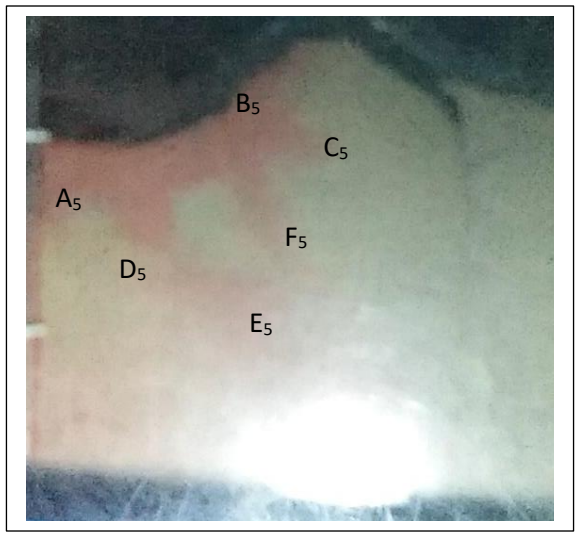

Fig 4.32(c): Development of phreatic surface for 5 hrs.

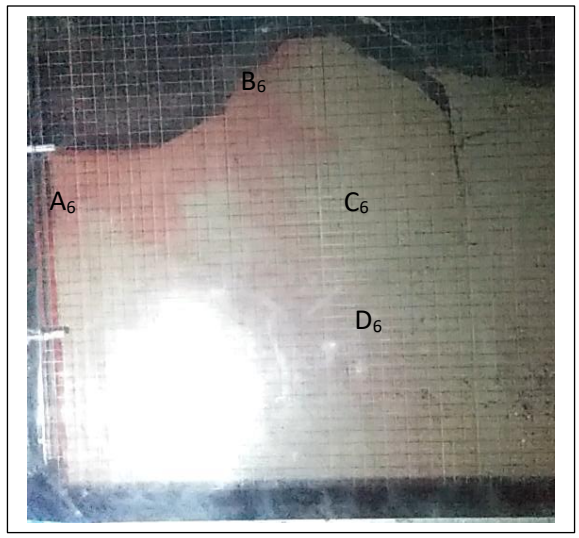

Fig 4.32(d): Development of phreatic surface for 6 hrs.

4.8.1.10 Dynamics of phreatic surface Single Tidal Cycle: Effect of Rise up and Draw-Down rate (3*B*/8 position 5m length)

During single cycle tests with a rate of rise up / drawdown, the variation in dynamics in phreatic surface has been shown in **Figures –4.33(a),4.33(b)**. The variation of the phreatic surface in upstream side with respect to time=3hrs. and 6hrs. respectively has also been shown in the respective figures. The LTL has been kept at zero position and only the increase and decrease in water level from LTL to HTL and HTL to LTL has been made. Points A, B, C, D, E has been marked with progress of time to illustrate the propagation of flow.

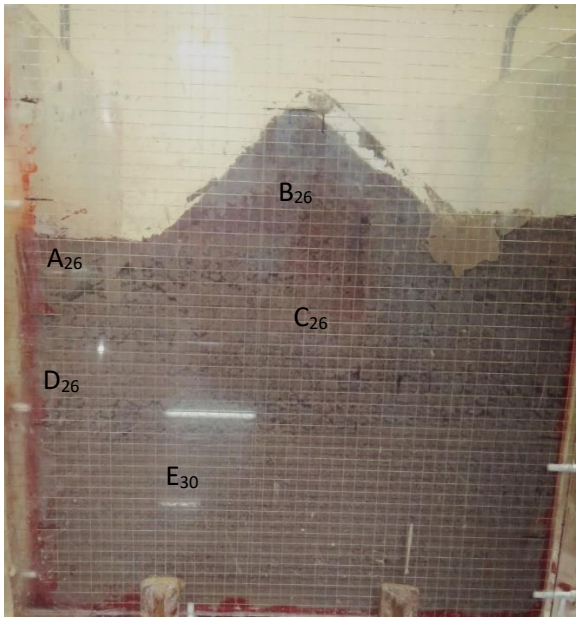

Fig 4.33(a): Development of phreatic surface for 3 hrs.

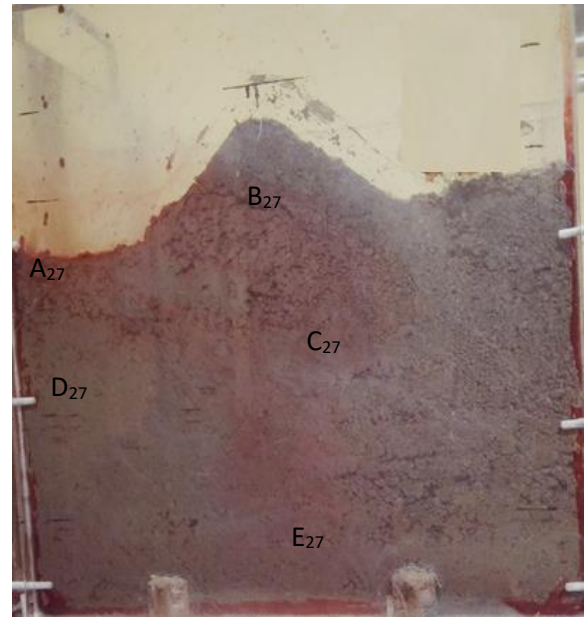

Fig 4.33(b): Development of phreatic surface for 6 hrs.

4.8.1.11 Dynamics of phreatic surface Single Tidal Cycle: Effect of Rise up and Drawdown rate (3*B*/8 position 10m length)

During single cycle tests with a rate of rise up / drawdown, the variation in dynamics in phreatic surface has been shown in **Figures –4.34(a),4.34(b),4.34(c),4.34(d),4.34(e)**. The variation of the phreatic surface in upstream side with respect to time=1hr., 3hrs.,4hrs.,5hrs. and 7hrs. respectively has also been shown in the respective figures. The LTL has been kept at zero position and only the increase and decrease in water level from LTL to HTL and HTL to LTL has been made. Points A, B, C, D, E has been marked with progress of time to illustrate the propagation of flow.

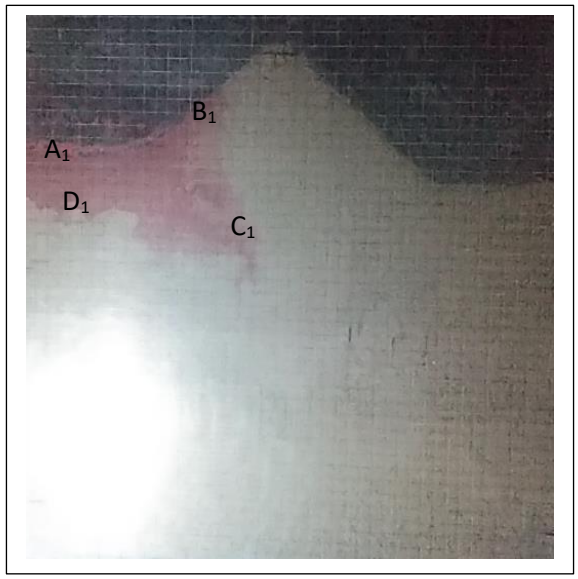

Fig 4.34(a): Development of phreatic surface for 1 hour

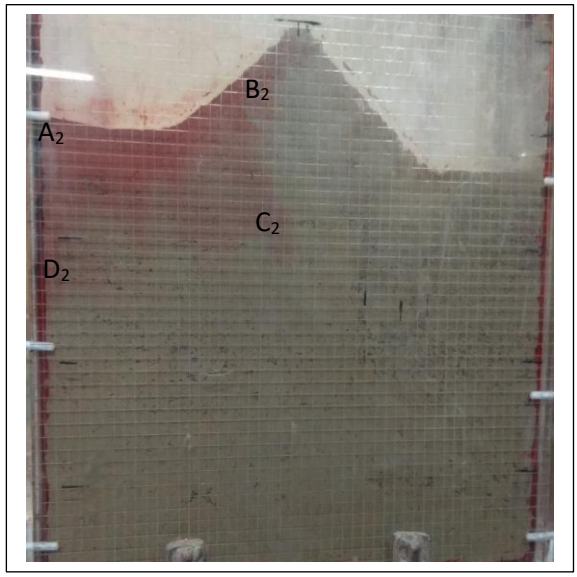

Fig 4.34(b): Development of phreatic surface for 3 hrs.

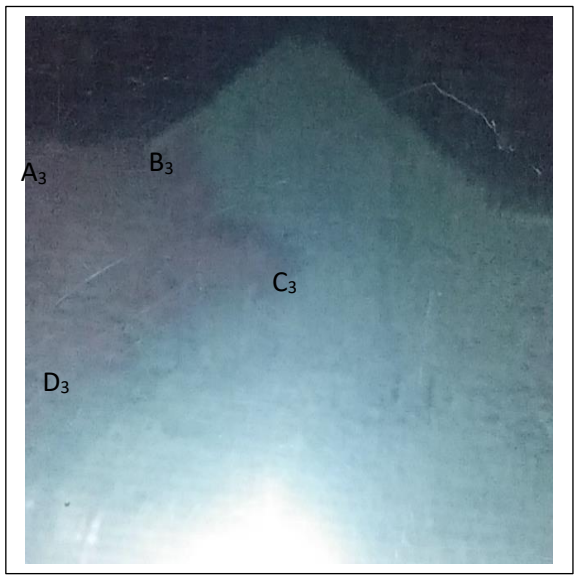

Fig 4.34(c): Development of phreatic surface for 4 hrs.

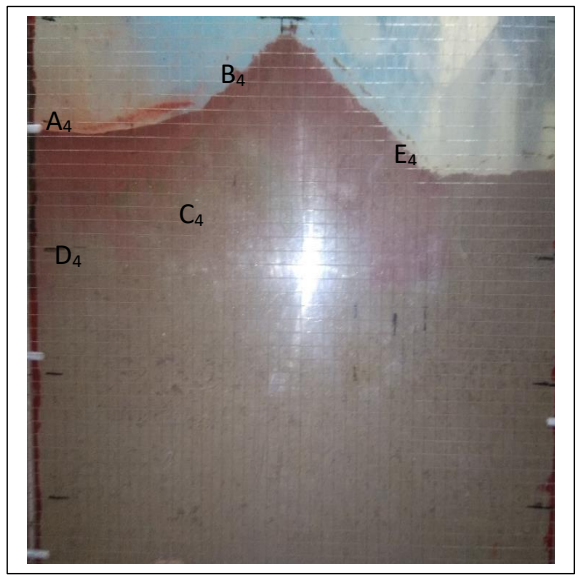

Fig 4.34(d): Development of phreatic surface for 5 hrs.

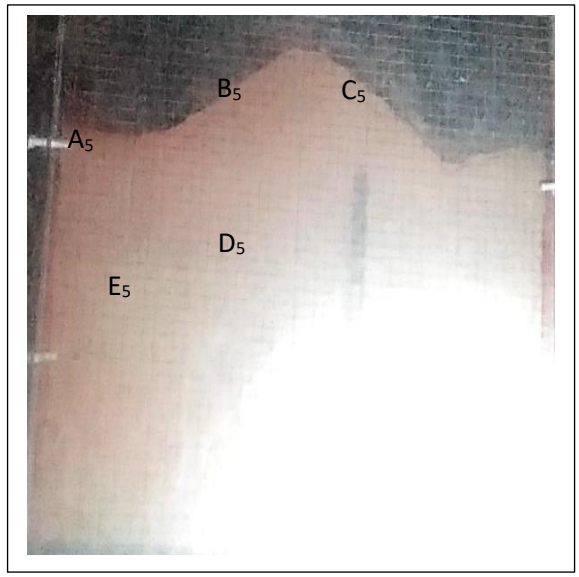

Fig 4.34(e): Development of phreatic surface for 7 hrs.

4.8.1.12 Dynamics of phreatic surface Single Tidal Cycle: Effect of Rise up and Drawdown rate (3*B*/8 position 15m length)

During single cycle tests with a rate of rise up / drawdown, the variation in dynamics in phreatic surface has been shown in **Figures –4.35(a),4.35(b),4.35(c),4.35(d)**. The variation of the phreatic surface in upstream side with respect to time=1hr., 3hrs., 5hrs. and 6hrs. respectively has also been shown in the respective figures. The LTL has been kept at zero position and only the increase and decrease in water level from LTL to HTL and HTL to LTL has been made. Points A, B, C, D, E has been marked with progress of time to illustrate the propagation of flow.

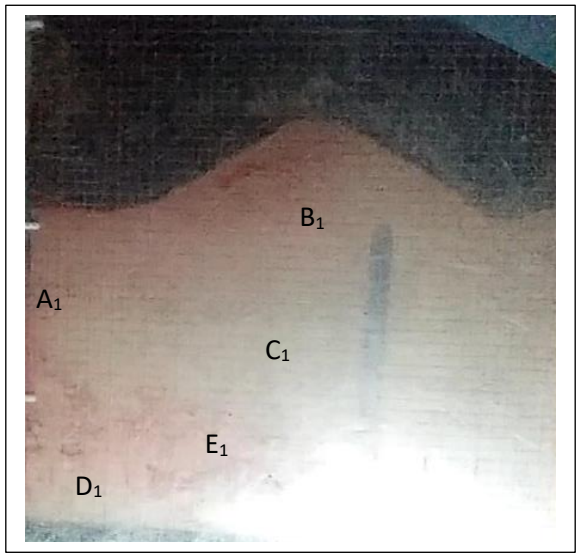

Fig 4.35(a): Development of phreatic surface for 1 hour

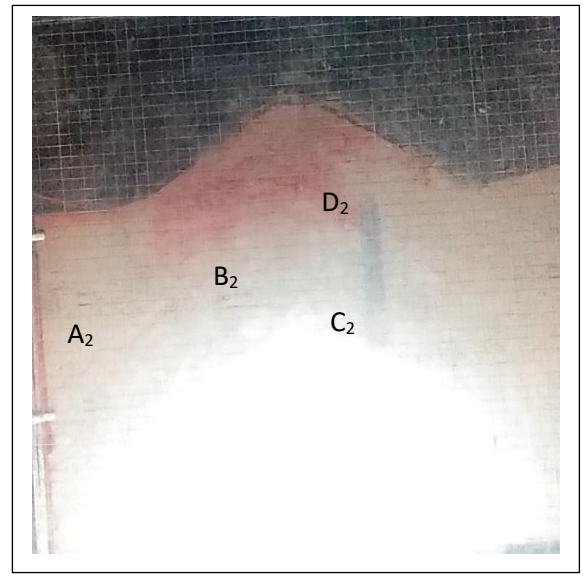

Fig 4.35(b): Development of phreatic surface for 3 hrs.

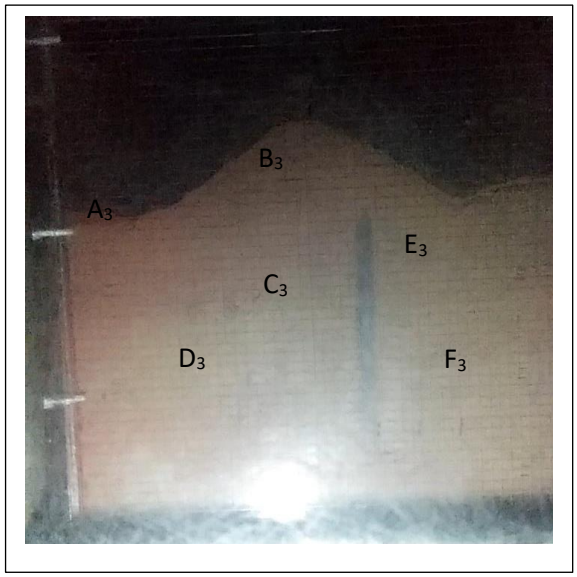

Fig 4.35(c): Development of phreatic surface for 5 hrs.

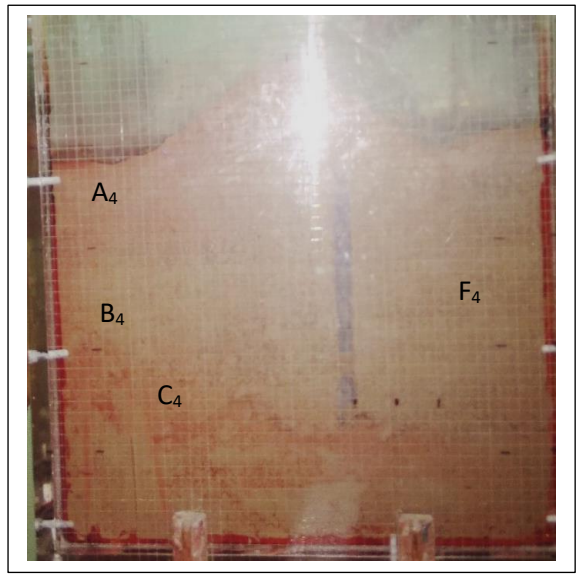

Fig 4.35(d): Development of phreatic surface for 6 hrs.

4.8.1.13 Dynamics of phreatic surface Single Tidal Cycle: Effect of Rise up and Drawdown rate (3*B*/8 position 20m length)

During single cycle tests with a rate of rise up / drawdown, the variation in dynamics in phreatic surface has been shown in **Figures –4.36(a),4.36(b),4.36(c)**. The variation of the phreatic surface in upstream side with respect to time=1hr., 2hrs., 3hrs., 4hrs., 5hrs., 6hrs., 7hrs., 8hrs., 9hrs., 10hrs., 11hrs. and 12hrs. respectively has also been shown in the respective figures. the increase and decrease in river water level from LTL to HTL and HTL to LTL has been made. Points A, B, C, D, E has been marked with progress of time to illustrate the propagation of flow.

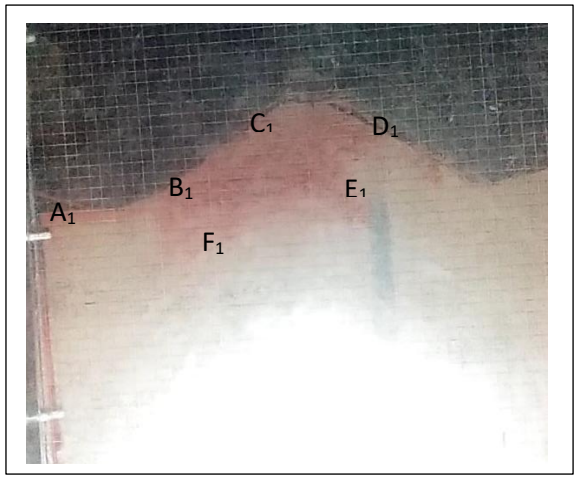

Fig 4.36(a): Development of phreatic surface for 1 hour

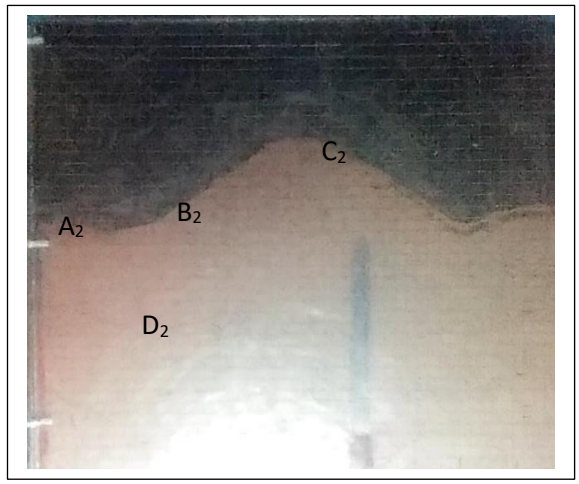

Fig 4.36(b): Development of phreatic surface for 3 hrs.

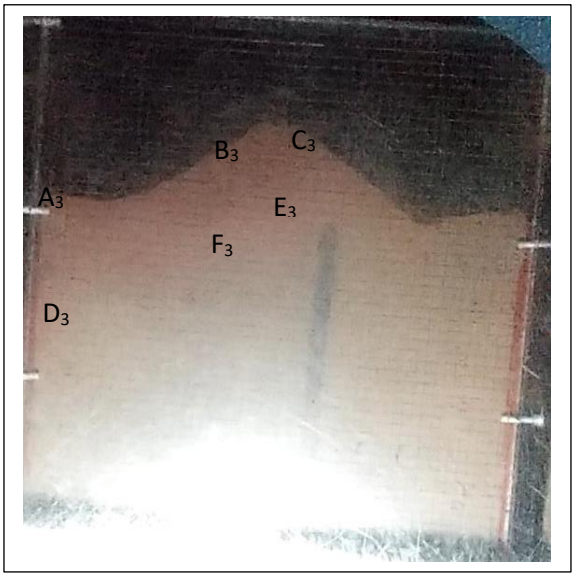

Fig 4.36(c): Development of phreatic surface for 6 hrs.

4.8.2 PRESENTATION OF FLUID FLOW VECTOR AND FLOWNET

The experimental results of centrifuge modeling after image processing through MATLAB PIV processing have been presented as follows. Fast Fourier Transform (FFT) cross correlation have been used to digitally examine the track the flow from two digital images. The PIV results give a clear representation of the stream flow and flow vector in the modelling of the dam. Based on the images obtained from the experiments streamlines, obtained flow vector from each experimental model have been illustrated in the following sections.

4.8.2.1 EMBANKMENT WITH-OUT CUT OFF STEADY STATE CONDITION

The flownet has been developed for different cases under steady seepage condition and also in different time intervals by image processing through PIV. The experimentally obtained phreatic surface, flownet and pattern of fluid flow vector in an embankment has been shown for in Figure 4.37(a).

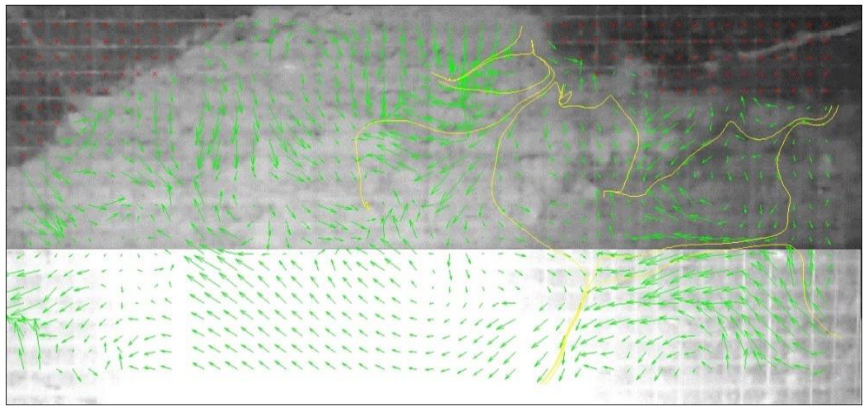

Figure 4.37(a): Phreatic Surface and flownet Development for steady state condition

4.8.2.2 EMBANKMENT WITH CUT OFF STEADY STATE CONDITION

The flownet has been developed for different cases under steady seepage condition and also in different time intervals by image processing through PIV. The experimentally obtained phreatic surface, flownet and pattern of fluid flow vector in an embankment has been shown for in Figure 4.38(a) to 4.38(l).

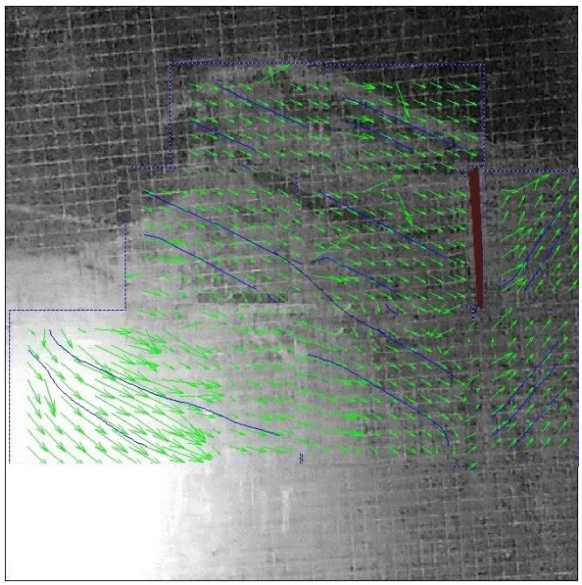

4.38(a): Flownet for *B*/8 position 5m long sheet pile

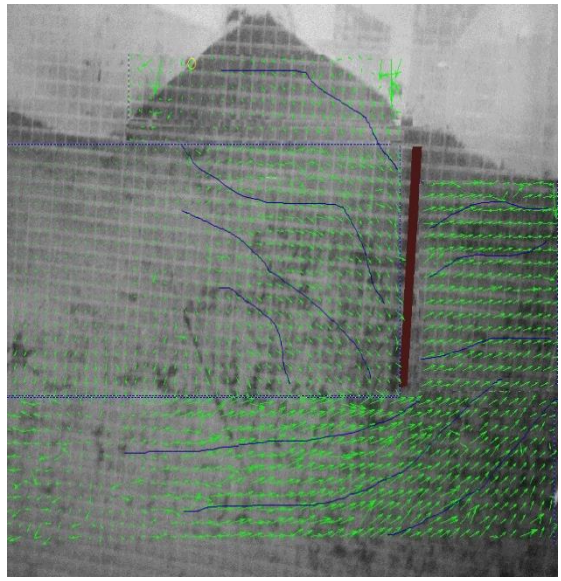

4.38(b): Flownet for *B*/8 position 10m long sheet pile

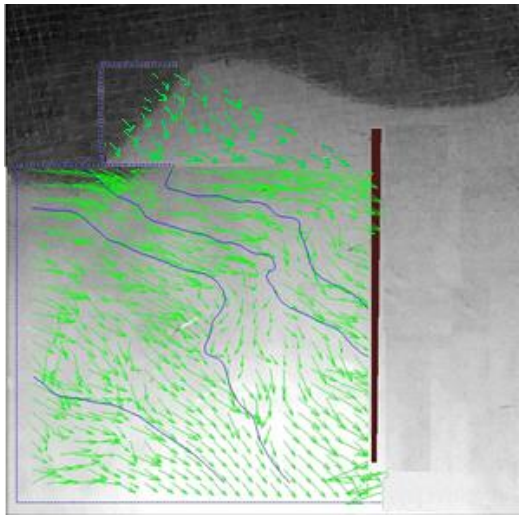

4.38(c): Flownet for *B*/8 position 15m long sheet pile

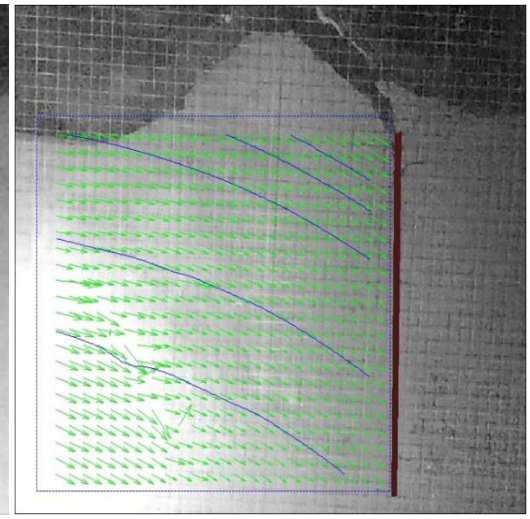

4.38(d): Flownet for *B*/8 position 20m long sheet pile

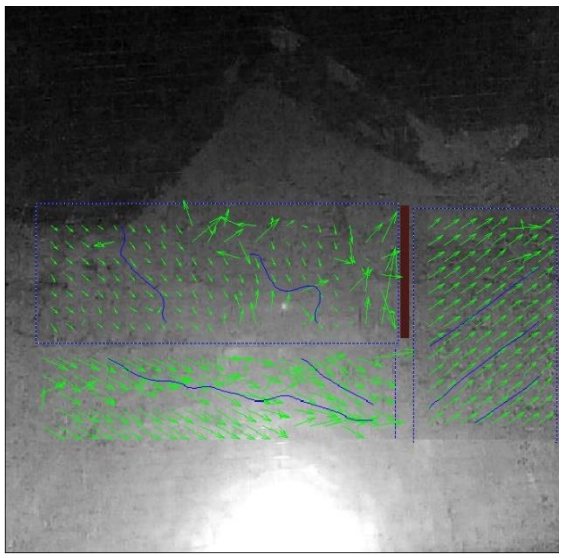

4.38(e): Flownet for *2B*/8 position 5m long sheet pile

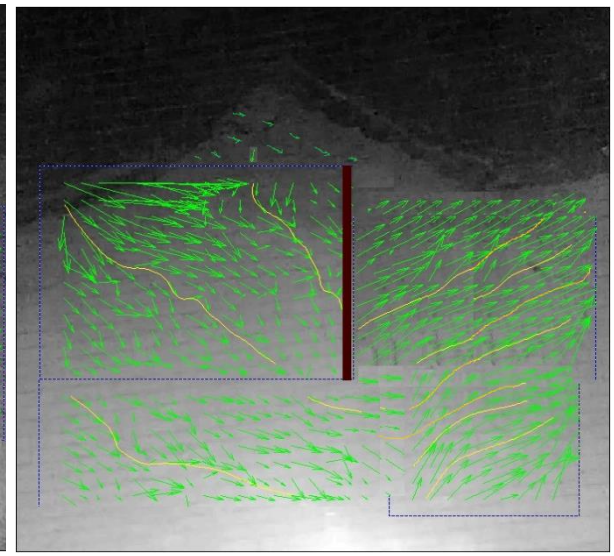

4.38(f): Flownet for *2B*/8 position 10m long sheet pile

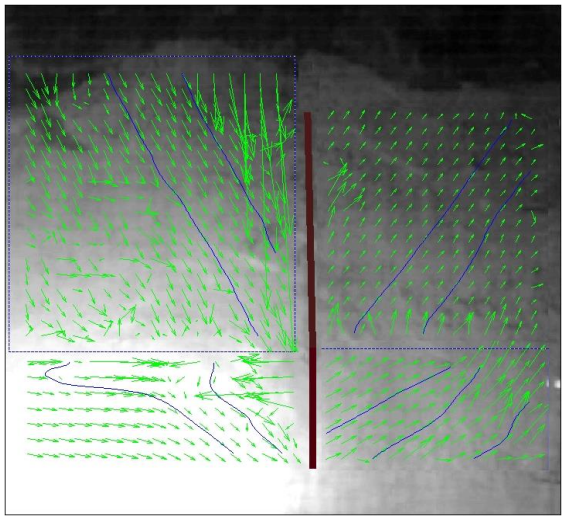

4.38(g): Flownet for *2B*/8 position 15m long sheet pile

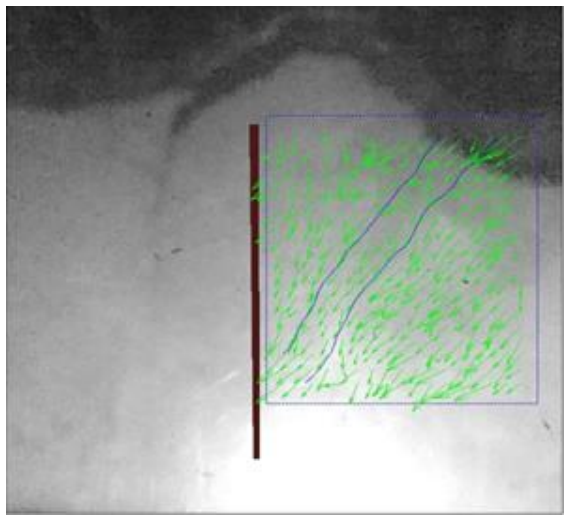

4.38(h): Flownet for *2B*/8 position 20m long sheet pile

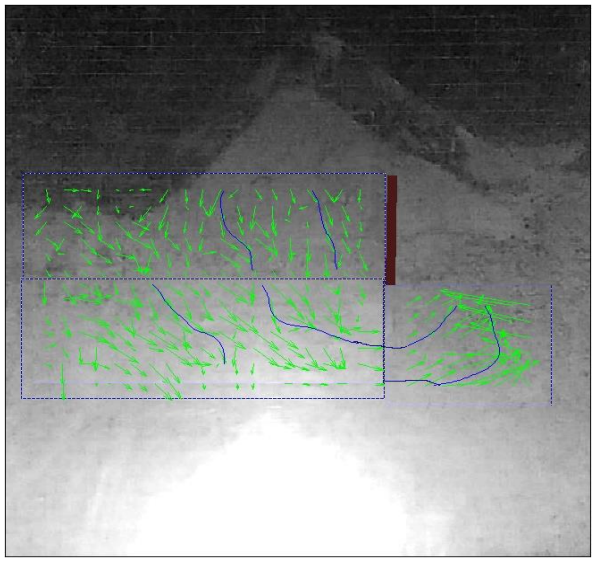

4.38(i): Flownet for *3B*/8 position 5m long sheet pile

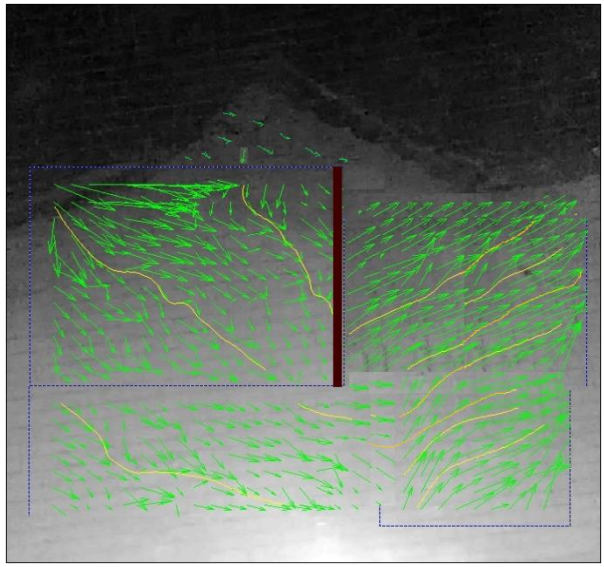

4.38(j): Flownet for *3B*/8 position 10m long sheet pile

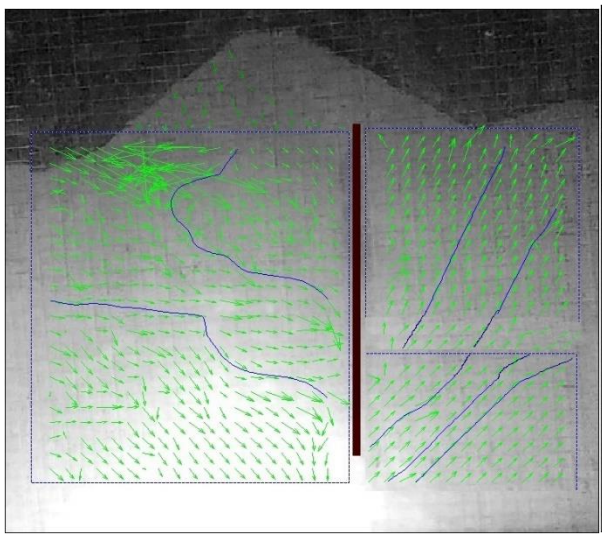

4.38(k): Flownet for *3B*/8 position 15m long sheet pile

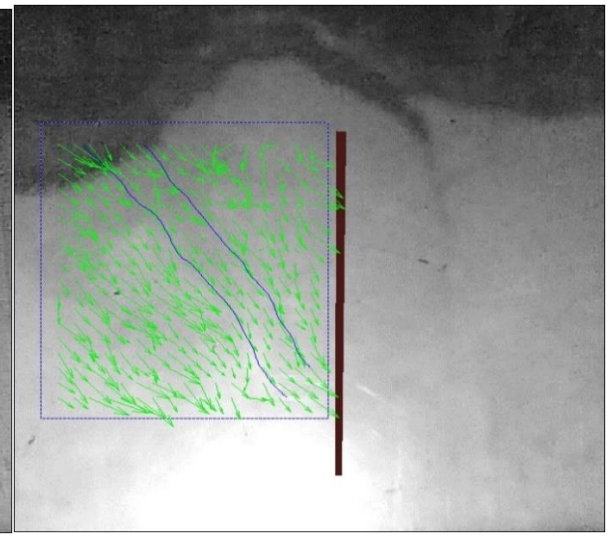

4.38(l): Flownet for *3B*/8 position 20m long sheet pile

4.8.2.3 EMBANKMENT WITH-OUT CUT OFF TRANSIENT STATE CONDITION

The flownet has been developed for different cases under steady seepage condition and also in different time intervals by image processing through PIV. The experimentally obtained phreatic surface, flownet and pattern of fluid flow vector in an embankment has been shown for Tidal cycle of 2 hours, 4hours, 6 hours has been shown accordingly in Figure 4.39(a) to 4.39(c) respectively.

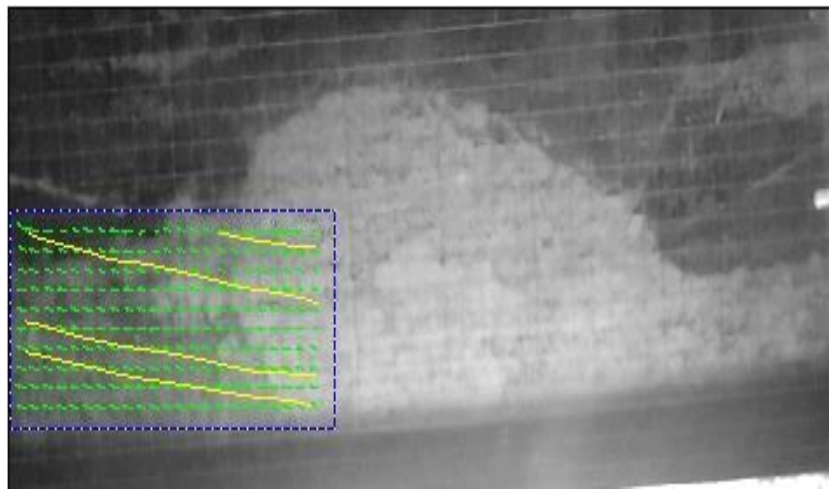

Figure 4.39(a): Phreatic Surface and flownet development for tidal cycle 2 hrs.

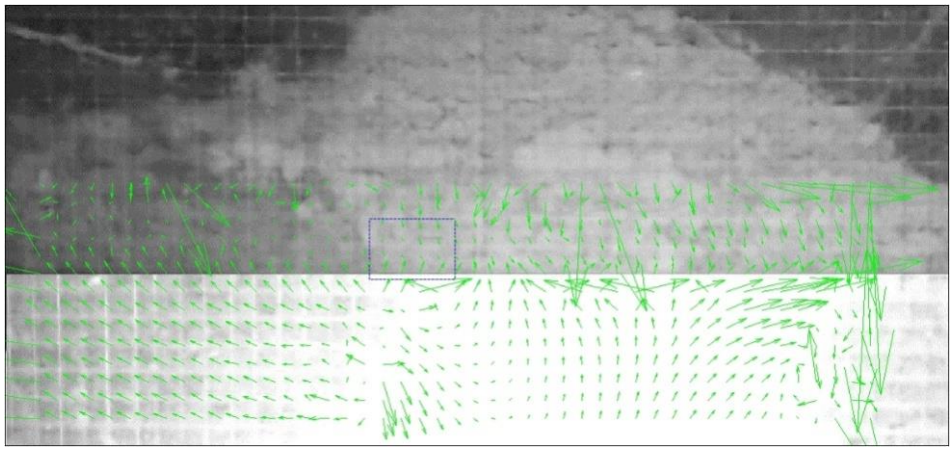

Figure 4.39(b): Phreatic Surface and flownet development for tidal cycle 4 hrs.

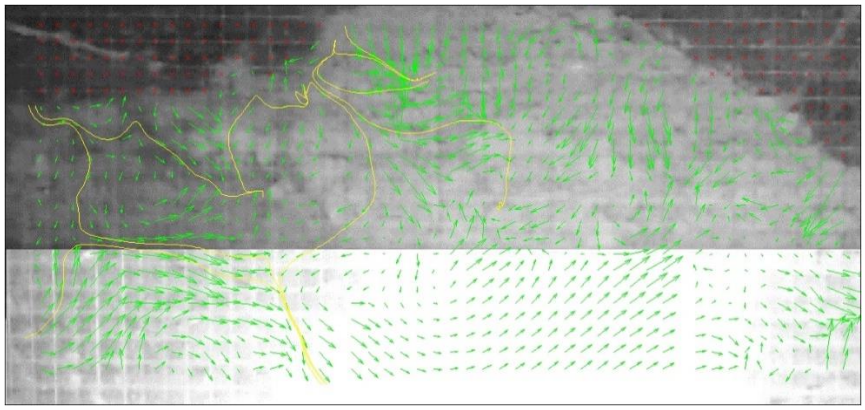

Figure 4.39(c): Phreatic Surface and flownet development for tidal cycle 6 hrs.

4.8.2.4 EMBANKMENT WITH-OUT CUT OFF TRANSIENT STATE CONDITION

Flownet and fluid flow vector obtained from PIV analysis have been presented in this section for different sheet pile position and location.

4.8.2.4.1 Flownet and fluid flow vector (*B*/8 position 5m length)

The flownet has been developed for different cases of 1hour, 3 hours, 5hours, 7 hours has been shown accordingly in Figure 4.40(a),4.40(b),4.40(c),4.40(d) respectively. Stream line has been plotted through flow tracking technique. The measured velocity and vorticity contour distributions from particle images from interpolated particle images are shown manifested in figures. Furthermore, PIV gives the visualization of magnitudes and gives values the x-y components of velocity for the flow different points, at different times in matrix form. Blue line represents stream line and flow vector have been represented by green arrow. It has been observed that at upstream side the position of fluid flows in the downward

direction along the length of sheet pile. At the position of sheet pile there is an abrupt jump of fluid flow vector.

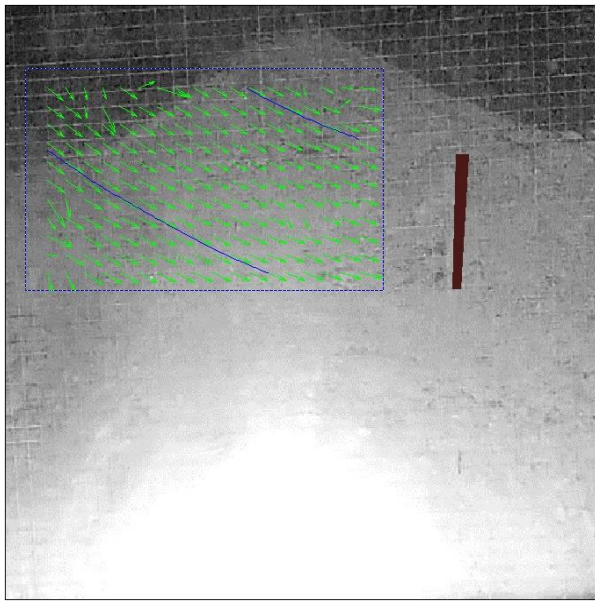

Fig 4.40(a): Flownet under rise up condition (for 5 m long sheet file at *B*/8 from downstream end), time=1 hour

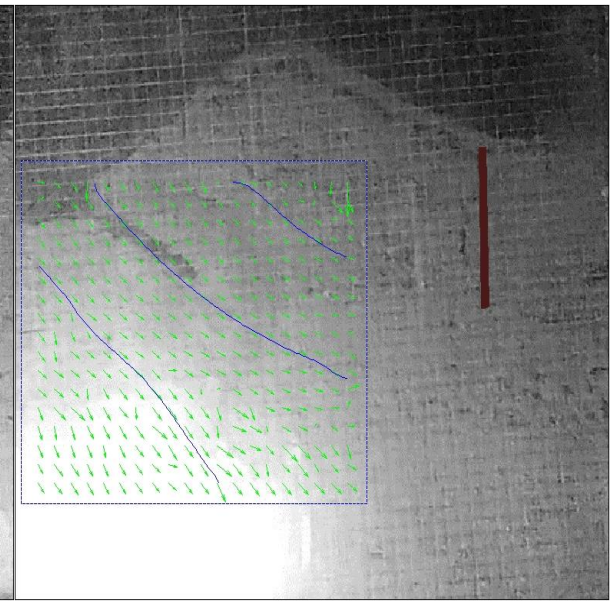

Fig 4.40(b): Flownet under rise up condition (for 5 m long sheet file at *B*/8 from downstream end), time=3 hrs.

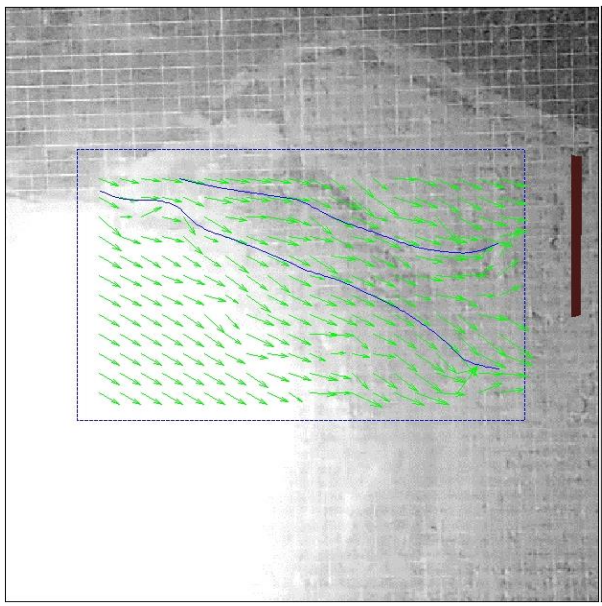

Fig 4.40(c): Flownet under rise up condition (for 5 m long sheet file at *B*/8 from downstream end), time=5 hrs.

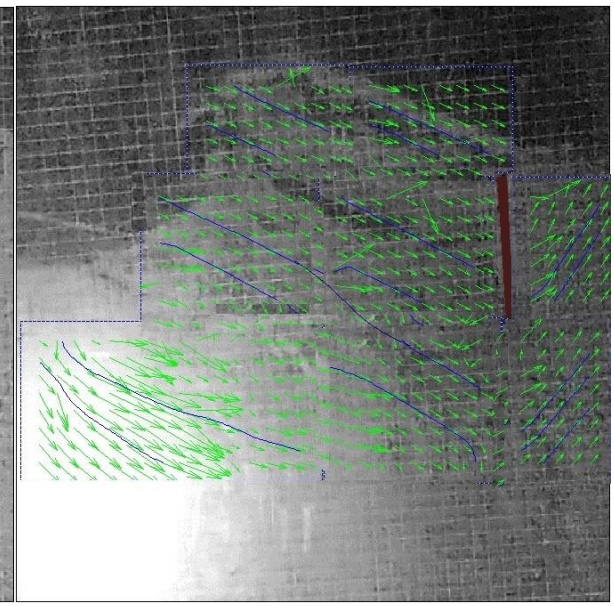

Fig 4.40(d): Flownet under rise up condition (for 5 m long sheet file at *B*/8 from downstream end), time=7 hrs.

4.8.2.4.2 Flownet and fluid flow vector (*B*/8 position 10m length)

The flownet has been developed for different cases of 1hour, 2 hours, 3hours, 4hours, 6 hours ,8 hours has been shown accordingly in Figure 4.41(a), 4.41(b), 4.41(c), 4.41(d), 4.41(e), 4.41(f) respectively. Stream line has been plotted through flow tracking technique. The measured velocity and vorticity contour distributions from particle images from interpolated particle images are shown manifested in figures. Furthermore, PIV gives the visualization of magnitudes and gives values the x-y components of velocity for the flow different points, at different times in matrix form. Blue line represents stream line and flow vector have been represented by green arrow. It has been observed that at upstream side the position of fluid flows in the downward direction along the length of sheet pile. At the position of sheet pile there is an abrupt jump of fluid flow vector.

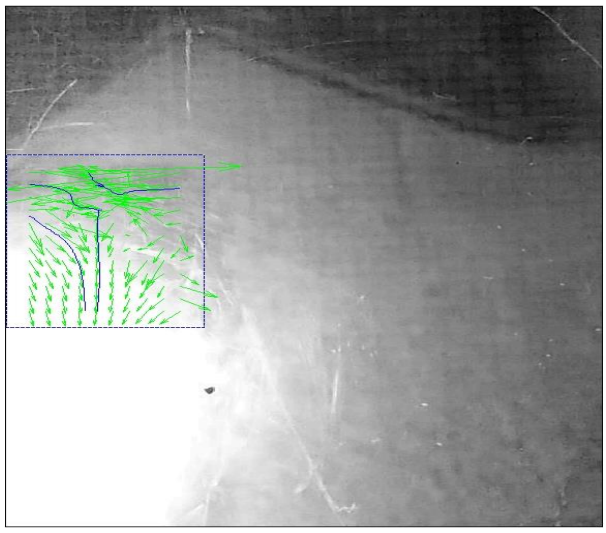

Fig 4.41(a): Flownet under rise up condition (for 10 m long sheet file at *B*/8 from downstream end), time=1 hour

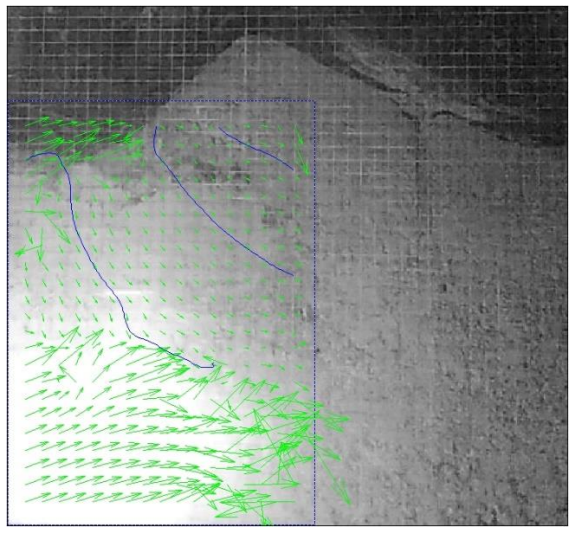

Fig 4.41(b): Flownet under rise up condition (for 10 m long sheet file at *B*/8 from downstream end), time=2 hrs.

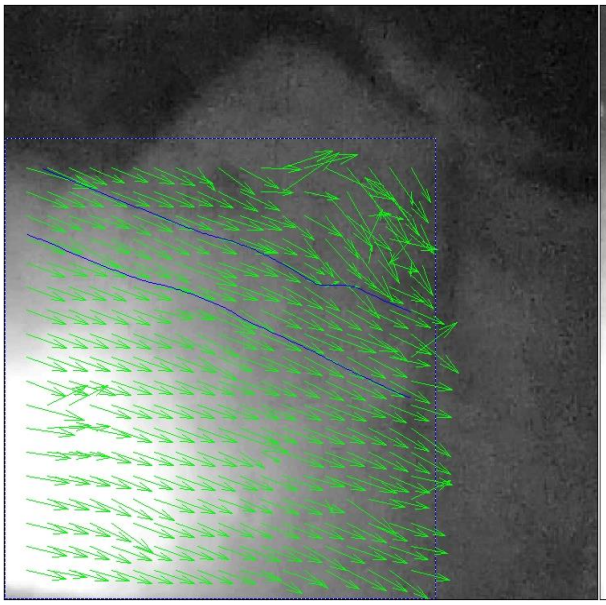

Fig 4.41(c): Flownet under rise up condition (for 10 m long sheet file at *B*/8 from downstream end), time=3 hrs.

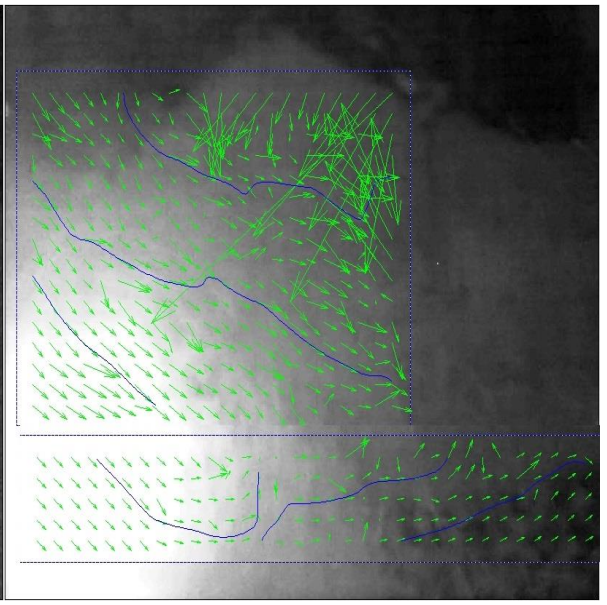

Fig 4.41(d): Flownet under rise up condition (for 10 m long sheet file at *B*/8 from downstream end), time=4 hrs.

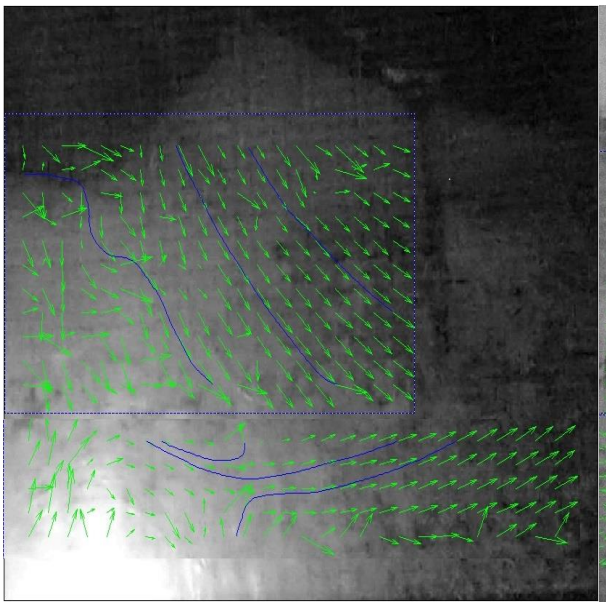

Fig 4.41(e): Flownet under rise up condition (for 10 m long sheet file at *B*/8 from downstream end), time=6 hrs.

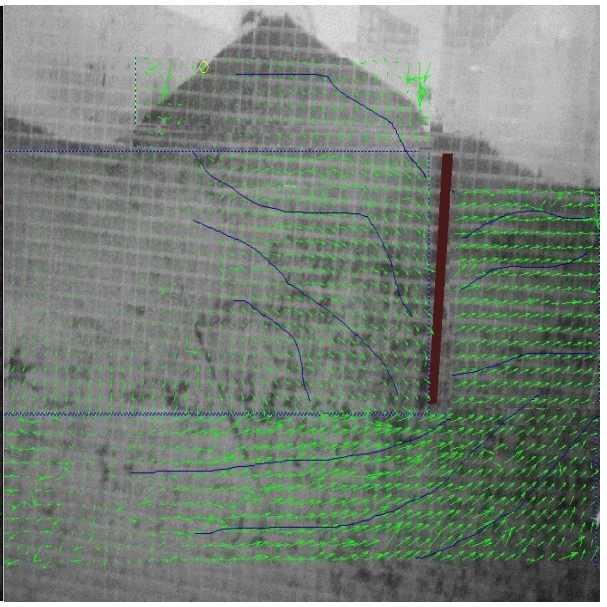

Fig 4.41(f): Flownet under rise up condition (for 10 m long sheet file at *B*/8 from downstream end), time=8 hour

4.8.2.4.3 Flownet and fluid flow vector (*B*/8 position 15m length)

The flownet has been developed for different cases of 1hour, 3 hours, 4hours, 6 hours has been shown accordingly in Figure 4.42(a),4.42(b),4.42(c),4.42(d) respectively. Stream line has been plotted through flow tracking technique. The measured velocity and vorticity contour distributions from particle images from interpolated particle images are shown manifested in figures. Furthermore, PIV gives the visualization of magnitudes and gives values the x-y components of velocity for the flow different points, at different times in matrix form. Blue line represents stream line and flow vector have been represented by green arrow. It has been observed that at upstream side the position of fluid flows in the downward direction along the length of sheet pile. At the position of sheet pile there is an abrupt jump of fluid flow vector.

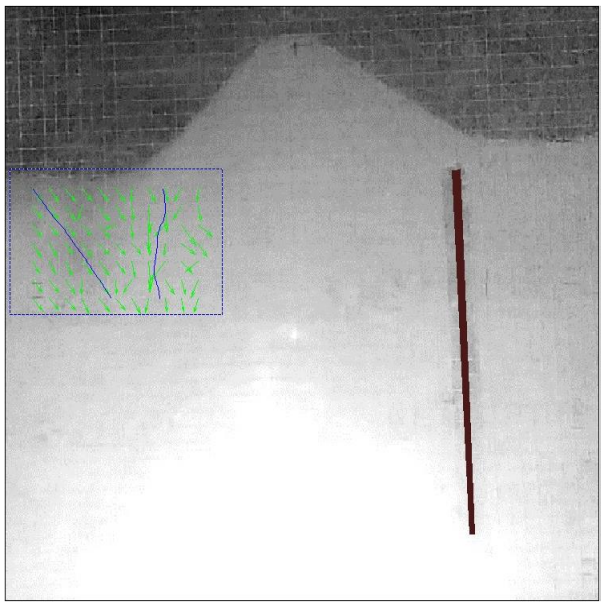

Fig 4.42(a): Flownet under rise up condition (for 15 m long sheet file at *B*/8 from downstream end), time=1 hour

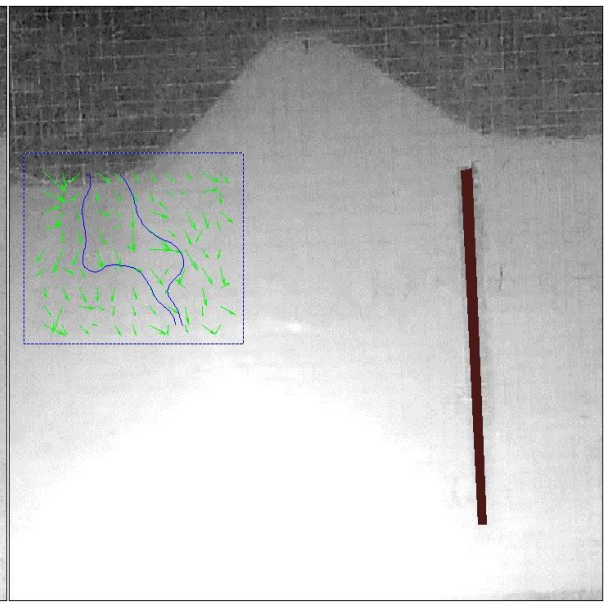

Fig 4.42(b): Flownet under rise up condition (for 15 m long sheet file at *B*/8 from downstream end), time=3 hrs.

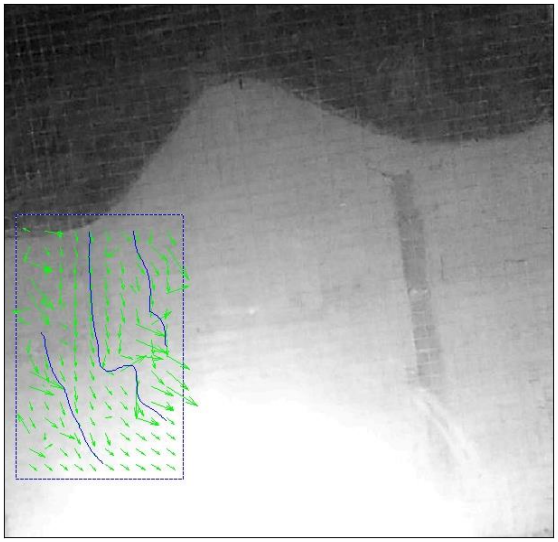

Fig 4.42(c): Flownet under rise up condition (for 15 m long sheet file at *B*/8 from downstream end), time=4 hrs.

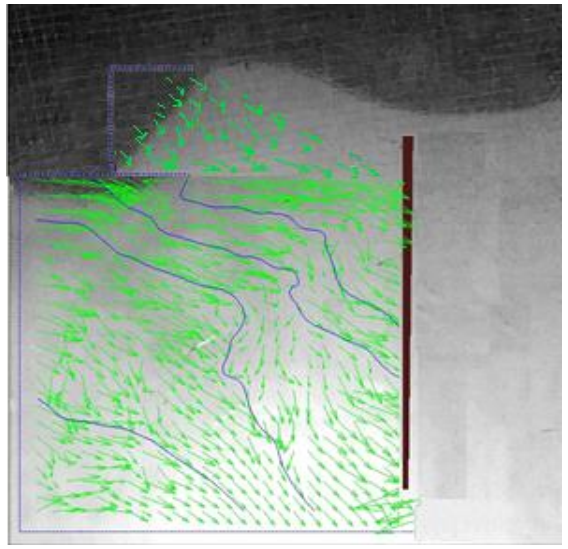

Fig 4.42(d): Flownet under rise up condition (for 15 m long sheet file at *B*/8 from downstream end), time=6 hrs.

4.8.2.4.4 Flownet and fluid flow vector (*B*/8 position 20m length)

The flownet has been developed for different cases of 1hour, 2 hours, 3hours, 5 hours, 7 hours has been shown accordingly in Figure 4.43(a),4.43(b),4.43(c),4.43(d),4.43(e) respectively. Stream line has been plotted through flow tracking technique. The measured velocity and vorticity contour distributions from particle images from interpolated particle images are shown manifested in figures. Furthermore, PIV gives the visualization of magnitudes and gives values the x-y components of velocity for the flow different points, at different times in matrix form. Blue line represents stream line and flow vector have been represented by green arrow. It has been observed that at upstream side the position of fluid flows in the downward direction along the length of sheet pile. At the position of sheet pile there is an abrupt jump of fluid flow vector.

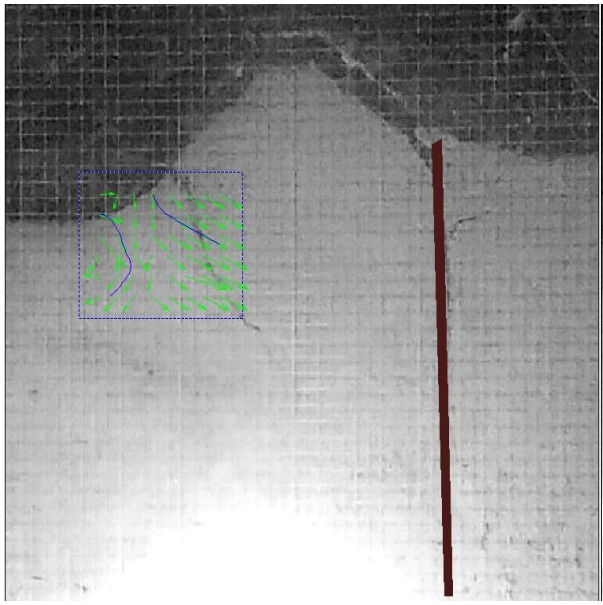

Fig 4.43(a): Flownet under rise up condition (for 20 m long sheet file at *B*/8 from downstream end), time=1 hour

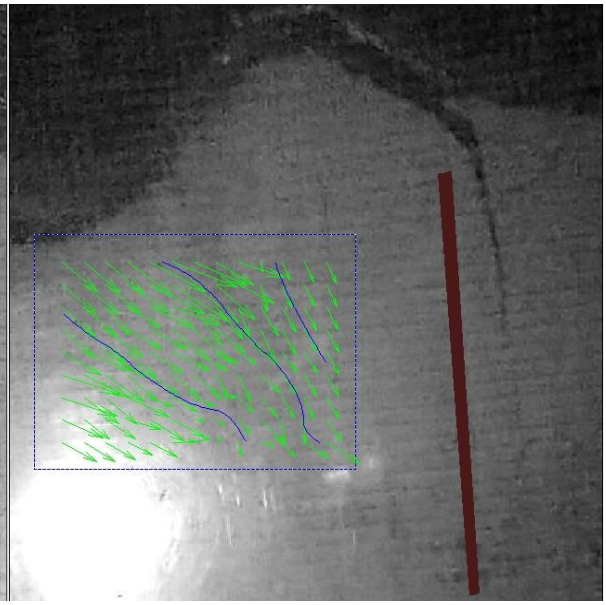

Fig 4.43(b): Flownet under rise up condition (for 20 m long sheet file at *B*/8 from downstream end), time=2 hrs.

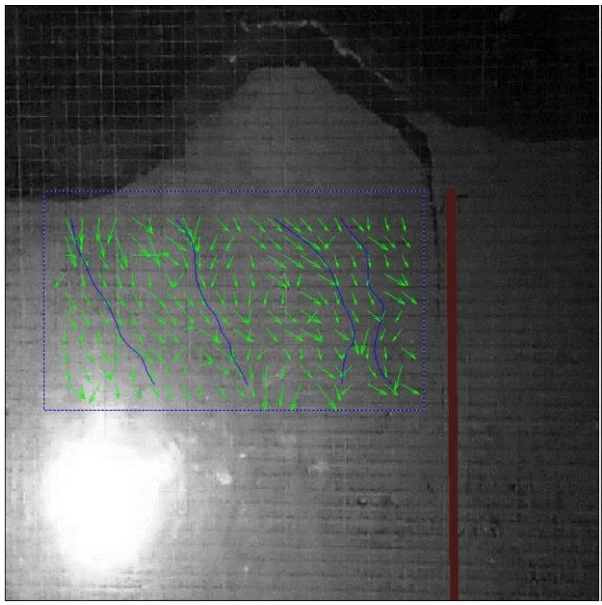

Fig 4.43(c): Flownet under rise up condition (for 20 m long sheet file at *B*/8 from downstream end), time=3 hrs.

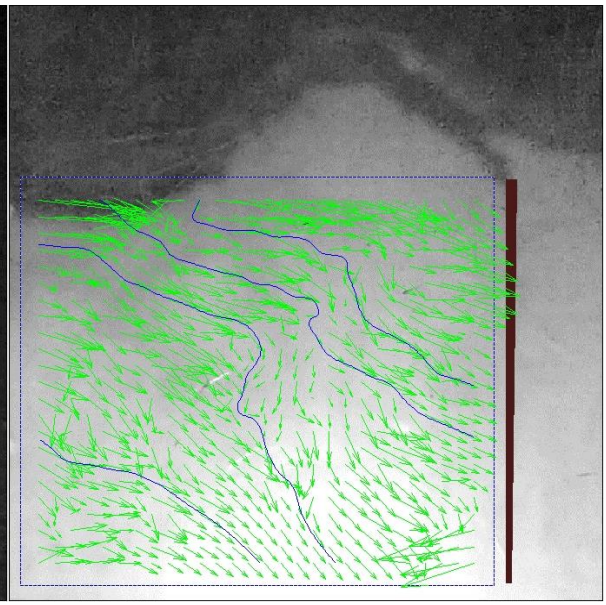

Fig 4.43(d): Flownet under rise up condition (for 20 m long sheet file at *B*/8 from downstream end), time=5 hrs.

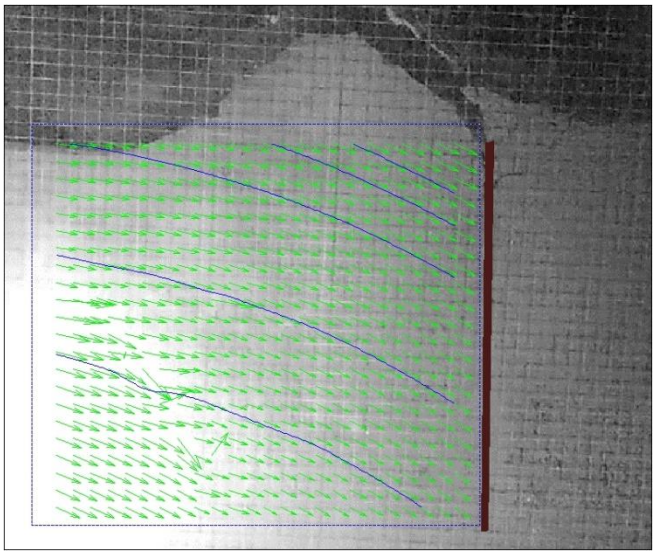

Fig 4.43(e): Flownet under rise up condition (for 20 m long sheet file at *B*/8 from downstream end), time=7 hrs.

4.8.2.4.5 Flownet and fluid flow vector (2*B*/8 position 5m length)

The flownet has been developed for different cases of 1hour, 2 hours, 3hours, 5 hours, 7hours has been shown accordingly in Figure 4.44(a),4.44(b),4.44(c),4.44(d),4.44(e) respectively. Stream line has been plotted through flow tracking technique. The measured velocity and vorticity contour distributions from particle images from interpolated particle images are shown manifested in figures. Furthermore, PIV gives the visualization of magnitudes and gives values the x-y components of velocity for the flow different points, at different times in matrix form. Blue line represents stream line and flow vector have been represented by green arrow. It has been observed that at upstream side the position of fluid flows in the downward direction along the length of sheet pile. At the position of sheet pile there is an abrupt jump of fluid flow vector.

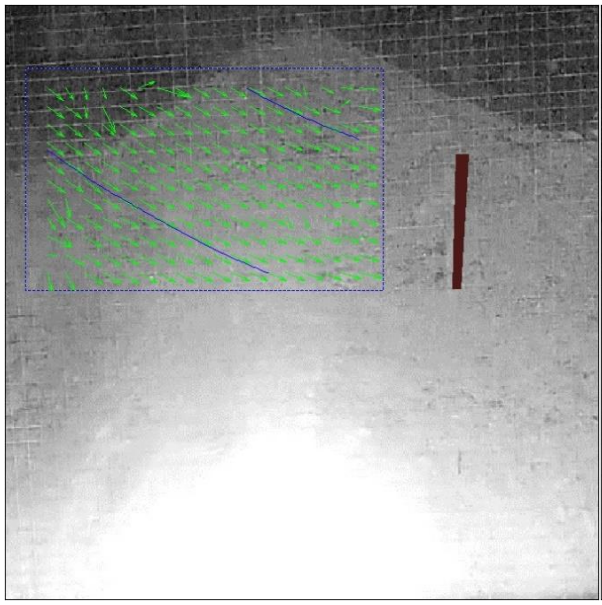

Fig 4.44(a): Flownet under rise up condition for 5 m long sheet file at 2*B*/8 from downstream end, time=1 hour

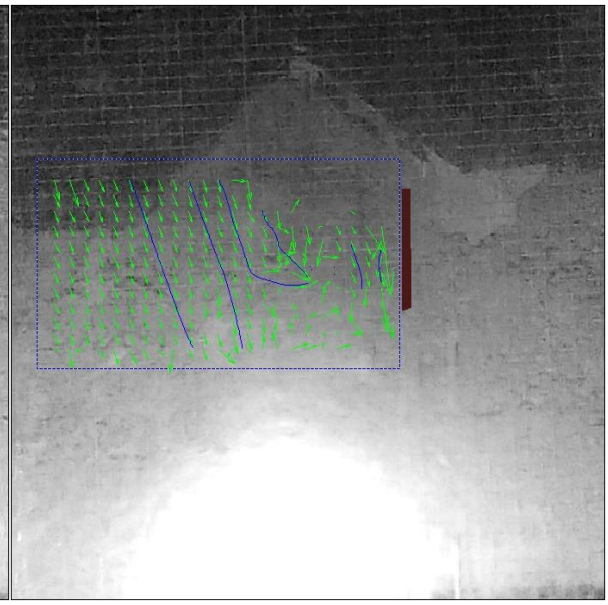

Fig 4.44(b): Flownet under rise up condition for 5 m long sheet file at 2*B*/8 from downstream end, time=2 hrs.

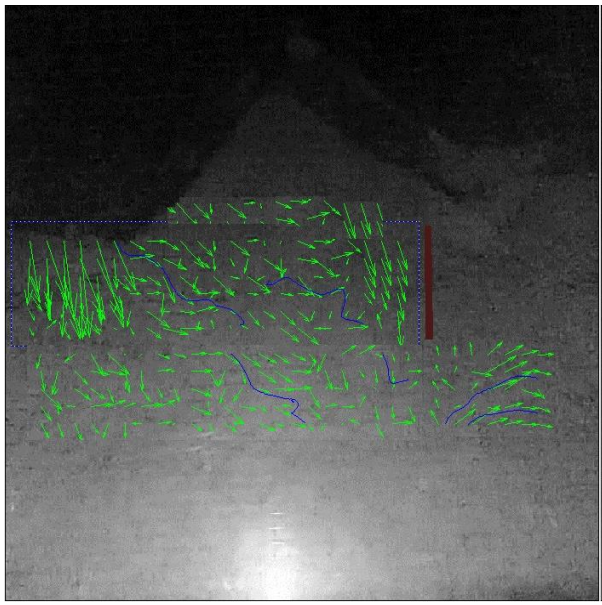

Fig 4.44(c): Flownet under rise up condition for 5 m long sheet file at 2*B*/8 from downstream end, time=3 hrs.

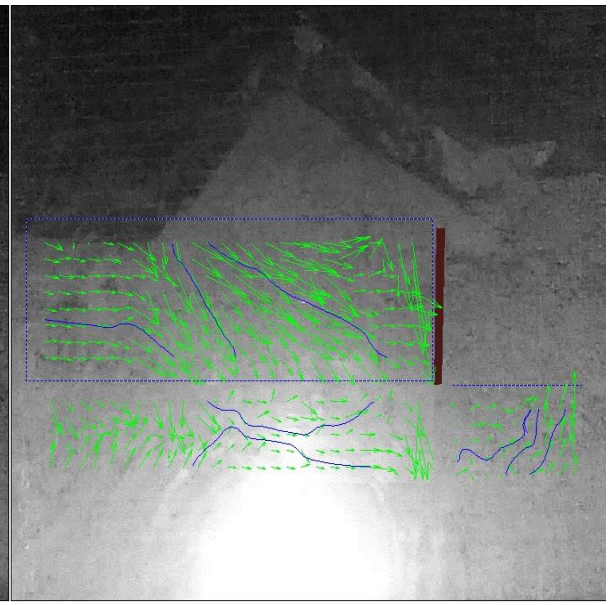

Fig 4.44(d): Flownet under rise up condition for 5 m long sheet file at 2*B*/8 from downstream end, time=5 hrs.

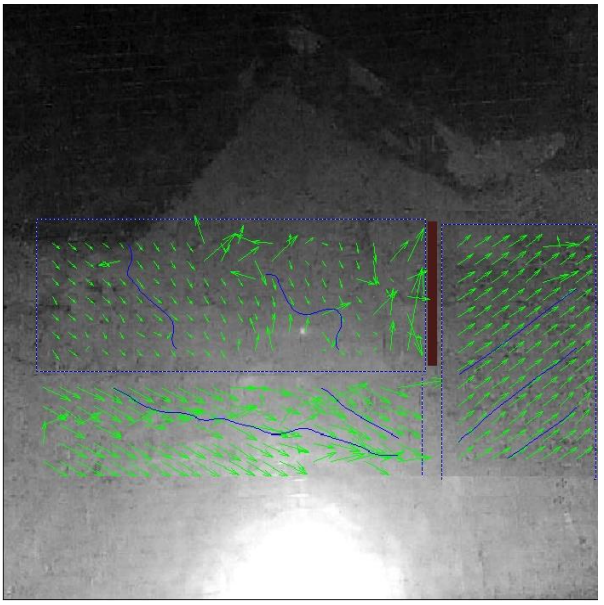

Fig 4.44(e): Flownet under rise up condition for 5 m long sheet file at 2*B*/8 from downstream end, time=7 hrs.

4.8.2.4.6 Flownet and fluid flow vector (2*B*/8 position 10m length)

The flownet has been developed for different cases of 1hour, 3 hours, 6 hours has been shown accordingly in Figure 4.45(a),4.45(b),4.45(c) respectively. Stream line has been plotted through flow tracking technique. The measured velocity and vorticity contour distributions from particle images from interpolated particle images are shown manifested in figures. Furthermore, PIV gives the visualization of magnitudes and gives values the x-y components of velocity for the flow different points, at different times in matrix form. Blue line represents stream line and flow vector have been represented by green arrow. It has been observed that at upstream side the position of fluid flows in the downward direction along the length of sheet pile. At the position of sheet pile there is an abrupt jump of fluid flow vector.

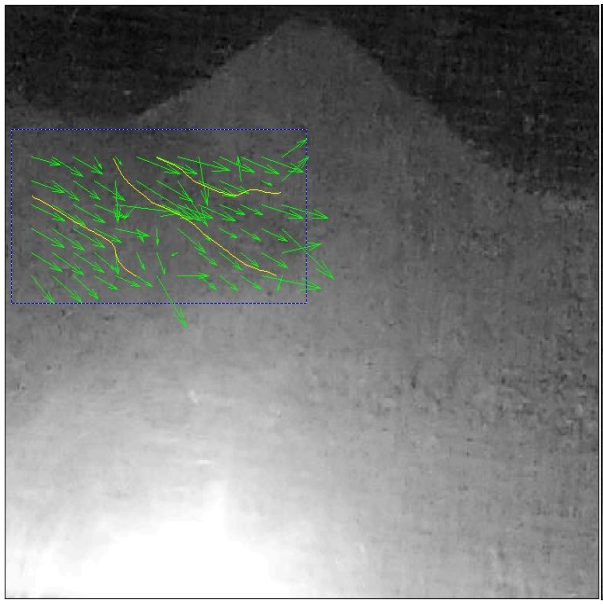

Fig 4.45(a): Flownet under rise up condition for 10 m long sheet file at 2*B*/8 from downstream end, time=1 hour

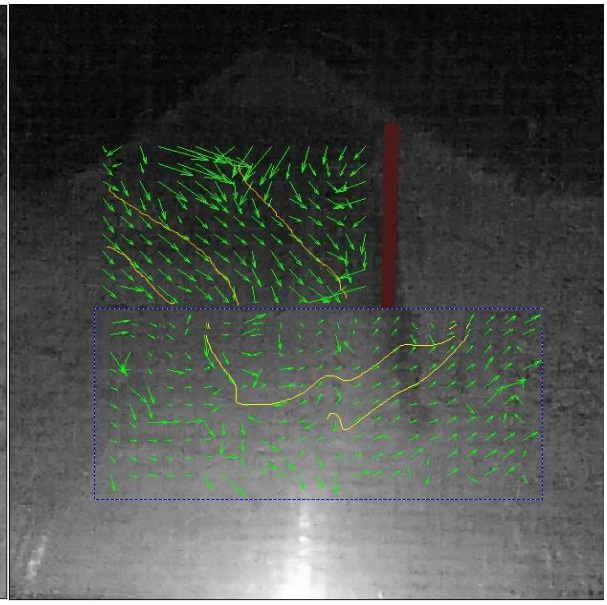

Fig 4.45(b): Flownet under rise up condition for 10 m long sheet file at 2*B*/8 from downstream end, time=3 hrs.

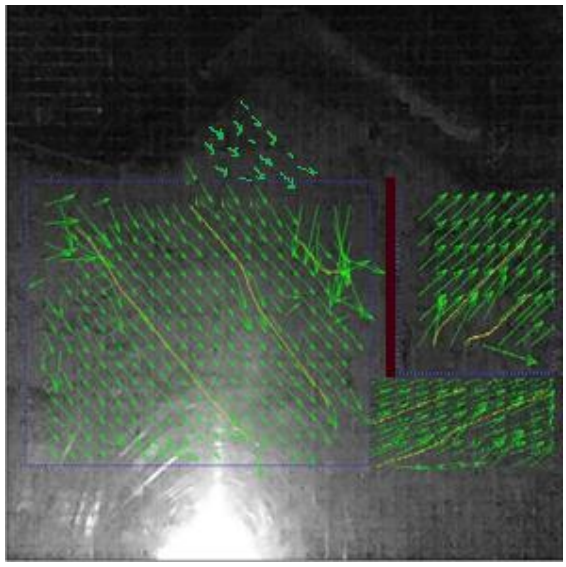

Fig 4.45(c): Flownet under rise up condition for 10 m long sheet file at 2*B*/8 from downstream end, time=6 hrs.

4.8.2.4.7 Flownet and fluid flow vector (2*B*/8 position 15m length)

The flownet has been developed for different cases of 1hour, 2 hours, 5hours, 7 hours has been shown accordingly in Figure 4.46(a),4.46(b),4.46(c),4.46(d) respectively. Stream line has been plotted through flow tracking technique. The measured velocity and vorticity

contour distributions from particle images from interpolated particle images are shown manifested in figures. Furthermore, PIV gives the visualization of magnitudes and gives values the x-y components of velocity for the flow different points, at different times in matrix form. Blue line represents stream line and flow vector have been represented by green arrow. It has been observed that at upstream side the position of fluid flows in the downward direction along the length of sheet pile. At the position of sheet pile there is an abrupt jump of fluid flow vector.

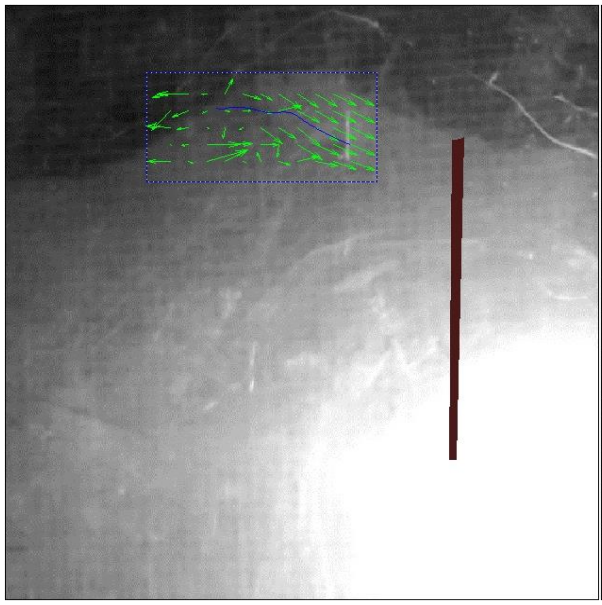

Figure 4.46(a): Flownet under rise up condition for 15 m long sheet file at 2*B*/8 from downstream end, time=1 hour

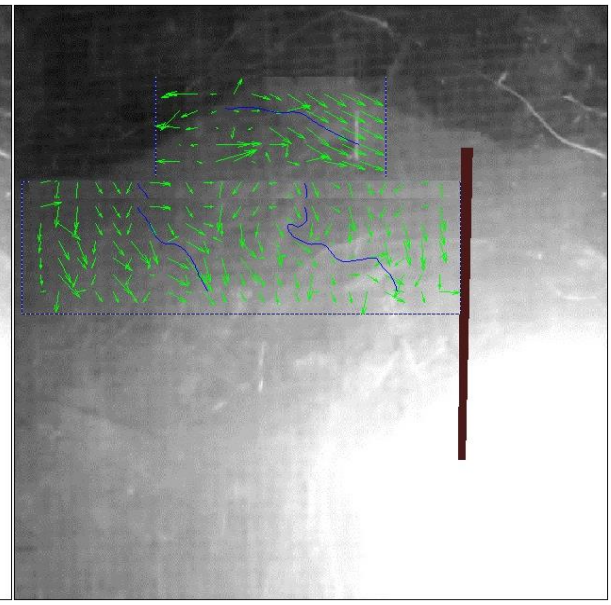

Figure 4.46(b): Flownet under rise up condition for 15 m long sheet file at 2*B*/8 from downstream end, time=2 hrs.

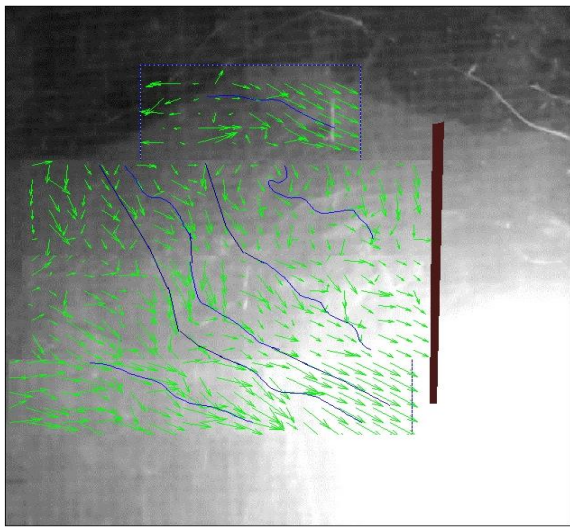

Figure 4.46(c): Flownet under rise up condition for 15 m long sheet file at 2*B*/8 from downstream end, time=5 hrs.

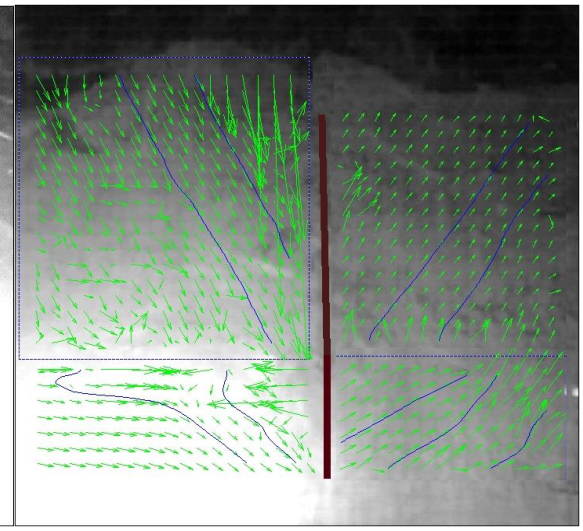

Figure 4.46(d): Flownet under rise up condition for 15 m long sheet file at 2*B*/8 from downstream end, time=7 hrs.

4.8.2.4.8 Flownet and fluid flow vector (2*B*/8 position 20m length)

The flownet has been developed for different cases of 1hour, 2 hours, 4hours, 6 hours has been shown accordingly in Figure 4.47(a),4.47(b),4.47(c),4.47(d) respectively. Stream line has been plotted through flow tracking technique. The measured velocity and vorticity contour distributions from particle images from interpolated particle images are shown manifested in figures. Furthermore, PIV gives the visualization of magnitudes and gives values the x-y components of velocity for the flow different points, at different times in matrix form. Blue line represents stream line and flow vector have been represented by green arrow. It has been observed that at upstream side the position of fluid flows in the downward direction along the length of sheet pile. At the position of sheet pile there is an abrupt jump of fluid flow vector.

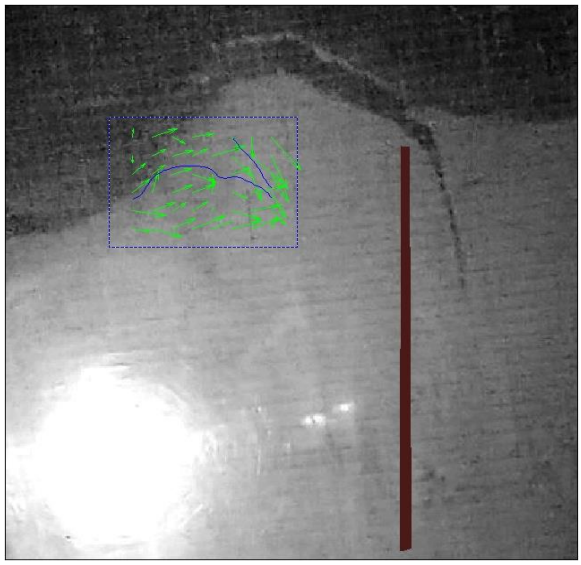

Figure 4.47(a): Flownet under rise up condition for 20 m long sheet file at 2*B*/8 from downstream end, time=1 hour

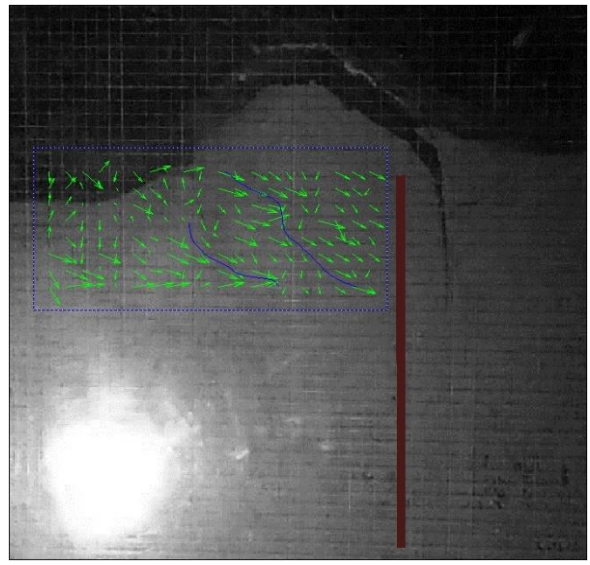

Figure 4.47(b): Flownet under rise up condition for 20 m long sheet file at 2*B*/8 from downstream end, time=2 hrs.

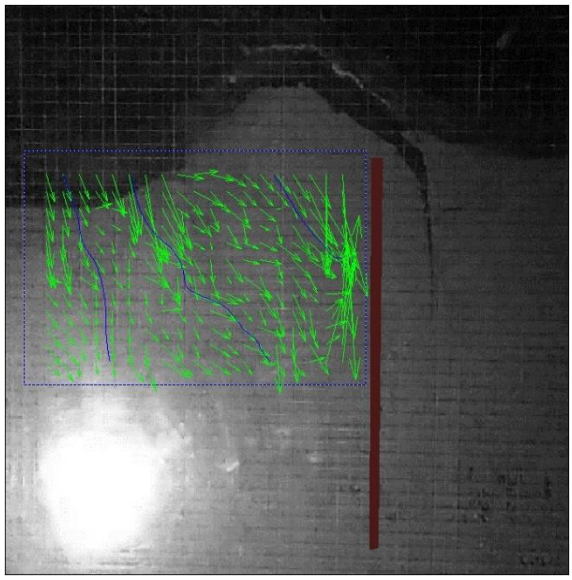

Figure 4.47(c): Flownet under rise up condition for 20 m long sheet file at 2*B*/8 from downstream end, time=4 hrs.

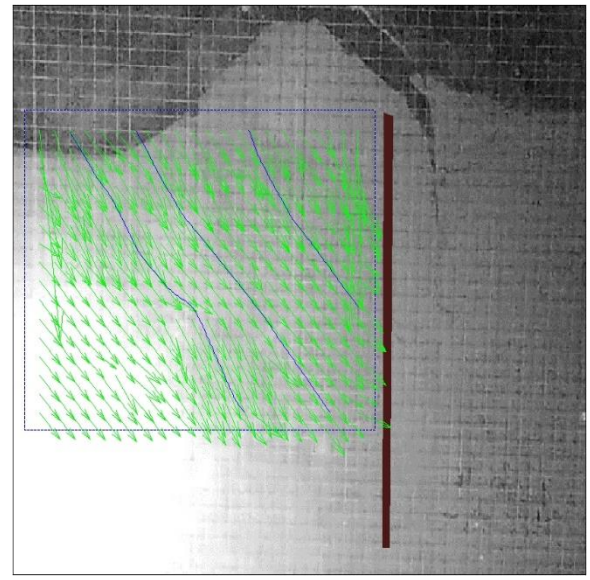

Figure 4.47(d): Flownet under rise up condition for 20 m long sheet file at 2*B*/8 from downstream end, time=6 hrs.

4.8.2.4.9 Flownet and fluid flow vector (3*B*/8 position 5m length)

The flownet has been developed for different cases of 1hour, 3 hours,5hours, 7 hours has been shown accordingly in Figure 4.48(a),4.48(b),4.48(c),4.48(d) respectively. Stream line has been plotted through flow tracking technique. The measured velocity and vorticity contour distributions from particle images from interpolated particle images are shown manifested in figures. Furthermore, PIV gives the visualization of magnitudes and gives values the x-y components of velocity for the flow different points, at different times in matrix form. Blue line represents stream line and flow vector have been represented by green arrow. It has been observed that at upstream side the position of fluid flows in the downward direction along the length of sheet pile. At the position of sheet pile there is an abrupt jump of fluid flow vector.

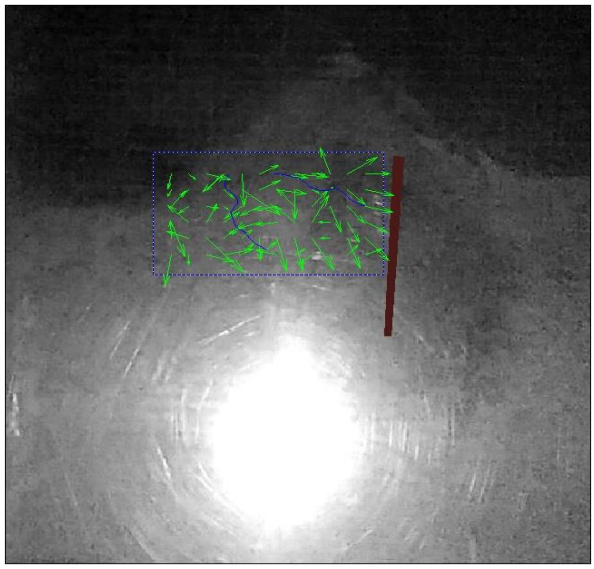

Figure 4.48(a): Flownet under rise up condition for 5 m long sheet file at 3*B*/8 from downstream end, time=1 hour

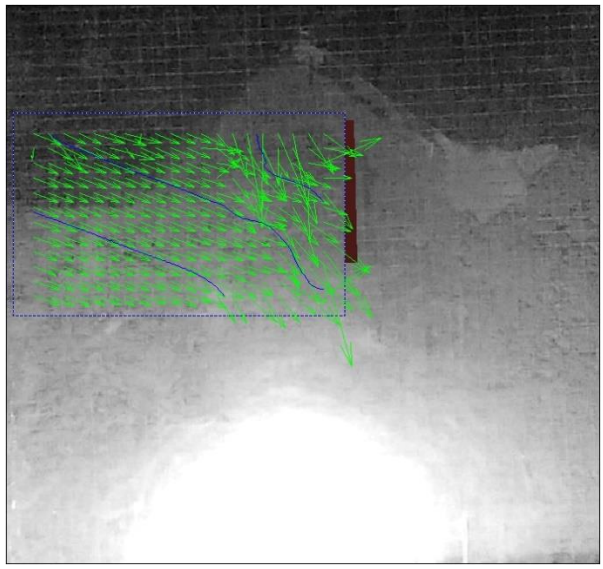

Figure 4.48(b): Flownet under rise up condition for 5 m long sheet file at 3*B*/8 from downstream end, time=3 hrs.

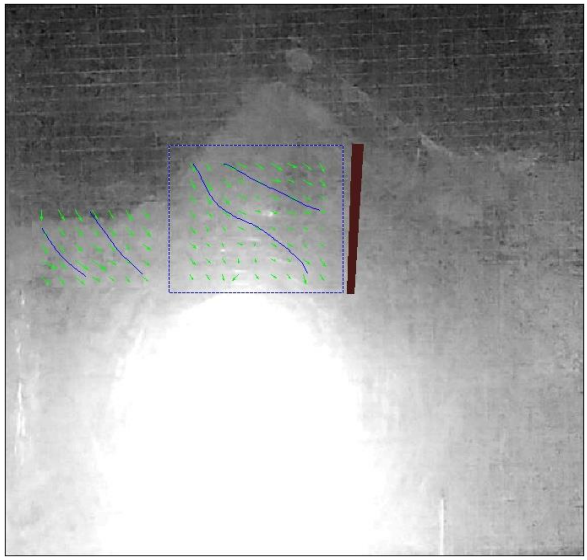

Figure 4.48(c): Flownet under rise up condition for 5 m long sheet file at 3*B*/8 from downstream end, time=5 hrs.

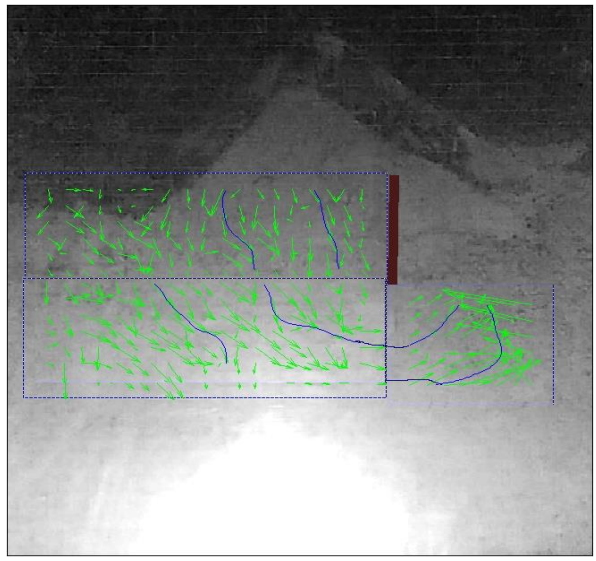

Figure 4.48(d): Flownet under rise up condition for 5 m long sheet file at 3*B*/8 from downstream end, time=7 hrs.

4.8.2.4.10 Flownet and fluid flow vector (3*B*/8 position 10m length)

The flownet has been developed for different cases of 1hour, 2 hours, 3hours, 5 hours, 6 hours, 8 hours respectively. Streamline has been shown accordingly in Figure 4.49(a),4.49(b),4.49(c),4.49(d),4.49(e),4.49(f) respectively. Stream line has been plotted through flow tracking technique. The measured velocity and vorticity contour distributions from particle images from interpolated particle images are shown manifested in figures. Furthermore, PIV gives the visualization of magnitudes and gives values the x-y components of velocity for the flow different points, at different times in matrix form. Blue line represents stream line and flow vector have been represented by green arrow. It has been observed that at upstream side the position of fluid flows in the downward direction along the length of sheet pile. At the position of sheet pile there is an abrupt jump of fluid flow vector.

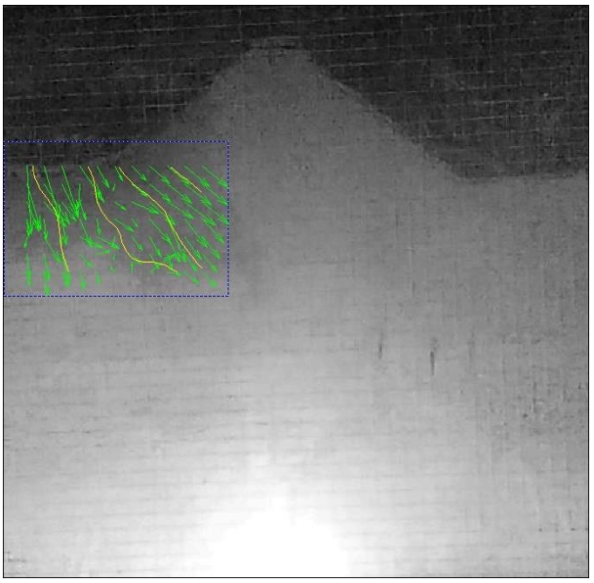

Figure 4.49(a): Flownet under rise up condition for 10 m long sheet file at 3*B*/8 from downstream end, time=1 hour

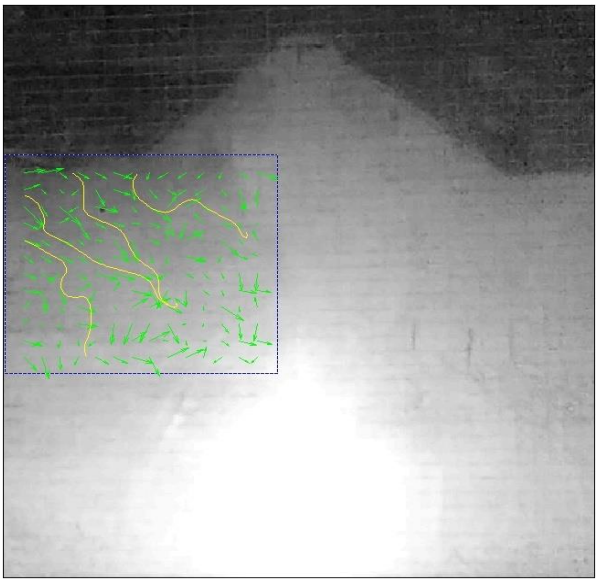

Figure 4.49(b): Flownet under rise up condition for 10 m long sheet file at 3*B*/8 from downstream end, time=2 hrs.

Figure 4.49(c): Flownet under rise up condition for 10 m long sheet file at 3*B*/8 from downstream end, time=3 hrs.

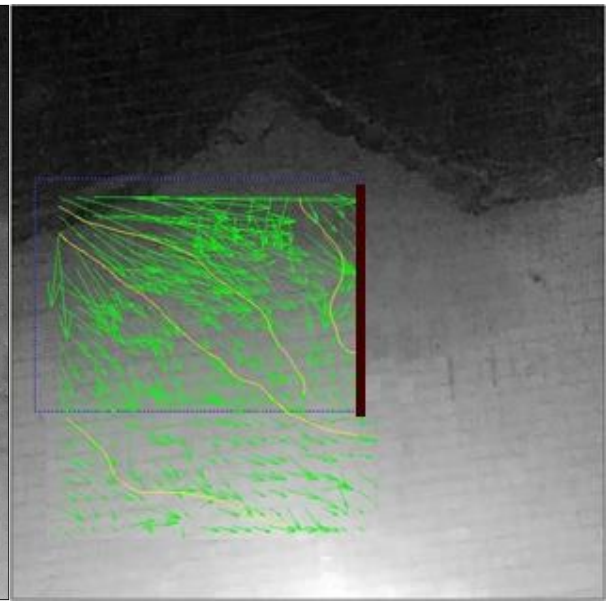

Figure 4.49(d): Flownet under rise up condition for 10 m long sheet file at 3*B*/8 from downstream end, time=5 hrs.

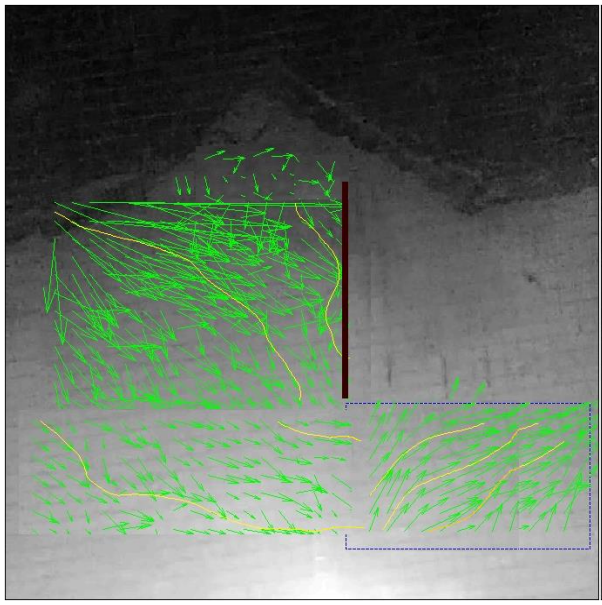

Figure 4.49 (e): Flownet under rise up condition for 10 m long sheet file at 3*B*/8 from downstream end, time=6 hrs.

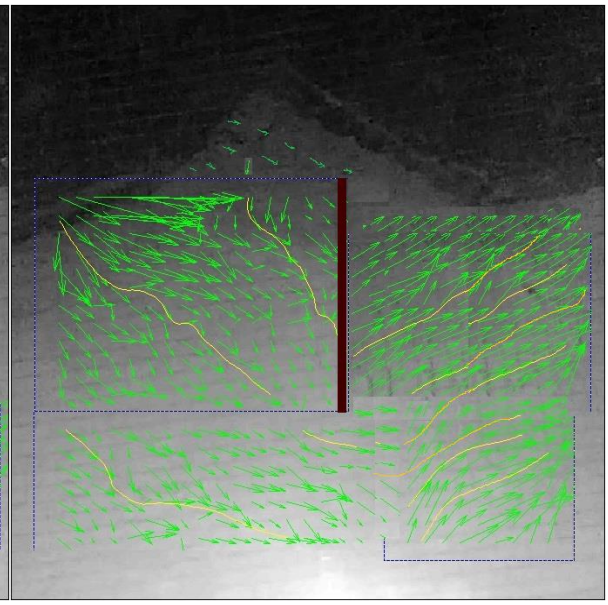

Figure 4.49(f): Flownet under rise up condition for 10 m long sheet file at 3*B*/8 from downstream end, time=8 hrs.

4.8.2.4.11 Flownet and fluid flow vector (3*B*/8 position 15m length)

The flownet has been developed for different cases of 1hour, 3 hours, 5hours, 7 hours has been shown accordingly in Figure 4.50(a),4.50(b),4.50(c),4.50(d) respectively. Stream line has been plotted through flow tracking technique. The measured velocity and vorticity contour distributions from particle images from interpolated particle images are shown

manifested in figures. Furthermore, PIV gives the visualization of magnitudes and gives values the x-y components of velocity for the flow different points, at different times in matrix form. Blue line represents stream line and flow vector have been represented by green arrow. It has been observed that at upstream side the position of fluid flows in the downward direction along the length of sheet pile. At the position of sheet pile there is an abrupt jump of fluid flow vector.

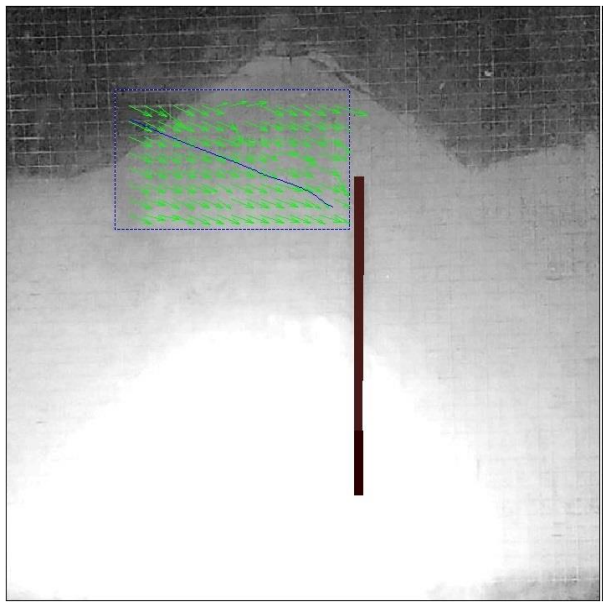

Figure 4.50(a): Flownet under rise up condition for 15 m long sheet file at 3*B*/8 from downstream end, time=1 hour

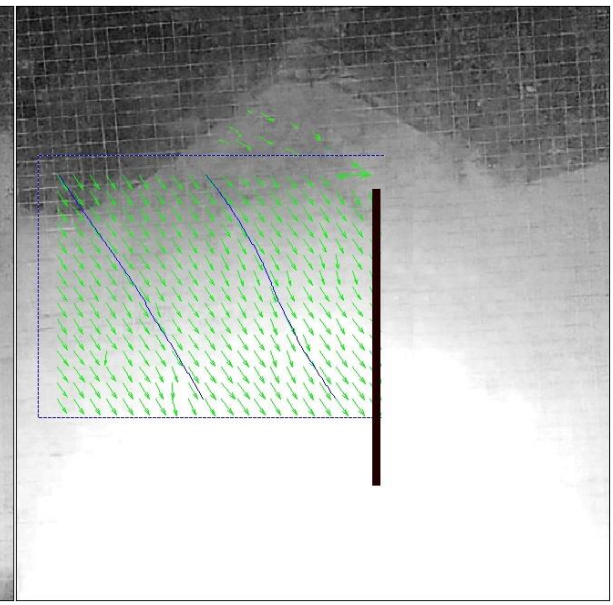

Figure 4.50(b): Flownet under rise up condition for 15 m long sheet file at 3*B*/8 from downstream end, time=3 hrs.

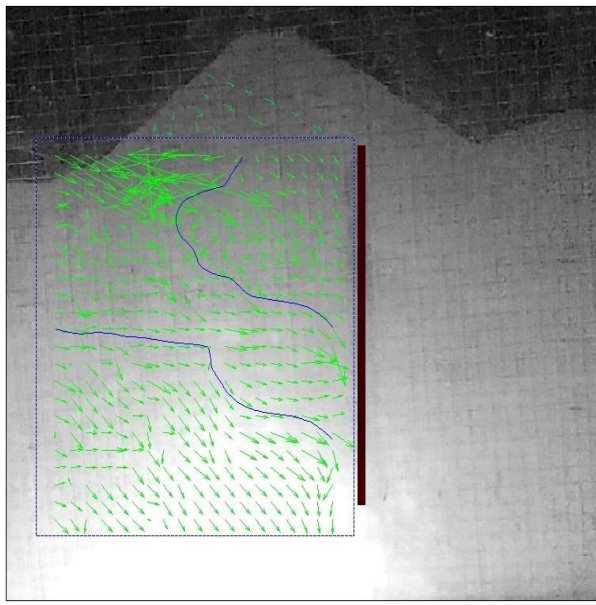

Figure 4.50(c): Flownet under rise up condition for 15 m long sheet file at 3*B*/8 from downstream end, time=5 hrs.

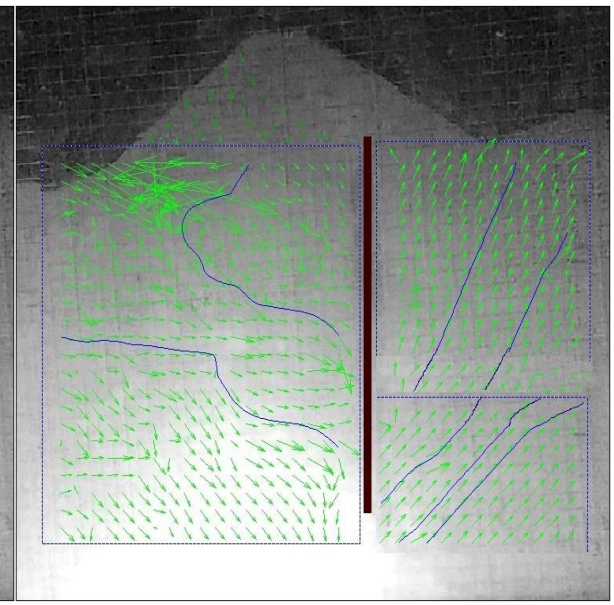

Figure 4.50(d): Flownet under rise up condition for 15 m long sheet file at 3*B*/8 from downstream end, time=7 hrs.

4.8.2.4.12 Flownet and fluid flow vector (3*B*/8 position 20m length)

The flownet has been developed for different cases of 1hour, 3 hours, 5hours, 8 hours has been shown accordingly in Figure 4.51(a),4.51(b),4.51(c),4.51(d) respectively. Stream line has been plotted through flow tracking technique. The measured velocity and vorticity contour distributions from particle images from interpolated particle images are shown manifested in figures. Furthermore, PIV gives the visualization of magnitudes and gives values the x-y components of velocity for the flow different points, at different times in matrix form. Blue line represents stream line and flow vector have been represented by green arrow. It has been observed that at upstream side the position of fluid flows in the downward direction along the length of sheet pile. At the position of sheet pile there is an abrupt jump of fluid flow vector.

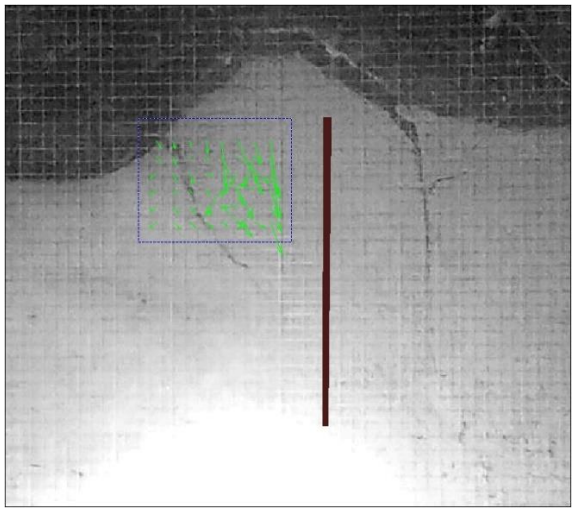

Figure 4.51(a): Flownet under rise up condition for 20 m long sheet file at 3*B*/8 from downstream end, time=1 hour

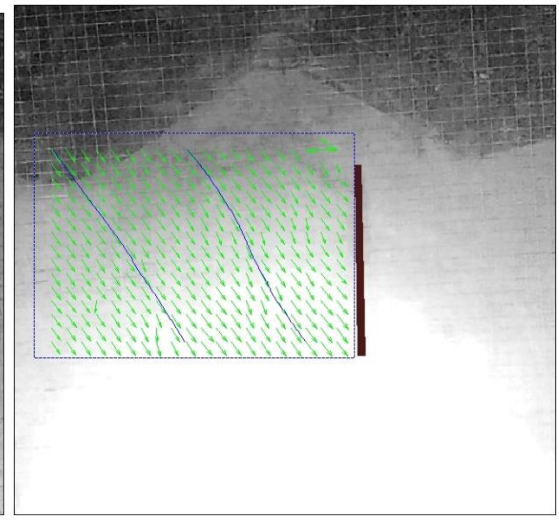

Figure 4.51(b): Flownet under rise up condition for 20 m long sheet file at 3*B*/8 from downstream end, time=3 hrs.

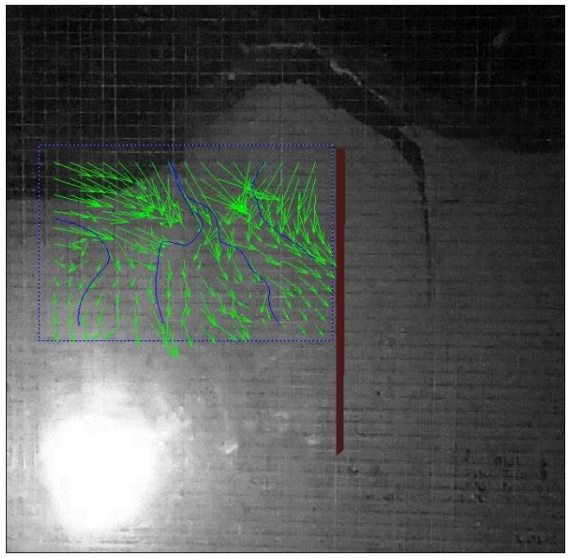

Figure 4.51(c): Flownet under rise up condition for 20 m long sheet file at 3*B*/8 from downstream end, time=5 hrs.

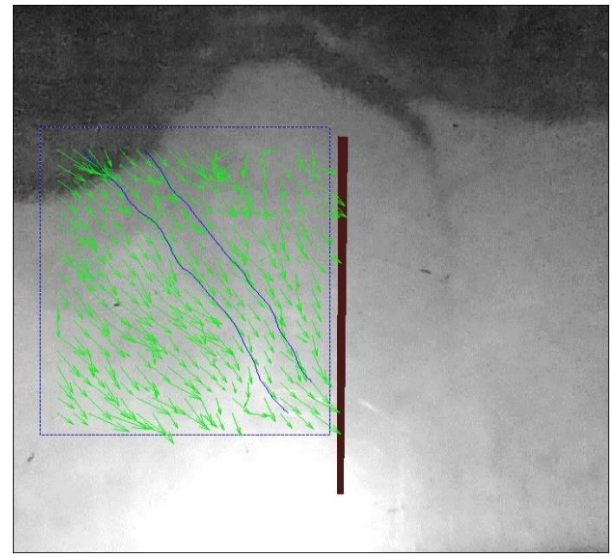

Figure 4.51(d): Flownet under rise up condition for 20 m long sheet file at 3*B*/8 from downstream end, time=8 hrs.

4.9 EXPERIMENTAL OBSERVATIONS FOR FLUID FLOW VECTOR

In the experimental investigation by centrifuge modelling the observation of magnitudes and values of the x-y components of velocity for the flow at different points, obtained with the help of PIV analysis, at different times have been estimated and plotted as shown in figures.

Figure 4.52(a) to 4.62(b) represents plotting of magnitude including direction of fluid flow vector in vertical direction in pixel form. Distance and velocity components in vertical direction have been plotted in the form of pixel/frame through PIV analysis. Figure 4.52(a) to 4.52(b) represent fluid flow vector in pixel form analyzed by PIV for 5m length of sheet pile positioned at B/8 position from downstream end for different position from the top along the horizontal direction. Figure 4.53(a) to 4.53(b) represent fluid flow vector in pixel form analyzed by PIV for 10m length of sheet pile positioned at *B*/8 position from downstream end for different position from the top along the horizontal alignment. Figure 4.54(a) to 4.54(b) represents fluid flow vector in pixel form analyzed by PIV for 15m length of sheet pile positioned as *B*/8 position from downstream end for different position from the top along the horizontal alignment. Figure 4.55(a) to 4.55(b) represents fluid flow vector in pixel form analyzed by PIV for 20m length of sheet pile positioned as *B*/8 position from downstream end for different position from the top along the horizontal alignment. Figure 4.56(a) to 4.56(b) represents fluid flow vector in pixel form analyzed by PIV for 5m length of sheet pile positioned as 2*B*/8 position from downstream end for different position from the top along the horizontal alignment. Figure 4.57(a) to 4.57(b) represents fluid flow vector in pixel form analyzed by PIV for 10m length of sheet pile positioned as 2*B*/8 position from downstream end for different position from the top along the horizontal alignment. Figure 4.58(b) represents fluid flow vector in pixel form analyzed by PIV for 15m length of sheet pile positioned as 2*B*/8 position from downstream end for different position from the top along the

horizontal alignment. Figure 4.59(a) to 4.59(b) represents fluid flow vector in pixel form analyzed by PIV for 20m length of sheet pile positioned as 2*B*/8 position from downstream end for different position from the top along the horizontal alignment. Figure 4.60(a) represents fluid flow vector in pixel form analyzed by PIV for 5m length of sheet pile positioned as 3*B*/8 position from downstream end for different position from the top along the horizontal alignment. Figure 4.61(a) to 4.61(b) represents fluid flow vector in pixel form analyzed by PIV for 10m length of sheet pile positioned as 3*B*/8 position from downstream end for different position from the top along the horizontal alignment. Figure 4.62(a) to 4.62(b) represents fluid flow vector in pixel form analyzed by PIV for 15m length of sheet pile positioned as 3*B*/8 position from downstream end for different position from the top along the horizontal alignment. Figure 5.14(a) to 5.14(b) represents fluid flow vector in pixel form analyzed by PIV for 20m length of sheet pile positioned as 3*B*/8 position from downstream end for different position from the top along the horizontal alignment.

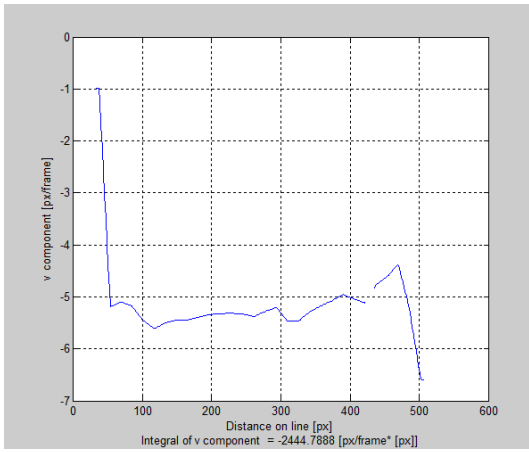

Fig 4.52 (a)

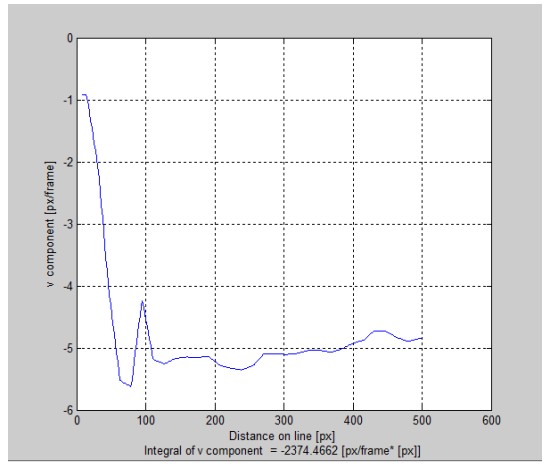

Fig 4.52 (b)

Figure 4.52: Results from experimental investigation *B*/8 position 5m length (a) 5m from the top of dam (b) 10 m from the top of dam

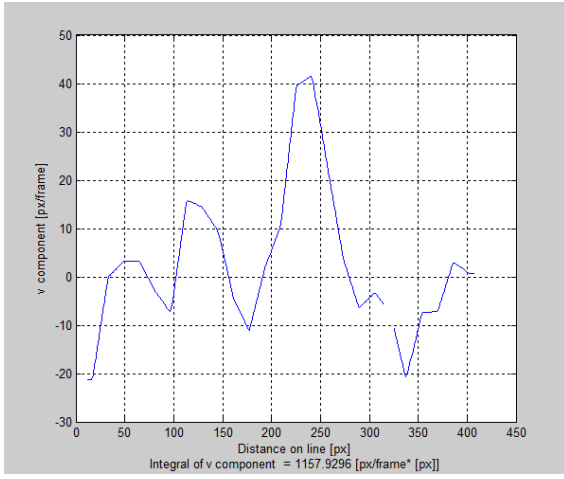

Figure 4.53: Results from experimental investigation *B*/8 position 10m length at 5m from the top of dam

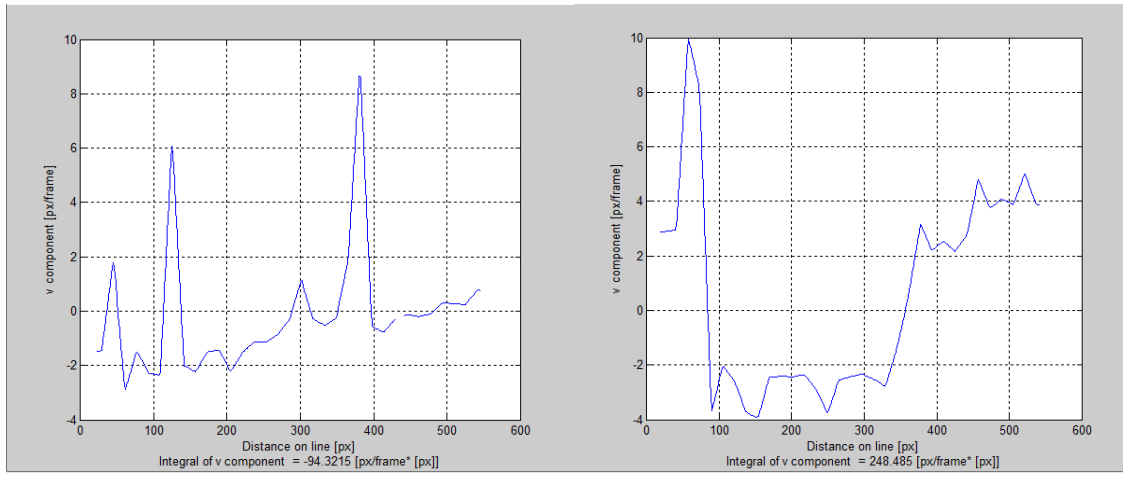

Fig 4.54 (a) Fig 4.54 (b)

Fig 4.54Result from experimental investigation *B*/8 position 15m length (a) 5m from the top of dam (b) 15 m from the top of dam

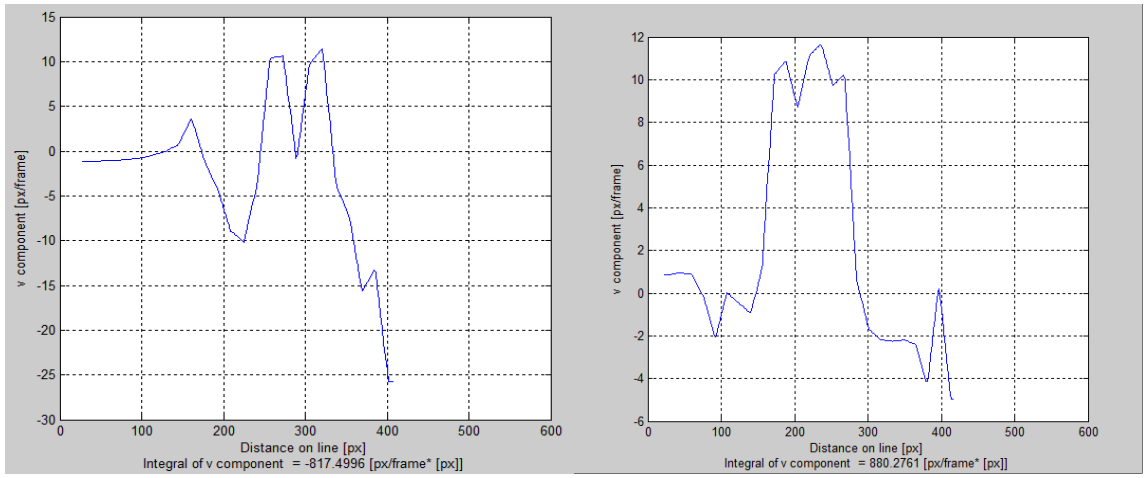

Fig 4.55 (a) Fig 4.55 (b)

Fig 4.55 Result from experimental investigation 20m long sheet pile for *B*/8 position (a) 5m from the top of dam (b) 10 m from the top of dam

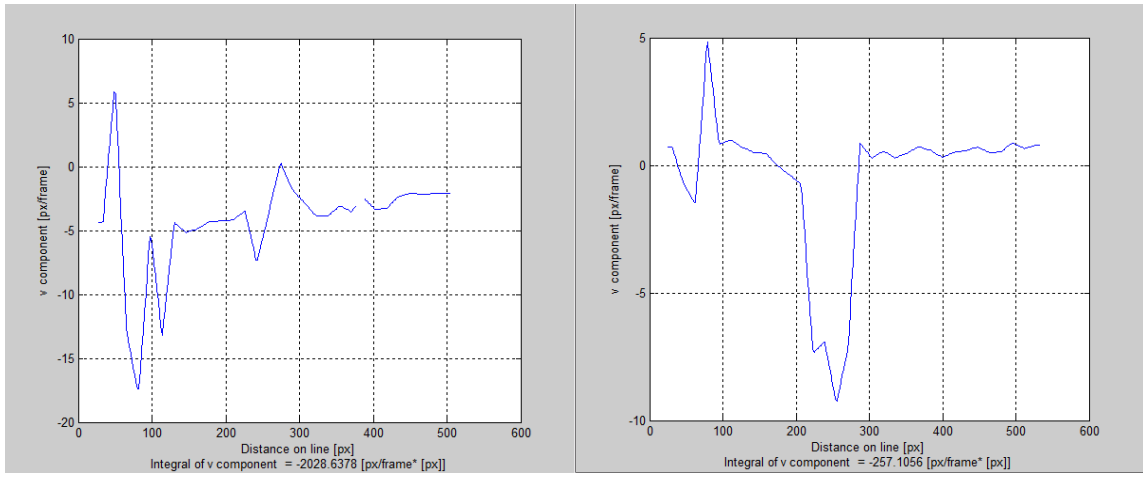

Fig 4.56 (a) Fig 4.56 (b)

Fig 4.56: Result from experimental investigation 2*B*/8 position 5m length (a) 5m from the top of dam (b) 10 m from the top of dam

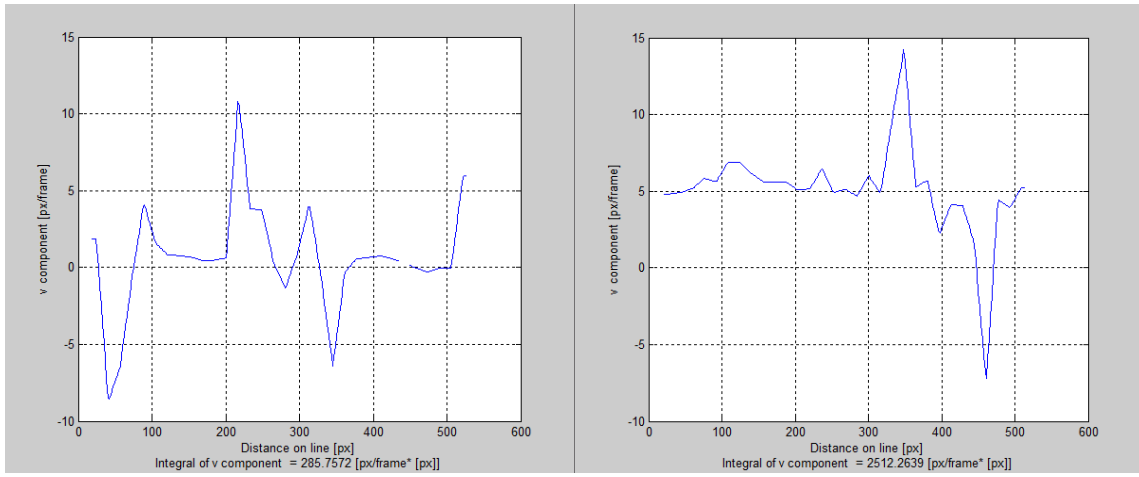

Fig 4.57 (a) Fig 4.57 (b)

Fig 4.57: Result from experimental investigation 2*B*/8 position 10m length (a) 5m from the top of dam (b) 10 m from the top of dam

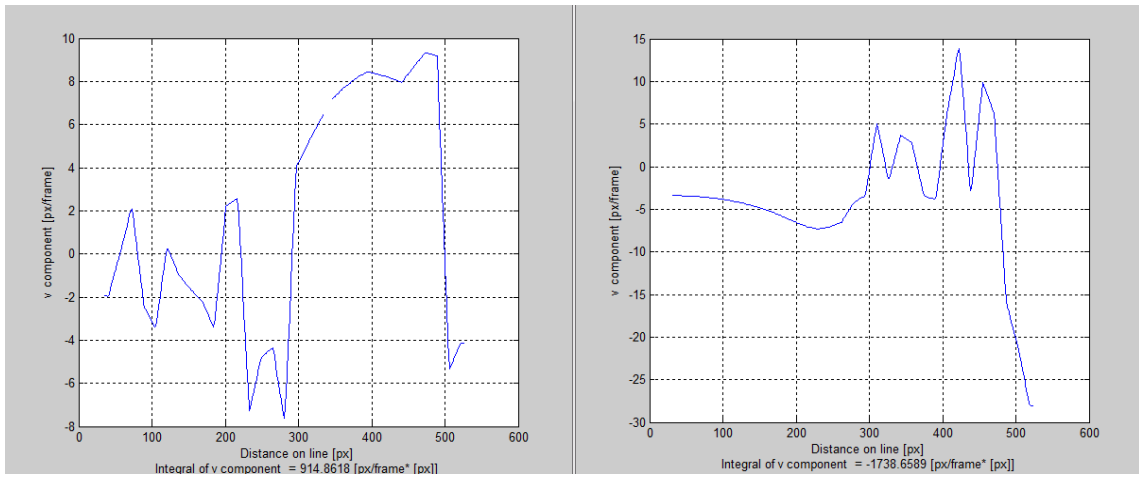

Fig 4.58 (a) Fig 4.58 (b)

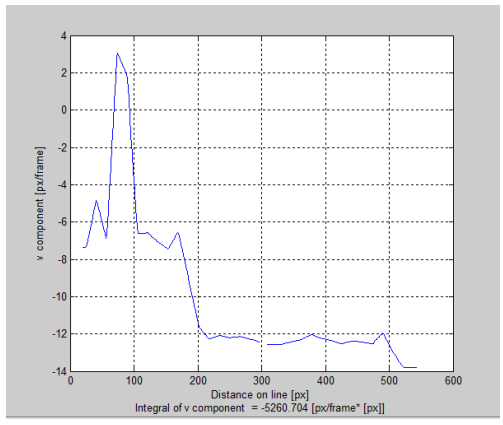

Fig 4.58 (c)

Fig 4.58: Result from experimental investigation 2*B*/8 position 15m length (a) 5m from the top of dam (b) 10 m from the top of dam (c)15 m from the top of dam

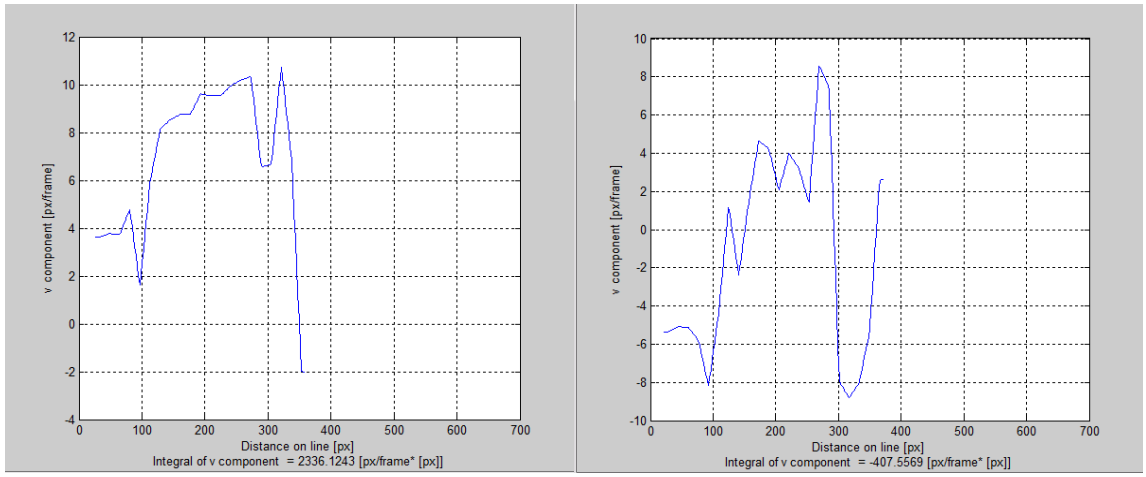

Fig 4.59 (a) Fig 4.59 (b)

Fig 4.59: Result from experimental investigation 2*B*/8 POSITION 20m length (a) 5m from the top of dam (b) 15 m from the top of dam

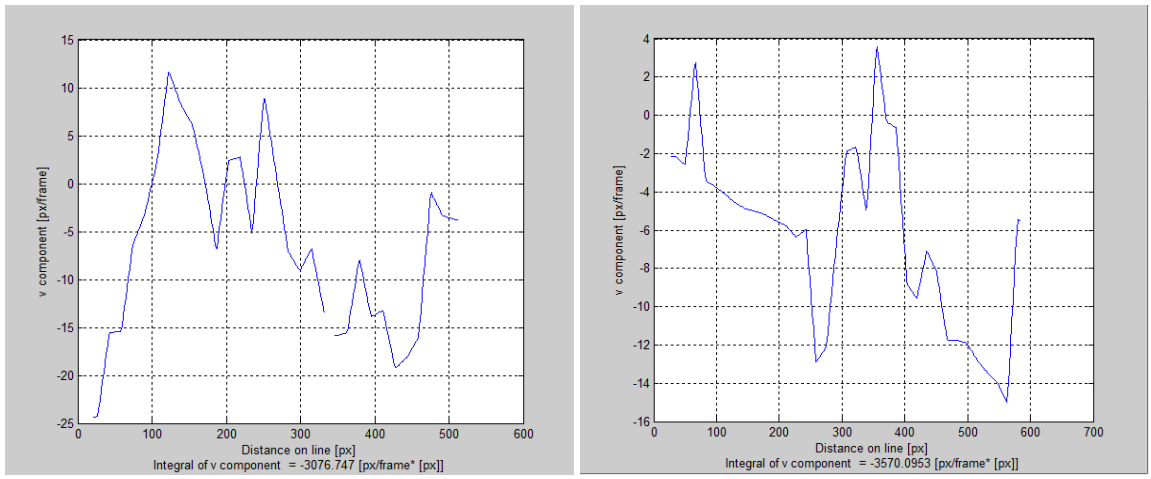

Fig 4.60(a) **Fig 4.60 (b)**

Fig 4.60: Result from experimental investigation 3*B*/8 position 5m length (a) 5m from the top of dam (b) 10 m from the top of dam

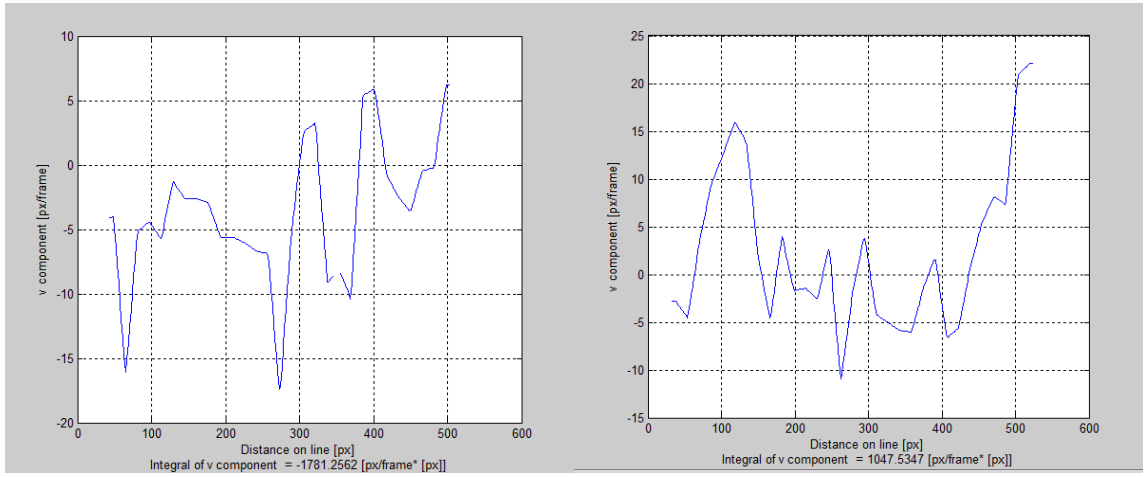

Figure. 4.61(a) Figure. 4.61(b)

Fig 4.61: Result from experimental investigation 3*B*/8 position 10m length (a) 5m from the top of dam (b) 15 m from the top of dam

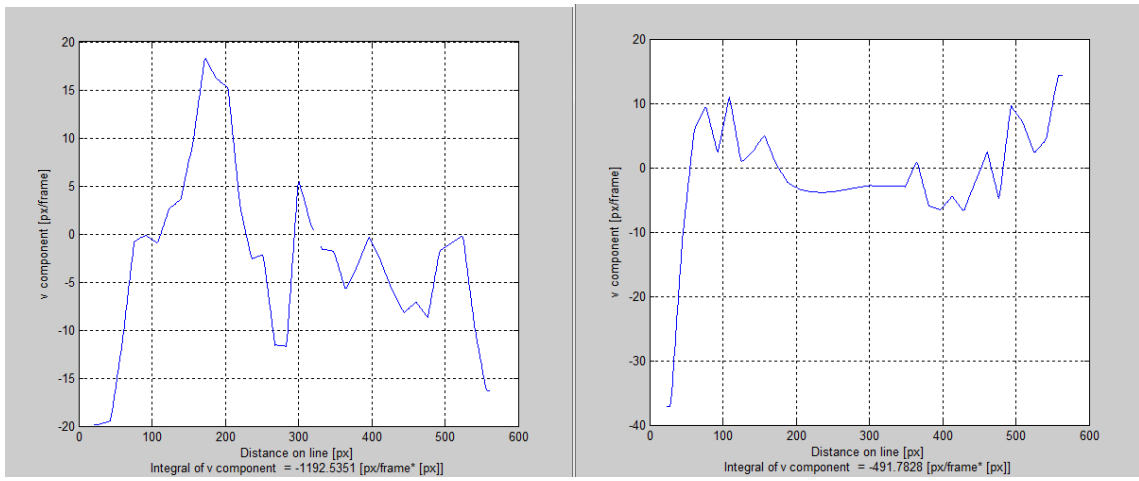

Figure. 4.62(a) Figure. 4.62(b)

Fig 4.62: Result from experimental investigation 3*B*/8 position 15m length (a) 10m from the top of dam (b) 15 m from the top of dam

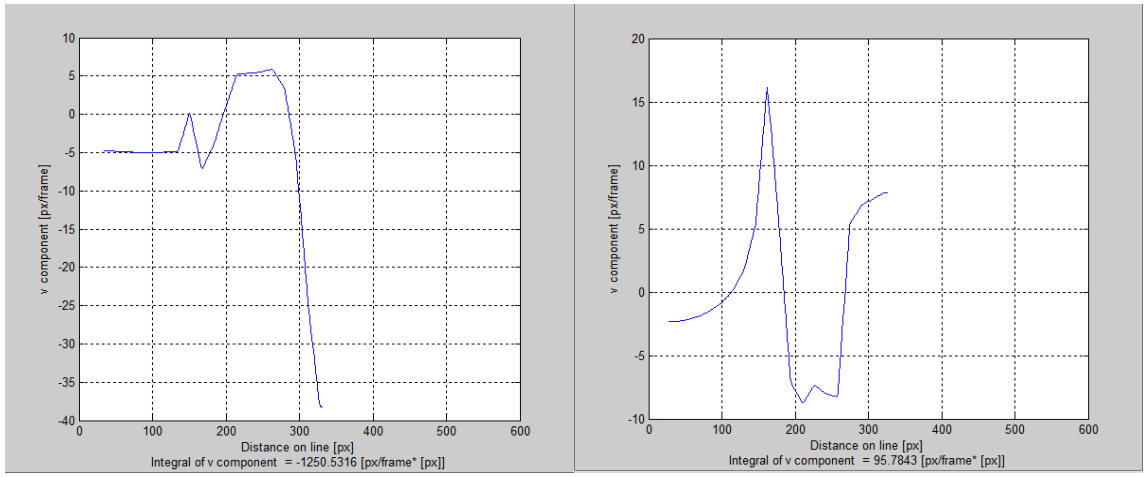

Figure. 4.63(a) Figure. 4.63(b)

Fig 4.63 Result from experimental investigation 3*B*/8 position 20m length (a) 5m from the top of dam (b) 10 m from the top of dam

4.10 USE OF EXPERIMENTAL MODEL

The experimental results presented in this chapter have been discussed in chapter five with relevance to numerical results to study seepage analysis done in the present research.

CHAPTER FIVE

DISCUSSION ON RESULTS

5.1 GENERAL

Based on the numerical and experimental results presented in chapter 3 and chapter 4 respectively an attempt has been made in this chapter to interpret the results to gain an insight into the seepage behavior of an earthen embankment dam with and without sheet pile (considered as seepage cutoff) under steady and transient states for both static and seismic conditions. The results have been presented in the form of different parametric variations, such as, variation of flownet pattern, fluid flow vector, pore water pressure, soil pressure, factor of safety against piping, overall factor of safety and those are illustrated in the following sections.

5.2 FLOW NET PATTERN

The flow net obtained by MATLAB, SEEP/W and FLAC 2D softwares are presented under steady state and transient state for a model earthen dam with and without sheet pile respectively.

5.2.1 STEADY STATE

An attempt has been made to observe the effect of location and length of sheet pile, used, as seepage cutoff. It has been observed from Figure 3.11 to 3.13 presented in chapter 3, that similar flow net pattern occurs with-out sheet pile condition as found in results obtained for MATLAB, FLAC 2D and SEEP/W. Flow net pattern obtained under steady state condition with varying sheet pile positions and locations have been shown from Figure 3.14(a) to 3.16(l) in chapter 3. From the presentation of results, it has been observed that sheet pile acts as a fluid barrier effectively. At every position and length of sheet pile the pattern of flow net matches with one another as found from these softwares. The flow net construction by the basic approach using Laplace's equation for seepage through MATLAB and the same obtained by FLAC 2D and SEEP/W appears to be similar for respective cases. Therefore, further part of the investigation has been carried out with FLAC 2D and SEEP/W. It has been observed that as the Sheet pile moves away from the downstream end the field of the flownet near the downstream end is becoming more or more similar to the case with no sheet-pile. When sheet pile is shifted towards the downstream end then the average dimension of last element of flow line is decreases. It also observed from that for any fixed position when sheet pile length increases seepage path increases.

In case of steady seismic condition, it has been observed that the phreatic surface is becoming parallel to the boundary of the dam and equipotential lines are more curvilinear than in case of steady flow.

5.2.2 TRANSIENT STATE

In case of transient state, it has been observed that the extent of the phreatic surface at the top of dam body increases continuously with the falling of the upstream water level. When the upstream water level starts rising from the point of lowest water level of a typical cycle, the extent of the phreatic surface decreases starting from the particular water level. The unsaturated region continuously reduces with rise up and increases with drawdown. The location of phreatic line gradually approaches towards that under steady state with the lapse of the time during rise up.

From the variation of the phreatic surface within the embankment during a typical cycle it has been observed that when the upstream water level goes to the highest point of the cycle in each stage, the phreatic surface rises accordingly on the upstream side. But there is slight rise of phreatic surface near the downstream end as shown from Figure 3.17(a) to 3.55(h) (presented in chapter three).

On the other hand, when the upstream water level is at the lowest point of the cycle in a stage, the part of the phreatic surface near upstream end is higher than that of the upstream water level. This is due to the slow movement of the water inside the dam than compared with that for the water level in the previous stage. The Figures 3.17(a) to Figures 3.17(c), (Result from MATLAB analysis), Figures 3.18(a) to Figure 3.18(d) (Result from FLAC 2D analysis), Figures 3.19(a) to Figure 3.17(d) (Result from SEEP/W analysis) as presented in chapter three, reveal that the phreatic surface shows a tendency to fall towards downward direction along that of flow of water as in this case the upstream boundary becomes a flow line. On the contrary in case of steady state this is equipotential line. Hence prominent change in stream line and equipotential line occurs with time. From the presentation of results, it has been observed that sheet pile acts as a fluid barrier effectively. At every position and length of sheet pile the pattern of flow net matches with one another as found from experimental and numerical investigations.

In case of multiple cycle minor change in phreatic surface has been observed as presented figure 3.56(a) in chapter three. Seepage It has been observed that the location of the phreatic surface shifts to a slightly higher elevation within a particular zone after each cycle for multiple cycle. Equipotential total head contour due to transient during single tidal cycle has been observed. It has been observed that a zone has been developed at river embankment interface through rise up stage. The equipotential total head is observed to slowly increase in this zone with rise up half cycle time. During drawdown this zone dissipated slowly till the end of single cycle (t= 12 hrs.). This zone is termed as “Zone of influence”. It is seen that this zone still persists in upper parts of upstream slope when next tidal cycle is to come. This indicates that during single tidal cycle, excess water head induced due to transient seepage during rise up did not dissipate at the end of drawdown stage, for certain regions within this zone. No change in total head induced during tidal cycle is observed in the interior part of the embankment which are outside of Zone of Influence.

The variation is observed up to a certain distance from the upstream face, beyond which no variation in phreatic surface is observed. At the end of 120 cycles, this zone has been measured as 0.25 metres approximately from the upper slope for this particular study. However, the elevational shift in phreatic surface is marginal. This phenomenon is similar for all numerical studies of varying sheet pile positions and lengths. The seismic condition at transient state has been considered to vary with time and three particular times, one at the beginning of rise up, one at the end of rise up and another at middle of the half cycle during both rise up and drawdown have been considered. Thus 1 hour, 6 hours and 8 hours have been considered for transient seismic cases.

In case of transient seismic state, it has been observed that in each case in 1 hour the extent of flownet is very small. In 6 hours, it is increasing due to rise of upstream water level whereas in 8 hours it is further decreasing with starting of drawdown condition.

5.3FLUID FLOW VECTOR

An attempt has been made in this section to study the development of fluid flow vector with variation of time without and with sheet pile depending on sheet pile lengths and positions. In each case fluid flow vectors have been plotted along the horizontal profile at distances of 2m, 7m and12m from top of the dam to study its variation within the dam body as well as foundation of the dam. The purpose of this fluid flow vector study is to investigate the effectiveness of sheet pile against erosion caused by piping. In the following sections the influence of sheet pile position and length on fluid flow vector has been investigated under steady state and transient state for both seismic and non-seismic conditions.

5.3.1 STEADY STATE

Fluid flow vector is defined as discharge per unit area i.e. in the unit of velocity. Numerical and experimental findings have been illustrated in this section.

5.3.1.1 Numerical observations

Figure 5.1(a) and Figure 5.1(b) show the flow vector diagram and phreatic surface of earthen dam without and with sheet pile respectively for non-seismic condition, as obtained from output of FLAC 2D. Similar observations has been made for all the cases. The figures indicate that presence of sheet pile is likely to save the downstream end from piping failure since water is flowing along sheet pile without affecting the downstream end much.

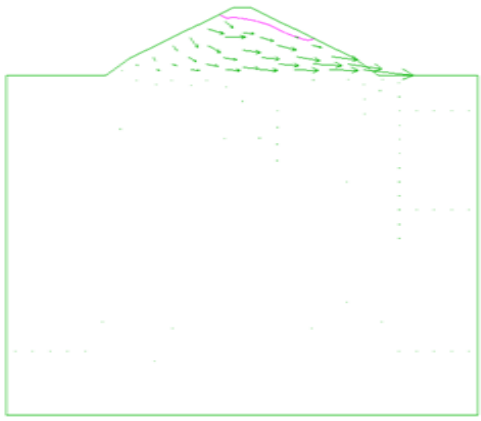

Figure 5.1(a): Fluid flow vector of embankment with-out sheet pile (OBTAINED FROM FLAC2D)

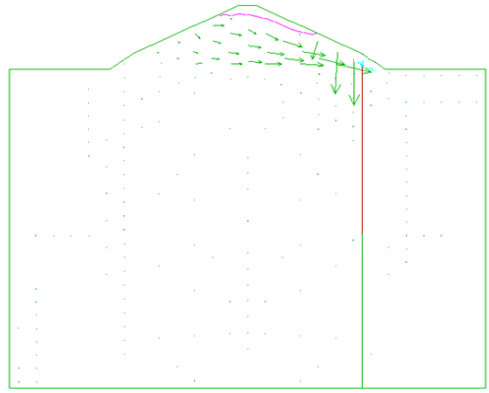

Figure 5.1(b): Fluid flow vector of embankment with sheet pile condition (OBTAINED FROM FLAC2D)

As the head difference increases, the magnitude of pore fluid velocity increases especially around the tip of the sheet pile and it also has been observed that fluid flow velocity is maximum around the sheet pile wall and the velocity decreases further away from the sheet pile.

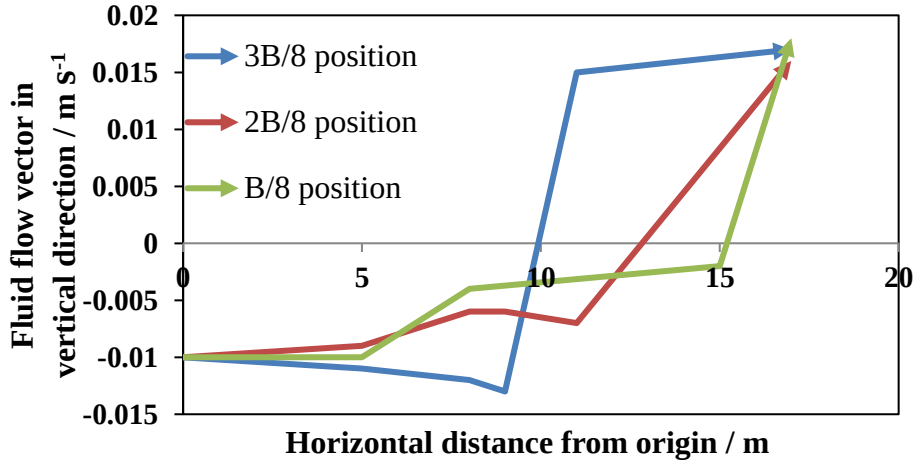

Fig. 5.2(a): Typical graph showing fluid flow vector in vertical direction for different sheet pile position (5m from the top)

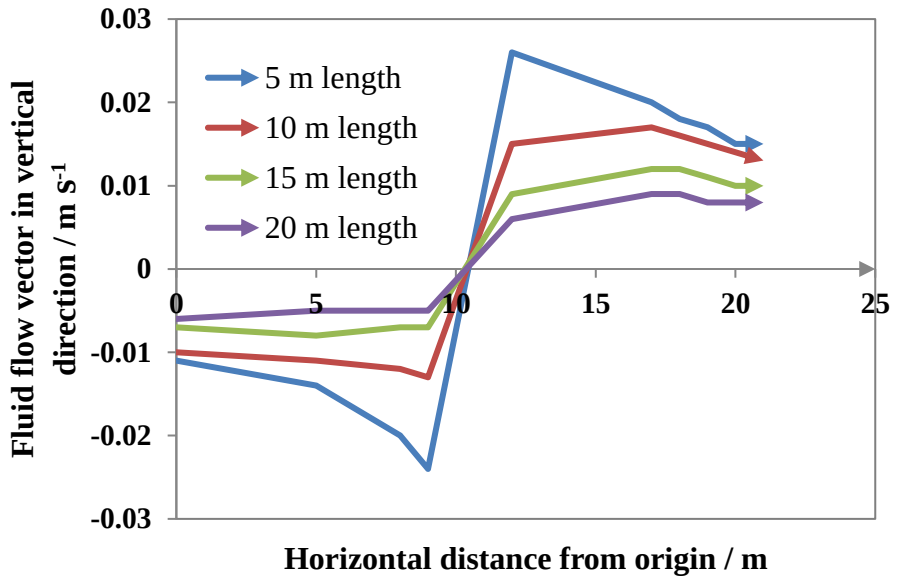

Fig. 5.2(b): Fluid flow vector in vertical direction for different sheet pile length at fixed position of 3*B*/8 (5m from the top).

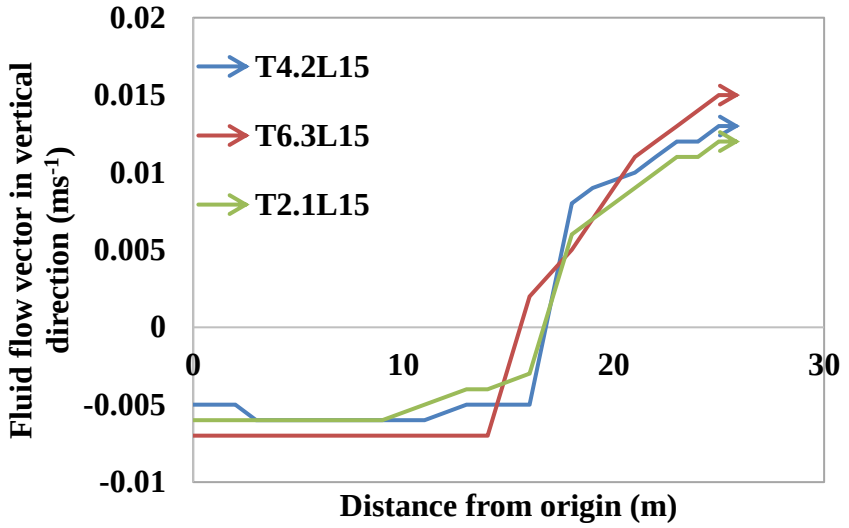

Fig. 5.2(c): Typical graph showing fluid flow vector in vertical direction for different sheet pile position (12m from the top)

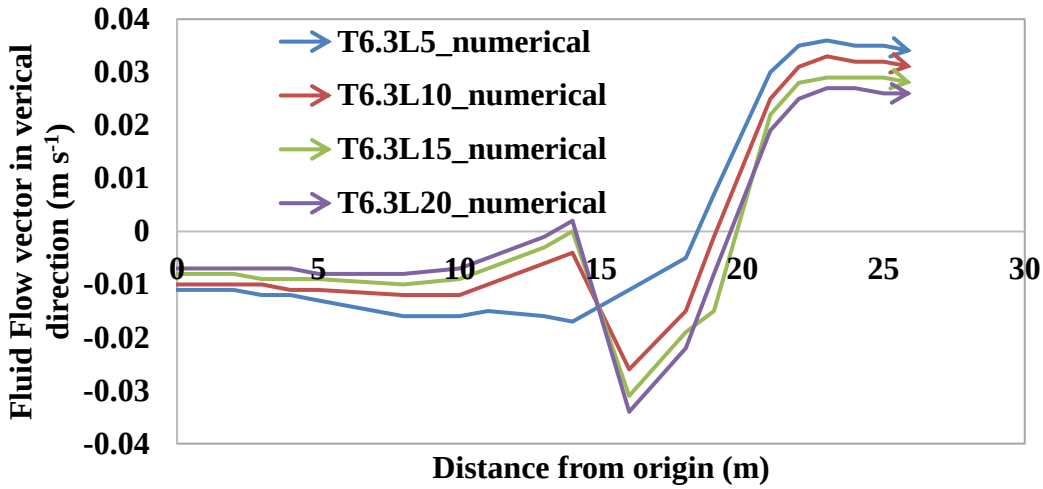

Fig. 5.2(d): Fluid flow vector in vertical direction for different sheet pile length at fixed position of 3*B*/8 (12 m from the top).

Figure 5.2(a) and Figure 5.2(b) present the graph of fluid flow vectors at a depth of 3m below the base of the dam i.e. 7m from the top for different positions of a typical 10m length sheet pile and for different length of sheet pile at a typical location of 3*B*/8 from downstream end respectively for non-seismic condition. Figure 5.2(c) and Figure 5.2(d) present the variation of of fluid flow vectors with distance at a depth of 8m below the base of the dam i.e. 12m from the top, for different positions of a typical 15m length sheet pile and for different lengths of sheet pile at a typical location of 3*B*/8 from downstream end respectively for non-seismic condition. Similar variation has been observed for all the cases under static condition. It is observed from Figure 5.2(a) and Figure 5.2 (c) that maximum flow vector occurs at sheet pile position. This maximum value is highest for 3*B*/8 position of sheet pile from downstream end. For each case the flow vector is increased at the sheet pile position indicating vertical flow along sheet pile. Irrespective of length and position, negative flow vector occurs at the upstream side of sheet pile. The negative signs arise due to fluid flow in the downward direction along the length of sheet pile. At the position of sheet pile there is an abrupt jump of fluid flow vector. At the upstream side of sheet pile, fluid flow vector decreases along the length and at the downstream side of sheet pile it increases with length. From Figure 5.2(b) and Figure 5.2 (d) it is observed that for the same position of sheet pile in case of different sheet pile lengths fluid flow vector is maximum for 5 meter length than those for 10m, 15m, 20m length. It is observed that the slope of fluid flow vector graph at sheet pile position at 7m from the top of the dam is 50% more than 12m from the top of the dam. As sheet pile length increases flow vector reduces indicating quantity of fluid flow is less when sheet pile length is more. Due to this fact the path traced by the percolating water *i.e.* creep length increases and thereby hydraulic gradient is reduced. Hydraulic gradient always decreases in the direction of *water* flow. It has also been observed from figure 5.2 (c) that decrease of fluid flow vector for 20m length of sheet pile on the downstream end is 30% less compared to 5m length of sheet pile and 13% less compared to 15m length of sheet pile at 3*B*/8 position. It has

also been observed that fluid flow vector on the downstream end is 13.33% less in case of *B*/8 position compared to 2*B*/8 position and 3*B*/8 position and on an average for another position. It has been also been observed that at 12m from the top of the dam the fluid flow vector for all the cases on the upstream side is on an average 40 % less compared to 7m from the top of the dam. At the position and surrounding zone of sheet pile towards downstream end sharpness of fluid flow vector is more at 7m from the top of dam for all cases compared to 12m from the top of the dam. In this way the fluid flow vector decreases as sheet pile moves towards downstream end and it is maximum for least length.

5.3.1.2 Comparison of experimental observations and numerical study for steady state

In the experimental investigation by centrifuge modelling the visualization of magnitudes and values the x-y components of velocity for the flow different points, obtained with the help of PIV analysis, at different times have been estimated and plotted in matrix form. From the PIV analysis in the present study fluid flow vector in the vertical direction have been obtained.

It is further to mention that variation of fluid flow vector obtained under static condition is found to be similar as obtained from both experimental and numerical results and this is clear from the graphs shown in figure 5.15(a) to 5.15(b).

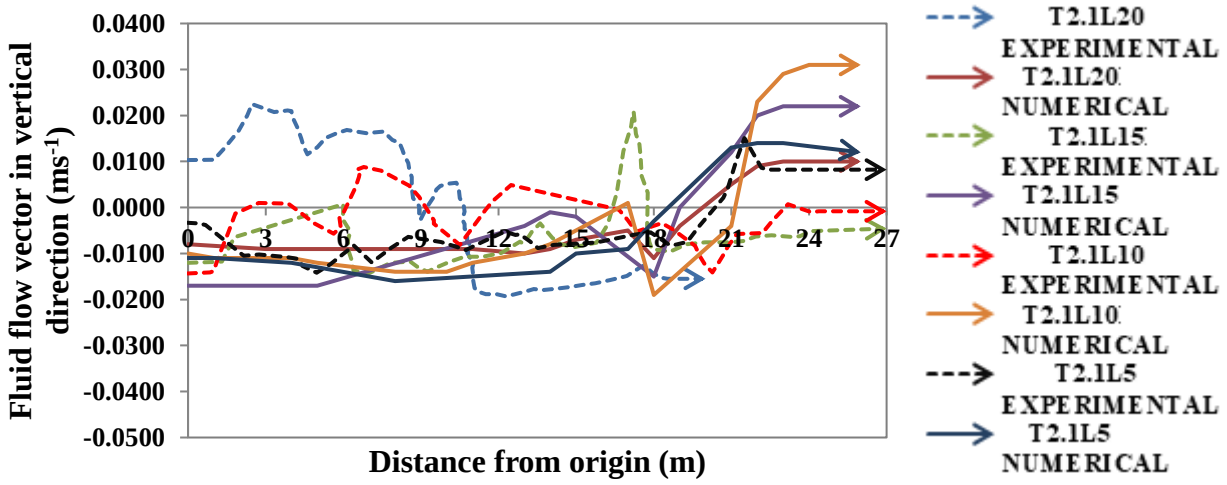

Fig 5.3(a)Result From experimental investigation and numerical analysis for *B*/8 position at 7 m from the top of dam

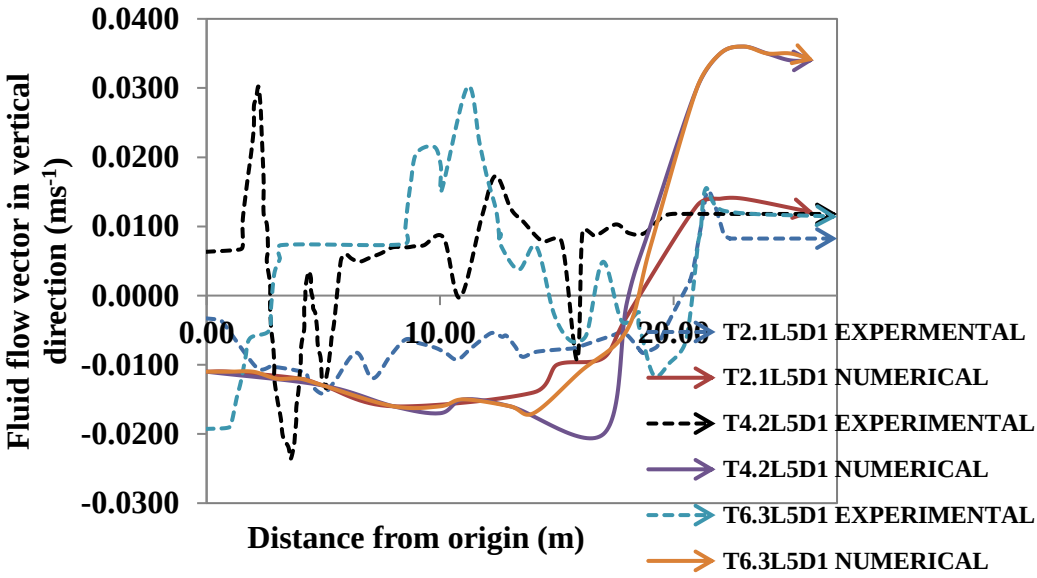

Fig 5.3(b) Result From experimental investigation and numerical analysis for *5m* length of sheet pile at 7m from the top of dam

The trend of variation of fluid flow vector appears to be similar as obtained from experimental and numerical studies with minor variation with initial higher experimental values, which lowers towards downstream.

5.3.1.3 Seismic condition under steady state

For seismic conditions the graphs for fluid flow vector have been presented in Figure 5.4 (a) for *B*/8 position 15m length of sheet pile at 7m from the top of the dam. Figure 5.4 (b) and Figure 5.4 (c) presents fluid flow vector for 3*B*/8 position at 15m length of sheet pile for 7m from the top of the dam and 12m from the top of the dam respectively.

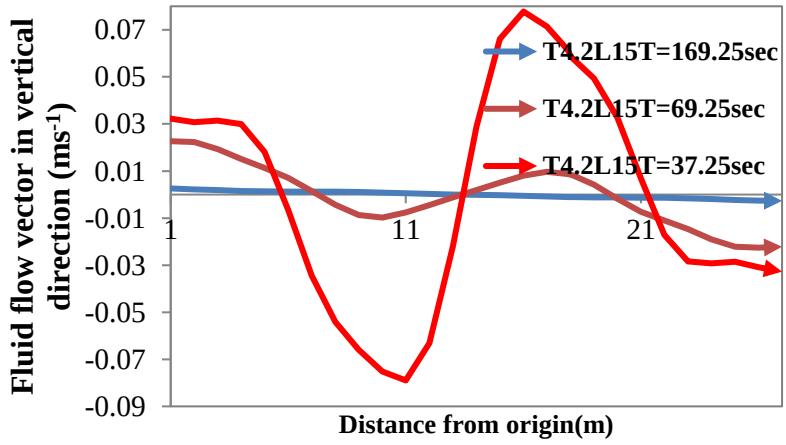

Fig 5.4 (a): Fluid flow vector in vertical direction of 15 m length for *B*/8 position from the downstream end for acceleration time= 37.25 sec, 69.25 sec, 169.25 sec. (at 7m from the top)

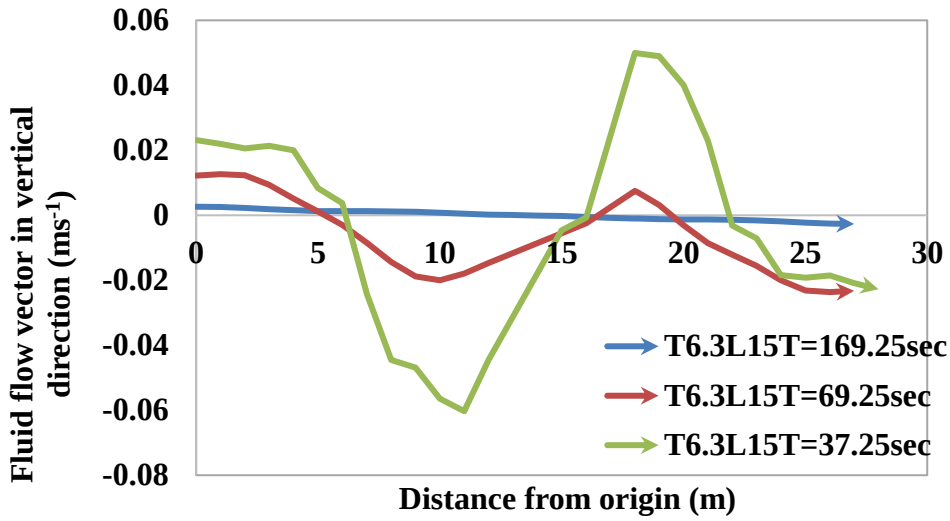

Fig 5.4 (b): Fluid flow vector in vertical direction of 15 m length for 3*B*/8 position from the downstream end for acceleration time= 37.25 sec, 69.25 sec, 169.25 sec. (at 7 m from the top)

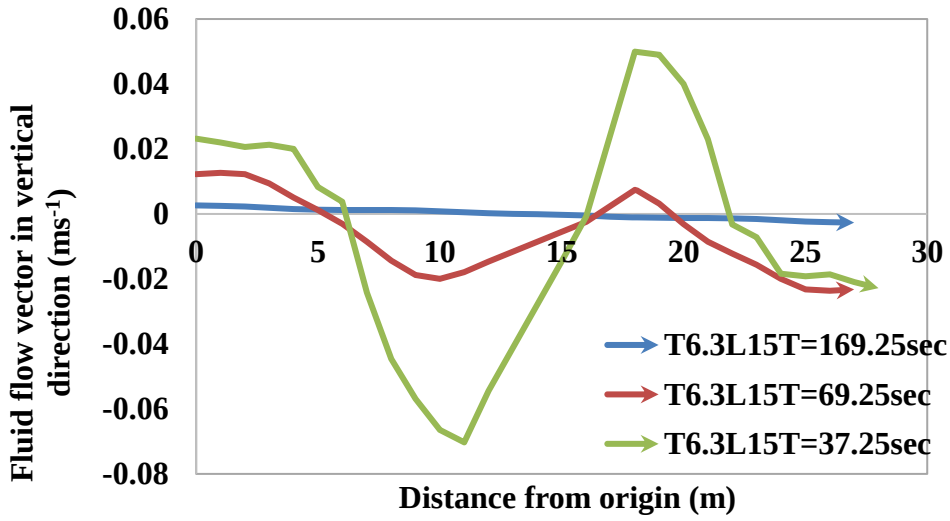

Fig 5.4 (c): Fluid flow vector in vertical direction of 15 m length for 3*B*/8 position from the downstream end for acceleration time= 37.25 sec, 69.25 sec, 169.25 sec. (at 12 m from the top)

It has been observed from the figures that variation of fluid flow vector appears to be irregular for seismic conditions with and without sheet piles. This may be due to variation of seismic force with time. It has further been observed that for any time, variation of fluid flow vector follows the trend for that under static condition. It has been clearly observed that for peak acceleration (at time=37.25 seconds) the magnitude of fluid flow vector in both upstream and downstream side is maximum. In addition to this it has been observed that at

the end of seismic duration (time=169.25 seconds) the magnitude of fluid flow vector for both upstream and downstream side is less compared to that for peak acceleration period. Fluid flow vector is found to fall at sheet pile position for seismic condition when the position is towards downstream end. But when it is mainly towards upstream end it is found to similar to that for static condition. Thus, sheet pile is more effective towards downstream end under seismic condition since it is resisting upward movement of water beyond sheet pile position probably due to more movement of sheet pile under seismic condition. Similar pattern of variation of fluid flow vector has been observed for all the positions of sheet pile and that also for different lengths.

5.3.2 TRANSIENT STATE

5.3.2.1 Numerical study under transient state

The fluid flow vector graphs have been plotted for different time intervals for rise up and drawdown along a horizontal direction at 7m and 12m depths, which have been shown in figure 5.5(a) to 5.7(o) for different sheet pile lengths and positions.

5.3.2.1.1 At 7m from the top of the dam

Figures 5.5(a) to 5.5(b) shows the fluid flow vector for 3*B*/8 position for sheet pile length of 10m and 15m. Figure 5.5(c) to 5.5(d) present fluid flow vector for 2*B*/8 position for sheet pile length of 10m and15m. Figures 5.5(e) to 5.5(f) show fluid flow vector for *B*/8 position respectively for sheet pile lengths of 10m and 15m.

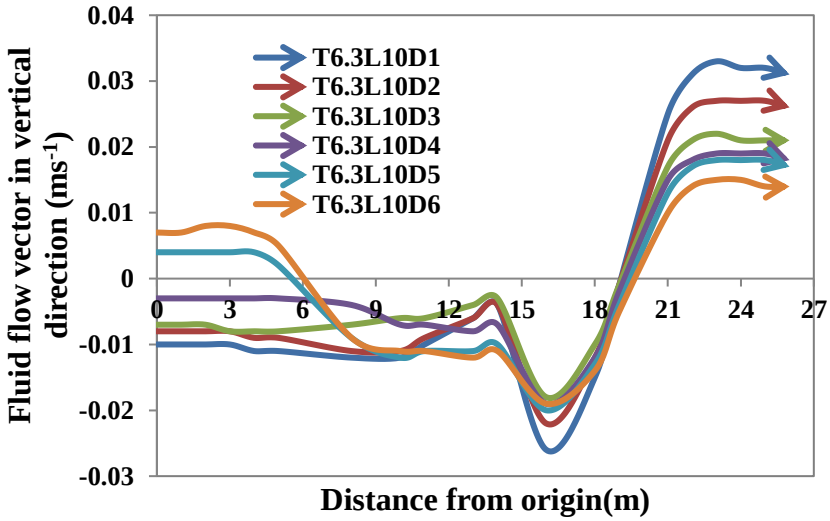

Fig 5.5(a): Fluid flow vector in vertical direction for 10 m long sheet pile with position at 3*B*/8 from the downstream end

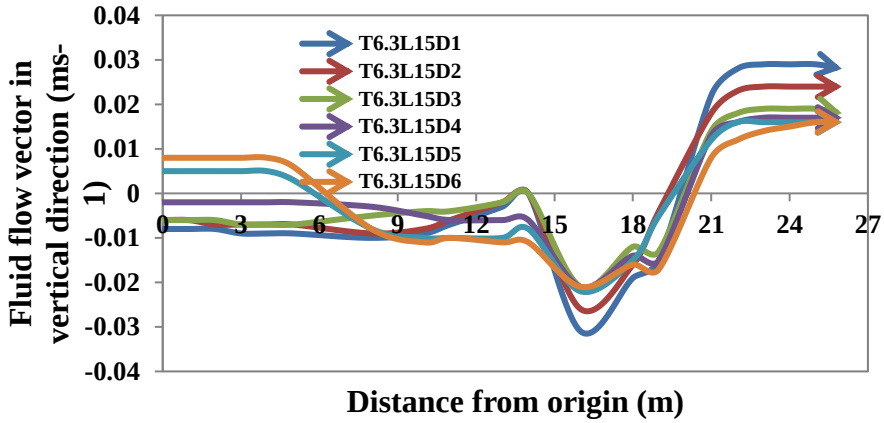

Fig 5.5(b): Fluid flow vector in vertical direction for 15 m long sheet pile with position at 3*B*/8 from the downstream end

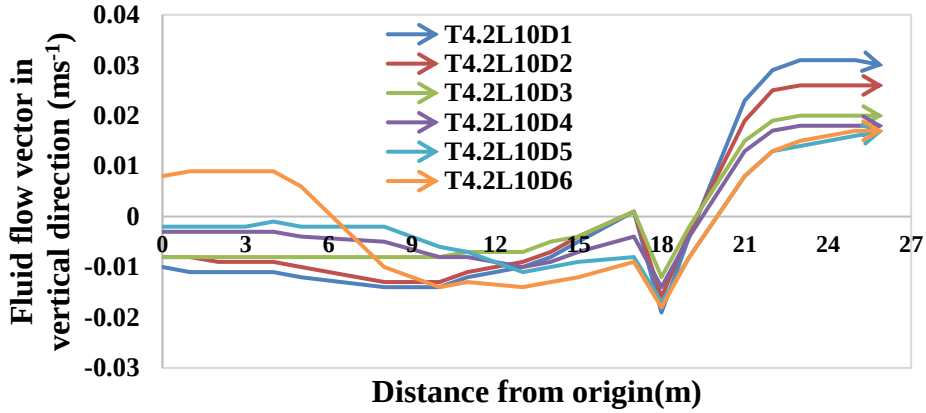

Fig 5.5(c): Fluid flow vector in vertical direction for 10 m long sheet pile with position at 2*B*/8 from the downstream end

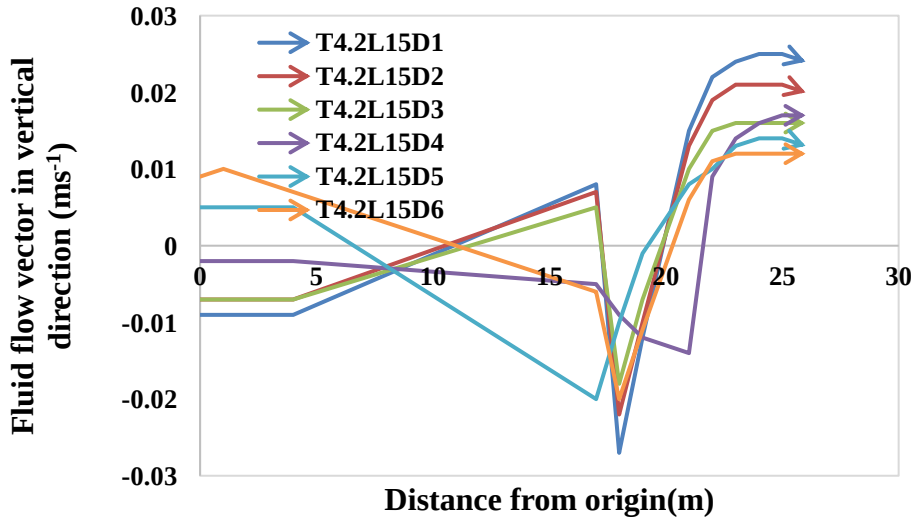

Fig 5.5(d): Fluid flow vector in vertical direction for 15 m long sheet pile with position at 2*B*/8 from the downstream end

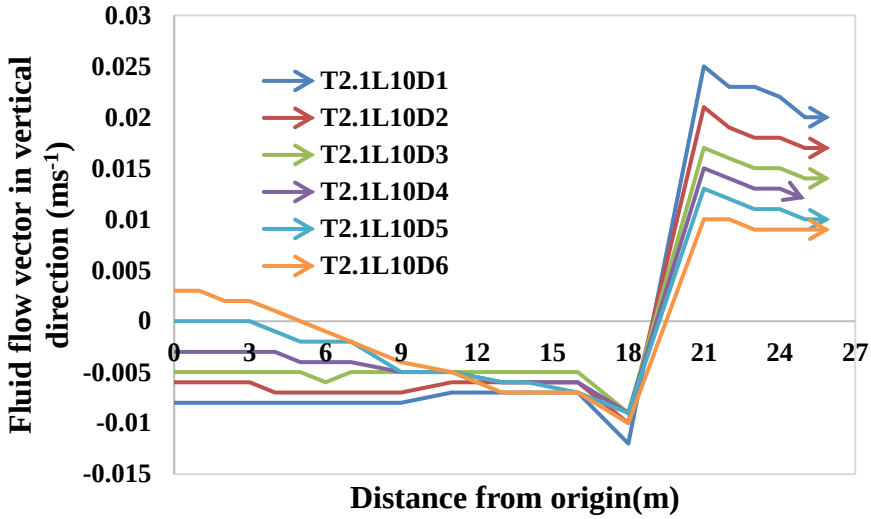

Fig 5.5(e): Fluid flow vector in vertical direction for 10 m long sheet pile with position at *B*/8 from the downstream end

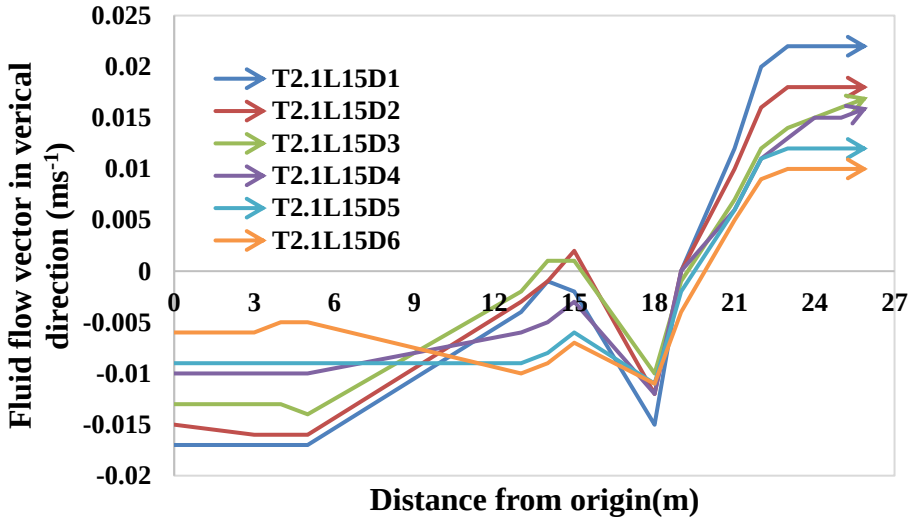

Fig 5.5(f): Fluid flow vector in vertical direction for 15 m long sheet pile with position at *B*/8 from the downstream end

It has been observed from the figures that with progress of time under rise- up condition, with increase of upstream water level fluid flow vector is higher indicating downward direction of flow on upstream side. Under drawdown condition, direction of fluid flow vector tends to move in upward direction. Beyond sheet pile the fluid flow vector increases in magnitude by approximately 5% in upward direction with increase of water level under rise up condition. Under drawdown condition it decreases in magnitude in downward direction. This reduction of variation of fluid flow vector is due to change of flownet pattern.

The comparison of fluid flow vector for full rise up and drawdown condition in respect of sheet pile position and length has been presented in this section. Figures 5.6(a) to Figure 5.6

(h) present numerical results for different sheet pile positions for 5m, 10m, 15m and 20m long sheet pile respectively under full rise up and full drawdown conditions. Figures 5.6(i) to Figure 5.6 (k) present numerical results at 3*B*/8 position from downstream end for 5m, 10m, 15m and 20m long sheet pile under rise up and drawdown conditions respectively. Figures 5.6(l) to Figure 5.6 (n) present numerical results at 2*B*/8 position from downstream end for 5m, 10m, 15m and 20m long sheet pile under rise up and drawdown conditions respectively. Figures 5.6(o) to Figure 5.6 (q) present numerical results at *B*/8 position from downstream end for 5m, 10m, 15m and 20m long sheet pile under rise up and drawdown conditions respectively.

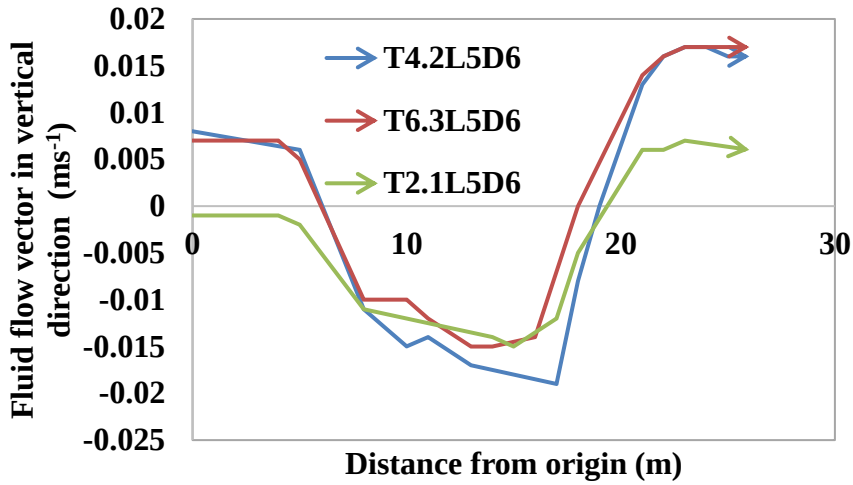

Fig 5.6(a): Fluid flow vector in vertical direction for 5m long sheet pile at 7m from the top under full drawdown condition

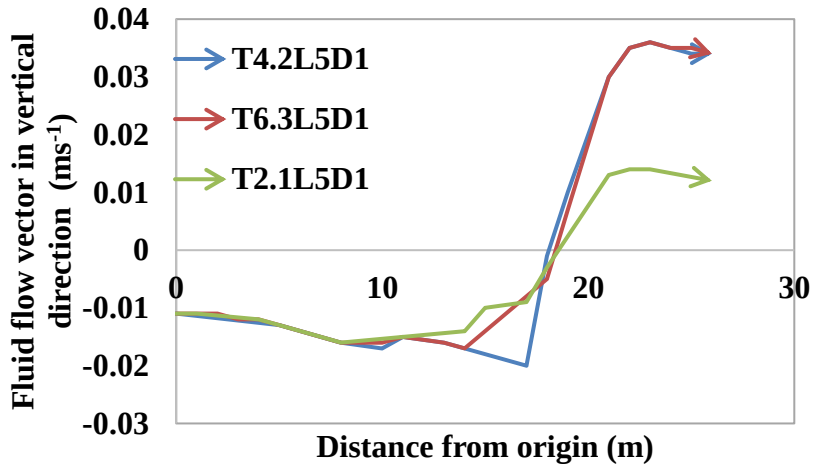

Fig 5.6(b): Fluid flow vector in vertical direction for 5m long sheet pile at 7m from the top under full rise up condition

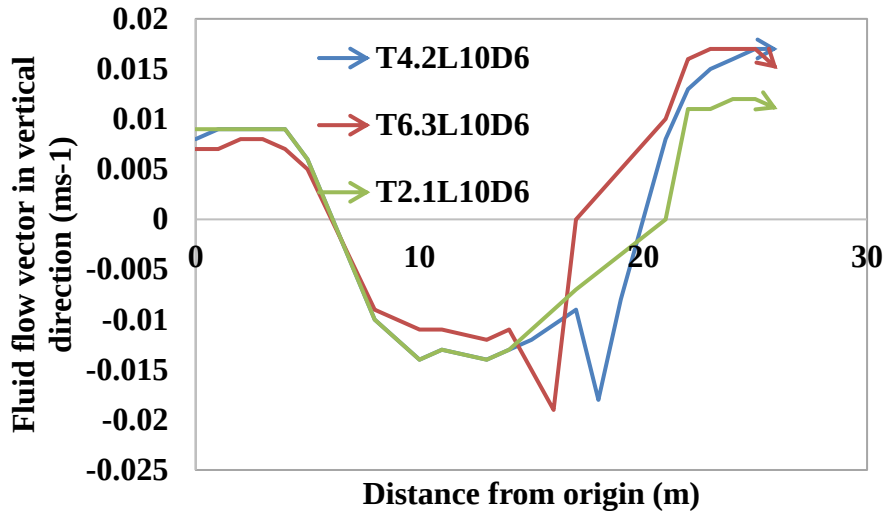

Fig 5.6(c): Fluid flow vector in vertical direction for 10m long sheet pile at 7m from the top under full drawdown condition

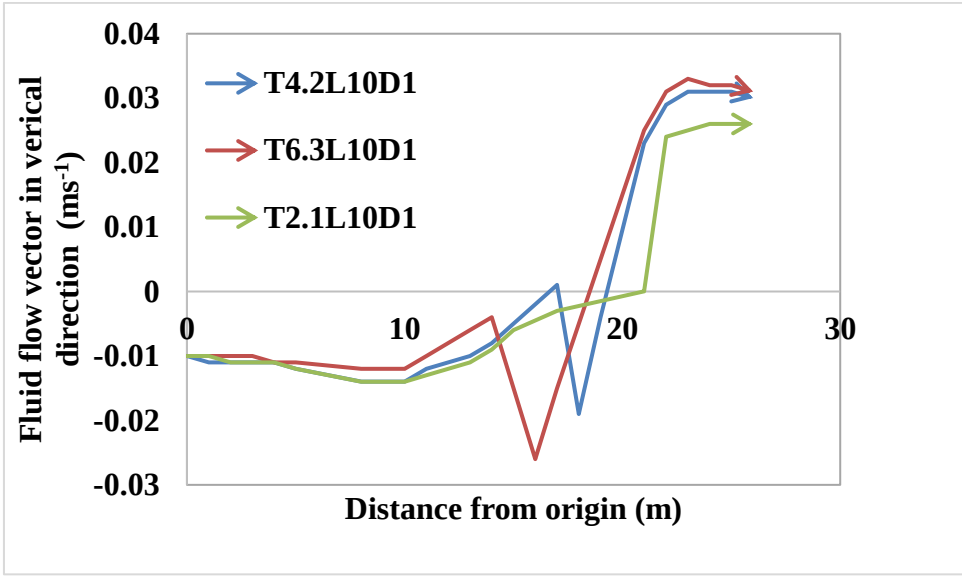

Fig 5.6(d): Fluid flow vector in vertical direction for 10m long sheet pile at 7m from the top under full rise up condition

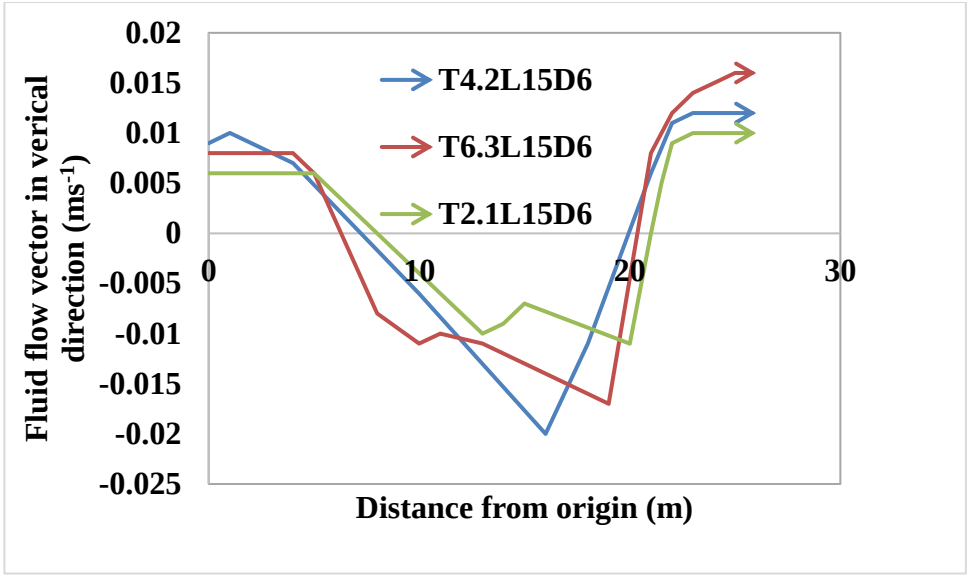

Fig 5.6(e): Fluid flow vector in vertical direction for 15m long sheet pile at 7m from the top under drawdown condition

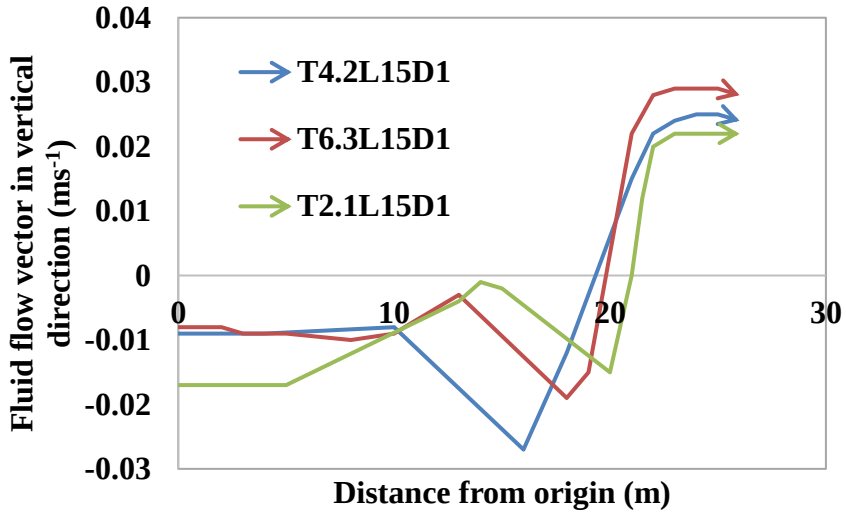

Fig 5.6(f): Fluid flow vector in vertical direction for 15m long sheet pile at 7m from the top under rise up condition

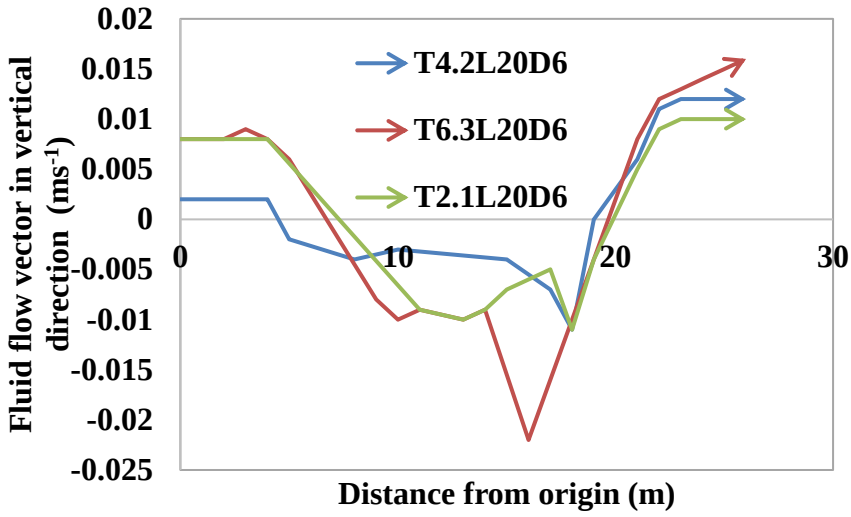

Fig 5.6(g): Fluid flow vector in vertical direction for 20m long sheet pile at 7m from the top under drawdown condition

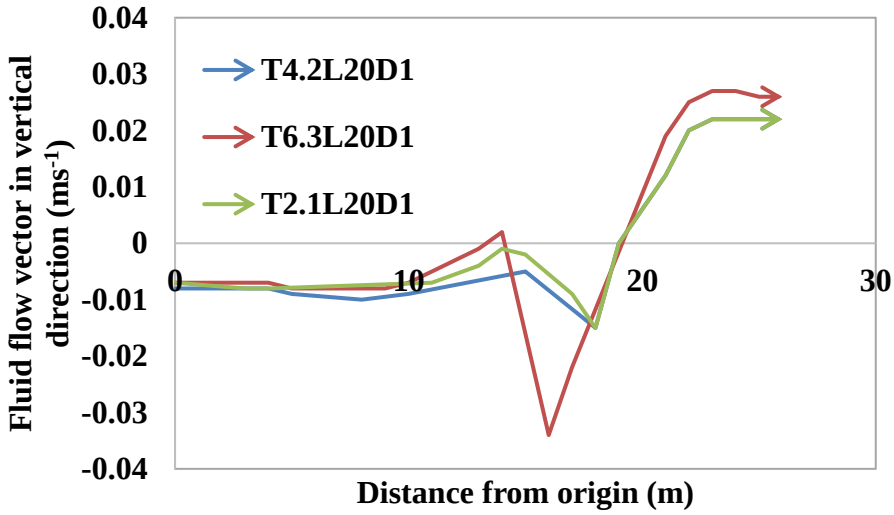

Fig 5.6(h): Fluid flow vector in vertical direction for 20m long sheet pile at 7m from the top under rise up condition

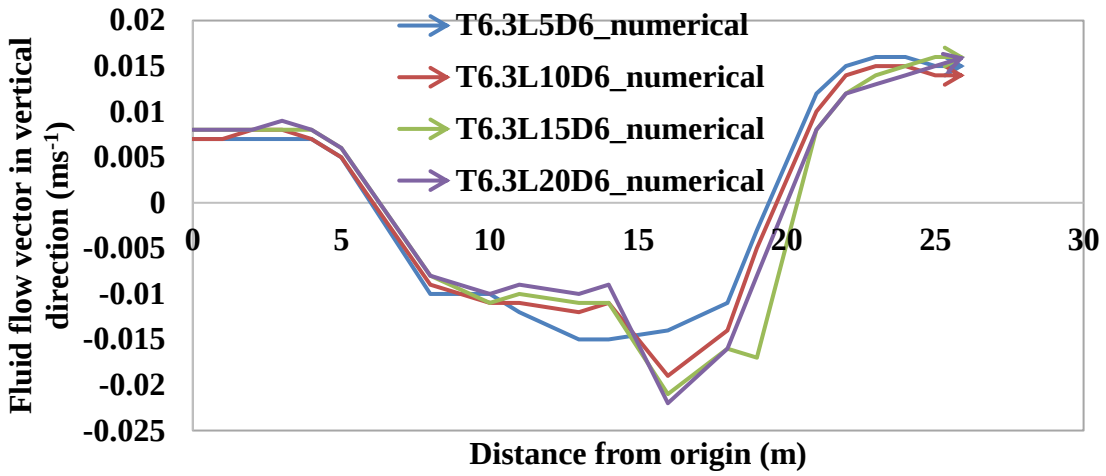

Fig 5.6(i): Fluid flow vector in vertical direction at 3*B*/8 position for different sheet pile length at 7m from the top under drawdown condition

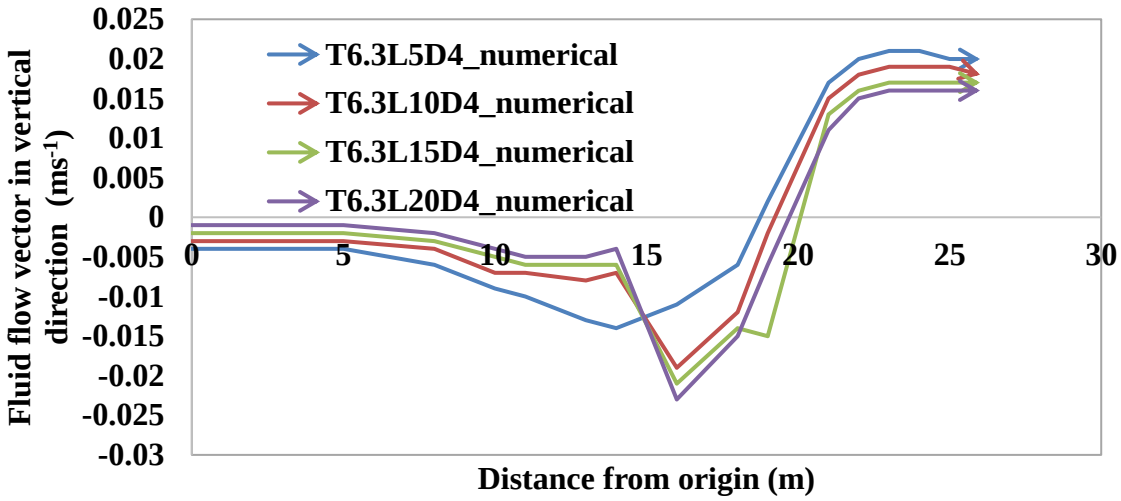

Fig 5.6(j): Fluid flow vector in vertical direction at 3*B*/8 position for different sheet pile length at 7m from the top under rise up condition

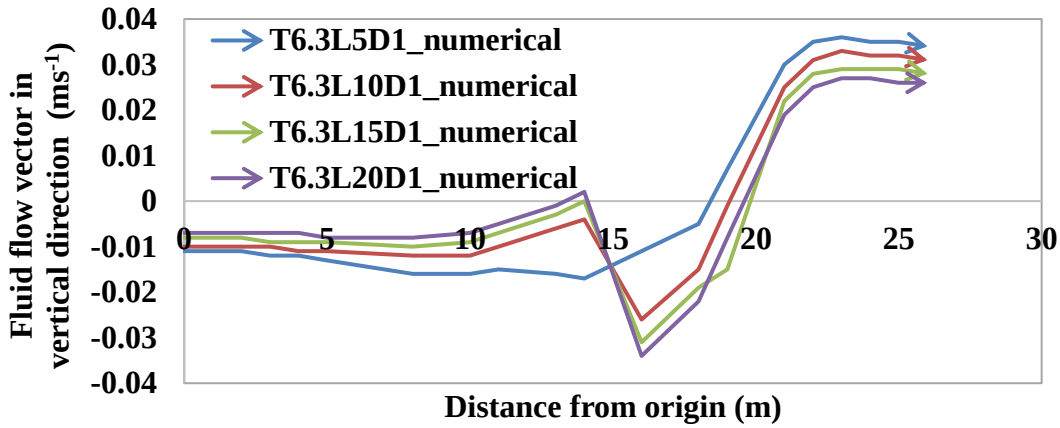

Fig 5.6(k): Fluid flow vector in vertical direction at 3*B*/8 position for different sheet pile length at 7m from the top under full rise up condition

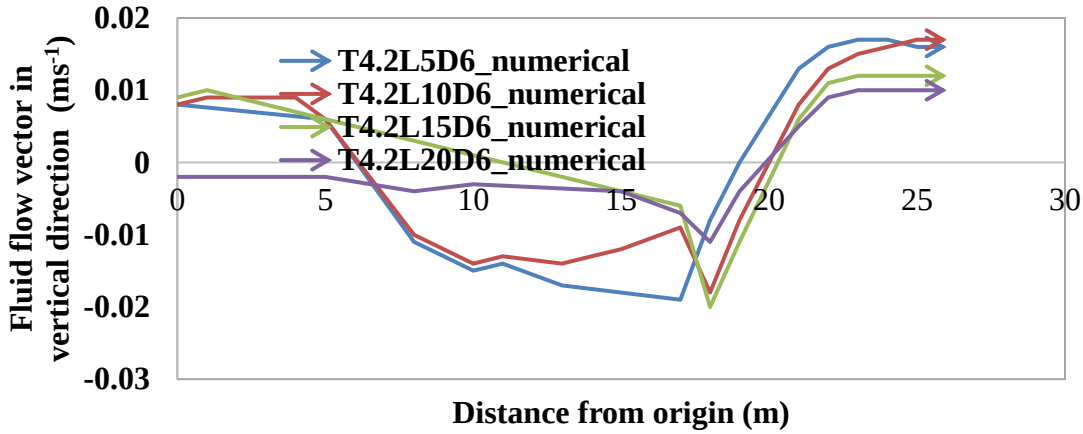

Fig 5.6(l): Fluid flow vector in vertical direction at 2*B*/8 position for different sheet pile length at 7m from the top under full drawdown condition

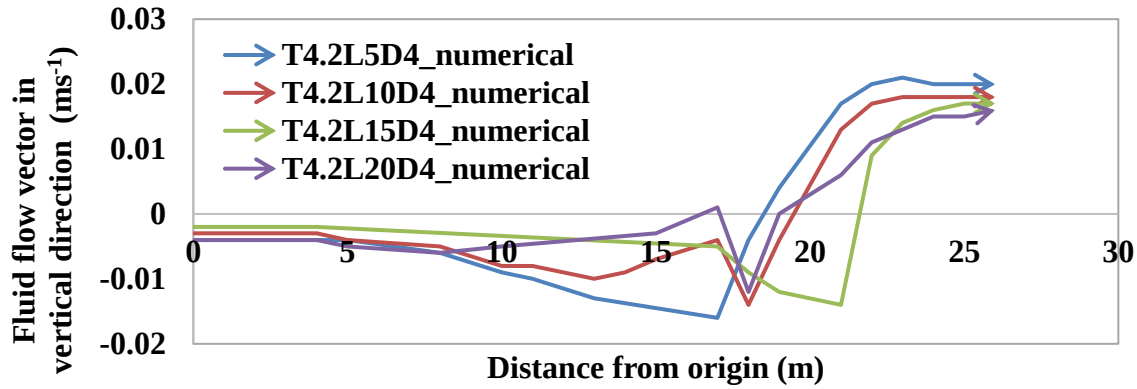

Fig 5.6(m): Fluid flow vector in vertical direction at 2*B*/8 position for different sheet pile length at 7m from the top under rise up condition

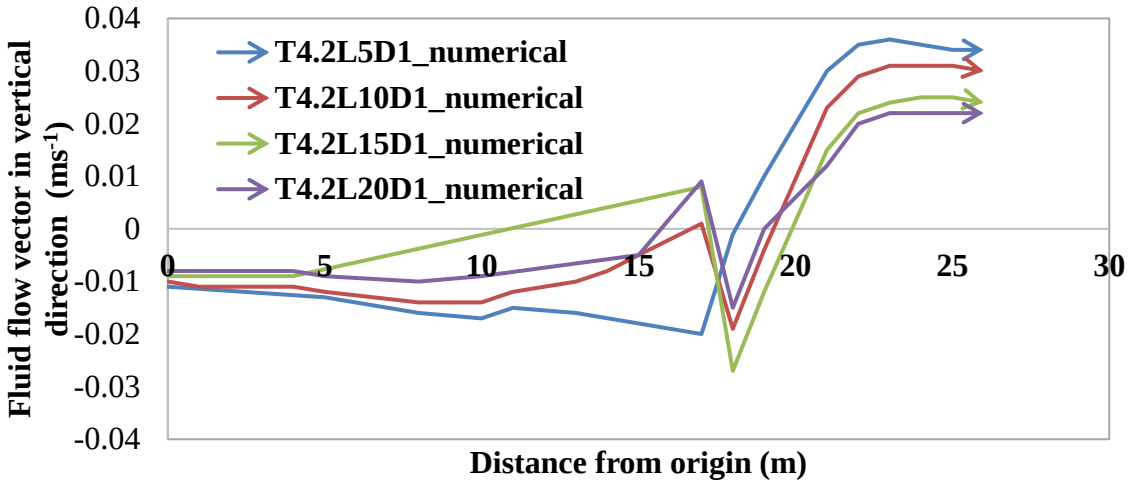

Fig 5.6(n): Fluid flow vector in vertical direction at 2*B*/8 position for different sheet pile length at 7m from the top under full rise up condition

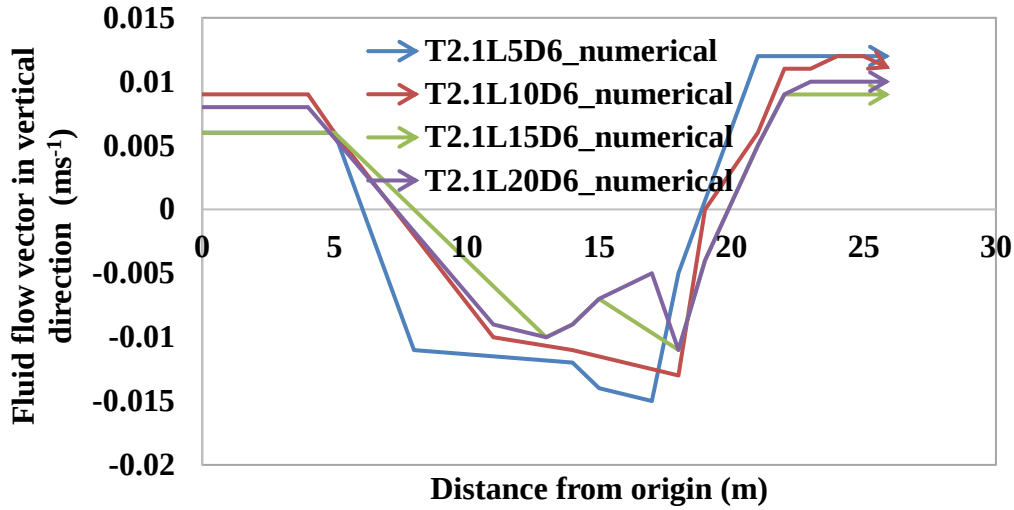

Fig 5.6(o): Fluid flow vector in vertical direction at *B*/8 position for different sheet pile length at 7m from the top under full drawdown condition

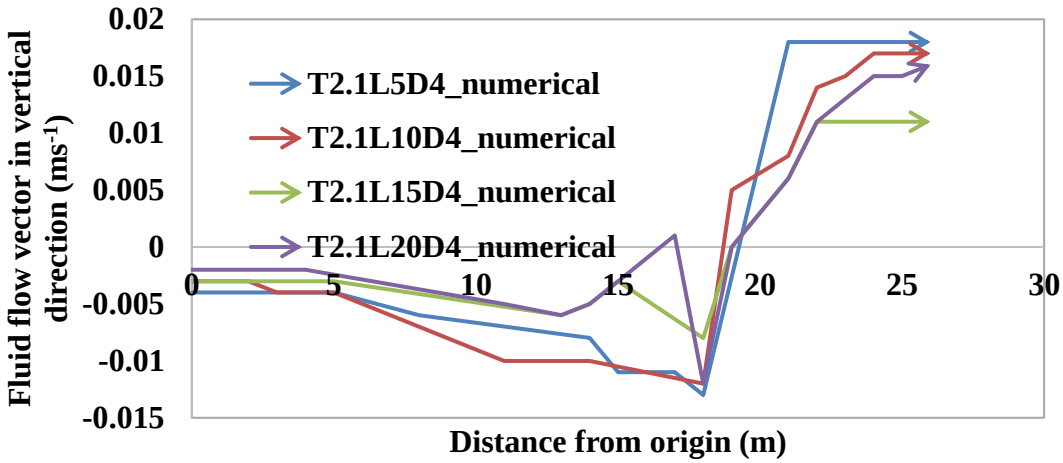

Fig 5.6(p): Fluid flow vector in vertical direction at *B*/8 position for different sheet pile length at 7m from the top under rise up condition

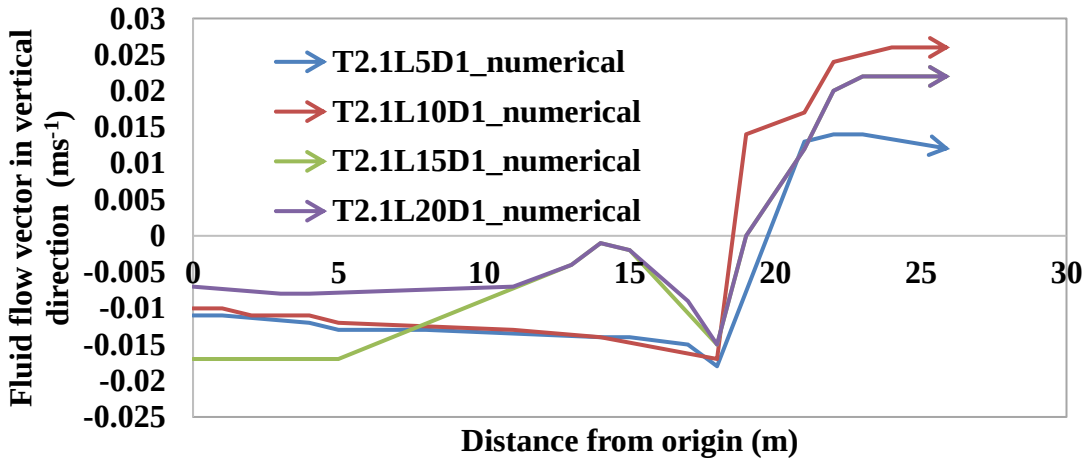

Fig 5.6(q): Fluid flow vector in vertical direction at *B*/8 position for different sheet pile length at 7m from the top under full rise up condition

5.3.2.1.2 At 12m from the top of the dam

The results have been observed at 12m from the top of the dam along its horizontal profile. Figures 5.7(a) to 5.7(d) present the fluid flow vector for 3B/8 position for sheet pile length of 5m, 10m,15m and 20m. Figures 5.7(e) to 5.7(h) present fluid flow vector for 2B/8 position for sheet pile length of 5m, 10m,15m and 20m. Figures 5.7(i) to 5.7(l) presents fluid flow vector for 2*B*/8 position for sheet pile length of 5m, 10m,15m and 20m. Figures 5.7(m) to 5.7(o) presents fluid flow vector for 2*B*/8 position for sheet pile length of 5m, 10m,15m and 20m under drawdown condition, rise up condition and full rise up condition.

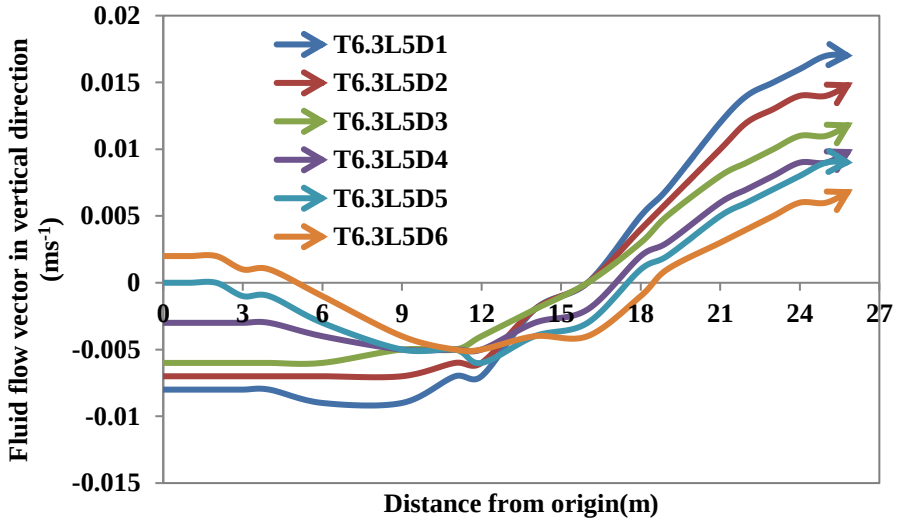

Fig 5.7(a): Fluid flow vector in vertical direction of 5 m length for 3*B*/8 position from the downstream end

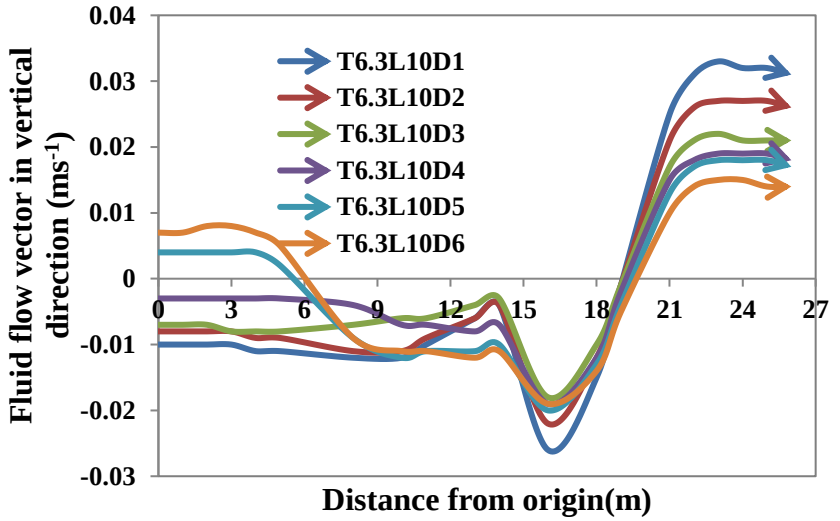

Fig 5.7(b): Fluid flow vector in vertical direction of 10 m length for 3*B*/8 position from the downstream end

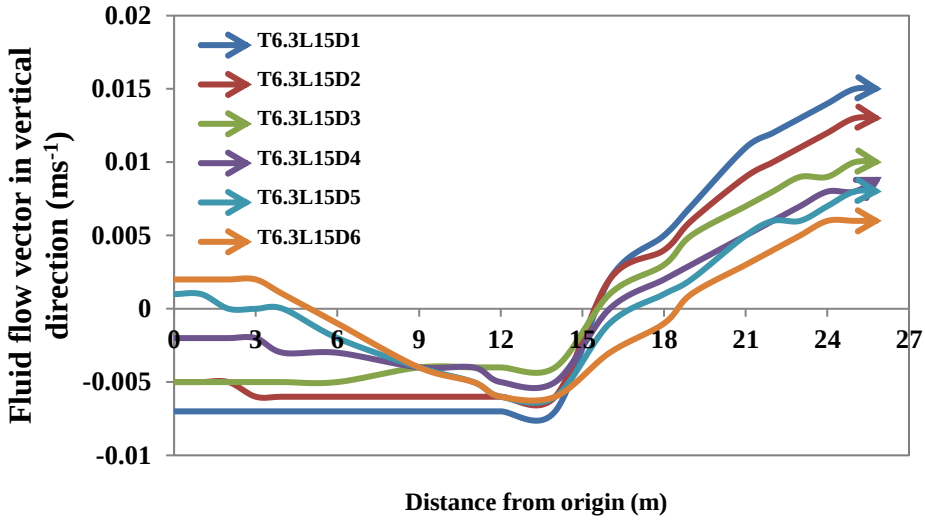

Fig 5.7(c): Fluid flow vector in vertical direction of 15 m length for 3*B*/8 position from the downstream end

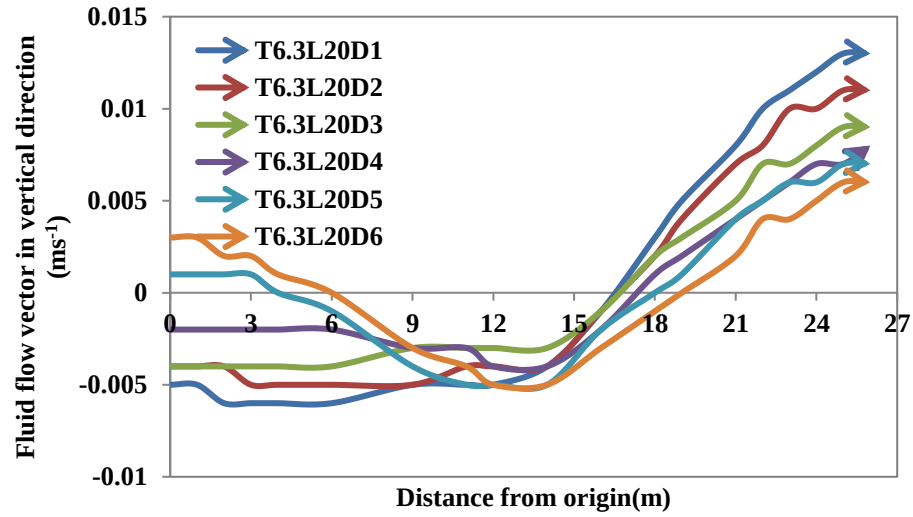

Fig 5.7(d): Fluid flow vector in vertical direction of 20 m length for 3*B*/8 position from the downstream end

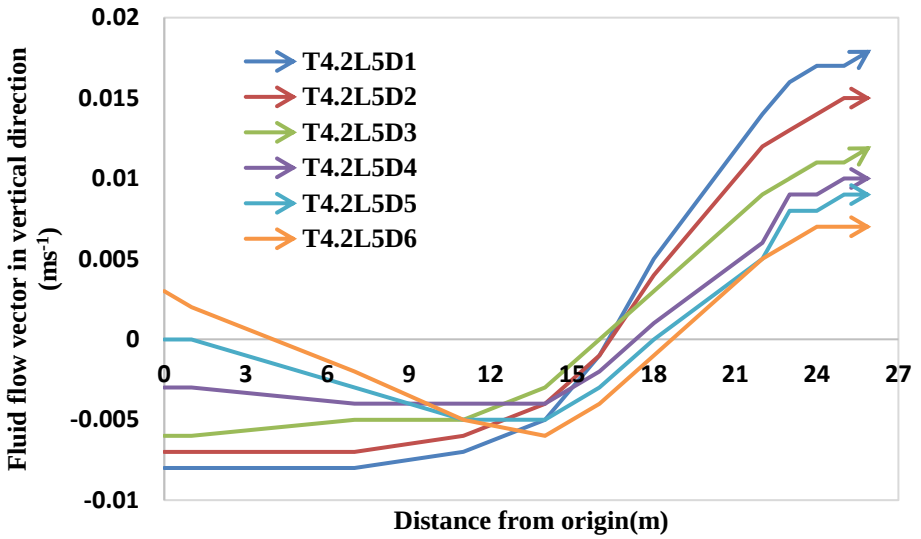

Fig 5.7(e): Fluid flow vector in vertical direction of 5 m length for 2*B*/8 position from the downstream end

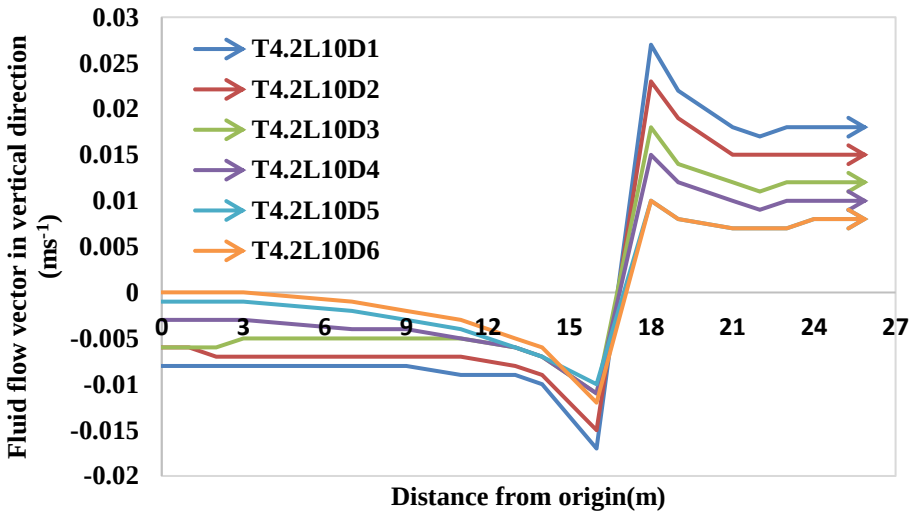

Fig 5.7(f): Fluid flow vector in vertical direction of 10 m length for 2*B*/8 position from the downstream end

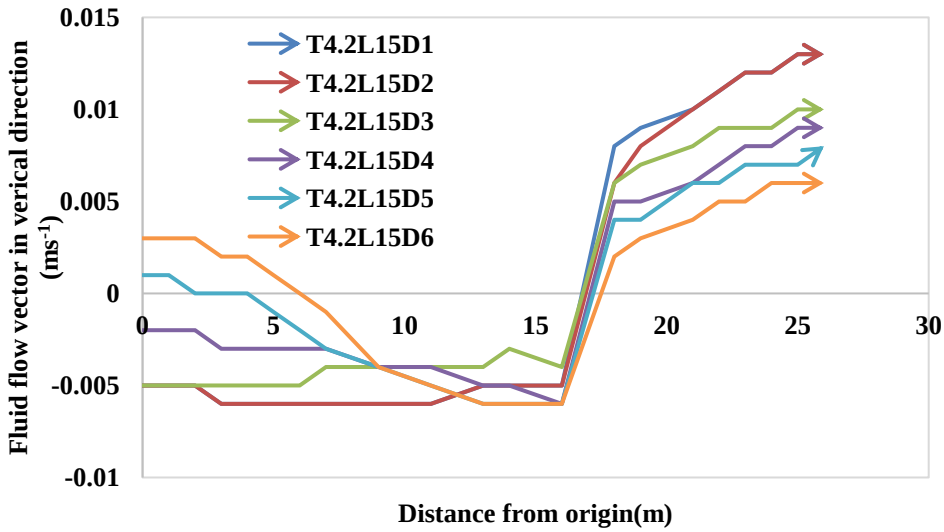

Fig 5.7(g): Fluid flow vector in vertical direction of 15 m length for 2*B*/8 position from the downstream end

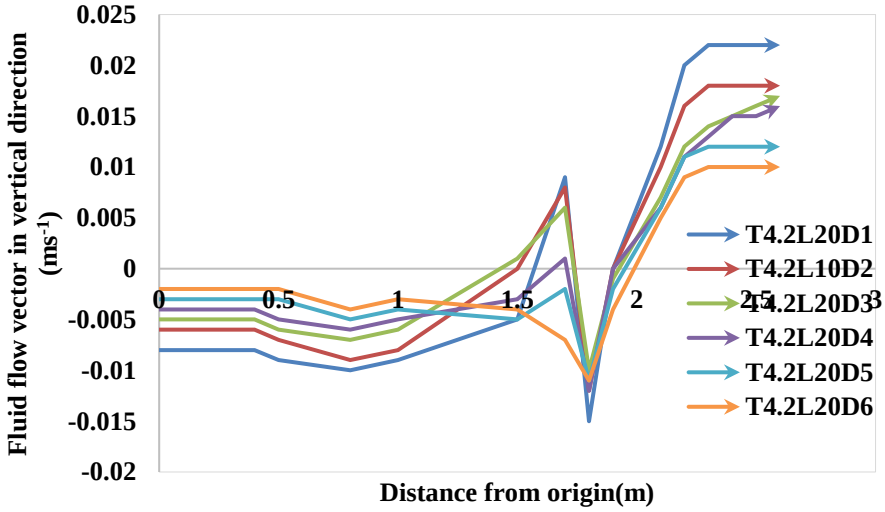

Fig 5.7(h): Fluid flow vector in vertical direction of 20 m length for 2*B*/8 position from the downstream end

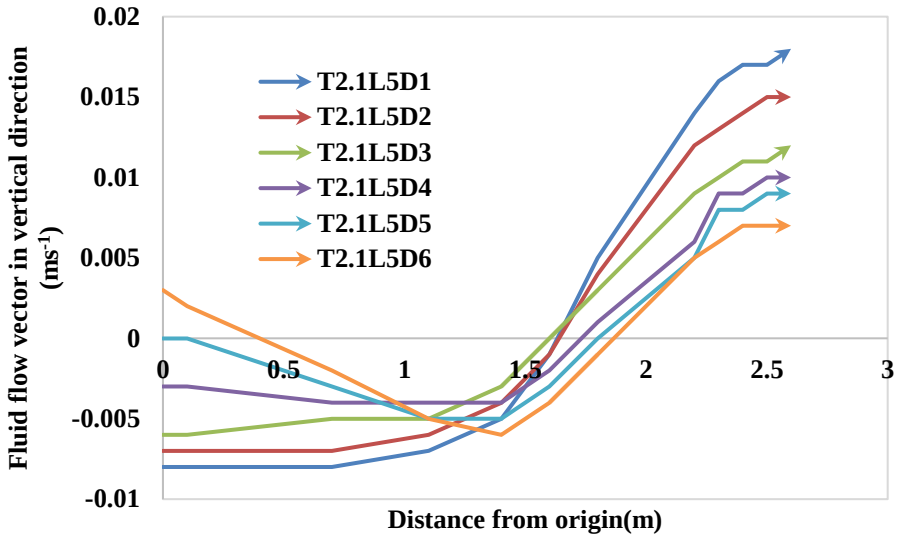

Fig 5.7(i): Fluid flow vector in vertical direction of 5 m length for *B*/8 position from the downstream end

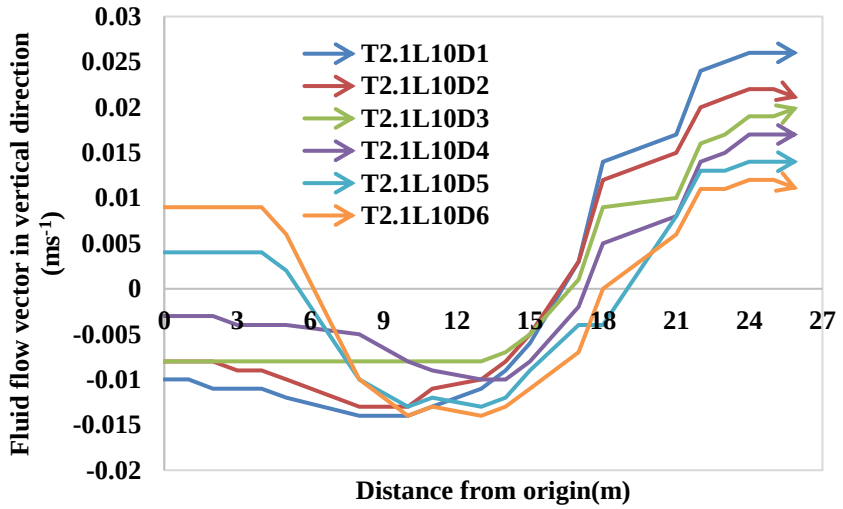

Fig 5.7(j): Fluid flow vector in vertical direction of 10 m length for *B*/8 position from the downstream end

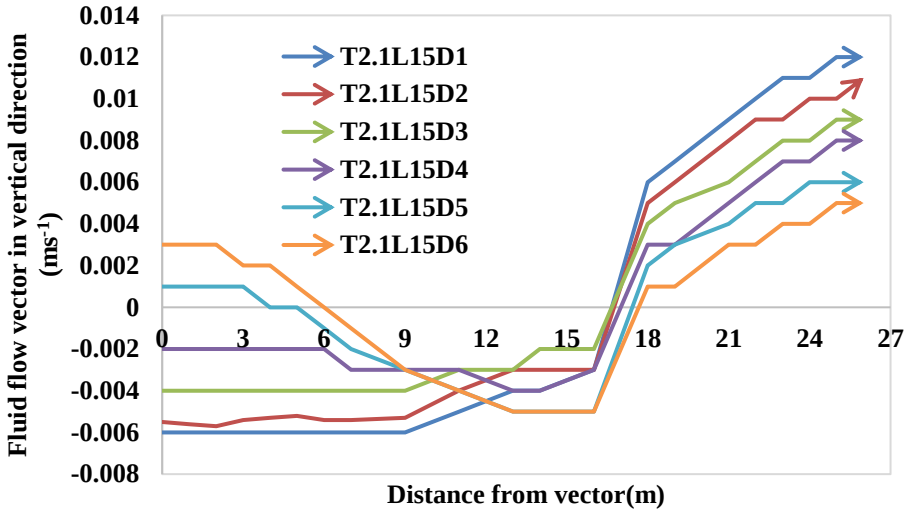

Fig 5.7(k): Fluid flow vector in vertical direction of 10 m length for *B*/8 position from the downstream end

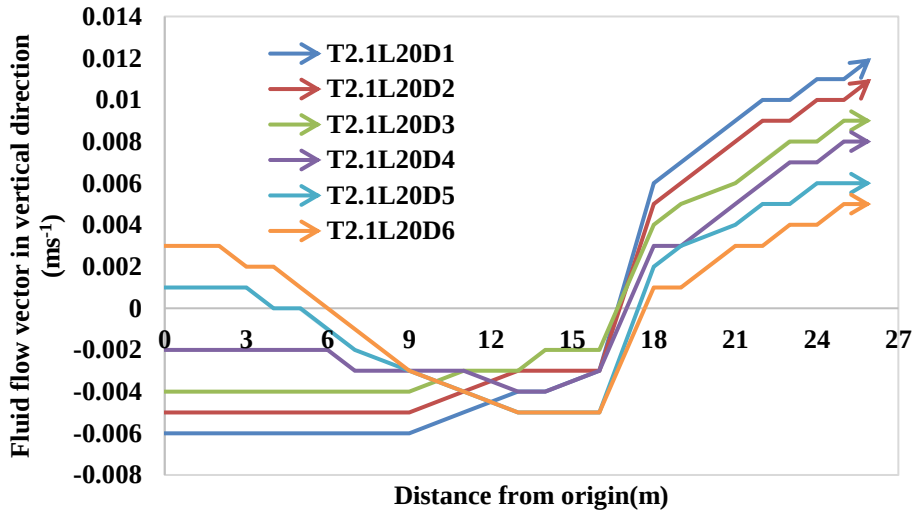

Fig 5.7(l): Fluid flow vector in vertical direction of 20 m length for *B*/8 position from the downstream end

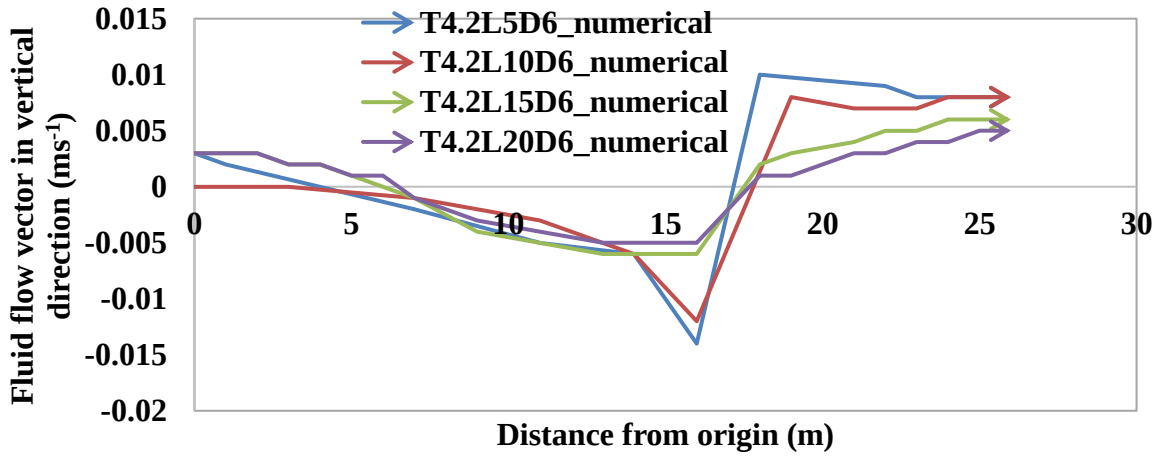

Fig 5.7(m): Fluid flow vector in vertical direction at 2*B*/8 position for different sheet pile length at 12m from the top under full drawdown condition

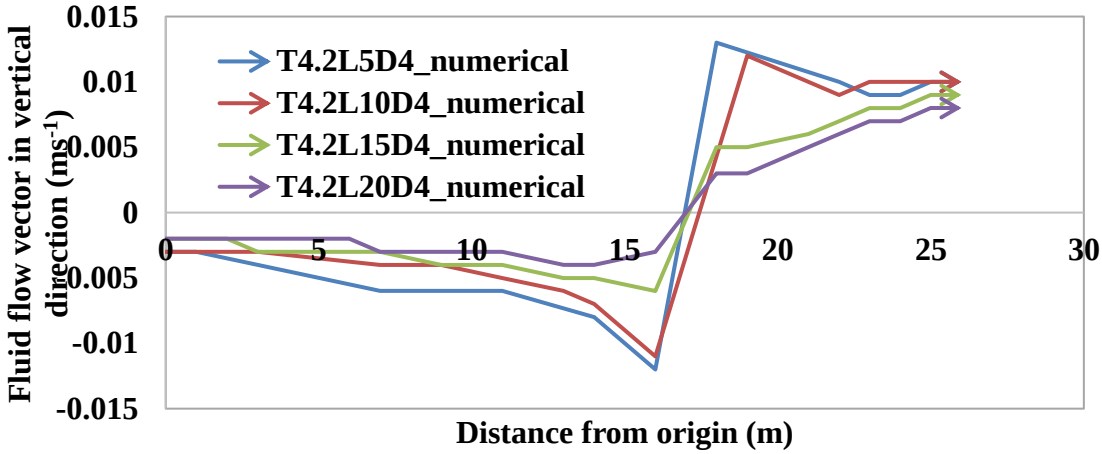

Fig 5.7(n): Fluid flow vector in vertical direction at 2*B*/8 position for different sheet pile length at 12m from the top under rise up condition

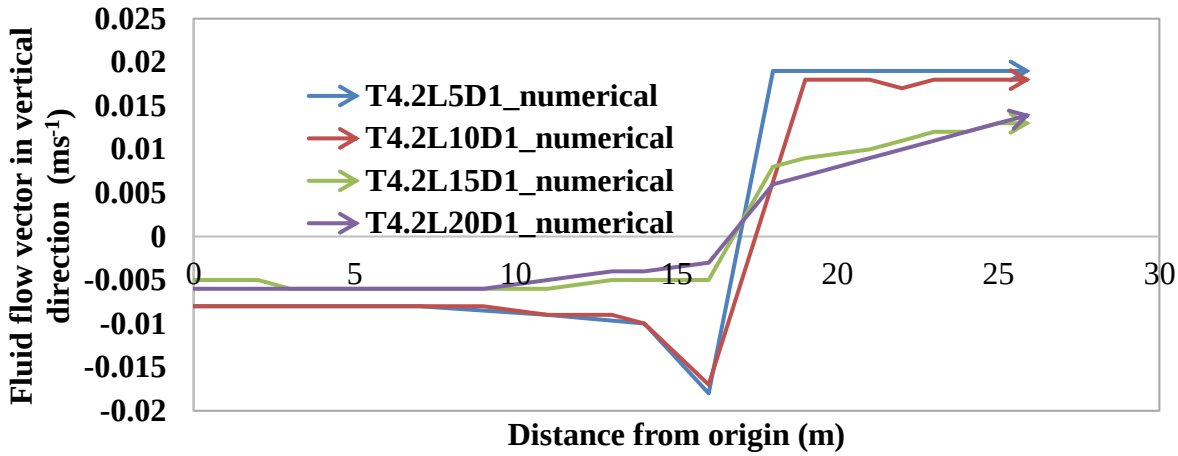

Fig 5.7(o): Fluid flow vector in vertical direction at 2*B*/8 position for different sheet pile length at 12m from the top under full rise up condition

However, for 12m depth with progress of time under rise up condition with increase of upstream water level fluid flow vector is higher indicating downward direction of flow on upstream side. Under drawdown condition direction of fluid flow vector tends to more in upward direction. As observed for 12m depth in this case also beyond sheet pile the fluid flow vector increases in magnitude by approximate 5% in upward with increase of water level under rise up condition. Under drawdown condition it decreases in magnitude in downward direction. This reduction of variation of fluid flow vector is due to change of flownet pattern. This is due to the fact that with increase of depth below base of the dam fluid flow is less and it is going towards the boundary of zone of flow from reservoir through the soil having low hydraulic conductivity.

5.3.2.2 Comparison of numerical study and experimental observations under transient state

Figure 5.8(a) presents fluid flow vector of experimental and numerical observations for *B*/8 position of different sheet pile length. Figure 5.8(b) shows fluid flow vector of experimental and numerical observations for 2*B*/8 position of different sheet pile length. Figure 5.8(c) presents fluid flow vector of experimental and numerical observations for 3*B*/8 position of different sheet pile length. Figure 5.8(d) shows fluid flow vector of experimental and numerical observations for 5m long sheet pile different sheet pile position. Figure 5.8(e) presents fluid flow vector of experimental and numerical observations for 10m long sheet pile different sheet pile position. Figure 5.8(e) shows fluid flow vector of experimental and numerical observations for 15m long sheet pile different sheet pile positions. Figure 5.8(f) presents fluid flow vector of experimental and numerical observations for 20m long sheet pile for different sheet pile positions. Experimental and numerical values appear to agree to each other as has been observed from the figures 5.8(a) to 5.8(g). It is observed from the figures that the variation of fluid flow vector is following similar trend in cases of both experimental

and numerical results. However, the water flow beyond sheet pile is not being indicated by the experimental results. This occurs probably due to the fact that in the experimental set up soil beyond the sheet pile is not getting fully saturated due to the sheet pile barrier.

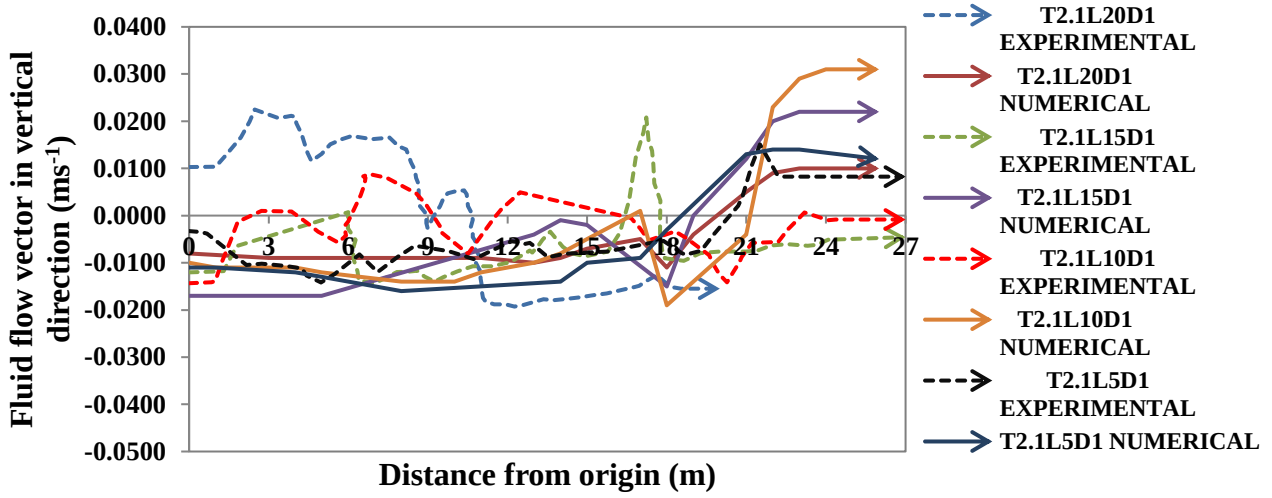

Fig 5.8(a): Fluid flow vector in vertical direction for *B*/8 position from the downstream end at 7m from the top (Numerical and experimental investigation)

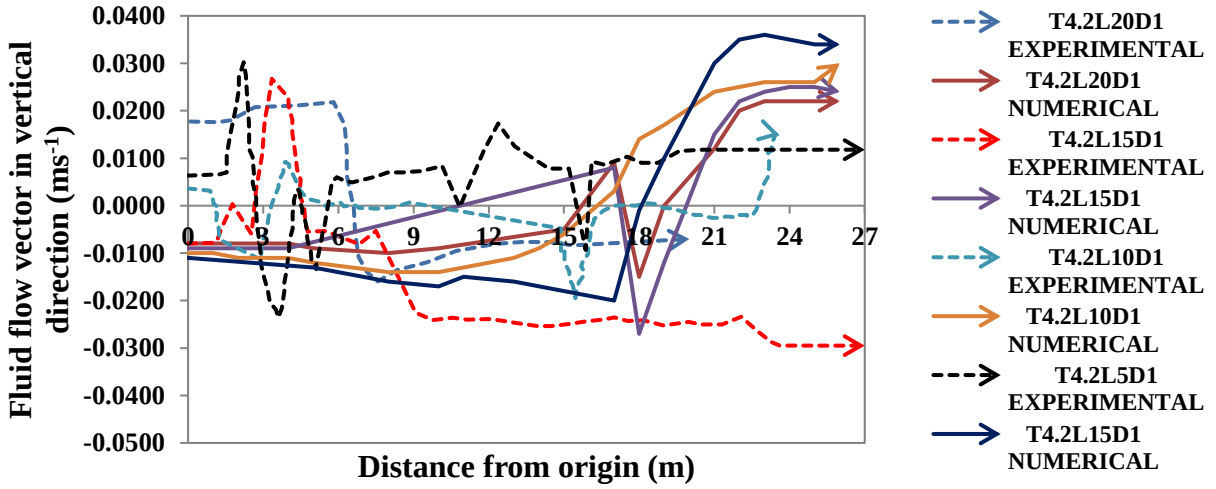

Fig 5.8(b): Fluid flow vector in vertical direction for 2*B*/8 position from the downstream end at 7m from the top (Numerical and experimental investigation)

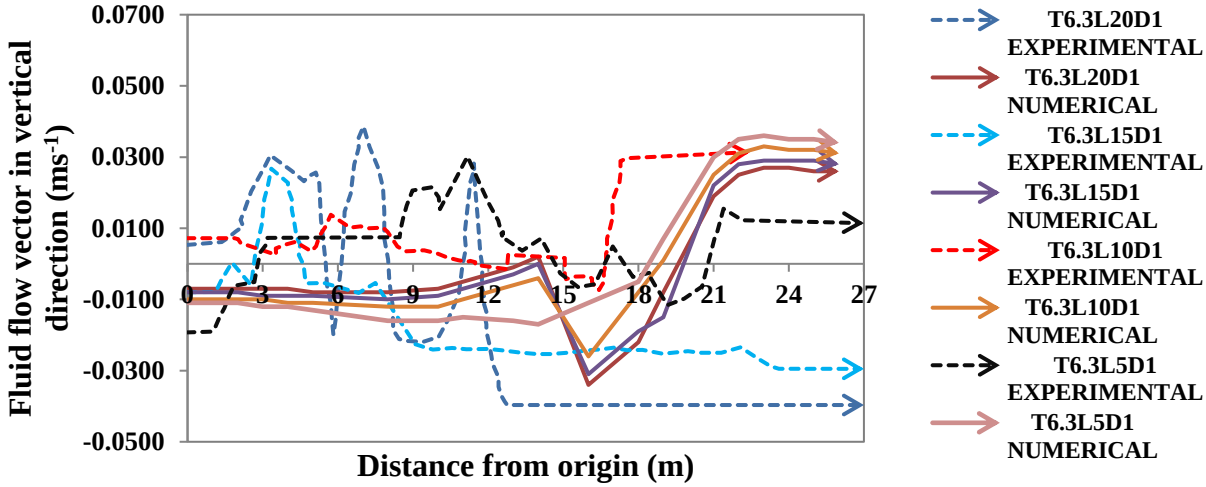

Fig 5.8(c): Fluid flow vector in vertical direction for 3*B*/8 position from the downstream end at 7m from the top (Numerical and experimental investigation)

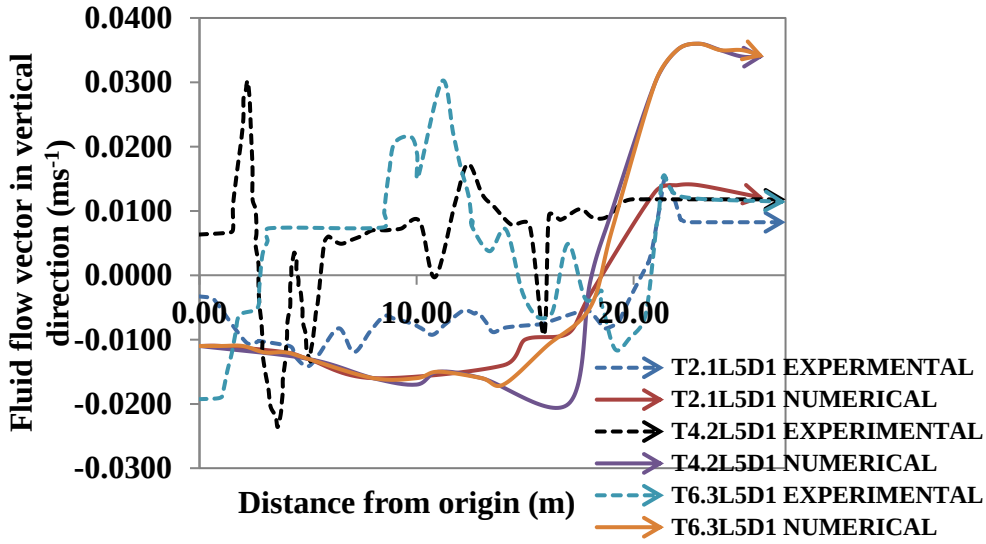

Fig 5.8(d): Fluid flow vector in vertical direction for 5m length at different position from the downstream end at 7m from the top (Numerical and experimental investigation)

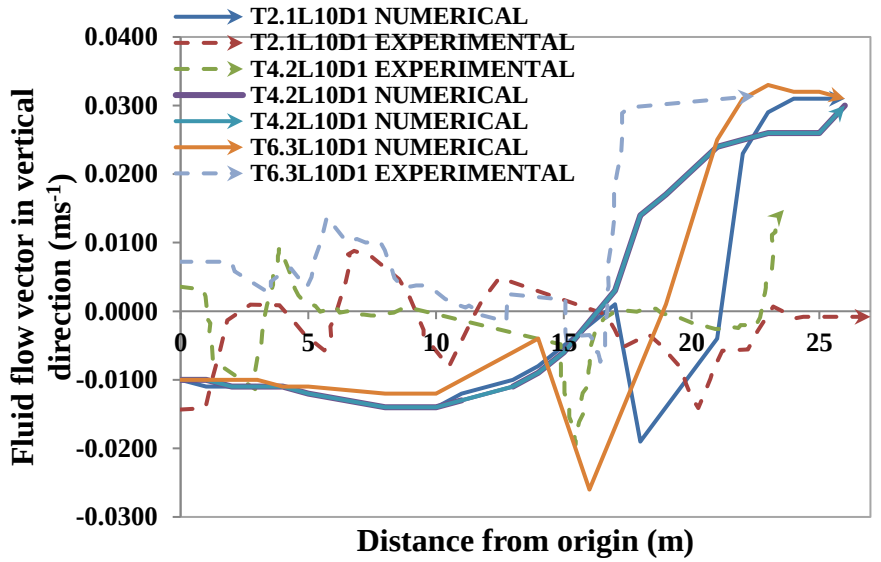

Fig 5.8(e): Fluid flow vector in vertical direction for 15m length at different position from the downstream end at 10m from the top (Numerical and experimental investigation)

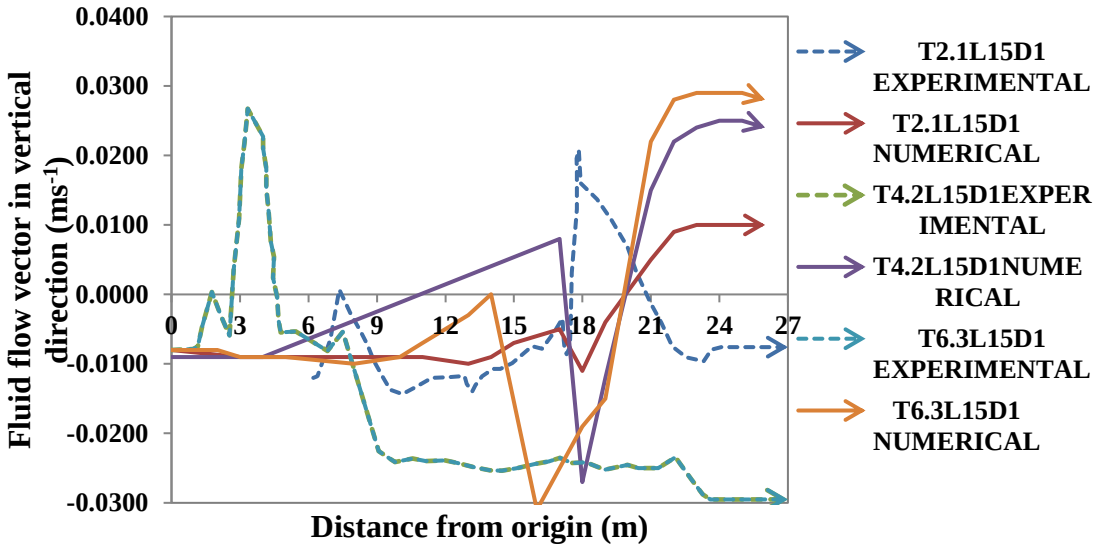

Fig 5.8(f): Fluid flow vector in vertical direction for 15m length at different position from the downstream end at 7m from the top (Numerical and experimental investigation)

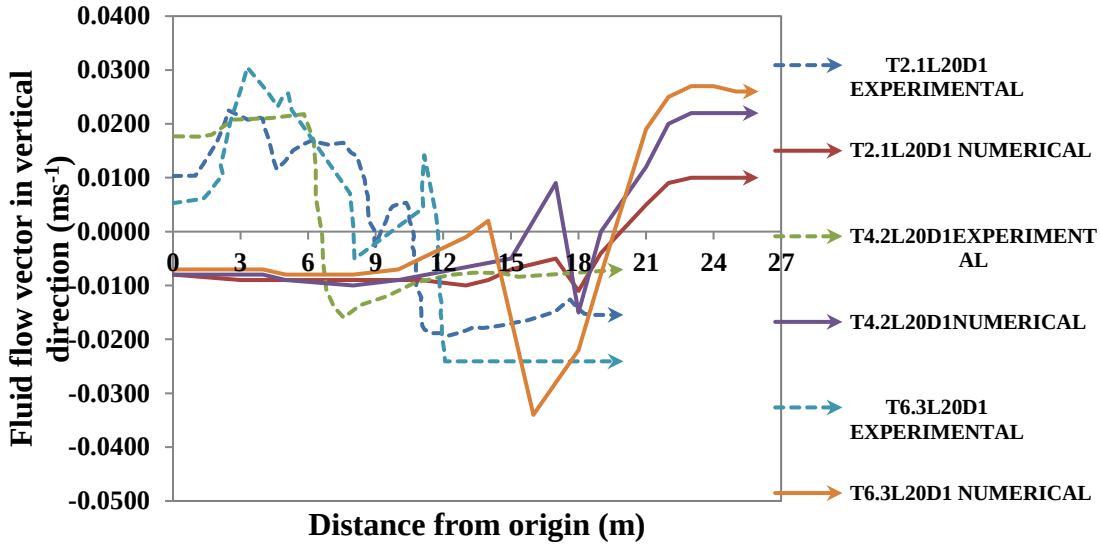

Fig 5.8(g): Fluid flow vector in vertical direction for 20m length at different position from the downstream end at 7m from the top (Numerical and experimental investigation)

It is observed that fluid flow vector increases on the upstream side with time but decreases on the downstream side beyond the sheet pile for any given time. This is probably due to the fact that sheet pile increases the creep length and thereby reduces the flow. It is further observed that when water height is more on the upstream side fluid flow vector becomes negative indicating overall downward flow as water is flowing from the upstream slope line which is a flow line in this case. It is found that for different sheet pile positions and also for different lengths of sheet pile the variation of fluid flow vector is similar to that as in case of steady state condition. This is clearly observed from the fluid flow vector graphs shown in figures 5.8(a) to 5.8(g).

5.3.2.3 Seismic condition under transient state

Fluid flow vector has been plotted for different sheet pile positions and lengths at time=37.25 sec in case of seismic study. Figure 5.9(a) to Figure 5.9 (c) presents fluid flow vector in vertical direction for 3*B*/8, 2*B*/8 and *B*/8 position respectively for different sheet pile length at seismic acceleration time=37.25 sec at 7m from the top of the dam. Figure 5.9(d) shows fluid flow vector in vertical direction for 15 m long sheet pile at different position at seismic acceleration time=37.25 sec at 7m from the top of the dam. Figure 5.9(e) to Figure 5.9 (g) presents Fluid flow vector in vertical direction for 3*B*/8, 2*B*/8 and *B*/8 position respectively for different sheet pile lengths at seismic acceleration time=37.25 sec at 12m from the top of the dam.

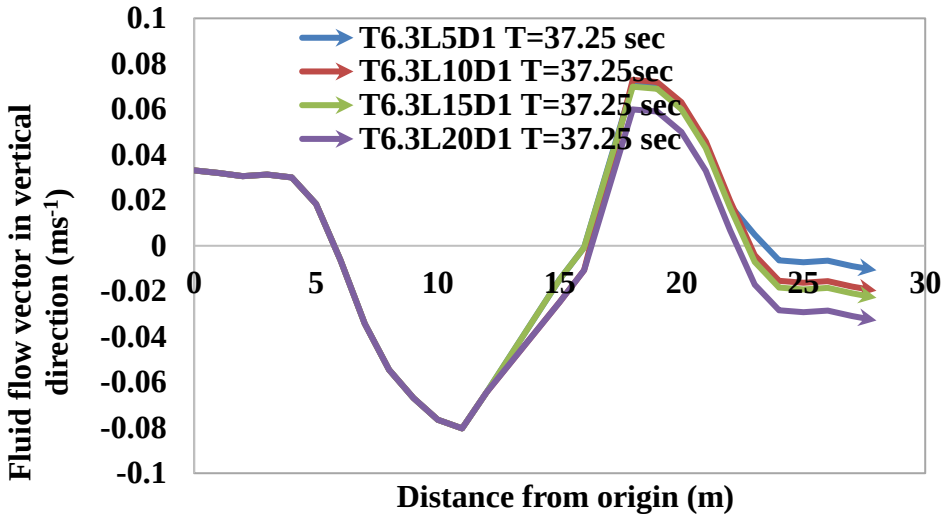

Fig 5.9(a): Fluid flow vector in vertical direction for 3*B*/8 position from the downstream end for different sheet pile length at 7m from the top

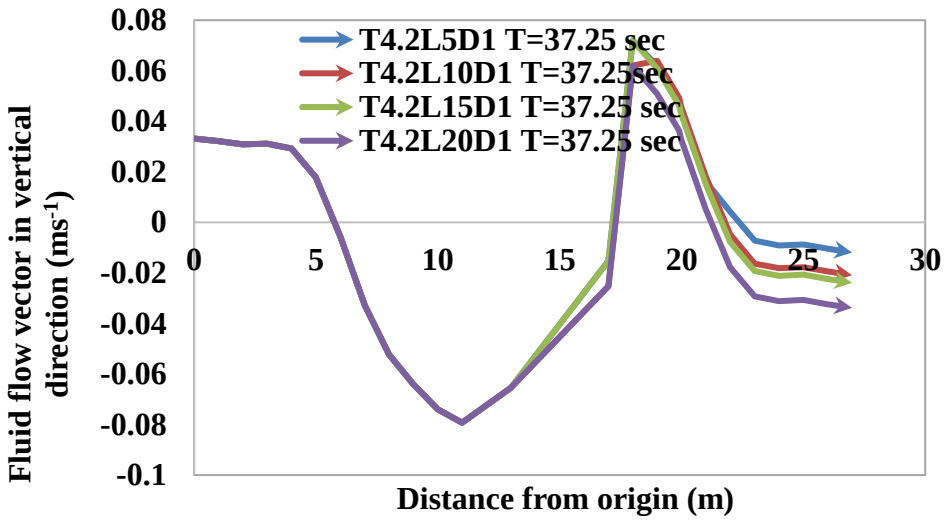

Fig 5.9(b): Fluid flow vector in vertical direction for 2*B*/8 position from the downstream end for different sheet pile length at 7m from the top

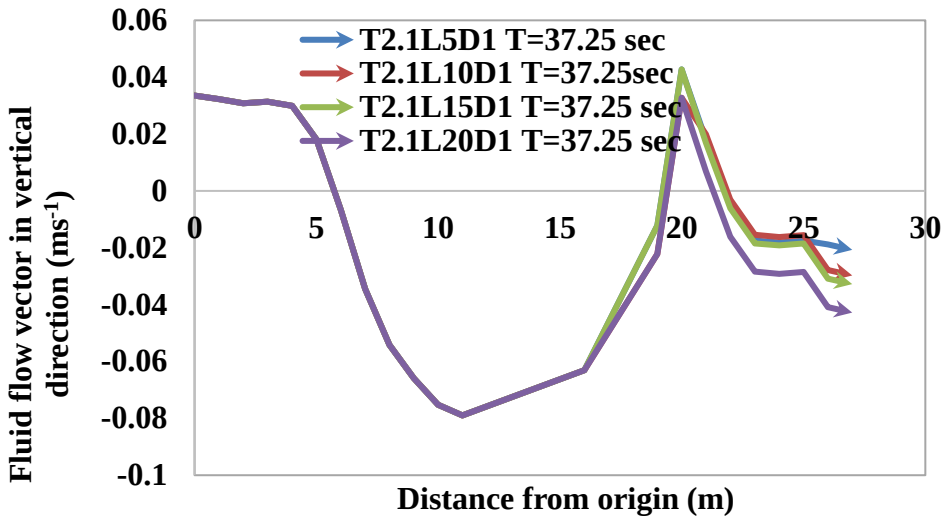

Fig 5.9(c): Fluid flow vector in vertical direction for *B*/8 position from the downstream end for different sheet pile length at 7m from the top

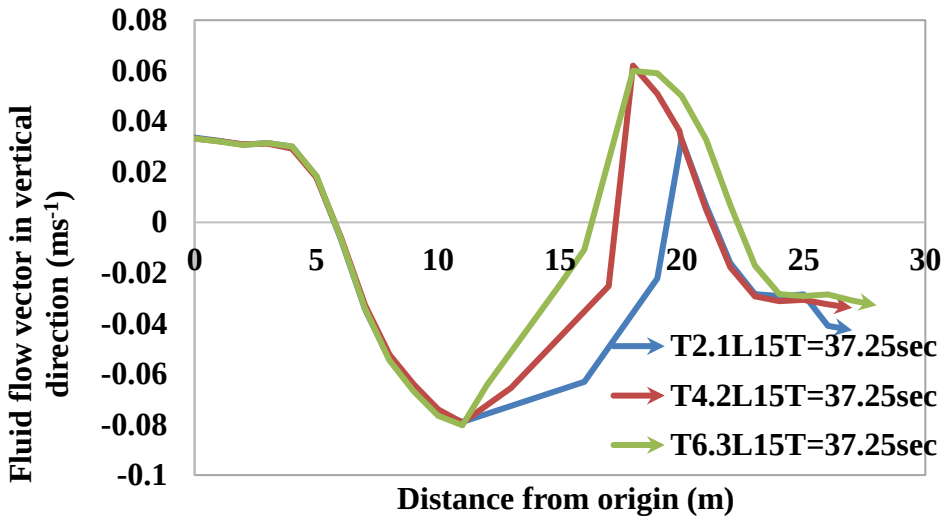

Fig 5.9(d): Fluid flow vector in vertical direction for *15 m* long sheet pile from the at different position from downstream end at 7m from the top

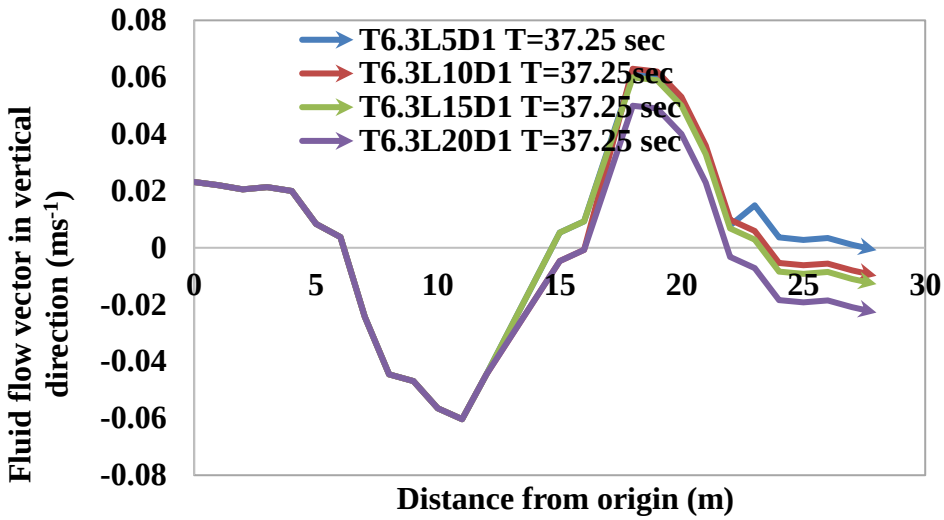

Fig 5.9(e): Fluid flow vector in vertical direction for 3*B*/8 position from the downstream end for different sheet pile length at 12m from the top

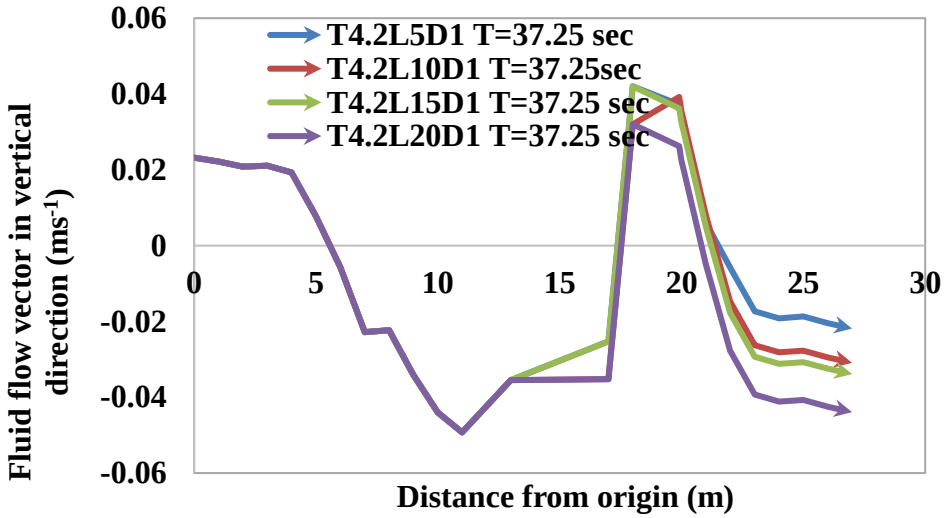

Fig 5.9(f): Fluid flow vector in vertical direction for 2*B*/8 position from the downstream end for different sheet pile length at 12m from the top

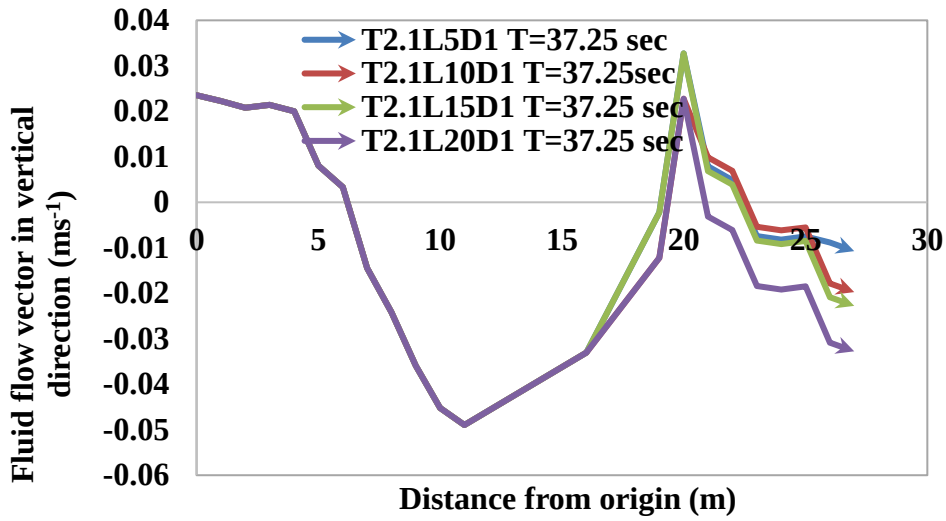

Fig 5.9(g): Fluid flow vector in vertical direction for *B*/8 position from the downstream end for different sheet pile length at 12m from the top

In case of seismic condition for any given time the analysis has been done in the same way as adopted for analysis under steady state condition. Variation of fluid flow vector under seismic condition and in case of transient flow is very much irregular and increases and decreases respectively at the time of increase and decrease of seismic force. The variation of fluid flow vector is not found to be influenced much by length and position of sheet pile. However maximum magnitude of fluid flow vector reduces as sheet pile shifts towards downstream end. This is probably due to the movement of sheet pile under seismic condition.

5.4 PORE WATER PRESSURE (PWP) VARIATION

Pore water pressure for different cases have been studied in this section. In each case pore water pressures have been plotted along the horizontal direction at 2m, 7m and12m from top to study its variation within the body as well as in foundation of the dam. The study has been done under steady state as well as for rise- up and drawdown conditions, for a working head of 3.5 m considering the rate of 0.583 m/hour (Refer to page Chapter1) for half cycle and also for multiple cycles.

5.4.1 PWP VARIATION IN FOUNDATION

5.4.1.1 STEADY STATE

Pore water pressure variation in foundation for different sheet pile positions of varying sheet pile lengths for both static and seismic conditions has been discussed in this section based on numerical and experimental results.

5.4.1.1.1 Numerical observations

Figure 5.10(a) shows the variation of pore pressure with change of sheet pile position for its fixed length under a particular water head. It is observed from the figure that, in general the pore pressure is higher at the upstream of sheet pile than it is at its downstream. It is further observed that at the location of sheet pile there is an abrupt decrease of pore water pressure. Thereafter it suddenly increases sharply. The abrupt change is sharp when sheet pile position is at a distance of 3*B*/8 from downstream. The change gradually reduces for position of sheet pile at 2*B*/8 and *B*/8 from downstream end. It therefore appears that sheet pile helps to reduce the pore pressure allowing flow of water along its length. The effect of pore pressure variation is more pronounced as sheet pile position proceeds towards the upstream. This is obvious as the flow path has to terminate near the downstream end. Thus, the seepage cutoff is more effective when the sheet pile position shifts more towards upstream end. It is also observed that irrespective of sheet pile position, the pore pressure at downstream end is more or less same. At the downstream end pore pressure becomes of similar order irrespective of sheet pile position.Thus, the effect of cutoff is more towards upstream probably due to availability of more creep length on downstream side. It is also observed from the Figure 5.10(b) that for all sheet pile positions pore pressure is high on the upstream side of sheet pile and it reduces along the sheet pile itself. The magnitude of the negative pore pressure (soil suction) is controlled by surface tension at the air-water boundaries within the pores and is governed by grain size. This observation justifies the use of sheet pile as seepage cutoff as pore pressure is getting reduced at sheet pile location. Figure 5.10(c) shows insignificant effect of sheet pile length on pore pressure variation along a particular position of sheet pile.

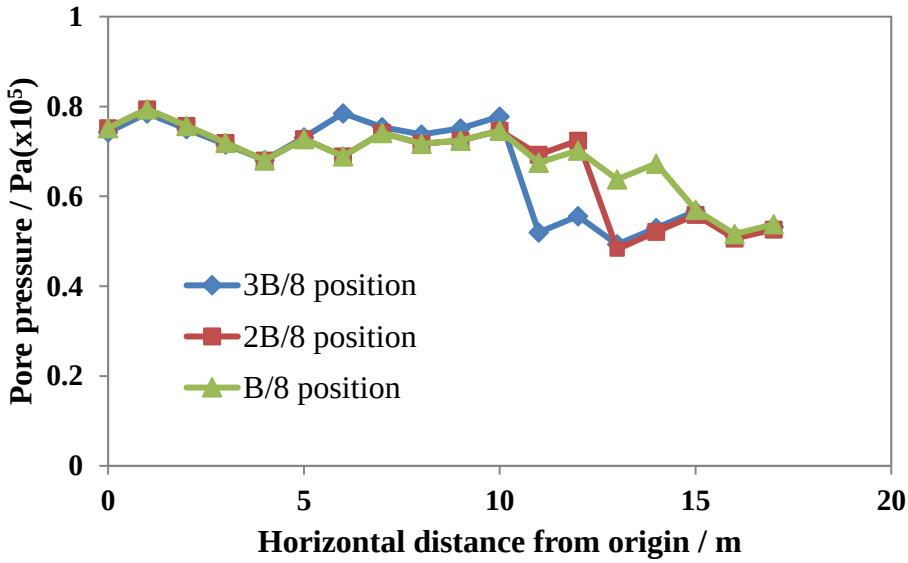

Fig 5.10(a): Pore pressure variation for 20m length sheet pile for different sheet pile positions 2m below the base of earthen dam at 7m from the top of dam

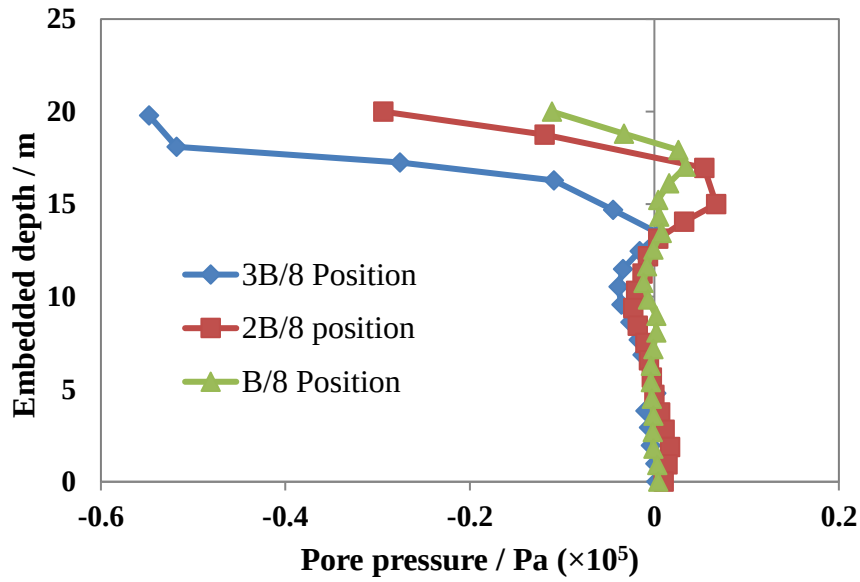

Fig 5.10(b): Pore pressure variation (along the sheet pile) for 20m long sheet pile for different sheet pile positions

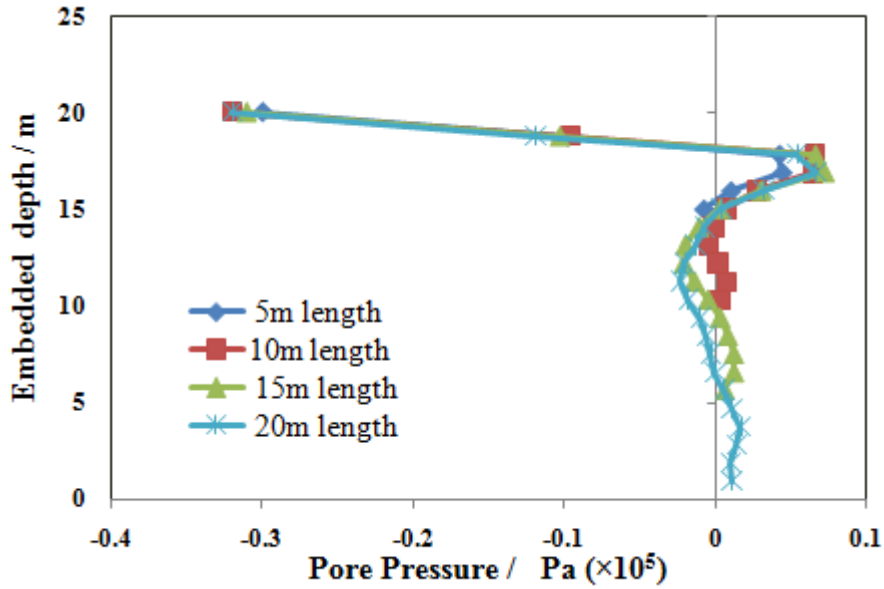

Fig 5.10(c): Pore pressure variation (along the sheet pile) for different sheet pile lengths for a *B*/8 sheet pile position.

5.4.1.1.2 Comparison between numerical and experimental results

It is further to mention that variation of pore water pressure obtained under static condition are found to be similar as obtained from both experimental and numerical results and this is clear from the graphs shown in Figure 5.11(a) to 5.11(b). However, all the positions of sheet pile the experimental value of pore pressure has been observed to be higher than those obtained in numerical results. Figure 5.11(c) presents pore water pressure variation for numerical and experimental observation at 12m position from the top of the dam at 3*B*/8 position for different length of sheet pile. Figure 5.11(d) presents pore water pressure variation for numerical and experimental observation at 12m position from the top of the dam for 10m long sheet pile at different sheet pile position. The difference between experimental and numerical values appear to be within a reasonable range of (±)20%.

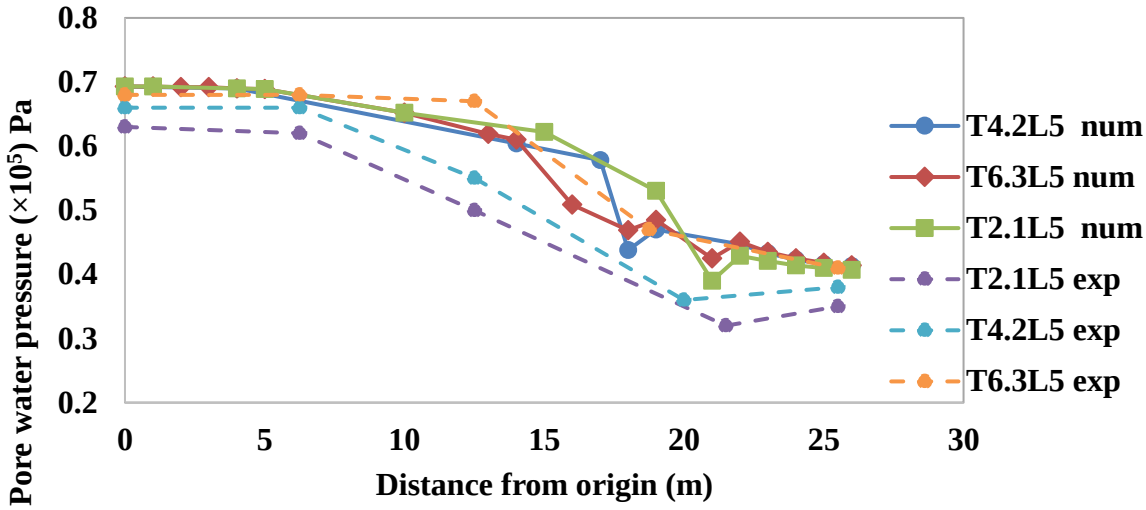

Fig 5.11(a): Pore pressure variation (along the sheet pile) for different sheet pile positions for a 5m length sheet pile (at 7m from the top of the dam)

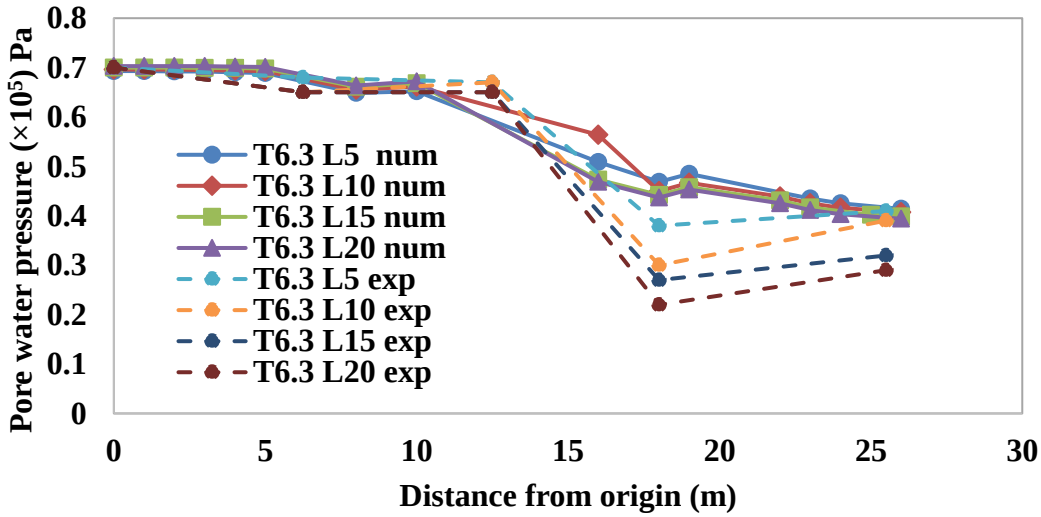

Fig 5.11(b): Pore pressure variation for different sheet pile length for 3*B*/8 position (at 7m from the top of the dam)

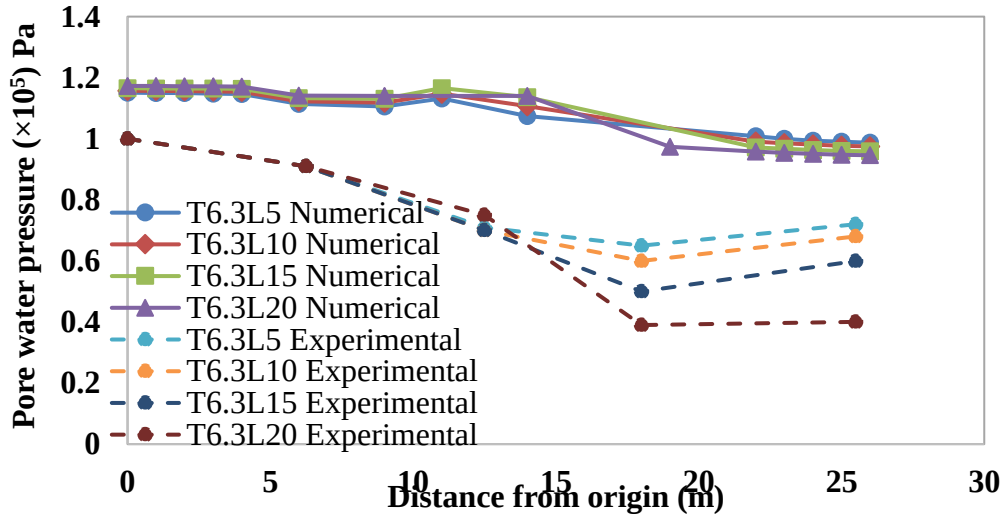

Fig 5.11(c): Pore pressure variation at for different sheet pile length at 3*B*/8 position sheet pile (at 12m from the top of the dam)

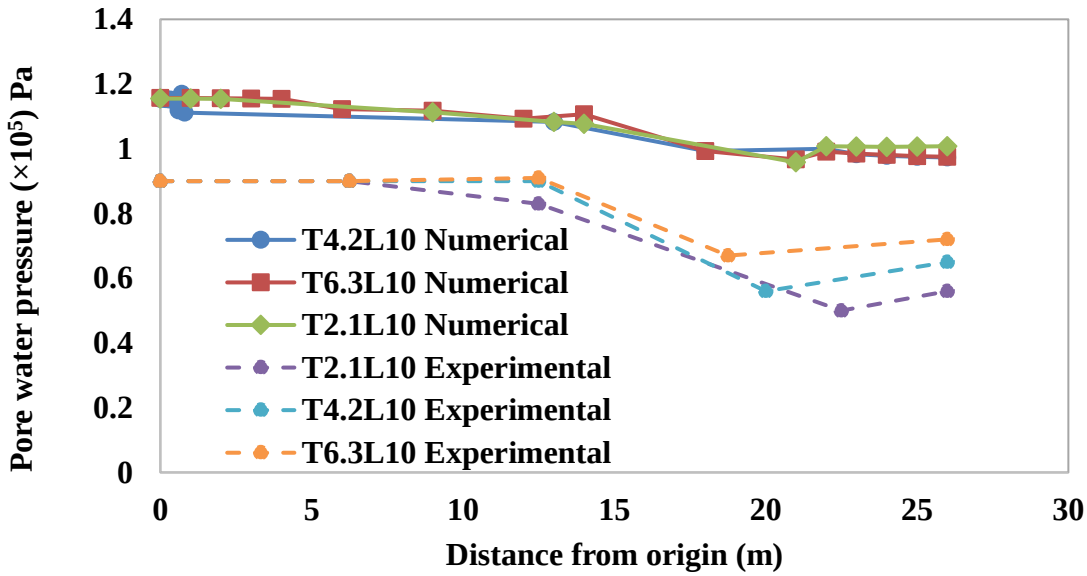

Fig 5.11(d): Pore pressure variation for different sheet pile positions for a 10m length sheet pile (at 12m from the top of the dam)

It is observed that for any water height, at the location of sheet pile there is an abrupt decrease of pore water pressure. Thereafter it suddenly increases sharply. The effect of pore pressure variation is more pronounced as sheet pile position proceeds towards the upstream. This is obvious as the flow path has to terminate near the downstream end. Experimentally it has been found that when sheet pile shifted from 2*B*/8 position to *B*/8 towards the downstream end average percentage change in pore water pressure is 16.00 %.

5.4.1.1.3 Observations for seismic study

Trend of variation of pore water pressure, as observed in steady state static case, is found to be similar under steady state seismic conditions. For seismic conditions the graphs for pore water pressure have been presented in Figure 5.12 (a) to 5.12(e). It has been observed that variation of pore pressure appears to be erratic for seismic conditions with and without sheet piles as may be observed from the figures 5.12 (a) to 5.12(c). This may be due to variation of seismic force with time. It has further been observed that for any particular time variation of pore water pressure follows the trend similar to that for static condition. Figure 5.12 (d) to 5.12(e) presents pore water pressure variation for 10m and 15m length for different sheet pile position at 12m from the top of the dam.

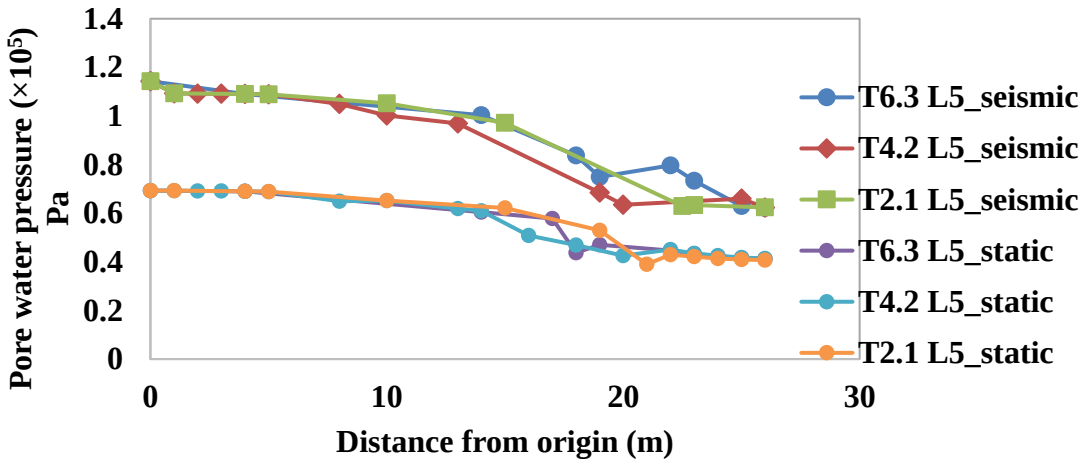

Fig 5.12(a): Pore pressure variation for different sheet pile positions for a 5m length sheet pile position at 7m from the top of the dam.

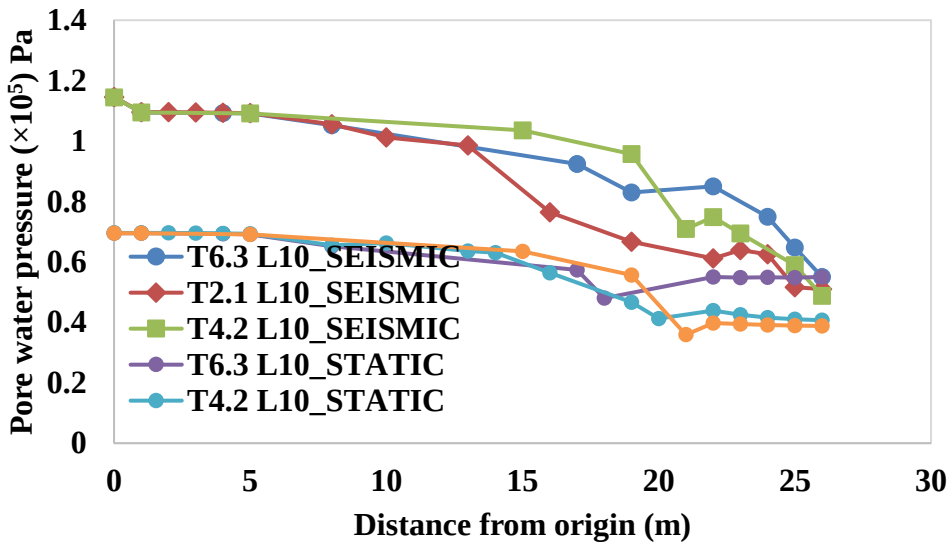

Fig 5.12(b): Pore pressure variation for different sheet pile positions for a 10m length sheet pile position at 7m from the top of the dam.

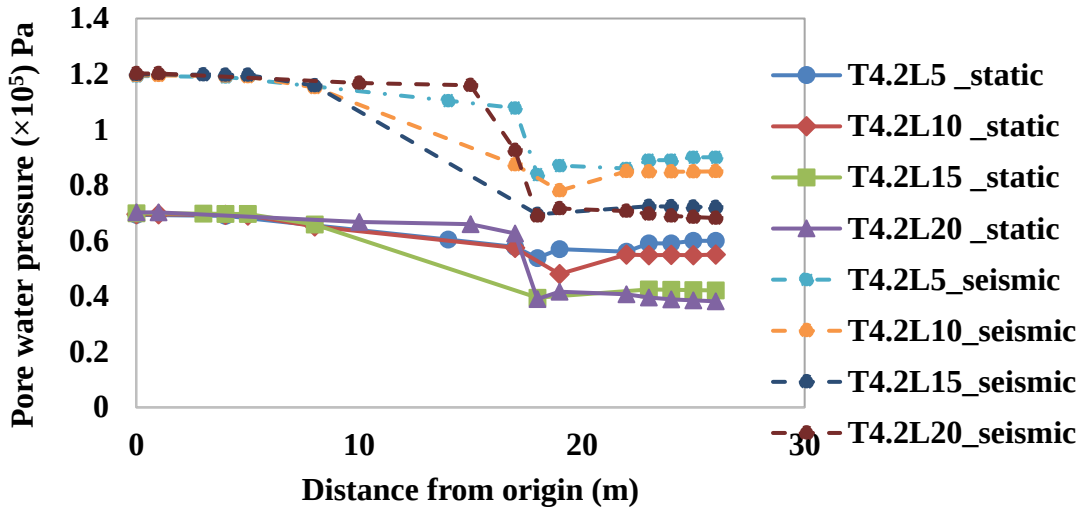

Fig 5.12(c): Pore pressure variation for 2*B*/8 position from downstream end for different length of sheet pile at 7m from the top of the dam.

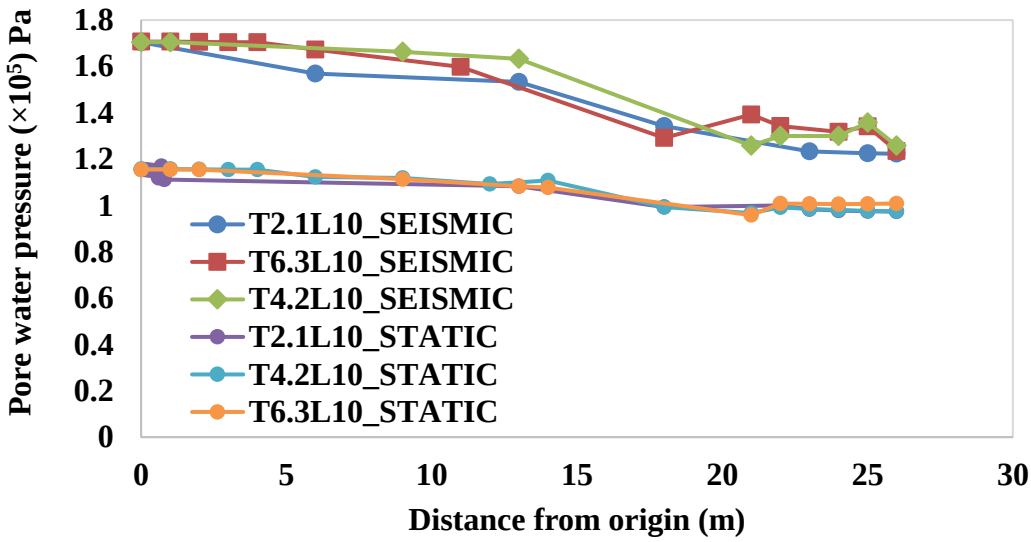

Fig 5.12(d): Pore pressure variation for different sheet pile positions for a 10m length sheet pile position at 12m from the top of the dam.

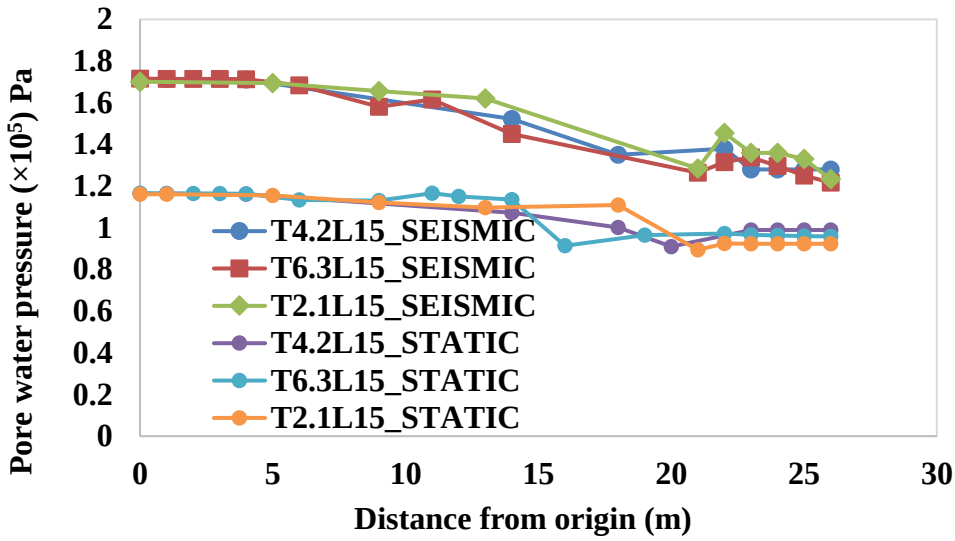

Fig 5.12(e): Pore pressure variation for different sheet pile positions for a 15m length sheet pile position at 12m from the top of the dam.

It has been observed from the figures that in seismic case pore water pressure increases up to 20% at the upstream side whereas at downstream side increases up to 10%-15% compared to respective static condition at 7m from the top of dam. Further, it has been observed from the figures that in seismic case pore water pressure increases up to 50% at the upstream side whereas at downstream side increases up to 15%-20% compared to respective static condition at 12m from the top of dam. This is due to seismic effect which is responsible for increase of pore pressure.

5.4.1.2 TRANSIENT STATE

Pore water pressure variation at foundation for different sheet pile positions and of varying sheet pile lengths for both static and seismic conditions has been discussed in this section based on numerical observations and experimental results.

5.4.1.2.1 Numerical results

It is observed from Figure 5.13(a) to Figure 5.14(l) that pore water pressure increases on the upstream side with time but decreases on the downstream side beyond the sheet pile at any given time. This is probably attributed to the fact that sheet pile increases the creep length and thereby reduces the flow. It is found that for different sheet pile positions, and also for different lengths of sheet pile the variation of pore water pressure is similar to that as in cases of steady state condition.

5.4.1.2.1.1. Numerical observations at 7m from the top of the dam

Pore water pressure variation in an earthen embankment in foundation at a level of 7m below the top of dam has been presented from Figure 5.13(a) to 5.13(l). Figure 5.13(a) to 5.13(d) presents the pore water pressure variation for 3*B*/8 position for sheet pile length of 5m, 10m,15m and 20m. Figures 5.13(e) to 5.13(h) show pore water pressure variation for 2*B*/8 position for sheet pile length of 5m, 10m,15m and 20m. Figures 5.13(i) to 5.126(l) show pore water pressure variation for 3*B*/8 position for sheet pile length of 5m, 10m,15m and 20m.

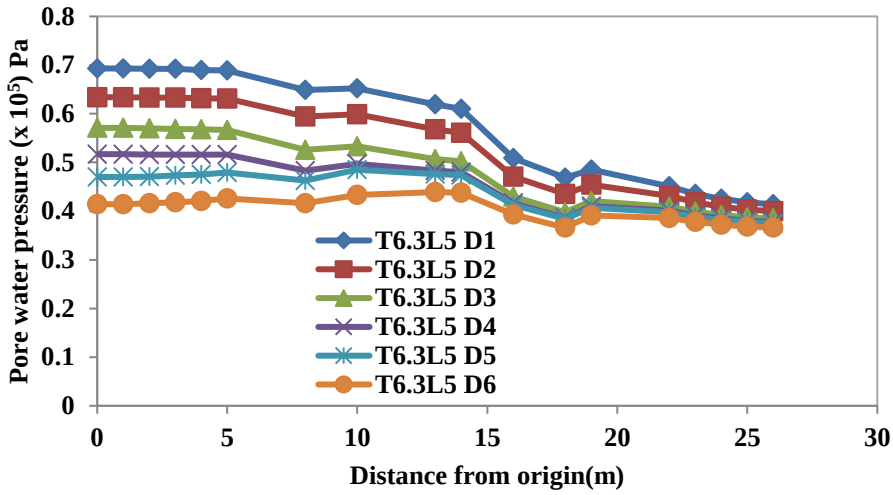

Fig 5.13(a): Pore water pressure variation of 5 m length for 3*B*/8 position from the downstream end

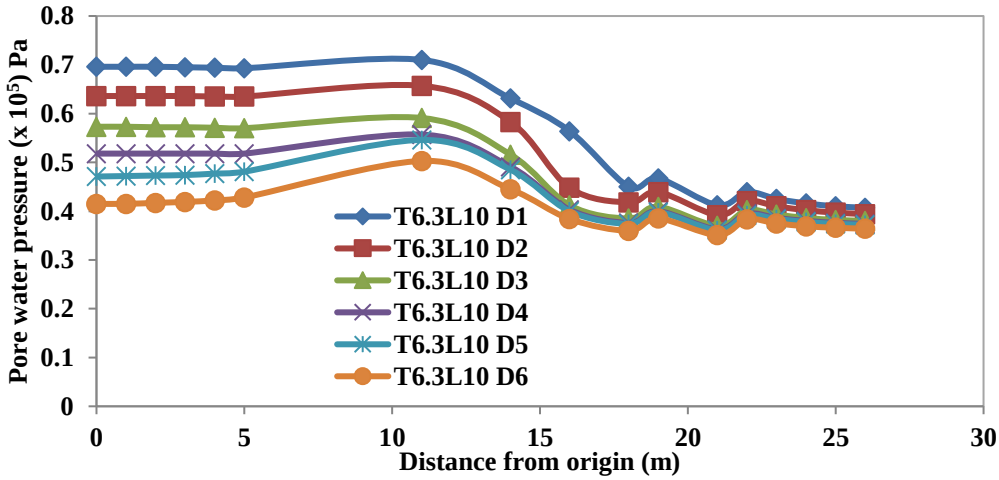

Fig 5.13(b): Pore water pressure variation of 10 m length for 3*B*/8 position from the downstream end

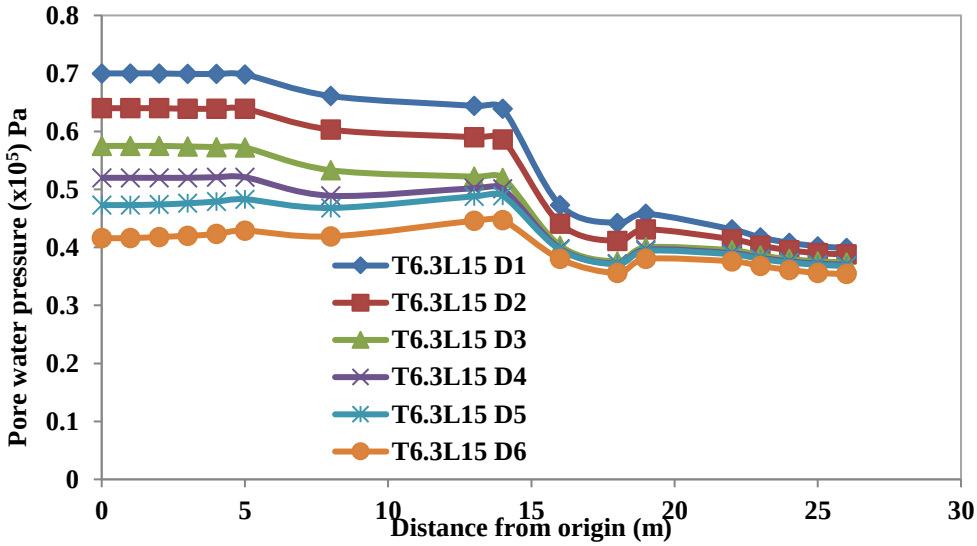

Fig 5.13(c): Pore water pressure variation of 15 m length for 3*B*/8 position from the downstream end

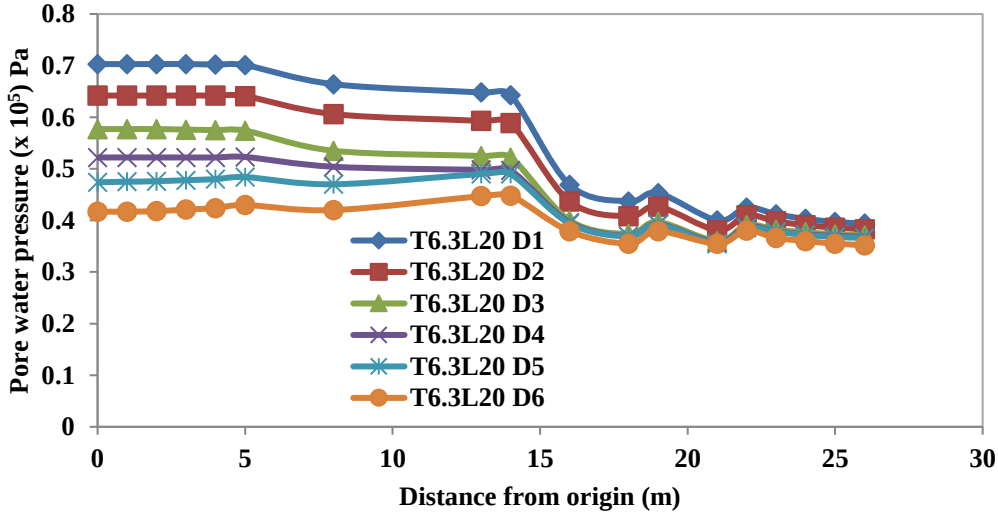

Fig 5.13(d): Pore water pressure variation of 20 m length for 3*B*/8 position from the downstream end

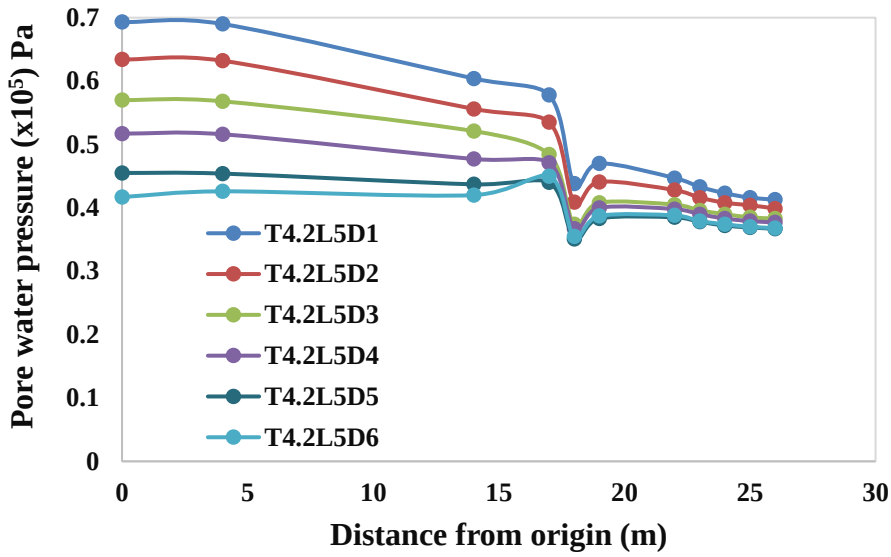

Fig 5.13(e): Pore water pressure variation of 5 m length for 2*B*/8 position from the downstream end

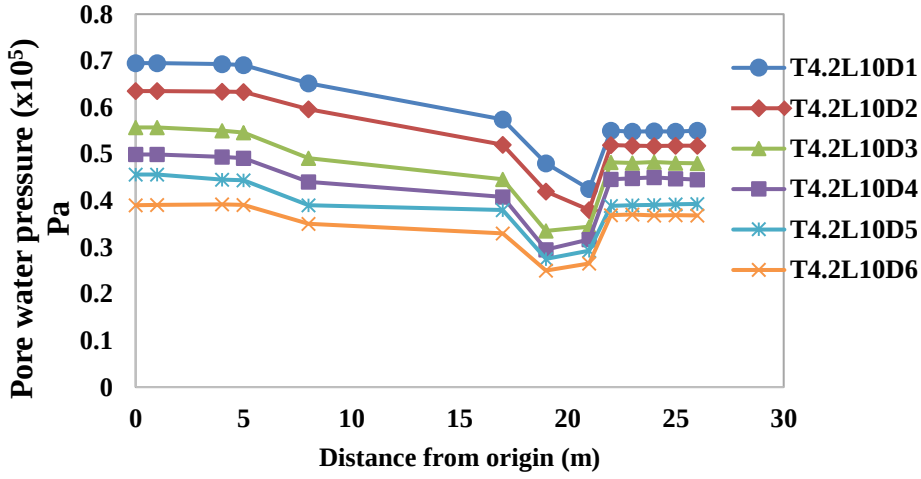

Fig 5.13(f): Pore water pressure variation of 10 m length for 2*B*/8 position from the downstream end

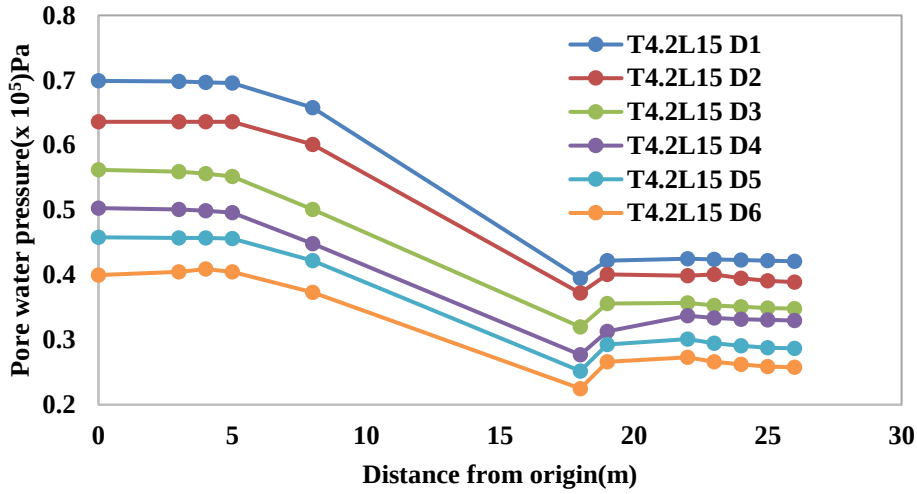

Fig 5.13(g): Pore water pressure variation of 15 m length for 2*B*/8 position from the downstream end

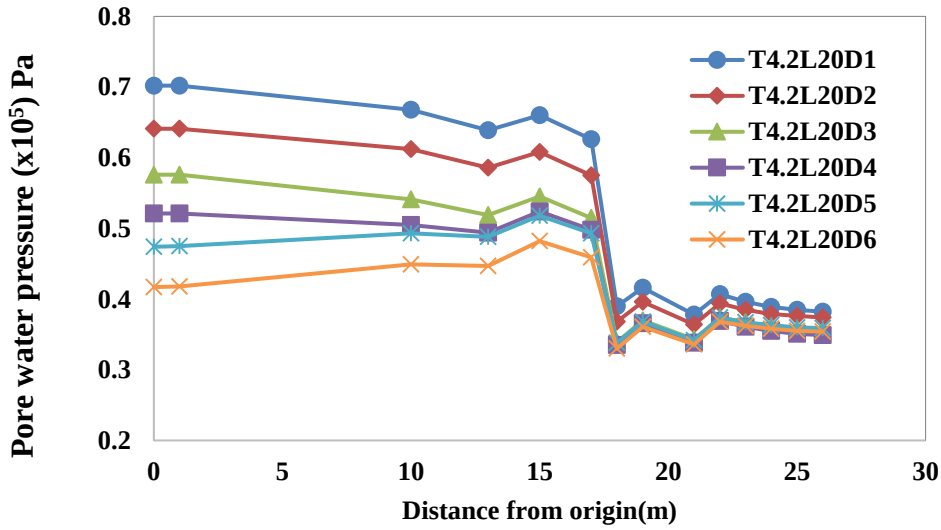

Fig 5.13(h): Pore water pressure variation of 20 m length for 2*B*/8 position from the downstream end

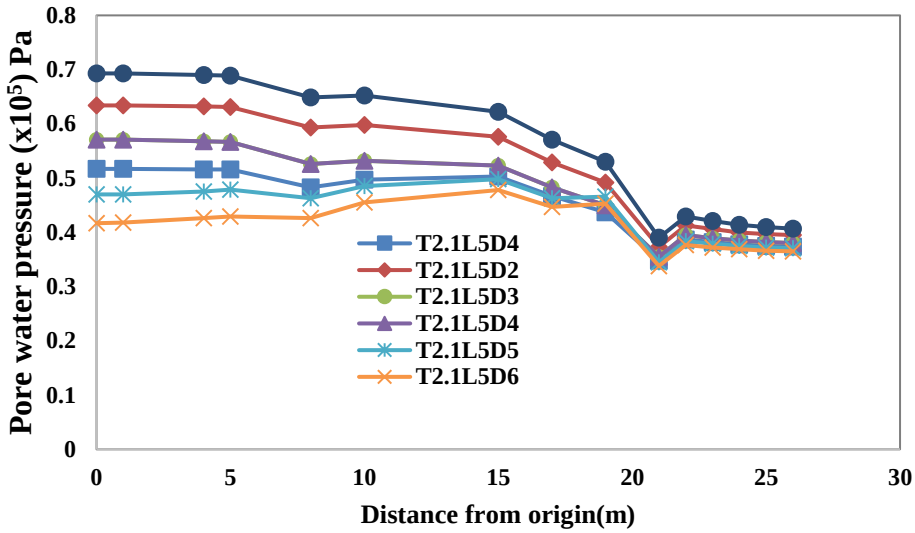

Fig 5.13(i): Pore water pressure variation of 5m length for *B*/8 position from the downstream end

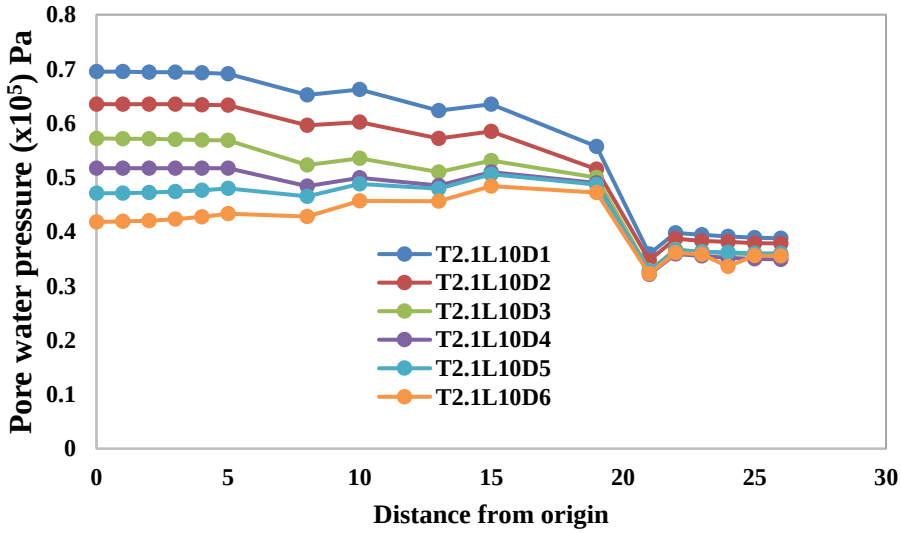

Fig 5.13(j): Pore water pressure variation of 10m length for *B*/8 position from the downstream end

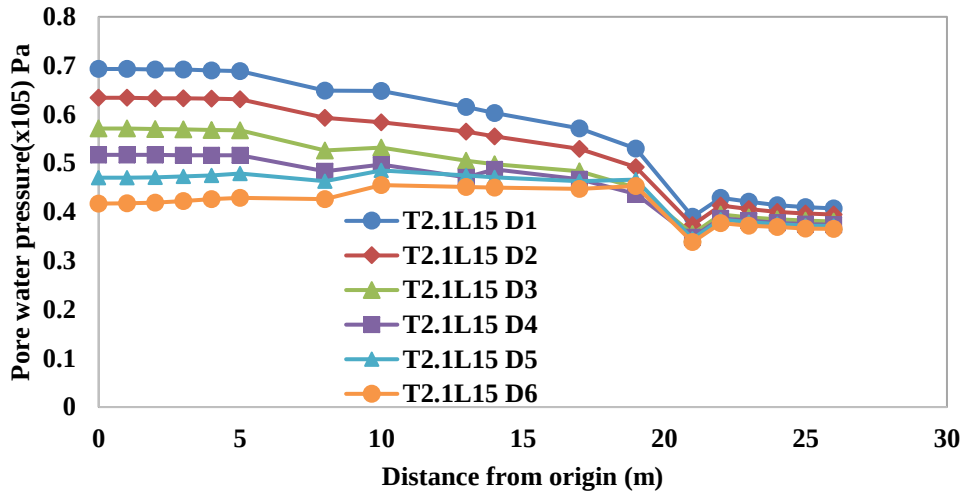

Fig 5.13(k): Pore water pressure variation of 15m length for *B*/8 position from the downstream end

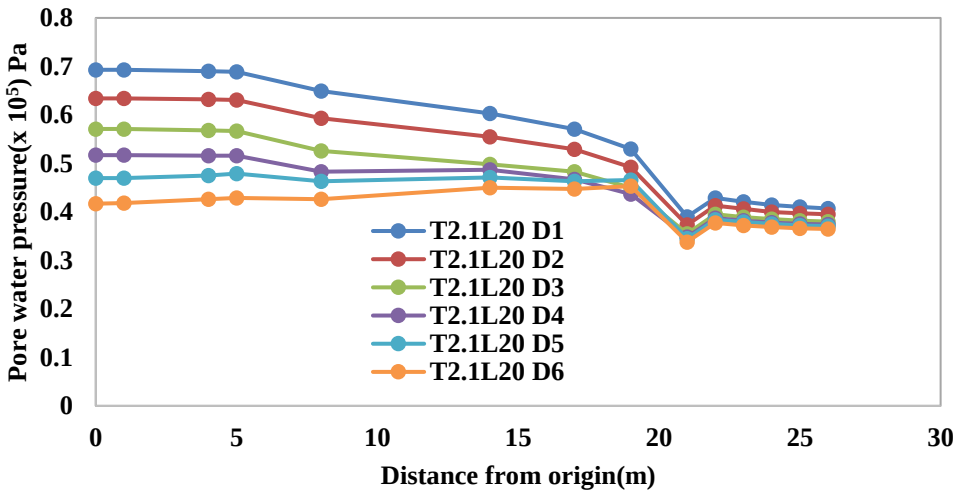

Fig 5.13(l): Pore water pressure variation of 20m length for *B*/8 position from the downstream end

It has been observed from the figures that at full drawdown condition the reduction of pore water pressure is on and average 42.58% compared to full rise up condition at the upstream slope. It has been further observed that at the position of sheet pile there is abrupt change of pore water pressure. The abrupt change of pore water pressure varies from 35.00% to 57.58% on an average at the position of sheet pile for variation of length of 5m to 20m. It has been further observed that at downstream end the reduction of pore water pressure under full drawdown condition is 10%-15% less compared to rise up condition.

5.4.1.2.1.2. Numerical observations at 12m from the top of the dam

Pore water pressure variation in an earthen embankment at foundation level of 10m below the top of dam has been presented from Figures 5.14(a) to 5.14(l). Figures 5.14(a) to 5.14(d) present the pore water pressure variation for 3*B*/8 position for sheet pile length of 5m, 10m,15m and 20m. Figures 5.14(e) to 5.14(h) present pore water pressure variation for 2*B*/8 position for sheet pile length of 5m, 10m,15m and 20m. Figures 5.14(i) to 5.127(l) show pore water pressure variation for *B*/8 position for sheet pile length of 5m, 10m,15m and 20m.

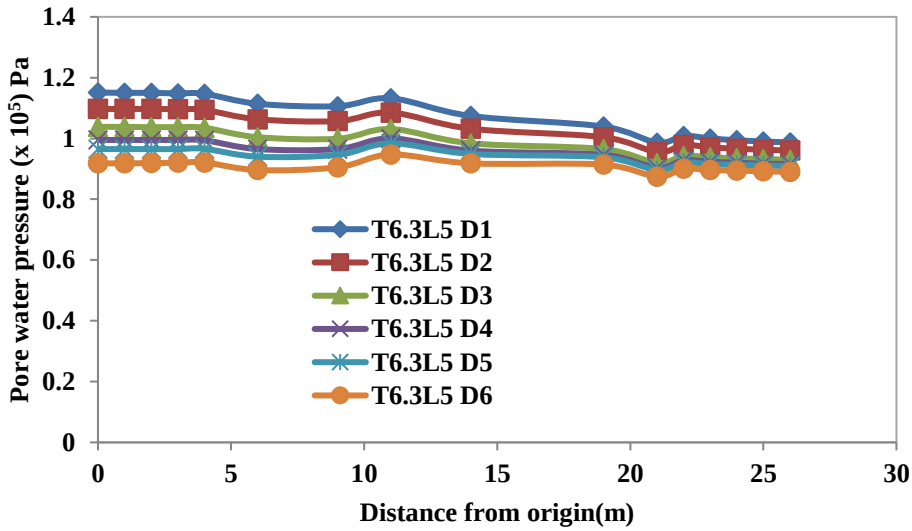

Fig 5.14(a): Pore water pressure variation of 5m length for 3*B*/8 position from the downstream end (at 12m from the top of dam)

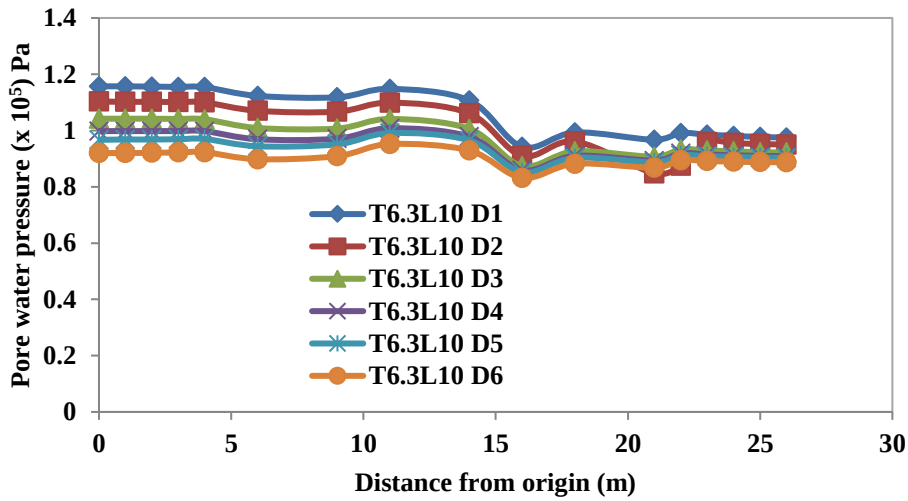

Fig 5.14(b): Pore water pressure variation of 10m length for 3*B*/8 position from the downstream end (at 12m from the top of dam)

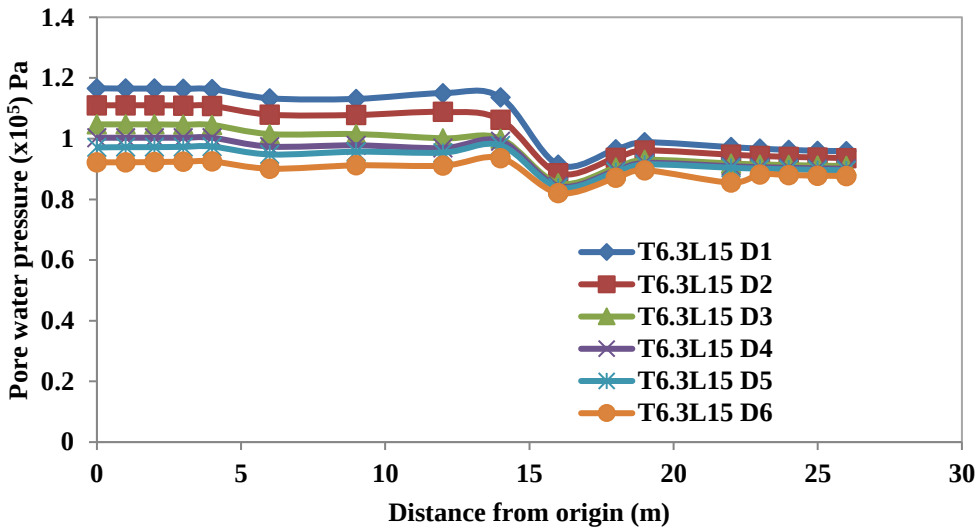

Fig 5.14(c): Pore water pressure variation of 15m length for 3*B*/8 position from the downstream end (at 12m from the top of dam)

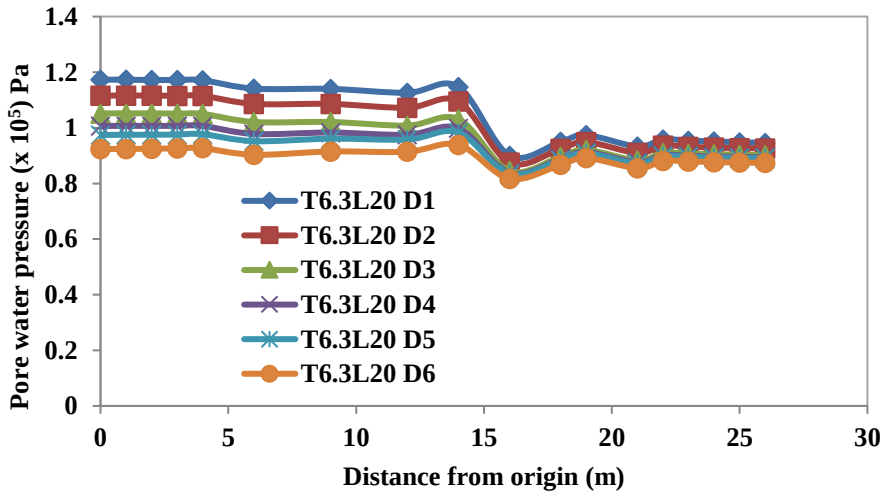

Fig 5.14(d): Pore water pressure variation of 20m length for 3*B*/8 position from the downstream end (at 12m from the top of dam)

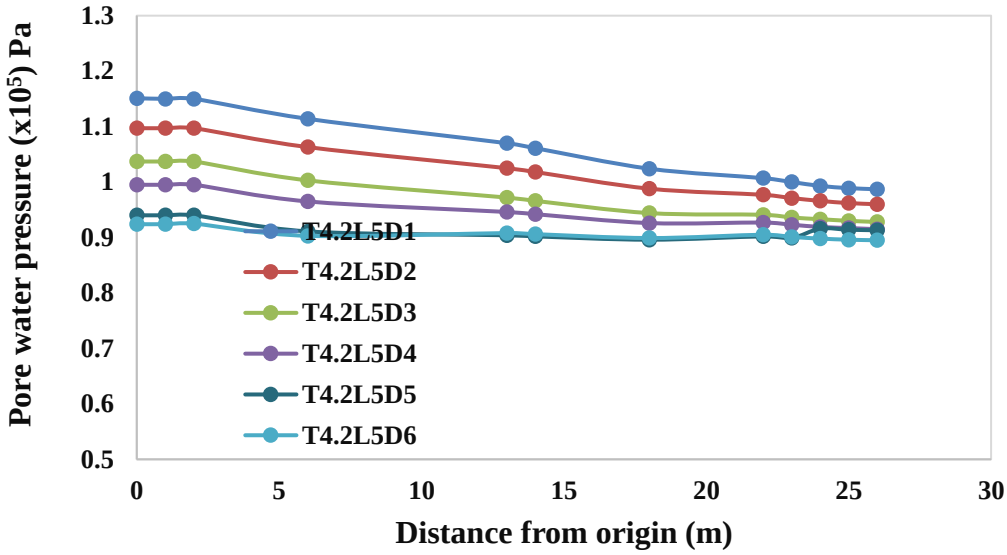

Fig 5.14(e): Pore water pressure variation of 5m length for 2*B*/8 position from the downstream end (at 12m from the top of dam)

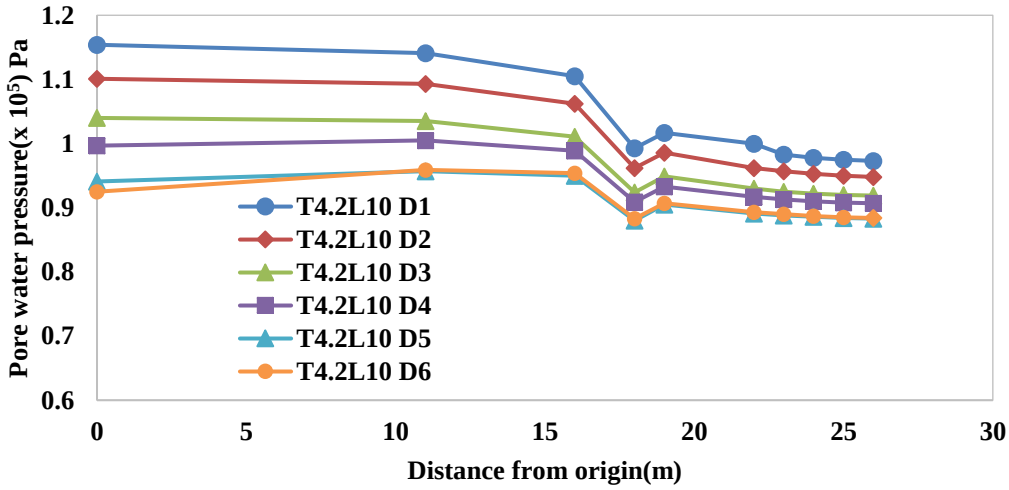

Fig 5.14(f): Pore water pressure variation of 10m length for 2*B*/8 position from the downstream end (at 12m from the top of dam)

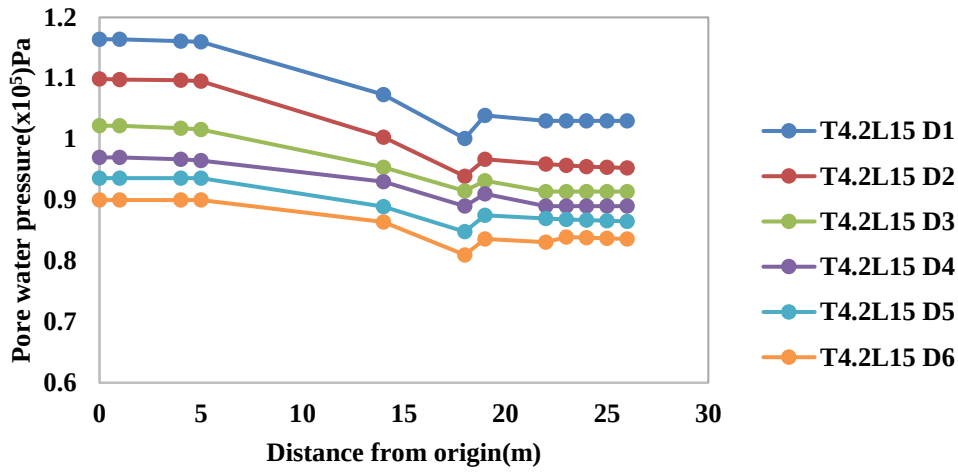

Fig 5.14(g): Pore water pressure variation of 15m length for 2*B*/8 position from the downstream end (at 12m from the top of dam)

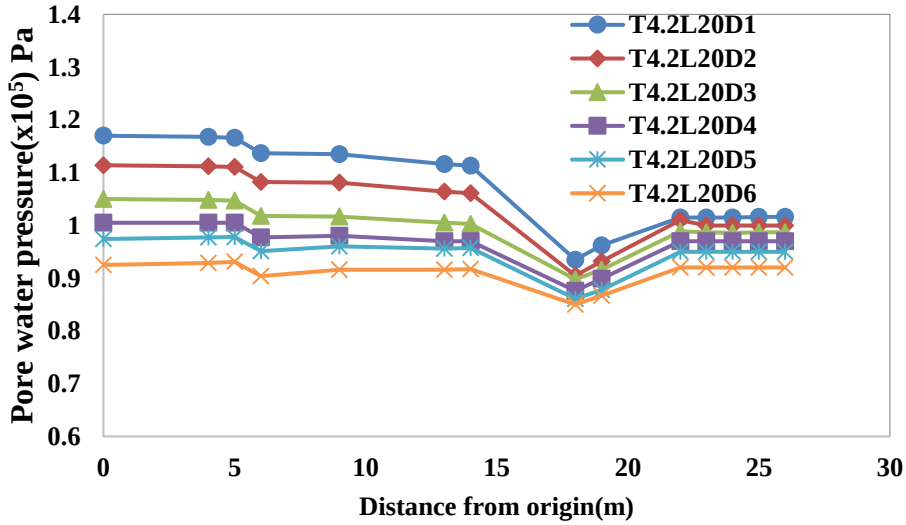

Fig 5.14(h): Pore water pressure variation of 20m length for 2*B*/8 position from the downstream end (at 12m from the top of dam)

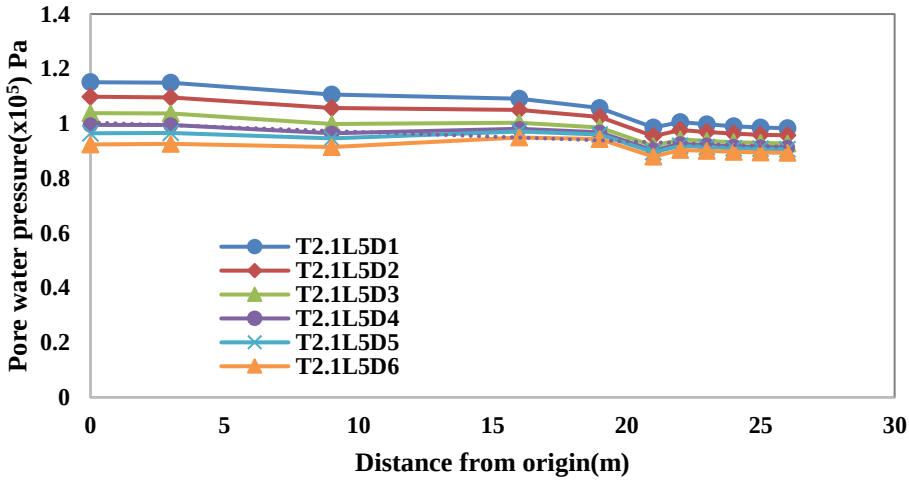

Fig 5.14(i): Pore water pressure variation of 5m length for *B*/8 position from the downstream end (at 12m from the top of dam)

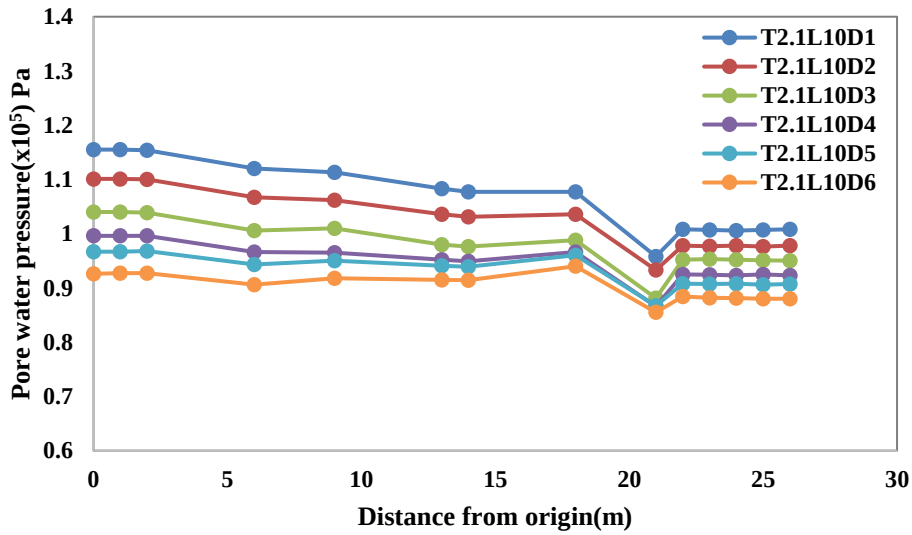

Fig 5.14(j): Pore water pressure variation of 10m length for *B*/8 position from the downstream end (at 12m from the top of dam)

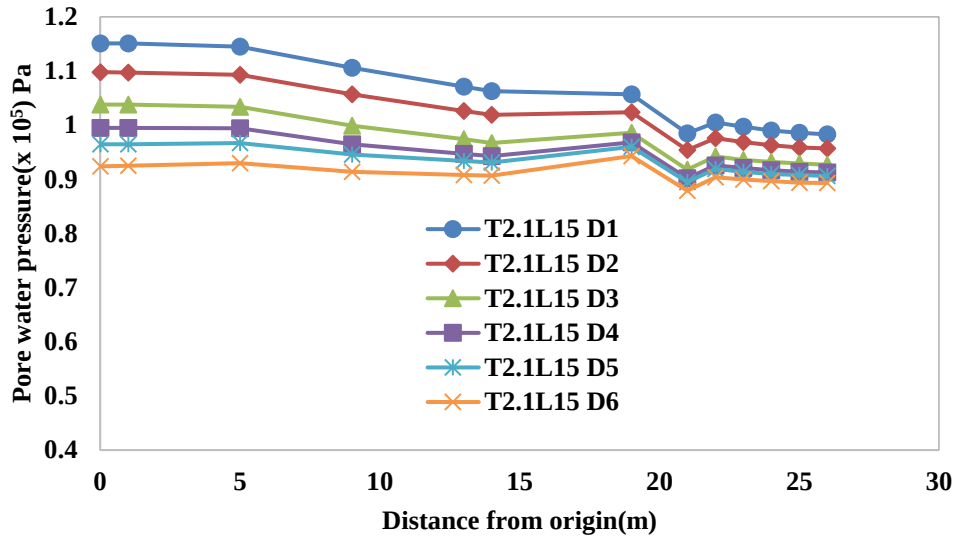

Fig 5.14(k): Pore water pressure variation of 15m length for *B*/8 position from the downstream end (at 12m from the top of dam)

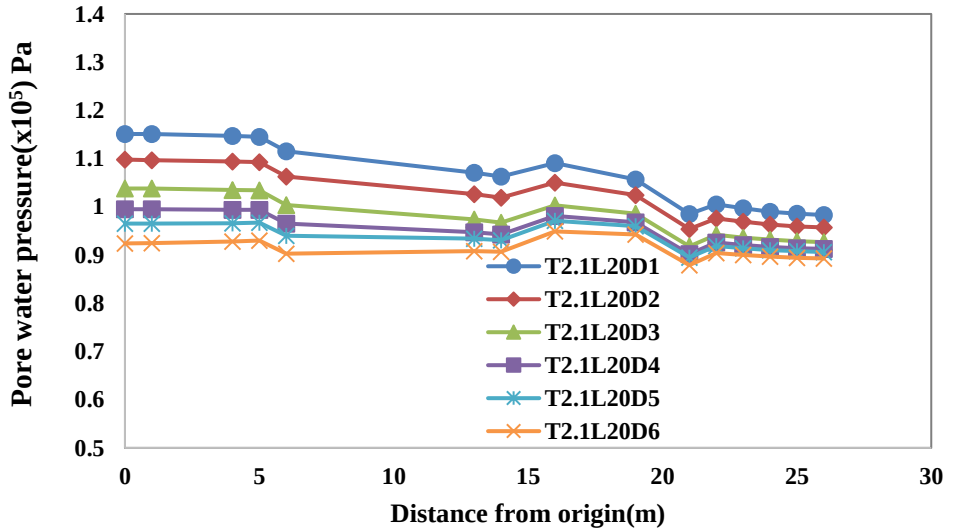

Fig 5.14(l): Pore water pressure variation of 20m length for *B*/8 position from the downstream end (at 12m from the top of dam)

It is observed from the figures that for any water height, at the location of sheet pile there is an abrupt decrease of pore water pressure. Thereafter it suddenly increases sharply. The effect of pore pressure variation is more pronounced as sheet pile position proceeds towards the upstream. This is obvious as the flow path must terminate near the downstream end. This means that the trend of variation of pore pressure along horizontal direction from upstream end is like that obtained for steady state condition in cases of without sheet pile as well as with sheet pile for different lengths and positions. It has been observed from the figures that at full drawdown condition the reduction of pore water pressure is on an average 33.00% compared to full rise up condition at the upstream slope. The abrupt change of pore water

pressure varies from 33.00% to 40% on an average, at the position of sheet pile for variation of length of 5m to 20m. It has been also observed that at the position of sheet pile there is abrupt change of pore water pressure. It has been further observed that at downstream end the reduction of pore water pressure under full drawdown condition is on and average 20%-22% less compared to that for rise up condition.

5.4.1.2.2 Comparison of pore water pressure from numerical and experimental observations

5.4.1.2.2.1 Pore water pressure variation at 7m from the top of the dam

Experimental and numerical observations in transient state considering both rise up and drawdown condition have been presented in this section from figure 5.15(a) to 5.15(l). Pore water pressure variation 7m from the top of the dam along a horizontal profile of different points of 6.25m, 12.5m, 15m and 22.5m from the upstream end has been presented for both rise up and drawdown conditions. Pore water pressure variation for both rise up and drawdown conditions at 3*B*/8 position along the horizontal profile of 7m from the top has been presented in figures 5.15(a),5.15(b),5.15(c), 5.15(d) for 5m,10m, 15m and 20m long sheet pile respectively. Pore water pressure variation for both rise up and drawdown conditions at 2*B*/8 position along the horizontal profile of 7m from the top has been presented in figures 5.15(e),5.15(f),5.15(g), 5.15(h) for 5m,10m, 15m and 20m long sheet pile respectively. Pore water pressure variation for both rise up and drawdown conditions at *B*/8 position along the horizontal profile of 7m from the top has been presented in figures 5.15(i),5.15(j),5.15(k), 5.15(l) for 5m,10m, 15m and 20m long sheet pile respectively. Variation of pore water pressure at 7m from the top of the dam in respect of sheet pile length has been presented in Figures 5.16(a) to 5.16(h). Out of these Figures 5.16(a) and 5.16(b) present experimental and numerical results for full drawdown and rise up conditions respectively for 5m long sheet pile at 7m from the top of the dam Figures 5.16(c) and 5.16(d) show experimental and numerical results for full drawdown and rise up conditions respectively for 10m long sheet pile at 7m from the top of the dam. Figures 5.16(e) and 5.16(f) present experimental and numerical results for full drawdown and rise up conditions respectively for 15m long sheet pile at 7m from the top of the dam. Figures 5.16(g) and 5.16(h) show experimental and numerical results for full drawdown and rise up conditions respectively for 5m long sheet pile at 7m from the top of the dam. Variation of pore water pressure at 7m from the top of the dam in respect of sheet pile position has been presented in Figure 5.16(i) to 5.16(n). Figures 5.16(i) and 5.16(j) present experimental and numerical results for full drawdown and rise up conditions respectively at 3*B*/8 position at 7m from the top of the dam Figures 5.16(k) and 5.16(l) present experimental and numerical results for full drawdown and rise up conditions respectively at 2*B*/8 position at 7m from the top of the dam. Figures 5.16(m) and 5.16(n) shows experimental and numerical results for full drawdown and rise up conditions respectively at *B*/8 position at 7m from the top of the dam.

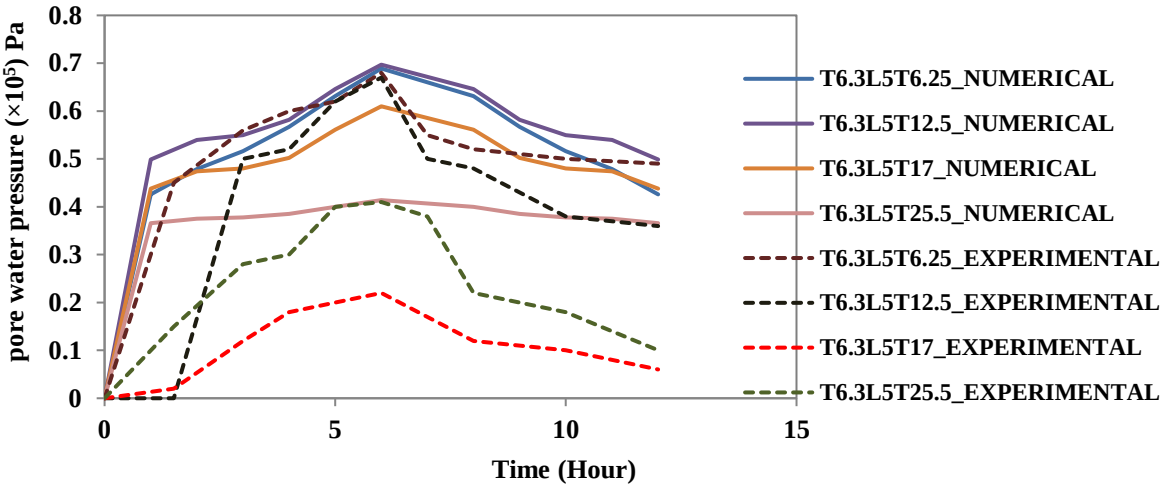

Figure. 5.15(a) Pore water pressure variation of 5m long sheet pile at 3*B*/8 position under full rise up and drawdown condition at 7m position (Experimental and numerical investigation)

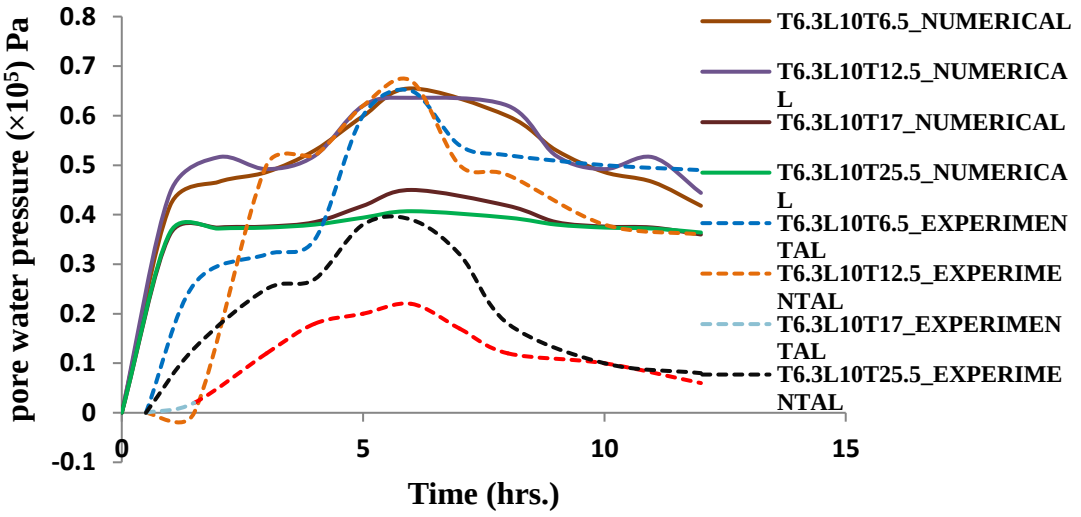

Figure. 5.15(b) Pore water pressure variation of 10m long sheet pile at 3*B*/8 position under full rise up and drawdown condition at 7m position (Experimental and numerical investigation)

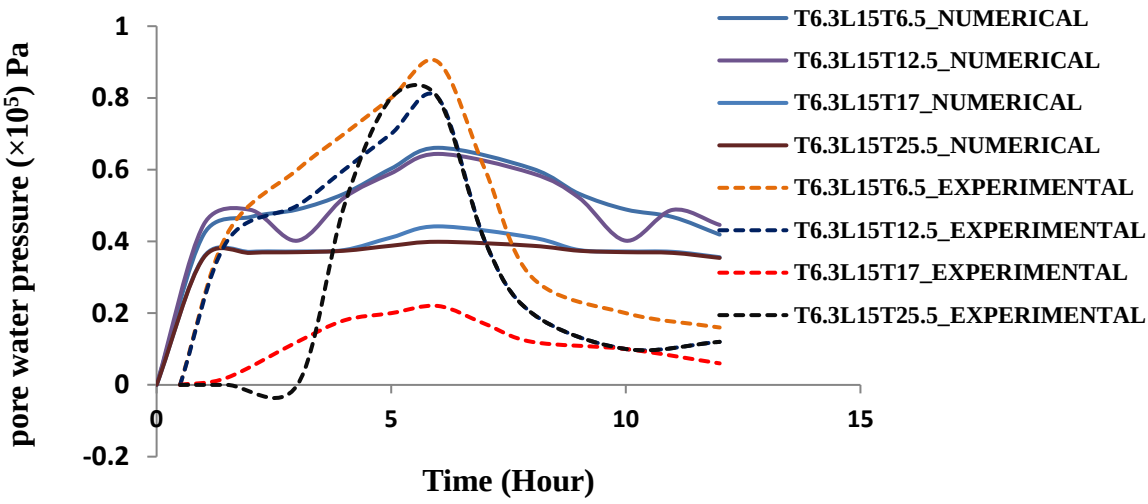

Figure. 5.15(c) Pore water pressure variation of 3*B*/8 position under full rise up and drawdown condition at 7m position (Experimental and numerical investigation)

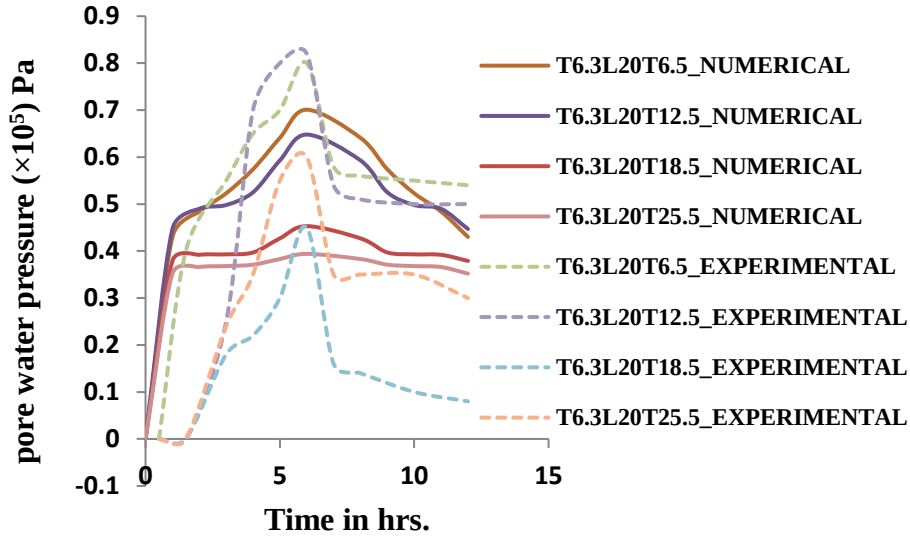

Figure. 5.15(d) Pore water pressure variation of 3*B*/8 position under full rise up and drawdown condition at 7m position (Experimental and numerical investigation)

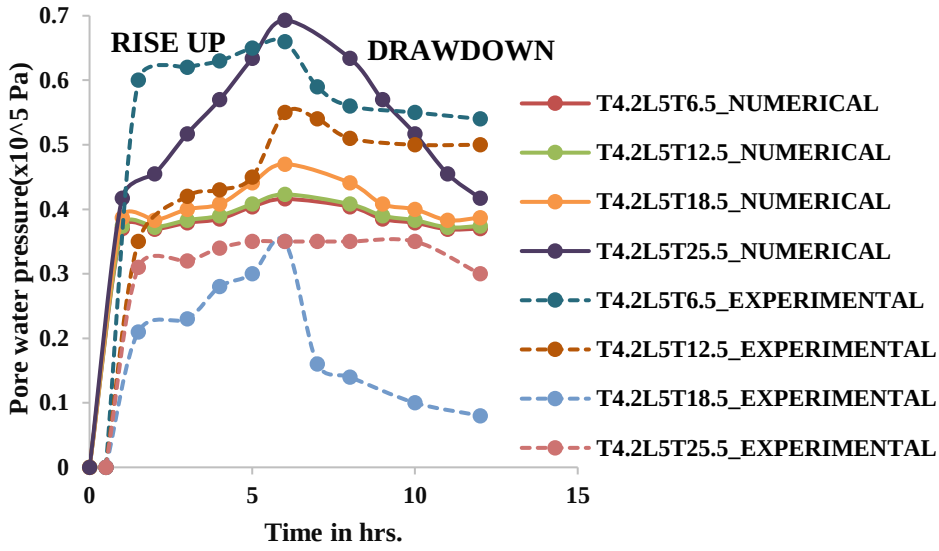

Figure. 5.15(e): Pore water pressure variation of 2*B*/8 position under full rise up and drawdown condition at 7m position (Experimental and numerical investigation)

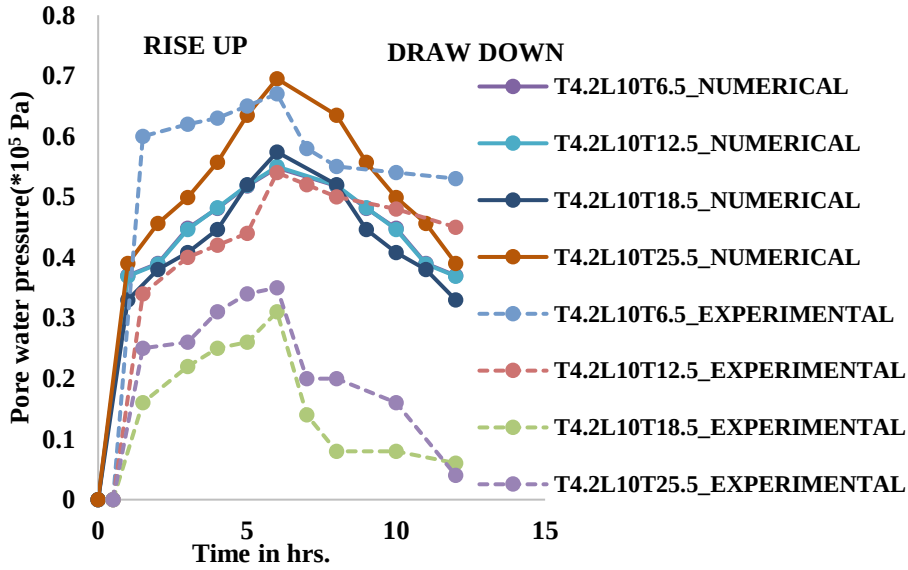

Figure. 5.15(f): Pore water pressure variation of 2*B*/8 position under full rise up and drawdown condition at 7m position (Experimental and numerical investigation)

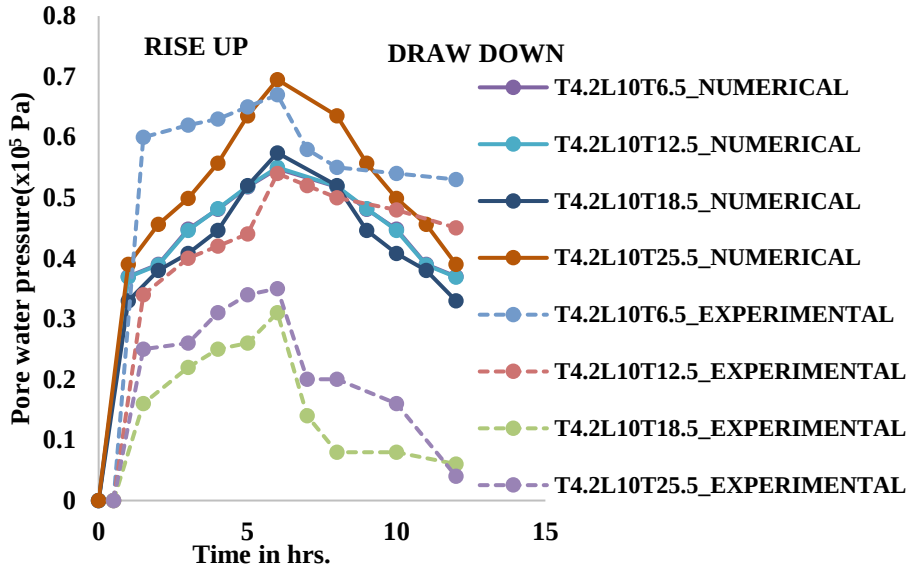

Figure. 5.15(g): Pore water pressure variation of 2*B*/8 position under full rise up and drawdown condition at 7m position (Experimental and numerical investigation)

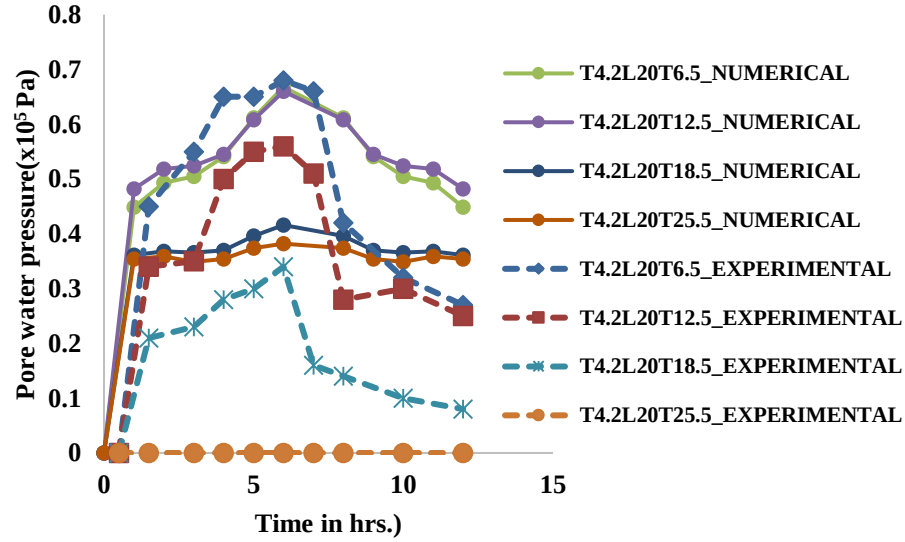

Figure. 5.15(h): Pore water pressure variation of 2*B*/8 position under full rise up and drawdown condition at 7m position (Experimental and numerical investigation)

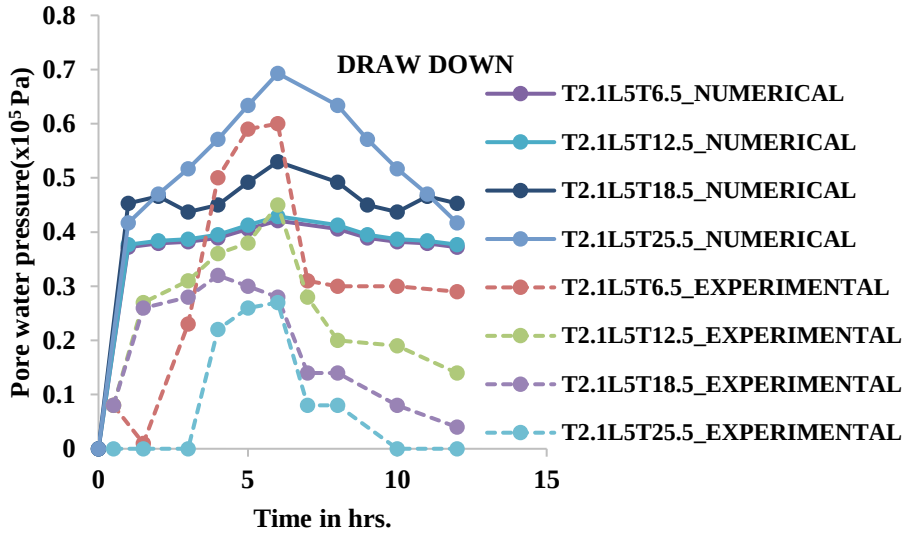

Figure. 5.15(i): Pore water pressure variation of *B*/8 position under full rise up and drawdown condition at 7m position (Experimental and numerical investigation)

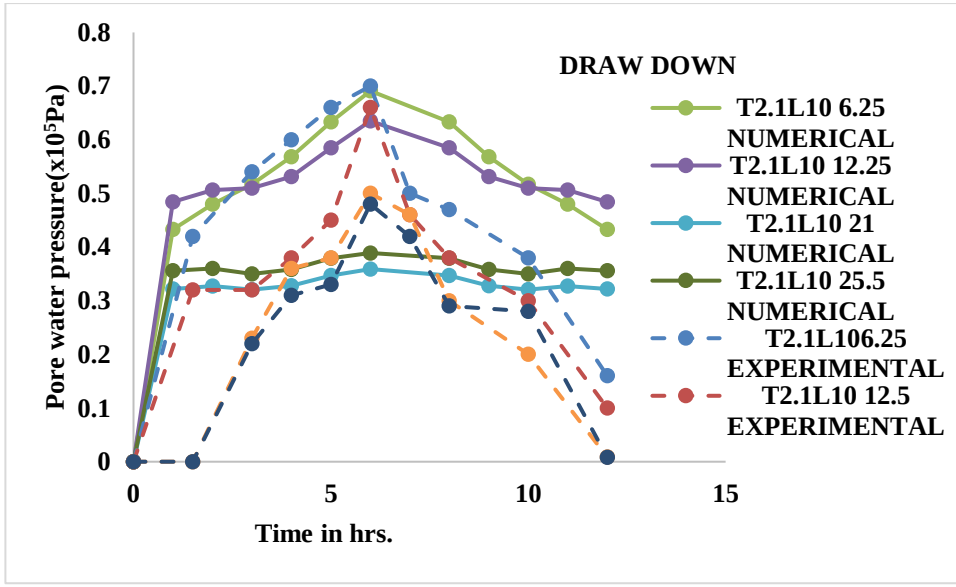

Figure. 5.15(j): Pore water pressure variation of *B*/8 position under full rise up and drawdown condition at 7m position (Experimental and numerical investigation)

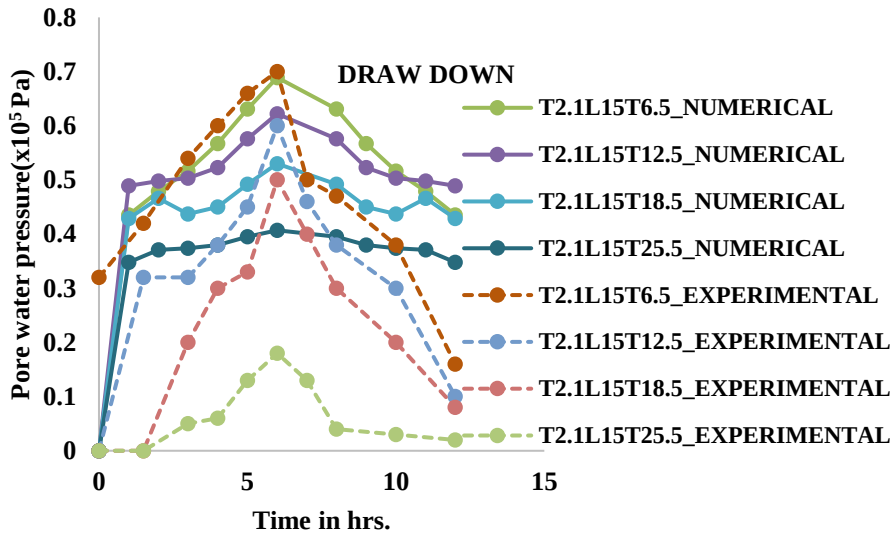

Figure. 5.15(k): Pore water pressure variation of *B*/8 position under full rise up and drawdown condition at 7m position (Experimental and numerical investigation)

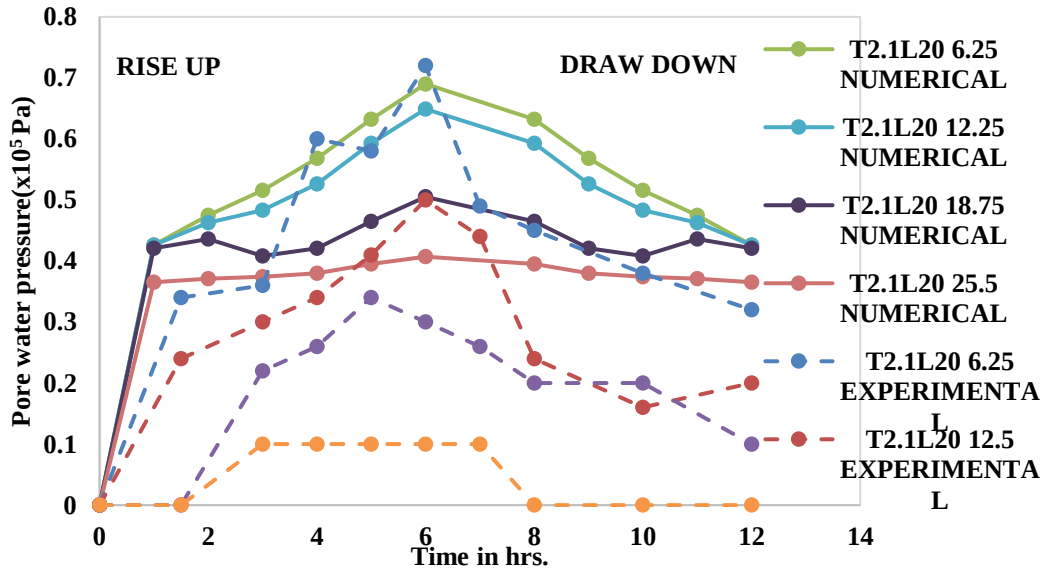

Figure. 5.15(l): Pore water pressure variation of *B*/8 position under full rise up and drawdown condition at 7m position (Experimental and numerical investigation)

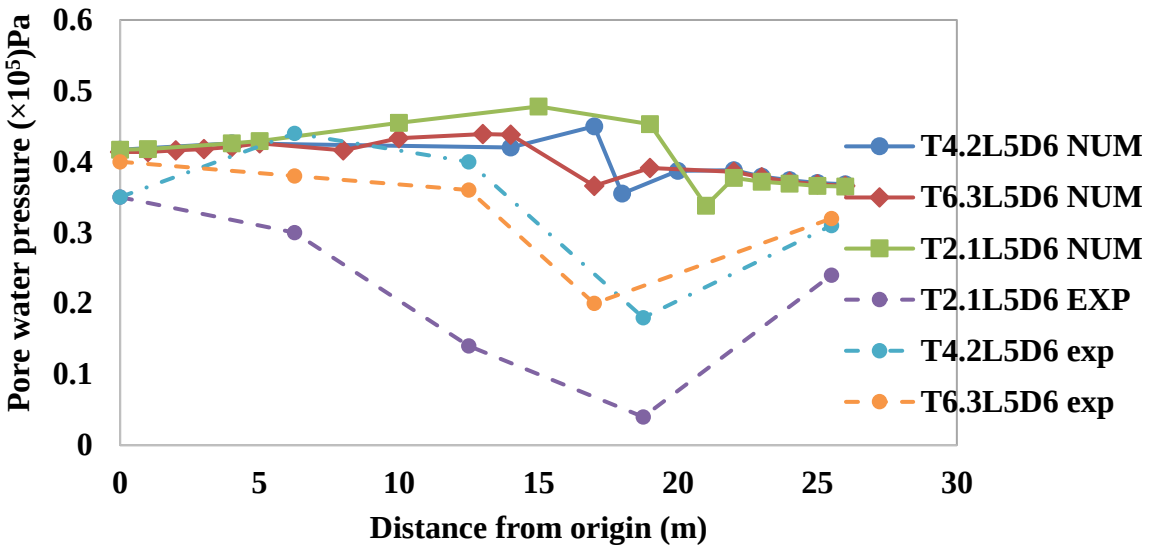

Figure. 5.16(a) Pore water pressure variation of 5m long sheet pile under full drawdown condition at 7m position (Experimental and numerical investigation)

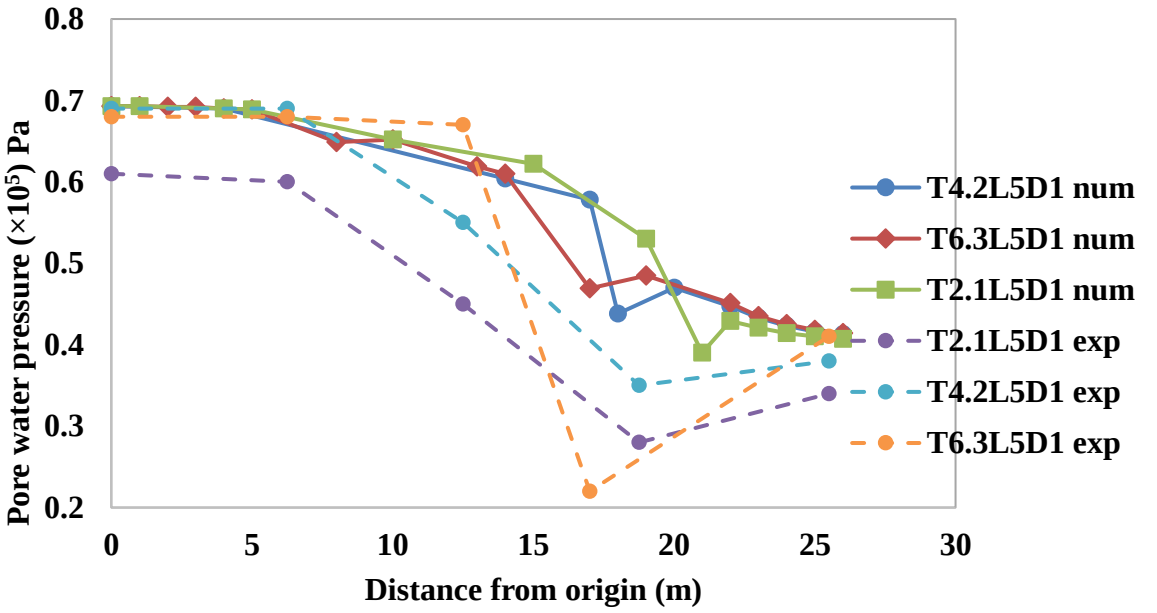

Figure. 5.16(b) Pore water pressure variation of 5m long sheet pile under full drawdown condition at 7m position (Experimental and numerical investigation)

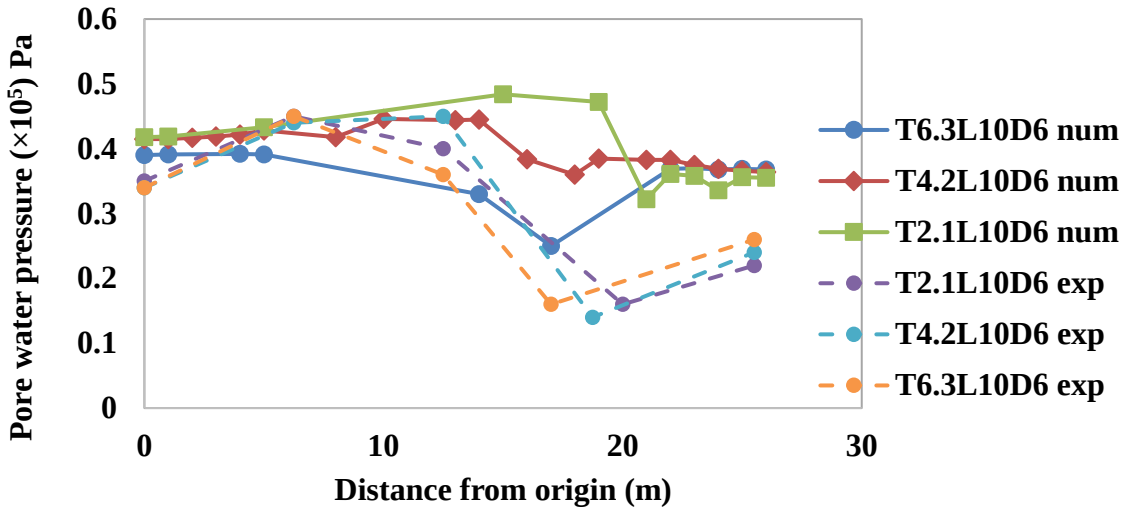

Figure. 5.16(c) Pore water pressure variation of 10m long sheet pile under full drawdown condition at 7m position (Experimental and numerical investigation)

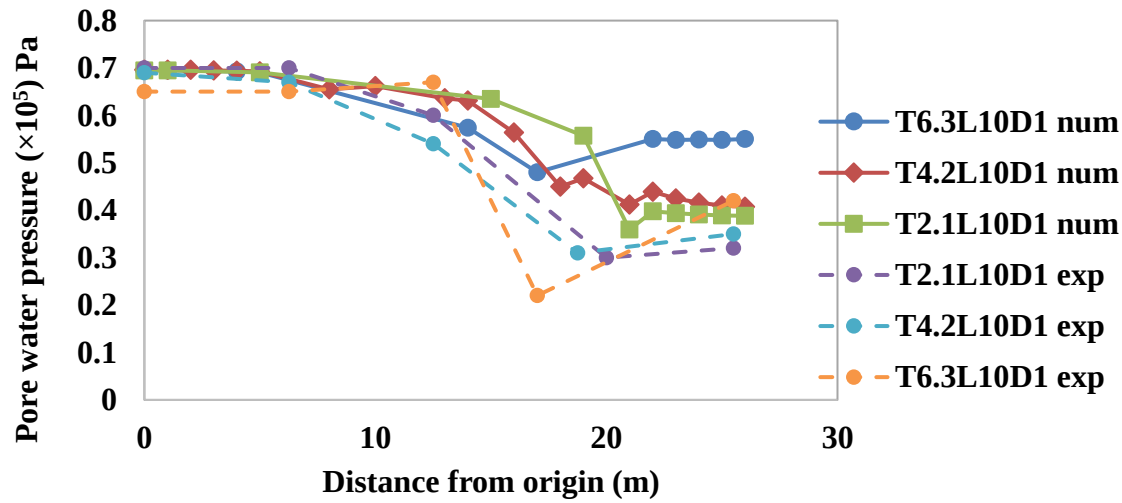

Figure. 5.16(d) Pore water pressure variation of 10m long sheet pile under full rise up condition at 7m position (Experimental and numerical investigation)

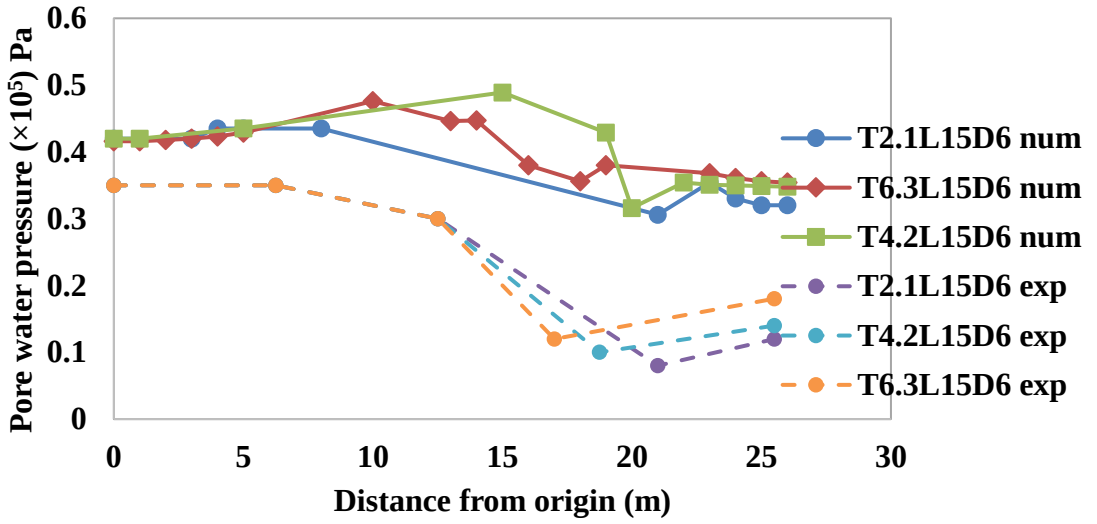

Figure. 5.16(e) Pore water pressure variation of 15m long sheet pile under full drawdown condition at 7m position (Experimental and numerical investigation)

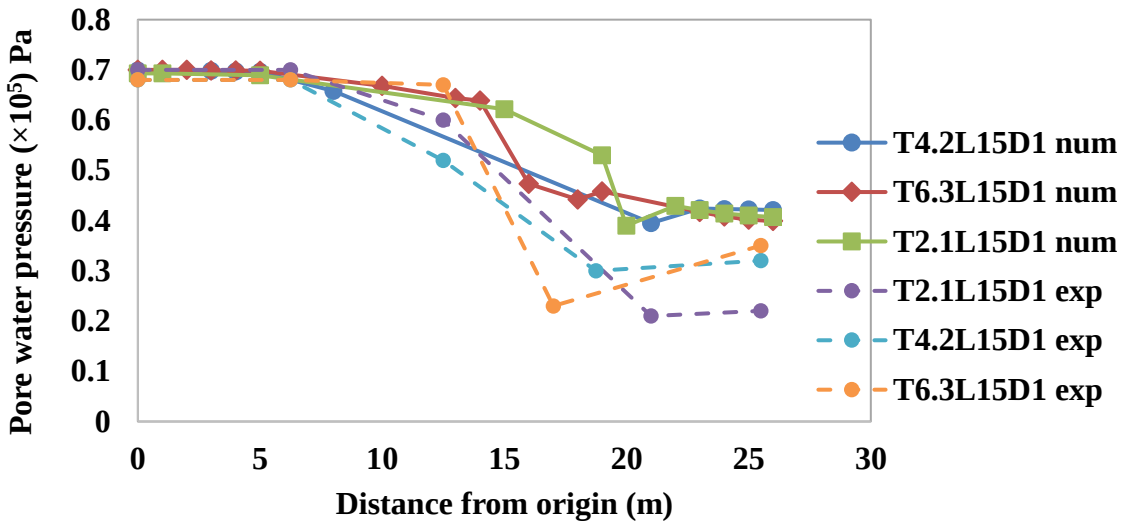

Figure. 5.16(f) Pore water pressure variation of 15m long sheet pile under full rise up condition at 7m position (Experimental and numerical investigation)

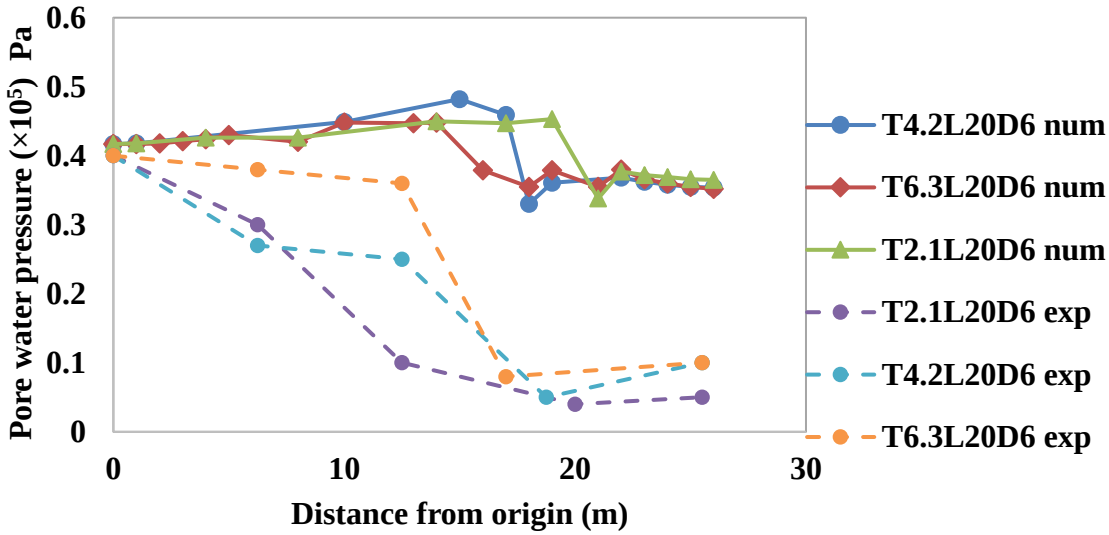

Figure. 5.16(g) Pore water pressure variation of 20m long sheet pile under full drawdown condition at 7m position (Experimental and numerical investigation)

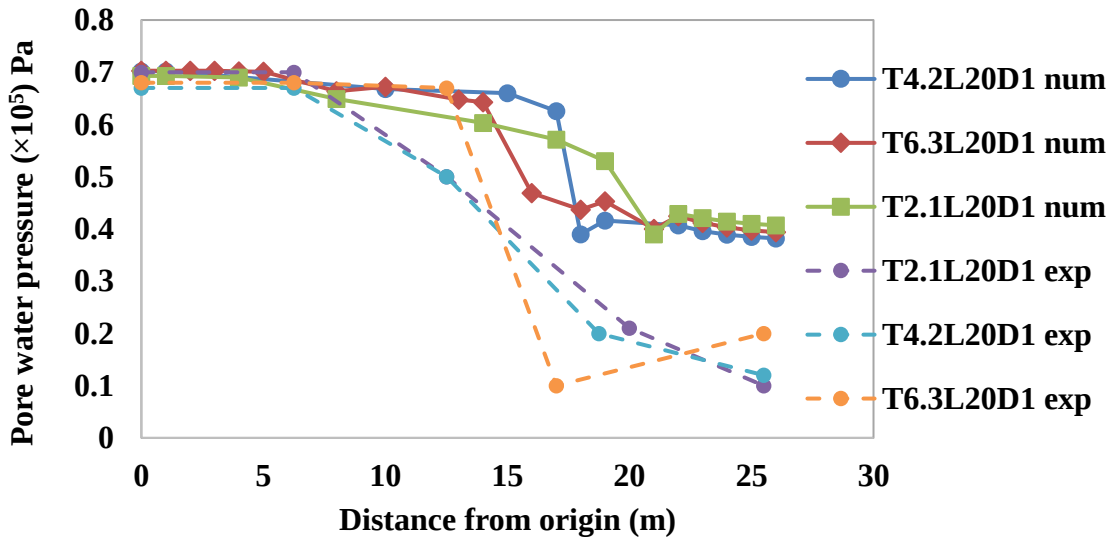

Figure. 5.16(h) Pore water pressure variation of 20m long sheet pile under full rise up condition at 7m position (Experimental and numerical investigation)

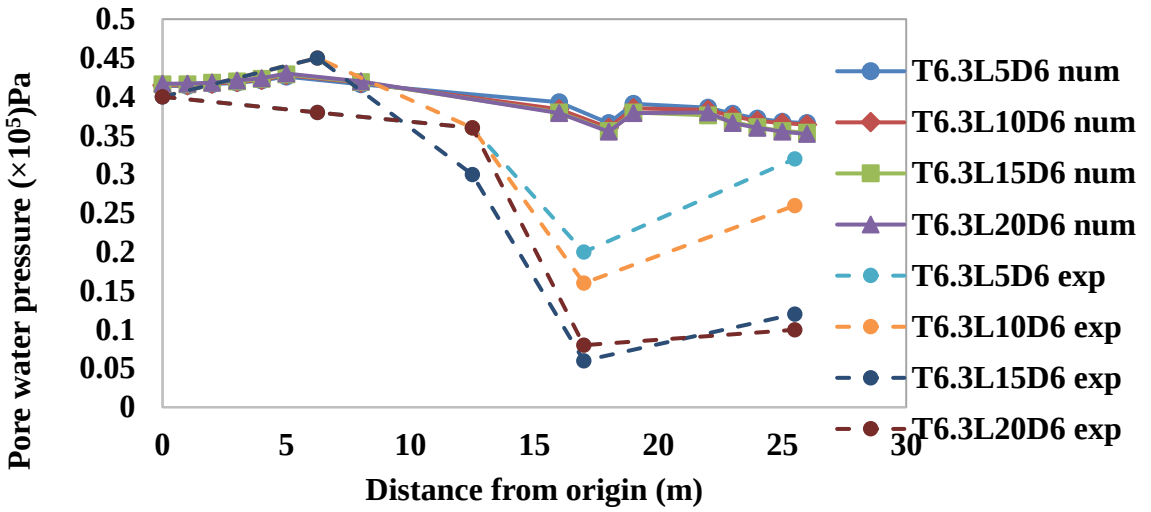

Figure. 5.16(i) Pore water pressure variation of different length of sheet pile at 3*B*/8 position under full drawdown condition at 7m position (Experimental and numerical investigation)

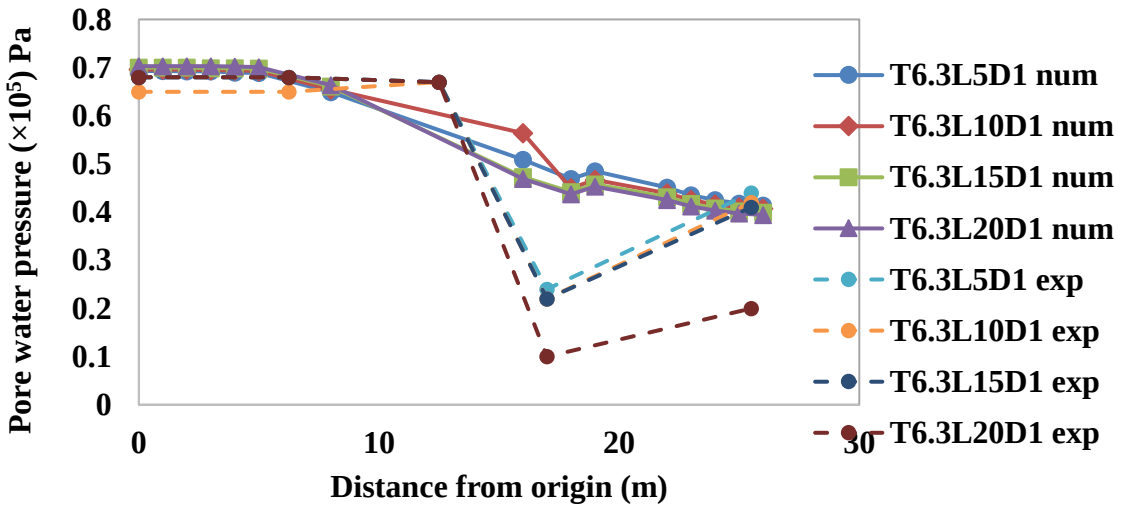

Figure. 5.16(j) Pore water pressure variation of different length of sheet pile at 3*B*/8 position under full rise up condition at 7m position (Experimental and numerical investigation)

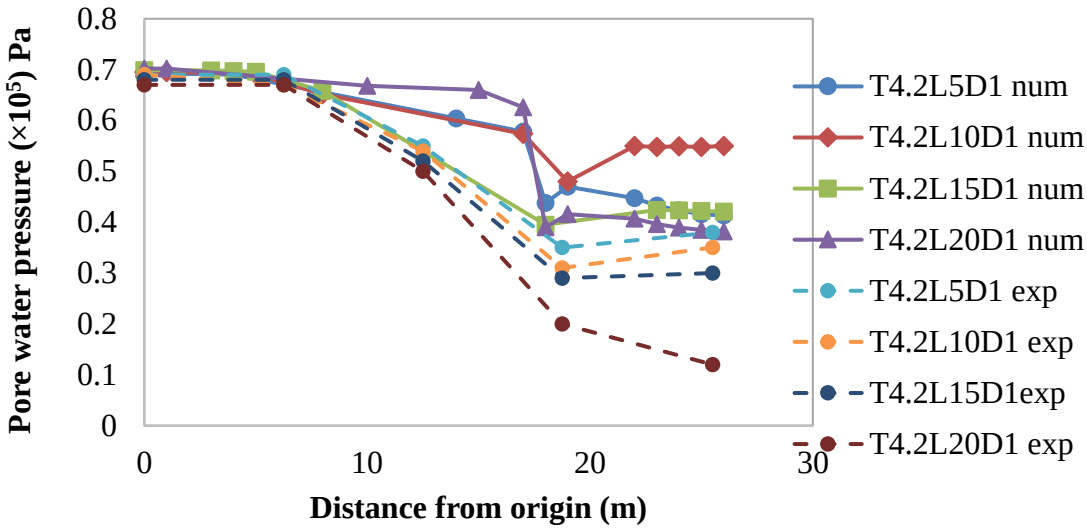

Figure. 5.16(k) Pore water pressure variation of different length of sheet pile at 2*B*/8 position under full rise up condition at 7m position (Experimental and numerical investigation)

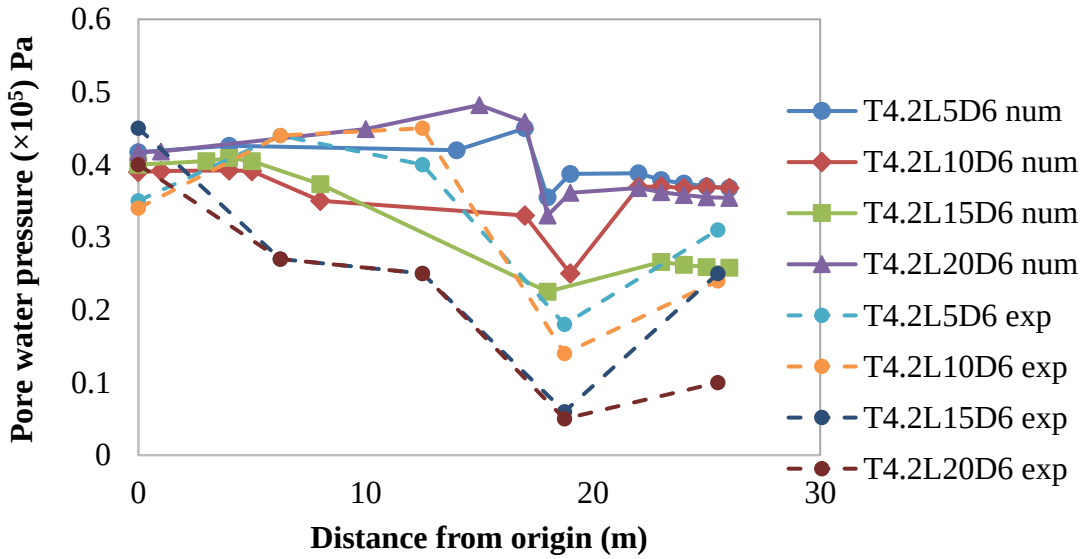

Figure. 5.16(l) Pore water pressure variation of different length of sheet pile at 2*B*/8 position under full drawdown condition at 7m position (Experimental and numerical investigation)

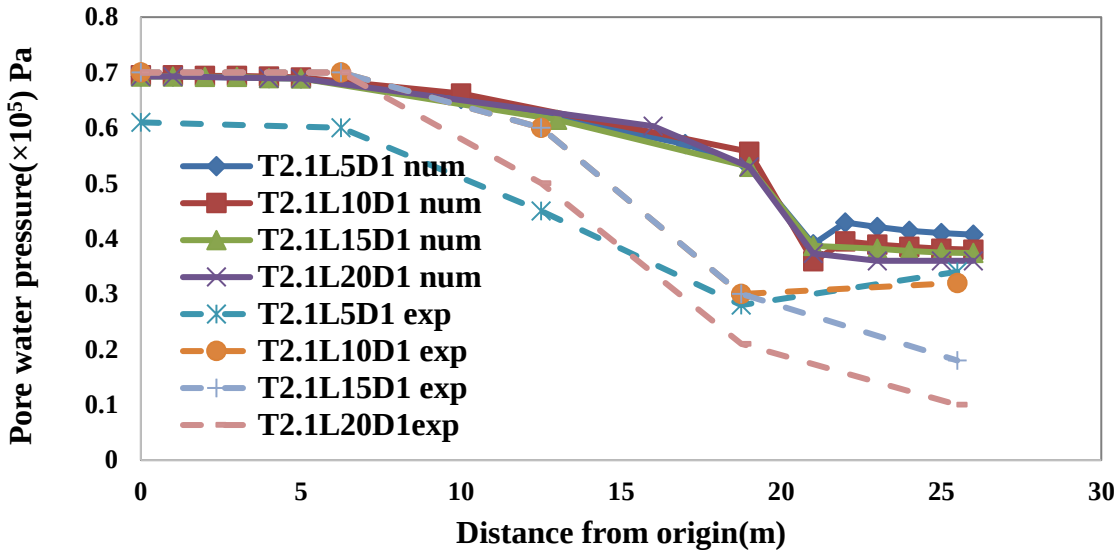

Figure. 5.16(m) Pore water pressure variation of different length of sheet pile at *B*/8 position under full rise up condition at 7m position (Experimental and numerical investigation)

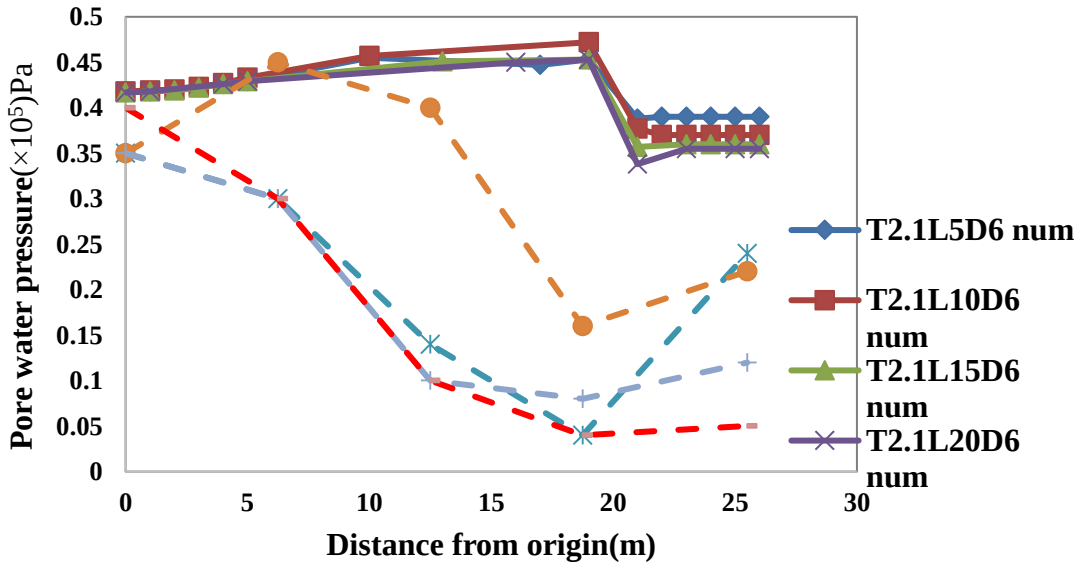

Figure. 5.16(n) Pore water pressure variation of different length of sheet pile at *B*/8 position under full drawdown condition at 7m position (Experimental and numerical investigation)

It is observed from the figures that the magnitude of variation of pore pressure at downstream end is less compared to the upstream side. It has been observed that at 3*B*/8 position for full drawdown condition at downstream end pore water pressure is approximately 28.00% less compared to that on the upstream slope. It has further been observed that at 2*B*/8 position for full drawdown condition at downstream end pore water pressure is approximately 30.00%

less compared to that on the upstream slope. In addition to this, for sheet pile position of *B*/8 position, at full drawdown condition at downstream end pore water pressure is approximately 33.00% less compared to that on the upstream slope. Effectiveness of seepage barrier has been observed at *B*/8 position compared to 2*B*/8 and 3*B*/8 positions. Further It has been seen that for full rise up condition the magnitude of variation of pore pressure at downstream end for 2*B*/8 and 3*B*/8 positions approximately are 45.00% and 50% less respectively compared to the upstream side slope at *B*/8 position, whereas at 2*B*/8 and 3*B*/8 positions, reduction for pore water pressure is 2*B*/8 and 3*B*/8 positions is approximately 42.00% and 40.00% respectively. The effectiveness of sheet pile in terms of pore water pressure has been shown in Table. 5.1 and Table 5.2.

Table 5.1: Percentage change of pore water pressure variation under rise up condition at 7m from the top of the dam

Percentage change in pore water pressure with respect to without sheet pile case at full rise up condition at downstream end			
	Sheet pile position from downstream end		
Sheet pile length	***3B*/8 Position**	***2B*/8 Position**	***B*/8 Position**
5 m long	20.5%	22.61%	23.93%
10 m long	21.12%	23.73%	25.23%
15 m long	21.30%	23.93%	27.47%
20 m long	28.22%	28.41%	33.64%

Table 5.2: Percentage change of pore water pressure variation under drawdown condition at 7m from the top of the dam

Percentage change in pore water pressure with respect to without sheet pile case at full drawdown condition at downstream end			
	Sheet pile position from downstream end		
Sheet pile length	***3B*/8 Position**	***2B*/8 Position**	***B*/8 Position**
5 m long	9.11%	16.88%	23.28%
10 m long	19.11%	21.11%	36.36%
15 m long	19.778%	22.66%	50.00%
20 m long	21.33%	34.44%	57.48%

It appears from the Table 5.1 and Table 5.2 that due to the changes of the sheet pile length pore water pressure also changes. It has been quantifying that for 5m length of sheet pile reduction of pore water pressure at the downstream end is approximately 30% whereas for the placement of 10m, 15m and 20m long sheet pile the reduction of pore water pressure is approximately 33%, 40% and 50% respectively. It is also observed from the tables that for 5m length to 20m length the decrease of pore pressure is varying from 20.5% to 28.22% for 3*B*/8 position, whereas for B/8 position it varies from 23.93% to 33.64%. It further appears from the table 5.2 that for 5m length to 20m length the decrease of pore pressure is varying from 9.11% to 21.33% for 3*B*/8 position whereas for B/8 position it varies from 23.28% to

57.48%. Thus maximum effectiveness of sheet pile is obtained for 20m long pile at B/8 position (near downstream end) with maximum decrease of pore water pressure of 57.48% with respect to pore pressure without sheet pile at 7m below the top of the dam under maximum drawdown.

5.4.1.2.2.2 Pore water pressure variation at 12m from the top of the dam

Experimental and numerical observations in transient state considering both rise up and drawdown conditions have been presented in this section from figures 5.17(a) to 5.17(l). Pore water pressure variation at 10m from the top of the dam along horizontal direction at different points at distances of 6.25m, 12.5m, 15m and 22.5m from the upstream end has been presented for both rise up and drawdown conditions. Pore water pressure variation for both rise up and drawdown conditions at 3*B*/8 position at 12m from the top has been presented in figures 5.17(a),5.17(b),5.17(c), 5.17(d) for 5m,10m, 15m and 20m long sheet pile respectively. Pore water pressure variation for both rise up and drawdown conditions at 2*B*/8 position along horizontal direction at 12m from the top has been presented in figures 5.17 (e) for 10m long sheet pile respectively. Figures 5.17(f) and 5.17(g) present experimental and numerical results for full drawdown and rise up conditions respectively for 5m long sheet pile at 12m from the top of the dam Figures 5.17(i) and 5.17(j) show experimental and numerical results for full drawdown and rise up conditions respectively of 10m long sheet pile at 12m from the top of the dam. Figures 5.17(k) and 5.17(l) present experimental and numerical results for full drawdown and rise up conditions respectively for 15m long sheet pile at 12m from the top of the dam.

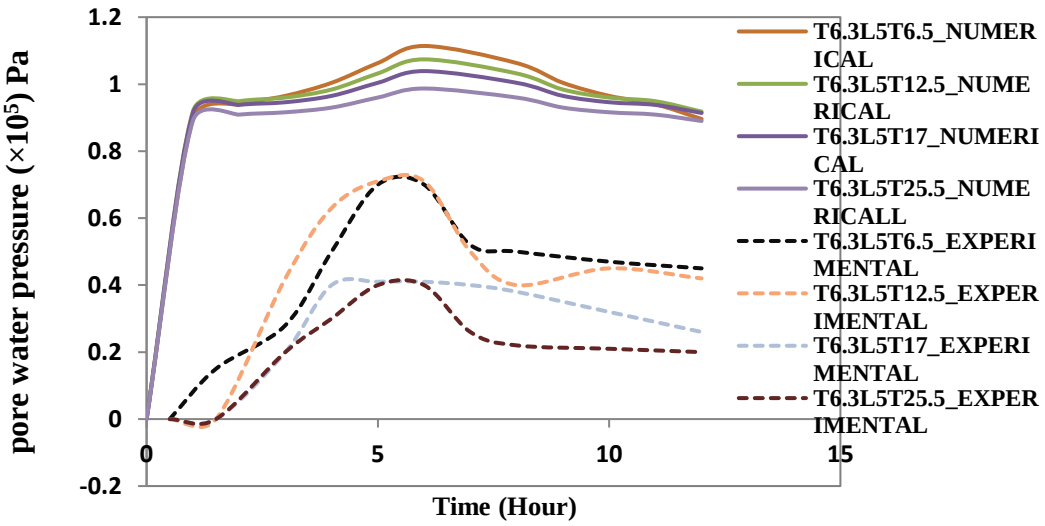

Figure. 5.17(a) Pore water pressure variation of 3*B*/8 position under full rise up and drawdown condition at 12m position (Experimental and numerical investigation)

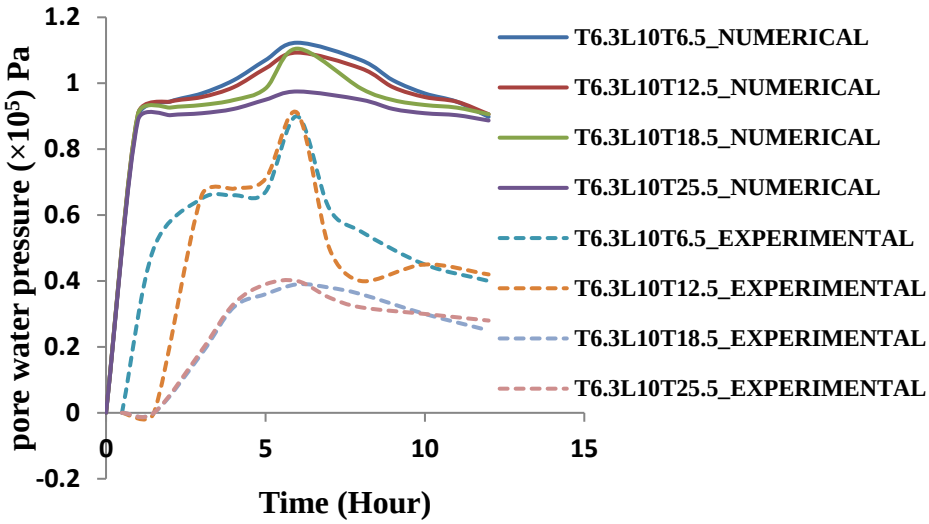

Figure. 5.17(b) Pore water pressure variation of 3*B*/8 position under full rise up and drawdown condition at 12m position (Experimental and numerical investigation)

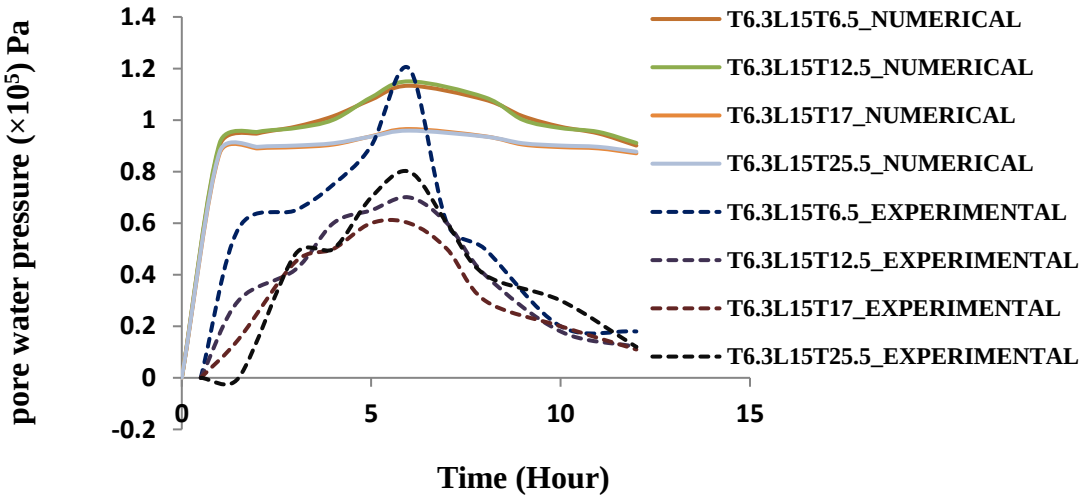

Figure. 5.17(c) Pore water pressure variation of 3*B*/8 position under full rise up and drawdown condition at 12m position (Experimental and numerical investigation)

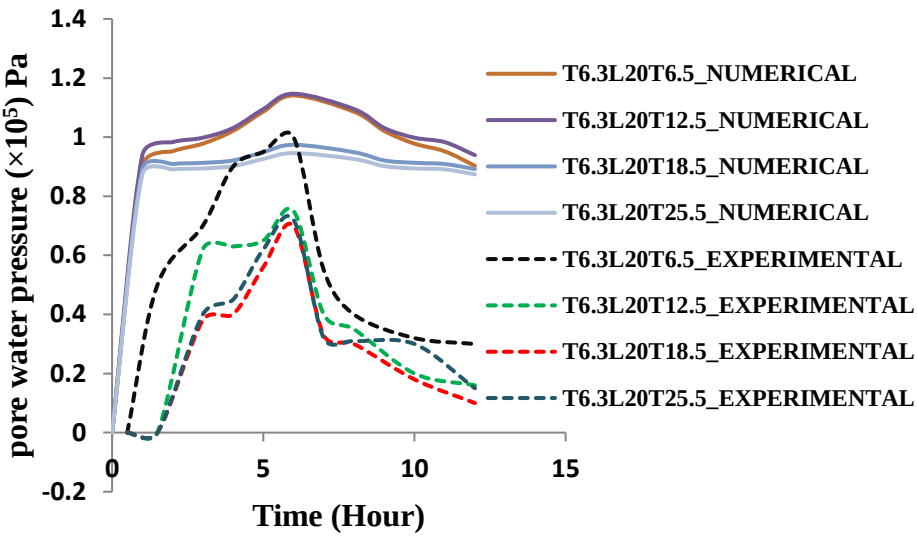

Figure. 5.17(d) Pore water pressure variation of 3*B*/8 position under full rise up and drawdown condition at 12m position (Experimental and numerical investigation)

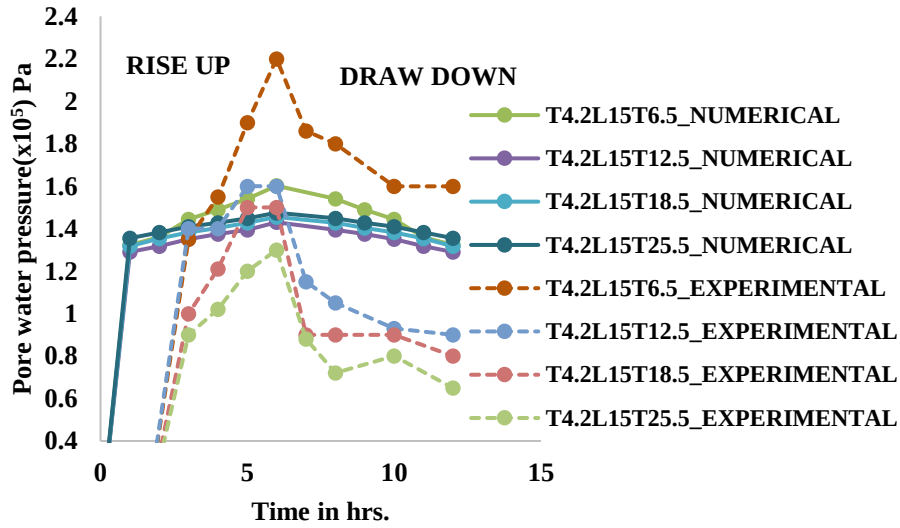

Figure. 5.17(e) Pore water pressure variation of 2B/8 position under full rise up and drawdown condition at 12m position (Experimental and numerical investigation)

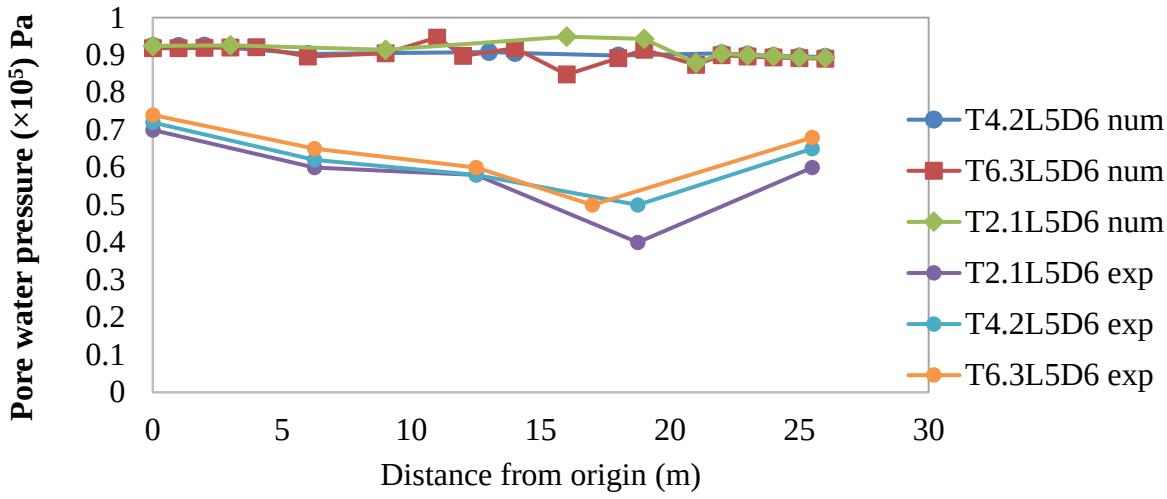

Figure. 5.17(f) Pore water pressure variation of 5m long sheet pile under full drawdown condition at 12m position (Experimental and numerical investigation)

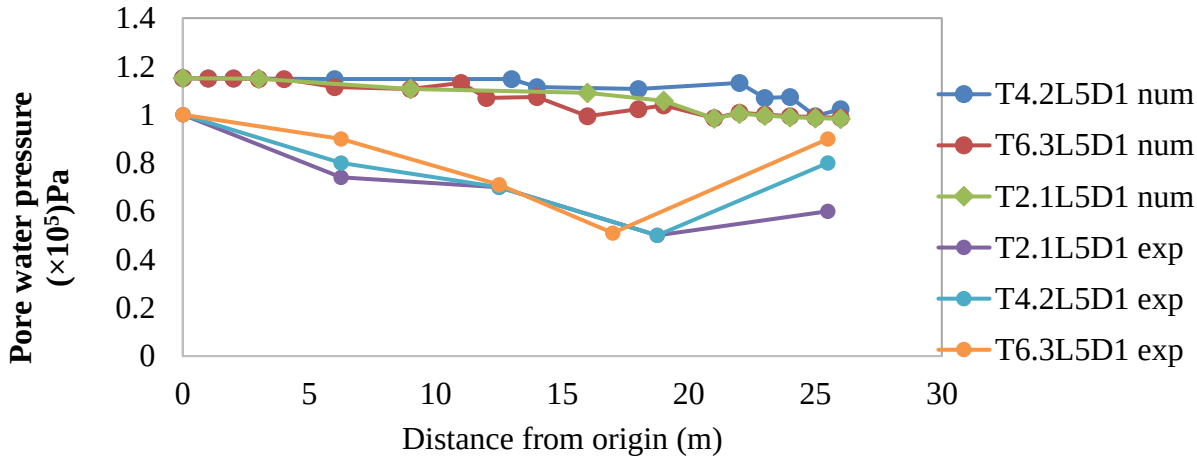

Figure. 5.17(g) Pore water pressure variation of 5m long sheet pile under full rise up condition at 12m position (Experimental and numerical investigation)

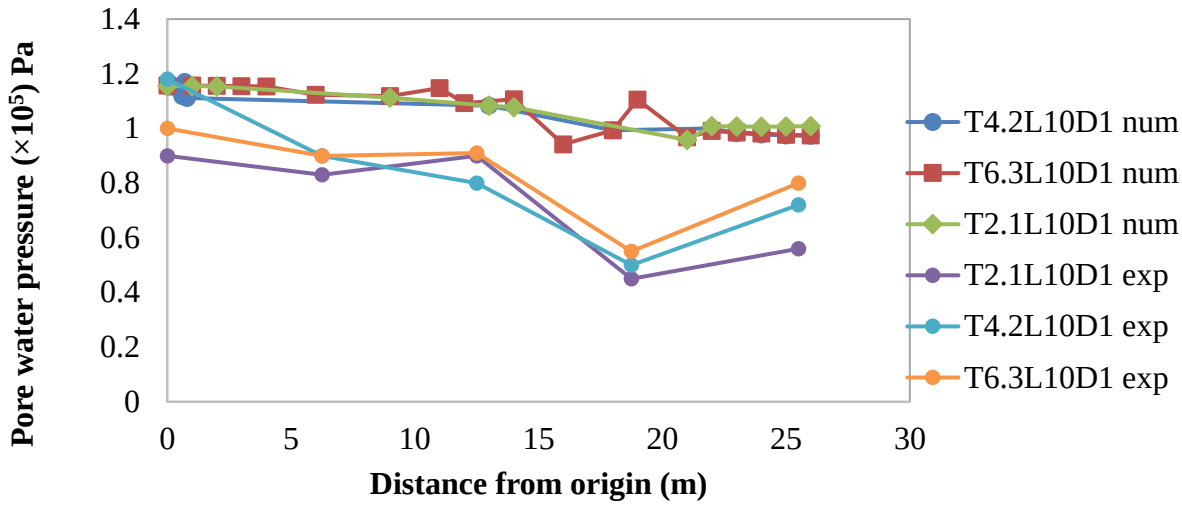

Figure. 5.17(h) Pore water pressure variation of 10m long sheet pile under full rise up condition at 12m position (Experimental and numerical investigation)

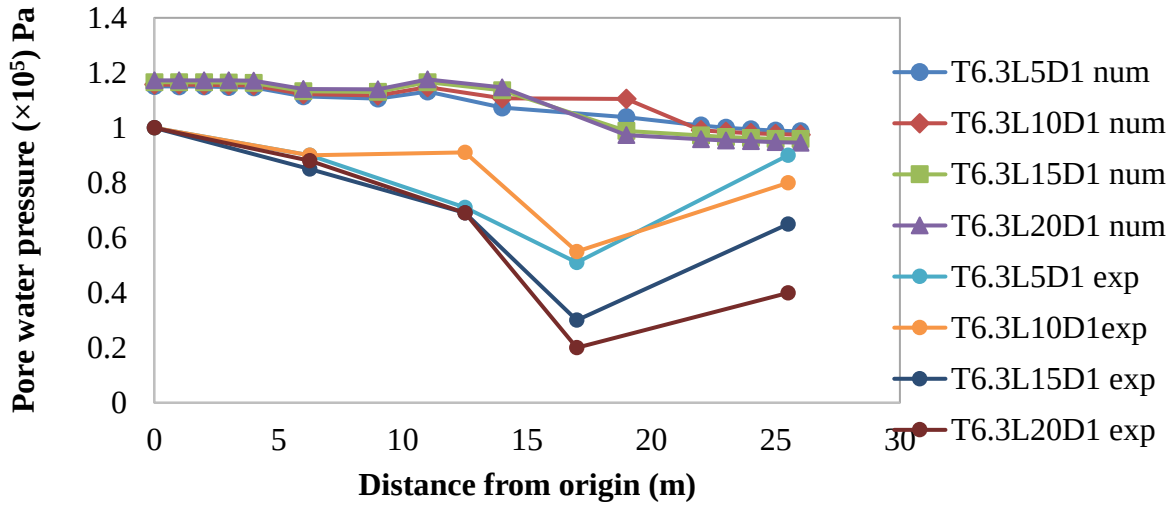

Figure. 5.17(i) Pore water pressure variation of B/8 position sheet pile under full rise up condition at 12m position (Experimental and numerical investigation)

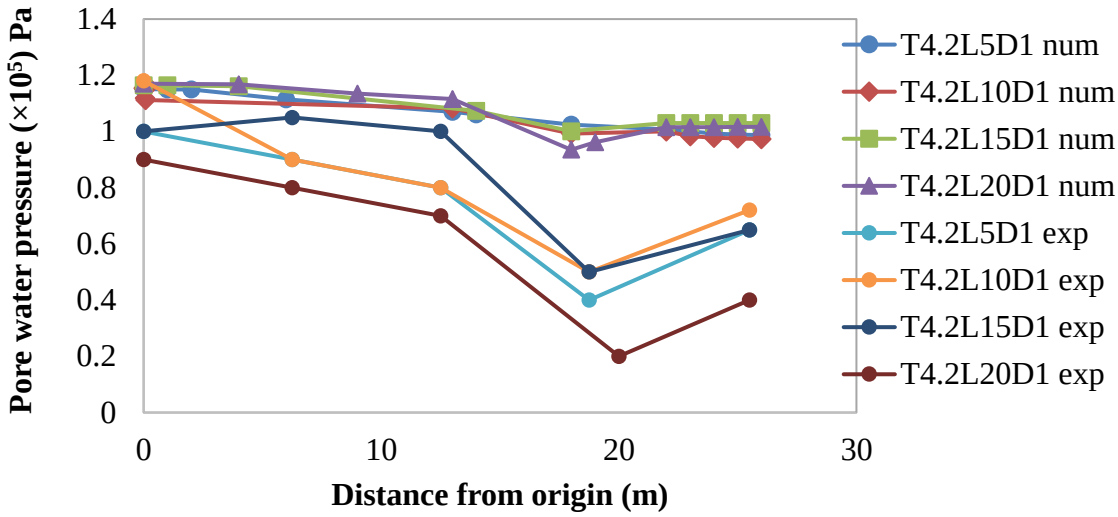

Figure. 5.17(j) Pore water pressure variation of 5m long sheet pile under full rise up condition at 12m position (Experimental and numerical investigation)

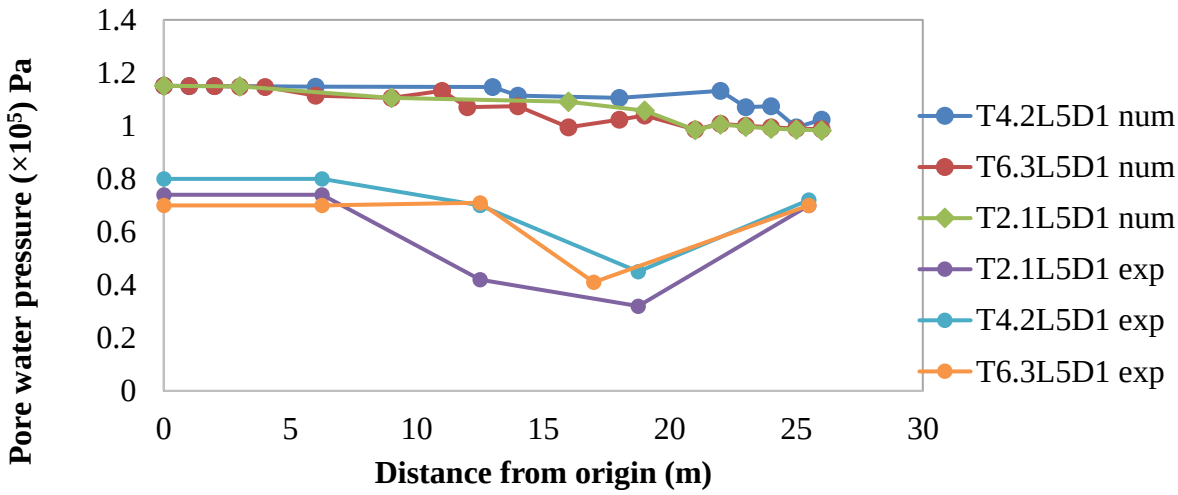

Figure. 5.17(k) Pore water pressure variation of 5m long sheet pile under full rise up condition

It has been observed from the figures that pore water pressure on downstream slope has been reduced approximately by 15%-20% compared to upstream slope at the position of 12m from the top of the dam. Tables 5.3 and Table 5.4 present percentage of decrease of pore water pressure variation for different sheet pile positions and lengths.

Table 5.3: Percentage change of pore water pressure variation under rise up condition at 12m from the top of the dam

Percentage change in pore water pressure with respect to without sheet pile case at full rise up condition at downstream end			
	Sheet pile position from downstream end		
Sheet pile length	***3B*/8 Position**	***2B*/8 Position**	***B*/8 Position**
5 m long	7.75%	17.75%	18.083%
10 m long	9.75%	18.75%	19.5%
15 m long	14.167%	19.42%	23.33%
20 m long	16.66%	21.16%	28.33%

Table 5.4: Percentage change of pore water pressure variation at drawdown condition at 12m from the top of the dam

Percentage change in pore water pressure with respect to without sheet pile case at full drawdown condition at downstream end			
	Sheet pile position from downstream end		
Sheet pile length	***3B*/8 Position**	***2B*/8 Position**	***B*/8 Position**
5 m long	8.48%	9.49%	9.78%
10 m long	8.58%	11.11%	10.40%
15 m long	10.91%	12.72%	15.55%
20 m long	11.71%	13.03%	29.29%

It appears from the Table 5.3 and Table 5.4 that due to the changes of the sheet pile length pore water pressure also changes. It is also observed from the tables that for 5m length to 20m length the decrease of pore pressure is varying from 7.57% to 16.66% for 3*B*/8 position, whereas for B/8 position it varies from 18.083% to 28.33%. It further appears from the Table 5.4 that for 5m length to 20m length the decrease of pore pressure is varying from 8.48% to 11.71% for 3*B*/8 position whereas for *B*/8 position it varies from 9.78% to 29.29%. Thus maximum effectiveness of sheet pile is obtained for 20m long pile at B/8 position (near downstream end) with maximum decrease of pore water pressure of 29.29% with respect to pore pressure without sheet pile at 12m below the top of the dam under maximum drawdown.

It is thus seen that pore pressure reduction at 7m level is more than that at 12m depth. This is obvious since water must reach the downstream water head, crossing the sheet pile barrier, which has been considered at the base of the dam.

5.4.1.2.3 Observations for seismic study

In case of seismic condition for any given time the analysis has been done in the same way as adopted for analysis under steady state condition considering three particular times. Variation of pore water pressure under seismic condition in case of transient flow is very much erratic and increases and decreases respectively at the time of increase and decrease of seismic acceleration. This is clearly observed from the pore water pressure graphs shown in figures 5.18(a) to 5.18(f). These figures present variation of pore water pressure along horizontal

direction parallel to dam base at a depth of 7m from the top of the dam for sheet pile lengths of 5m, 10m, 15m and 20m respectively at different position of *B*/8, 2*B*/8 and 3*B*/8 from downstream end respectively.

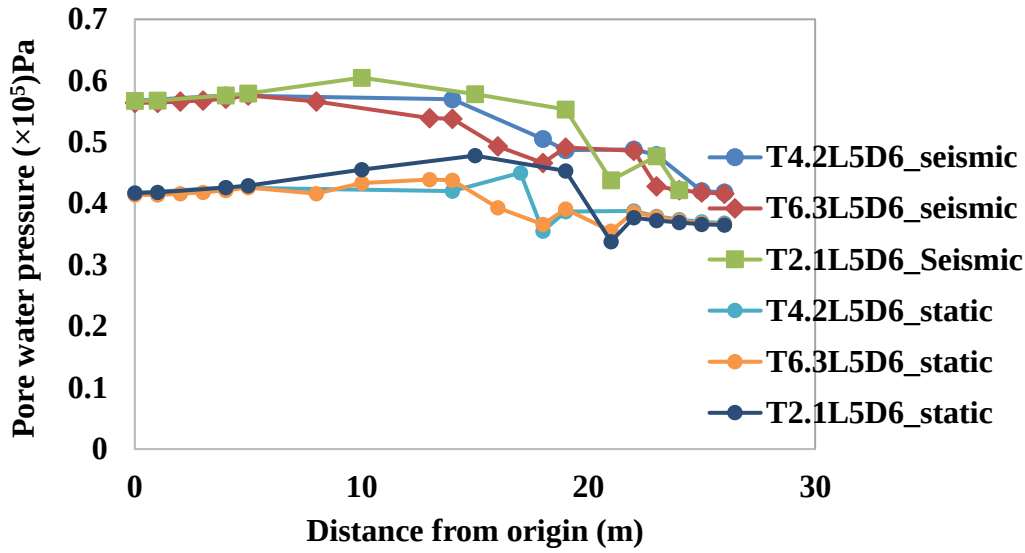

Figure. 5.18(a) Pore water pressure variation of 5m long sheet pile under full drawdown condition (at 7m position from top)

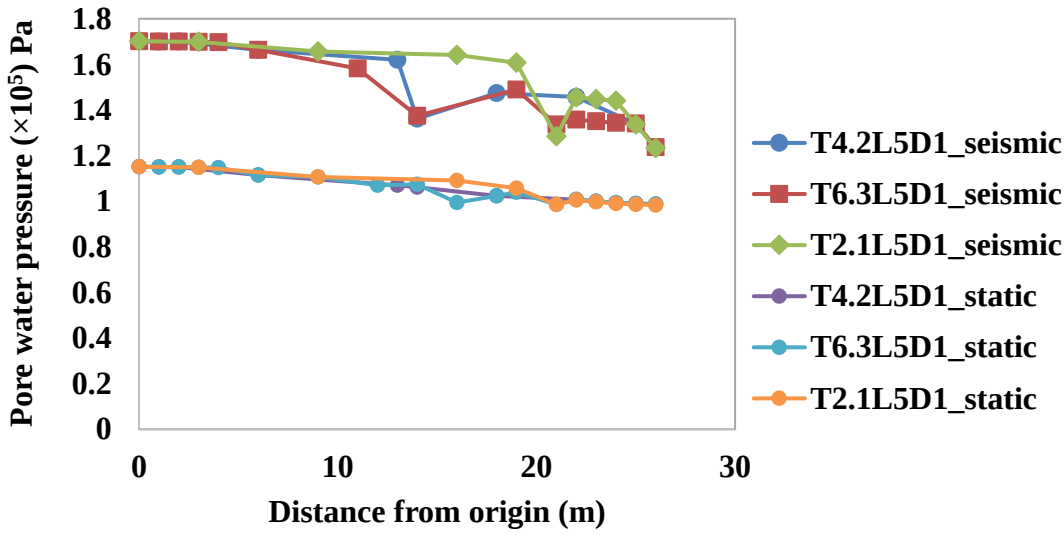

Figure. 5.18(b) Pore water pressure variation of 5m long sheet pile under full rise up condition (at 12m position from top)

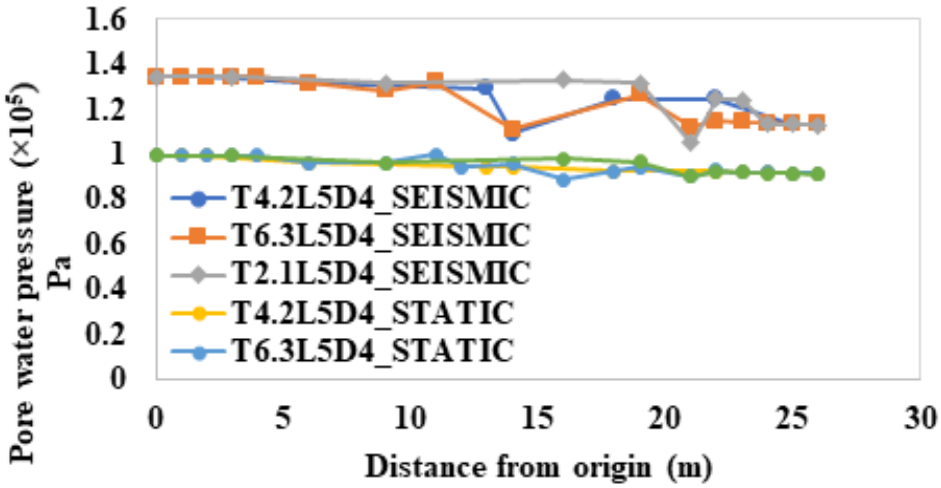

Figure. 5.18(c) Pore water pressure variation of 5m long sheet pile under rise up condition (at 12m position from top)

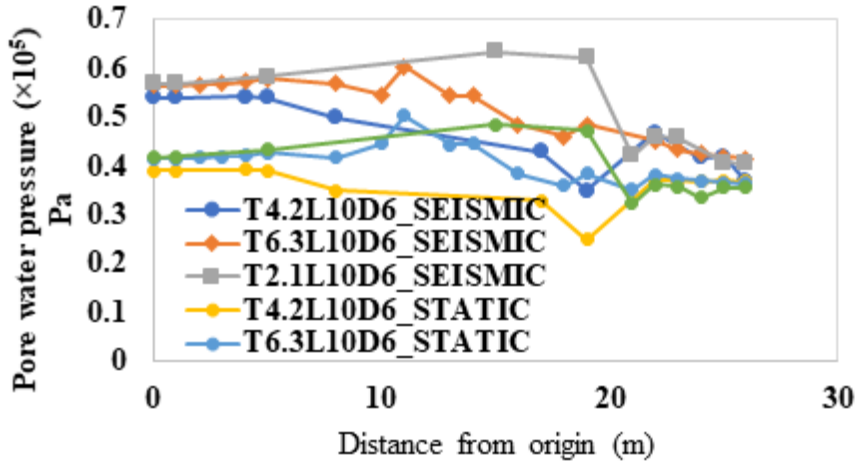

Figure. 5.18(d) Pore water pressure variation of 10m long sheet pile under full drawdown condition (at 7m position from top)

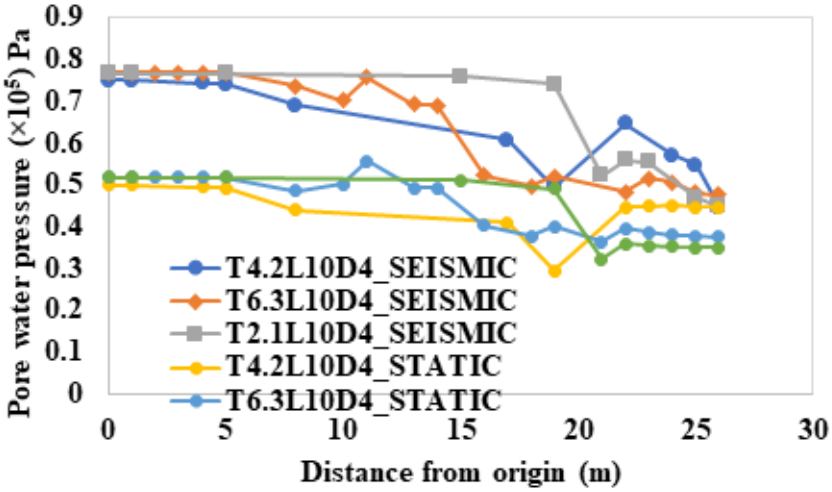

Figure. 5.18(e) Pore water pressure variation of 10m long sheet pile under rise up condition (at 7m position from top)

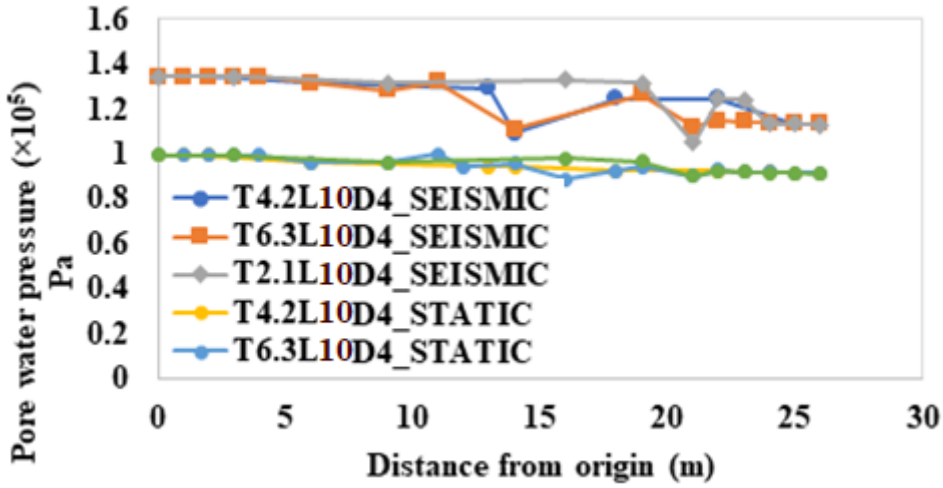

Figure. 5.18(f) Pore water pressure variation of 10m long sheet pile under rise up condition (at 12m position from top)

It has been observed from the figures that in seismic case pore water pressure increases up to 20% at the upstream side whereas at downstream side increases up to 10-15% compared to respective static condition. This is due to seismic effect which is responsible for increase of pore pressure.

5.4.2 PORE WATER PRESSURE VARIATION WITHIN DAM BODY

5.4.2.1 STATIC CONDITION

Figure 5.19 (a) presents pore water pressure developed in the dam body at 2m from the top along the horizontal cross section of the dam. In figure 5.19 (a) Pore water pressure has been plotted experimentally and numerically for fixed hydraulic head of 3.5 m. A non-linear variation pattern has been obtained for all the cases. It is observed from the figure that for both the working heads maximum pore pressure occurs at about 11m from the origin (extreme upstream point of the base), with a continually rising trend and beyond this point pore pressure decreases towards the downstream. This may be attributed to gradual building up of pore pressure within the dam body from upstream side during seepage through a medium of low permeability. The pore pressure dissipates on the downstream side as pore water finds its way towards downstream.

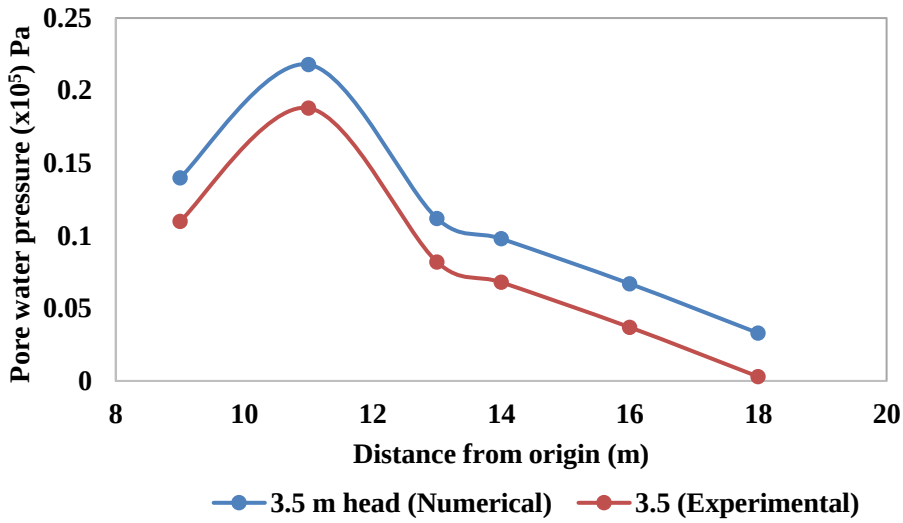

Figure. 5.19(a) Pore water pressure variation in steady state condition for *B*/8 position 5m length at 2m from the top.

Similar observation has been made for all lengths of sheet pile. Hence a typical 5m long sheet pile has been considered to illustrate the phenomenon for *B*/8, 2*B*/8 and 3*B*/8 positions of different sheet pile length. It has been observed that variation of length in sheet pile is not affecting the pore pressure within the dam body.

5.4.2.2 SEISMIC CONDITION

Figure 5.19(b) presents the pore water pressure variation along the horizontal direction of 2m position from the top of the dam for 5m long sheet pile at different sheet pile positions.

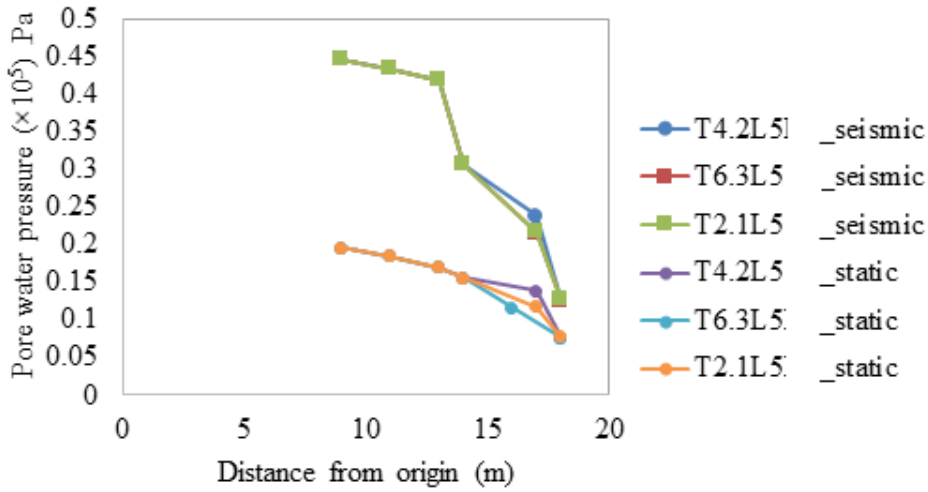

Figure. 5.19(b) Pore water pressure variation in steady state condition

It is also observed from the figure 5.19(b) that under seismic condition pore water pressure increases towards the downstream. Due to this phenomenon phreatic surface moves upward. It has been also observed that at upstream side pore water pressure increases up to 45% whereas at downstream increment is up to 10% on an average due to seismic effect.

5.4.2.3 TRANSIENT STATE CONDITION

5.4.2.3.1 Single tidal cycle under static condition

Pore water pressure along the horizontal center line of the dam body has been estimated from numerical modeling in case of transient seepage of time variation in 1 hour, 2 hours, 3 hours, 4 hours, 5 hours and 6 hours in rise up condition and after that 7 hours, 8 hours, 9 hours and 10 hours, 11 hours and 12 hours in drawdown condition. Figure5.20(a) (for rise up condition) and 5.20 (b) (for drawdown condition) present pore water pressure at the middle of the dam along horizontal direction from origin. Figure 5.20(c) shows variation of pore water pressure at different points along the horizontal direction at 2m from the top of dam. Figure 5.20(d) it has been shown that experimental results appear to follow similar trend with numerical one

In the figures variation of the upstream tidal head with respect to cycle time has been indicated. The LTL has been kept at zero position and only the increase and decrease in river water level from LTL to HTL and HTL to LTL is plotted. The Zone of rise up, defined can be clearly identified by the co-ordinates of the points which show a variation in pore water pressure (PWP) head during the tidal cycle.

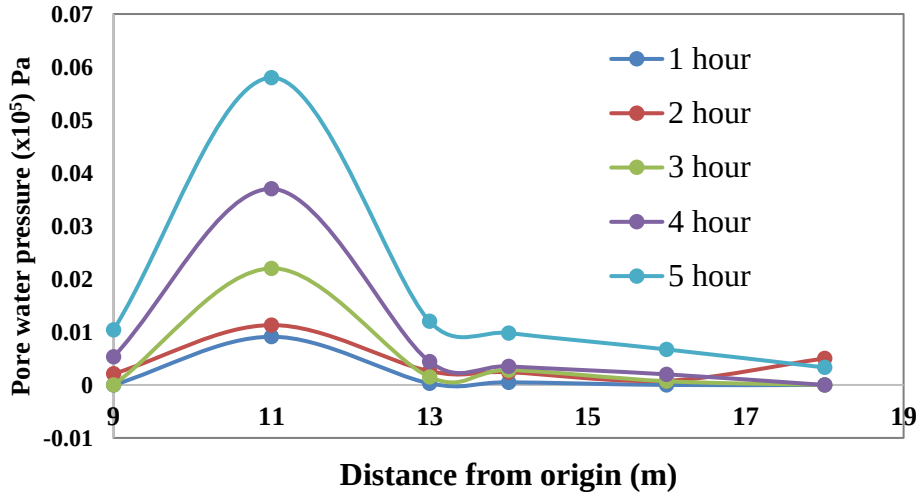

Figure. 5.20 (a) Pore water pressure variation in rise up condition (Numerical)

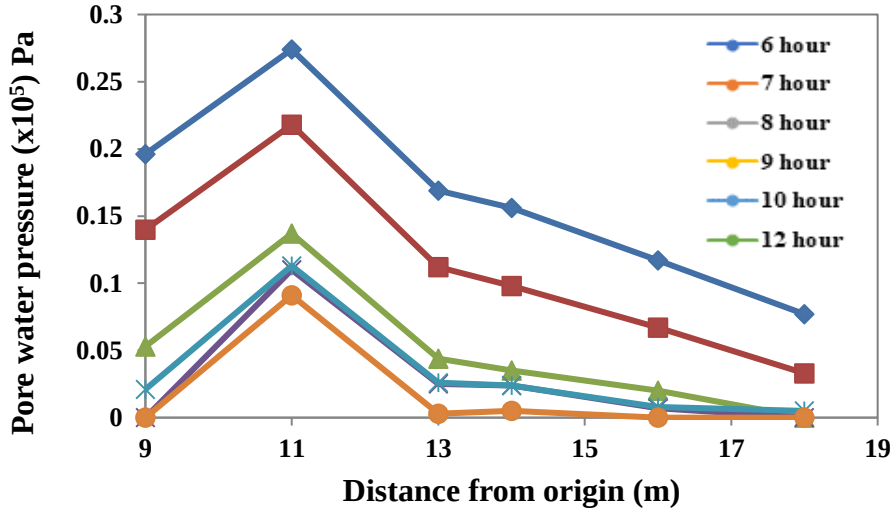

Figure. 5.20 (b) Pore water pressure variation in drawdown condition (Numerical)

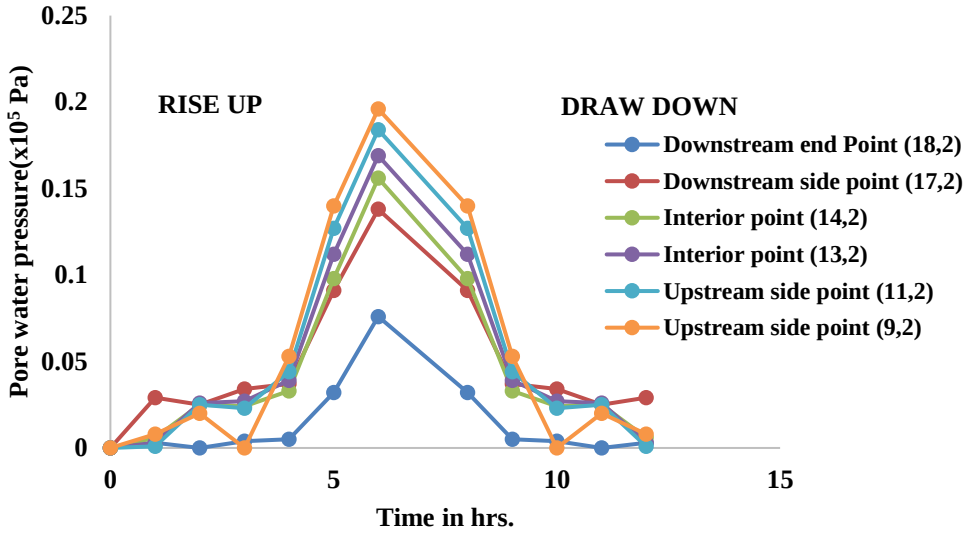

Figure. 5.20 (c) Pore water pressure variation in rise up and drawdown condition (Numerical)

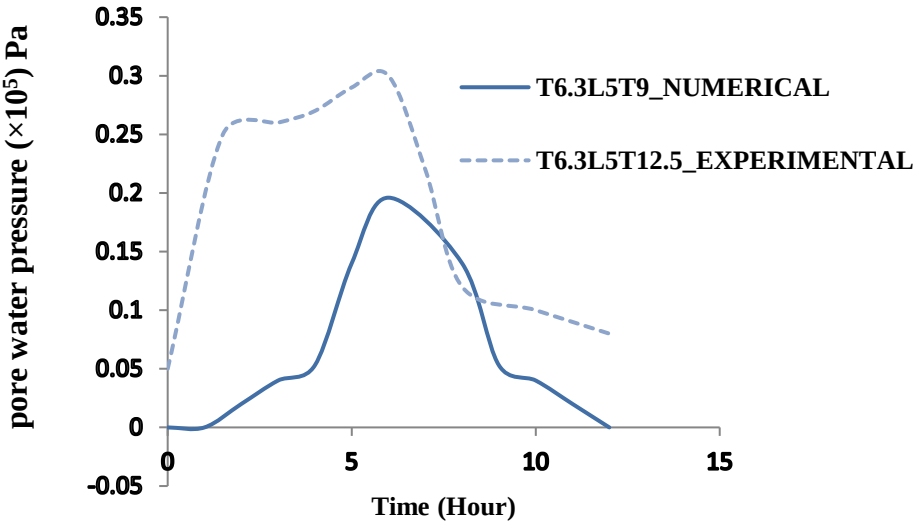

Figure. 5.20 (d) Pore water pressure variation (Experimental and numerical investigation)

It has been observed from the figures that for rise up and drawdown conditions variation of pore water pressure is more pronounced on upstream slope compared to the downstream side. From Figure 5.20(d) it has been shown that experimental results appear to follow similar trend with numerical one. Occurrence of maximum value

obtained from numerical study is found at similar location in case of experimental results, although experimental values are found to be quite higher.

It is further observed that for both the cases of rise up and draw down pore pressure initially increases up to about 9m for rise up condition and 11m for drawdown condition. Then it decreases towards the downstream. The reason may be attributed to the same aspect as discussed for steady seepage case in the previous section. It is further observed that with increase of time pore pressure is increasing for rise up condition and decreasing for drawdown condition. Thus, for increasing head pore pressure is increasing during rise up and vice versa for drawdown.

It has been seen that in the upstream side slope, there is an initial gradual increase in PWP head during rise up, followed by a sharp steep increase near the half cycle time zone, which is followed by a decrease in pore water pressure during Drawdown. However, the rate of increase of pore water pressure during drawdown has been observed to be much lower than that during rise up.

At the end of a single cycle, it has been observed that there is a net gain in pore water pressure for all portions within the body of the dam.

From the Figure 5.20 (c) it has been noticed that the pore water pressure variation with respect to time is maximum for upstream side point of the dam. The maximum effect in respect of pore water pressure variation on transient seepage has been observed at the entry point of the embankment.

5.4.2.3.2 Single tidal cycle under seismic condition

Figure 5.20(e) and Figure 5.20(f) present pore water pressure variation under static and seismic condition for full rise up for a particular case of full rise up and full drawdown condition. Similar observation has been found for all cases.

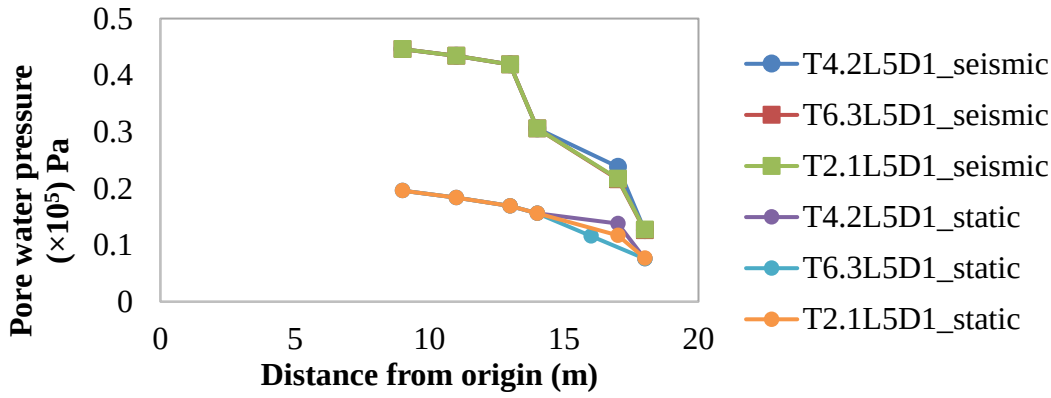

Figure 5.20(e): Pore water pressure variation with respect to time (For different location

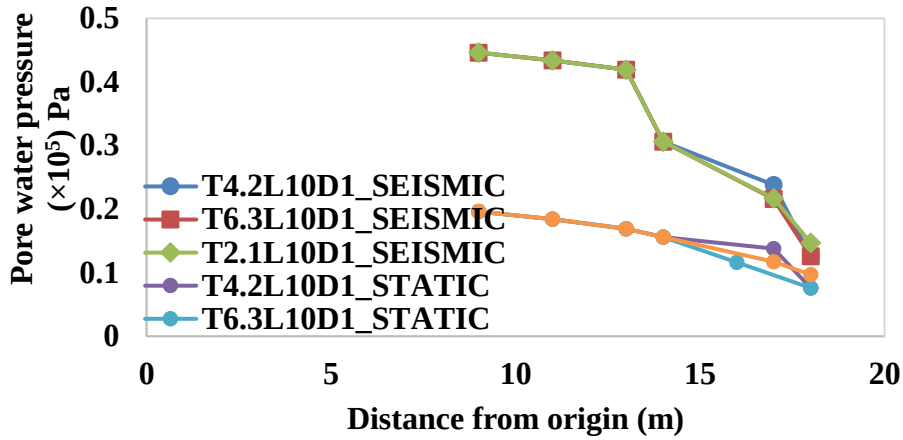

Figure 5.20(f): Pore water pressure variation with respect to time (For different location

From the figures it is observed that under seismic condition pore water pressure increases by 50% on an average on upstream side compared to static condition. From the figures it is obtained that under seismic condition pore water pressure increases by 15% on an average on downstream side compared to static condition.

5.4.2.3.3 Multiple tidal cycle

The effect of multiple tidal cycles on the above-mentioned parameters was also investigated. Figure 5.21(a) presents effect of multiple tidal cycle at the foundation level. Figure 5.21(b) shows effect of multiple tidal cycle at the dam body. 120 number of cycles was run to get an idea of the cumulative effect of the same on the embankment. The magnitude of net gain in pore water pressure is maximum for lowest cycle. It shows from the corresponding figure at upstream side effect of multiple tidal cycle is more pronounced than downstream end.

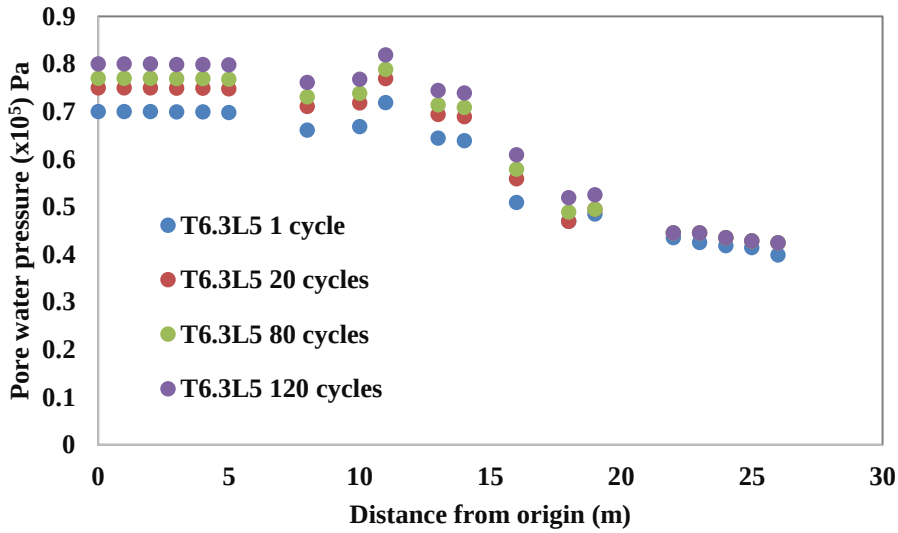

Figure 5.21(a): variation of pore water pressure for 3*B*/8 position 5 m length

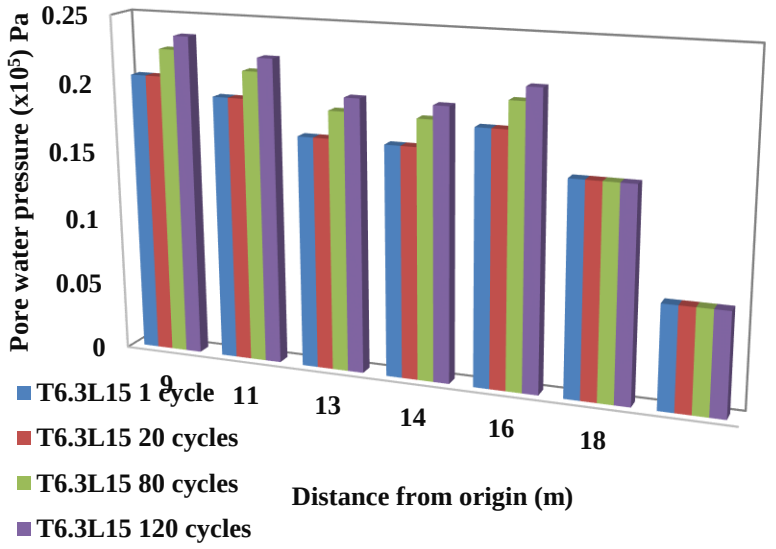

Figure 5.21(b): Variation of pore water pressure at the dam body

It has been observed from the figures that pore water pressure is decreasing towards downstream end. Ultimately increase of pore water pressure on upstream side is 14.00% and there is no appreciable change of pore water pressure on downstream side compared to static condition. Effect of multiple tidal cycle i.e. 1 single, 20 cycle, 80 cycle and 120 cycle is making a cyclic change in pore water pressure, which is resulting in slight change in pore water pressure at upstream end and practically no change in pore water pressure in downstream end for the number of multiple tidal cycle.

5.4.3 PORE PRESSURE ALONG BASE

Estimated pore water pressure at different time intervals, along horizontal distance from origin at the base, have been plotted in Figure 5.22 (a) and Figure 5.22(b) for drawdown and rise up conditions respectively.

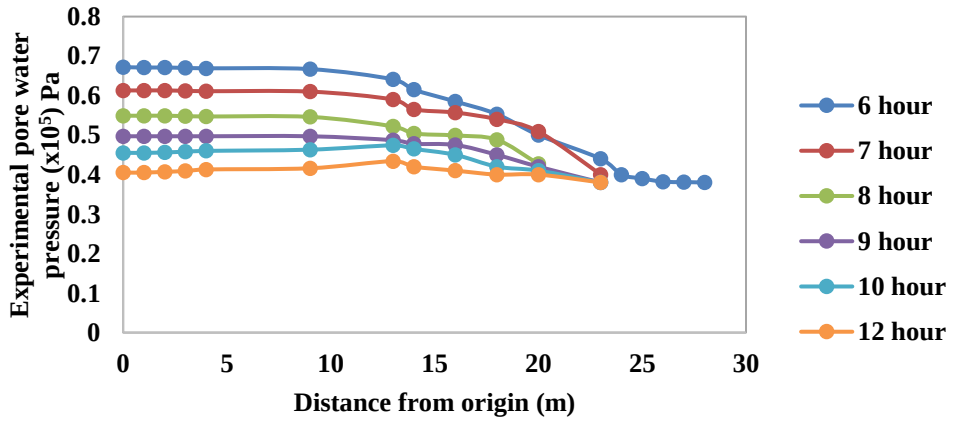

Figure 5.22 (a): Pore water pressure variation at the foundation level in drawdown condition

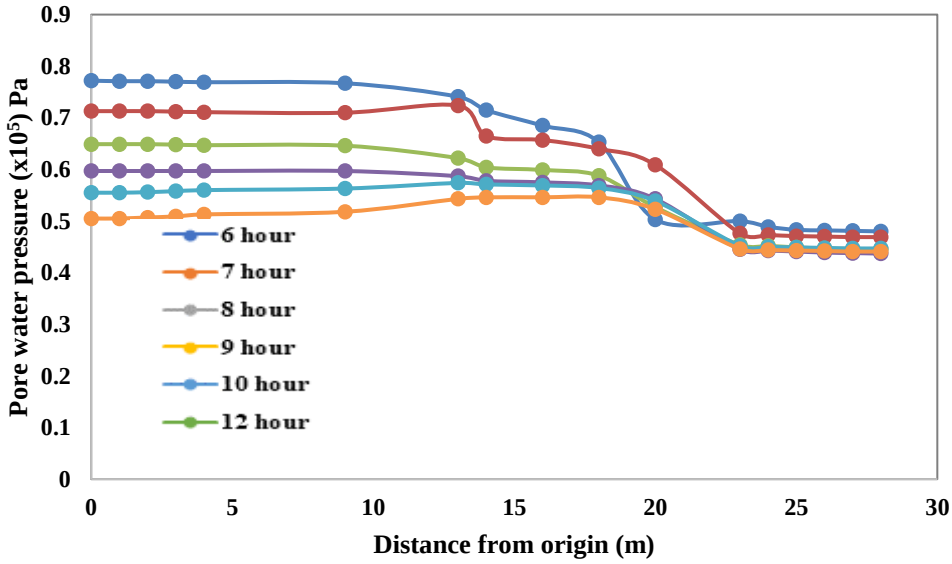

Figure 5.22 (b): Pore water pressure variation at the foundation level in drawdown condition (Numerical)

It is seen from the figures that pore water pressure gradually increases a little for rise up condition and remains almost same for drawdown condition up to about 15m for both the cases. The pore pressure increases a little for rise up condition and decreases for drawdown condition towards downstream. The change of pore pressure for a typical cycle is illustrated in Figures 5.22(a) and 5.22(b). From these figures, it is observed that the pressure at the upstream side at the base varies accordingly with the variation of the upstream water level. In other words, the pore pressure at the upstream side of base is dependent upon the position of the phreatic surface. The pore pressure at the downstream of base varies due to variation of the phreatic surface for different sheet pile positions and lengths. But when the water level on the upstream face approaches towards the lowest position at dam base, the downstream portion of the dam experiences a lower pore pressure as water flow paths are further restricted due to the effectiveness of sheet pile.

5.5. SOIL PRESSURE

Soil pressures coming on both sides of sheet piles at different depths have been obtained for different conditions and development of soil pressure under different conditions has been studied in the following sections.

5.5.1 STEADY STATE

5.5.1.1 STEADY STATE STATIC CONDITION

The soil pressure on both sides of sheet pile for each case has been obtained. Soil pressure for sheet piles of different lengths located at 2*B*/8 position from downstream end is plotted against embedded depth in Figure 5.23(a). It appears from the figure that soil pressure lies on negative side of sheet pile up to sheet pile length of 5m. It further appears from the figure that when the length is quite less, no net soil pressure is produced on the downstream side. Again

when pile length is 10m or more, soil pressure on downstream side increases. This is probably due to the fact that with less sheet pile length the pile acts as a rigid one, with negligible effect of pressure on downstream side. When the pile length is appreciable it becomes flexible with pressure coming on both sides. In Figure 5.23(b), soil pressure has been plotted for 20m length and located at a distance of *B*/8, 2*B*/8 and 3*B*/8 from downstream end. In case of same length of sheet pile, when position of sheet pile moves towards downstream end, value of soil pressure for both upstream and downstream sides gradually decreases. Point of zero soil pressure is found to move upward from bottom when sheet pile moves towards upstream side from downstream end. Towards downstream side the soil mass inducing pressure on sheet pile is becoming limited with less magnitude of pressure.

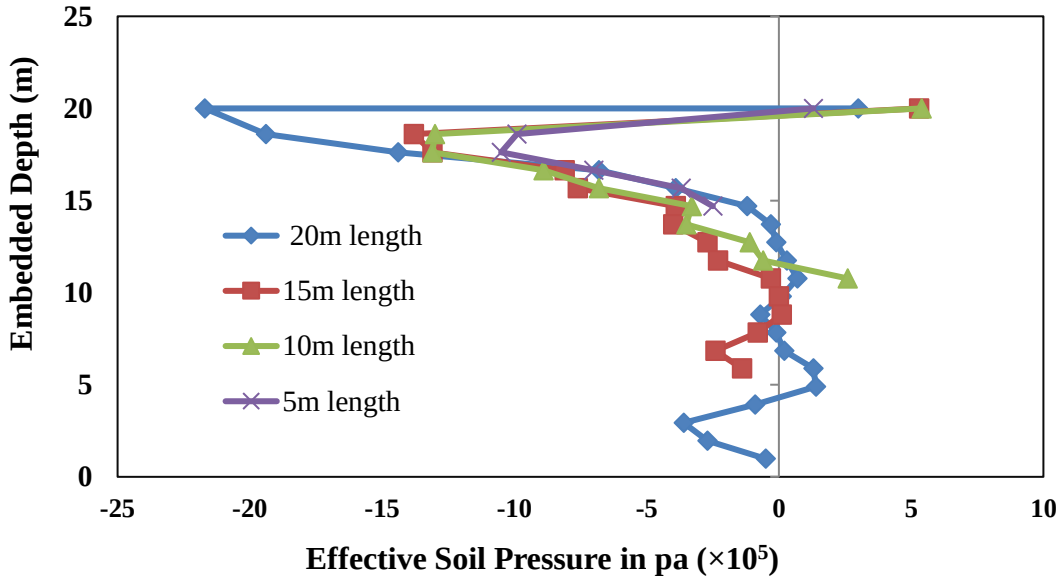

Fig 5.23(a): Soil pressure diagram for different sheet pile length at 2*B*/8 position

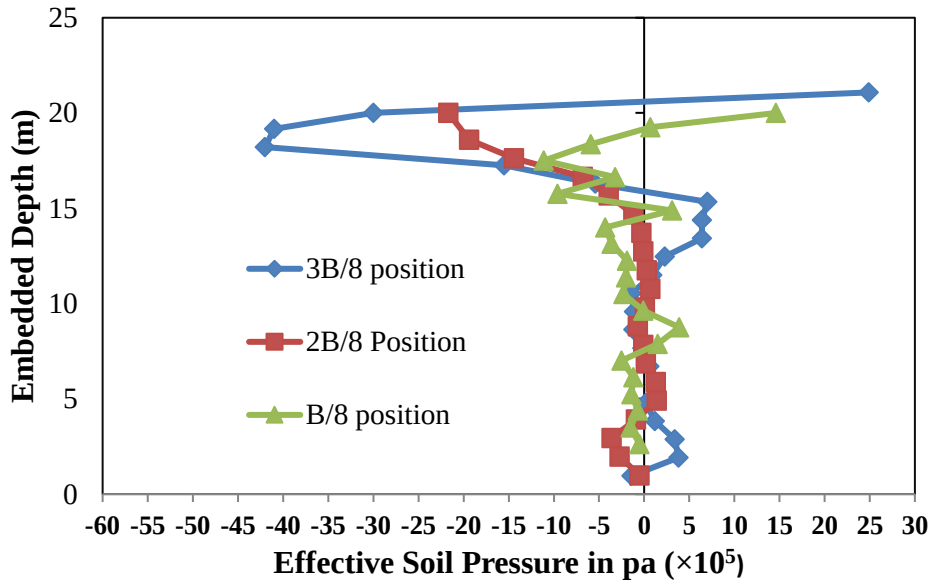

Fig 5.23(b): Soil pressure diagram for different sheet pile position for 20m long sheet pile

5.5.1.2 STEADY STATE SEISMIC CONDITION

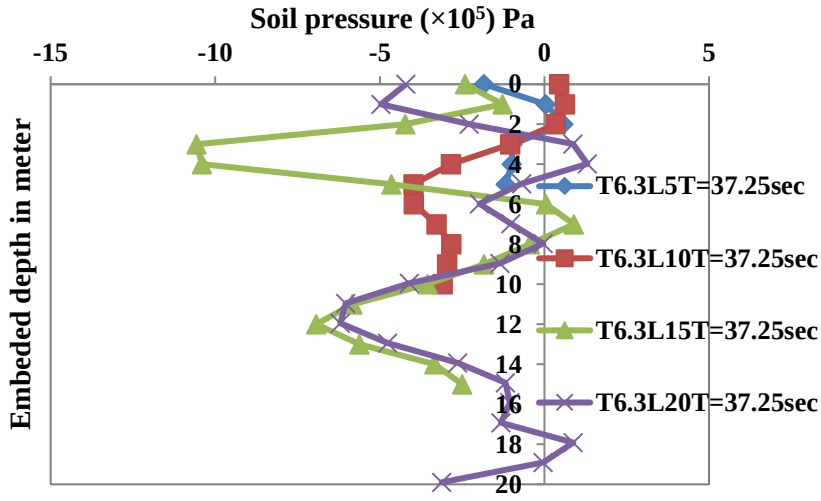

Fig 5.23(c): Soil pressure diagram for different sheet pile length under seismic condition

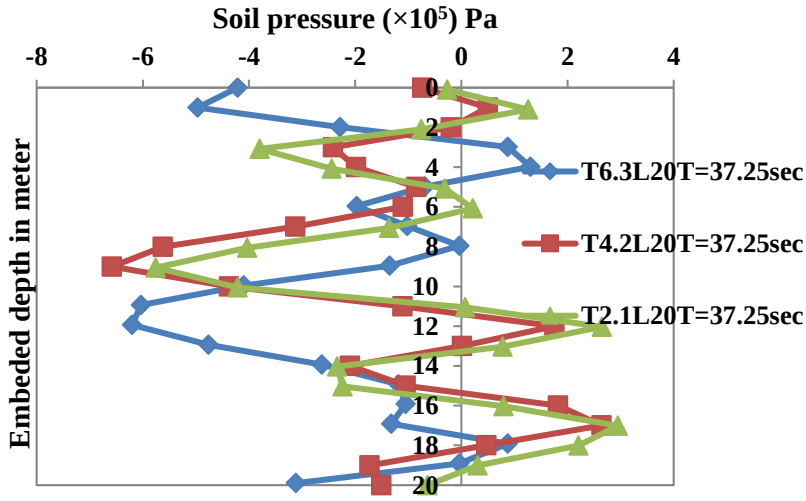

Fig 5.23(d): Soil pressure diagram for different sheet pile position of 20 m length under seismic condition

For seismic conditions the soil pressure diagrams have been drawn along the length of sheet piles as shown in figure 5.23(c) to 5.23 (d). It is observed from the figures that the variation of soil pressure on upstream and downstream sides of sheet pile is reduced to a considerable extent. The maximum 50% reduction of soil pressure occurs at 3B/8 position. This is probably due to the seismic effect on sheet pile -soil system existing below the body of the dam as the effect increases the pore water pressure and thereby reduces the effective soil pressure.

5.5.2 TRANSIENT CASE

5.5.2.1 TRANSIENT STATIC CONDITION

The soil pressure diagrams have been plotted for transient cases with rise up and drawdown conditions from figure 5.24 (a) to 5.24(i).

It is observed from the figures that during rise up pore water pressure increases with time lapse whereas for drawdown condition pore water pressure decreases. Hence soil pressure decreases in rise up condition and increases in drawdown condition respectively for all cases. However, the value of soil pressure increases or reduces to a small extent probably due to variation of seepage pressure in transient state. In case of transient condition as the sheet pile is shifted towards upstream side the soil pressure increases in magnitude for any length of sheet pile. When sheet pile moves towards downstream end soil pressure reduces probably due to less effect of weight of embankment.

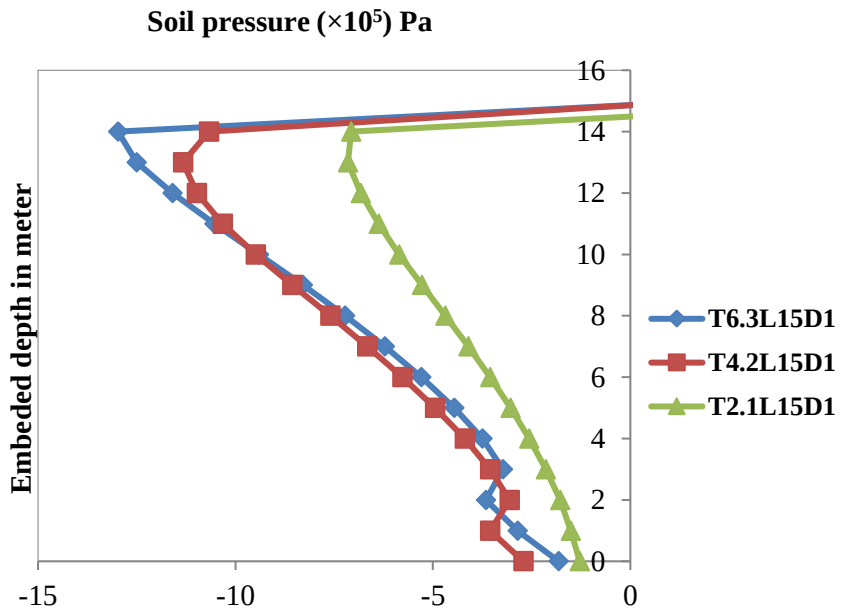

Fig 5.24(a): Soil pressure diagram for different sheet pile position of 15 m length under rise up condition

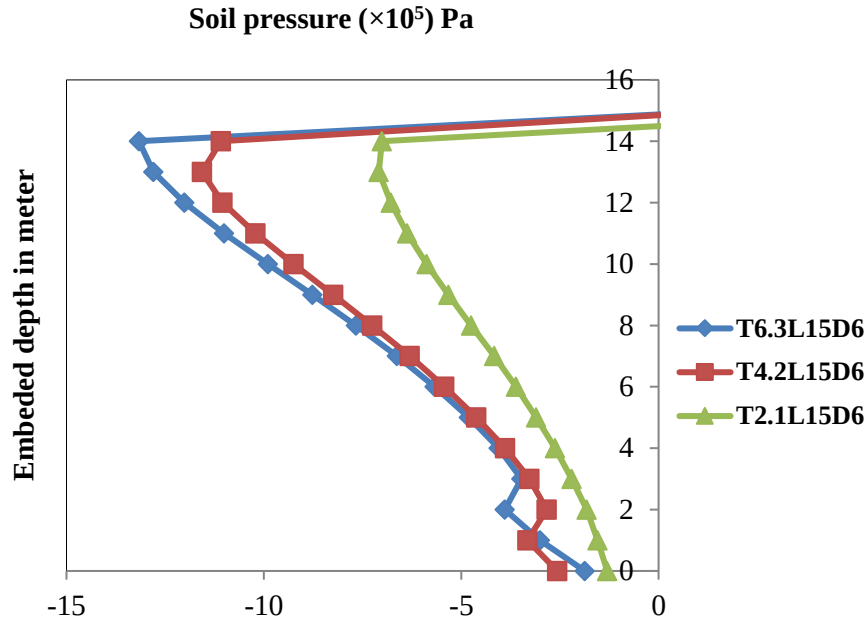

Fig 5.24(b): Soil pressure diagram for different sheet pile position of 15 m length under drawdown condition

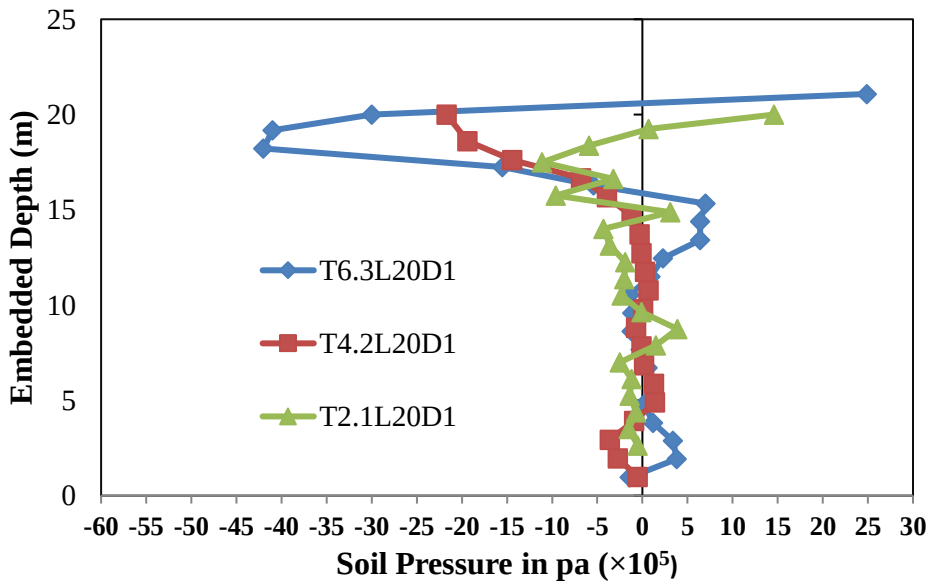

Fig 5.24(c): Soil pressure diagram for different sheet pile position of 20 m length under rise up condition

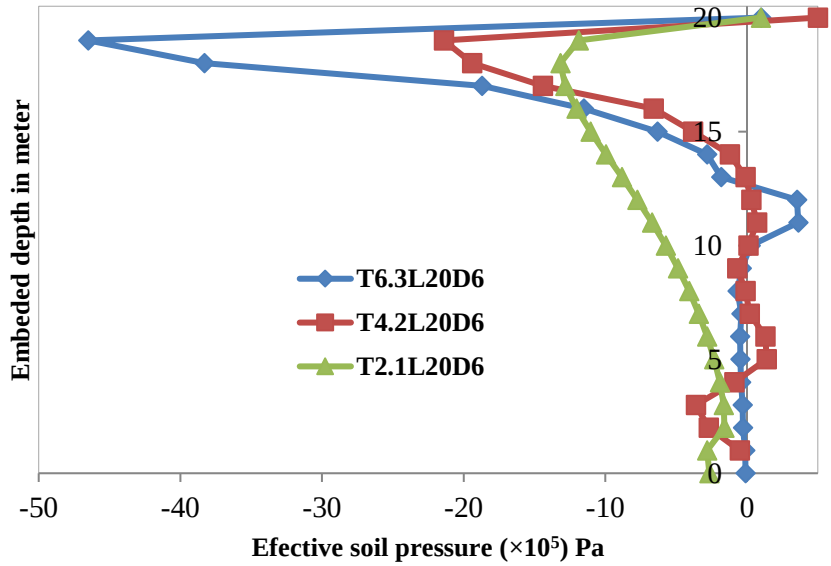

Fig 5.24(d): Soil pressure diagram for different sheet pile position of 20 m length under drawdown condition

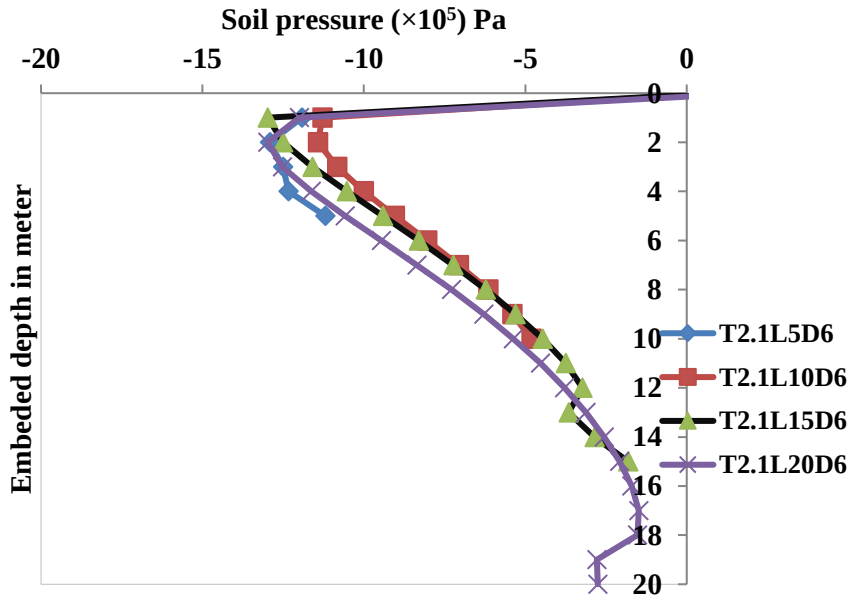

Fig 5.24(e): Soil pressure diagram for *B*/8 position under drawdown condition

5.5.2.2 TRANSIENT SEISMIC CONDITION

In case of seismic condition, the soil pressure abruptly rises following the same trend as found in seismic cases under steady state condition.

Soil pressure under seismic condition has been presented in Figure. 5.24(f) to Figure 5.24(k). Figure 5.24(f) to Figure 5.24(i) presents soil pressure at peak acceleration time=37.25 sec for

rise up condition for 5m, 10m , 15m and 20m long sheet pile. Figure 5.24(j) shows soil pressure under rise up condition for 3*B*/8 position of sheet pile for different length. Figure 5.24(k) presents soil pressure under rise up condition for 2*B*/8 position of sheet pile for different acceleration time.

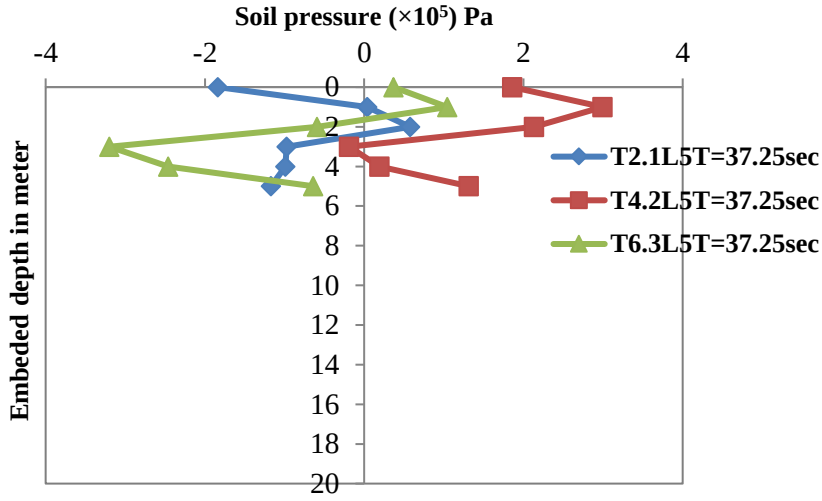

Fig 5.24(f): Soil pressure diagram for 5m long sheet pile under rise up condition (seismic)

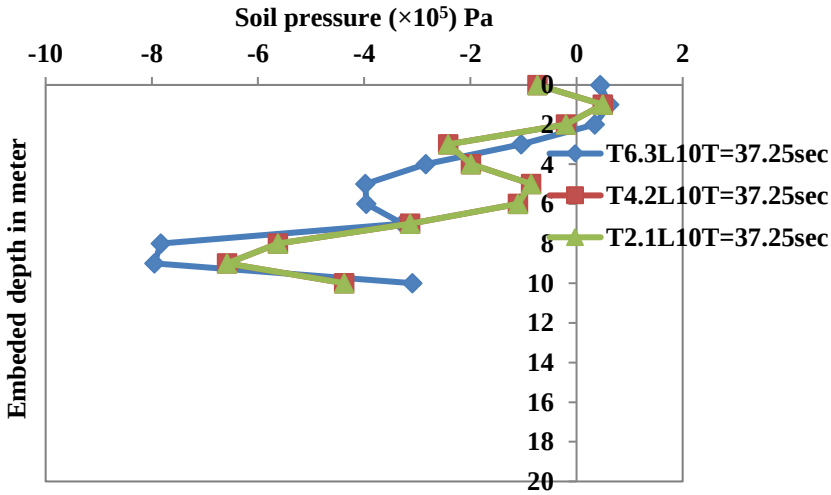

Fig 5.24(g): Soil pressure diagram for 10m long sheet pile under rise up condition (seismic condition)

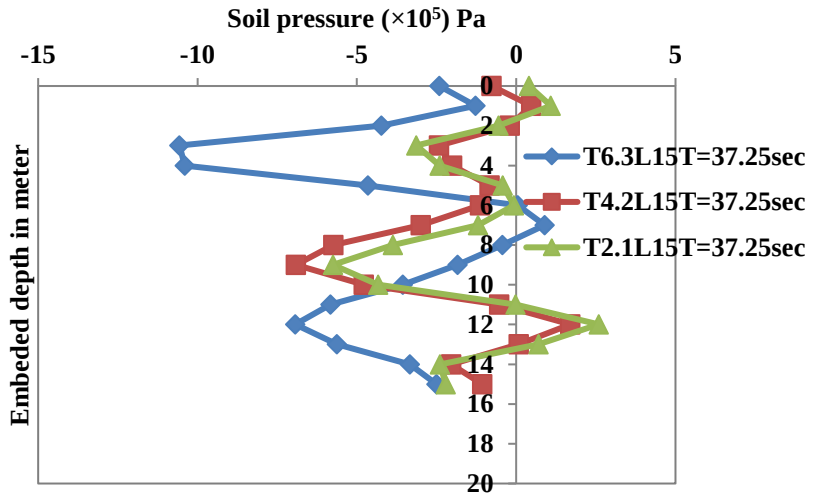

Fig 5.24(h): Soil pressure diagram for 15m long sheet pile under rise up condition (seismic condition)

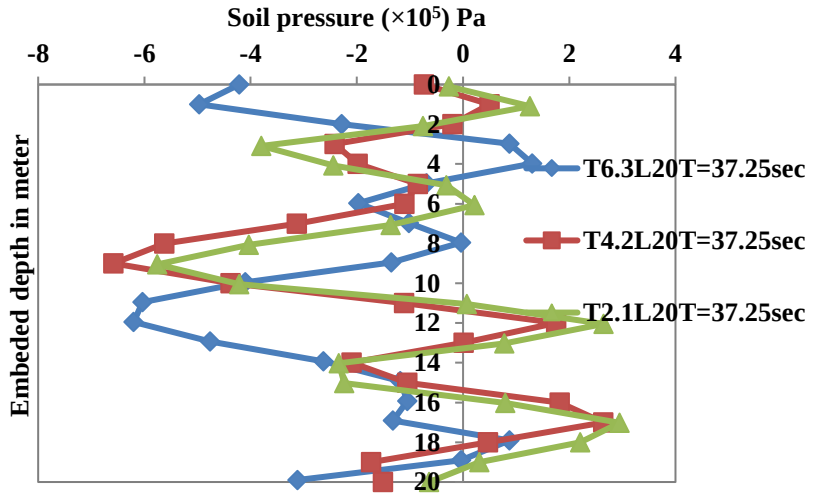

Fig 5.24(i): Soil pressure diagram for 20m long sheet pile under rise up condition (seismic condition)

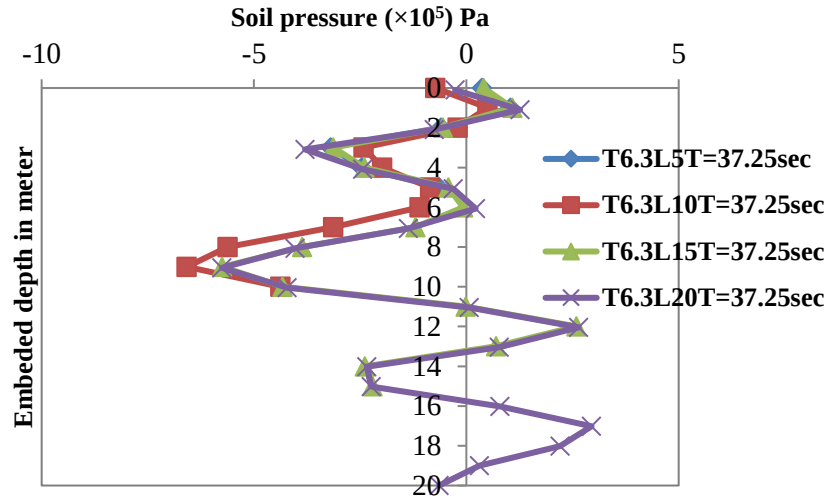

Fig 5.24(j): Soil pressure diagram for 3*B*/8 position under rise up condition (seismic condition)

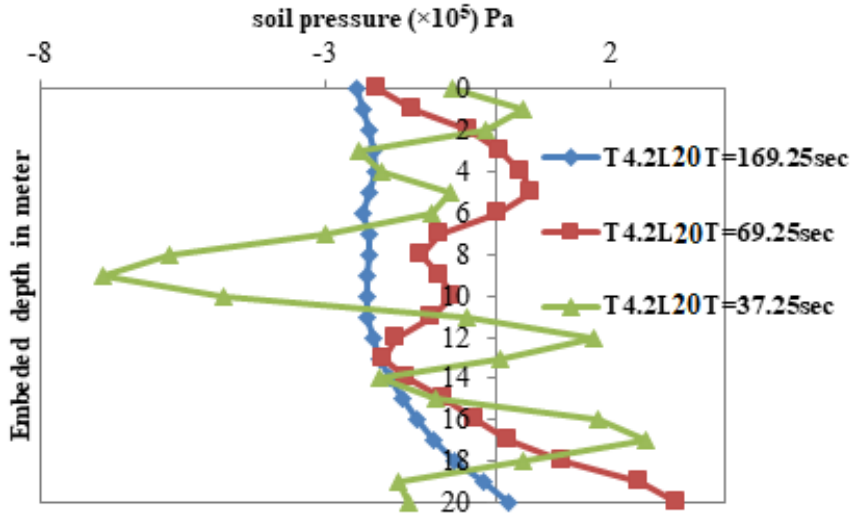

Fig 5.24(k): Soil pressure diagram for 2*B*/8 position under rise up condition (seismic condition)

In seismic condition for any position and length of sheet pile, soil pressure is found to be irregular depending on the magnitude of seismic acceleration. When seismic acceleration is less soil pressure is remaining on upstream side of the sheet pile probably due to seismic effect for which it is behaving as a rigid one. It is observed that soil pressure is erratic in case of seismic acceleration. From Figure 5.24(k) it has been observed that soil pressure is maximum for peak seismic acceleration. Magnitude of soil pressure is less than that under static condition. It has been observed that peak magnitude decreases by maximum of 76% compared to static condition for 3B/8 position. This is due to combined behavior of sheet pile and soil in seismic cases for higher acceleration as soil movement is more and this may create more soil pressure on sheet pile.

5.6 FACTOR OF SAFETY(FOS)

Overall stability is a failure mode where, embedded sheet pile wall has been assumed to displace along the soil mass in terms of sliding and rotation under slope stability mechanism failure. Global stability analysis has been evaluated in soft soil using FLAC 2D software satisfying all conditions of static equilibrium. In the present study sheet pile has been modeled using no gap condition. The no gap slip surface is considered below the dam toe, i.e. to prevent potential slip surface passing through the wall. Due to this the stiffness of the sheet pile wall has been assumed to be higher than surrounding soil. Factor of safety based on piping only can be defined further with respect to critical hydraulic gradient at the dam toe on downstream side.

Factor of safety has been obtained using the effective shear strength characterization. The section of trial slip surface has been done by the Entry and Exit Method with gradual radii increments in stages. A total of 726 trial slip surfaces by default have been taken and the minimum Factor of Safety has been recorded. Both overall factor of safety and that against piping have been obtained for all numerical cases of steady and transient states. Factor of safety against piping has been also found for experimental cases.

5.6.1 Overall factor of safety

In this section an attempt has been made to study the change of factor of safety for steady state and transient state as well as under seismic and non-seismic conditions. The factor of safety against stability has been obtained from the output of SEEP/W software and overall stability considering both slope stability and piping condition have been obtained from FLAC 2D.

5.6.1.1 STEADY STATE UNDER STATIC AND SEISMIC CONDITIONS

In FLAC2D software Shear Strength method determines a factor of safety based on a defined maximum unbalanced force for a failure surface utilizing the stress/strain characteristics for the soil. (Reference: Itasca 2005). The overall factor of safety considers both piping and overall stability of the dam. In Figure 5.25(a) overall factor of safety has been plotted against different sheet pile positions and different sheet pile lengths. It is observed from the figures that for a fixed length of sheet pile overall factor of safety remains almost same for any position of sheet pile. When length of sheet pile increases, overall factor of safety increases appreciably. It appears from the figures that factor of safety increases by maximum 16% to 17% for both static and seismic conditions with sheet pile, compared to factor of safety without sheet pile condition. This is probably attributed to the fact that for any position of sheet pile, a fixed seepage length is not affecting the stability but increase of flow path

reduces the chance of piping and hence increases the factor of safety. It also includes the factor of safety against stability of slope.

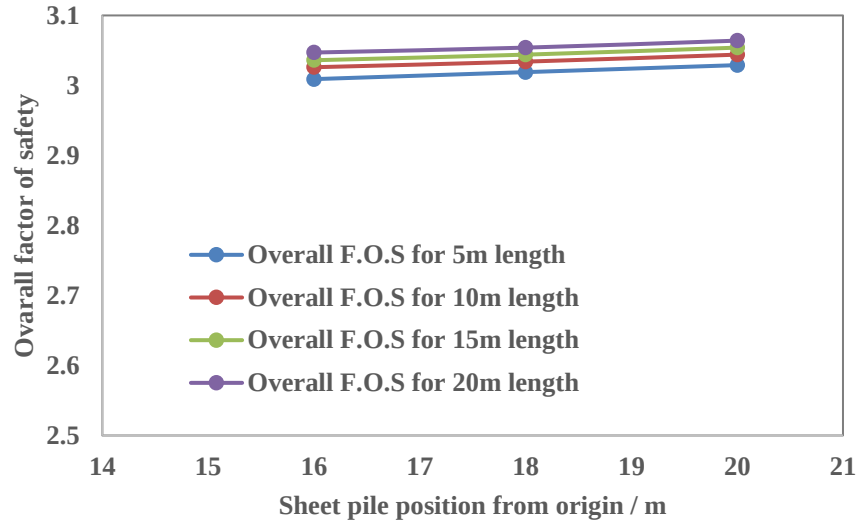

Fig. 5.25(a): Variation of Overall Factor of safety with different sheet pile positions under static condition

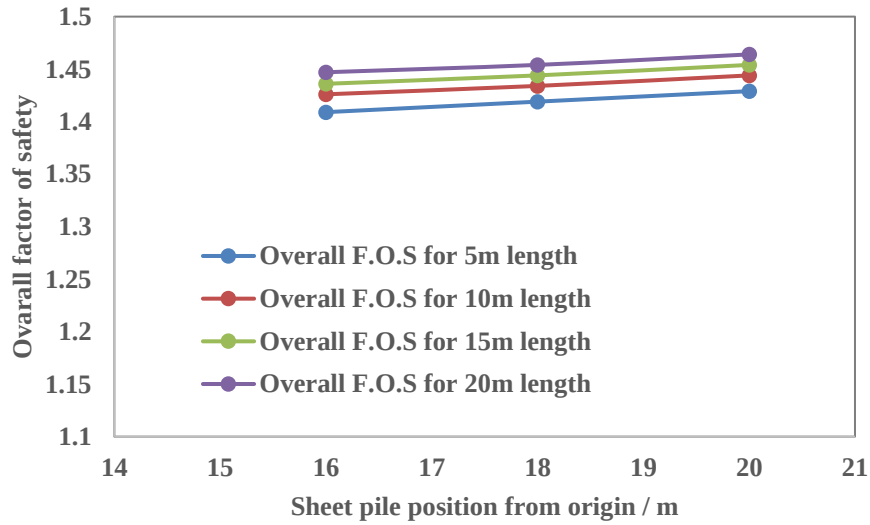

Fig. 5.25(b): Variation of Overall Factor of safety with different sheet pile positions under seismic condition

For steady state condition with maximum water level at 3.5 m, the FOS obtained for different sheet pile position and length varies from 3.009 to 3.064 as shown in Figure 5.25(a). The results showed that the FOS satisfied the minimum required FOS, which is 1.5 (Ref: IS code 7894 of 1975). During steady state condition, the ponded water will exert external force on the upstream surface to counter balance the internal force exerted by the pore water pressure.

In seismic cases under steady state condition as pore water pressure increases the factor of safety is also reduced by 45% to 50% compared to corresponding static cases due to increase of seepage force as is shown in Figure 5.25(a) and Figure 5.25(b).

5.6.1.2 TRANSIENT STATE (SINGLE TIDAL CYCLE)

The factor of safety for transient case under static and seismic condition has been estimated with the help of FLAC2D and presented in Table 5.5 and Table 5.6. Figure 5.25 (c) presents factor of safety for static condition under rise up and drawdown conditions in 3D surfacing for typical cases of B/8 position, 5m length, B/8 position , 20m length, 2B/8 position , 15m length and 3B/8 position, 10m length respectively. Figures 5.25(d) and 5.25(e) show that effect of rise up and drawdown on factor of safety of earthen dam for a typical case of 15m long sheet pile with variation of sheet pile position and these figures have been drawn as column presentation for static and seismic conditions respectively. Figures 5.25(f) and 5.25(g) show the effect of rise up and drawdown on factor of safety of earthen dam for different sheet pile lengths with fixed sheet pile position at B/8 from downstream end in column presentation for static and seismic conditions respectively.

Table 5.5: Factor of safety under static condition

STATIC CONDITION														
		Time (hrs.)												
Sheet pile position	Sheet pile length	0	1	2	3	4	5	6	7	8	9	10	11	12
B/8	5	2.40	2.42	2.43	2.44	2.98	2.98	3.03	2.98	2.59	2.49	2.39	2.19	1.99
	10	2.60	2.62	2.62	2.63	3.21	3.22	3.27	3.21	2.79	2.68	2.58	2.36	2.14
	15	2.64	2.66	2.67	2.68	3.27	3.28	3.33	3.27	2.84	2.73	2.62	2.40	2.18
	20	2.69	2.71	2.72	2.73	3.33	3.34	3.39	3.33	2.90	2.78	2.67	2.45	2.22
2B/8	5	2.39	2.41	2.42	2.43	2.97	2.97	3.01	2.97	2.58	2.48	2.38	2.18	1.98
	10	2.51	2.53	2.54	2.55	3.11	3.12	3.16	3.11	2.70	2.60	2.49	2.28	2.07
	15	2.58	2.60	2.61	2.62	3.20	3.21	3.25	3.20	2.78	2.67	2.57	2.35	2.13
	20	2.64	2.66	2.67	2.68	3.27	3.28	3.33	3.27	2.84	2.73	2.62	2.40	2.18
3B/8	5	2.38	2.40	2.41	2.42	2.96	2.96	3.01	2.96	2.57	2.47	2.37	2.17	1.97
	10	2.50	2.52	2.53	2.54	3.10	3.11	3.16	3.10	2.69	2.59	2.48	2.27	2.06
	15	2.57	2.59	2.60	2.61	3.19	3.20	3.25	3.19	2.77	2.66	2.55	2.34	2.12
	20	2.62	2.64	2.65	2.66	3.25	3.26	3.31	3.25	2.82	2.71	2.60	2.38	2.16

Table 5.6: Factor of safety under seismic condition

SEISMIC CONDITION														
		Time (hrs.)												
Sheet pile position	Sheet pile length	0	1	2	3	4	5	6	7	8	9	10	11	12
B/8	5	1.003	1.022	1.03	1.039	1.376	1.379	1.381	1.376	1.185	1.085	0.985	0.785	0.585
	10	1.018	1.037	1.045	1.054	1.391	1.394	1.396	1.391	1.2	1.1	1	0.8	0.6
	15	1.028	1.047	1.055	1.064	1.401	1.404	1.406	1.401	1.21	1.11	1.01	0.81	0.61
	20	1.038	1.057	1.065	1.074	1.411	1.414	1.416	1.411	1.22	1.12	1.02	0.82	0.62
2B/8	5	0.993	1.012	1.02	1.029	1.366	1.369	1.371	1.366	1.175	1.075	0.975	0.775	0.575
	10	1.008	1.027	1.035	1.044	1.381	1.384	1.386	1.381	1.19	1.09	0.99	0.79	0.59
	15	1.018	1.037	1.045	1.054	1.391	1.394	1.396	1.391	1.2	1.1	1.00	0.8	0.6
	20	1.028	1.047	1.055	1.064	1.401	1.404	1.406	1.401	1.21	1.11	1.01	0.81	0.61
3B/8	5	0.983	1.002	1.01	1.019	1.356	1.359	1.361	1.356	1.165	1.065	0.965	0.765	0.565
	10	1	1.019	1.027	1.036	1.373	1.376	1.378	1.373	1.182	1.082	0.982	0.782	0.582
	15	1.01	1.029	1.037	1.046	1.383	1.386	1.388	1.383	1.192	1.092	0.992	0.792	0.592
	20	1.021	1.04	1.048	1.057	1.394	1.397	1.399	1.394	1.203	1.103	1.003	0.803	0.603

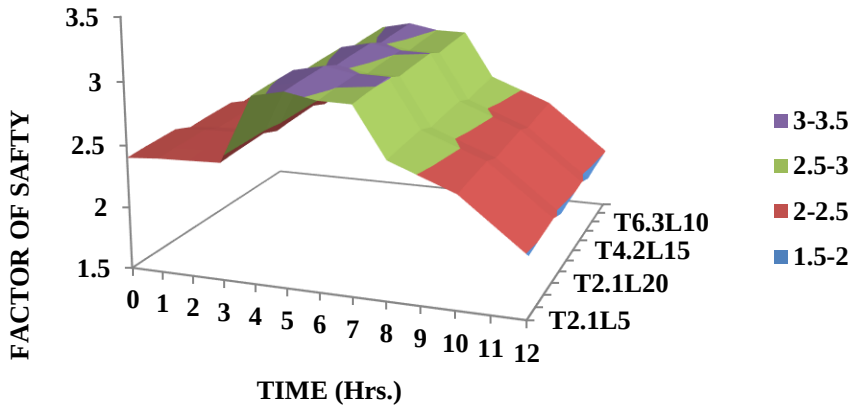

Figure. 5.25 (c) Factor of safety against time for different sheet pile condition

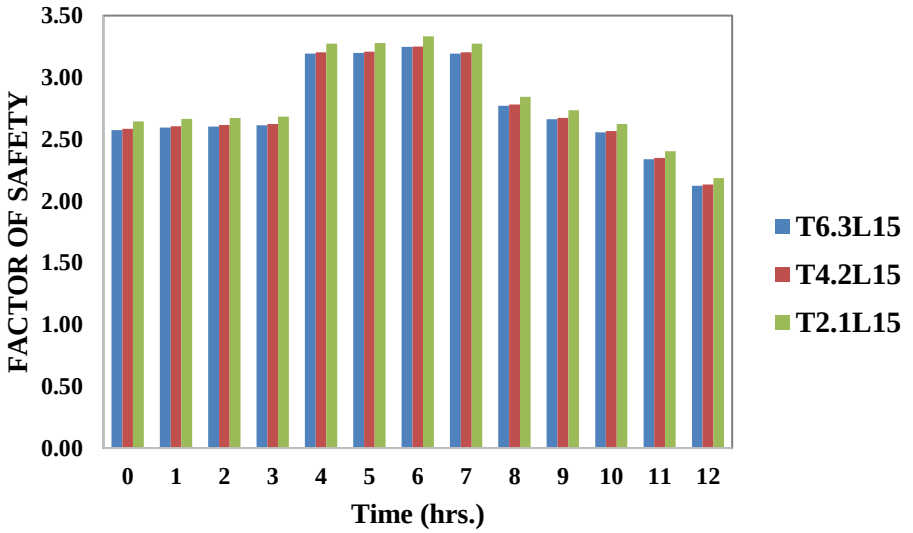

Figure. 5.25 (d) Factor of safety against time at different position for 15m long sheet pile under static condition

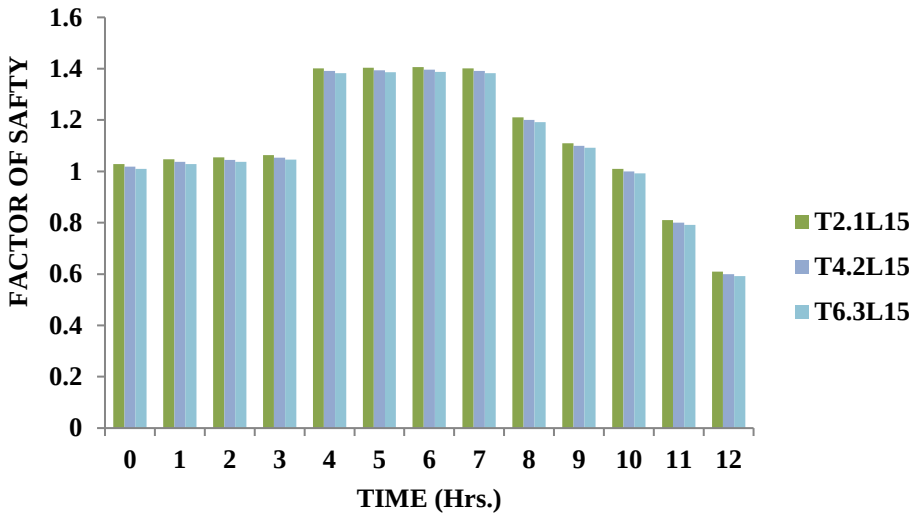

Figure. 5.25 (e) Factor of safety against time at different position for 15m long sheet pile under seismic condition

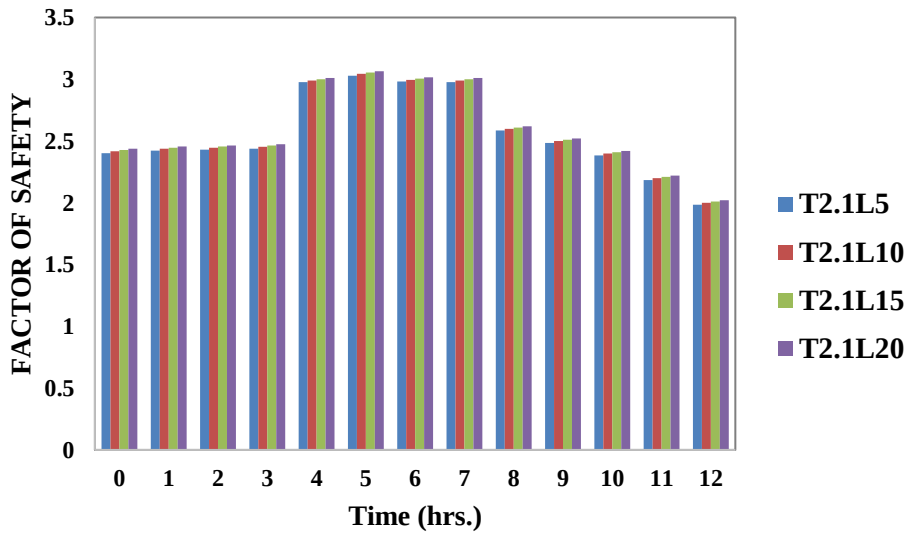

Figure. 5.25 (f) Factor of safety against time at *B*/8 position for different sheet pile length under static condition

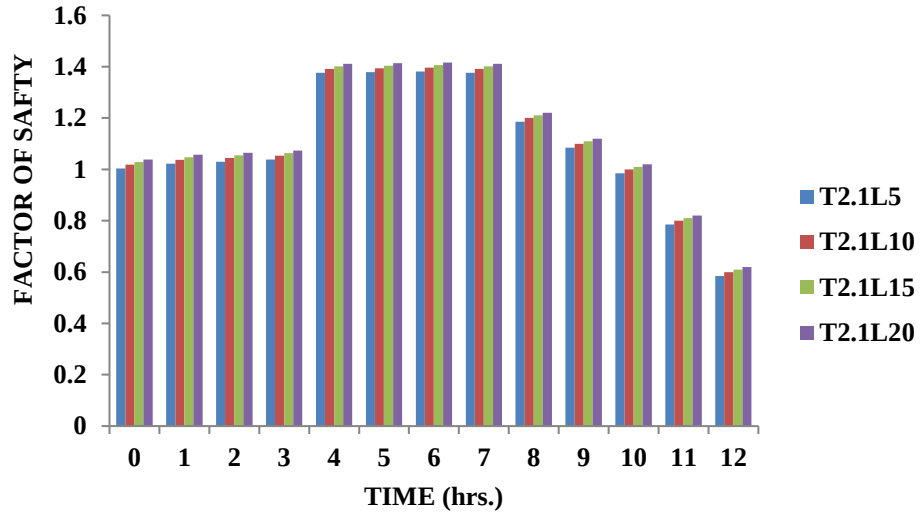

Figure. 5.25 (g) Factor of safety against time at *B*/8 position for different sheet pile length under seismic condition

It appears from the tables and figures that the factor of safety increases during rise up condition and decreases during drawdown condition. This is due to reduction in stabilizing moment of water thrust on upstream side of dam during drawdown condition and increase in stabilizing moment under rise up condition.

Compared to the steady state condition the factor of safety increases by 10% in rise up condition and decreases by 5%-10% in drawdown condition.

It is observed that factor of safety decreases on an average by 30% for transient state seismic condition, compared to steady state seismic condition condition as is observed from Figure 5.25 (b) and Table 5.6.

5.6.1.2.1 Effect of rise up and drawdown on Factor of Safety for variation position and length of sheet pile

An attempt has been made to observe the effect of rise up and drawdown on earthen dam for different sheet pile positions and lengths. It is observed from Table 5.6 that for a fixed length, if position of sheet pile moves towards downstream end under rise up, factor of safety increases and it decreases during drawdown. This occurs due to increase of stabilizing moment of water during rise up and decrease of stabilizing moment of water during drawdown respectively. The change in factor of safety during drawdown also may occur due to the fact that when water level reduces, the seeping water that is percolating inside the embankment is not reduced immediately with no reduction of seepage force; this effect is termed as mounding effect. Due to mounding effect at the time of drawdown factor of safety reduces

The increase of factor of safety during rise up is about 7% to 10% as sheet pile moves for B/8 to 3B/8 position. The decrease of FOS is about is 6% to 10% for drawdown condition as

sheet pile moves for *B*/8 position to 3*B*/8 position for any given length during drawdown. It is further observed from Table 5.6 that as sheet pile length changes from 5m to 20m the FOS changes from on and average 15% to 35% under both rise up and drawdown conditions for any position of sheet pile. Thus, it is observed the sheet pile length has predominant influence on factor of safety than sheet pile position. This is due to increase of creep length with increase of sheet pile length. This is further observed that for any length and position of sheet pile the FOS reduces by 56% during rise up and 40% during drawdown, on and average. Thus it becomes obvious that drawdown condition is vulnerable during transient state.

5.6.1.2.2 TRANSIENT STATE (MULTIPLE TIDAL CYCLE)

For multiple cycle Factor of safety with number of cycles has been computed and shown in Figure 5.25(h). It has been observed from the figure that in case of multiple tidal cycle factor of safety is gradually reduced. In case of 120 cycles reduction of factor of safety is 8.3%, 26% and 40%, on an average, compared to 80 cycles, 20 cycles and single tidal cycle respectively for typical B/8 position, where maximum factor of safety occurs. This is due to residual strain which is accumulated with number of cycles leading to failure in case of transient state.

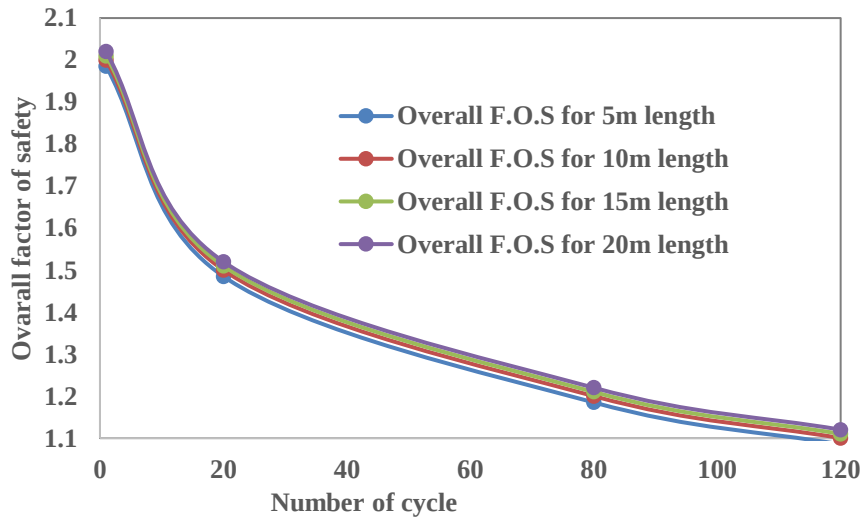

Figure. 5.25 (h) Factor of safety against time at *B*/8 position for different sheet pile length under multiple tidal cycle

5.6.2 FACTOR OF SAFETY AGAINST PIPING

Factor of safety against piping has been determined with respect to critical hydraulic gradient at the last field on downstream end along some flow path. It has been calculated manually as the ratio of head loss to length of seepage path through the field considered. This has been studied for both static and transient states.

5.6.2.1 STEADY STATE

Figure 5.26(a) shows the variation of factor of safety against piping with sheet pile lengths. It is observed that for a fixed sheet pile length, factor of safety against piping decreases when sheet pile position moves away from downstream end. When sheet pile moves from downstream end exit gradient increases and chance of piping is reduced. As sheet pile position is shifted towards the downstream end, the average flow length of the extreme field of flow net at downstream end increases which causes reduction in exit gradient. Thus, the factor of safety against piping increases. In Figure 5.26(a), factor of safety against piping has been plotted against sheet pile position measured from downstream end for different sheet pile lengths. It is observed from the figure that for any fixed position of sheet pile, exit gradient reduces with sheet pile length. It is also observed that when exit gradient reduces factor of safety against piping increases, reducing the probability of piping failure. As sheet pile length increases seepage path increases, reducing the exit gradient and thus also reducing the chance of piping failure. Similar observation was made by Perri et al (2012).

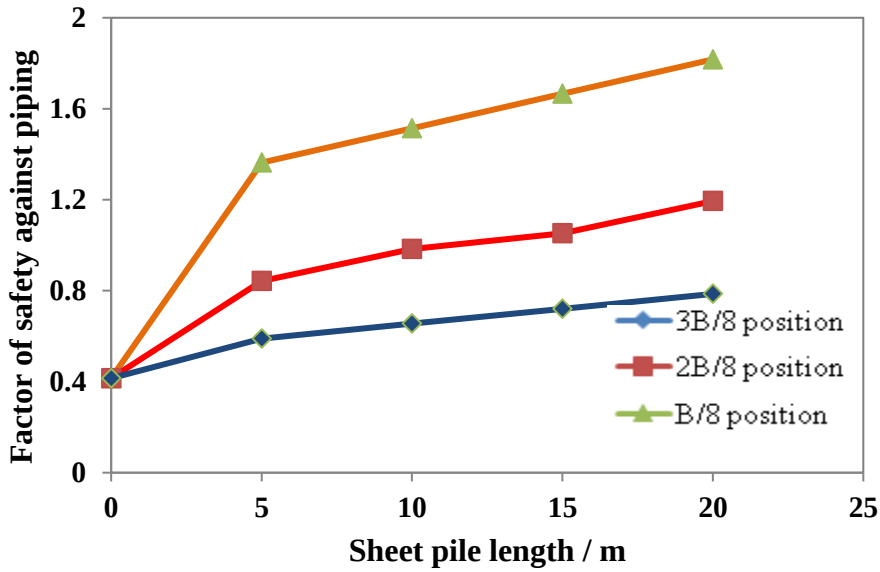

Fig.5.26(a): Variation of factor of safety against piping with sheet pile length

5.6.2.2 TRANSIENT STATE

In case of transient state condition, factor of safety against piping has been presented in Table 5.7. Figure 5.26 (a) presents factor of safety against piping under rise up and drawdown conditions in 3D surfacing for typical cases of B/8 position; 5m length, B/8 position; 20m length, 2B/8 position; 15m length ,3B/8; position 10m length and 3B/8; position 20m length respectively in column presentation. Figures 5.26(b) to 5.26 (d) present factor of safety against piping for different lengths at fixed positions of sheet pile of B/8, 2B/8 and 3B/8. Factor of safety against piping for fixed lengths and different positions of sheet pile has been presented in Figure 5.26(e) to 5.26 (h). It has been observed that for rise up condition factor of safety against piping gradually reduces with increase of waterhead, whereas for drawdown

condition factor of safety against piping gradually increases. A zone of crack has been found to clearly develop with each subsequent cycle in the region shown in the figure 5.27(a) to 5.27(d). Thus, it appears that effect of position is predominant compared to that of length, although for any given position factor of safety against piping increases with increase of length. Figure. 5.27(a) presents crack development in an earthen embankment in centrifuge modeling. Figure. 5.27(b) presents crack development in an earthen embankment in practical South 24 parganas site (REF: DEPARTMENT OF DISASTER MANAGEMENT, WEST BENGAL). Figure. 5.27(c) to Figure. 5.27(d) present factor of safety against piping and crack development through theoretical approach using MATLAB software.

Table 5.7: Factor of safety against piping under static condition

			Time (hrs.)												
Sl No.	sheet pile position from Downstream end	sheet pile position from Downstream end	0	1	2	3	4	5	6	7	8	9	10	11	12
1	N.A		1.88	1.5	1.2	1	0.8	0.6	0.5	0.6	0.8	1	1.2	1.5	1.88
2	5	B/8	2	1.995	1.975	1.885	1.685	1.605	1.6	1.605	1.685	1.885	1.975	1.995	2
3	10	B/8	2.02	2.015	1.995	1.905	1.705	1.585	1.58	1.585	1.705	1.905	1.995	2.015	2.02
4	15	B/8	2.04	2.035	2.015	1.925	1.725	1.585	1.58	1.585	1.725	1.925	2.015	2.035	2.04
5	20	B/8	2.06	2.055	2.035	1.945	1.745	1.606	1.601	1.606	1.745	1.945	2.035	2.055	2.06
6	5	2B/8	1.9	1.895	1.875	1.785	1.585	1.305	1.3	1.305	1.585	1.785	1.875	1.895	1.9
7	10	2B/8	1.902	1.897	1.877	1.787	1.587	1.485	1.48	1.485	1.587	1.787	1.877	1.897	1.902
8	15	2B/8	1.904	1.899	1.879	1.789	1.589	1.545	1.51	1.545	1.589	1.789	1.879	1.899	1.904
9	20	2B/8	1.906	1.901	1.881	1.791	1.603	1.55	1.5	1.55	1.603	1.791	1.881	1.901	1.906
10	5	3B/8	1.89	1.885	1.775	1.685	1.485	1.005	1	1.005	1.485	1.685	1.775	1.885	1.89
11	10	3B/8	1.892	1.887	1.795	1.705	1.505	1.35	1.3	1.35	1.505	1.705	1.795	1.887	1.892
12	15	3B/8	1.894	1.889	1.815	1.725	1.565	1.48	1.4	1.48	1.565	1.725	1.815	1.889	1.894
13	20	3B/8	1.896	1.891	1.835	1.745	1.602	1.5	1.45	1.5	1.602	1.745	1.835	1.891	1.896

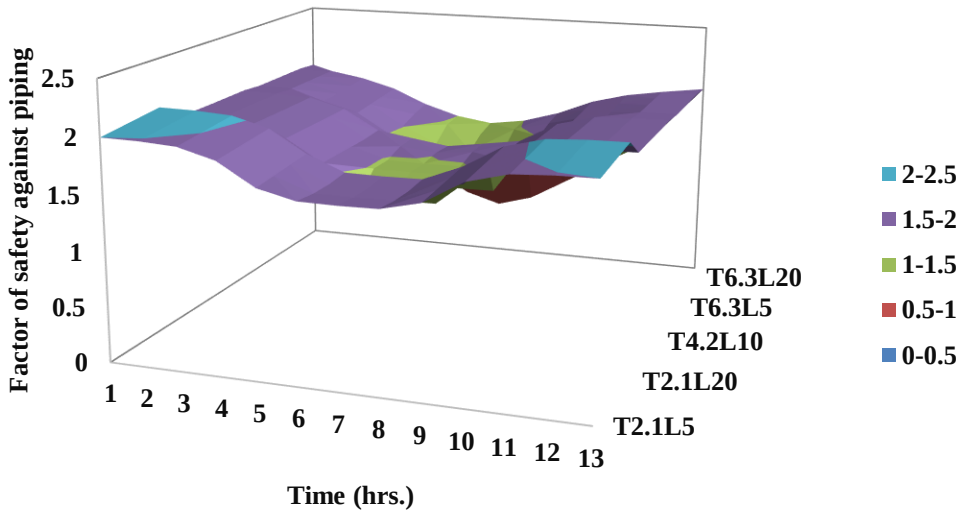

Figure. 5.26(a) Factor of safety against piping for different sheet pile condition

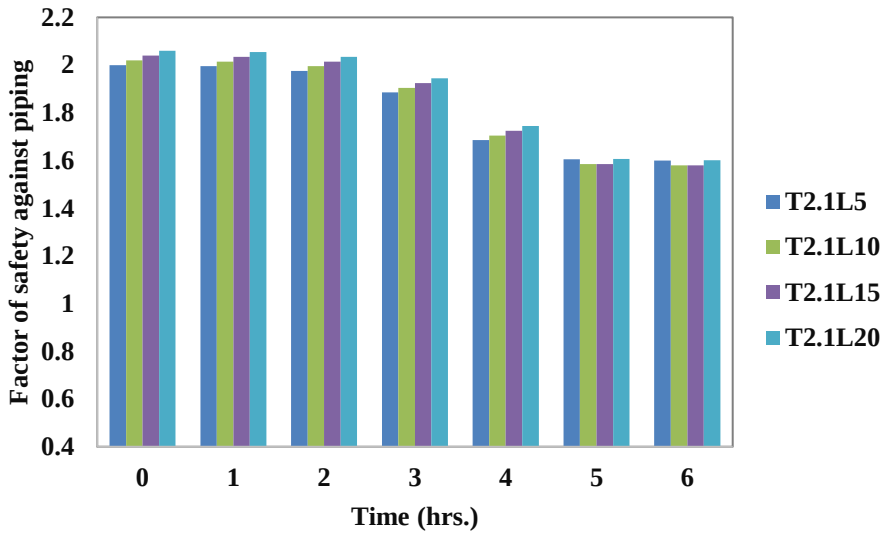

Figure. 5.26(b) Factor of safety against piping for *B*/8position sheet pile position

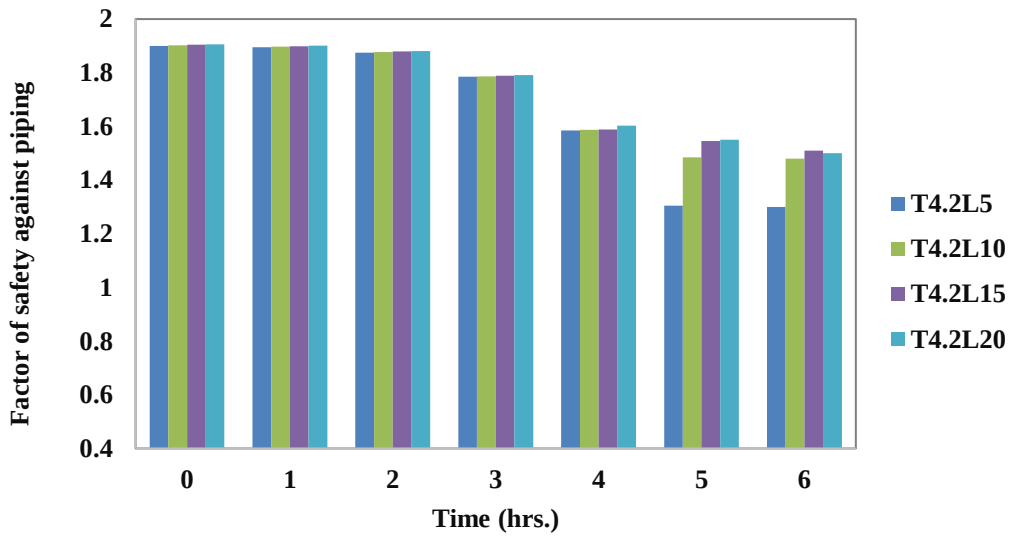

Figure. 5.26(c) Factor of safety against piping for 2*B*/8position sheet pile position

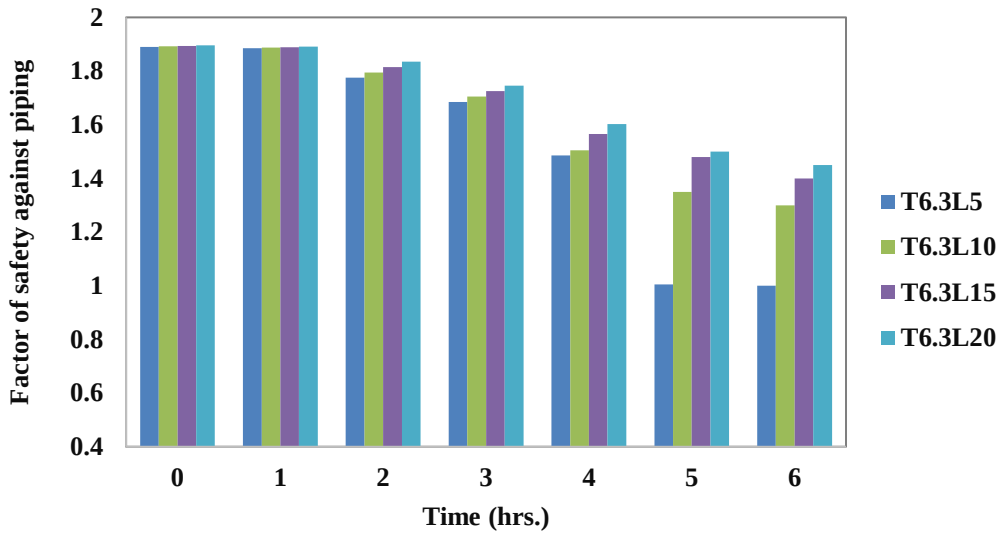

Figure. 5.26(d) Factor of safety against piping for 3*B*/8position sheet pile position

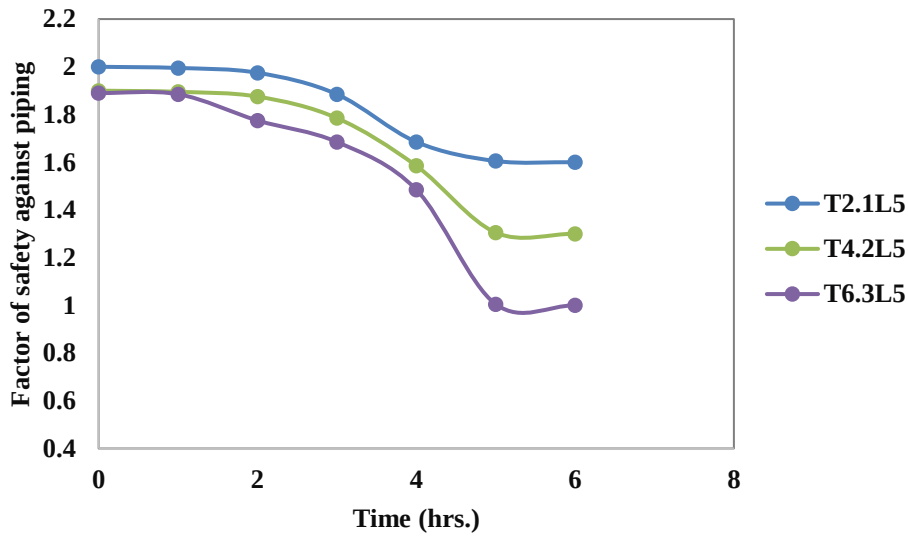

Figure. 5.26(e) Factor of safety against piping for 5m long sheet pile

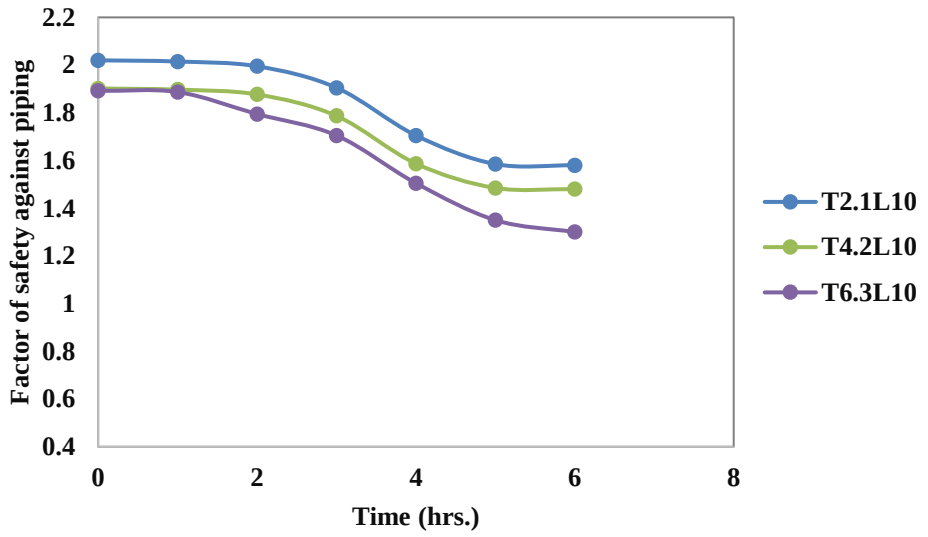

Figure. 5.26(f) Factor of safety against piping for 10m long sheet pile

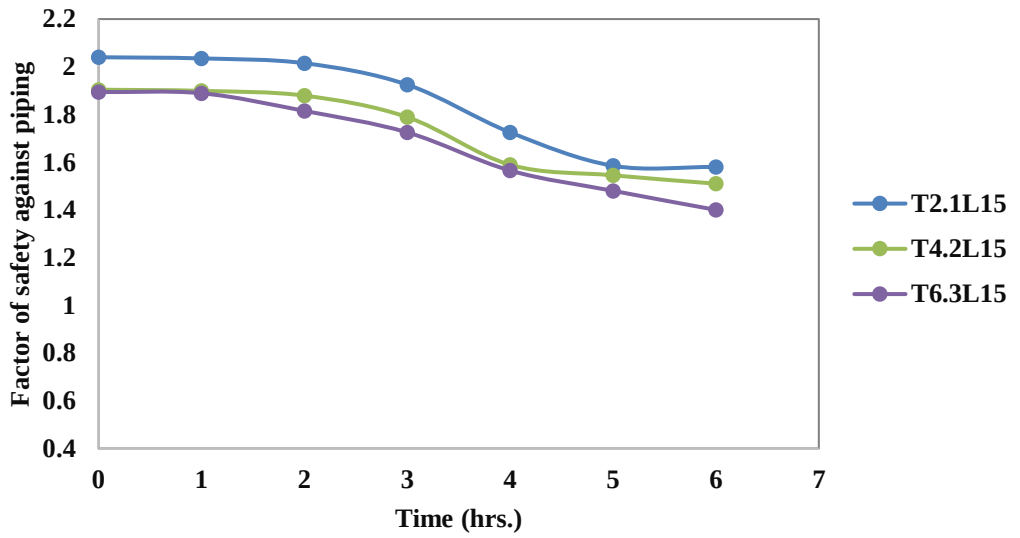

Figure. 5.26(g) Factor of safety against piping for 15m long sheet pile

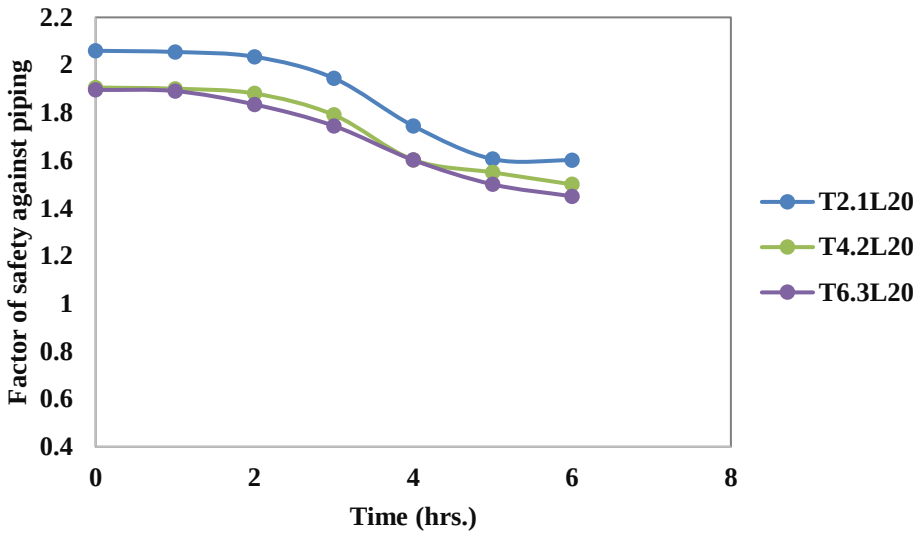

Figure. 5.26(h) Factor of safety against piping for 20m long sheet pile

It is observed from the table 5.7 that for full rise up condition factor of safety against piping is minimum and for full drawdown condition factor of safety against piping is maximum. This may be explained by the fact that this region undergoes both build up and release of pore water pressure during each tidal cycle. Crack is developed gradually on both upstream and downstream sides during each consecutive cycle and leads to failure at the end due to piping. The piping phenomenon occurs due to increase of exit gradient beyond the value of critical gradient.

It has been observed that factor of safety against piping reduces with varying water head condition with time. In case of drawdown condition factor of safety against piping increases with varying water head with time. For a given length as the sheet pile position shifts towards downstream end, factor of safety against piping increases due to increase of length of last field of flownet along flow path, thereby exit gradient reduces and factor of safety against piping increases. For increase of length of sheet pile, as creep length increases, exit gradient reduces and thereby factor of safety against piping increases. It has been seen that at full rise up condition considering 5m of sheet pile at *B*/8 position factor of safety against piping increases up to 37.00% compared to 3*B*/8 position whereas this is approximately 18.75% for 2*B*/8 position, compared to 3*B*/8 position. It is also observed that factor of safety against piping increases by 5% to 10% due to increase of sheet pile length.

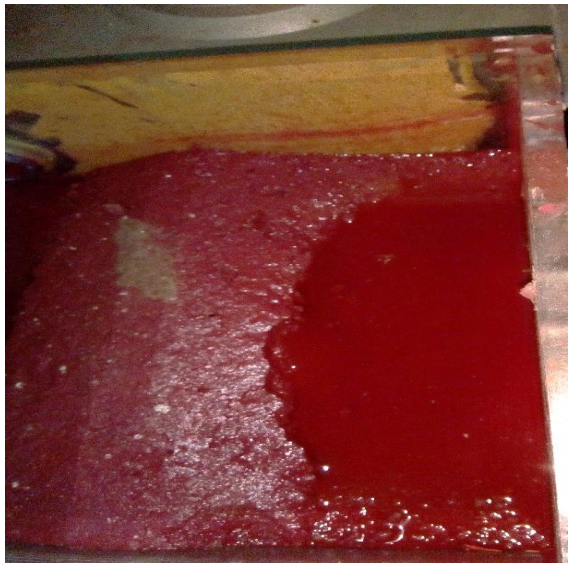

Figure 5.27(a)

Figure 5.27(b)

Figure 5.27 Crack developed under effect of tidal cycle a) in the centrifuge model b)Real time crack developed in embankment at Sundar ban site. (Reference: www.google.co.in/search sundarban crack developed)

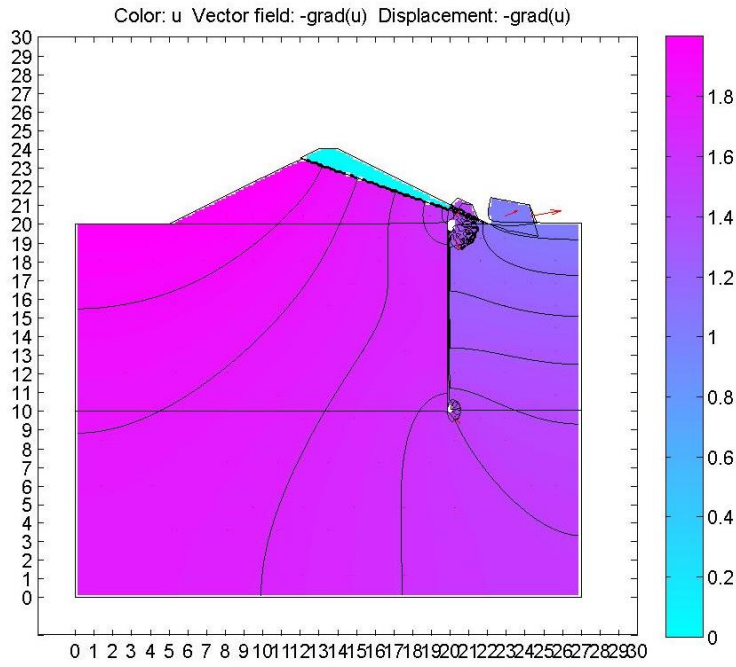

Figure 5.27 (c) Crack developed under effect of tidal cycle in MATLAB Software at *B*/8 position 10m long sheet pile (Theoretical)

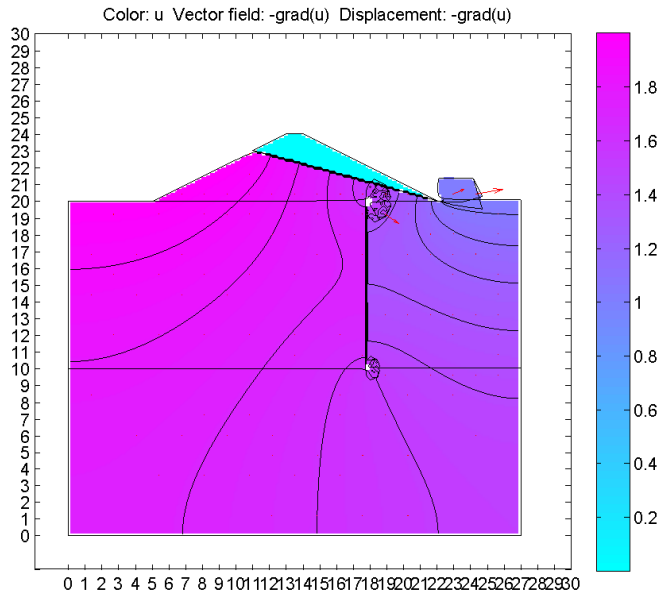

Figure 5.27 (d) Crack developed under effect of tidal cycle in MATLAB Software at 2*B*/8 position 10m long sheet pile (Theoretical)

5.7 STATISTICAL MODELING

A statistical modeling has been developed in this section considering independent variables (Sheet pile length, Sheet pile position and time) and the dependent variable (Fluid flow vector, Overall factor of safety, Factor of safety against piping, Pore water pressure variation) to form a generalized equation to predict the reliability of the model and to predict the factor of safety of a similar dam through some generalized equation. For the formulation of generalized equation MATLAB have been used to develop the equation through statistical modeling.

Linear Regression (LR) analysis, Artificial Neural Network (ANN) are the machine learning technique to capture the functional relationship among the design parameters i.e. Factor of safety against piping, overall Factor of safety, Pore water pressure variation to evaluate the correlation i.e. upstream slope, height of the dam, water table fluctuation corresponding to time and also sheet pile position and length. Determination of Factor of Safety against piping (Fp), overall factor of safety and pore water pressure variation has been possible to predict by deep learning technique for different geometry of embankment and different sheet pile position and length.

5.7.1 Prediction of factor of safety against piping with fluid flow vector, pore water pressure (Steady State)

Factor of safety against piping can be predicted in terms of pore water pressure and fluid flow vector. Figure 5.28(a), Figure 5.28(b), Figure 5.28(c) presents the regression modeling in terms of dependent and independent variables.

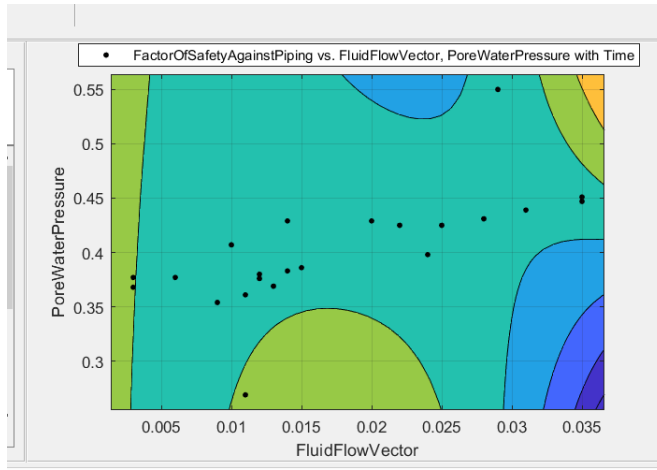

5.28(a)

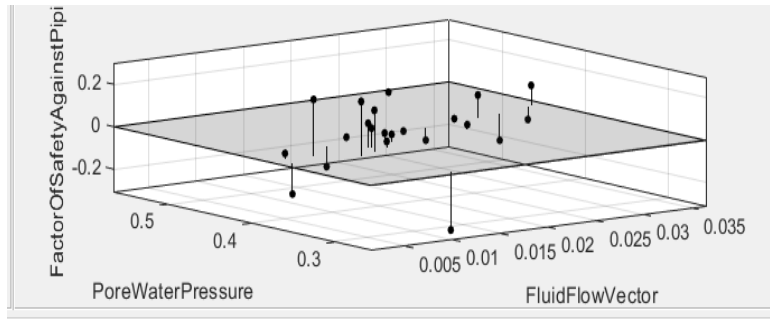

5.28(b)

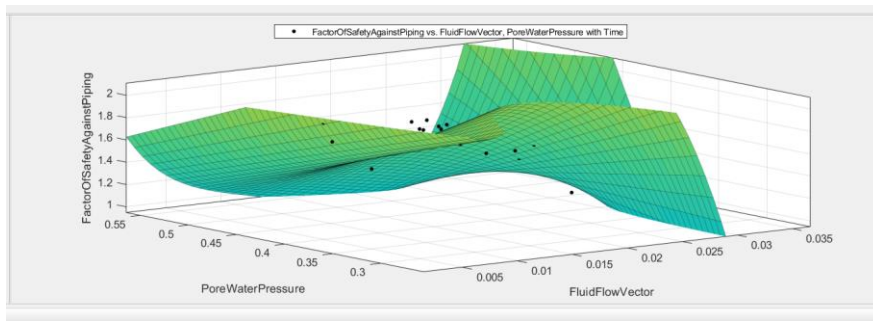

5.28(c)

Figure 5.28: Statistical modeling corelating dependent and independent variable (a) contour (b)coordinate(c) 3D surface

The generalized equation for factor of safety against piping, (with 95% confidence bounds) and R-square: 0.8512 is given by equation (5.1)

$$Fp = 1.789 + 0.0002307\ x - 0.3002\ y - 0.4997\ x^2 - 0.07234\ x\ y - 0.1701\ x^3 + 0.1833\ x^2\ y + 0.1528\ x^4 + 0.1177\ x^3 y \quad (5.1)$$

where x is normalized by mean= 0.01736 and Standard deviation = 0.00985 and y is normalized by mean 0.4014 and Standard deviation 0.05257

5.7.2 Prediction of factor of safety against piping with sheet pile length and position with time (Transient State)

Factor of safety against piping can be predicted in terms of pore water pressure and fluid flow vector. Figure 5.29(a), Figure 5.29(b), Figure 5.29(c) presents the regression modeling in terms of dependent and independent variable.

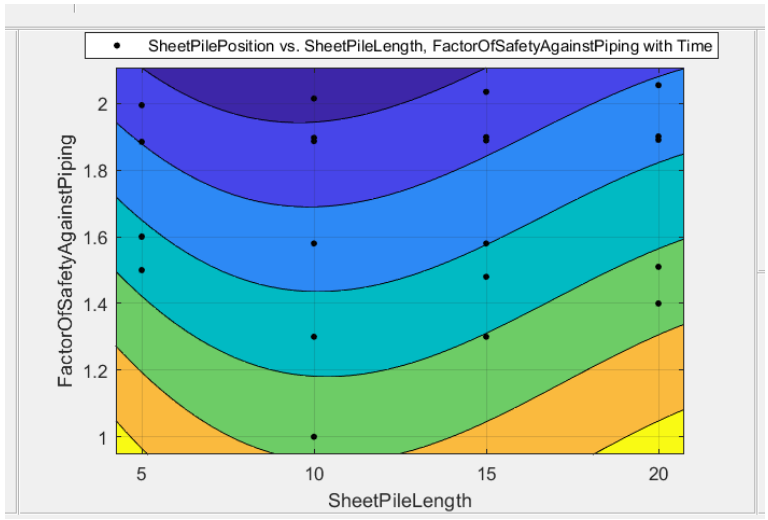

5.29(a)

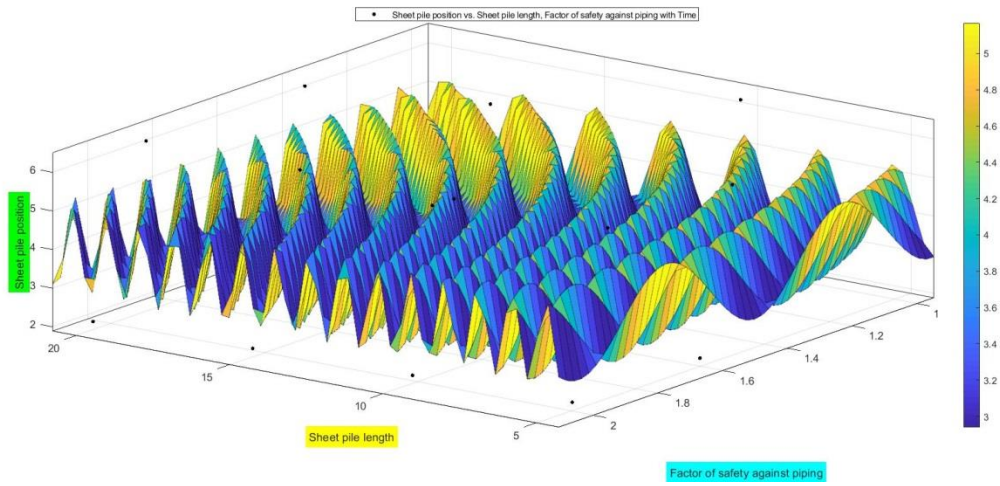

5.29(b)

Figure 5.29: Statistical modeling corelating dependent and independent variable (a) contour (b) 3D surface

The generalized equation for factor of safety against piping, (with 95% confidence bounds) is given by equation (5.2)

$$F_p=4.504+1.111\times\sin(0.8618\times\pi\times L\times T)+8.271\times e^{-(4.767\times T)^2} \quad (5.2)$$

Where, *L*=sheet pile length, *T*=Sheet pile position

5.7.3 Correlation of overall factor of safety against under static condition between pore water pressure, fluid flow vector, piping with sheet pile length and position with time

Thus, it is possible to predict factor of safety and factor of safety against piping for the model embankment for the range of parameters under study.

The prediction of factor of safety with respect to pore water pressure, fluid flow vector, piping with sheet pile length and position with time has been studied and represent in the following figures 5.30(a) to 5.30(k). The regression results have been presented in Table 5.8. The generalized equation has been presented in Table 5.9.

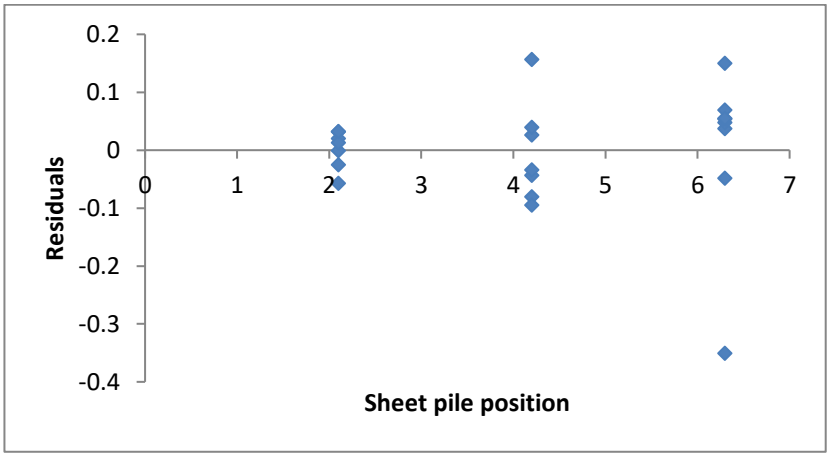

Figure 5.30(a): Sheet pile position Residual Plot

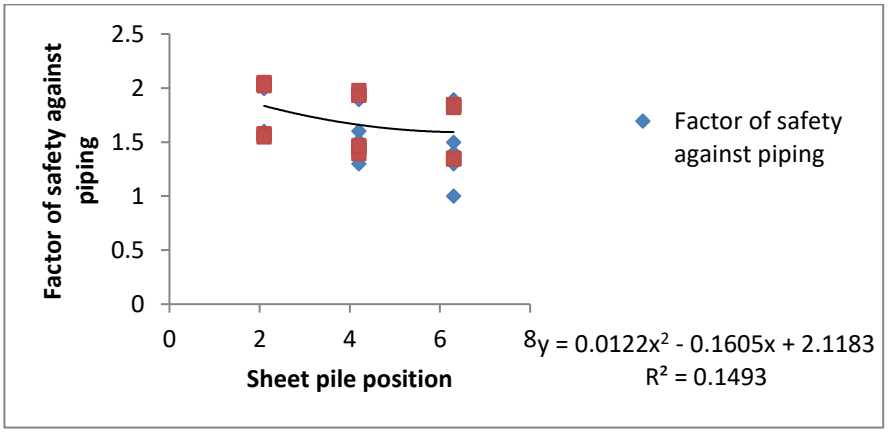

Figure 5.30(b): Sheet pile position Line Fit Plot

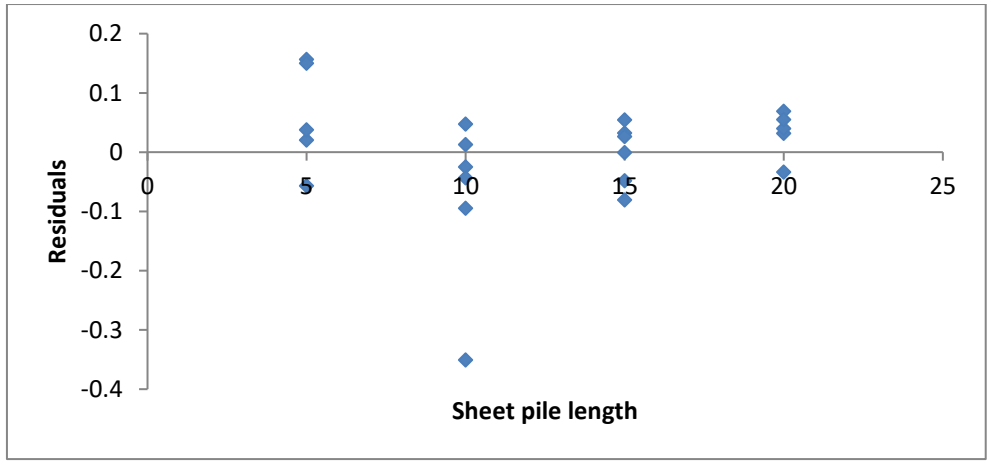

Figure 5.30(c): Sheet pile length Residual Plot

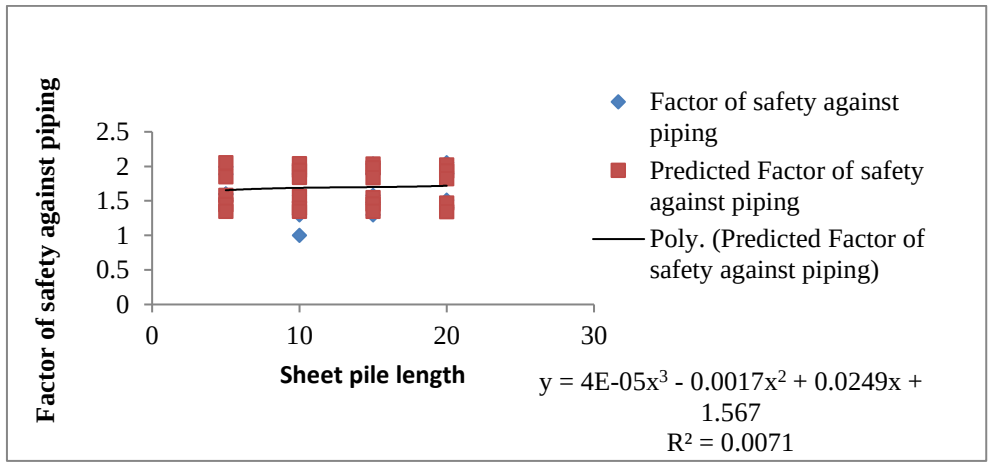

Figure 5.30(d): Sheet pile length Line Fit Plot

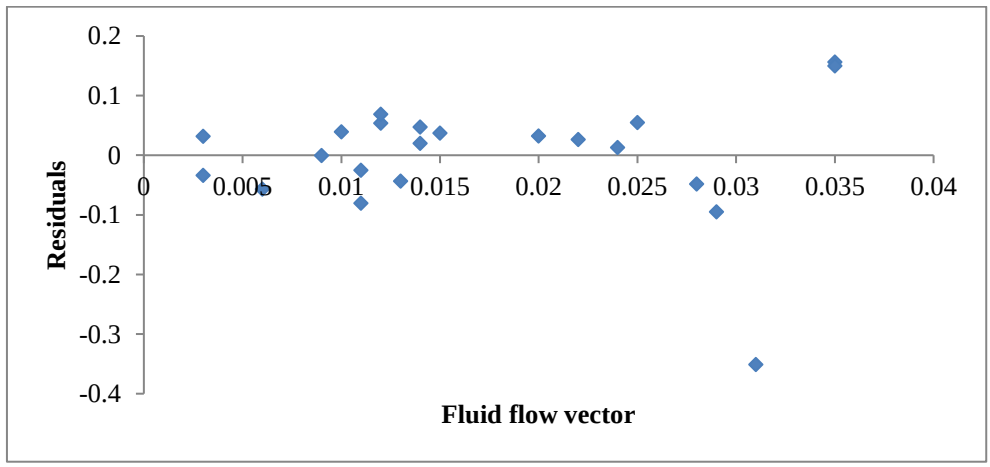

Figure 5.30(e): Fluid flow vector Residual Plot

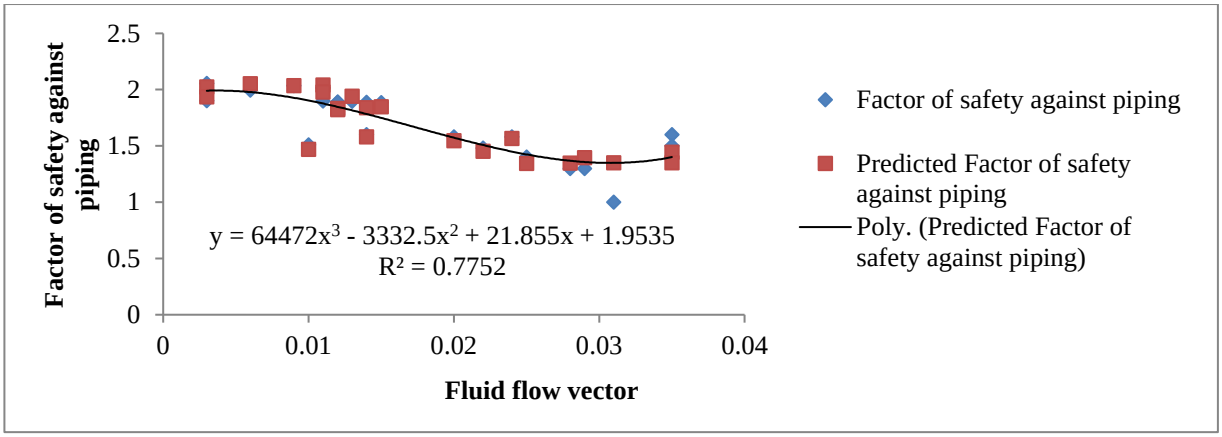

Figure 5.30(f): Fluid flow vector Line Fit Plot

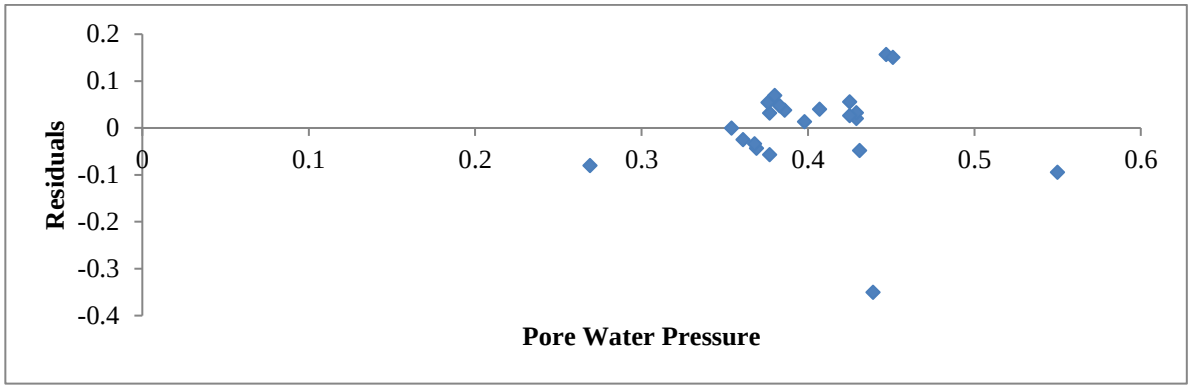

Figure 5.30(g): Pore Water Pressure Residual Plot

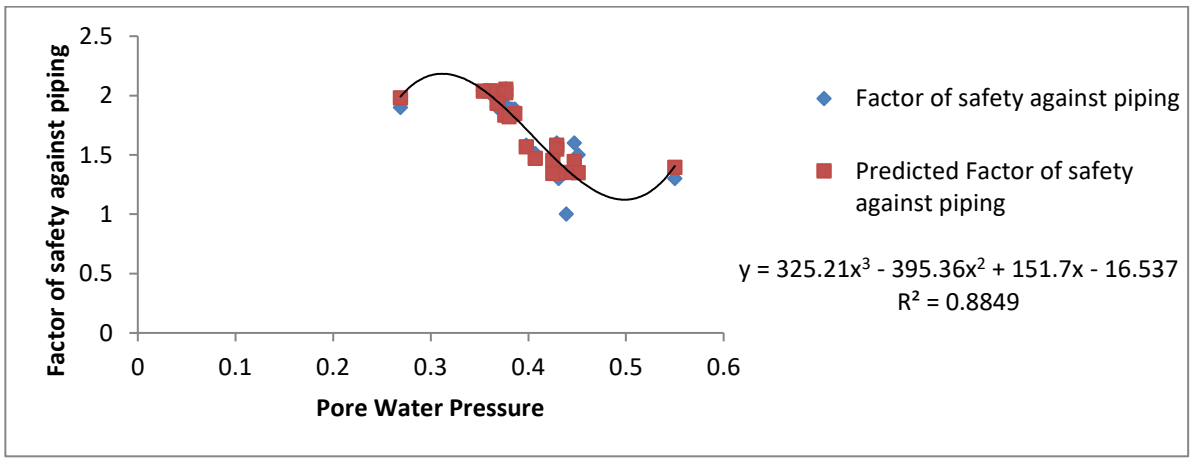

Figure 5.30(h): Pore Water Pressure Line Fit Plot

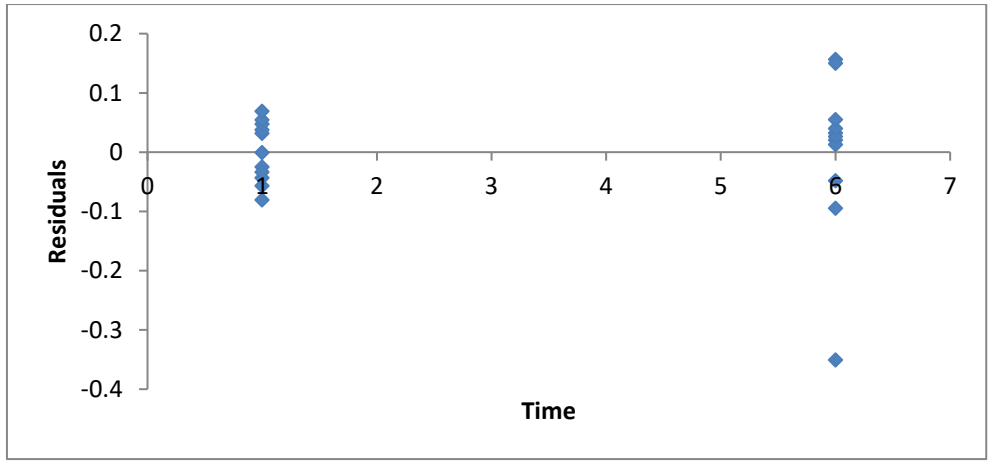

Figure 5.30(i): Time Residual Plot

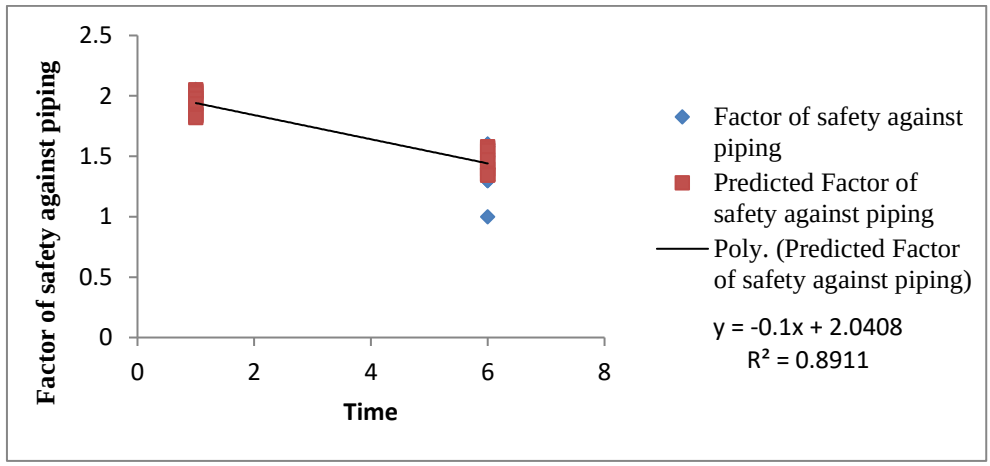

Figure 5.30(j): Time Line Fit Plot

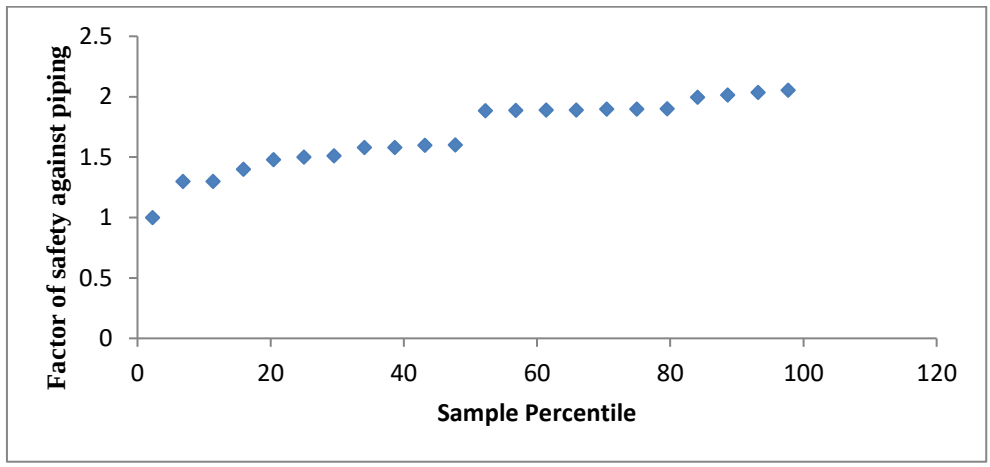

Figure 5.30(k): Normal Probability Plot

Figures 5.30(a) to 5.30(k) show different statistical plots and Table 5.8 presents statistical table with mean, median, mode and standard deviation. Table 5.9 presents the generalized equation of factor of safety against piping for different parameter as dependent variable.

Table 5.8: Statistical table

Sheet pile position		*Sheet pile length*		*Fluid flow vector*		*Time*	
Mean	4.2	Mean	12.5	Mean	0.017	Mean	3.5
Median	4.2	Median	12.5	Median	0.014	Median	3.5
Mode	2.1	Mode	5	Mode	0.011	Mode	1
Standard Deviation	1.75152 1078	Standard Deviation	5.7104 0241	Standard Deviation	0.009 537	Standard Deviation	2.55 377

Table 5.9: Equation for variation of Factor of safety against piping

Dependent Variable	**Independent Variable**	**EQUATION**
Factor of safety against piping	Pore water pressure variation (P_P)	$y = 325.8P_P^3 - 395.23P_P^2 + 151.7P_P - 16.537$
Factor of safety against piping	Fluid flow vector(y_f)	$y = 64472\ y_f^{\ 3} - 3332.5\ y_f^{\ 2} + 21.855\ y_f + 1.9535$
Factor of safety against piping	Sheet pile length (L)	$y = 4E\text{-}05\ L^{\ 3} - 0.0017\ L^{\ 2} + 0.0249\ L + 1.567$
Factor of safety against piping	Sheet pile position(T)	$y = 0.0122\ T^2 - 0.1605\ T + 2.118$
Factor of safety against piping	Time (t)	$y = -0.1t + 2.0408$

Thus, it is possible to predict the factor of safety against piping and factor of safety for the model embankment for the range of parameters under study.

5.7.4 Correlation of overall factor of safety against under seismic condition between sheet pile length and position with time

The prediction of factor of safety under seismic condition with respect to pore water pressure, fluid flow vector, piping with sheet pile length and position with time has been studied and represent in the following figures 5.31(a) to 5.31(g). Table 5.10 presents the generalized equation of factor of safety against under seismic condition for different parameter as dependent variable.

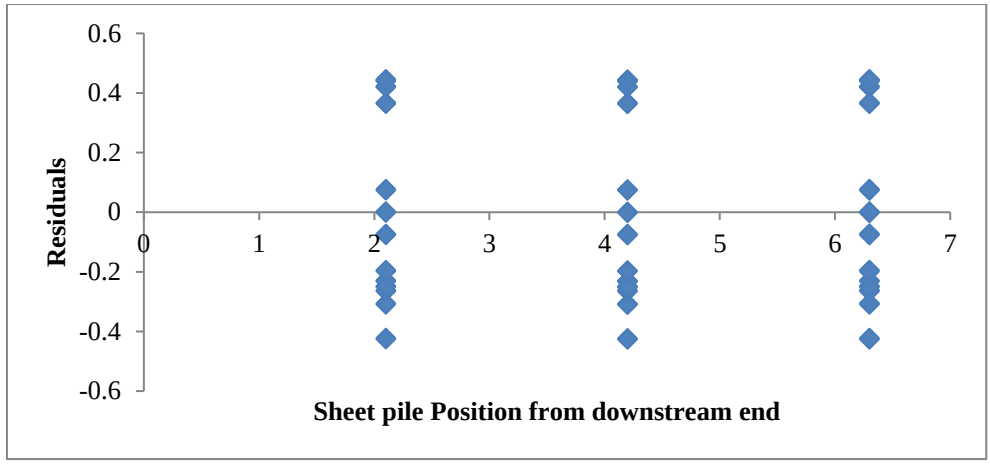

Figure 5.31(a): Sheet pile position Residual Plot

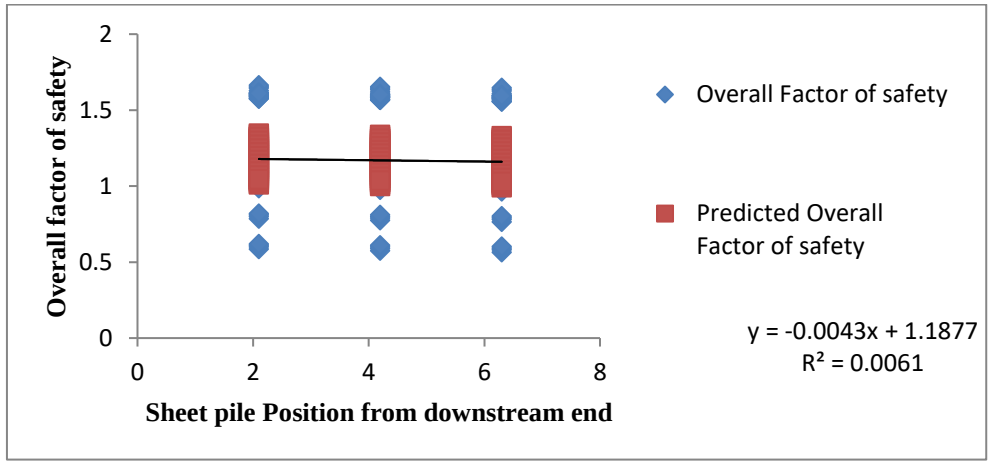

Figure 5.31(b): Sheet pile position Line fit Plot

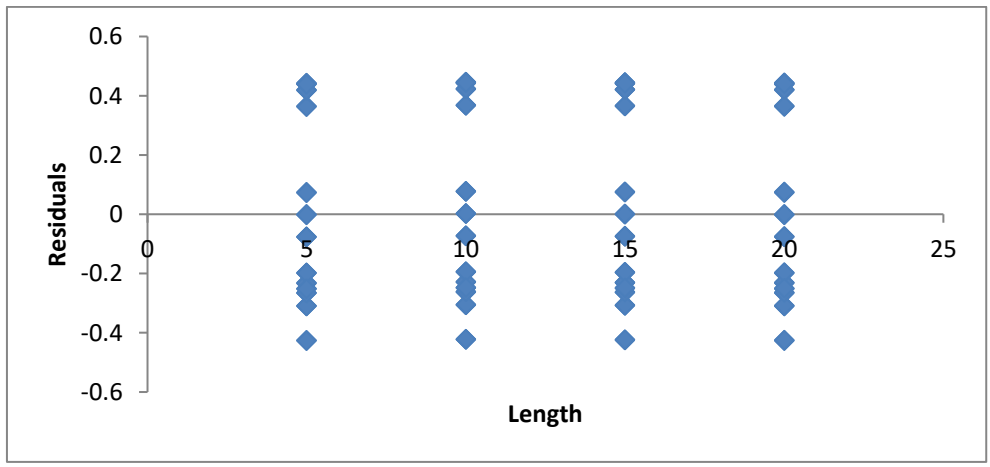

Figure 5.31(c): Sheet pile Length Residual Plot

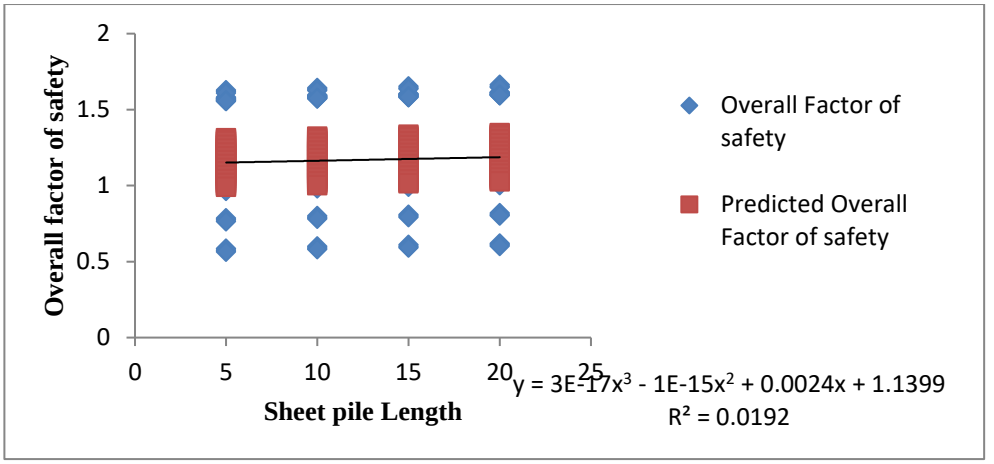

Figure 5.31(d): Sheet pile Length line fit Plot

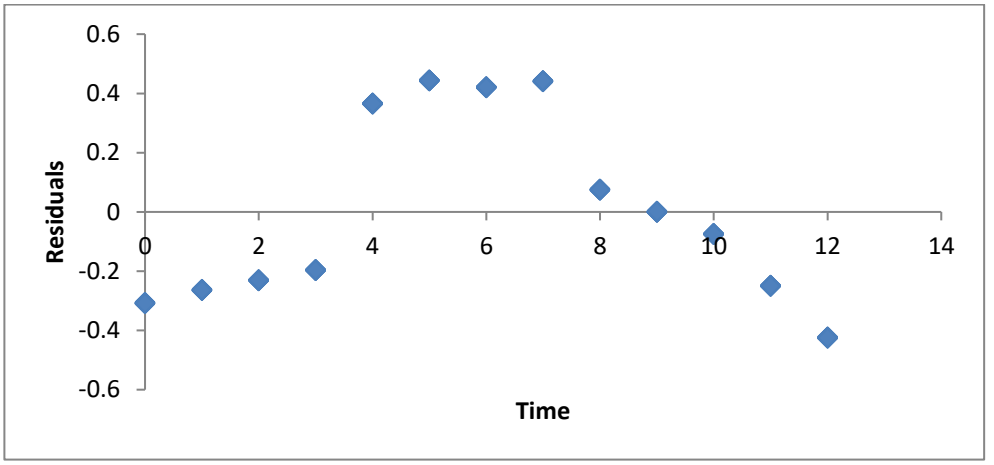

Figure 5.31(e): Time residual Plot

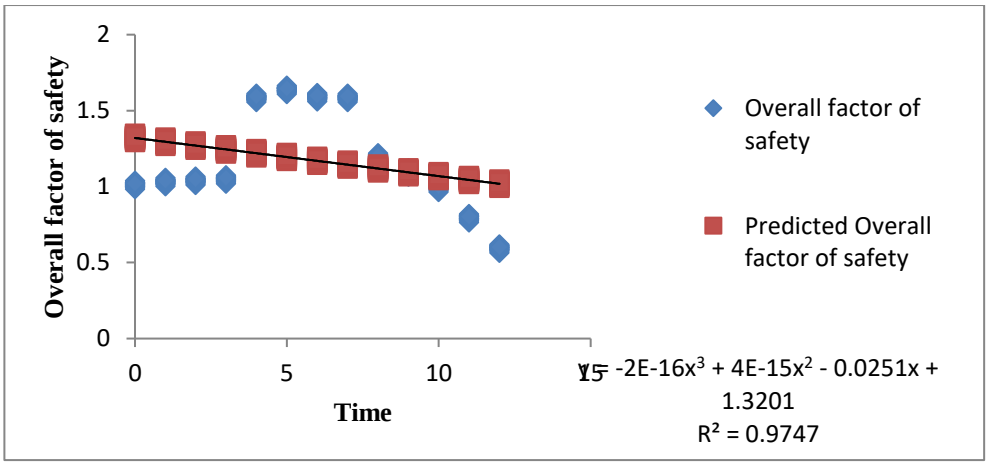

Figure 5.31(f): Time Line fit Plot

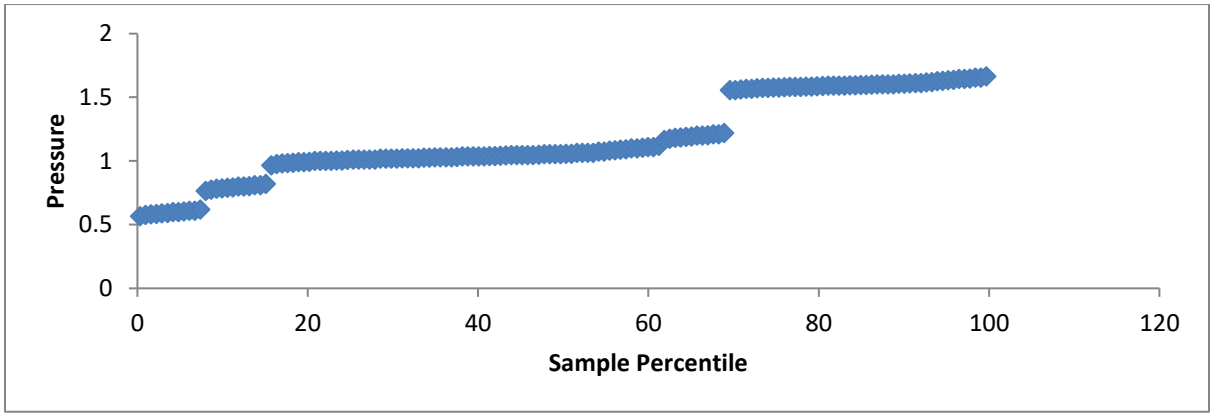

Figure 5.31(g): Normal probability Plot

Table 5.10: Equation for variation of Factor of safety under seismic condition

Dependent Variable	**Independent Variable**	**EQUATION**
Overall Factor of safety	Sheet pile length (L)	Fs = 3E-17L^3 - 1E-15L^2 + 0.0024L + 1.1399
Overall Factor of safety	Sheet pile position(T)	Fs = 0.0043T + 1.1877
Overall Factor of safety	Time (t)	Fs = 2E-16t^3 + 4E-15t^2 - 0.0251t + 1.3201

Thus, it is possible to predict the overall factor of safety and factor of safety for the model embankment for the range of parameters under study.

5.7.5 PREDICTION OF OVERALL FACTOR OF SAFETY

In order to, predict Factor of safety in generalized form an attempt has been made to forecasting data for changes in dam geometry, length of sheet pile and position of sheet pile for steady state and transient state for both static and seismic condition. This has been done by Support Vector Machine (SVM), Decision Tree, Linear Discriminant and K-Nearest Neighbor with principal component analysis (PCA). In SVM each data is plotted as a point in n-dimensional space (where n is number of features) and classification is performed by finding the hyper-plane. Medium Tree & Course Tree classification learner algorithm on this particular dataset with PCA technique show 15.9% accuracy which is less considerable to predict the validity of this model based on this dataset. Figure 5.32(a) presents scatter plot for prediction model for $\frac{Width\ of\ dam\ (B)}{Height\ of\ dam(H)}$ ratio with factor of safety. Figure 5.32(b) presents

scatter plot for prediction model for slope of dam (m) with factor of safety. Thus, it is possible to predict factor of safety and factor of safety against piping for the model embankment for the range of parameters under study.

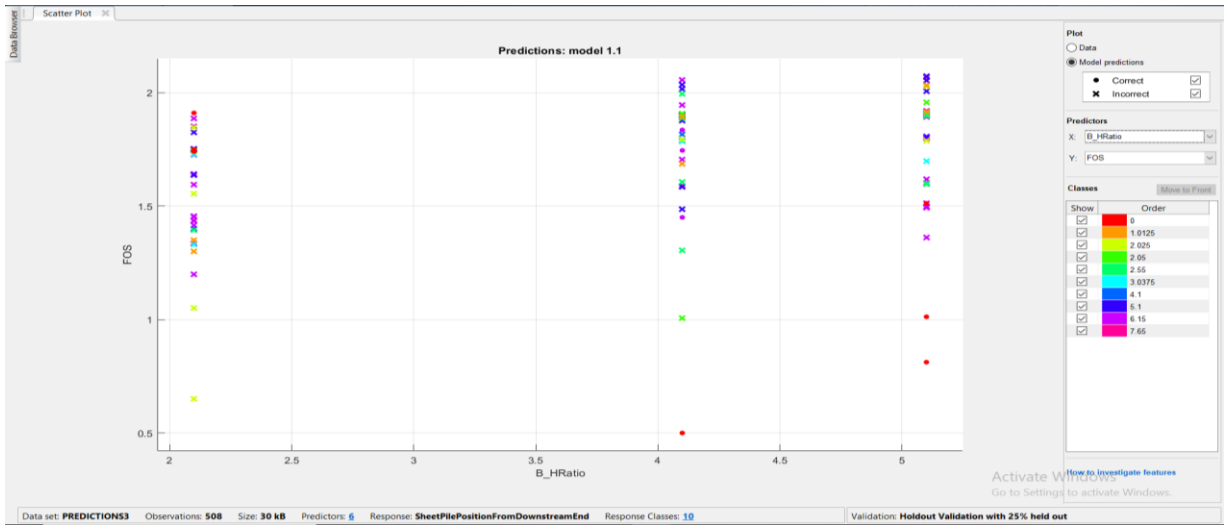

Figure 5.32(a): Scatter plot for prediction model for B/H ratio and factor of safety (FOS) as predictors using PCA

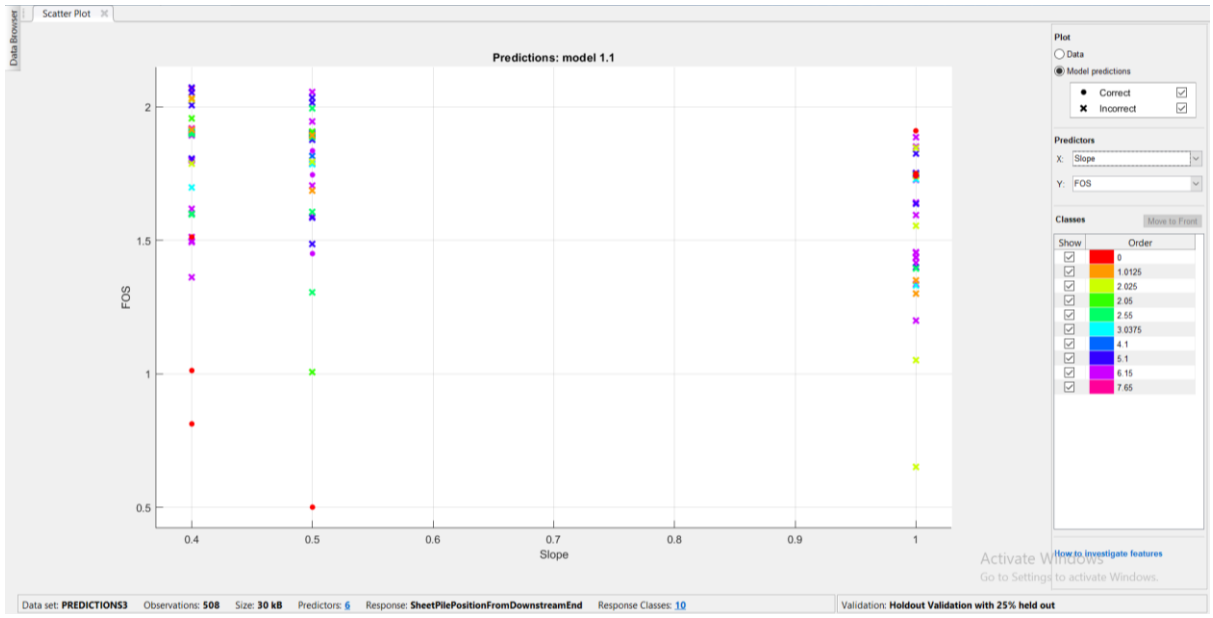

Figure 5.32(b) : Scatter plot for prediction model using slope & factor of safety (FOS) as predictors using PCA

Gaussian process regression (GPR) models are nonparametric kernel-based probabilistic models computing the prediction intervals using the trained model. It is intended to be accessible to a general readership and focuses on practical examples and high-level

explanations. Gaussian process regression has been successfully applied to predict a correlation where it is useful as the priors over different functions can also be modelled, thereby assessing an optimized sheet pile position and location. The built-in kernel (covariance) functions with same length scale for predicting overall factor of safety for static condition is, Squared Exponential Kernel and for seismic condition is Rational Quadratic Kernel. Using the regression learner to get various types of solutions and models and training them with the data such that the predictors of the Overall Factor of safety are the positions of B/8, 2B/8, 3B/8 and lengths of 5m, 10m, 15m, 20m with time variation from 1hr. to 6 hrs. and 6 hrs. to 12 hrs. A square smoothing spline with the degrees of freedom 4, determined by 21 folds cross validation within the training set. From this predicted result, the primary data set is one again used to get a polynomial fitting equation (poly-fitn function) with two-degree solutions. Figure 5.33 (a), Figure 5.33(b) and Figure 5.33 (c) presents true response and predicted response of overall factor of safety under static condition.

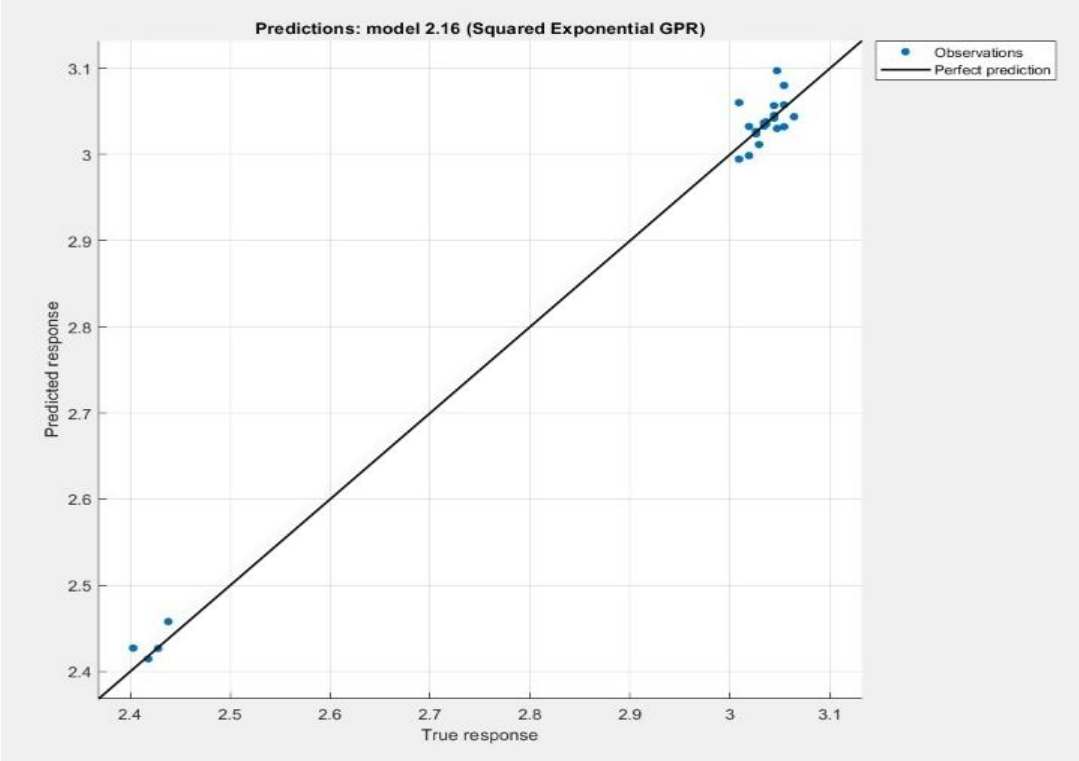

Figure 5.33(a) : True response and predicted response using PCA in predictor model for static condition

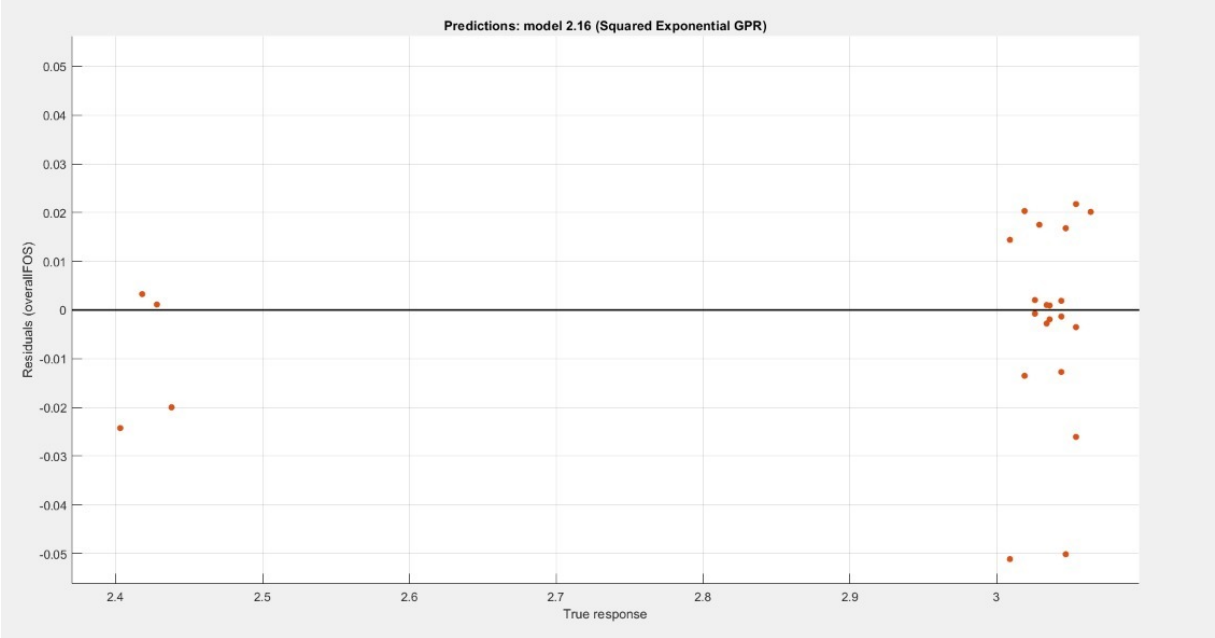

Figure 5.33(b): Residuals vs. True response using PCA in predictor model for static condition

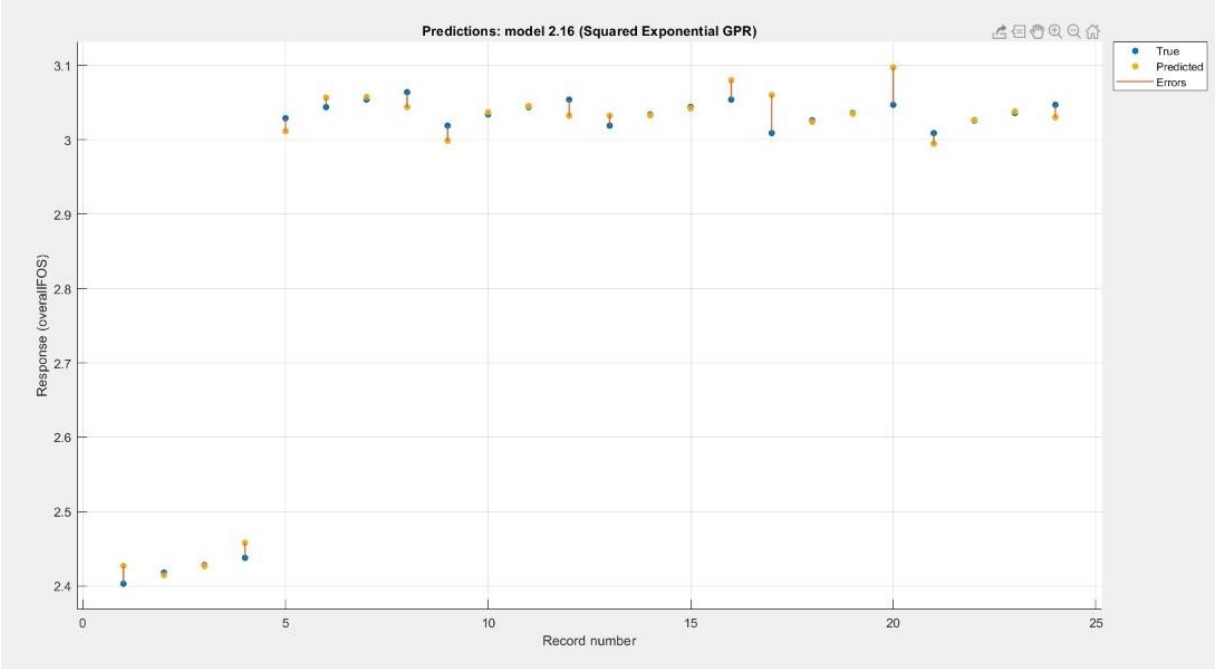

Figure 5.33(c): Residuals vs. Record number using PCA in predictor model for static condition

Optimized equation of overall factor of safety under static condition considering second degree polynomial has been presented in equation (5.3),

$$Optimized\ Overall\ FoS \text{ (Under static condition)} = -0.03520 \times x_1^2 - 9.0 \times 10^{-05} \times (x_1 x_2) - 0.02900 \times (x_1 x_3) + 0.47156 \times x_1 - 0.00012 \times x_2^2 - 0.000217 \times (x_2 x_3) + 0.00717 \times x_2 - 1.88 \times 10^{12} \times x_3^2 + 1.317 \times 10^{13} \times x_3 - 1.12 \times 10^{13} \quad (5.3)$$

$x_1 = Position\ of\ sheet\ pile\ from\ downstream\ end$
$x_2 = Sheet\ pile\ length$
$x_3 = Time\ in\ hr.$

Results revealed that two have very low RMSE (Root Mean Squared Error). The lowest being the model using SEGPR or Squared Exponential GPR method (Squared Exponential Gaussian Process Regression) under the effect of PCA (Principal Component Analysis) set at a variance of 97% and numeric component=1, giving an RMSE= 0.0764 (least of all models). Next this solution is made into a structural predictive model to predict the Factor of safety for a similar data of 24 members with the input of the same data set as the position/length has fixed values and the time factor gives a very low change of the Factor of safety.

Figure 5.33 (d), Figure 5.33(e) and Figure 5.33 (f) presents true response and predicted response of overall factor of safety under seismic condition.

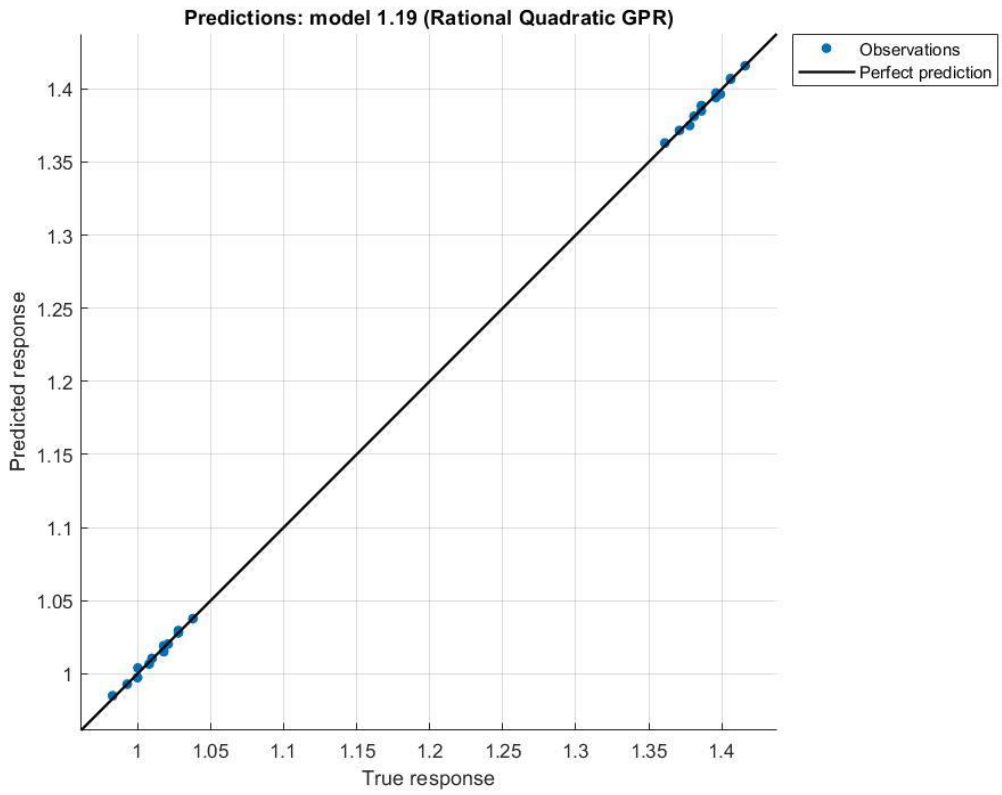

Figure 5.33(d) : True response and predicted response using PCA in predictor model for seismic condition

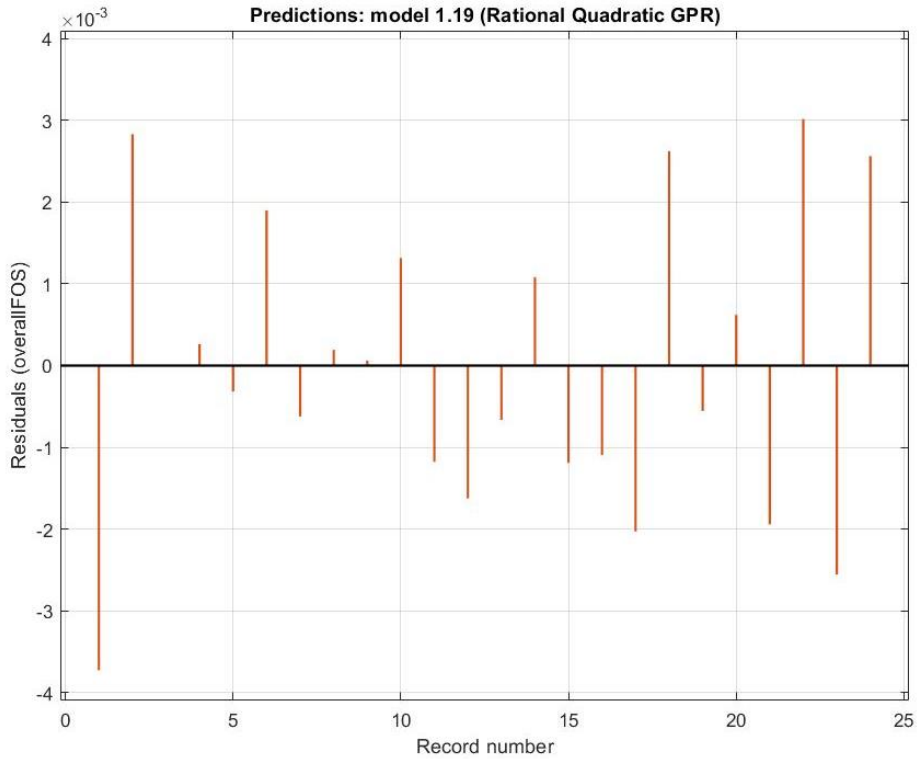

Figure 5.33(e): Residuals vs. True response using PCA in predictor model for seismic condition

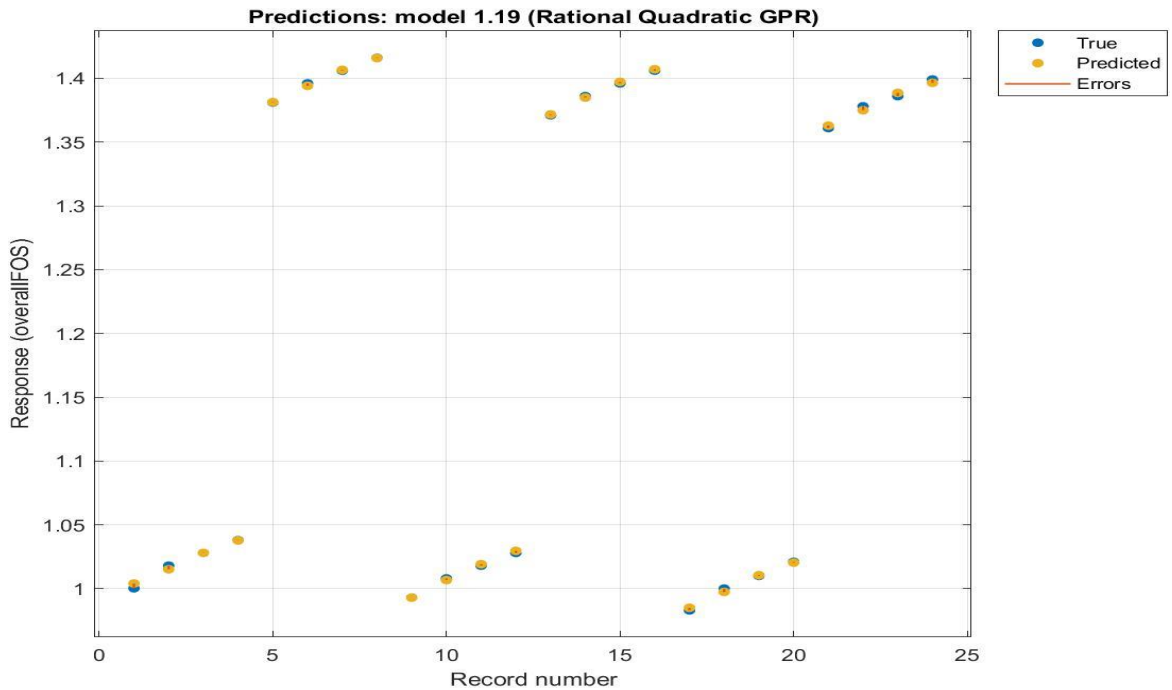

Figure 5.33(f): Residuals vs. Record number using PCA in predictor model for seismic condition

Optimized equation of overall factor of safety under seismic condition considering second degree polynomial has been presented in equation (5.4),

$$Optimized\ Overall\ FoS\ (\text{Under seismic condition}) = 3.620\times10^{-05}\times x_1^{\,2} + 1.583\times10^{-05}(x_1x_2) - 4.712\times10^{-05}(x_3) - 0.0046x_1 - 3.743\times10^{-05}\times x_2^{\,2} - 1.131\times10^{-05}\,(x_2x_3) + 0.003x_2 + 1.18\times10^{18}(\times x_3^{\,2}) - 8.2\times10^{8}\times x_3 + 7.09\times10^{8} \quad (5.4)$$

$x_1 = Position\ of\ sheet\ pile\ from\ downstream\ end$
$x_2 = Sheet\ pile\ length$
$x_3 = Time\ in\ hr.$

Results revealed that two have very low RMSE (Root Mean Squared Error). The lowest being the model using SEGPR or Squared Exponential GPR method (Squared Exponential Gaussian Process Regression) under the effect of PCA (Principal Component Analysis) set at a variance of 97% and numeric component=1, giving an RMSE= 9.87×10^{-4} (least of all models). Next this solution is made into a structural predictive model to predict the Factor of safety for a similar data of 24 members with the input of the same data set as the position/length has fixed values and the time factor gives a very low change of the Factor of safety.

Optimized position of sheet pile has been evaluated in terms of factor of safety correlating the generalized solution. Figure 5.33 (g) and Figure 5.33 (h) presents optimized position and length in terms of Factor of safety in a vector space variating sheet pile length and position. Figure 5.33 (i) presents optimization of factor of safety for both static and seismic condition.

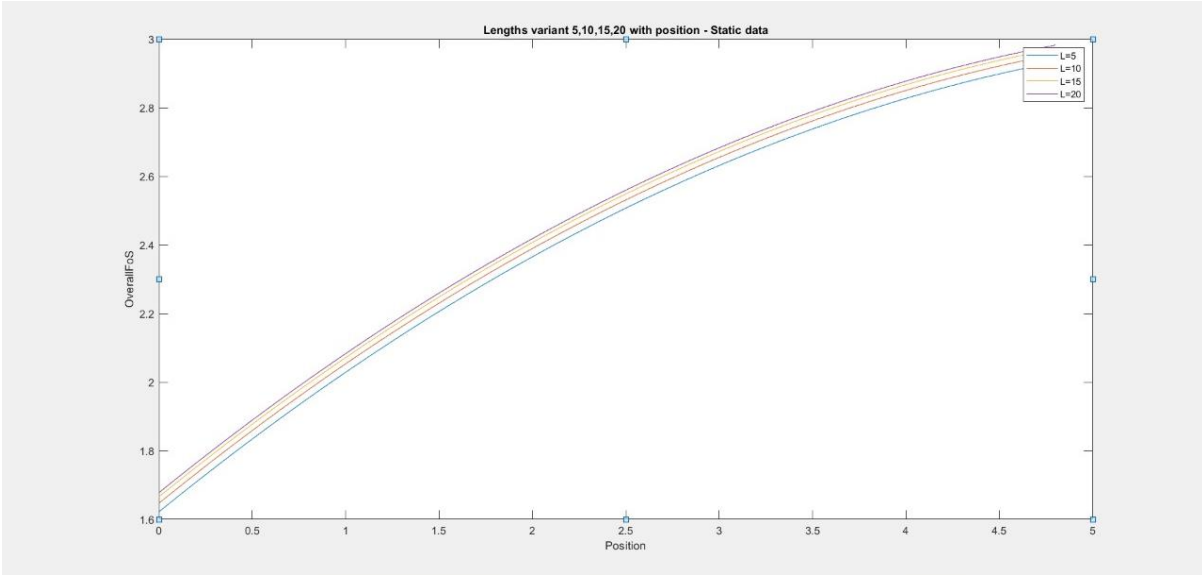

Figure 5.33(g): Optimization of factor of safety with respect to sheet pile position and sheet pile length under static condition

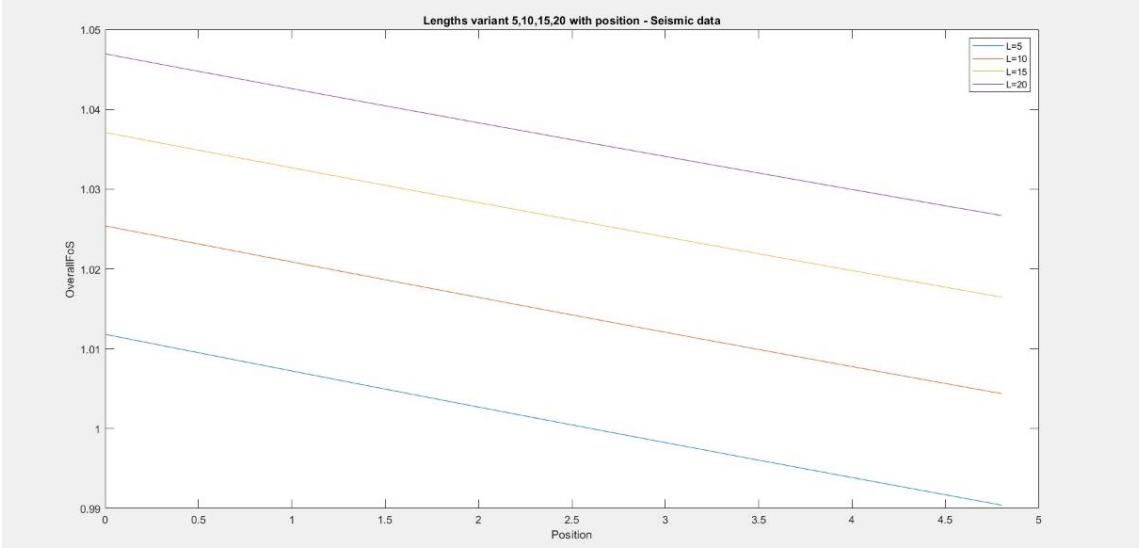

Figure 5.33(h): Optimization of factor of safety with respect to sheet pile position and sheet pile length under seismic condition

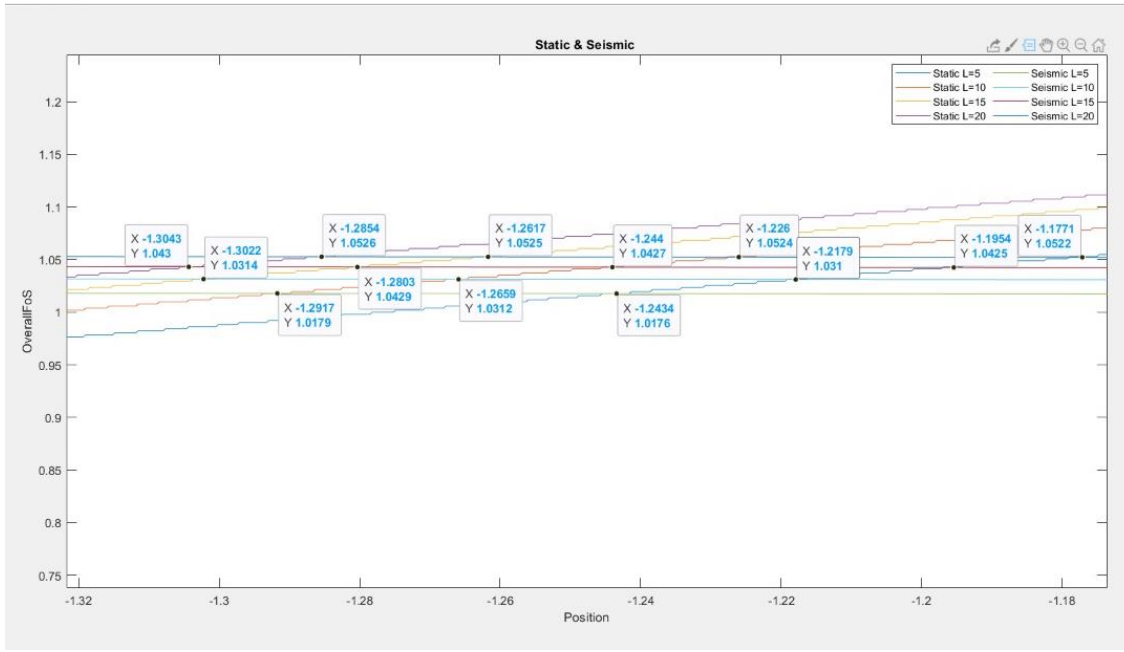

Figure 5.33(i): Optimization of factor of safety with respect to sheet pile position and sheet pile length under both static and seismic condition

From Figure 5.33 (g), Figure 5.33 (h) and Figure 5.33 (i) it has been found that optimized sheet pile length is 15m for both static and seismic condition in the data space. Optimizing sheet pile length at 15m it has been further observed that optimized sheet pile position lies at *B/7* from downstream end.

After Statistical Analysis, it has been found that most advantageous location and length of sheet pile become *B/7* from downstream end and 0.88 times the base width of the dam respectively under both static and seismic condition for both steady and transient seepage.

CHAPTER SIX

SUMMARY, CONCLUSIONS AND FURTHER SCOPE

6.1 SUMMARY

A dam is constructed across a river, as a barrier, to impound water in the reservoir to use it for various purposes like irrigation; navigation etc. Seepage through and below an earthen dam plays an important role in determining the stability of the dam. The present study has been carried out to analyze both steady and transient seepage (under tidal variation) in case of a water front earthen embankment dam. With this in view the seepage behavior of a model dam, made of clayey soil and of 1m top width, 17m bottom width and 4m height has been studied. The foundation of the dam has also been made clayey down to 20m depth to simulate soil condition of a location at South 24 Parganas in West Bengal; India. In the numerical analysis part finite element and finite difference methods have been adopted to study the dynamics of phreatic line and flow net. Numerical modeling has been done with FLAC2D and SEEP/W after validating by MATLAB. Two-dimensional numerical analyses have been carried out with the help of FLAC-2D. The flow net has been drawn by SEEP/W software using the finite element method for solving steady state and transient state seepage analysis. Further to establish the reliability of the study, flow net has been drawn by solving Laplce's partial differential equation with the help of partial differential equation solver in MATLAB. An experimental investigation has also been performed on similar model dam in geotechnical centrifuge simulating steady state and transient state with single and multiple tidal cycles. The study has been done both under steady seepage and rise up-drawdown conditions (transient state) to simulate tidal effect of river of the same region considered for the study. For the transient state the tidal head has been varied in a linear pattern. Rise up half cycle time i.e. time taken by the riverside water to rise from LTL to HTL has been taken as 6 hours. Draw down Half Cycle time i.e. time taken by the riverside water to fall from HTL to LTL has also been taken as 6 hours. The present work has been performed considering a single tidal cycle duration as 12 hours and multiple cycle duration of 60 days or 120 cycles. The experimental output images of centrifuge modeling have been captured and thereafter processed through MATLAB- Raspberry Pi interfacing. Particle Image Velocimetry (PIV) processing have been done by Fast Fourier Transform (FFT) cross correlation. An attempt has been made further to evaluate the effectiveness of sheet pile as seepage barrier, varying sheet pile length and position for all cases. In this current study numerical and experimental investigations have been

performed with parametric variation of sheet pile length of 5m, 10m, 15m and 20m varying the sheet pile position *B*/8, 2*B*/8 and 3*B*/8 positions from the downstream end under steady and transient states for both seismic and static conditions.

Based on the experimental and numerical studies, flownet for each experimental and numerical case, variation of flow vector and pore water pressure have been studied within the dam body as well as within the foundation of the dam. Soil pressure on sheet piles have also been obtained on both sides of sheet pile along its length for different lengths and positions of sheet piles. Factor of safety against only piping and overall factor of safety, taking into account the stability of slope also has been estimated for all cases of steady and transient seepage under both seismic and non-seismic conditions. A statistical modeling has also been developed with the help of SPSS and MATLAB; considering independent variables as sheet pile length, sheet pile position and time and the dependent variables as fluid flow vector, overall factor of safety, factor of safety against piping, pore water pressure. This has been done to form a generalized equation to predict the reliability of the model and to predict the factor of safety of a similar dam through some generalized equation.

6.2 CONCLUSIONS

Transient stage analysis, under drawdown condition has been performed by several researchers but rise up condition has not been addressed properly. The contribution in this present study, is to study the effect of sheet pile as fluid barrier for both rise up and drawdown condition. Determination of flow-net by experimental modeling has not been well addressed by earlier researchers. But In this present investigation flownet has been obtained by PIV technique in experimental analysis. From the obtained flownet, in both numerical and experimental study, factor of safety against piping has been successfully obtained in rise up and drawdown condition. Furthermore, non-dimensional analysis has been performed in MATLAB 2018R, and an equation has been suggested of factor of safety, with respect of sheet pile position and length, for a fixed geometry and homogeneous soil property.

The following conclusions may be drawn from this present study:

A. For Static Steady State condition

1. Fluid flow vector decreases as sheet pile moves towards downstream end and it is maximum for least length and flow vector reduces with increase of sheet pile length.
2. Fluid flow vector is found to fall at sheet pile position for seismic condition when the position is towards downstream end. Variation of fluid flow vector under seismic

condition is very much erratic. It increases and decreases respectively at the time of increase and decrease of seismic force

3. At the downstream end, pore pressure becomes of similar order irrespective of sheet pile position. Pore pressure is high on the upstream side of sheet pile and it reduces along the sheet pile itself for all sheet pile positions. Sheet pile length has insignificant effect on pore pressure variation along the sheet pile. In seismic case pore water pressure increases up to 20% at the upstream side whereas at downstream side increases up to 10-15% compared to respective static condition.
4. Factor of safety against piping decreases when sheet pile position moves away from downstream end for a fixed sheet pile length. As the length of the sheet pile increases factor of safety against piping also increases.
5. Factor of safety against both piping and overall stability increase with sheet pile length. In case of piping, it is more predominant due to increase of creep length. It further appears that piping phenomenon is being more influenced than overall stability of dam by introduction of sheet pile.
6. For short sheet pile (5m), no net soil pressure is produced on the downstream side. When position of sheet pile is shifted towards downstream end, value of soil pressure for both upstream and downstream sides gradually decreases.
7. Under seismic condition the peak values of soil pressure on both sides of sheet pile become very high

For transient condition

1. The unsaturated region continuously reduces with rise up and increases with drawdown. In case of transient seismic state, in 1 hour the extent of flownet is very small and it is increasing due to rise of upstream water level whereas it is further decreasing with starting of drawdown condition.

2. The location of the phreatic surface,at thr river-embankment interface, shifts to a slightly higher elevation within a particular zone after each cycle in case of multiple tidal cycle condition. The elevational shift in phreatic surface is marginal. The location of phreatic line gradually approaches towards that under steady state with the lapse of the time during rise up.

3. Variation of fluid flow vector under seismic condition and in case of transient flow is very much irregular and increases and decreases respectively at the time of increase and

decrease of seismic force. The variation of fluid flow vector is not found to be influenced much by length and position of sheet pile.

4. Beyond sheet pile the fluid flow vector increases in magnitude by approximate 5% in upward with increase of water level under rise up condition. Under drawdown condition it decreases in magnitude in downward direction.
5. Pore pressure reduction at 7m level is 28.28% more than that at 12m depth.
6. At 12.0 m depth, for 5m length to 20m length the decrease of pore pressure is varying from 7.57% to 16.66% for 3*B*/8 position, whereas for B/8 position it varies from 18.083% to 28.33% under rise up condition and the same for drawdown condition is varying from 8.48% to 11.71% for 3*B*/8 position whereas for *B*/8 position it varies from 9.78% to 29.29%.
7. variation of length in sheet pile is not affecting the pore pressure within the dam body and pore pressure at the mid horizontal level of the dam body increases up to about middle during rise up. At upstream side pore water pressure increases up to 45% whereas at downstream increment is up to 10% on an average due to seismic effect.
8. Under seismic condition pore water pressure increases on an average 50% on upstream side compared to static condition. Under seismic condition pore water pressure increases on an average 15% on downstream side compared to static condition.
9. Pore water pressure gradually increases a little for rise up condition and remains almost same for drawdown condition up to about 15m for both the cases. The pore pressure increases a little for rise up condition and decreases for drawdown condition towards downstream.
10. Pore water pressure is decreasing towards downstream end. Ultimately increase of pore water pressure on upstream side is 14.00% more and there is no change of pore water pressure on downstream side compared to static condition. Effect of multiple tidal cycle is pronounced at upstream end of change of pore water pressure for the number of multiple tidal cycle i.e. 1 single, 20 cycle, 80 cycle and 120 cycle.
11. variation of soil pressure on upstream and downstream sides of sheet pile is reduced to a considerable extent. The maximum 50% reduction of soil pressure occurs at 3B/8 position.

12. Magnitude of soil pressure is less than that under static condition. It has been observed that peak magnitude decreases by maximum of 76% compared to static condition for 3*B*/8 position.

13. Factor of safety increases by maximum 16% to 17% for both static and seismic conditions with sheet pile, compared to factor of safety without sheet pile condition.

14. In seismic cases under steady state condition as pore water pressure increases the factor of safety is also reduced by 45% to 50% compared to corresponding static cases due to increase of seepage force

15. Compared to the steady state condition the factor of safety increases by 10% in rise up condition and decreases by 5%-10% in drawdown condition.

16. Factor of safety decreases on an average by 30% for transient state seismic condition, compared to steady state seismic condition.

    The decrease of FOS is about is 6% to 10% for drawdown condition as sheet pile moves for *B*/8 position to 3*B*/8 position for any given length during drawdown. It is further observed that as sheet pile length changes from 5m to 20m the FOS changes from on and average 15% to 35% under both rise up and drawdown conditions for any position of sheet pile.

17. In case of 120 cycles reduction factor of safety is 8.3%, 26% and 40%, on an average, compared to 80 cycles, 20 cycles and single tidal cycle respectively.

18. Under full rise up condition considering 5m of sheet pile at *B*/8 position factor of safety against piping increases up to 37.00% compared to 3*B*/8 position whereas this is approximately 18.75% for 2B/8 position, compared to 3*B*/8 position.

19. Factor of safety against piping increases by 5% to 10% due to increase of sheet pile length.

20. The generalized equation of factor of safety against piping for different parameter i.e. Pore water pressure (P_p), Fluid flow vector (y_f), Sheet pile length (L), Sheet pile position (T) as dependent variable

    $F_p = 325.8P_P^3 - 395.23P_P^2 + 151.7P_P - 16.537$

    $F_p = 64472\ y_f^{\,3} - 3332.5\ y_f^{\,2} + 21.855\ y_f + 1.9535$

    $F_p = 4E\text{-}05\ L^{\,3} - 0.0017\ L^{\,2} + 0.0249\ L + 1.567$

    $F_p = 0.0122\ T^2 - 0.1605\ T + 2.118$

The generalized equation of factor of safety against piping for different parameter i.e. Sheet pile length (*L*), Sheet pile position (*T*) with progress of time as dependent variable,

F_p=4.504+1.111×sin(0.8618×π×*L*×*T*)+8.271×$e^{-(4.767\times T)^2}$

21. The generalized optimized equation of overall factor of safety for different parameter i.e. Sheet pile length, Sheet pile position with progress of time as follows,

$Optimized\ Overall\ FoS$ (Under seismic condition)=3.620×10^{-05}× $x_1{}^2$ + 1.583×10^{-05}(x_1x_2) -4.712×10^{-05}(x_3) -0.0046x_1 -3.743×10^{-05}× $x_2{}^2$ -1.131×10^{-05} (x_2x_3) + 0.003x_2 + 1.18× 10^{18}(× $x_3{}^2$) -8.2× 10^8× x_3 + 7.09× 10^8

$Optimized\ Overall\ FoS$ (Under static condition)=-0.03520× $x_1{}^2$ -9.0×10^{-05}× (x_1x_2) -0.02900× (x_1x_3) + 0.47156× x_1 -0.00012× $x_2{}^2$ -0.000217× (x_2x_3) + 0.00717× x_2 -1.88×10^{12}× $x_3{}^2$ + 1.317×10^{13}× x_3 -1.12×10^{13}

$x_1 = Position\ of\ sheet\ pile\ from\ downstream\ end$

$x_2 = Sheet\ pile\ length$

$x_3 = Time\ in\ hr.$

22. Most advantageous location and length of sheet pile become *B/7* from downstream end and 0.88 times the base width of the dam respectively under both static and seismic condition for both steady and transient seepage.

6.3 FUTURE SCOPE OF WORK:

The following work may be carried out in the future in the following directions:

1. To carry out similar studies with varying soil parameters of embankment soil and foundation soil, and a number of working heads and varying geometry of dam section.
2. To study of effect of precipitation with inclusion of precipitation and infiltration parameters to investigate the stability of slopes for single and multiple tidal cycles.
3. To carry out centrifuge modelling with dams of different geometries with and without berms and having different upstream and downstream slopes with different upstream and downstream water heads under steady and transient states of seepage with tidal fluctuation.

REFERENCES

1. Ahmed-Zeki et al. (2000), " Monitoring the cut –off wall performance of upper Huia Dam", ASCE, GEO- INSTITUTE SPECIALITY CONFERENCE, USA, 9-12 April.

2. Aral Mustafa M., and Maslia Morris L. (1983), "Unsteady Seepage Analysis of Wallace Dam", J. Hydraul. Eng.109, pp.809-826.

3. Athania Shivakumar S. , Shivamanth , Solanki C. H. and Dodagoudar G. R. (2015), "Seepage and Stability Analyses of Earth Dam Using Finite Element Method" , International Conference On Water Resources, Coastal And Ocean Engineering (Icwrcoe 2015)), Elsevier , Aquatic Procedia 4, pp.876 – 883.

4. B. Kovács, I. Czinkota, L. Tolner, Gy. Czinkota (2003), "The determination of particle size distribution (PSD) of clayey and silty formations using the hydrostatic method"

5. Bligh, W.G. 1910. Dams, Barrages, and Weirs on Porous Foundations, *Engineering News*, **64**, (26), 708-710.

6. Boufadel, M.C., Suidan, M.T., Venosa, A.D., and Bowers, M.T. (1999), "Steady Seepage in Trenches and Dams: Effect of Capillary Flow", Journal of Hydraulic Engineering, Vol. 125, No. 3, March 1999, pp. 286-294.

7. Boufadel Michel C., Suidan Makram T.,Venosa Albert D. (1999), "Effect of Unsaturated Flow on Steady Seepage" , ASCE, Waterpower congress 1999.

8. Byrne, P. M. (1991). "A cyclic Shear-Volume Coupling and Pore Pressure Model for Sand Proceeding"; Second International Conference on Recent Advances in Geotechnical Earthquake Engineering and Soil Dynamics, March 11-15,St.Louis,Missouri, Paper No.1-24.

9. B. Minasny, J. W. Hopmans, T. Harter, S. O. Eching, A. Tuli, and M. A. Denton (2004), "Neural Networks Prediction of Soil Hydraulic Functions for Alluvial Soils Using Multistep Outflow Data", PREDICTION OF SOIL HYDRAULIC FUNCTIONS, SOIL SCI. SOC. AM. J., VOL. 68, PP. 417-429.

10. Cala, M., and J. Flisiak. (2001), "Slope stability analysis with FLAC and limit equilibrium methods, FLAC and Numerical Modeling in Geomechanics.

11. Cargill Kenneth W. and Ko Hon-Yim, (1983), "CENTRIFUGAL MODELING OF TRANSIENT WATER FLOW", ASCE, 1983, 109(4): 536-555.

12. Casagrande A.(1937), "Seepage Through Dams. Journal of the New EnglandWaterWorks Association, republished in Contributions to Soil Mechanics1925-1940, BostonSociety of Civil Engineers", Boston, MA, pp. 295-336.

13. Cedergren, Harry R. (1977), "Seepage, Drainage and Flow nets", Wiley, ISBN 0-471-14179-8.

14. Chakraborty Debarghya and Choudhuri Deepankar (2009), "Investigation of the Behaviour of the Tailings Earthen Dam under Seismic Conditions", Department of Civil Engineering, Indian Institute of Technology Bombay, Powai, mumbai-400076,India.

15. Chang, C.S., (1987): "Boundary Element Method in Draw Down Seepage Analysis for Earth Dams'', Journal of Computing in Civil Engineering, ASCE, Vol. 1, No. 2, April 1987, pp. 83-98.

16. CHEN Q., ZHANG L.M., (2006), "Three-dimensional analysis of water infiltration into the Gouhou rockfill dam using satu-rated-unsaturated seepage theory", Can. Geotech. J., *43*, 449—461.

17. Das, B.K., (2005), "A Preliminary Study on Identification of Probable Causes of Failure of Existing Earthen Embankments around Sunderban", Unpublished M.E. Thesis Submitted to Jadavpur University, Kolkata.

18. David zumr and Milena císlerová (2010), "soil moisture dynamics in levees during flood events – Variably saturated approach", J. Hydrol. Hydromech., pp. 58-69.

19. Davies M.C.R. and Parry R.H.G. (1985), "Centrifuge Modelling of Embankments on Clay Foundations" Soils and Foundations Vol.25, No.4, 19-36, Dec. 1985, Japanese Society of Soil Mechanics and Foundation Engineering.

20. Das Arghya & Viswanadham B.V.S. (2010), "Geofiber reinforced slopes subjected to seepage: Centrifuge study" Department of Civil Engineering, IIT Bombay, Powai, Mumbai-400076 India Email: viswam@civil.iitb.ac.in

21. Desai C.S, (1988), "Case Studies through Material Modeling and Computation", 2nd International Conference on Case Histories in Geotechnical Engineering, Missouri University of Science & Technology.

22. De Alba, P., Chan, C. K. and Seed, H. B. (1975). "Determination of Soil Liquefaction Characteristics by Large-Scale Laboratory Test," Report NO. EERC 75-14, Earthquake Engineering Research Center, University of California, Berkeley, California. Martin et al. (1975)

23. D. Rice and J. Michael Duncan. 2010. Findings of Case Histories on the Long-Term Performance of Seepage Barriers in Dams, John J. Geotech. Geoenviron. Eng., 2010, 136(1): 2-15

24. Dvinoff, A. H., and Harr, M. E. (1971), "Phreatic surface location after drawdown" J. Soil Mech. Found. ASCE. January.

25. Fredlund , Lu and Feng (2011), "Combined Seepage and Slope Stability Analysis of Rapid Drawdown Scenarios for Levee Design" Geo-Frontiers, ASCE 2011.

26. Fell and Wan (2005), "estimating the probability of failure of embankment dams by internal erosion, piping within the foundation".

27. Fenton, G.A. and Griffiths, D.V. (1996), "Statistics of free surface flow through a stochastic earth dam." J Geotech Eng, ASCE, vol.122, no.6, pp.427-436.

28. Fenton, G.A. and Griffiths, D.V. (1997), "A mesh deformation algorithm for free surface problems." Int J Numer Anal Methods Geomech, vol.21, no.12, pp.817-824.

29. Fogg, G.E., and Senger, R.K., (1985), "Automatic Generation of Flow Nets with Conventional Ground-Water Modeling Algorithms", Published by Bureau of Economic Geology, The University of Texas at Austin, Vol. 23, No. 3, May-June 1985, pp. 336344.

30. GEOSTUDIO, 2004-2012 GEO-SLOPE International, Ltd. Calgary, Alberta, Canada T2P 2Y5.

31. Hansen David and Roshanfekr Ali (2012), "Assessment of Potential for Seepage-Induced Unraveling Failure of Flow-Through Rockfill Dams", Int. J. Geomech. 12 pp.560-573.

32. Hasani, H., Mamizadeh, J. and Karimi, H. (2013), "Stability of Slope and Seepage Analysis in Earth Fills Dams Using Numerical Models (Case Study: Ilam Dam-Iran)", *World Applied Sciences Journal*, **21**, (9), 1398-1402.

33. Higo Y., Oka F., Kimoto S., Kinugawa T., Lee C.-W., Doi T. (2013), "Dynamic centrifugal model test for unsaturated embankments considering seepage", Department of Civil and Earth Resources Engineering, Kyoto University, Japan, Proceedings of the 18th International Conference on Soil Mechanics and Geotechnical Engineering, Paris 2013 flow and the numerical analysis.

34. Maosong Huang and Cang-Qin Jia (2009), "Strength reduction FEM in stability analysis of soil slopes subjected to transient unsaturated seepage'' Computer and Geotechnics, Vol. 36, 1-2, pp.93-101.

35. Huang, Y.H.,(1986): "steady State Phreatic Surface in Earth Dam", Journal of Geotechnical Engineering, Vol. 112, No. 1, January 1986, pp. 93-98.

36. IS 7894 of 1975: Code of practice for stability analysis of earthen dams.

37. Itasca Consulting Group, Inc. 2002. FLAC- Fast Lagrangian Analysis of Continua, Volumes 1-8 of program documentation, Minneapolis, Minnesota.

38. Itasca. 2005. User's guide for FLAC version 5.0., Itasca India Consulting, Nagpur, India.

39. Kaustav Chatterjee, and Deepankar Choudhury (2012), "Seismic stability analyses of soil slopes using analytical and numerical approaches", Proceedings of the ISET Golden Jubilee Symposium.

40. Khalilzad Mahdi , Gabr M. A., and Hynes Mary Ellen, (2014), "Deformation-Based Limit State Analysis of Embankment Dams Including Geometry and Water Level Effects", Int. J. Geomech 04014086,pp.1-11.

41. Khassaf, S. I., Abdoul- Hameed, M. R., Shams Al-deen, N.N., (2013), "Slope Stability Analysis under Rapid Drawdown Condition and Siesmic Loads of Earth Dam (Case Study: Mandali Dam)", International Journal of Innovative Research in Science, Engineering and Technology, Vol.2, Issue 12, pp. 7114-7118.

42. Khosla, M.N., Bose, K.K. and Taylor, M.T. (1954), "Design of Weirs on Permeable Foundation", *CBIP, Malcha Marg, New Delhi*, Pub. No. 12.

43. K.F. Alsenousi and Hasan G. Mohamed (2008), "Effects of inclined cutoffs and soil foundation characteristics on seepage beneath hydraulic structures", Twelfth International Water Technology Conference, IWTC12 2008, Alexandria, Egypt 1597.
44. Lane, E.W. (1935). Security from Underseepage, *Trans. ASCE*, **100,** 1235.
45. Lane P. A., Griffiths D. V , (2000), "Assessment Of Stability Of Slopes Under Drawdown Conditions", J.Geotech. Geoenviron. Eng.126, pp.443-450.
46. Laplace, P. S., Memory on the approximations of the formulas which are functions of very large numbers. Same. Acad. roy. Sci. (Paris) (1782, 1785), 1-88. Complete Works of Laplace (Paris: Gauthier-Villars, 1878-1912) 10, 209-291.
47. P. Forchheimer (1880), "Wasserbewegung durch boden", Zeitschrift Ver D Ing, 45 (1901), pp. 1782-1788
48. Richardson, E.V., Simons, D.B. and Julian, P.Y., (1990), "Highways in the River Environment," Design and Training Manual, U.S. Department of Transportation, Federal Highway Administration, Washington D.C, (Civil Engineering Department Report, Colorado State University, 1987).
49. T. M. Le (2013), "Stability and Deformation of Sheet Pile Walls for Protecting Riverside Structures in the Mekong River Delta", American Society of Civil Engineers, Reston, Virginia, pp. 1349-1358.
50. T. Lee and C. H. Benson. (2000), "Flow past bench- scale vertical ground-water cutoff walls", *J. Geotechnical and Geoenvironmental Engineering*. **1256**,511-520.
51. Li, G.C, and Desai, C. (1983), "Stress and Seepage Analysis of Earth Dams", *Journal of Geotechnical Engineering, ASCE,***109**, (7), 946-960
52. López, Acosta N.P., Fuente de la H.A., Auvinet G., (2013), "Safety of a protection levee under rapid drawdown conditions. Coupled analysis of transient seepage and stability", Proceedings of the 18th International Conference on Soil Mechanics and Geotechnical Engineering, Paris
53. MATLAB 2014 a, MATHWORKS, Natick, UNITED STATES

54. Manzari Majid T. (1996), "Seismic Analysis of Soil Embankments", CMEE Department, George Washington University, Washington DC 20052.

55. Marsal, R.J. and Resendiz, D., (1971), "Effectiveness of Cutoffs in Earth Foundations and Abutments of Dams", Proceedings of the 4th Panamerican Conferance on Soil mechanics and Foundation Engineeering, American Society of Civil Engineers, San Juan, Puerto Rico, pp.237-312.

56. McCook, D (2004), "A comprehensive discussion on the mechanisms of piping and internal erosion failure mechanism", Annual association of state dam officials, 1-6.

57. Mishra, G.C, Singh,A.K., (2005), "Seepage through a Levee", International Journal ofGeomechanics, ASCE, Vol. 5, No. 1, March 2005, pp. 74-79.

58. Moayed R. Ziaie, Rashidian V., Izadi E., (2012), "Evaluation of Phreatic Surface in Homogenous Dams with different drainage systems", Innovative Dam & Levee Design and Construction, pp.619-626.

59. Morgenstern, N.R., and Price, V.E., (1965), "The Analysis of the Stability of General Slip Surfaces", Geotechnique, Vol. 15, pp. 79-93.

60. Perri., J,F, and Shewbridge. S, E, and Cobos-Roa.,D, A, and Green.,R, K, (2012), "Steady State Seepage Pore Water Pressures Influence in the Slope Stability Analysis of Levees",*GeoCongress , ASCE.*

61. Pham HTV, Fredlund DG. (2003), "The application of dynamic programming to slope stability analysis", Canadian Geotechnical Journal **40**(4): 830-847.

62. Richards Kevin, S.,. and Reddy Krishna, R.. (2005), "Slope Failure of Embankment Dam under Extreme Flooding Conditions:Comparison of Limit Equilibrium and Continuum Models" , *GSP 140 Slopes and Retaining Structures under Seismic and Static Conditions, ASCE.*

63. Rakhshandehroo and Pourtouiserkani (2013), "predicting doroodzan dam hydraulic behavior during rapid drawdown", IJST, Transactions of Civil Engineering, Vol. 37, No. C2, pp 301-310.

64. Robert J.Huzjak, Adam B. Prochaska and James A. Olsen, (2008), "Transient seepage analyses of soil-cement uplift pressures during reservoir drawdown", Biennial Geotechnical conference 2008.

65. Schmertmann j.h., (2006), "Estimating slope stability re-duction due to rain infiltration moulding", Journal of Geo-technical and Geoenvironmental Engineering, 132, 9, 1219—1228.

66. Schofield Andrew N. and Steedman R Scott (1988), "State of the Art Report RECENT DEVELOPMENT on Dynamic MODEL TESTING IN GEOTECHNICAL ENGINEERING", Cambridge University Engineering Department, Trumpington Street,Cambridge,U.K, Proceedings of Ninth World Conference on Earthquake Engineering, August 2-9,1988, Tokyo-Kyoto, JAPAN(Vol. VIII).

67. Sherard. J. L., Woodward. R. J., Gizienski. S.F., and Clevenges. W. A. (1963), "The mechanics of piping in earth and earth-rock dams.", John Wiley & Sons, New York.

68. Thieu, N.T.M., Fredlund, M.D., Fredlund,D.G., and Hung, V.Q., (2001), "Seepage Modeling in a Saturated/Unsaturated Soil System", International Conference on Management of the Land and Water Resources, MLWR, October 20-22, 2001Hanoi, Vietnam

69. Timothy D. Stark, Navid H. Jafari, J. Sebastian Lopez Zhindon and Ahmed Baghdady. 2017. Unsaturated and Transient Seepage Analysis of San Luis Dam, *J. Geotechnical and Geoenvironmental Engineering*. 143(2): 04016093

70. Turnbull, W.J., Mansur, C.I., (1961), "Investigation of Underseepage – Mississippi River levees". Trans. ASCE 126, 1429–1485

71. U.S. Army Corps of Engineers CECW-ED Washington, DC 20314-1000 Manual No.1110-2-2502 29 September 1989 Engineering and Design RETAINING AND FLOOD WALLS.

72. VandenBerge Daniel R., Duncan J. Michael and Brandon Thomas L., (2015), "Limitations of Transient Seepage Analyses for Calculating Pore Pressures during External Water Level Changes", J. Geotech. Geoenviront. Eng.141.

73. Wenjun Dong (2005),"Finite Element Soil-Pile-Interaction Analysis of Floodwall in Soft Clay", Ph.D., P.E., M. ASCE and Neil T. Schwanz, P.E., MVD Geotechnical Regional Technical Specialist

74. Xu G. M., L. Zhang and Liu S. S. (2005) ,'Preliminary Study of Instability Behavior of Levee on Soft Ground during Sudden Drawdown' , Slopes and Retaining Structures Under Seismic and Static Conditions.

75. Yamagami, T., and Ueta, Y. (1988), "Search for noncircular slip surfaces by the Morgenstern-Price method." Proc., 6th Int. Conf. on Numerical Methods in Geomechanics, 1219–1223.

76. Y. Hata, K. Ichii, and Tokida Ken-ichi (2011), "A probabilistic evaluation of the size of earthquake induced slope failure for an embankment", Georisk: Assessment and Management of Risk for Engineered Systems and Geohazards, pp. 1-16.

77. Zou, Jin-Zhang, and Williams, David J. and Xiong Wen-Lin (1995), "Search for critical slip surfaces based on finite element method"Canadian Geotechnical Journal, 1995, 32(2): 233-246, https://doi.org/10.1139/t95-026.

78. Thusyanthan N. I. & Madabhushi S.P.G. (2003) "Scaling of Seepage Flow Velocity in Centrifuge Models" CUED/D-SOILS/TR326.

79. United States Society on Dams "Strength of Materials for Embankment Dams", February 2007

80. USACE (1989), U.S. Army Corps of Engineers CECW-ED Washington, DC 20314-1000 Manual No.1110-2-2502 29 September 1989 Engineering and Design RETAINING AND FLOOD WALLS.

81. VAN GENUCHTEN, M.Th (1980), "A closed-form equation for predicting the hydraulic conductivity of unsaturated soils." Soil Sci. Soc. Am. J., 44:892-898.

82. William Meyer, R. L. Schuster and M. A. Sabol. (1994), " POTENTIAL FOR SEEPAGE EROSION OF LANDSLIDE DAM", J. Geotech. Engrg., 1994, 120(7): 1211-1229

83. Zheng Y. R., Shi W. M., Kong W. X. , Lei W. J., (2005), "Determination of the phreatic-line under reservoir drawdown condition" , Slopes and Retaining Structures Under Seismic and Static Conditions